

Graduate Texts in Physics

Sérgio Luiz Morelhão

Computer Simulation Tools for X-ray Analysis

Scattering and Diffraction Methods

LEYBOLD®

 Springer

Graduate Texts in Physics

Series Editors

Professor Richard Needs
Cavendish Laboratory
JJ Thomson Avenue
Cambridge CB3 0HE, UK
rn11@cam.ac.uk

Professor William T. Rhodes
Department of Computer and Electrical Engineering and Computer Science
Imaging Science and Technology Center
Florida Atlantic University
777 Glades Road SE, Room 456
Boca Raton, FL 33431, USA
wrhodes@fau.edu

Professor Susan Scott
Department of Quantum Science
Australian National University
Science Road
Acton 0200, Australia
susan.scott@anu.edu.au

Professor H. Eugene Stanley
Center for Polymer Studies Department of Physics
Boston University
590 Commonwealth Avenue, Room 204B
Boston, MA 02215, USA
hes@bu.edu

Professor Martin Stutzmann
Walter Schottky Institut
TU München
85748 Garching, Germany
stutz@wsi.tu-muenchen.de

Graduate Texts in Physics publishes core learning/teaching material for graduate- and advanced-level undergraduate courses on topics of current and emerging fields within physics, both pure and applied. These textbooks serve students at the MS- or PhD-level and their instructors as comprehensive sources of principles, definitions, derivations, experiments and applications (as relevant) for their mastery and teaching, respectively. International in scope and relevance, the textbooks correspond to course syllabi sufficiently to serve as required reading. Their didactic style, comprehensiveness and coverage of fundamental material also make them suitable as introductions or references for scientists entering, or requiring timely knowledge of, a research field.

More information about this series at <http://www.springer.com/series/8431>

Sérgio Luiz Morelhão

Computer Simulation Tools for X-ray Analysis

Scattering and Diffraction Methods



Springer

Sérgio Luiz Morelhão
Institute of Physics
University of São Paulo
São Paulo, Brazil

The author wish to acknowledge LD Didactic for sponsoring the translation of this book from Portuguese, its original language.

ISSN 1868-4513

Graduate Texts in Physics

ISBN 978-3-319-19553-7

DOI 10.1007/978-3-319-19554-4

ISSN 1868-4521 (electronic)

ISBN 978-3-319-19554-4 (eBook)

Library of Congress Control Number: 2015944087

Springer Cham Heidelberg New York Dordrecht London

© Springer International Publishing Switzerland 2016

This work is subject to copyright. All rights are reserved by the Publisher, whether the whole or part of the material is concerned, specifically the rights of translation, reprinting, reuse of illustrations, recitation, broadcasting, reproduction on microfilms or in any other physical way, and transmission or information storage and retrieval, electronic adaptation, computer software, or by similar or dissimilar methodology now known or hereafter developed.

The use of general descriptive names, registered names, trademarks, service marks, etc. in this publication does not imply, even in the absence of a specific statement, that such names are exempt from the relevant protective laws and regulations and therefore free for general use.

The publisher, the authors and the editors are safe to assume that the advice and information in this book are believed to be true and accurate at the date of publication. Neither the publisher nor the authors or the editors give a warranty, express or implied, with respect to the material contained herein or for any errors or omissions that may have been made.

Printed on acid-free paper

Springer International Publishing AG Switzerland is part of Springer Science+Business Media (www.springer.com)

*To my wife Marilza and daughters Thalia and
Larissa for caring and understanding of my
dedication to this project.*

Book Credits

Translation into English:
Luana Guedes, Gary Fray
Prioridade Consultoria Ltda.



For sponsoring the translation of this book from Portuguese, its original language.
LD DIDACTIC GmbH, Leyboldstr. 1, 50354 Hürth, Germany

LEYBOLD®

Preface

This book is dedicated to students who need to assimilate extensive knowledge in a short period of time. The international scientific production has increased at a breakneck pace, demanding more dynamic approaches and synergies between different areas of knowledge. Mastering X-ray scattering and diffraction methods means to be competent to work in an infinity of areas, studying the various systems where the organizational understanding of matter at the atomic scale is necessary. Since the discovery of X-radiation, its use as an investigative tool has always been in wide expansion provided by advances in instrumental and computational resource. The current development in the fields of medicine and technology has as one of its supporting pillars the structural analysis offered by X radiation. One of the greatest difficulties faced by beginners in the effective use of this fantastic tool is in analyzing the experimental results. Few are the situations where it is possible to extract structural information directly from the experiments. In most situations, computer programs are necessary for simulating the interaction of radiation with matter. The advent of intense radiation sources and the rapid development of nanotechnology constantly create challenges for solutions beyond those offered by the already settled techniques. Preparing new researchers for this scenario of rapid and drastic changes requires more than teaching physical phenomena theories, it also calls for teaching how to implement them in a simple and efficient way. In this book, the fundamental concepts needed to analyze a wide range of materials (macromolecules, liquids, nanoparticles, polymers, amorphous, polycrystals, small-molecule crystals, and protein crystals) using scattering and diffraction techniques are demonstrated through computer simulation tools. The chapters follow an ascending order going from disordered to ordered matter, covering various types of samples and targeting a unification of theoretical approaches. There are exercises that go with each topic presented, which are proposed and solved. There are more than 80 routines in MatLab developed for solving the exercises. Therefore, besides X-ray physics, this book also offers a practical programming course in modern, high-level language with an infinity of graphic and mathematical resources.

Acknowledgements

I would like to thank Professor Márcia C. A. Fantini and technician Társis M. Germano of the Laboratory of Crystallography, Institute of Physics-USP, for encouraging words and technical help along the preparation of this book. Discussions with other professors and students, in particular Professor Mauro S. D. Cattani, Prof. Leandro R. S. Barbosa, Prof. Giancarlo E. S. Brito, Ms. Gaspar Darin, and Dr. Raul O. Freitas, were very useful to enlighten some topics and have contributed to the final form in which ideas are presented here.

Contents

1 Fundamentals of X-Ray Physics	1
1.1 Radiation–Electron (Free Electron) Elementary Interaction	1
1.1.1 Polarization Effects	2
1.1.2 Radiation Field	5
1.1.3 Coherence Lengths	8
1.2 Scattering of X-Rays by Distributions of Free Electrons	12
1.2.1 Mathematical Tools: Fourier Transform	15
1.2.2 Distributions of One Electron and the Compton Scattering ..	19
1.3 Atoms and Molecules	23
1.3.1 Spherically Symmetrical Atoms	23
1.3.2 Scattering by Single Molecules and the “Phase Problem” ..	28
1.3.3 Compton Scattering by Atoms	33
1.4 X-Ray Absorption	38
1.4.1 Linear Attenuation Coefficient	39
1.4.2 Atomic Resonance	42
1.4.3 Semi-classical Approach of Atomic Resonance: Electron Elastically Bound	45
1.4.4 Kramers–Kronig Relations	48
1.4.5 Absorption Modulation by Rescattering of Photoelectrons...	50
2 Low Correlated Systems: Gases and Dilute Solutions	59
2.1 Monatomic Gas	59
2.2 Dispersed Molecules: Random Orientations	63
2.3 Small Angle Scattering	67
2.3.1 Macromolecules	68
2.3.2 Particles of Uniform Density	69
2.3.3 Morphology of Particles	71
2.3.4 Polydisperse Systems and Dispersion of Size	74
3 Complex Systems	81
3.1 Internal Correlations in Particles	84
3.1.1 Molecules, Proteins, and Discrete Particles in General	86

3.1.2	Particles of Random Conformation	94
3.2	Arbitrary Correlations Between Particles	100
3.2.1	Mutual Interference	102
3.2.2	Volume Effects	102
3.2.3	Liquids and Colloidal Suspensions	109
3.2.4	Radial Distribution Function	110
3.2.5	Amorphous	117
4	Crystals	127
4.1	Elements of X-Ray Crystallography	128
4.1.1	Unit Cell and Crystalline Lattice	128
4.1.2	Structure Factors and Diffracted Intensities	134
4.2	Truncation of the Crystal Lattice	138
4.3	Atomic Disorder in Crystalline Structures	142
4.3.1	Thermal Vibrations	142
4.3.2	Occupancy Factor	147
5	Applications of Kinematic Diffraction	151
5.1	Working in the Reciprocal Space	152
5.2	Powder Diffractometry	157
5.2.1	Relative Intensities in Polycrystalline Samples	158
5.3	Single Crystal Diffractometry	165
5.3.1	With Monochromatic Radiation	165
5.3.2	With Polychromatic Radiation	170
5.4	Protein Crystals	174
6	Dynamical Diffraction	179
6.1	Recursive Equations	180
6.1.1	Standing Waves	186
6.2	Kinematic Limit	187
6.3	Refraction Index for X-Rays	189
7	Worked Examples	195
7.1	PDDF Analysis of Lysozyme	195
7.1.1	Contents	195
7.1.2	Loading Intensity Data	196
7.1.3	Inverse Fourier Transform	196
7.1.4	Gyration Radius	197
7.2	PDF Analysis of Gold Nanoparticles	197
7.2.1	Contents	198
7.2.2	Loading Intensity Data	198
7.2.3	Structural Function $S(Q)$	199
7.2.4	Background Correction	199
7.2.5	Normalizing $S(Q)$	200
7.2.6	Fourier Analysis	201
7.3	XRD Analysis of Alumina	201
7.3.1	Contents	203

7.3.2	Loading Intensity Data	203
7.3.3	Adjusting the Background Intensity	204
7.3.4	XRD Pattern Simulation from a CIF	204
7.3.5	Comparison of Experimental and Simulated Patterns	205
7.4	Measurement of Absorption Edge.....	206
7.4.1	Contents	207
7.4.2	Experimental Data	207
7.4.3	Transmission Coefficients	208
7.4.4	Photoelectric Absorption Cross-Section	208
A	Electric Dipole Radiation by a Free Electron	211
B	MatLab Routines	213
	Bibliography	283
	Index	287

Chapter 1

Fundamentals of X-Ray Physics

1.1 Radiation–Electron (Free Electron) Elementary Interaction

In the classical description of electromagnetic radiation, X-rays are waves similar to radio, TV, and light waves, but with a much smaller wavelength, λ of the order of 1 Å (10^{-10} m). The wave nature of X-rays give rises to the phenomena of interference at an atomic scale, which provide the various scattering and diffraction techniques that will be covered in this book. Moreover, there is also a quantum description of the electromagnetic fields based on the particle nature of electromagnetic radiation, which means that it behaves as a beam of photons created and annihilated by interacting with matter. Absorption and detection of X-ray photons are intrinsically quantum phenomena explored in techniques for analyzing materials by absorption spectroscopy and X-ray fluorescence. The radiation–electron interaction that gives rise to an absorption process occurs mainly with atomic electrons, i.e., with bound electrons in general. In this section we address the elementary interaction of X-rays with free electrons.

There are only two relevant elementary interactions of X-rays with free electrons: elastic scattering and inelastic scattering, which are also often called Thomson scattering and Compton scattering, respectively. The conservation laws of linear momentum and energy prevent a free electron from annihilating (absorbing) a photon, converting all the energy of the photon,

$$\mathcal{E}[\text{eV}] = \frac{2\pi\hbar c}{\lambda} = \frac{12398.5}{\lambda[\text{\AA}]} , \quad (1.1)$$

into its own kinetic energy. In the Compton effect, only part of the photon energy is converted into the electron's kinetic energy. The scattered photon has slightly lower energy (larger λ), which consists of an inelastic scattering. Because it is

a manifestation of the particle nature (quantum) of the electromagnetic field, the scattering by the Compton effect destroys any phase correlation with the incident wave and hence there is no interference effects related to this inelastic scattering process. Although the intensity of the Compton scattering is present as a background intensity without a correlation with the atomic structure of the materials, it is often neglected or subtracted from the experimental data of the coherent scattering of X-rays.

In addition to the scattering processes, there is also the absorption by the vacuum in a process where the X-ray photons are annihilated in the creation of electron-positron pairs. The probability of a photon to be annihilated and give origin to an electron-positron pair is very small and, in general, is not taken into account by analytical techniques of materials. Therefore, the elementary interaction of X-rays with free electrons is essentially an elastic scattering process treatable by classical electromagnetic theory, as done by J.J. Thomson in the late nineteenth century where the incident radiation of angular frequency ω is described as a function of the position vector \mathbf{r} , and of the time t , by a plane wave such as

$$\mathbf{E}(\mathbf{r}, t) = \mathbf{E}_0 e^{\pm i(\omega t - \mathbf{k}\cdot\mathbf{r})}. \quad (1.2)$$

The incidence direction is given by wavevector $\mathbf{k} = k\hat{s}$, of modulus $k = 2\pi/\lambda = \omega/c$. Although the electromagnetic wave has both electric, \mathbf{E} , and magnetic, \mathbf{B} , fields where $\mathbf{k} \cdot \mathbf{E} = \mathbf{k} \cdot \mathbf{B} = \mathbf{E} \cdot \mathbf{B} = 0$, it is common to represent the X-ray electric field only, as in (1.2).

1.1.1 Polarization Effects

In the presence of the electric field of an incident X-ray beam, a free electron is forced to vibrate and begins to radiate in a similar way to electrons in a dipole antenna. There is no emission of radiation in the direction along the length of the antenna. It is a characteristic of the electric dipole radiation and can be understood as a consequence of the Biot–Savart law. Thus, if the X-ray wave is linearly polarized, that is $\mathbf{E}_0 = E_0\hat{e}$, the radiation from the electron is null in the direction of the versor \hat{e} . On the other hand, the radiation is maximum in the electron's plane perpendicular to versor \hat{e} , as depicted in Fig. 1.1a.

In X-ray physics, the observation direction \hat{s}' , of the scattered radiation is in general given by the angle 2θ measured from the incidence direction \hat{s} , Fig. 1.1b. Both directions, incidence and observation, define a virtual plane named “incidence plane.” A complete description of the scattering requires \mathbf{E}_0 to be specified with respect to the incidence plane, which is done through versors

$$\hat{\sigma} = \hat{s} \times \hat{s}' / \sin 2\theta \quad \text{and} \quad \hat{\pi} = \hat{\sigma} \times \hat{s}, \quad (1.3)$$

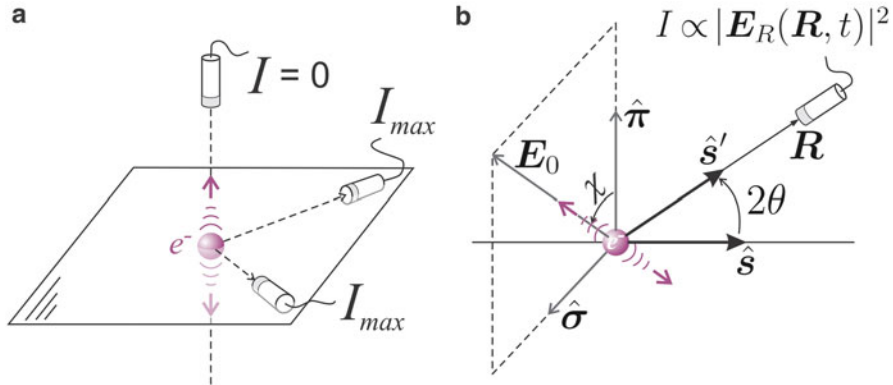


Fig. 1.1 Electron in forced vibration. (a) The scattered intensity is maximum, $I = I_{\max}$, on the plane containing the electron and perpendicular to the vibration direction, and is null, $I = 0$, along this direction. (b) Electric field vector \mathbf{E}_0 of the incident radiation described with respect to $\hat{\sigma} = \hat{s} \times \hat{s}' / \sin 2\theta$ and $\hat{\pi} = \hat{\sigma} \times \hat{s}$ directions. Incidence direction: \hat{s} . Observation position of the scattered intensity: $\mathbf{R} = R\hat{s}'$. Incidence plane: the plane that contains both \hat{s} and \hat{s}' directions

perpendicular and parallel to the incidence plane, respectively, Fig. 1.1b. In the case of linearly polarized radiation such as synchrotron radiation, we have

$$\hat{\epsilon} = \cos(\chi)\hat{\pi} + \sin(\chi)\hat{\sigma}. \quad (1.4)$$

For $2\theta = 0$, the amplitude of scattering is maximum and independent of the polarization angle χ . But, for $2\theta = 90^\circ$ the amplitude is null if $\chi = 0$, Fig. 1.1a.

The vectorial polarization factor (Appendix A),

$$\mathcal{P}(\hat{s}') = \hat{s}' \times (\hat{\epsilon} \times \hat{s}'), \quad (1.5)$$

summarizes the polarization effects in the scattered electric field, $\mathbf{E}_R(\mathbf{R}, t) = \mathcal{P}(\hat{s}') \mathbf{E}_R(R, t)$, observed at point $\mathbf{R} = R\hat{s}'$, Fig. 1.1b. The measurable intensity I is proportional to the field square modulus, i.e., $I \propto |\mathbf{E}_R(\mathbf{R}, t)|^2 = |\mathcal{P}(\hat{s}')|^2 |\mathbf{E}_R(R, t)|^2$.

Note 1.1: The classical intensity of an electromagnetic field is defined as energy per unit of time per unit of area, that is Joules ($\text{J}/\text{s m}^2$). In X-ray physics, intensity means the number of photons detected in a given interval of time. Comparing with the classical definition of intensity,

$$I = \frac{\text{classic intensity } \left(\frac{\text{J}}{\text{s m}^2} \right) \times \text{detection area } (\text{m}^2)}{\text{photon energy, } \mathcal{E} (\text{J})}.$$

To exemplify the use of polarization factors, let us choose $\hat{s} = [0, 0, 1]$, $\hat{\pi} = [1, 0, 0]$, $\hat{\sigma} = [0, 1, 0]$, $\hat{e} = [\cos \chi, \sin \chi, 0]$ and $\hat{s}' = [\sin 2\theta, 0, \cos 2\theta]$, which provides by (1.5) the general expression

$$\mathcal{P} = [\cos \chi \cos^2 2\theta, \sin \chi, -\cos \chi \cos 2\theta \sin 2\theta] \quad (1.6)$$

as a function of χ . Hence, for σ and π polarizations, we have:

$$\mathcal{P} = \begin{cases} \hat{\sigma}, & |\mathcal{P}|^2 = 1 \text{ if } \hat{e} = \hat{\sigma} (\chi = 90^\circ, \sigma \text{ polarization}) \\ \cos 2\theta [\cos 2\theta, 0, -\sin 2\theta], & |\mathcal{P}|^2 = \cos^2 2\theta \text{ if } \hat{e} = \hat{\pi} (\chi = 0, \pi \text{ polarization}) \end{cases}$$

In the case of unpolarized X-rays generated by compact sources—sealed tubes and rotating anodes without beam conditioning devices such as monochromators and/or focusing optics—the scattered intensity is the intensity average over all possible values of χ , i.e., $I \propto \langle |\mathcal{P}|^2 \rangle |E_R(R, t)|^2$ where

$$\langle |\mathcal{P}|^2 \rangle = \langle \sin^2 \chi \rangle + \langle \cos^2 \chi \rangle \cos^2 2\theta = \frac{1}{2}(1 + \cos^2 2\theta) \quad (1.7)$$

is the scalar polarization factor.

...

Exercise 1.1. It is known that crystals are used to filter (making monochromatic) and direct X-ray beams. (a) An unpolarized X-ray beam is reflected by a crystal at an angle of $2\theta = 90^\circ$. What is the reflected beam's polarization? (b) In experiments where angular and spectral high resolutions are required, a typical monochromator is the 4-reflection monochromator. What is the polarization of the monochromatized beam when $2\theta = 45.3^\circ$ in each reflection?

Answer (a): The resulting polarization is linear: $\mathcal{P} = [0, \sin \chi, 0]$ for each component χ of the unpolarized beam, Fig. 1.1b. As χ ranges from 0 to 2π , the polarization factor is

$$\langle |\mathcal{P}|^2 \rangle = \langle \sin^2 \chi \rangle = 1/2.$$

Answer (b): By taking $\hat{s} = [0, 0, 1]$ as the direction of the incident beam and according to the scheme in Fig. 1.2, the reflected beam directions \hat{s}'_n ($n = 1, \dots, 4$), are

$$\hat{s}'_1 = [\sin 2\theta, 0, \cos 2\theta], \quad \hat{s}'_2 = [0, 0, 1], \quad \hat{s}'_3 = [-\sin 2\theta, 0, \cos 2\theta] \quad \text{and} \quad \hat{s}'_4 = [0, 0, 1].$$

Since $\mathcal{P}_0 = \hat{e} = [\cos \chi, \sin \chi, 0]$ stands for a given component of polarization of the incident beam,

$$\mathcal{P}_n = \hat{s}'_n \times (\mathcal{P}_{n-1} \times \hat{s}'_{n-1})$$

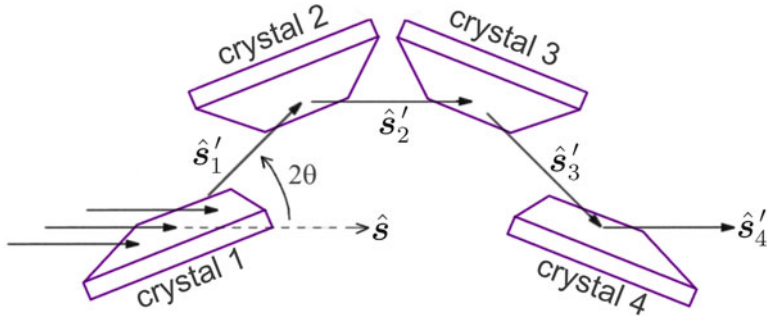


Fig. 1.2 The four-reflection monochromator

is the polarization after n reflections. As $\mathcal{P}_4 = [\cos^4 2\theta, 0, 0]$ for $\chi = 0$ and $\mathcal{P}_4 = [0, 1, 0]$ for $\chi = 90^\circ$, we have $\mathcal{P}_4(\chi) = [\cos^4 2\theta \cos \chi, \sin \chi, 0]$, and hence,

$$\langle |\mathcal{P}_4|^2 \rangle = \frac{1}{2} (1 + \cos^8 2\theta) = 0.53 \quad (\text{nearly linear polarization}) .$$

...

1.1.2 Radiation Field

We already know how to take into account polarization effects in the scattered radiation by a free electron, but we still have to calculate the amplitude of scattering $E_R(R, t)$. Since the polarization is considered through vector \mathcal{P} , $E_R(R, t)$ is simply the radiation field in the electron's plane perpendicular to the acceleration (vibration) direction.

The radiated field by an accelerated charge is derived directly from Maxwell's equations as demonstrated in many textbooks of classical electromagnetism.¹ In the International System of units, this derivation results in

$$E_R(R, t) = \frac{e}{4\pi\epsilon_0 c^2 R} \ddot{z}(t') \quad (1.8)$$

where $\ddot{z}(t')$ is the electron acceleration perpendicular to the observation plane, Fig. 1.1a, at a time instant $t' = t - R/c$, generating the field at a distance R and time instant t . The electron is accelerated in response to the incident electric field, (1.2), that is

¹Classical Electrodynamics, J.D. Jackson; Foundations of Electromagnetic Theory, J.R. Reitz and F.J. Milford; ...etc. See also Appendix A.

$$\ddot{z}(t') = \frac{-e}{m} E(\mathbf{r} = 0, t') = \frac{-e}{m} E_0 e^{\pm i\omega t'} = \frac{-e}{m} E_0 e^{\pm i(\omega t - kR)} \quad (1.9)$$

where e and m are the electron charge (in modulus) and mass, respectively. By replacing in (1.8) we have

$$\frac{E_R(R, t)}{E_0} = - \left(\frac{e^2}{4\pi\epsilon_0 mc^2} \right) \frac{e^{\pm i(\omega t - kR)}}{R} = -r_e \frac{e^{\pm i(\omega t - kR)}}{R}. \quad (1.10)$$

$r_e = 2.818 \times 10^{-5}$ Å is called classical electron radius or Thomson scattering length. Note that the amplitude of scattering is proportional to $1/R$. This ensures that the total radiated power is constant over any spherical surface of radius R around the electron. Also note the negative sign in (1.10), indicating that the scattered field has a 180° phase lag with respect to the incident X-ray wave. Taking the polarization effect into account, the full expression of the field scattered by the electron at the origin, $\mathbf{r} = 0$, and observed at position \mathbf{R} , is

$$E_R(\mathbf{R}, t) = \mathcal{P} E_R(R, t) = -r_e \mathcal{P} E_0 \frac{e^{\pm i(\omega t - k' \cdot \mathbf{R})}}{R} \quad (1.11)$$

where \mathbf{k}' is the wavevector of the scattered radiation. Since it is an elastic scattering, $|\mathbf{k}'| = k = 2\pi/\lambda$ (same λ of the incident wave).

Although the essential points of the scattering theory are synthesized in the above equations, there still lacks of establishing a practical bridge between theory and experiment. To this end, we assume an incident X-ray beam with a photon flux Φ per square meter per second, which in terms of incident amplitude E_0 , is given by

$$\Phi = \frac{\text{classical intensity}}{\mathcal{E}} = \frac{\frac{1}{2}\epsilon c |E_0|^2}{\mathcal{E}}. \quad (1.12)$$

c is the speed of light, and ϵ is the dielectric permittivity. In a detector placed at position \mathbf{R} , covering a solid angle $d\Omega$, the intensity of scattered radiation according to (1.11) is

$$I_{Th} = \overbrace{\left(\frac{\frac{1}{2}\epsilon c \langle |\mathcal{P}|^2 \rangle |E_R|^2}{\mathcal{E}} \right)}^{\text{scattered photons/m}^2/\text{s}} \overbrace{R^2 d\Omega}^{m^2} = \Phi \left(\frac{\langle |\mathcal{P}|^2 \rangle |E_R|^2}{|E_0|^2} \right) R^2 d\Omega = \Phi \langle |\mathcal{P}|^2 \rangle r_e^2 d\Omega \quad (1.13)$$

where $\langle |\mathcal{P}|^2 \rangle r_e^2$ is the differential cross-section $(\frac{d\sigma}{d\Omega})_{Th}$, of the Thomson scattering; a quantity independent of the photon energy.

Considering all directions in space, the total intensity scattered by one electron is obtained by integration of (1.13):

$$I_{tot} = \Phi r_e^2 \int \langle |\mathcal{P}|^2 \rangle d\Omega = \Phi \sigma_{Th} . \quad (1.14)$$

$\sigma_{Th} = 8\pi r_e^2/3 = 6.6525 \times 10^{-29} \text{ m}^2 = 0.66525 \text{ barn}$ is the total cross-section of the Thomson scattering.

...

Exercise 1.2. (a) What is the flux Φ to provide 1 photon/s inside a cubic volume V , of edge $L = 0.1 \text{ mm}$? (b) What is the classical intensity, or beam power P per unit of area (W/cm^2), for photons of wavelength $\lambda = 1.23985 \text{ \AA}$?

Answer (a): If I is the incident intensity perpendicular to a face of the cube, the flux will be $\Phi = I/L^2$. Since L/c is the time for a photon to cross the volume, we will have 1 photon/s inside the cube when $I = c/L$, which leads to $\Phi = c/L^3 = c/V = 3 \times 10^{20} \text{ photons/m}^2/\text{s}$.

Answer (b): $P = \Phi \mathcal{E} = (3 \times 10^{20})(10^{-4})(10^4)(1.6 \times 10^{-19}) = 48 \text{ W/cm}^2$.

Exercise 1.3. Determine the total intensity I_{tot} , scattered by a small cube-shaped GaAs (gallium arsenide²) sample of 0.1 mm edge, fully placed in an X-ray beam with cross section $S_0 = 0.5 \times 0.5 \text{ mm}^2$ and intensity $I_0 = 10^6 \text{ cps}$ (cps = counts per second), Fig. 1.3a. Neglect interference and diffraction phenomena, absorption, and re-scattering.

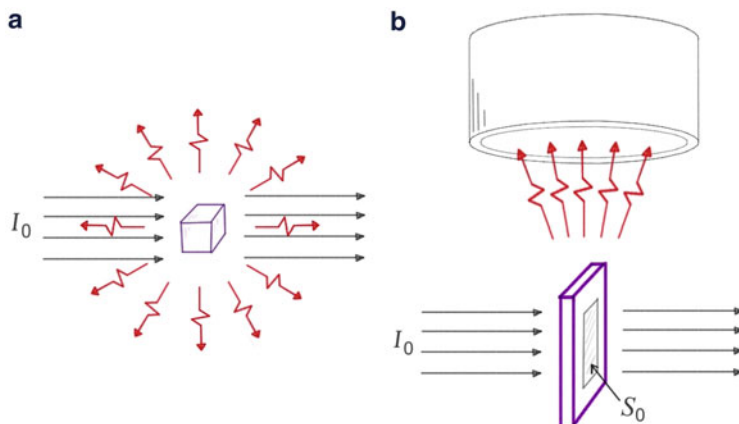


Fig. 1.3 Samples (a) smaller and (b) larger than the cross section S_0 , of the incident beam of intensity $I_0 = \Phi S_0$

²GaAs: cubic unit cell with 4 Ga ($Z = 31$), 4 As ($Z = 33$), and edge of 5.6534 \AA

Answer:

$$I_{tot} = \Phi \rho V \sigma_{Th} = \frac{10^6}{(5 \times 10^{-4})^2} \frac{256}{(5.6534 \times 10^{-10})^3} (10^{-4})^3 6.6525 \times 10^{-29} = 377 \text{ cps.}$$

Φ : photon flux per second ($= I_0/S_0$); ρ : volumetric density of electrons (e^-/m^3); V : sample volume.

Exercise 1.4. A plate-shaped GaAs sample with thickness $T = 0.1 \text{ mm}$ and area larger than the cross section S_0 of the X-ray beam of intensity $I_0 = 10^6 \text{ cps}$ is placed perpendicular to the incidence direction. (a) What is the value of I_{tot} ? (b) A detector of circular window with angular acceptance of $\Delta = 20^\circ$ is positioned at $2\theta = 90^\circ$, Fig. 1.3b. What are the detector readings, I_σ and I_π , in the σ and π polarizations?

Answer (a):

$$I_{tot} = \frac{I_0}{S_0} \rho S_0 T \sigma_{Th} = 10^6 \frac{256}{(5.6534 \times 10^{-10})^3} (10^{-4}) 6.6525 \times 10^{-29} = 9425 \text{ cps.}$$

$S_0 T$: sample volume illuminated by the X-ray beam.

Answer (b): In σ polarization, $\langle |\mathcal{P}|^2 \rangle \simeq 1$ within the detector window so that

$$\int \langle |\mathcal{P}|^2 \rangle d\Omega \simeq \int d\Omega = \int_0^{2\pi} \int_0^{\Delta/2} \sin \gamma d\gamma d\varphi = 2\pi [1 - \cos(\Delta/2)] \simeq \frac{\pi}{4} \Delta^2 \quad \text{and}$$

$$I_\sigma = I_0 \rho T r_e^2 \int \langle |\mathcal{P}|^2 \rangle d\Omega \simeq I_0 \rho T \left(\frac{3 \sigma_{Th}}{8\pi} \right) \frac{\pi}{4} \Delta^2 = 9425 \frac{3}{32} \left(20 \frac{\pi}{180} \right)^2 = 108 \text{ cps.}$$

In π polarization, the variation of $\langle |\mathcal{P}|^2 \rangle$ within the detector window must be taken into account, otherwise the calculated intensity will be null. Hence,

$$\begin{aligned} \int \langle |\mathcal{P}|^2 \rangle d\Omega &= \overbrace{\int_0^{2\pi} \int_0^{\Delta/2} \underbrace{\cos^2(\pi/2 - \gamma) \sin(\gamma)}_{\langle |\mathcal{P}|^2 \rangle} d\gamma d\varphi}^{\text{circular symmetry around } \hat{s}} = \frac{\pi}{6} [8 + \cos(3\Delta/2) - 9 \cos(\Delta/2)] \simeq \frac{3\pi}{8} \Delta^4 \\ \text{and} \quad I_\pi &= I_0 \rho T \left(\frac{3 \sigma_{Th}}{8\pi} \right) \frac{3\pi}{8} \Delta^4 = 9425 \frac{9}{64} \left(20 \frac{\pi}{180} \right)^4 = 20 \text{ cps.} \end{aligned}$$

...

1.1.3 Coherence Lengths

Whenever we represent the X-ray beam by a plane wave, e.g. (1.2), it is important to have in mind that this representation is valid within a limited region of the space of relative distances, whose dimensions are given in terms of coherence lengths.

Interference and diffraction phenomena occur within this region of coherence. That is the importance in knowing the coherence properties of a given X-ray beam.

The longitudinal coherence length C_L tells us how far along the beam propagation direction two electrons can be so that it is still possible to obtain information on their relative position from the interference of the scattered fields. The loss of longitudinal coherence comes exclusively from the fact that there is no X-ray source with null spectral width. Thus, to deduce the value of C_L let's take λ_1 and λ_2 as the minimum and maximum wavelengths defining the spectral width $\Delta\lambda = \lambda_2 - \lambda_1$ around $\lambda = \sqrt{\lambda_1 \lambda_2}$ (geometric mean value). Starting from (1.2) of a plane wave frozen in time, $t = 0$, we want to calculate the distance Δx so that

$$\mathbf{E}_0 e^{ik_1 \Delta x} = \mathbf{E}_0 e^{ik_2 \Delta x}$$

where $k_{1,2} = 2\pi/\lambda_{1,2}$. This leads to $k_2 \Delta x = k_1 \Delta x - 2\pi$ and therefore to $\Delta x = 2\pi/(k_1 - k_2)$. The longitudinal coherence length is defined as half the value of Δx , or

$$C_L \stackrel{\text{def}}{=} \frac{1}{2} \Delta x = \frac{1}{2} \left(\frac{1}{\lambda_1} - \frac{1}{\lambda_2} \right)^{-1} = \frac{1}{2} \frac{\lambda_1 \lambda_2}{\lambda_2 - \lambda_1} = \frac{1}{2} \frac{\lambda^2}{\Delta\lambda}. \quad (1.15)$$

The transverse coherence length C_T tells us how far in a perpendicular direction to the beam propagation direction, two electrons can be so that it is still possible to obtain information of their relative position from the interference of the scattered fields. The loss of transverse coherence comes exclusively from the fact that there is no X-ray beam with null angular divergence. Thus, to deduce the value of C_T we will take $\Delta\mathbf{k} \simeq k\delta\hat{\mathbf{y}}$ where $\hat{\mathbf{y}}$ is perpendicular to the central ray direction and δ is the angular divergence so that the beam spreads between \mathbf{k} and $\mathbf{k} + \Delta\mathbf{k}$. From (1.2) of a plane wave, we want to calculate the distance Δy so that

$$\mathbf{E}_0 e^{\pm i(\omega t - \mathbf{k} \cdot \hat{\mathbf{y}} \Delta y)} = \mathbf{E}_0 e^{\pm i[\omega t - (\mathbf{k} + \Delta\mathbf{k}) \cdot \hat{\mathbf{y}} \Delta y]}. \quad .$$

This leads to $\Delta\mathbf{k} \cdot \hat{\mathbf{y}} \Delta y = k\delta\Delta y = 2\pi$ and therefore to $\Delta y = \lambda/\delta$. The transverse coherence length is defined as half the value of Δy , or

$$C_T \stackrel{\text{def}}{=} \frac{1}{2} \Delta y = \frac{\lambda}{2\delta}. \quad (1.16)$$

In Fig. 1.4, by using geometric construction of wave fronts we can see the formation of a region of coherence with coherence lengths C_L and C_T .

...

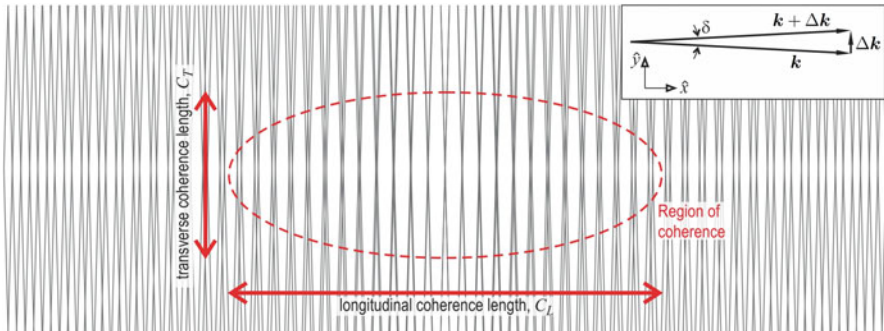


Fig. 1.4 Region of coherence formed by plane waves with spectral width $\Delta\lambda/\lambda = 0.02$ and angular divergence $\delta = 3^\circ$ (~ 52.4 mrad), implying in $C_L = 25\lambda$ and $C_T = 9.5\lambda$. Vector scheme used for calculating C_T , (1.16), is shown at the *upper right corner*

Exercise 1.5. A sealed tube with Cu target of effective size³ of $1.0 \times 1.0 \text{ mm}^2$ is the X-ray source. (a) What are the longitudinal and transverse coherence lengths of the K_α radiation when it hits a sample at 50 cm from the target? Note: ignore the intensity difference between lines $K_{\alpha 1}$ and $K_{\alpha 2}$. (b) A monochromator crystal allows angular decomposition of the tube spectrum. By taking 0.10 mrad as the monochromator angular acceptance and 2.0 eV as the spectral width of the characteristic main line, $K_{\alpha 1}$, estimate how much more coherent is the monochromatic radiation.

Answer (a): The K_α radiation is composed by two characteristic lines $K_{\alpha 1}$ and $K_{\alpha 2}$, with wavelengths $\lambda_1 = 1.540562 \text{ \AA}$ and $\lambda_2 = 1.54439 \text{ \AA}$, respectively. Therefore,

$$\frac{\Delta\lambda}{\lambda} = \frac{\lambda_2 - \lambda_1}{\sqrt{\lambda_1 \lambda_2}} = \frac{0.00383}{1.54247} = 2.48 \times 10^{-3},$$

implying in a longitudinal coherence length

$$C_L = \frac{1}{2} \frac{\lambda^2}{\Delta\lambda} = \frac{1.54247}{2 \times 2.48 \times 10^{-3}} = 3.11 \times 10^2 \text{ \AA} (0.031 \mu\text{m}).$$

The angular divergence is basically determined by effective target size and sample position, which leads to $\delta = 1.0/500 = 2.0 \text{ mrad}$, and a transverse coherence length

$$C_T = \frac{\lambda}{2\delta} = \frac{1.54247}{2 \times 0.0020} = 3.9 \times 10^2 \text{ \AA} (0.039 \mu\text{m}).$$

³Target size from the point of view of the sample.

Answer (b): For line $K_{\alpha 1}$ with $\Delta E = 2.0 \text{ eV}$, it follows from (1.1) that

$$\frac{\Delta\lambda}{\lambda} = \frac{\Delta E}{E} = \frac{2.0}{8048} = 2.5 \times 10^{-4},$$

increasing the longitudinal coherence length by a factor of 10, i.e.,

$$C_L = \frac{\lambda}{2} \left(\frac{\Delta E}{E} \right)^{-1} = \frac{1.540562}{2 \times 2.5 \times 10^{-4}} = 3.1 \times 10^3 \text{ Å} (0.31 \mu\text{m}),$$

and the transverse coherence length,

$$C_T = \frac{1.540562}{2 \times 0.00010} = 7.7 \times 10^3 \text{ Å} (0.77 \mu\text{m}),$$

by a factor of 20 due to the reduction in the angular divergence of the monochromatic beam.

...

Section Summary

— X-ray incident wave:

$$\boxed{\mathbf{E}(\mathbf{r}, t) = E_0 \hat{\boldsymbol{\epsilon}} e^{\pm i(\omega r - \mathbf{k} \cdot \mathbf{r})}}$$

— Photon energy:

$$\boxed{\mathcal{E}[\text{eV}] = \hbar |\mathbf{k}| c = \frac{2\pi \hbar c}{\lambda} = \frac{12398.5}{\lambda [\text{\AA}]}}$$

— Vectorial polarization factor (scattered wavevector $\mathbf{k}' = \frac{2\pi}{\lambda} \hat{\mathbf{s}'}$):

$$\boxed{\mathcal{P}(\hat{\mathbf{s}'}) = \hat{\mathbf{s}'} \times (\hat{\boldsymbol{\epsilon}} \times \hat{\mathbf{s}'})}$$

— Scalar polarization factor:

$$\boxed{\langle |\mathcal{P}|^2 \rangle = \begin{cases} 1 & \sigma - \text{polarization} \\ \cos^2 2\theta & \pi - \text{polarization} \\ \frac{1}{2}(1 + \cos^2 2\theta) & \text{unpolarized radiation} \end{cases}}$$

— Classical electron radius:

$$r_e = \left(\frac{e^2}{4\pi\epsilon_0 mc^2} \right) = 2.818 \times 10^{-5} \text{ Å}$$

— Scattered wave (electron at origin, observer at \mathbf{R}):

$$\mathbf{E}_K(\mathbf{R}, t) = -r_e \mathcal{P} E_0 \frac{e^{\pm i(\omega t - \mathbf{k}' \cdot \mathbf{R})}}{R}$$

— Scattered intensity by an electron:

$$I_{Th}(\hat{\mathbf{s}}') = \Phi \langle |\mathcal{P}(\hat{\mathbf{s}}')|^2 \rangle r_e^2 d\Omega$$

— Differential cross-section (Thomson scattering):

$$\left(\frac{d\sigma}{d\Omega} \right)_{Th} = \langle |\mathcal{P}|^2 \rangle r_e^2$$

— Total cross-section (Thomson scattering):

$$\sigma_{Th} = \frac{8\pi}{3} r_e^2 = 6.6525 \times 10^{-29} \text{ m}^2 = 0.66525 \text{ barn}$$

— Coherence lengths:

$$C_L = \frac{\lambda^2}{2\Delta\lambda} = \frac{\lambda}{2} \frac{\mathcal{E}}{\Delta\mathcal{E}} \text{ (longitudinal)} \quad \text{and} \quad C_T = \frac{\lambda}{2\delta} \text{ (transverse)}$$

1.2 Scattering of X-Rays by Distributions of Free Electrons

Coherent scattering of X-rays by a distribution of electrons generates the phenomenon of interference between scattered waves by each electron of the distribution. This physical phenomenon is the fundamental principle of many X-ray scattering and diffraction techniques. We will first discuss the simple interference process where the X-ray photons interact only once with the distribution, which means that effects of radiation re-scattering by the distribution itself are despising in this first approach. In general, this approach applies to dispersed distributions such as liquids and gases, solids with low structural order at atomic scales, or highly ordered solids (crystals) with submicron dimensions.

A distribution of electrons in equilibrium have as an implicit fact the existence of attractive electromagnetic forces (positive charges), maintaining the stability of the distribution and giving origin to electrons in bound states. In most cases, we are going to deal with atomic electrons where the electronic distributions are

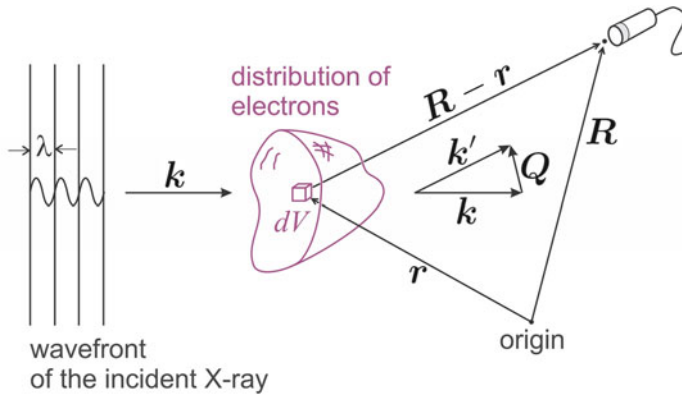


Fig. 1.5 Thomson scattering by a volumetric distribution of free electrons described with respect to an arbitrary origin

different arrangements of atoms that characterize the materials. The conservation laws of momentum and energy allow a bound electron to fully annihilate (absorb) an X-ray photon, so that the scattering and interference processes presented herein will be subsequently corrected to take into account radiation absorption and atomic resonance effects.

Such distributions can be described by volumetric electron density functions, $\rho(\mathbf{r})$. The Thomson scattering of each element of volume dV , containing $\rho(\mathbf{r}) dV$ electrons is analogous to that calculated in (1.11), but with the difference that scattering electrons no longer have positions coincident with the origin, i.e., with $\mathbf{r} = 0$. Before we deduct the total scattering by a volumetric distribution of electrons, we will rewrite (1.8) for the case of an electron placed at a position \mathbf{r} with respect to an arbitrary origin, as shown in Fig. 1.5, which provides

$$E_R(|\mathbf{R} - \mathbf{r}|, t) = \frac{e}{4\pi\epsilon_0 c^2 |\mathbf{R} - \mathbf{r}|} \ddot{z}(\mathbf{r}, t') . \quad (1.17)$$

$|\mathbf{R} - \mathbf{r}|$ is the distance between the electron and the observation point of the radiated field—equivalent to the distance R in (1.8). The acceleration equation, (1.9), also changes because the electron is no longer at $\mathbf{r} = 0$, so

$$\ddot{z}(\mathbf{r}, t') = \frac{-e}{m} E(\mathbf{r}, t') = \frac{-e}{m} E_0 e^{\pm i(\omega t' - \mathbf{k} \cdot \mathbf{r})} \quad (1.18)$$

where $t' = t - |\mathbf{R} - \mathbf{r}|/c$. With this, it is relatively simple to see that for an arbitrary origin the general form of (1.11) is

$$E_R(\mathbf{R}, t) = -r_e \mathcal{P} E_0 \frac{e^{\pm i(\omega t - \mathbf{k} \cdot \mathbf{R} - \mathbf{r})}}{|\mathbf{R} - \mathbf{r}|} . \quad (1.19)$$

Note that \mathbf{R} is still the observation position, Fig. 1.5, but the direction of the scattered radiation is now given by

$$\hat{\mathbf{s}}' = \frac{\mathbf{R} - \mathbf{r}}{|\mathbf{R} - \mathbf{r}|}, \quad (1.20)$$

so that $k|\mathbf{R} - \mathbf{r}| = \mathbf{k}' \cdot (\mathbf{R} - \mathbf{r})$ in (1.19), which is identical to (1.11) when $\mathbf{r} = 0$.

The field scattered by the electron distribution,

$$\mathbf{E}_d(\mathbf{R}, t) = \int \rho(\mathbf{r}) \mathbf{E}_R(\mathbf{R}, t) dV = -r_e \mathcal{P} E_0 e^{\pm i\omega t} \int \rho(\mathbf{r}) \frac{e^{\pm i[(\mathbf{k}' - \mathbf{k}) \cdot \mathbf{r} - \mathbf{k}' \cdot \mathbf{R}]}}{|\mathbf{R} - \mathbf{r}|} dV, \quad (1.21)$$

corresponds to the integration of (1.19) multiplied by the number of electrons in each element of volume. The interference phenomenon is fully governed by the phase factor $e^{\pm i(\mathbf{k}' - \mathbf{k}) \cdot \mathbf{r}}$ in the above integral, which extends throughout the distribution volume illuminated by the incident beam with phase coherence. We will analyze cases in which the distributions have very small dimensions, e.g. atomic dimensions. For extensive distributions, the integration volume is limited by the coherence lengths of the X-ray beam, typically of the order of a few microns (10^{-6} m), see Exercise 1.5. Since the observation distance R is in scale of meters, we have that inside the integration volume the value of $|\mathbf{R} - \mathbf{r}|$ is practically constant, as well as the wavevector $\mathbf{k}' = k\hat{\mathbf{s}}'$, scattered in the observation direction. These facts allow a major simplification in (1.21), originating the far field expression

$$\mathbf{E}_d(\mathbf{R}, t) \cong -r_e \mathcal{P} E_0 \frac{e^{\pm i(\omega t - \mathbf{k}' \cdot \mathbf{R})}}{R} \int \rho(\mathbf{r}) e^{\pm i\mathbf{Q} \cdot \mathbf{r}} dV = [\mathbf{E}_R(\mathbf{R}, t)]_{\mathbf{r}=0} F(\mathbf{Q}) \quad (1.22)$$

where the origin is taken as any point within the integration volume, for instance, the distribution's center of gravity. The reciprocal vector

$$\mathbf{Q} = \mathbf{k}' - \mathbf{k} = \frac{2\pi}{\lambda} (\hat{\mathbf{s}}' - \hat{\mathbf{s}}), \quad (1.23)$$

is also constant in the integration volume, and

$$F(\mathbf{Q}) = \int \rho(\mathbf{r}) e^{\pm i\mathbf{Q} \cdot \mathbf{r}} dV. \quad (1.24)$$

The far field scattered by a distribution of free electrons is the field scattered by a single electron multiplied by the form factor $F(\mathbf{Q})$, which depends on both the form of the distribution and the observation direction $\hat{\mathbf{s}}'$ (implicit in the reciprocal vector \mathbf{Q}). As a result, the scattering intensity is

$$I(\mathbf{Q}) = I_{Th} |F(\mathbf{Q})|^2 \quad (1.25)$$

where I_{Th} is the Thomson scattering intensity by an electron, (1.13).

1.2.1 Mathematical Tools: Fourier Transform

Although (1.25) is relatively simple and compact, understanding all the physics implicit in it is not a trivial matter. Before showing the importance of $F(Q)$ in the study of the atomic structure of materials, we need to recall some mathematical tools such as Dirac delta function, Fourier transform, and convolution of functions.

The Dirac delta function in one-dimension $\delta(x)$ satisfies the following relationships:

$$\delta(x) = \begin{cases} \infty & \text{if } x = 0 \\ 0 & \text{if } x \neq 0 \end{cases}, \quad \int_{-\infty}^{+\infty} \delta(x) dx = 1, \text{ and } \int_{-\infty}^{+\infty} f(x) \delta(x - x_0) dx = f(x_0) \quad (1.26)$$

for any continuous function $f(x)$. From the various mathematical expressions of a delta function, one that will be useful is

$$\delta(x) = \lim_{h \rightarrow \infty} \int_{-h}^{+h} e^{\pm 2\pi i q x} dq = \lim_{h \rightarrow \infty} \frac{\sin(2\pi h x)}{\pi x} \quad (1.27a)$$

or

$$\delta(q) = \lim_{a \rightarrow \infty} \int_{-a}^{+a} e^{\pm 2\pi i q x} dx = \lim_{a \rightarrow \infty} \frac{\sin(2\pi a q)}{\pi q} \quad (1.27b)$$

where the qx product is dimensionless, i.e. $[qx] = 1$. If x has dimension of length, $[\delta(x)] = \text{m}^{-1}$ and $[\delta(q)] = \text{m}$.

The Fourier transform (FT) of function $f(x)$ is defined by

$$F(q) = \text{FT}\{f(x)\} = \int_{-\infty}^{+\infty} f(x) e^{+2\pi i q x} dx, \quad (1.28)$$

using the signal “+” in the phase factor according to the *International Tables for Crystallography* (Coppens 2010). Therefore, the inverse FT for recovering the original function $f(x)$ is

$$\begin{aligned} \text{FT}^{-1}\{F(q)\} &= \int_{-\infty}^{+\infty} F(q) e^{-2\pi i x q} dq = \int_{-\infty}^{+\infty} \left(\int_{-\infty}^{+\infty} f(x') e^{+2\pi i q x'} dx' \right) e^{-2\pi i x q} dq = \\ &= \int_{-\infty}^{+\infty} f(x') \left(\int_{-\infty}^{+\infty} e^{+2\pi i q(x' - x)} dq \right) dx' = \int_{-\infty}^{+\infty} f(x') \delta(x' - x) dx' = f(x). \end{aligned} \quad (1.29)$$

The convolution of two functions, for instance $f(x)$ and $g(x)$, is represented by “ $*$ ” as in

$$c(u) = f(x) * g(x) = \int_{-\infty}^{+\infty} f(x) g(u - x) dx. \quad (1.30)$$

Regarding convolution of functions, there are two very useful math operations:

1. The FT of a convolution is equal to the product of FTs,

$$\begin{aligned} \text{FT}\{f(x) * g(x)\} &= \int c(u) e^{2\pi i qu} du = \int \left(\int f(x) g(u - x) dx \right) e^{2\pi i qu} du = \\ &= \int f(x) e^{2\pi iq x} \left(\int g(u - x) e^{2\pi i(u-x)q} du \right) dx = \int f(x) e^{2\pi iq x} dx \int g(x') e^{2\pi iq x'} dx' = \\ &= F(q) G(q) = \text{FT}\{f(x)\} \text{FT}\{g(x)\}. \end{aligned} \quad (1.31)$$

2. The FT of a product is equal to the convolution of FTs,

$$\begin{aligned} \text{FT}\{f(x) g(x)\} &= \int f(x) g(x) e^{2\pi iq x} dx = \int f(x) \int g(x') \delta(x - x') e^{2\pi iq x'} dx' dx = \\ &= \int f(x) \int g(x') \left(\int e^{2\pi i(x-x')q'} dq' \right) e^{2\pi iq x'} dx' dx = \\ &= \int \left(\int f(x) e^{2\pi ix q'} dx \right) \left(\int g(x') e^{2\pi i(q-q')x'} dx' \right) dq' = \\ &= \int F(q') G(q - q') dq' = F(q') * G(q') = \text{FT}\{f(x)\} * \text{FT}\{g(x)\}. \end{aligned} \quad (1.32)$$

From the definition of the Fourier transform (FT), (1.28), it can be seen that the form factor $F(\mathbf{Q})$ is the three-dimensional FT of the electronic density. Since the FT was defined with the phase signal “+”, the same signal has to be chosen for the form factor phase in (1.24). Henceforth, the incident X-ray wave will have also to be represented with the phase signal “+” in (1.2), that is, only

$$\mathbf{E}(\mathbf{r}, t) = E_0 e^{+i(\omega t - \mathbf{k} \cdot \mathbf{r})} \quad (1.33)$$

is a representation consistent with the FT definition. This means that⁴

⁴If you have difficulty comparing (1.34) and (1.35) with (1.28) and (1.29) due to the absence of the number 2π in the phase factor, you can reset the reciprocal vector to make this number explicit, such that $\mathbf{Q} = 2\pi \mathbf{q}$ where $\mathbf{q} = (\hat{s}' - \hat{s})/\lambda$. $dV_Q = dQ_x dQ_y dQ_z = (2\pi)^3 dq_x dq_y dq_z = (2\pi)^3 dV_q$.

$$F(\mathbf{Q}) = \int \rho(\mathbf{r}) e^{+i\mathbf{Q}\cdot\mathbf{r}} dV = \text{FT}\{\rho(\mathbf{r})\} \quad \text{and} \quad (1.34)$$

$$\rho(\mathbf{r}) = \text{FT}^{-1}\{F(\mathbf{Q})\} = \frac{1}{(2\pi)^3} \int F(\mathbf{Q}) e^{-i\mathbf{Q}\cdot\mathbf{r}} dV_Q. \quad (1.35)$$

...

Exercise 1.6. (a) Calculate the general form factor expression for electron densities with radial symmetry. (b) In the case of a spherical and uniform electron distribution with radius a , obtain the scattered intensity curve, $I(Q)$, and determine the angular spreading of the scattering as a function of the distribution's radius.

Answer (a): Due to radial symmetry

$$F(\mathbf{Q}) = F(Q) = \text{FT}\{\rho(r)\} = \int \rho(r) e^{iQr} dr,$$

implying that the solution is independent of the direction of vector \mathbf{Q} . Defining $\hat{z} = [0, 0, 1]$ as the reciprocal vector direction,

$$\mathbf{Q} = Q\hat{z} = [0, 0, Q], \quad \mathbf{r} = r [\sin\gamma \cos\varphi, \sin\gamma \sin\varphi, \cos\gamma],$$

$$\mathbf{Q} \cdot \mathbf{r} = Qr \cos\gamma, \quad \text{and} \quad dV = r^2 \sin\gamma dr d\gamma d\varphi.$$

$$\begin{aligned} \therefore F(Q) &= \int_0^{2\pi} \int_0^\pi \int_0^\infty \rho(r) r^2 [\cos(Qr \cos\gamma) + i \overbrace{\sin(Qr \cos\gamma)}^{\text{=0 (odd function)}}] \sin\gamma dr d\gamma d\varphi = \\ &= 2\pi \int_0^\infty \rho(r) r dr \int_0^\pi r \sin\gamma \cos(Qr \cos\gamma) d\gamma = \frac{2\pi}{Q} \int_0^\infty \rho(r) r dr \underbrace{\int_{-Qr}^{+Qr} \cos w dw}_{\text{where } w=Qr \cos\gamma} = \\ &= \int_0^\infty \rho(r) 4\pi r^2 \left[\frac{\sin(Qr)}{Qr} \right] dr, \end{aligned} \quad (1.36)$$

whose numerical or analytical solution depends on the explicit form of the function $\rho(r)$.

Answer (b): By replacing $\rho(r) = \rho s(r)$ where $s(r) = 1$ if $r \leq a$ and $s(r) = 0$ if $r > a$ in (1.36), we have

$$\begin{aligned} F(Q) &= \frac{4\pi\rho}{Q^3} \underbrace{\int_0^{Qa} v \sin v dv}_{v=Qr} = \frac{4\pi\rho}{Q^3} [\sin v - v \cos v]_0^{Qa} = \\ &= 3 \left[\frac{\sin(Qa) - (Qa) \cos(Qa)}{(Qa)^3} \right] \rho V = \Theta(Qa) \rho V. \end{aligned} \quad (1.37)$$

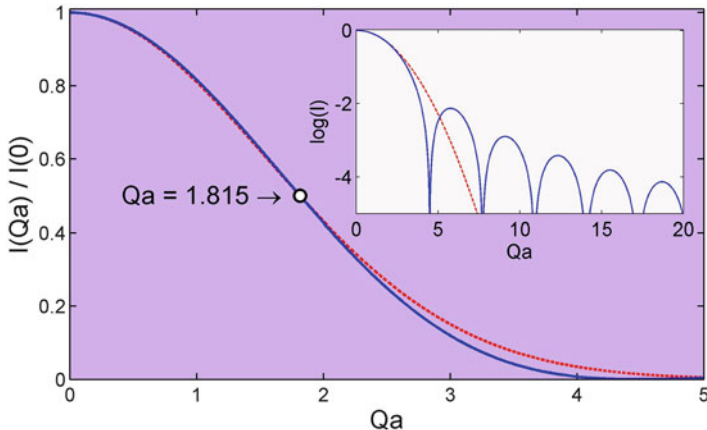


Fig. 1.6 Relative intensity $I(Qa)/I(0)$ (blue line), scattered by a uniform spherical electron density. Exponential decay $\exp[-\alpha(Qa)^2]$ (red line), with $\alpha = 0.21$ is shown for the sake of comparison. *Inset:* relative intensity on a logarithmic scale. The first minimum occurs at $Qa = 4.4934$. [exsphere.m]

$V = 4\pi a^3/3$ is the volume occupied by the ρV electrons of the distribution. The scattered intensity

$$\begin{aligned} I(Q) &= I_{Th} |F(Q)|^2 = I_{Th} \rho^2 V^2 [\Theta(Qa)]^2 = \\ &= I_{Th} \rho^2 V^2 9 \left[\frac{\sin(Qa) - (Qa) \cos(Qa)}{(Qa)^3} \right]^2, \end{aligned} \quad (1.38)$$

has a maximum value, at $Q = 0$, proportional to the square of the number of electrons, i.e. $I(0) = I_{Th} \rho^2 V^2$. The $I(Qa)/I(0)$ curve shown in Fig. 1.6 was calculated by using the `exsphere.m` routine (MatLab).⁵ It allows us to estimate the angular spreading by half height of the maximum intensity where $I(Qa = 1.815)/I(0) = 1/2$. [Note: to find the $Qa = 1.815$ value, numerically calculate the root of the function $y(x) = 2I(x)/I(0) - 1$.] Since

$$Q = |\mathbf{Q}| = \frac{2\pi}{\lambda} |\hat{s}' - \hat{s}| = \frac{4\pi}{\lambda} \sin \theta, \quad (1.39)$$

the half maximum condition implies a scattering angle 2θ that satisfies $\sin(2\theta/2) = 1.815 \lambda / 4\pi a$, and hence

$$2\theta_{1/2} = 2 \sin^{-1} \left(0.1444 \frac{\lambda}{a} \right) \simeq 0.3 \frac{\lambda}{a} \quad (\text{for } \lambda < a). \quad (1.40)$$

...

⁵Routines in MatLab (extension *.m) or C++ (*.c) are available in Appendix B.

1.2.2 *Distributions of One Electron and the Compton Scattering*

Any electron exists only as a probability distribution. In the Thomson treatment of scattered radiation, the electron's position was given as fully localized in \mathbf{r} . However, since the electron is a very light particle (low mass), the wave characteristics of the electron have to be considered. The probability density function $|\psi(\mathbf{r})|^2$, so that $\int |\psi(\mathbf{r})|^2 dV = 1$, is what really characterizes the coherent scattering produced by a single electron. This implies that the scattering of one electron already shows interference effects, which are considered when calculating the form factor

$$f_e(\mathbf{Q}) = \int |\psi(\mathbf{r})|^2 e^{i\mathbf{Q}\cdot\mathbf{r}} dV = \text{FT}\{|\psi(\mathbf{r})|^2\}, \quad (1.41)$$

of the probability density. Thus, the intensity of the scattered radiation with phase coherence by one electron is given by

$$I_{cohe}(\mathbf{Q}) = I_{Th}|f_e(\mathbf{Q})|^2. \quad (1.42)$$

Except for the condition where $Q = 0$, the coherent intensity is always less than the intensity I_{Th} scattered by a single electron (1.13). At first sight, the I_{Th} calculation seems wrong because it was obtained from an ideal classical hypothesis (electron with defined position), or it may seem that it is only valid for very localized probability distributions described by delta functions, i.e., $|\psi(\mathbf{r})|^2 = \delta(\mathbf{r} - \mathbf{r}_0)$ where \mathbf{r}_0 is the electron's position, and substituting this in (1.41) and (1.42) we will have

$$f_e(\mathbf{Q}) = \text{FT}\{\delta(\mathbf{r} - \mathbf{r}_0)\} = e^{i\mathbf{Q}\cdot\mathbf{r}_0} \quad \text{and} \quad I_{cohe}(\mathbf{Q}) = I_{Th} \quad \forall \quad \mathbf{Q}.$$

But, the value of I_{Th} is correct and it actually represents the intensity scattered by one electron.⁶ It just lacks reassessing the process of photon-electron interaction from the perspective of quantum electrodynamics (QED), which means taking into account the wave-particle duality of both the electromagnetic radiation and the electron. The wave aspect generates the coherent scattering part, I_{cohe} , and the particle aspect generates an incoherent part, I_{Comp} , which is the Compton scattering. The self-interference produced by the electron probability density itself is what determines if the radiation behaves like a wave or like a particle.

For free-electrons, the result of the photon-electron interaction is restricted to two possibilities represented by the diagrams in Fig. 1.7. The diagrams are identical before the interaction: a photon with wavelength λ intercepting an electron e^- . However, the result of the interaction depends on the value of $|f_e(\mathbf{Q})|^2$. If for a given

⁶Within the non-relativistic approximation, which is reasonable for X-rays up to a few tens of keV. The exact value of I_{Th} comes from the Klein–Nishina formula, see, for example, Lovesey and Collins (1996, p. 250, eq. 7.8).

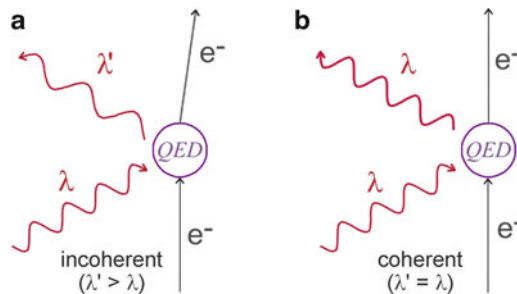


Fig. 1.7 Photon-electron interaction and manifestation of the electromagnetic radiation wave-particle duality. **(a)** Corpuscular aspect: incoherent scattering, $\lambda' > \lambda$, Compton effect. **(b)** Wave aspect: coherent scattering, $\lambda' = \lambda$, interference phenomena. The relative fraction between coherent and incoherent scattering depends on the self-interference produced by the spatial probability density function of the electron (1.41)

Q the self-interference is totally destructive, i.e. $|f_e(\mathbf{Q})|^2 = 0$, Compton scattering is the result, Fig. 1.7a. On the other hand, if the self-interference is totally constructive, $|f_e(\mathbf{Q})|^2 = 1$, coherent scattering is the result, Fig. 1.7b. In an intermediate condition where $|f_e(\mathbf{Q})|^2 < 1$, from a total of N interaction, $N|f_e(\mathbf{Q})|^2$ interactions will result in coherent scattering and $N(1 - |f_e(\mathbf{Q})|^2)$ interactions will result in Compton scattering. Therefore, the Compton scattering intensity is simply given by

$$I_{Comp}(\mathbf{Q}) = I_{Th}(1 - |f_e(\mathbf{Q})|^2). \quad (1.43)$$

Intuitively one would expect that the corpuscular aspect of the radiation is more evident when the electron is localized. But what happens is exactly the opposite. The more localized the electron, the lower the probability of Compton scattering, e.g., Fig. 1.8.

To correct the experimental intensity I_{exp} , scattered by a distribution of electrons from the background (incoherent) intensity generated by the Compton effect, it is necessary to sum over the individual contributions of all electrons. Therefore, the coherent intensity scattered by the distribution will be

$$I(\mathbf{Q}) = I_{exp} - I_{Th} \sum_j (1 - |f_e(\mathbf{Q})|^2)_j = I_{exp} - I_{Th} \sum_j (1 - |\text{FT}\{|\psi_j(\mathbf{r})|^2\}|^2) \quad (1.44)$$

where j runs over all electrons of the distribution, whose wave functions are the $\psi_j(\mathbf{r})$.⁷ Understand well the meaning of this expression: the background intensity due to Compton effect depends only on the self-interference of each electron. The interference of the fields scattered by electrons does not affect the Compton

⁷Situation valid when the binding energies of all electrons can be neglected. The case of bound electron is discussed in Sect. 1.3.3.

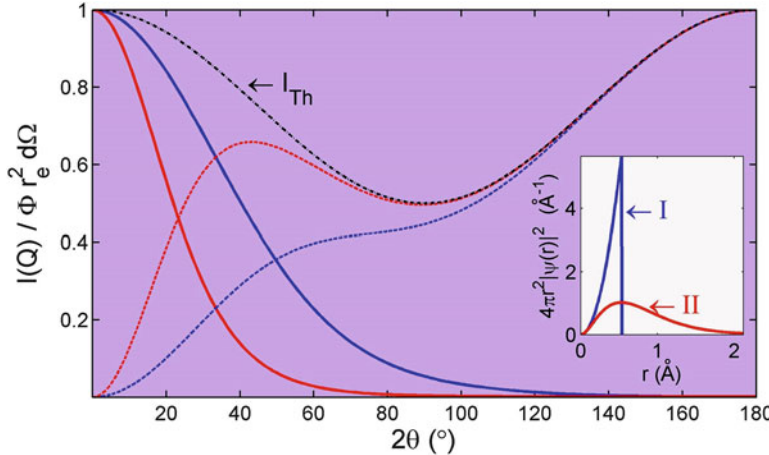


Fig. 1.8 Coherent and incoherent (Compton) intensities scattered by one electron with different probability density functions $|\psi(r)|^2$ (inset). I: I_{cohe} (blue line) and I_{Comp} (blue dashed line). II: I_{cohe} (red line) and I_{Comp} (red dashed line). In both cases, $I_{cohe} + I_{Comp} = I_{Th}$ (black dashed line) and $\lambda = 1.54$. [excompton.m]

effect, but greatly increases the contribution of the coherent scattering. This makes the correction by (1.44) very small compared to the total intensity of the coherent scattering, and then, $I(\mathbf{Q}) \simeq I_{exp}$ in most analytical techniques of materials by X-rays.

...

Exercise 1.7. Compare the coherent and incoherent scattered intensities using the following probability density functions for one electron: $|\psi_1(r)|^2 = 3/4\pi a^3$ uniform within a sphere of radius $a = 0.5 \text{\AA}$ (null outside the sphere); and $|\psi_{II}(r)|^2 = e^{-2(r/a)}/\pi a^3$. [Note: consider non-polarized radiation and neglect any electron binding energy.]

Answer: The coherent and incoherent intensities are given, respectively, by

$$I_{cohe}(\mathbf{Q}) = I_{Th} |f_e(\mathbf{Q})|^2 = \Phi \langle |\mathcal{P}|^2 \rangle r_e^2 |f_e(\mathbf{Q})|^2 d\Omega \quad \text{and}$$

$$I_{Comp}(\mathbf{Q}) = I_{Th} (1 - |f_e(\mathbf{Q})|^2) = \Phi \langle |\mathcal{P}|^2 \rangle r_e^2 (1 - |f_e(\mathbf{Q})|^2) d\Omega .$$

For the uniform radial distribution, from (1.37), $f_e(\mathbf{Q}) = \text{FT}\{|\psi_1(\mathbf{r})|^2\} = \Theta(Qa)$, and for the distribution type orbital 1s of hydrogen, it comes from (1.36) that (Pirenne 1946)

$$f_e(Q) = \text{FT}\{|\psi_{\text{II}}(\mathbf{r})|^2\} = \frac{4}{a^3} \int_0^\infty r^2 e^{-2(r/a)} \left[\frac{\sin(Qr)}{Qr} \right] dr = \frac{1}{[1 + (Qa/2)^2]^2}.$$

Taking also into account the polarization coefficient, $\langle |\mathcal{P}|^2 \rangle = [1 + \cos^2(2\theta)]/2$, the intensities scattered by this two distributions are compared in Fig. 1.8.

...

Section Summary

— Scattered wave by one electron at \mathbf{r} (observer at \mathbf{R}):

$$\boxed{\mathbf{E}_R(\mathbf{R}, t) = -r_e \mathcal{P} E_0 \frac{e^{i[\omega t - \mathbf{k}' \cdot \mathbf{R} + (\mathbf{k}' - \mathbf{k}) \cdot \mathbf{r}]}}{|\mathbf{R} - \mathbf{r}|}}$$

— Scattered wave by an electronic density $\rho(\mathbf{r})$, far field approximation:

$$\boxed{\mathbf{E}_d(\mathbf{R}, t) \simeq \mathbf{E}_R(\mathbf{R}, t)_{r=0} \int \rho(\mathbf{r}) e^{i(\mathbf{k}' - \mathbf{k}) \cdot \mathbf{r}} dV}$$

— Reciprocal vector ($\mathbf{k}' \angle \mathbf{k} = 2\theta$):

$$\boxed{\mathbf{Q} = \mathbf{k}' - \mathbf{k} \quad \text{and} \quad Q = |\mathbf{Q}| = \frac{4\pi}{\lambda} \sin \theta}$$

— Form factor $F(\mathbf{Q})$, and Fourier transform (FT):

$$\boxed{F(\mathbf{Q}) = \text{FT}\{\rho(\mathbf{r})\} = \int \rho(\mathbf{r}) e^{i\mathbf{Q} \cdot \mathbf{r}} dV}$$

— Inverse FT:

$$\boxed{\rho(\mathbf{r}) = \text{FT}^{-1}\{F(\mathbf{Q})\} = \frac{1}{(2\pi)^3} \int F(\mathbf{Q}) e^{-i\mathbf{Q} \cdot \mathbf{r}} dV_Q}$$

— Form factor for spherically symmetric electron density [(1.36)]

$$\boxed{F(Q) = \int_0^\infty \rho(r) 4\pi r^2 \left[\frac{\sin(Qr)}{Qr} \right] dr}$$

— Form factor for uniform sphere of radius a and volume V [(1.37)]

$$\boxed{F(Q) = \Theta(Qa) V = 3 \left[\frac{\sin(Qa) - (Qa) \cos(Qa)}{(Qa)^3} \right] V}$$

— Form factor for one electron with wave function $\psi(\mathbf{r})$:

$$f_e(\mathbf{Q}) = \text{FT}\{|\psi(\mathbf{r})|^2\}$$

— Coherent scattering by one electron:

$$I_{cohe}(\mathbf{Q}) = I_{Th}|f_e(\mathbf{Q})|^2 = \Phi r_e^2 \langle |\mathcal{P}|^2 \rangle |f_e(\mathbf{Q})|^2 d\Omega$$

— Incoherent (Compton) scattering by one electron:

$$I_{Comp}(\mathbf{Q}) = I_{Th}(1 - |f_e(\mathbf{Q})|^2) = \Phi r_e^2 \langle |\mathcal{P}|^2 \rangle (1 - |f_e(\mathbf{Q})|^2) d\Omega$$

1.3 Atoms and Molecules

The coherent scattering of an atom is characterized exclusively by the electronic cloud. The high frequency of the X-rays, of the order of 10^{18} Hz, and the nucleus inertia (mass) make the coherent scattering by nuclear charge practically null. The nuclear charge affects only electronic properties, differentiating one atom from another by the number of electrons (atomic number Z) and by the energies of electron shells and atomic orbitals (electron bound states). The orbital energies are relevant to the X-ray absorption and atomic resonance effects, as we shall see in the next chapter. For now, a neutral or ionized atom will be treated only as a distribution of free electrons, described by the electron density

$$\rho_a(\mathbf{r}) = \sum_{j=1}^Z |\psi_j(\mathbf{r})|^2, \quad (1.45)$$

where $|\psi_j(\mathbf{r})|^2$ is the probability density of an occupied orbital, so that $\int \rho_a(\mathbf{r}) dV = Z$.

1.3.1 Spherically-symmetrical Atoms

The amplitude of the coherent scattering produced by an atom is proportional to the atomic form factor

$$f(\mathbf{Q}) = \text{FT}\{\rho_a(\mathbf{r})\} = \sum_{j=1}^Z \text{FT}\{|\psi_j(\mathbf{r})|^2\}, \quad (1.46)$$

(1.34) with f instead of F , also called atomic scattering factor. The values of $f(Q)$ for all atoms and ions are calculated by using wave functions of atoms with many electrons,⁸ or experimentally measured, when feasible, from monatomic gases. Due to accuracy and availability of theoretical values over a wide range in Q , these are the values actually used in the simulation of X-ray scattering experiments. They are tabulated values, not directly as a function of Q , but as a function of

$$\sin \theta / \lambda = Q / 4\pi \quad (1.47)$$

where θ is half the scattering angle, which is conventionally called 2θ , Fig. 1.1b. The dependence only with the module Q of the reciprocal vector is a consequence of the atom's spherical symmetry (or revolution symmetry) assumed in the calculations. That's not exactly right for atoms with incomplete shells, or atoms in chemical bonding with distorted electronic clouds. However, the greatest contribution to the coherent scattering comes from the inner shells, so that there are few situations where these facts are relevant, and only in these particular situations they are taken into account.⁹

Due to the frequent need of using atomic scattering data in simulation routines, i.e. of interpolating tabulated values, the following parametric equation has been employed:

$$f(Q) = \sum_{n=1}^4 a_n e^{-b_n (\frac{Q}{4\pi})^2} + c. \quad (1.48)$$

a_n , b_n , and c are adjustable parameters that allow us to reproduce the theoretical values of $f(Q)$.¹⁰ Thus, for each atom or ion there is a set of nine values, commonly called Cromer–Mann coefficients, some of which are shown in Table 1.1.

Note 1.2: Knowledge of atomic scattering factors is extremely important in X-ray physics. Thus, for a better use of this book, the reader should have on hand a routine that provides $f(Q)$, e.g. routine `ASFQ.m` (Appendix B).

...

Exercise 1.8. Choose one atom and an ion of this atom, for example Ga and Ga^{3+} .
 (a) Plot $f(Q)$ for at least two photon energies \mathcal{E} . What changes in $f(Q)$ with the

⁸The wave functions of atoms with many electrons are obtained through multiple methods depending on the atomic number and ionization state. For detailed references see, for example, Prince (2006, pp. 554 and 565).

⁹Giacovazzo (2002, p. 160). See also Prince (2006, § 6.1.1.4).

¹⁰In the Q range between 25 and 75 \AA^{-1} , $f(Q)$ values are obtained through other parametric equation, e.g. Prince (2006, p. 565).

Table 1.1 Cromer–Mann coefficients for a few atoms and ions (Source: Prince (2006, pp. 578–580))

Atom	a_1	a_2	a_3	a_4	b_1	b_2	b_3	b_4	c
C	2.3100	1.0200	1.5886	0.8650	20.8439	10.2075	0.5687	51.6512	0.2156
Ga	15.2354	6.7006	4.3591	2.9623	3.0669	0.2412	10.7805	61.4135	1.7189
Ga ³⁺	12.6920	6.6988	6.0669	1.0066	2.8126	0.2279	6.3644	14.4122	1.5355
As	16.6723	6.0701	3.4313	4.2779	2.6345	0.2647	12.9479	47.7972	2.5310

Note that $\sum a_n + c = f(0) \simeq Z$

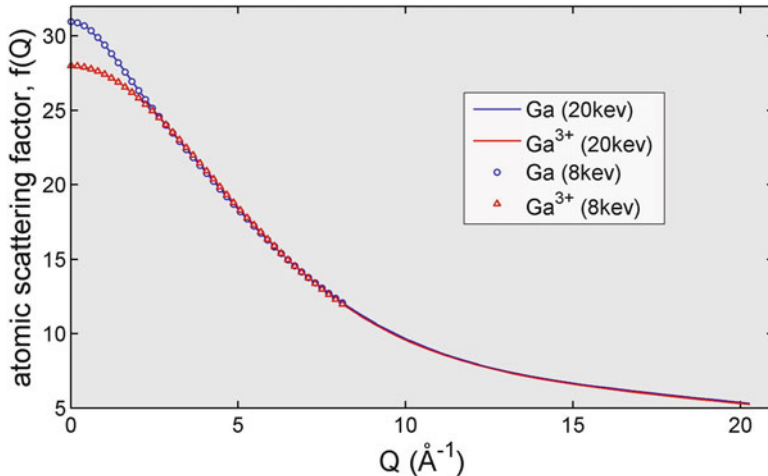


Fig. 1.9 Atomic scattering factors for Ga ($Z = 31$) and Ga^{3+} ($Z = 28$) as a function of Q for X-ray energies $\mathcal{E} = 8$ and 20 keV . [exasf.m]

energy? (b) In a polar graphic where $x = f(Q) \cos 2\theta$ and $y = f(Q) \sin 2\theta$, show the dependence of the atomic scattering factor with the scattering angle and the energy of the photons. What changes in $f(2\theta)$ with the energy? (c) How does the atom ionization affect the scattering amplitude?

Answer (a): As can be seen in Fig. 1.9, $f(Q)$ does not depend on the energy. Only the accessible Q range is limited by energy since the maximum value of Q is

$$Q_{\max} = \frac{4\pi}{\lambda} \overbrace{\sin \theta}^{\stackrel{=}1} = \frac{4\pi}{hc} \mathcal{E} = 1.0135 [\text{\AA}^{-1}/\text{keV}] \mathcal{E}. \quad (1.49)$$

For example, for photons of 8 and 20 keV, $f(Q)$ goes up to $Q = Q_{\max} \approx 8$ and 20\AA^{-1} , respectively, when the scattering angle is the largest possible, i.e. $2\theta = 180^\circ$. For other scattering angles, $Q = Q_{\max} \sin \theta$.

Answer (b): Polar graphics of $f(Q)$ as a function of $2\theta = 2\sin^{-1}(Q/Q_{\max})$ are shown in Fig. 1.10. As the photon energy increases, the coherent scattering becomes more restricted to the direct beam direction.

Answer (c): In the direction of the direct beam, $Q = 0$, ionization changes the amplitude of the scattering according to the ion charge value in number of electrons. As Q increases, the ionization ceases to affect the scattering amplitude, decreasing the difference in $f(Q)$ values between ion and neutral atom.

...

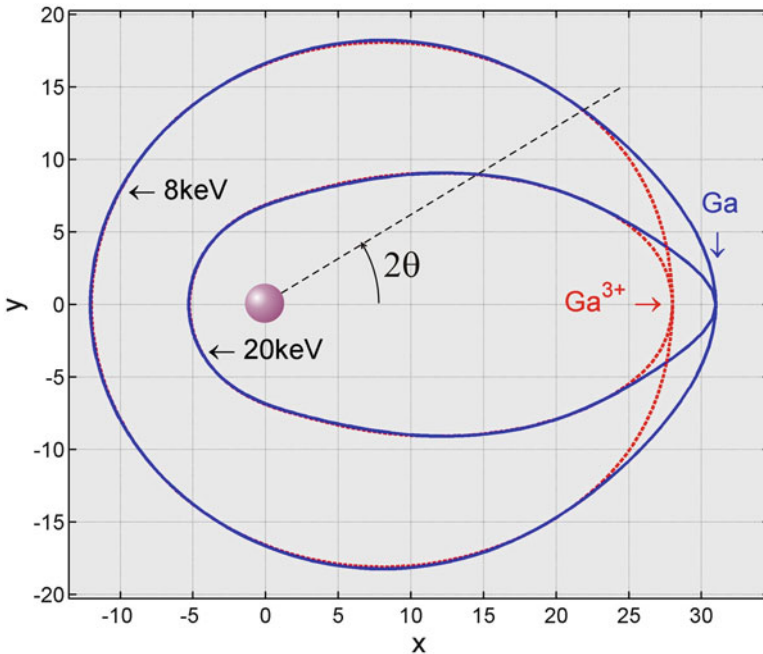


Fig. 1.10 Atomic scattering factors for Ga and Ga^{3+} as a function of the scattering angle 2θ for X-rays of 8 and 20 keV. Coordinates $x = f(Q) \cos 2\theta$ and $y = f(Q) \sin 2\theta$. [exasf.m]

1.3.1.1 Coherent Scattering Cross-Section for Isolated Atoms

When an atom is isolated to the point in which there is no interference effects with fields scattered by other atoms, the integrated value of the coherent intensity with respect to all directions of the space is equal to $\Phi \sigma_R$. The coherent scattering cross-section

$$\sigma_R(\mathcal{E}, Z) = r_e^2 \int \langle |\mathcal{P}|^2 \rangle |f(Q)|^2 d\Omega = \exp \left\{ \sum_{n=0}^3 c_n [\ln(\mathcal{E})]^n \right\} \quad (1.50)$$

is characteristic of each element and may be obtained in three ways: numerical integration of $|f(Q)|^2$; interpolation of tabulated values (Hubbell et al. 1975); or through the parametric equation (or analytic function) given above with the c_n coefficients (McMaster et al. 1969), `sgrayleigh.m` routine. A comparison between the numerical integration and the analytical solution is shown in Fig. 1.11. The significance of the value of σ_R is related to the linear attenuation effect of the incident beam, as discussed in Sect. 1.4.1.

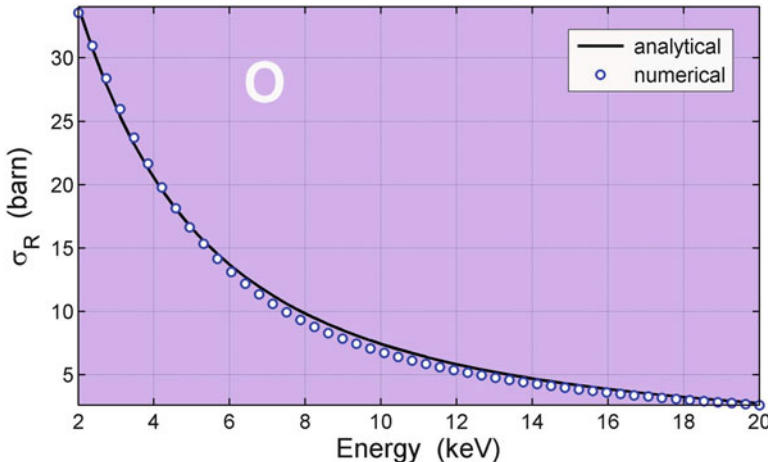


Fig. 1.11 Coherent scattering cross-section for oxygen. Comparison of analytical and numerical solutions. 1 barn = 10^{-28} m^2 [exsgr.m]

1.3.2 Scattering by Single Molecules and the “Phase Problem”

For any atom or ion $f(0) = Z$, Fig. 1.9, indicating that the interference of scattered waves by electrons in the electronic cloud around the atom is fully constructive in the incident beam direction, regardless of the used energy. In any other fixed direction, $2\theta \neq 0$, the amplitude of the atom’s coherent scattering decreases with the increase of energy, Fig. 1.10, fact that is clearly seen by the reduction in the cross-section σ_R , Fig. 1.11. The total constructive interference at $Q = 0$ is a physical fact, described through the FT of the electronic density, (1.34), and it is independent of the distribution nature, whether the distribution consists of one electron probability density or of many atoms.

In determining the various atomic structures, whether molecules dispersed in gas, in solution, or in crystalline or amorphous solids, it is important to analyze what happens outside the $Q = 0$ condition. The X-ray crystallography largely consists of methods for measuring coherent intensities $I(Q)$, covering Q values in the range of 10^{-3} to 10^2 \AA^{-1} , as well as of methods for suitably treating the intensities measured from each type of sample or material under investigation. It is difficult to determine the atomic structure from the intensity measures since the phase information of the form factors are lost in the measurements. For example, consider the electronic density

$$\rho(\mathbf{r}) = \sum_a \rho_a(\mathbf{r} - \mathbf{r}_a) = \sum_a \int \rho_a(\mathbf{r}') \delta(\mathbf{r} - \mathbf{r}_a - \mathbf{r}') dV' = \sum_a \rho_a(\mathbf{r}) * \delta(\mathbf{r} - \mathbf{r}_a) \quad (1.51)$$

of a discrete arrangement of atoms, such as in single molecules, where the index a runs over all atoms whose positions are given by \mathbf{r}_a . Using the property that the FT of a convolution is equal to the product of the FTs, (1.31), the form factor of the arrangement will be

$$F(\mathbf{Q}) = \text{FT}\{\rho(\mathbf{r})\} = \sum_a \text{FT}\{\rho_a(\mathbf{r})\} \text{FT}\{\delta(\mathbf{r} - \mathbf{r}_a)\} = \sum_a f_a(Q) e^{iQ \cdot \mathbf{r}_a} = |F(\mathbf{Q})| e^{i\phi(\mathbf{Q})}. \quad (1.52)$$

Since the atomic scattering factors $f_a(Q)$ are known, e.g. (1.48), the scattered intensity can be easily calculated for any given set of atomic positions through (1.25), $I(\mathbf{Q}) = I_{Th} |F(\mathbf{Q})|^2$. The difficulty is in determining the positions from intensity measurements. $I(\mathbf{Q}) \Rightarrow |F(\mathbf{Q})|$, but this is not enough to obtain

$$\rho(\mathbf{r}) = \text{FT}^{-1} \{ |F(\mathbf{Q})| e^{i\phi(\mathbf{Q})} \} \quad (1.53)$$

because the phase values $\phi(\mathbf{Q})$ are unknown. This problem is fundamental in crystallography, and it is commonly called the “phase problem.” For each type of sample there is a procedure to be adopted for structural analysis, and that’s why X-ray crystallography is a very extensive area. A widely used resource is structure modeling and simulation of scattered intensities. Skills in computer and curve fitting methods are crucial in applied X-ray physics. Practice in data analysis leads to the development of a good intuition about the correlations between reciprocal space, accessible through $I(\mathbf{Q})$, and real space, i.e. the aspect of $\rho(\mathbf{r})$. In Chap. 2, we will begin the analysis of the scattering by atomic arrangements that represent typical systems often studied in the laboratory. If you want, you can skip to Chap. 2, which is perfectly understandable without taking into account the Compton scattering and radiation absorption effects (Sect. 1.4).

...

Exercise 1.9. In order to record the scattered intensity by a single molecule, an X-ray film or a phosphor-base photostimulated plate, known as image plate, is mounted in the shape of a cylinder around the position where the radiation strikes the molecule, as diagrammed in Fig. 1.12. The radiation is linearly polarized along the cylinder axis. (a) Define a coordinate system for locating each film pixel from the center of the molecule. What are the versors \hat{s} and $\hat{\epsilon}$, the pixel position vector \mathbf{R} , and the versor \hat{s}' in this coordinate system? (b) What is the solid angle $d\Omega$, corresponding to each pixel? (c) Write down a routine for calculating the molecule form factor as a function of its orientation, assuming that the molecule is an aromatic ring where the C–C bond length is $d = 140$ pm. (d) Calculate the intensity distributed over the film for a given molecule orientation. What is the scattered intensity (without considering the incident-transmitted beam) in the central pixel, coordinates $(0, 0)$?

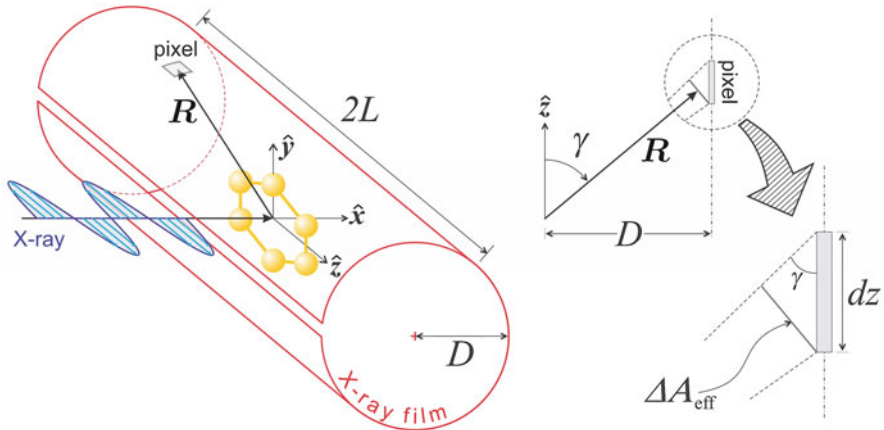


Fig. 1.12 Radiation detector (X-ray film or image plate) positioned in a cylindrical shape around a single molecule. X-ray beam linearly polarized along the detector (cylinder) axis

Answer (a): $\hat{s} = [1, 0, 0]$ (incident beam direction), $\hat{e} = [0, 0, 1]$ (polarization along the cylinder axis), $\mathbf{R} = [D \cos \phi, D \sin \phi, z]$ (position of each pixel) where D is the cylinder (film) radius, and

$$\hat{s}'(z, \phi) = \frac{\mathbf{R}}{|\mathbf{R}|} = \frac{[D \cos \phi, D \sin \phi, z]}{\sqrt{D^2 + z^2}}$$

is the beam direction scattered in the pixel of coordinates (z, ϕ) .

Answer (b): γ being the polar angle between \hat{s}' and the cylinder axis, the effective area of each pixel viewed from the center of the molecule, Fig. 1.12, is

$$\Delta A_{\text{eff}} = \sin \gamma \overbrace{D d\phi dz}^{\text{pixel area}} = \frac{D}{R} D d\phi dz = \frac{D^2 d\phi dz}{\sqrt{D^2 + z^2}}$$

$$\therefore d\Omega(z) = \frac{\Delta A_{\text{eff}}}{R^2} = \frac{D^2 d\phi dz}{(D^2 + z^2)^{3/2}}.$$

Answer (c): The aromatic ring is initially on the yz plane perpendicular to the incident beam and the n -th atom is at position

$$\mathbf{r}_n^{(0)} = d [0, \cos(n\pi/3), \sin(n\pi/3)].$$

Around the x axis the molecule has a six-fold symmetry (positions repeat every $360^\circ/6$), so that the rotation matrix

$$\mathcal{R}_X(\theta_x) = [1, 0, 0; 0, \cos \theta_x, -\sin \theta_x; 0, \sin \theta_x, \cos \theta_x]$$

only makes a difference to θ_x in the range from 0 to $\pi/3$. [Note: “;” is used to end a line in the matrix.] For a general orientation of the molecule, rotation matrices around the axes y and z are also required:

$$\mathcal{R}_Y(\theta_y) = [\cos \theta_y, 0, -\sin \theta_y; 0, 1, 0; \sin \theta_y, 0, \cos \theta_y] \quad \text{and}$$

$$\mathcal{R}_Z(\theta_z) = [\cos \theta_z, \sin \theta_z, 0; -\sin \theta_z, \cos \theta_z, 0; 0, 0, 1].$$

The total molecule spin is then given by the sequence of rotations:

$$\mathcal{R}(\theta_x, \theta_y, \theta_z) = \mathcal{R}_X(\theta_x) \mathcal{R}_Y(\theta_y) \mathcal{R}_Z(\theta_z),$$

and the final atomic positions are

$$\mathbf{r}_n = \mathbf{r}_n^{(0)} \mathcal{R}(\theta_x, \theta_y, \theta_z).$$

[Note: position vectors represented by 1×3 line matrices, $\mathbf{r}_n \equiv [\mathbf{r}_n]_{1 \times 3}$. For column matrix representation, the rotation matrices are transposed, $[\mathbf{r}_n]_{3 \times 1} = [\mathbf{r}_n]_{1 \times 3}^t = \mathcal{R}^t(\theta_x, \theta_y, \theta_z) [\mathbf{r}_n^{(0)}]_{1 \times 3}^t = \mathcal{R}_Z(-\theta_z) \mathcal{R}_Y(-\theta_y) \mathcal{R}_X(-\theta_x) [\mathbf{r}_n^{(0)}]_{3 \times 1}$.] Given a molecule orientation $(\theta_x, \theta_y, \theta_z) \rightarrow \mathbf{r}_n$, the molecule form factor

$$F_M(\mathbf{Q}) = f_C(Q) \sum_{n=1}^6 e^{i \mathbf{Q} \cdot \mathbf{r}_n}$$

is calculated for each pixel specified by the versor $\hat{s}'(z, \phi)$, so that $\mathbf{Q}(z, \phi) = (2\pi/\lambda) [\hat{s}'(z, \phi) - \hat{s}]$ and $F_M(\mathbf{Q}) \rightarrow F_M(z, \phi)$.

Answer (d): To calculate the intensity $I(\mathbf{Q})$ on the film, let us take $D = 50$ mm (cylinder radius) and $L = 200$ mm where $2L$ is the total cylinder length so that $z \in [-L, L]$. Since the molecule has few atoms, the intensity distribution is relatively smooth and there is no need for high resolution films with very small pixels. For 2 mm pixel of area $D d\phi dz = 4 \text{ mm}^2$ where $dz = 2 \text{ mm}$ and $d\phi = 1/25 \text{ rad}$, there will be a total of 31,400 pixels in the film.

The intensity expression is given by

$$I(z, \phi) = \Phi r_e^2 \langle |\mathcal{P}|^2 \rangle d\Omega(z) |F_M(z, \phi)|^2 = \Phi r_e^2 M(z, \phi)$$

where $\langle |\mathcal{P}|^2 \rangle = |\mathcal{P}(\hat{s}')|^2 \rightarrow |\mathcal{P}(z, \phi)|^2 = |\hat{s}'(z, \phi) \times [\hat{\mathbf{e}} \times \hat{s}'(z, \phi)]|^2$, (1.5). An example is shown in Fig. 1.13 for which the scattered intensity in the central pixel is

$$I(0, 0) = \underbrace{\Phi r_e^2}_{= 1 \text{ cps}} \underbrace{|\mathcal{P}(0, 0)|^2}_{= 1} \left(\frac{D d\phi dz}{D^2} \right) [6f_C(0)]^2 = \frac{4}{50^2} 36^2 \simeq 2 \text{ cps}.$$

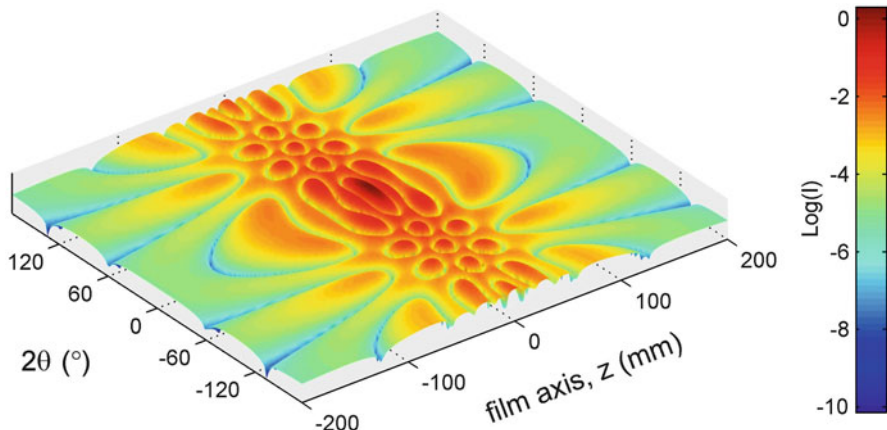


Fig. 1.13 Intensity pattern for a benzene molecule oriented in the xz plane (Fig. 1.12), orientation matrix $\mathcal{R}(30^\circ, 0, 90^\circ)$. X-rays of 20 keV, and flux so that $\Phi r_e^2 = 1$ cps [benzeneonpsp.m]

Exercise 1.10. (a) Using a photon distribution routine in which the probability of detecting a photon is proportional to the intensity on the film pixels, estimate the minimum number of photons required to visualize the intensity pattern in Fig. 1.13. (b) For a flux $\Phi = 1/r_e^2 = 1.26 \times 10^{25}$ cps/cm², what is the exposure time to make the experiment feasible?

Answer (a): With 10^4 photons, it is already possible to identify details of the molecule interference pattern, see image with 10^5 photons in Fig. 1.14.

Answer (b): The total intensity distributed on the film, $I_{image} = \Phi r_e^2 \sum_j M_j$, corresponds to the sum of pixel intensities, specified herein by the subscript j . The number of photons collected in a time interval Δt will be $\mathcal{N} = I_{image} \Delta t$. In the case of the intensity pattern in Fig. 1.13, already calculated for $\Phi r_e^2 = 1$ cps, $M = \sum_{j=1}^{31400} M_j = 82.1$, and thus

$$\Delta t = \frac{\mathcal{N}}{\Phi r_e^2 M} = \frac{10^4}{82.1} = 121.8 \text{ s.}$$

To make the experiment feasible, the total flux required is at least $\Phi \Delta t = 121.8/r_e^2 = 1.5 \times 10^{27}$ photons/cm², but for a sufficiently short exposure time to ensure detection of the diffraction pattern prior to any movement of the molecule. Ultra short X-ray pulses, with duration in the order of femtoseconds, are produced by free electron laser (FEL). With the current technology, a 70 fs pulse may have a power of up to 10^{16} W/cm² for 1.8 keV photons (Chapman et al. 2011), implying a total flux of 2.4×10^{18} photons/cm². Although for the detection of a single molecule diffraction pattern these values of photon flux and energy are much lower than necessary, new advances in the X-ray production technologies can make such experiments conceivable within a few years, as what happened in the 90s when

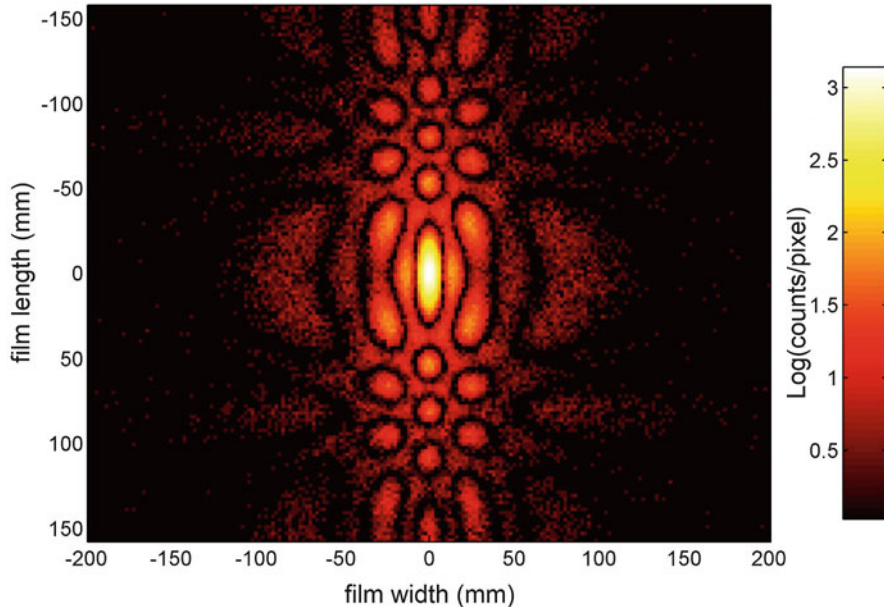


Fig. 1.14 X-ray scattering by a single benzene molecule. Data acquisition simulated with a statistic of 10^5 counts from the intensity pattern in Fig. 1.13 [photonsonpsp.m]

the third generation of synchrotron sources dramatically changed the experimental paradigms of X-ray physics (Als-Nielsen and McMorrow 2001).

...

1.3.3 Compton Scattering by Atoms

In a first approximation, the incoherent scattering (Compton) produced by an atom of atomic number Z would be calculated in a manner that is similar to that indicated in (1.44),

$$I_{Comp}(Q) \simeq I_{Th} \sum_{j=1}^Z (1 - |\text{FT}\{|\psi_j(\mathbf{r})|^2\}|^2) = I_{Th} \mathcal{S}(Q, Z) , \quad (1.54)$$

with the wave functions $\psi_j(\mathbf{r})$ of many electron atoms, the same that are used for calculating the atomic scattering factors $f(Q)$, (1.46). However, the Compton effect

for an atomic electron occurs only when the transfer energy¹¹ is higher than the electron binding energy in the atom. Consequently, (1.54) only provides a good estimate for all elements of the periodic table in the range of γ -rays or hard X-rays with energies above 100 keV. In the range of a few tens of keV, in which most X-ray sources operate, not all electrons represented by the wave functions $\psi_j(\mathbf{r})$ contribute to the incoherent scattering generated by the atom in a given angle 2θ . The value of I_{Comp} for an atom is predominantly determined by the outermost electrons, while the electrons that do not contribute are accounted as those related by the Pauli exclusion principle, so that $\text{FT}\{\psi_j(\mathbf{r}) \psi_k^*(\mathbf{r})\} \neq 0$. This fact allows the correction of the incoherent scattering function¹²

$$\mathcal{S}(Q, Z) = \sum_j (1 - |\text{FT}\{|\psi_j(\mathbf{r})|^2\}|^2) - \sum_j \sum_{k \neq j} |\text{FT}\{\psi_j(\mathbf{r}) \psi_k^*(\mathbf{r})\}|^2, \quad (1.55)$$

only by adding an extra term (double summation), whose value is calculated using the wave functions $\psi_j(\mathbf{r})$ of the atom ground-state.

Note 1.3: A full table of $\mathcal{S}(x, Z)$ values where $x = \sin \theta / \lambda = Q/4\pi$ can be obtained in the article by Hubbell et al. (1975), which is partially reproduced in the International Tables for Crystallography (Prince 2006, p. 658). There still does not exist an equation in the case of incoherent scattering function for interpolating the tabulated values. Therefore, for each intermediate value of $x = Q/4\pi$ between those available in the tables an interpolation routine is needed, e.g. routine `csfQ.m` in Appendix B. But there is a parametric equation (McMaster et al. 1969) for the incoherent scattering cross-section,

$$\sigma_C(\mathcal{E}, Z) = r_e^2 \int \langle |\mathcal{P}|^2 \rangle \mathcal{S}(Q, Z) d\Omega = \exp \left\{ \sum_{n=0}^3 c_n [\ln(\mathcal{E})]^n \right\} \quad (1.56)$$

where the c_n coefficients are tabulated for Z from 1 to 92, see routine `sgcompton.m`. The integration of the incoherent intensity in all space directions eliminates the dependence with the reciprocal vector, making the Compton cross-section of each element a function only of energy. The tabulated $\sigma_C(\mathcal{E}, Z)$ values are also available in Hubbell et al. (1975). Figure 1.15 shows a comparison between the numerical solution of the above integral, using linear interpolation of the tabulated $\mathcal{S}(Q, Z)$ values, and the analytical solution in (1.56).

¹¹Energy transferred to the electron, equal to the difference $\mathcal{E} - \mathcal{E}'$, between the incident and scattered photon energies. For an electron with initial moment zero, the transfer energy is determined by the well-known Compton effect formula: $\mathcal{E}' = \mathcal{E}/[1 + \tau(1 - \cos 2\theta)]$ where $\tau = \mathcal{E}/mc^2$ (Lovesey and Collins 1996).

¹²Prince (2006, p. 659, 7.4.3.5). See also Cattani (2011).

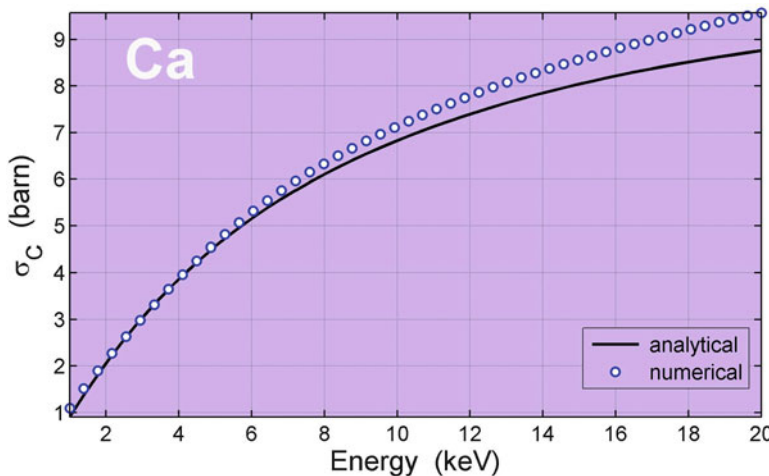


Fig. 1.15 Incoherent (Compton) scattering cross-section for Ca. Comparison of analytical and numerical solutions. The latter obtained by linear interpolation of $S(Q, Z)$ [exsgc.m]

Over the past century, the Compton effect had fundamental importance in the development of quantum physics, as well as in other chapters of the history of high energy and solid state physics. Nowadays, the Compton scattering helps investigating the electron linear momentum in a ground state atom and in the study of magnetic materials (Lovesey and Collins 1996). Understanding the relationship between the Compton scattering and the electron momentum is relatively simple, you just have to redo the scattering kinematics calculations assigning an initial nonzero momentum to the electron. The energy difference $\mathcal{E} - \mathcal{E}'$ between the incident and scattered photons no longer has a single value at a defined scattering angle, and now presents a distribution of values directly proportional to the moment distribution of the atomic electrons. In the study of magnetic materials, the interaction of the incident magnetic wavefield with the electron spin, which is very small compared to the charge scattering at low energies, becomes dominant in the region of hard X-rays, above 60 keV, a fact that provides information about the spin density in an atom. However, this book is focused on applications of coherent scattering for structural analysis of materials. Nevertheless, it is necessary to be aware of the presence of the Compton scattering and, when appropriate, know how to remove the contributions of incoherent scattering from the experimental data.

...

Exercise 1.11. Using the tabulated values of function $S(Q, Z)$, compare the coherent and incoherent scattered intensities by an atom as a function of scattering angle, and polarization.

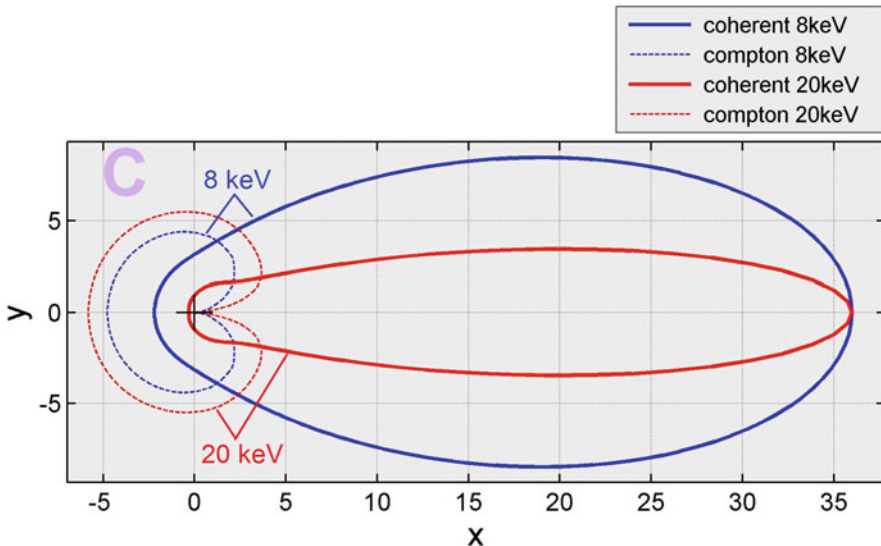


Fig. 1.16 Coherent and incoherent (Compton) intensities scattered by the carbon atom. X-rays of 8 and 20 keV. Coordinates: $x = I(Q) \cos(2\theta)$ and $y = I(Q) \sin(2\theta)$ where $I(Q) = I_{Th} |f(Q)|^2$ (coherent) and $I(Q) = I_{Th} S(Q, Z)$ (incoherent). Flux so that $I_{Th} = \Phi r_e^2 \langle |\mathcal{P}|^2 \rangle d\Omega = 1 \text{ cps}$ (σ polarization) [excsf.m]

Answer: For an atom of atomic number Z , the coherent and incoherent intensities are given by $I_{Cohe}(Q) = I_{Th} |f(Q)|^2$ and $I_{Comp}(Q) = I_{Th} S(Q, Z)$, respectively. In Fig. 1.16, the functions $|f(Q)|^2$ and $S(Q, Z)$ of the carbon atom ($Z = 6$) are compared as a function of the scattering angle 2θ . At $2\theta = 180^\circ$, $S(Q_{max}, Z) < Z$ but approaches to Z as $Q_{max} \rightarrow \infty$, reflecting the fact that with increasing radiation energy all the binding energies of the Z electrons become smaller than the transfer energy. On the other hand, $|f(0)|^2 = Z^2$ for any radiation energy. Both contributions, coherent and incoherent, are equally affected by the polarization coefficient $\langle |\mathcal{P}|^2 \rangle$, which is equal to 1 only in the σ polarization. For instance, in the π polarization both intensities are multiplied by the $\cos^2(2\theta)$ factor, so that they are canceled at 90° from the incident beam direction.

...

Suggestion: With routine `excsf.m`, check the influence of X-ray polarization in the coherent and incoherent intensities scattered by an atom.

Section Summary

— Electron density of atoms:

$$\rho_a(\mathbf{r}) = \sum_j |\psi_j(\mathbf{r})|^2$$

— Atomic scattering factor:

$$f(Q) = \text{FT}\{\rho_a(\mathbf{r})\}$$

— Parametric formula (Cromer–Mann coefficients: a_n , b_n , and c):

$$f(Q) = \sum_{n=1}^4 a_n e^{-b_n(Q/4\pi)^2} + c$$

— Coherent intensity scattered by an isolated atom:

$$I(Q) = I_{Th} |f(Q)|^2$$

— Parametric formula of the coherent scattering cross-section (McMaster et al. 1969):

$$\sigma_R(\mathcal{E}, Z) = \exp \left\{ \sum_{n=0}^3 c_n [\ln(\mathcal{E})]^n \right\} \simeq r_e^2 \int \langle |\mathcal{P}|^2 \rangle |f(Q)|^2 d\Omega$$

— Electron density of a discrete arrangement of atoms, e.g. molecule:

$$\rho(\mathbf{r}) = \sum_a \rho_a(\mathbf{r}) * \delta(\mathbf{r} - \mathbf{r}_a)$$

— Form factor of a discrete arrangement of atoms:

$$F(Q) = \text{FT}\{\rho(\mathbf{r})\} = \sum_a \text{FT}\{\rho_a(\mathbf{r})\} \text{FT}\{\delta(\mathbf{r} - \mathbf{r}_a)\} = \sum_a f_a(Q) e^{iQ \cdot \mathbf{r}_a}$$

— Coherent intensity scattered by the arrangement of atoms:

$$I(Q) = I_{Th} |F(Q)|^2$$

— Incoherent (Compton) intensity scattered by an atom:

$$I_{Comp}(Q) = I_{Th} \mathcal{S}(Q, Z)$$

$\mathcal{S}(Q, Z)$: incoherent scattering function (Hubbell et al. 1975; Prince 2006)

— Parametric formula of the Compton scattering cross-section (McMaster et al. 1969):

$$\sigma_C(\mathcal{E}, Z) = \exp \left\{ \sum_{n=0}^3 c_n [\ln(\mathcal{E})]^n \right\} \simeq r_e^2 \int \langle |\mathcal{P}|^2 \rangle \mathcal{S}(Q, Z) d\Omega$$

...

1.4 X-Ray Absorption

The optical properties of a material medium are described in general by macroscopic parameters such as magnetic permeability, dielectric permittivity, polarizability, conductivity, etc. By definition, these parameters are the average values of the response of the medium to an external electromagnetic field. This approach is completely justified in the case of electromagnetic waves with wavelengths much larger than the interatomic distances; visible light has a λ of hundreds of nanometers (400–700 nm), while the distances between neighboring atoms in a solid are typically around tenths of nanometers (0.2–0.5 nm). Also within this approach, the mobility of the electrons is a key parameter for the attenuation of the wave amplitude as it propagates in the medium. Resistance to the microscopic electric currents induced by the electric field is responsible for absorbing the wave energy by Joule effect,¹³ causing the medium to heat up.

In the case of X-rays, since the wavelengths are of the order of atomic diameters, the concepts of mean macroscopic values of the medium are not sufficient in themselves to describe the wave fields established in the medium when it is excited by the incident radiation. For example, the very high frequency of X radiation, of the order of 3×10^{18} Hz ($= c/\lambda$), produces zero displacements of the electrons in the material compared to atomic dimensions. This means that there is no radiation absorption by the resistivity of the material, as is the case of visible and infrared light. The amplitude of vibration of electrons in response to the electric field is very small for there to be dissipation of the wave energy by Joule heating effect. Therefore, the average properties of the medium in molecular scales have very little influence on absorbing the radiation in the X-ray range. In other words, X-ray photons do not excite vibrational states of molecules.

At a level of first principles, the X radiation absorption process is far from the classical approach, which means that X-ray absorption is a purely quantum process at an atomic scale without any analogy with classical systems. The annihilation of photons occurs by electronic transitions from quantum core-levels (K or L shell) to discrete or continuous states available around the atom, resulting in both electrical currents in the sample (photocurrents) and free electrons with a certain kinetic energy (photoelectron). After each transition come processes of filling the hole giving rise to fluorescence emissions and Auger electrons.¹⁴ The photons emitted by fluorescence, besides having less energy than the primary photon, they do not preserve any phase coherence with the incident X-ray wave. They are scattered in all directions without any correlation with the sample's atomic structure and so without showing any interference effects. However, the fluorescent X-rays are characteristic

¹³Any resistance to the movement of electrons that increases the vibrations of the molecules in the material.

¹⁴Electrons ejected by absorption of fluorescence photons within a simplified description of this process considering that the Auger electrons satisfy the energy balance for the photoelectric effect with fluorescence photons. For more details, search for Auger spectroscopy.

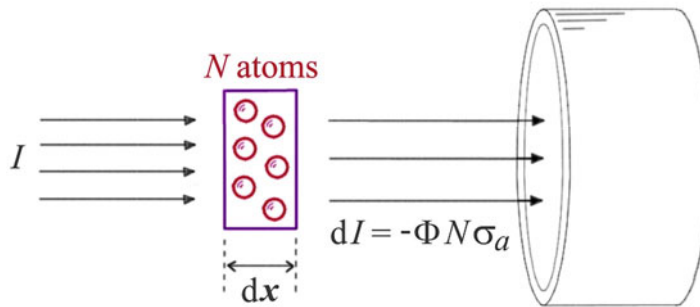


Fig. 1.17 Attenuation dI of the intensity I by N atoms with an absorption cross-section of σ_a , submitted to a flux Φ of photons per second

of each element, just like fingerprints, denouncing the presence of the elements that make up the sample, even in minute quantities in the order of parts per million (ppm).

1.4.1 Linear Attenuation Coefficient

From the experimental point of view, the description of the absorption process for a given element is summarized in cross-section σ_a . It tells us that by putting N atoms in a flux Φ of photon per area unit per second, we will have $N \Phi \sigma_a$ photons absorbed per second, Fig. 1.17. The cross-section leads to the linear attenuation coefficient μ , which is responsible for the attenuation of the X-rays when they travel through a material medium.

To simplify the deduction of the attenuation coefficient, we initially assume a material composed of a single chemical element containing η atoms per volume unit. The attenuation of a beam's intensity when crossing a layer of thickness dx in the material will be

$$\begin{aligned} dI &= I(x + dx) - I(x) = - \underbrace{\frac{N}{\eta S dx}}_{\eta S \Phi} \Phi \sigma_a = - \underbrace{\frac{I(x)}{S \Phi}}_{\frac{1}{\mu}} \underbrace{\mu}_{\eta \sigma_a} dx \\ \Rightarrow \quad I(x) &= I_0 e^{-\mu x}. \end{aligned} \quad (1.57)$$

[Note: S is the cross section of the incident beam of intensity I_0 and propagation direction \hat{x} .] In the case of a material made of different chemical elements

$$\mu = \sum_n (\eta \sigma_a)_n = \sum_n \left(\frac{N_A \sigma_a}{M} \right)_n \rho_n = \sum_n \left(\frac{\mu}{\rho} \right)_n \rho_n. \quad (1.58)$$

N_A is the Avogadro's number, M is the molar mass, and ρ_n is the mass density of the element n in the material.

According to (1.58), the attenuation coefficient is independent from the relative arrangement of atoms, depending only on their concentration in a given volume of material. Although this is the dominant fact for the attenuation process of X-rays, it is entirely true only when the absorption cross-section of every atom is independent of the local environment in which the atom is inserted. It turns out that the quantum states available around an atom suffer disturbances from the presence of neighboring atoms, changing the values of σ_a in relation to the values expected for isolated atoms. Attenuation coefficient measurements as a function of the energy, i.e. measurements of $\mu(\mathcal{E})$, are the basis of X-ray absorption spectroscopy techniques, providing information of the chemical bonds and the atomic arrangement in the vicinity of a particular atom of the material. Before the end of this section we will discuss in more detail the influence of the environment on the absorption cross-section, Sect. 1.4.5.

1.4.1.1 Scattering Cross-Section and the Linear Attenuation

It is important to notice that the linear attenuation is affected by any process that reduces the intensity of the incident X-ray beam as it penetrates in a given material. So, besides the photoelectric absorption, which in fact annihilates X-ray photons, the coherent and incoherent scattering processes, when they remove photons from the direct beam, also contribute to the total cross-section

$$\sigma = \sigma_a + \sigma_C + \sigma_R , \quad (1.59)$$

responsible for the beam's effective linear attenuation. σ_R and σ_C are the cross-sections of the coherent and incoherent scattering, (1.50) and (1.56), respectively.

In the energy range of X-rays between 1 and 100 keV, the scattering processes contribute with less than 10 % in the value $\sigma \simeq \sigma_a$, so that the linear attenuation, as a general rule, is predominantly a photoelectric absorption effect. The exception to this rule is due to the interference phenomena of coherent scattering since the tabulated values of σ_R are valid for isolated atoms. In materials with a certain order at the atomic level, the occurrence of constructive interference away from the direction of the direct beam can significantly change the cross-section σ_R and, consequently, the linear attenuation. For example, in an ideal gas where interference effects between atoms hardly occur, σ_R corresponds to the table. In an amorphous material, however, there is a predominance of destructive interference in any direction away from the direct beam, and thus $\sigma_R \approx 0$. In a crystal undergoing diffraction—strong diffracted beams— σ_R rises above the tabulated values.¹⁵ But as the orientation

¹⁵In perfect crystals of a certain thickness, the condition of diffraction gives rise to the formation of standing waves that do not coincide with the atomic positions, causing a sharp drop in photoelectric

is changed, the crystal leaves the condition of diffraction, and the constructive interference outside the direct beam is extinguished and $\sigma_R \rightarrow 0$. The cross-section of the Compton effect, σ_C , is the only contribution to the linear attenuation of the beam that does not change due to correlations of atomic positions in the materials.

In the past, it was common to use tables of mass attenuation coefficient (μ/ρ) , (1.58), as a function of characteristic energies of the main materials used as target in X-ray tubes such as Cu, Ag, Mo, etc., cf. Prince (2006, p. 230). The great facility that we have today to conduct experiments with synchrotron sources where the energy can be continuously adjusted over a wide range of values has diminished the practicality of the (μ/ρ) tables. Today, the values (μ/ρ) are calculated depending on the energy from the scattering cross-sections, σ_R and σ_C , and mainly from the photoelectric absorption cross-section σ_a (McMaster et al. 1969; Prince 2006). We will demonstrate later on how σ_a depends on the energy after the introduction of atomic resonance phenomenon, Sect. 1.4.2. However, when exact values of (μ/ρ) are required, special attention needs to be taken with the use of σ_R . In gases and liquid, σ_R should be considered, while in amorphous materials or single crystals outside the condition of diffraction, σ_R can be discarded. In polycrystalline materials there are always diffracted beams regardless of the radiation incidence angle in the sample, and therefore σ_R tends to always be higher than the tabulated values. Due to the interference phenomenon, the uncertainty in (μ/ρ) , or in the total cross-section σ , is difficult to account precisely since it depends on the particularities of each sample (Prince 2006).

...

Exercise 1.12. In the case of the K_α characteristic radiation of Cu [$\lambda = (2\lambda_{\alpha 1} + \lambda_{\alpha 2})/3 = 1.54184 \text{ \AA}$], the total cross-sections of the atoms C, N, O, and Ar are worth $\sigma(\text{C}) = 89.9 \text{ barn}$, $\sigma(\text{N}) = 173 \text{ barn}$, $\sigma(\text{O}) = 304 \text{ barn}$ and $\sigma(\text{Ar}) = 7.72 \times 10^3 \text{ barn}$, respectively.¹⁶ (a) In which of these values is the joint contribution of the scattering cross-sections relatively higher? (b) What are the mass attenuation coefficients (μ/ρ) in cm^2/g of these atoms? (c) Given: 23.2 % (O_2), 75.47 % (N_2), 1.28 % (Ar) and 0.046 % (CO_2) as the relative fractions of mass, w_n , of the main gases that make up dry air. What is the attenuation of an X-ray beam, Cu K_α , per linear meter of dry air at normal temperature and pressure (NTP) conditions? [Note: dry air density at 20 °C and 1 atm is $\rho_{\text{air}} = 1.204 \text{ kg/m}^3$.]

Answer (a): It is larger in $\sigma(\text{C})$, carbon, where

$$\sigma_R = 4.51 \text{ barn}, \quad \sigma_C = 2.56 \text{ barn}, \quad \text{and} \quad \frac{\sigma_R + \sigma_C}{\sigma(\text{C})} = 0.079, \text{ or } 7.9 \text{ \%}.$$

absorption. This phenomenon is known as anomalous transmission or Borrman effect (Batterman and Cole 1964, p. 681).

¹⁶Prince (2006, pp. 220–229).

The lower relative contribution of $\sigma_R + \sigma_C$ occurs for Ar, only 0.9 %. Routines `sgrayleigh.m` and `sgcompton.m`.

Answer (b): $(\mu/\rho) = N_A \sigma/M$, and hence it follows that $(\mu/\rho)_C = 4.51 \text{ cm}^2/\text{g}$, $(\mu/\rho)_N = 7.44 \text{ cm}^2/\text{g}$, $(\mu/\rho)_O = 11.5 \text{ cm}^2/\text{g}$, and $(\mu/\rho)_{Ar} = 116 \text{ cm}^2/\text{g}$.

Answer (c): With every meter of dry air the beam is attenuated by 69.2 % since $I/I_0 = e^{-1.177} = 0.308$.

$$\begin{aligned}\mu_{\text{air}} = \rho_{\text{air}} \sum_n (\mu/\rho)_n w_n &= (1.204) [(0.451) \underbrace{0.00013}_{w_C} + \\ &+ (0.744) \underbrace{0.7547}_{w_N} + (1.15) \underbrace{(0.2320 + 0.00033)}_{w_O} + (11.6) \underbrace{0.0128}_{w_{Ar}}] = 1.177 \text{ m}^{-1}.\end{aligned}$$

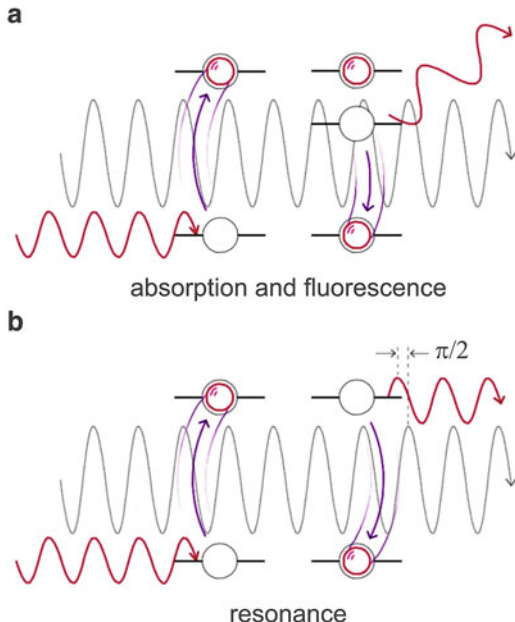
...

1.4.2 Atomic Resonance

The atomic resonance phenomenon is intrinsically related to the absorption and fluorescence processes. The mere existence of a quantum state available around the atom creates the probability of a core electron to interact with a photon and jump to the available state, whether to a discrete state of bound electron or to a continuous state of free electron (photoelectron). However, instead of the electron remaining at this level, which characterizes the absorption and fluorescence processes, Fig. 1.18a, the electron is stimulated by the field of the incident wave to return to its initial level, re-emitting the photon with a phase lag of $\pi/2$ in relation to the incident X-ray wave, Fig. 1.18b. Because of this phase correlation with the primary wave, the amplitude of resonant scattering has an imaginary term, which means that the atomic scattering factor $f(Q)$ ceases to be a purely real number since $e^{i\pi/2} = i$. Furthermore, it also becomes a function of the energy due to the dependence of resonance with the energy. In practical terms, we can say that the resonance implies $\text{Im}f(Q) \rightarrow f(Q, \mathcal{E})$ and $\text{Im}\{f(Q, \mathcal{E})\} \neq 0$.

Since the electronic transition responsible for the absorption is also the primary transition at resonance, Fig. 1.18, it is expected that the higher the absorption rate, meaning the cross-section σ_a , the greater also will be the contribution of the imaginary component of $f(Q, \mathcal{E})$. If the probability for the atom to remain in the excited state were zero, the amplitude of resonance would be a purely real number. To explicitly demonstrate the relationship between absorption and imaginary component, we will make a simple introduction to the phenomenon of resonance using the classical approach of forced oscillator. The approach by quantum mechanics based on the perturbation theories of the first and second order provides a more accurate idea of the absorption and resonance processes at the level of first principles, which are in terms of annihilation and creation of photons.

Fig. 1.18 (a) Absorption and fluorescence: X-ray photons eject electrons from core-levels (K or L shell) to empty quantum levels around the atom. The hole left by the ejected electron is filled by an electron from another atomic level, closing up the absorption process and generating fluorescence photons with less energy than the primary photons. (b) Atomic resonance: the primary wave field stimulates the electrons ejected to return to their initial state, re-emitting photons of the same energy but with a phase lag of $\pi/2$



In condensed matter physics, the quantum approach has been fundamental in the rapid development of modern techniques of material analysis using synchrotron X-ray sources and in the exploration of various phenomena related to the density of quantum states around the atoms (Lovesey and Collins 1996). In X-ray physics, as for the proper use of the concepts of absorption and resonance, it is important to keep in mind the following facts:

1. The total effect of the resonance in the atomic scattering factor is given by

$$f(Q, \mathcal{E}) = f_0(Q) + f'(\mathcal{E}) + i f''(\mathcal{E}) \quad (1.60)$$

where $f_0(Q)$ comes to represent the atomic scattering factor defined in (1.46).

2. The imaginary component is proportional to the absorption cross-section according to the relationship

$$f''(\mathcal{E}) = \mathcal{E} \sigma_a(\mathcal{E}) / 4\pi r_e \hbar c = \sigma_a(\mathcal{E}) / 2 r_e \lambda . \quad (1.61)$$

3. There are mathematical relationships between f' and f'' called Kramers–Kronig relations for determining f' from f'' and vice versa. Therefore, attenuation coefficient measurements lead to the experimental values of the correction terms of the atomic scattering factor:

$$\boxed{\text{Experiment}} \rightarrow \mu(\mathcal{E}) \rightarrow \sigma_a(\mathcal{E}) \rightarrow f''(\mathcal{E}) \rightarrow \boxed{\text{Kramers–Kronig}} \rightarrow f'(\mathcal{E}) .$$

The resonance amplitude $f' + if''$, often called dispersion correction terms or anomalous scattering factors, are available on the International Tables for Crystallography (Prince 2006) and also at some addresses on the world wide web. The tabulated values generally come from theoretical models for isolated atoms and are quite accurate away from the transition energies or absorption edges of the atoms in the sample. Contrary to what happens with the theoretical values of $f_0(Q)$ for isolated atoms, which, in addition to accurate are little affected by the presence of neighboring atoms, the experimental values of f' and f'' are more reliable in some situations since the theoretical models do not take into account the presence of neighboring atoms, whose effects can be quite significant in the vicinity of absorption edges.

Note 1.4: The theoretical values of the dispersion correction terms are essential in calculating the absorption cross-sections σ_a , through which the linear attenuation coefficients of the materials are estimated. In addition, several X-ray diffraction experiments explore the phenomenon of atomic resonance, for example, as a strategy for overcoming the phase problem in determining crystal structures.¹⁷ In this book we will do some exercises using the theoretical values of f' and f'' . Readers should have available a routine that allows them to quickly obtain these values. We have used the routine `fpfpp.m`.

...

Exercise 1.13. Choose an element with an absorption edge of around 10 keV. What is the effect of the atomic resonance in the coherent scattering cross-section $\sigma_R(\mathcal{E})$?
Answer:

$$\sigma_R(\mathcal{E}) = r_e^2 \int \langle |\mathcal{P}|^2 \rangle |f(Q, \mathcal{E})|^2 d\Omega .$$

$d\Omega = \sin \gamma d\gamma d\varphi$, so that $\langle |\mathcal{P}|^2 \rangle = (1 + \cos^2 \gamma)/2$ and $Q = 4\pi \sin(\gamma/2)/\lambda$ depend on the scattering angle $\gamma = 2\theta$. For Se, the values of $\sigma_R(\mathcal{E})$ with and without resonance are compared in Fig. 1.19. The real term of the resonance amplitude, $f'(\mathcal{E})$, reduces σ_R below and above the absorption edge at 12.6 keV, while the imaginary term, $f''(\mathcal{E})$, contributes toward increasing the cross-section above the edge.

...

¹⁷There is extensive literature on phasing methods by anomalous dispersion. See, for instance, Giacovazzo (2002) and Als-Nielsen and McMorrow (2001).

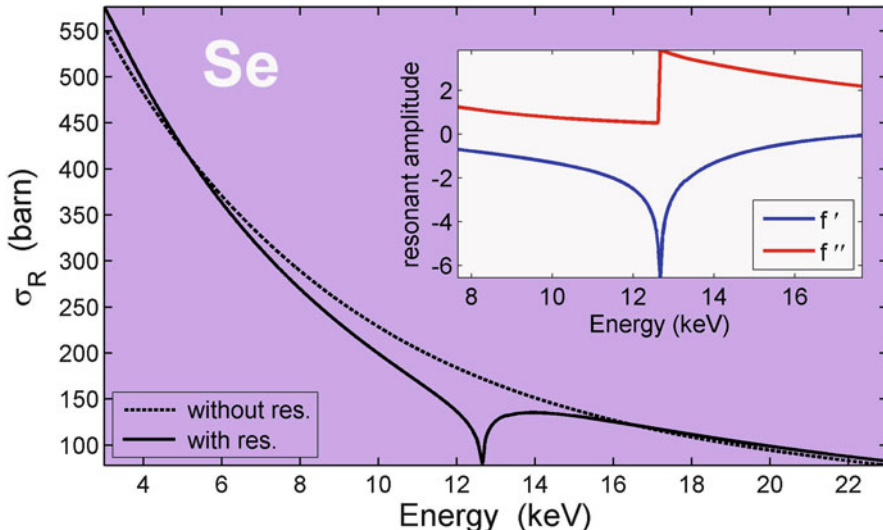


Fig. 1.19 Coherent scattering cross-section $\sigma_R(\mathcal{E})$ for Se. With (black line) atomic resonance correction: $f(Q, \mathcal{E}) = f_0(Q) + f'(\mathcal{E}) + i f''(\mathcal{E})$, (1.60). Without (black dashed line) correction: $f(Q, \mathcal{E}) = f_0(Q)$, (1.48). Inset: theoretical values of the atomic resonance amplitude, relativistic quantum model (Prince 2006) [exfpfpp.m]

1.4.3 Semi-classical Approach of Atomic Resonance: Electron Elastically Bound

The simplest way to demonstrate the resonance amplitude is by making an analogy with the field radiated by an elastically bound electron.¹⁸ There is a great similarity, within certain limitations, between the results obtained with the classical and quantum treatment. Reproduce this treatment here, which can be found in many textbooks, has the following objectives: (a) demonstrate that it is consistent with the convention adopted for the phase signal of the incident wave and Fourier transform, (1.33) and (1.34); and (b) deduce the mathematical relationships between resonance amplitude and absorption cross-section, Eq. (4.5), as well as between the real and imaginary components of the resonance amplitude.

A classic electron trapped by a restoring force with a resonance frequency of ω_n , and subject to a dissipative force proportional to the speed through the constant $m\Gamma$, has as its equation of movement $\ddot{z} + \Gamma \dot{z} + \omega_n^2 z = -(e/m)E_0 e^{i\omega t}$ when subjected to the electric field of the X-ray wave of frequency ω . The solution to this equation leads to the acceleration

¹⁸The original demonstration of the resonance amplitudes by elastically bound charges was made by Lord Rayleigh in the late eighteenth century. The coherent scattering by an atom, taking into account resonance effects or not, is often called Rayleigh scattering.

$$\ddot{z}(\mathbf{r}, t') = \frac{-e}{m} \left(\frac{\omega^2}{\omega^2 - \omega_n^2 - i\omega\Gamma} \right) E_0 e^{i(\omega t' - \mathbf{k} \cdot \mathbf{r})} \quad (1.62)$$

of the electron at the time instant t' and position \mathbf{r} regarding an arbitrary origin. Note that this equation is reduced to (1.18) if we turn off the restoring and dissipative forces ($\omega_n \rightarrow 0$ and $\Gamma \rightarrow 0$). By manipulating the frequency dependent term to obtain

$$\left(\frac{\omega^2}{\omega^2 - \omega_n^2 - i\omega\Gamma} \right) = 1 + f'_n(\omega) + if''_n(\omega), \quad (1.63)$$

and replacing the acceleration in the expression of the dipole radiation field, (1.17), we will have the amplitude of scattering of the resonant electron

$$\mathbf{E}_R(\mathbf{R}, t) = -r_e \mathcal{P} [1 + f'_n(\omega) + if''_n(\omega)] E_0 \frac{e^{i(\omega t - \mathbf{k}' \cdot \mathbf{R})}}{|\mathbf{R} - \mathbf{r}|} e^{i\mathbf{Q} \cdot \mathbf{r}}, \quad (1.64)$$

written to make explicit the terms $f'_n(\omega)$ and $f''_n(\omega)$ showing how the amplitude of scattering of an electron changes due to the effect of resonance.

The imaginary term in (1.63),

$$f''_n(\omega) = \frac{\omega^3 \Gamma}{(\omega^2 - \omega_n^2)^2 + \omega^2 \Gamma^2}, \quad (1.65)$$

implies in an amplitude of lagged scattering of 90° in relation to the incident wave and it is directly related to the dissipation of energy and, therefore, to the system's absorption cross-section, $\sigma_n(\omega)$. To demonstrate this fact, let us calculate the average power dissipated in the forced damped oscillator, which is given by

$$P(\omega) = - \left\langle \frac{d}{dt} (K + U) \right\rangle = - \left\langle \frac{d}{dt} \left(\frac{1}{2} m \dot{z}^2 + \frac{1}{2} m \omega_n^2 z^2 \right) \right\rangle = -m \langle \dot{z} (\ddot{z} + \omega_n^2 z) \rangle.$$

K : kinetic energy, U : potential energy, and from the equation of movement in the absence of external force $\ddot{z} + \omega_n^2 z = -\Gamma \dot{z}$. The speed \dot{z} can be obtained from (1.62), and thus

$$P(\omega) = m \Gamma \langle \dot{z}^2 \rangle = \frac{1}{2} m \Gamma |\dot{z}(\omega)|^2 = \underbrace{\frac{e^2 |E_0|^2}{2m}}_{4\pi r_e c \mathcal{E} \Phi} \frac{\omega^2 \Gamma}{(\omega^2 - \omega_n^2)^2 + \omega^2 \Gamma^2} = 4\pi r_e c \frac{f''(\omega)}{\omega} \mathcal{E} \Phi \quad (1.66)$$

where classic intensity of the incident wave is written depending on the flux and energy of the photons, i.e., $\frac{1}{2} \epsilon_0 c |E_0|^2 = \Phi \mathcal{E}$. According to the absorption cross-section definition, the number of photons absorbed per second is $\Phi \sigma_n(\omega)$, implying in the absorbed power $P(\omega) = \mathcal{E} \Phi \sigma_n(\omega)$. Compared to the (1.66), we arrive at the relation

$$\omega\sigma_n(\omega) = 4\pi r_e c f_n''(\omega) . \quad (1.67)$$

If now we include the resonant electron in an atom and recalculate the field scattered by the electron density $\rho_a(\mathbf{r})$, (1.45), we will have¹⁹

$$\mathbf{E}_{\text{atom}}(\mathbf{R}, t) = -r_e \mathcal{P} E_0 \frac{e^{i(\omega t - \mathbf{k}' \cdot \mathbf{R})}}{R} [\underbrace{\text{FT}\{\rho_a(\mathbf{r})\}}_{f_0(Q)} + f'_n(\omega) + i f''_n(\omega)] . \quad (1.68)$$

Since the photon energy is given by $\mathcal{E} = \hbar\omega$, this classic demonstration of resonance, (1.68), serves perfectly to illustrate both the origin of the dependence of the atomic scattering factor with the energy, as well as that the imaginary component is directly related to the resonance and absorption phenomena. However, up until now we have only considered an oscillator with a frequency of ω_n . Compared to the quantum treatment, this amounts to considering only the transition between two quantum levels whose energy difference is $\mathcal{E}_n = \hbar\omega_n$. As there are a number of states available, ranging from discrete states to the continuum of states for free electrons (photoelectrons), the total effect of resonance in the semi-classical model (James 1948) is given by the linear overlapping of resonance amplitudes, i.e.,

$$f'(\omega) + i f''(\omega) = \sum_n g_n [f'_n(\omega) + i f''_n(\omega)] \quad (1.69)$$

where g_n is the relative weight for all the possible electronic transitions of an atom, many times called oscillator strength. The values of g_n are essentially empirical in the classical treatment, but they also appear in the quantum treatment related to the probabilities of transitions, a fact that has partly justified²⁰ the classical model. The overlap in (1.69) also applies to the absorption cross-section of the atom

$$\sigma_a(\omega) = \sum_n g_n \sigma_n(\omega) = 4\pi r_e c f''(\omega)/\omega = 2r_e \lambda f''(\omega) , \quad (1.70)$$

thus demonstrating (1.61).

...

Exercise 1.14. It is known that the absorption cross-section, (1.70), has a behavior of the type $\sigma_a(\mathcal{E}) = A \mathcal{E}^n$ where n is a number close to -3 . (a) Choose an atom and on a log-log graph analyze by linear interpolation the behavior of the absorption

¹⁹Consider $\rho'_a(\mathbf{r}) \simeq \rho_a(\mathbf{r}) + [f'_n(\omega) + i f''_n(\omega)]\delta(\mathbf{r})$ as being the electronic density of the atom with one resonant electron, such that $\text{FT}\{\rho'_a(\mathbf{r})\} = \text{FT}\{\rho_a(\mathbf{r})\} + f'_n(\omega) + i f''_n(\omega)$. This is justified by the fact that there is no experimental evidence of the dependency of f'_n and f''_n with the scattering vector \mathbf{Q} , cf. Prince (2006, p. 253).

²⁰See Cohen-Tannoudji et al. (1978), complement A_{XIII}.

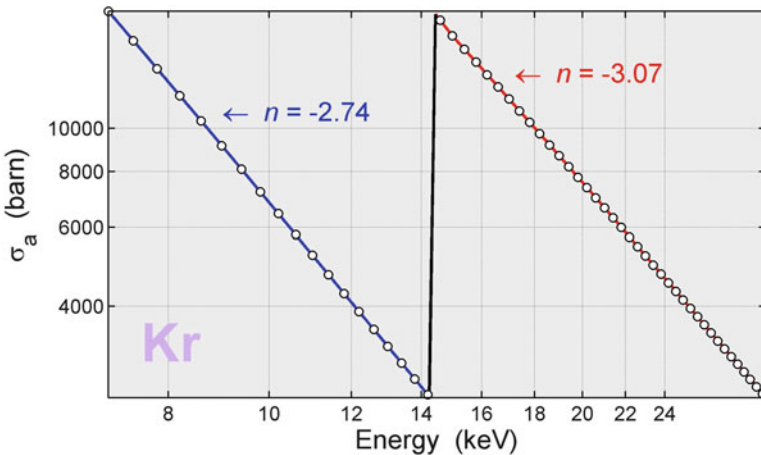


Fig. 1.20 Absorption cross-section for Kr near the K -edge. Theoretical values (circles), (1.70), and linear interpolations with function $\log(\sigma_a) = \log(A) + n \log(\mathcal{E})$ below and above the edge [exabscs.m]

cross-section below and above an absorption edge. (b) Why do the interpolation lines in the log-log scale have different inclinations on each side of the edge?

Answer (a): The theoretical curve of $\sigma_a(\mathcal{E})$ is obtained from the tabulated values of $f''(\mathcal{E})$. In the case of Kr shown in Fig. 1.20, the cross-section falls with \mathcal{E} elevated to the power of $n = -2.74$ and -3.07 below and above the K -edge at 14.3 keV, respectively.

Answer (b): The more accentuated slope of $\sigma_a(\mathcal{E})$ above the edge is due to the increase in the positive ionic charge of the atom after issuing the photoelectron.

...

1.4.4 Kramers–Kronig Relations

The mathematical relationship between the amplitudes $f'(\omega)$ and $f''(\omega)$ is deduced from general relations for complex functions. In the case of $F(z)$ being an analytic function in the complex plane of $z = x + iy$, satisfying two conditions: (1) singularities (poles) outside the real axis in a same sense along the imaginary axis; and (2) $\lim_{|z| \rightarrow \infty} [F(z)/(z - \omega)] = 0$. Then,

$$P \int_{-\infty}^{+\infty} \frac{F(x)}{x - \omega} dx = \lim_{\xi \rightarrow 0} \left(\int_{-\infty}^{\omega - \xi} \frac{F(x)}{x - \omega} dx + \int_{\omega + \xi}^{+\infty} \frac{F(x)}{x - \omega} dx \right) = -i\pi F(\omega). \quad (1.71)$$

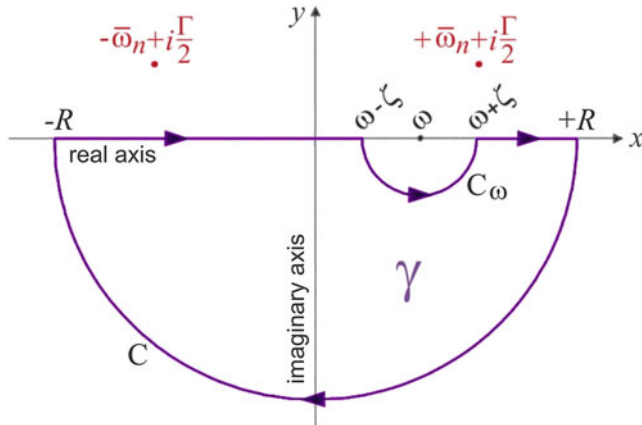


Fig. 1.21 Closed path γ divided into semicircle C , straight intervals $[-R, \omega - \zeta]$ and $[\omega + \zeta, +R]$, and smaller semicircle C_ω . The integral of $F(z)/(z - \omega)$ on the path is calculated for $R \rightarrow \infty$. The poles $\pm \bar{\omega}_n + i\Gamma/2$ of $F(z) = f'_n(z) + if''_n(z)$, (1.63), are outside the real axis in the positive sense of the imaginary axis. $\bar{\omega}_n^2 = \omega_n^2 - \Gamma^2/4$

The principal value integral, indicated by the letter P, follows directly from Cauchy's integral theorem (Arfken 1985): by choosing a closed path in the complex plane, passing through the real axis, but that does not contain singularities inside the contour as path γ in Fig. 1.21, it follows that

$$\oint_{\gamma} \frac{F(z)}{z - \omega} dz = P \int_{-\infty}^{+\infty} \frac{F(x)}{x - \omega} dx + \underbrace{\int_C \frac{F(z)}{z - \omega} dz}_{= 0 \text{ when } |z| \rightarrow \infty} + \underbrace{\int_{C_\omega} \frac{F(z)}{z - \omega} dz}_{= i\pi F(\omega)} = 0.$$

Path γ was chosen assuming poles of function $F(z)$ with positive imaginary components, such as $+i\Gamma/2$ in Fig. 1.21. Otherwise, in the case of negative imaginary components, the principal value would be positive, i.e. $P \int_{-\infty}^{+\infty} \frac{F(x)}{x - \omega} dx = +i\pi F(\omega)$ in (1.71).

Since $F(z)$ is a general function, we can replace it with $f'(z) + if''(z)$ as long as it meets the conditions (1) and (2) mentioned above and has poles with positive imaginary components. This is the case of the amplitudes $f'_n(z) + if''_n(z)$ in (1.63) and, therefore, of any linear combination of these amplitudes, e.g. (1.69). From this you can easily see the Kramers–Kronig relations as being

$$f'(\omega) = -\frac{1}{\pi} P \int_{-\infty}^{+\infty} \frac{f''(x)}{x - \omega} dx \quad \text{and} \quad f''(\omega) = \frac{1}{\pi} P \int_{-\infty}^{+\infty} \frac{f'(x)}{x - \omega} dx. \quad (1.72)$$

The dispersion terms are defined by positive values of frequency or of energy and because of this it is common to find these relations written as follows:

$$f'(\omega) = -\frac{2}{\pi} P \int_0^{+\infty} \frac{xf''(x)}{x^2 - \omega^2} dx \quad \text{and} \quad f''(\omega) = \frac{2\omega}{\pi} P \int_0^{+\infty} \frac{f'(x)}{x^2 - \omega^2} dx , \quad (1.73)$$

which are valid provided that $f'(x)$ and $f''(x)$ are, respectively, even and odd functions with respect to $x = 0$. To calculate them, multiply the numerator and denominator of the integrands in (1.72) by $x + \omega$. To write them in terms of energy $\mathcal{E} = \hbar\omega$, replace ω for \mathcal{E} and take x as a variable of integration on energy values.

1.4.5 Absorption Modulation by Rescattering of Photoelectrons

The cross-section σ_a of the photoelectric absorption by an atom is determined by the probability of transition between a quantum state of core electron with wave function $\psi_j(\mathbf{r})$, to free electron states with wave function $\psi_{free}(\mathbf{r})$. The simple fact that the core levels have very localized wave functions, to the point that $\psi_j(\mathbf{r}) \approx \delta(\mathbf{r})$, the probability of transition depends on the value of $\psi_{free}(\mathbf{r})$ only in the position $\mathbf{r} = 0$ of the “zero” atom from where the photoelectron is ejected. This fact results that $\sigma_a \propto |\psi_{free}(0)|^2$. For an isolated atom, the values of σ_a have been calculated and are known, see Note 1.4. But the presence of other atoms in the vicinity of the zero atom disturbs the free electron states, whose wave functions become $\psi'_{free}(\mathbf{r}) = \psi_{free}(\mathbf{r}) + \Delta\psi(\mathbf{r})$. Since

$$\begin{aligned} |\psi'_{free}(0)|^2 &\simeq |\psi_{free}(0)|^2 \left[1 + \frac{\Delta\psi(0) \psi_{free}^*(0) + \Delta\psi^*(0) \psi_{free}(0)}{|\psi_{free}(0)|^2} \right] = \\ &= |\psi_{free}(0)|^2 [1 + \chi(\mathcal{E})] , \end{aligned} \quad (1.74)$$

the cross-section

$$\sigma'_a(\mathcal{E}) = \sigma_a(\mathcal{E}) [1 + \chi(\mathcal{E})] \quad (1.75)$$

of the atom inserted in a material also begins to have an extra dependence on energy through the function $\chi(\mathcal{E})$. This extra dependence, implicit in the relation of $\Delta\psi(0)$ with the energy of the incident photon, is known as X-ray Absorption Fine Structure (XAFS) (Stöhr 1992; Newville 2004).

When the incident X-ray photon has energy \mathcal{E} , just above a given absorption edge with energy \mathcal{E}_b , the photoelectron is ejected from the atom to a free electron state with kinetic energy

$$K = \mathcal{E} - \mathcal{E}_b = \frac{\hbar^2 k_e^2}{2m} \quad \text{where} \quad k_e = \frac{\sqrt{2mK}}{\hbar} = 0.512315 \sqrt{K[\text{eV}]} \text{ \AA}^{-1} \quad (1.76)$$

is the module of the wavevector dictating the spatial evolution of the wave function, which propagates in all directions as a spherical wave²¹

$$\psi_{\text{free}}(\mathbf{r}) = \psi_{\text{free}}(0) \frac{a}{r} e^{ik_e r}.$$

Parameter a is related to the radius of the region around the atom zero where the $\psi_{\text{free}}(\mathbf{r})$ is evaluated in the calculation of the cross-section, i.e. $|\psi_{\text{free}}(r \leq a)| = |\psi_{\text{free}}(0)|$.

As the photoelectron propagates in the medium, it can be rescattered by the repulsive potential of the electron clouds from the neighboring atoms, producing a series of secondary waves $\Delta\psi_n(\mathbf{r})$, which makes up the perturbative wave

$$\Delta\psi(\mathbf{r}) = \sum_n \Delta\psi_n(\mathbf{r}) = \sum_n A_n \frac{k_e a_n}{k_e |\mathbf{r} - \mathbf{r}_n|} i e^{ik_e |\mathbf{r} - \mathbf{r}_n|}.$$

The imaginary number “ i ” stands for a phase shift of $\pi/2$ that appears in the exact solution of the secondary waves, cf. Appendix A in Stöhr (1992). The parameters a_n are introduced to limit the maximum amplitudes of the secondary waves in the regions $|\mathbf{r} - \mathbf{r}_n| \leq a_n$ where $|\Delta\psi_n(\mathbf{r})| = |A_n|$, so that each amplitude A_n represents the reflected fraction of the primary wave as it approaches the atom centered in the position \mathbf{r}_n , i.e.

$$A_n \propto \psi_{\text{free}}(0) \frac{a}{r_n} e^{i(k_e r_n + \delta_n)}.$$

The phase shifts δ_n of the secondary waves as well as the exact values of the amplitudes depend on the kinetic energy and atomic species of the neighboring elements. In a 1st-order approximation where further rescatterings (multiple scattering) of the secondary waves are neglected, the general form of the perturbative wave ends up being

$$\Delta\psi(\mathbf{r}) = \psi_{\text{free}}(0) \sum_n \frac{R_n(k_e) e^{i[k_e r_n + \delta_n(k_e)]}}{r_n k_e |\mathbf{r} - \mathbf{r}_n|} i e^{ik_e |\mathbf{r} - \mathbf{r}_n|}.$$

²¹(a) The solution to the Schrödinger equation for uniform potential in spherical coordinates (r, θ, ϕ) : $\nabla^2 \psi(r) = -k_e^2 \psi(r) \Rightarrow \partial^2[r\psi(r)]/\partial r^2 = -k_e^2[r\psi(r)] \Rightarrow r\psi(r) = A e^{\pm ik_e r}$. (b) The influences of the polarization of radiation and of the orbital angular momentum in the photoelectron emission direction are discarded in the approach of a spherically symmetric wave function, otherwise $\psi_{\text{free}}(0) \rightarrow \psi_{\text{free}}(0, \theta, \phi)$.

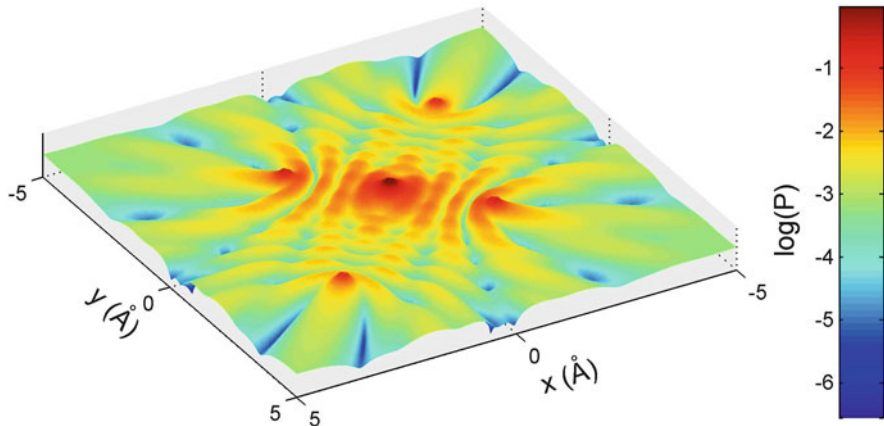


Fig. 1.22 Modulation in the probability density of the photoelectrons due to the presence of four neighboring atoms. $P = |\psi'_{free}(\mathbf{r})/\psi_{free}(0)|^2$. Photoelectrons with kinetic energy $K = 200$ eV, ejected from the atomic site $(0,0)$ [exexafsmap.m]

Besides the dependence with the neighboring element, $R_n(k_e)$ takes into account other factors that affect the amplitude of the reflected wave such as thermal vibrations, statistical distributions (disorder) of the distances r_n in the material, and the photoelectron's mean free path (Stöhr 1992). Figure 1.22 shows an illustrative example of how the waves rescattered in four neighboring coplanar atoms disturb the probability density $|\psi'_{free}(\mathbf{r})|^2$, creating regions of higher and lower probability of finding the photoelectron. But only the modulation in the position $\mathbf{r} = \mathbf{0}$ actually affects the photoelectric absorption, and therefore we have to be concerned only with the value of

$$\Delta\psi(0) = \psi_{free}(0) \sum_n \frac{R_n(k_e)}{k_e r_n^2} i e^{i[2k_e r_n + \delta_n(k_e)]},$$

whose contribution in (1.74) defines the function

$$\chi(k_e) = \frac{\Delta\psi(0)\psi_{free}^*(0) + \Delta\psi^*(0)\psi_{free}(0)}{|\psi_{free}(0)|^2} = \sum_n \frac{R_n(k_e)}{k_e r_n^2} \sin[2k_e r_n + \delta_n(k_e)]. \quad (1.77)$$

In the case of the example given in Fig. 1.22 where $r_{1,3} = 3.54 \text{ \AA}$ and $r_{2,4} = 2.12 \text{ \AA}$, the modulation provided by (1.77) on the cross-section σ_a of the atom zero due to the presence of the neighbors is shown in Fig. 1.23. Mn is taken as the atom zero for illustrative purposes only, as well as the functions $\delta_n(k_e)$ and $R_n(k_e)$, given in Fig. 1.24, which are used for the four neighboring atoms considered in the model. Compared to a real situation, the only effect not describable by (1.77) has to do with the phenomenon of multiple scattering of the photoelectrons. The phenomenon is dominant in the region of low kinetic energy, $K \lesssim 20 \text{ keV}$, and

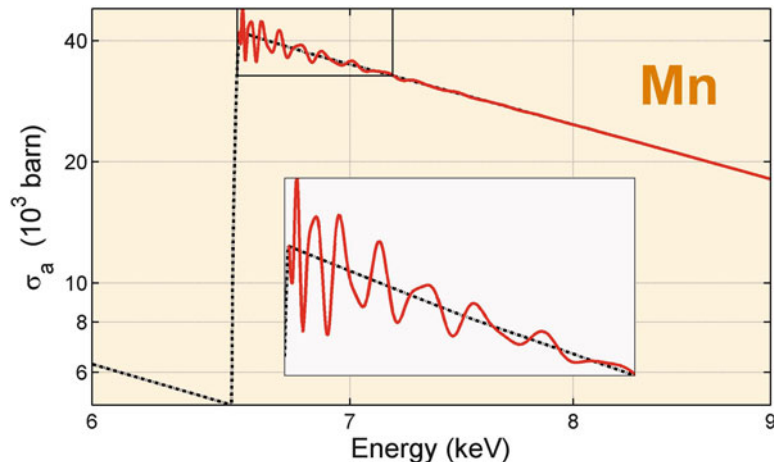


Fig. 1.23 Modulation in the absorption cross-section of Mn due to rescattering of photoelectrons. Demonstration considering four neighboring atoms arranged as shown in Fig. 1.22 [exexafs.m]

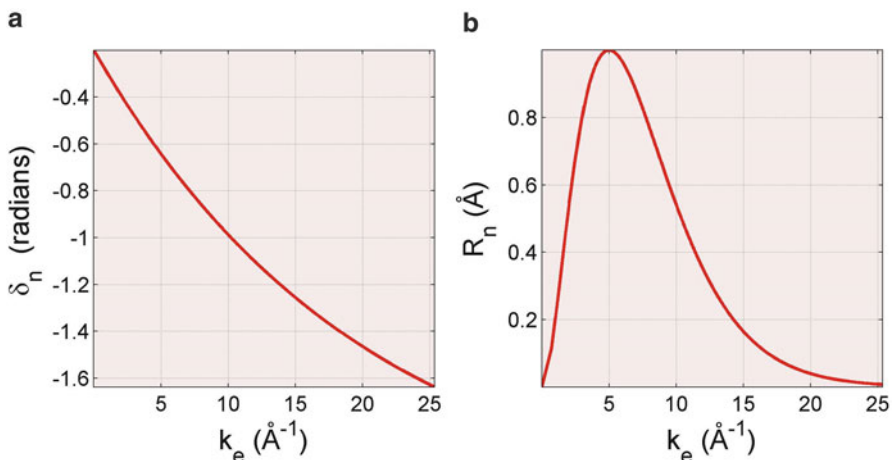


Fig. 1.24 Scattering properties of photoelectrons by the neighboring atoms considered in the simulated modulation of absorption cross-section in Fig. 1.23. (a) Variation in phase and (b) relative magnitude of the scattered wave function [exexafs.m]

is responsible for significant changes in the absorption cross-section very near the absorption edge. The detailed study of the Near-Edge X-ray Absorption Spectrum (NEXAFS) or also X-ray Absorption Near-Edge Spectroscopy (XANES) provides valuable information on the chemical bonds surrounding the atom zero and consists of an important method of structural investigation (Stöhr 1992).

Experimentally, function $\chi(k_e)$ is accessible by measuring either the linear attenuation coefficient or the fluorescence signal, depending mostly on how the

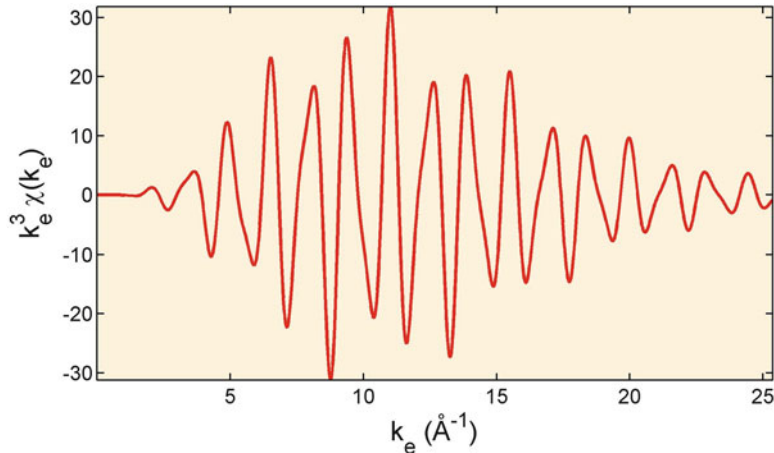


Fig. 1.25 Curve $k_e^3 \chi(k_e)$ refers to the modulation of σ_a shown in Fig. 1.23 [exexafs.m]

sample can be conditioned. In the case of conductive samples, it is also possible to monitor the photocurrent as a resource to access $\chi(k_e)$. Although conceptually simple, these experiments have a high degree of complexity due to the many factors that compromise the accuracy of the $\chi(k_e)$ measurements, and are only carried out in synchrotron facilities [Brazilian Synchrotron Light Laboratory (<http://lnls.cnptem.br/>), National Synchrotron Light Source-II (<http://www.bnl.gov/ps/>), Cornell High Energy Synchrotron Source (<http://www.chess.cornell.edu/>), Diamond Light Source (<http://www.diamond.ac.uk/>), European Synchrotron Radiation Facility (<http://www.esrf.eu/>), SPring-8 (<http://www.spring8.or.jp/en/>), Advanced Photon Source (<https://www1.aps.anl.gov/>), and many others] where it is possible to continuously vary the energy of the X-ray beam.

With the experimental $\chi(k_e)$ curve in hands, the general analysis is done with $k_e^m \chi(k_e)$ where $m = 1, 2$, or 3 , e.g. Fig. 1.25. One of the reasons for this procedure of multiplying by k_e^m is to minimize the contribution from the region of small k_e , strongly affected by multiple scattering of the photoelectrons, and at the same time magnify the modulations in an extended region above the absorption edge. Hence the technical name EXAFS (Extended XAFS), which uses indeed the (1.77) in materials analysis.

Among the technical subtleties are the functions $\delta_n(k_e)$ that need to be known for different neighbors. When $\delta_n(k_e)$ has a relatively small variation, such as the one in Fig. 1.24a, it is possible to use the Fourier analysis directly (Prince 2006)

$$F(u) = \left| \int k_e^m \chi(k_e) e^{2ik_e u} dk_e \right|^2, \quad (1.78)$$

to estimate interatomic distances between the atom zero and the nearby neighbors contributing to the EXAFS signal. The Fourier analysis of the signal in Fig. 1.25

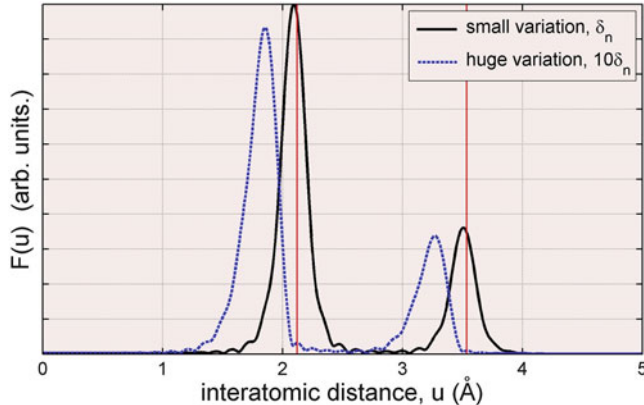


Fig. 1.26 Fourier analysis $F(u)$, (1.78), of the EXAFS signal in Fig. 1.25 (black line). Magnifying the phase variation of δ_n by a factor of 10 (blue dashed line), the displacements of the peaks of $F(u)$ regarding the expected values of r_n (marked with red lines) become more evident [exexafs.m]

results in two well-defined peaks centered at positions close to the values expected from r_n , as shown in Fig. 1.26. However in most situations, the analysis procedure is the simulation of the EXAFS signal using predetermined functions $\delta_n(k_e)$ whether by using standard samples or by theoretical calculations. The same applies to the reflection amplitudes for each kind of neighbor atom, which need to be known a priori to do the deconvolution of the information about atomic disorder and coordination number—number of neighboring atoms at a same distance r_n —contained in the EXAFS spectrum.²²

...

Exercise 1.15. From the XAFS signal, calculate $f'(\mathcal{E})$ and $f''(\mathcal{E})$ around the absorption edge of the atom zero.

Answer: Since $f''(\mathcal{E}) \propto \mathcal{E}\sigma_a(\mathcal{E})$, the XAFS signal disturbs f'' as it disturbs σ_a , which means $f''(\mathcal{E}) \rightarrow f''(\mathcal{E})[1 + \chi(\mathcal{E})]$. To obtain $f'(\mathcal{E})$ it is necessary to use one of the Kramers–Kronig relations in (1.73),

$$f'(\mathcal{E}) = -\frac{2}{\pi} P \int_0^{+\infty} \frac{xf''(x)}{x^2 - \mathcal{E}^2} dx \quad \therefore \quad f'(\mathcal{E}) \rightarrow f'(\mathcal{E}) - \frac{2}{\pi} P \int_0^{+\infty} \frac{xf''(x)\chi(x)}{x^2 - \mathcal{E}^2} dx .$$

²²For details on instrumentation, data collection methodology, and analysis of the EXAFS signal, read specialized literature such as Prince (2006), Als-Nielsen and McMorrow (2001), and Newville (2004).

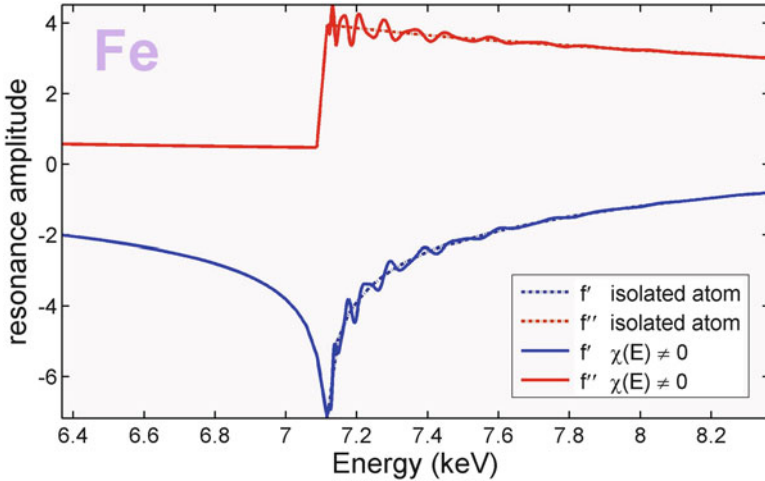


Fig. 1.27 Modulation of resonance amplitude of the Fe in presence of neighboring atoms. Model of four neighbors, Fig. 1.22 [exkk.m]

The values of $f''(\mathcal{E})$ are defined within the finite energy interval $[\mathcal{E}_{min}, \mathcal{E}_{max}]$. In the above integral, when $\mathcal{E} < \mathcal{E}_{min}$ or $\mathcal{E} > \mathcal{E}_{max}$ becomes $f''(\mathcal{E}) = f''(\mathcal{E}_{min})$ or $f''(\mathcal{E}) = f''(\mathcal{E}_{max})$, respectively. Figure 1.27 shows the resonance amplitudes for Fe as the atom zero.

...

Section Summary

— Atomic scattering factor with dispersion correction:

$$f(Q, \mathcal{E}) = f_0(Q) + f'(\mathcal{E}) + i f''(\mathcal{E})$$

— Absorption cross-section:

$$\sigma_a(\mathcal{E}) = 2r_e\lambda f''(\mathcal{E})$$

— Linear attenuation of intensity:

$$I(\mathcal{E}, x) = I_0 e^{-\mu(\mathcal{E})x}$$

— Linear attenuation coefficient:

$$\mu(\mathcal{E}) = \sum_n \left(\frac{N_A \rho}{M} \right)_n \sigma_n(\mathcal{E}) = \sum_n \left(\frac{\mu}{\rho} \right)_n \rho_n$$

— Total cross-section for the linear attenuation:

$$\sigma(\mathcal{E}) = \sigma_a(\mathcal{E}) + \sigma_C(\mathcal{E}) + \sigma_R(\mathcal{E})$$

— Modulation of the photoelectric absorption (XAFS):

$$\sigma'_a(\mathcal{E}) = \sigma_a(\mathcal{E}) [1 + \chi(\mathcal{E})]$$

— Term of modulation in the EXAFS approach:

$$\chi(k_e) = \sum_n \frac{R_n(k_e)}{k_e r_n^2} \sin[2k_e r_n + \delta_n(k_e)]$$

— Photoelectron wavevector with kinetic energy K :

$$k_e = \frac{\sqrt{2mK}}{\hbar} = 0.512315 \sqrt{K[\text{eV}]} \text{ \AA}^{-1}$$

Chapter 2

Low Correlated Systems: Gases and Dilute Solutions

The Kinematic Theory covers any description of the X-ray scattering process by a distribution of electrons where rescattering (with phase coherence) of the already scattered waves by the distribution has negligible effects. In other words, the scattered radiation is composed by photons that interacted once with the sample. Under these conditions, the scattered intensity, often called the kinematic intensity, is proportional to the form factor square module, (1.25). Material samples in a gaseous, liquid, or solid state are nothing more than atom systems with different degrees of correlation between the atomic positions, ranging from disperse systems, such as a gas, until strongly correlated systems as in a crystals. The Kinematic Theory describes very accurately the X-ray scattering by any of these systems, except only by highly perfect crystals with dimensions larger than a few microns. In this chapter we will begin in fact to discuss analysis methods of atomic systems by kinematic scattering of X-rays starting with the disperse system of lowest possible degree of correlation.

2.1 Monatomic Gas

By considering a discrete distribution of N atoms, as in (1.51), we come to the general expression of kinematic intensity

$$\begin{aligned} I(\mathbf{Q}) &= I_{Th} \left| \sum_{a=1}^N f_a(Q) e^{i\mathbf{Q} \cdot \mathbf{r}_a} \right|^2 = I_{Th} \sum_{a=1}^N \sum_{b=1}^N f_a(Q) f_b^*(Q) e^{i\mathbf{Q} \cdot (\mathbf{r}_a - \mathbf{r}_b)} = \\ &= I_{Th} \sum_{a=1}^N |f_a(Q)|^2 + I_{Th} \sum_{a=1}^N \sum_{b \neq a}^N f_a(Q) f_b^*(Q) e^{i\mathbf{Q} \cdot \mathbf{r}_{ab}} \end{aligned} \quad (2.1)$$

where $\mathbf{r}_{ab} = \mathbf{r}_a - \mathbf{r}_b$ and $f_b^*(Q) \neq f_b(Q)$ when the resonance amplitudes are taken into account, (1.60). At first this expression of intensity is valid for any type of sample scattering within the kinematic regime being especially useful in cases where it is feasible to discretize the electronic density atom-by-atom.

In the case of monatomic gas, $f_a(Q) = f_b(Q) = f(Q)$ and the \mathbf{r}_{ab} separations between pairs of atoms vary continuously over time so that

$$I(\mathbf{Q}) = \left[N + \sum_{a=1}^N \sum_{b \neq a}^N \cos(\mathbf{Q} \cdot \mathbf{r}_{ab}) \right] I_{Th} |f(Q)|^2 \quad (2.2)$$

corresponds to the instantaneous intensity scattered by the system. The coherent scattering cross-section of an atom, e.g. Fig. 1.11, has very small values, reaching at most a few thousand barns, $\sim 10^{-25} \text{ m}^2$. The scattered intensities are so weak that the intensity measures are in most cases done in relatively long times compared to the average time that the atoms in the gas take to move through the dimensions of the illuminated volume by the X-ray beam. A measure of $I(\mathbf{Q})$ therefore contains the temporal average value $\langle \dots \rangle_t$ of the double summation in (2.2). Since each atom has independent movements—a characteristic of disperse systems¹—the cosine temporal average is zero, i.e. $\langle \cos(\mathbf{Q} \cdot \mathbf{r}_{ab}) \rangle_t = 0$ for any pair of atoms, as long as $Q \neq 0$, making the term in brackets, $[\dots]$, contribute only with one factor of N . However, when $Q = 0$, the double summation is equal to $N(N - 1)$ and the term in brackets contributes with a factor N^2 . Note that in a random distribution of many atoms, the instantaneous intensity also obeys the relations $I(Q \neq 0) \propto N$ and $I(Q = 0) \propto N^2$, but in this case it is because of the statistical average null value of the cosine in the distribution. How different from zero should the \mathbf{Q} vector be for the average (temporal or statistical) of the cosine be null? Or, in other words, what is the function $I(\mathbf{Q})$ in the region where the multiplicative factor (term in brackets) changes from N to N^2 ? This function depends on shape and size of the gas volume illuminated by radiation or, more specifically, on the volume dimension perpendicular to the beam on the incidence plane. Quantitatively, the volume Fourier transform determines how far from $Q = 0$ we must look at the scattered radiation for the average of the cosines to be null. For a qualitative description, we can make a simple estimation of the scattering angle 2θ where the average is no longer null. From the definitions of versor $\hat{\mathbf{n}}$ and reciprocal vector \mathbf{Q} , (1.3) and (1.23), it is easy to verify that

$$\lim_{2\theta \rightarrow 0} \mathbf{Q} = Q\hat{\mathbf{n}} .$$

If D is the volume dimension in direction $\hat{\mathbf{n}}$, the vectorial product maximum value will be $\mathbf{Q} \cdot \mathbf{r}_{ab} = QD$. For the average cosines to be null we need $QD \geq 2\pi$, and thus

¹Ideal gases under normal temperature and pressure conditions stand for ideally disperse systems (Guinier and Fournet 1955).

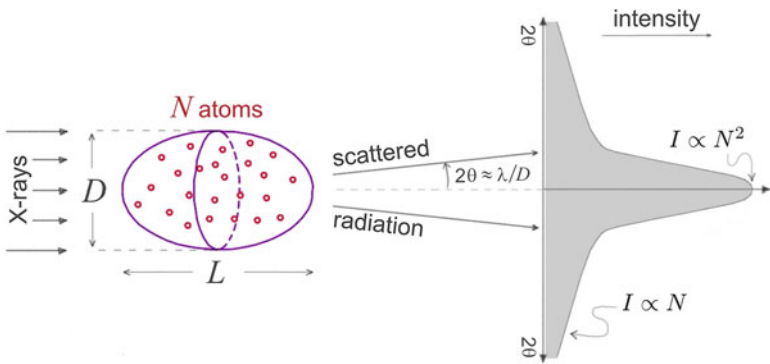


Fig. 2.1 Ultra-small angle region, $2\theta < \lambda/D$, where all the gas atoms scatter in phase, $I \propto N^2$. In real situations, D and L generally correspond to the transverse and longitudinal coherence lengths of the X-ray beam, as in Fig. 1.4

$$I(Q) = \begin{cases} NI_{Th}|f(Q)|^2 & \text{se } Q \geq 2\pi/D \quad (2\theta \geq \lambda/D) \\ N^2 I_{Th}|f(0)|^2 & \text{se } Q < 2\pi/D \quad (2\theta < \lambda/D) \end{cases} \quad (2.3)$$

as illustrated in Fig. 2.1.

Generally, D is the smallest value among sample size, beam transverse section, or beam transverse coherence length, (1.16). In practice, the value of D is large enough for the high intensity region—proportional to N^2 —to be indistinguishable from the direct beam. Away from the direct beam, the intensity is proportional to the number N of atoms and varies with Q according to the atomic scattering factor of the element in question, showing that experiments to directly measure $f(Q)$ are possible, in principle, in monatomic gases.

...

Exercise 2.1. Given a pictorial expression of coherent intensity

$$I(Q) = NI_{Th}|f(Q)|^2[1 + (N - 1)G(Q)]$$

where N is the number of atoms within the coherence volume $V \approx D^2L$. $G(Q) = \exp(-Q^2/2\sigma_Q^2)$, with $\sigma_Q = \pi/D$, is an empirical function used here to describe the intensity variation around the direct beam, (2.3). (a) Estimate the relative percentage R of photons scattered outside the direct beam in relation to the total number of photons scattered by the N atoms. Note: write the result as a function of volumetric density ϱ of atoms in the sample. (b) Using $D = 0.04 \mu\text{m}$ and $L = 0.03 \mu\text{m}$ as the coherence lengths for Cu radiation, Exercise 1.5, what is the value of R for gas argon (Ar) at standard conditions of temperature and pressure (STP)? (c) If in the

liquefied argon the smaller interatomic distances were in the order of 3.6 \AA , what is the value of R ? (d) Interpret the results.

Answer (a): The scattered intensity outside the direct beam is $I_1 = N \Phi \sigma_R$, (1.50). In the ultra-small angle region,² the intensity is $I_2 = 0.5 \pi N(N - 1) \Phi r_e^2 |f_{\text{Ar}}(0)|^2 (\lambda/D)^2$. Since $N - 1 \simeq \varrho V$,

$$R = 100 \frac{I_1}{I_1 + I_2} = \\ = 100 \frac{\sigma_R}{\sigma_R + 0.5\pi r_e^2 |f_{\text{Ar}}(0)|^2 (N - 1)(\lambda/D)^2} R \simeq 100 \frac{\sigma_R}{\sigma_R + 0.5\pi r_e^2 |f_{\text{Ar}}(0)|^2 L\lambda^2 \varrho} .$$

Answer (b): For 8 keV photons, $\sigma_R(\text{Ar}) = 63.9 \text{ barn}$ and $\lambda = 1.54 \text{ \AA}$. $f_{\text{Ar}}(0) = 18$ and $r_e^2 = 0.0794 \text{ barn}$. At STP the molar volume of an ideal gas is 24.467 L/Mol , $\varrho = 2.46 \times 10^7 \text{ atoms}/\mu\text{m}^3$ and $N = 1.2 \times 10^3$. Then,

$$R \simeq 100 \frac{63.9}{63.9 + 0.71} = 98.9 \% .$$

Answer (c): In a liquid, assuming that each atom occupies an average free volume of 46.7 \AA^3 , we have $\varrho = 2.14 \times 10^{10} \text{ atoms}/\mu\text{m}^3$ and $N = 1.0 \times 10^6$, which leads to

$$R \simeq 100 \frac{63.9}{63.9 + 615.7} = 9.4 \% .$$

Answer (d): The results in (b) and (c) show that measurable coherent intensity from disperse systems only occurs because the X-ray beam is not a perfect plane wave (infinity coherence lengths). Otherwise, the coherence volume would be as extensive as the macroscopic dimensions of the total illuminated volume by the X-ray beam, of the order of 1 mm^3 , containing about 10^{16} atoms (Ar gas) and resulting in $R = 0$, which means a completely destructive interference outside the direct beam. On the other hand, even with beams of finite coherence, liquid or solid samples where the atom density varies between 10^{10} and $10^{11} \text{ atoms}/\mu\text{m}^3$ have values of R practically null in the absence of constructive interferences (diffraction) produced by correlation of atomic positions in the sample. The use of X-ray equipment with focusing optics, providing high flux and low coherence, is therefore ideal for the study of low correlated systems.

...

²With $Q = (4\pi/\lambda) \sin(\gamma/2)$, $\int G(Q) d\Omega = 2\pi \int \exp\{-\alpha \sin^2(\gamma/2)\} \sin \gamma d\gamma \simeq 4\pi/\alpha = 0.5\pi (\lambda/D)^2$.

2.2 Dispersed Molecules: Random Orientations

Similar to the case of monatomic gas, the scattering by a gas of identical molecules is independent of the mutual interference between molecules,³ containing only internal structure information of the molecule. Other disperse molecular systems, such as low concentration solutions, may also exhibit scatterings free from mutual interference. Unlike atoms, molecules are 3-D structures that, in general, do not have spherical symmetry. Intensity measurements in such systems thus correspond to the sum of the scattered intensities by molecules in all possible orientations.

The molecule form factor F_M , (1.52), is calculated by adding up the contributions of all N_{at} molecule atoms, whose relative positions do not change (rigid molecules) and the redistributions of electrons in chemical bonds are neglected. The intensity scattered by a single molecule is then given by

$$I_M(\mathbf{Q}) = I_{Th} |F_M(\mathbf{Q})|^2 = I_{Th} \sum_{a=1}^{N_{at}} \sum_{b=1}^{N_{at}} f_a(Q) f_b^*(Q) e^{i\mathbf{Q}\cdot\mathbf{r}_{ab}}. \quad (2.4)$$

In a disperse system of N molecules, the scattered intensity outside the direct beam would be $N I_M(\mathbf{Q})$ if all molecules had the same spatial orientation. By the very fact that the system is sufficiently dispersed so that the molecules do not influence each other, the molecules have random orientations and all orientations with the same probability. The measurable intensity thus represents the average value of I_M ,

$$I(Q) = N \langle I_M(\mathbf{Q}) \rangle = N I_{Th} \sum_{a=1}^{N_{at}} \sum_{b=1}^{N_{at}} f_a(Q) f_b^*(Q) \langle e^{i\mathbf{Q}\cdot\mathbf{r}_{ab}} \rangle \quad (2.5)$$

is the coherent intensity scattered by the disperse system of N molecules randomly oriented. The interatomic distances r_{ab} inside the molecules are fixed for each pair of atoms, and the average is calculated over all orientations of these interatomic distances with respect to the reciprocal vector. The averaging is similar to the angular part solution of the integral in Exercise 1.6(a), i.e.,

$$\mathbf{Q} = Q\hat{\mathbf{z}} = [0, 0, Q], \quad \mathbf{r}_{ab} = r_{ab} [\sin \gamma \cos \varphi, \sin \gamma \sin \varphi, \cos \gamma],$$

$$\mathbf{Q} \cdot \mathbf{r}_{ab} = Q r_{ab} \cos \gamma, \quad \text{and}$$

$$\begin{aligned} \langle e^{i\mathbf{Q}\cdot\mathbf{r}_{ab}} \rangle &= \frac{1}{4\pi} \int_0^{2\pi} \int_0^\pi [\cos(Qr_{ab} \cos \gamma) + i \sin(Qr_{ab} \cos \gamma)] \sin \gamma d\gamma d\varphi = \\ &= \frac{1}{2Qr_{ab}} \underbrace{\int_{-Qr_{ab}}^{+Qr_{ab}} (\cos w + i \sin w) dw}_{\text{where } w=Qr_{ab} \cos \gamma} = \frac{\sin(Qr_{ab})}{Qr_{ab}}. \end{aligned}$$

³ Assuming X-ray beams with finite coherence lengths.

Thus,

$$I(Q) = N \langle I_M(Q) \rangle = N I_{Th} \sum_{a=1}^{N_{at}} \sum_{b=1}^{N_{at}} f_a(Q) f_b^*(Q) \frac{\sin(Qr_{ab})}{Qr_{ab}} = N I_{Th} P(Q). \quad (2.6)$$

For the sake of calculation efficiency, since $r_{ab} = r_{ba}$, the molecule's scattering power is rewritten as follows:

$$P(Q) = \sum_{a=1}^{N_{at}} |f_a(Q)|^2 + 2 \sum_{a=1}^{N_{at}-1} \sum_{b>a}^{N_{at}} \operatorname{Re}\{f_a(Q)f_b^*(Q)\} \frac{\sin(Qr_{ab})}{Qr_{ab}}, \quad (2.7)$$

so as to avoid double computing of the contribution of each atom pair. The sine function in the second term of $P(Q)$ appears solely due to the interference phenomenon between the molecule atoms, implying in a modulation of the scattered intensity as a function of Q .

The existence of an interference pattern in the scattering curve is more evident when evaluating the scattering curve normalized by $N I_{Th} \sum_a |f_a(Q)|^2$, the intensity that would be scattered by the system in case of total absence of interference owing to the atomic structure of each molecule. The interference pattern is thus characterized by the structural function

$$\begin{aligned} S(Q) &= \frac{I(Q)}{N I_{Th} \sum_a |f_a(Q)|^2} = \frac{P(Q)}{\sum_a |f_a(Q)|^2} = \\ &= 1 + \frac{2}{\sum_a |f_a(Q)|^2} \sum_a \sum_{b>a} \operatorname{Re}\{f_a(Q)f_b^*(Q)\} \frac{\sin(Qr_{ab})}{Qr_{ab}}, \end{aligned} \quad (2.8)$$

which has a maximum value equal to or slightly smaller than N_{at} at $Q = 0$, i.e. $S(Q=0) \lesssim N_{at}$, and oscillates around the unit for $Q \rightarrow \infty$.

...

Exercise 2.2. Consider a gas composed only of N benzene molecules, C₆H₆. (a) Neglecting the hydrogens, what is the structural function for this molecule? (b) Compare the intensity pattern of the gas with the one scattered by a single molecule in Fig. 1.13. (c) Decompose the interference pattern in the individual contributions of the molecule's characteristic interatomic distances. Which distance has greater weight? (d) How significant is the Compton scattering?

Answer (a): For a continuous distribution of orientations,

$$I(Q) = N I_{Th} 6|f_C(Q)|^2 \overbrace{\left[1 + 2 \frac{\sin(Qd)}{Qd} + 2 \frac{\sin(Qd\sqrt{3})}{Qd\sqrt{3}} + \frac{\sin(2Qd)}{2Qd} \right]}^{S(Q)} = \\ = N \Phi r_e^2 \langle |\mathcal{P}(\hat{s}')|^2 \rangle d\Omega 6|f_C(Q)|^2 S(Q)$$

is the intensity scattered by N molecules and $S(Q)$ is the structural function.

Answer (b): By using the same cylindrical detector geometry shown in Fig. 1.12,

$$Q(z, \phi) = \frac{2\pi\sqrt{2}}{\lambda} \left(1 - \frac{D \cos \phi}{\sqrt{D^2 + z^2}} \right)^{1/2}.$$

$\langle |\mathcal{P}(\hat{s}')|^2 \rangle$ and $d\Omega$ are those used in Exercise 1.9. Figure 2.2a shows the intensity pattern for the gas. It is highly concentrated around the direct beam and has much less details than the pattern for a single molecule in Fig. 1.14. However, the movement of the molecules does not affect the measurable intensities, allowing long exposures and improving statistical resolution of the scattering curve outside the direct beam. In practice the resolution is limited by background radiation (Compton) and by the dynamic range⁴ of the radiation detector.

Answer (c): In the benzene molecule, the interference pattern given by the structural function $S(Q)$ is defined by the superposition of three functions of the type $\sin(Qd)/Qd$, concerning to the distances $d = 140, 243$, and 280 pm, as shown in Fig. 2.2b. The weights are 2, 2, and 1, respectively.

Answer (d): To include the Compton scattering in Fig. 2.2a:

$$I(Q) = N I_{Th} 6 [|f_C(Q)|^2 S(Q) + \mathcal{S}(Z, Q)]$$

where the function $\mathcal{S}(Z, Q)$ is given by (1.56), with $Z = 6$ in the case of carbon. For 20 keV photons, Compton becomes more significant than the coherent scattering, i.e. $\mathcal{S}(Z, Q) > |f_C(Q)|^2 S(Q)$, when $Q > 3.5 \text{ \AA}^{-1}$ ($2\theta > 20^\circ$).

...

⁴Useful range of a radiation detector in intensity scales or dose per pixel.

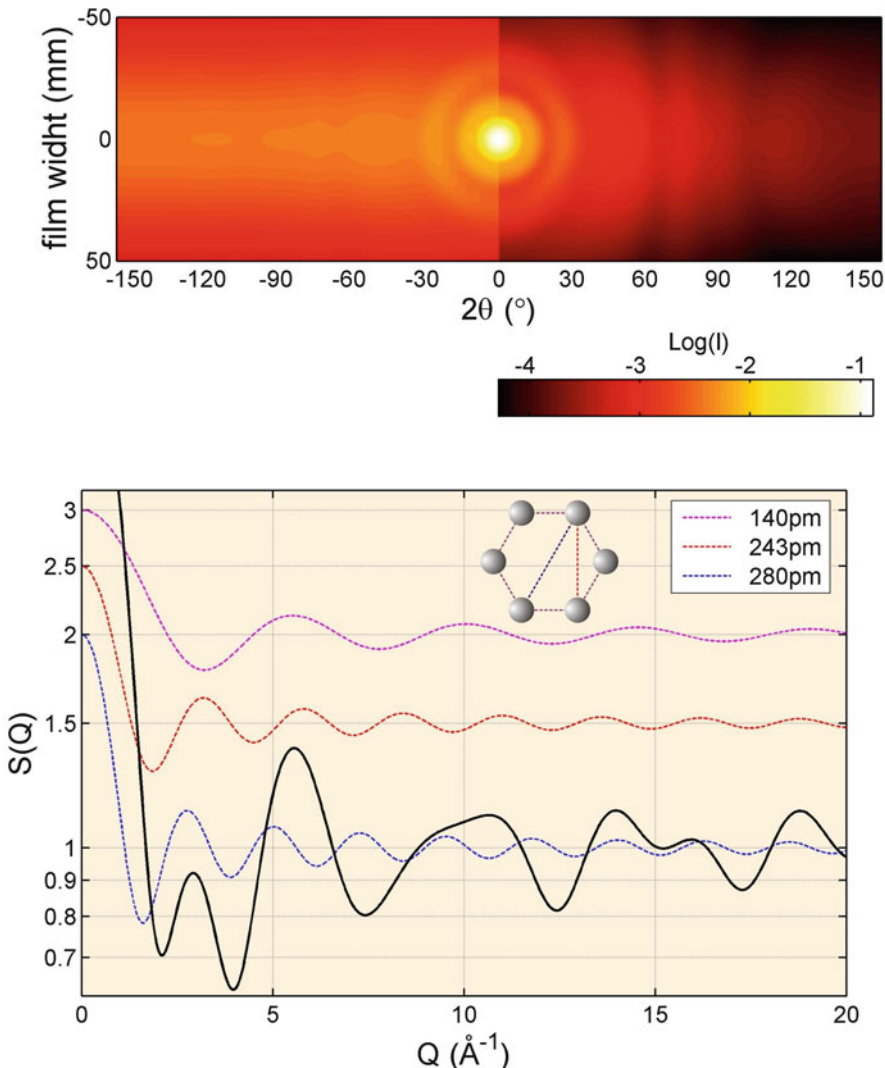


Fig. 2.2 (Top) Intensity scattered by N benzene molecules with random orientations. The background intensity from Compton scattering is considered only for carbon atoms and negative values of 2θ . X-rays of 20 keV, sample-film distance $D = 50$ mm, σ polarization, and flux so that $N\Phi r_e^2 = 1$ cps. (Bottom) Function $S(Q)$ (black line) for the benzene molecule, $S(0) = 6$. The individual contributions (dashed curves) of the three characteristic interatomic distances in the molecule are displaced in the ordinate axis for better viewing [benzenesaxs1.m, benzenesaxs2.m]

2.3 Small Angle Scattering

The analysis of $S(Q)$ in the large Q region would provide, in principle, information on minor values of r_{ab} . However, there are several experimental difficulties to access such information, one of them imposed by the maximum value of Q that is limited by the radiation energy, usually in the order of a few tens of keV, (1.49). This implies that, when studying disperse systems by X-ray scattering, the information on the smaller interatomic distances, in scale of angstrom, are only accessible at high angles, just where the atomic scattering factors are very reduced in comparison with the values at small angles and the Compton scattering is more intense, as can be seen in Fig. 1.16. Since low density of molecules and absence of long-range order are inherent properties of disperse systems, measurements with satisfactory statistical resolution of the coherent scattered intensity at high angles are most times impracticable in these systems.

On the other hand, measures of scattered intensity in the small Q region provide information about the largest interatomic distances of the order of physical dimensions of the molecules. To demonstrate this property of the small angle scattering, we take the limit of (2.6) when $Qr_{ab} \rightarrow 0$ so that

$$\begin{aligned} I(Q) &\approx N I_{Th} \sum_{a=1}^{N_{at}} \sum_{b=1}^{N_{at}} f_a(Q) f_b^*(Q) \left[1 - \frac{1}{6} (Qr_{ab})^2 \right] \\ &\approx N I_{Th} f_m^2(0) \sum_{a=1}^{N_{at}} \sum_{b=1}^{N_{at}} \left[1 - \frac{1}{6} (Qr_{ab})^2 \right] = N I_{Th} f_m^2(0) N_{at}^2 \left(1 - \frac{1}{3} Q^2 \langle r^2 \rangle \right). \end{aligned}$$

To get to the equation above, use

$$\lim_{x \rightarrow 0} \frac{\sin x}{x} \simeq \frac{x - x^3/6}{x} = 1 - \frac{1}{6} x^2$$

and replace $f_a(Q)f_b^*(Q)$ with $f_m^2(0)$ since $N_{at}^2 f_m^2(0)$ is the value of the summation when $Q = 0$, or for a more general definition: $f_m^2(Q) = N_{at}^{-2} |\sum_a f_a(Q)|^2$. Recalling that $e^{-x} \simeq 1 - x$ for $x \ll 1$, we obtain the intensity expression in the limit as Q approaches zero,

$$\lim_{Q \rightarrow 0} I(Q) = N I_{Th} f_m^2(0) N_{at}^2 e^{-\frac{1}{3} Q^2 \langle r^2 \rangle}. \quad (2.9)$$

$$\langle r^2 \rangle = \left(\frac{1}{2} \sum_{a=1}^{N_{at}} \sum_{b=1}^{N_{at}} r_{ab}^2 \right) / N_{at}^2 = \left(\sum_{a=1}^{N_{at}-1} \sum_{b>a}^{N_{at}} r_{ab}^2 \right) / N_{at}^2 \quad (2.10)$$

is the molecule mean square radius, thus demonstrating that the scattered intensity at small Q region is determined by the size of the molecules. The root-mean-square radius $R_g = \sqrt{\langle r^2 \rangle}$ is commonly called radius of gyration of the molecule.

2.3.1 Macromolecules

The atom-by-atom description is not restricted to cases of simple molecules. Thanks to the current computational facilities, exact calculations of both the radius of gyration and intensity are feasible even for giant molecular complexes containing tens of thousands of atoms. The protein database is one of the largest sources available on discrete structures (atom-by-atom). When a protein has its structure determined, in general by X-ray diffraction in the crystallized protein, it is available at the *Protein Data Bank* (<http://www.pdb.org/>). Among other format options, there are text files (*.pdb) in standard pdb format where the atomic coordinates are given in the lines starting with “ATOM” or “HETATM,” such as

```
-----
ATOM    84   N    LYS A 12      55.325  15.647  18.827  1.00 19.22          N
ATOM    85   CA   LYS A 12     55.370  17.014  18.328  1.00 22.23          C
.
.
.
HETATM 4716  C14  MYR A1006   29.904   5.219  -4.802  1.00 48.47          C
HETATM 4717  FE   HEM A 605   32.347   8.521  32.831  1.00 25.18          FE
-----
column: 1234567890123456789012345678901234567890123456789012345678901234567890
       1       2       3       4       5       6       7       8
```

where the atom with sequential number 85 is a carbon of the amino acid lysine (LYS) with coordinates $X = 55.370 \text{ \AA}$ (columns 31–38), $Y = 17.014 \text{ \AA}$ (columns 39 to 46), and $Z = 18.328 \text{ \AA}$ (columns 47–54). The symbol of the chemical element is given in columns 77 and 78. For more details about the pdb standard, see the file-format documentation also available at the pdb website.

In the Appendix B, the `saxs.c` routine written in C++ reads files in pdb format and returns $P(Q)$, $S(Q)$, and R_g calculated according to (2.7), (2.8), and (2.10), respectively. Although the calculation of $P(Q)$ through (2.7) is exact for any Q , it is a method of small computational efficiency. Later we will take a look at some approaches that make the calculation much more efficient and executable in MatLab™ in the experimentally accessible region of Q (small angle), but it will be interesting to have the exact calculation for the sake of comparison.

...

Exercise 2.3. With the known structure of a protein (file *.pdp), calculate its scattering power, $P(Q)$, and radius of gyration. (a) What is the mean number of electrons per atom effectively scattering X-rays? Relate this number with the expected value of $P(0)$. Note: despise hydrogens and chemical bonds, use $f_a(Q)$ for neutral atoms. (b) Which region of the $P(Q)$ curve has exponential decay with Q^2 ?

Answer (a): From (2.6) follows $P(0) = \left| \sum_{a=1}^{N_{at}} f_a(0) \right|^2$. Since at $Q = 0$ all the electrons scatter in phase, the mean effective number of electrons per atom is $f_m(0) = N_{at}^{-1} \sqrt{P(0)}$. In the case of the protein shown in Fig. 2.3, there are 4635 atoms (“ATOM” records in the 1N5U.pdb file): 784 N, 2926 C, 884 O, and 41 S. $P(0) = |784f_N(0) + 2926f_C(0) + 884f_O(0) + 41f_S(0)|^2 \simeq 9.469 \times 10^8$ if atomic

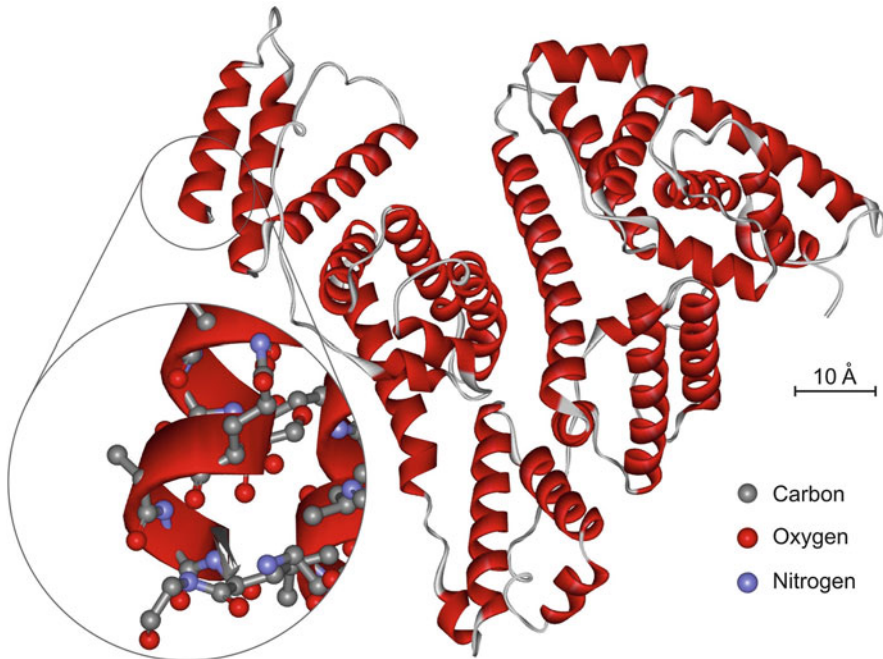


Fig. 2.3 Amino acid chains of human albumin, protein 1N5U in the *Protein Data Bank* (<http://www.pdb.org/>)

resonances are neglected, otherwise $P(0) = 9.547 \times 10^8$ for X-ray photons of 8 keV. So there are $f_m(0) = 6.6665$ effective electrons per atom.

Answer (b): In Fig. 2.4, $P(Q) = P(0) \exp(-\frac{1}{3}R_g^2 Q^2)$ from $Q = 0$ to approximately $Q = 0.08 \text{ \AA}^{-1}$ ($Q^2 = 0.0064 \text{ \AA}^{-2}$) where the value of $R_g = 27.9 \text{ \AA}$ was obtained by (2.10).

2.3.2 Particles of Uniform Density

Scattering properties in the region of small Q can be obtained in an equivalent manner to that shown for discrete molecules, starting from the assumption of particles of uniform density. When we look at the radiation scattered in a small enough angle so that the interatomic distances do not affect the scattering of X-rays, the electron density is rewritten as

$$\rho(\mathbf{r}) = \frac{F_M(0)}{v_p} s(\mathbf{r}) \simeq \frac{N_{at} f_m(0)}{v_p} s(\mathbf{r}) = \bar{\rho} s(\mathbf{r}) . \quad (2.11)$$

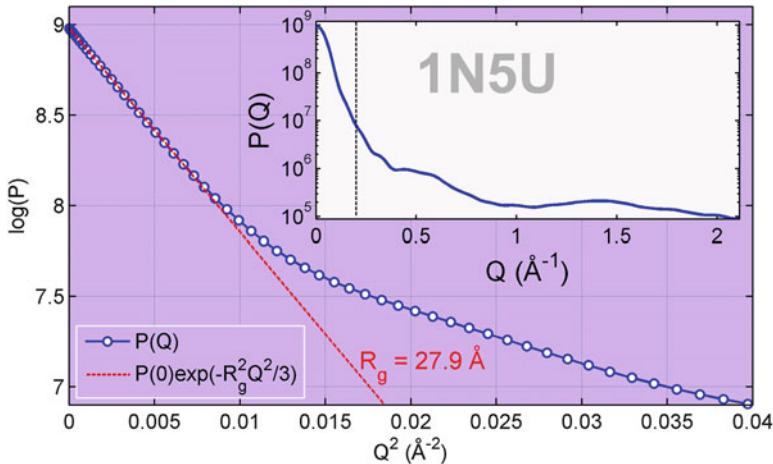


Fig. 2.4 Log(P) curve versus Q^2 in the region $Q < 0.2 \text{ \AA}^{-1}$ for human albumin (PDB ID: 1N5U). Inset: scattering power in an extended region of Q [saxs.c, ex1N5U.m]

$s(\mathbf{r})$ is the shape function: $s = 1$ (or 0) for \mathbf{r} inside (or outside) of the particle outline. $F_M(0) = \sum_a^{N_{at}} f_a(0) \simeq N_{at} f_m(0) = |\sum_a^{N_{at}} f_a(0)|$ is the effective number of electrons in the particle of volume v_p , so that $\bar{\rho} = N_{at} f_m(0)/v_p$ is the average density of electrons in the particle effectively scattering radiation. Thus, the new particle form factor for small angles, including cases of particles dispersed in a homogeneous medium with electron density ρ_0 , is

$$F'_M(Q) = (\bar{\rho} - \rho_0) \text{FT}\{s(\mathbf{r})\}. \quad (2.12)$$

Since the measurable intensity is the average $\langle \dots \rangle$ on all possible particle orientations, we have

$$I(Q) \simeq N I_{Th} \langle |F'_M(Q)|^2 \rangle = N I_{Th} (\bar{\rho} - \rho_0)^2 \langle |\text{FT}\{s(\mathbf{r})\}|^2 \rangle = N I_{Th} P(Q) \quad (2.13)$$

where the scattering power $P(Q)$ depends only on the particle shape and its density contrast with the medium.

The technique known as small angle X-ray scattering (SAXS) is widely used in the study of low correlated systems, particularly those systems where the particles have sizes in the range of 1–50 nm. Typically, $0.1^\circ < 2\theta < 10^\circ$ corresponds to the angular range analyzed by SAXS, depending on the particularities of each instrumental setup (Craievich 2002).

2.3.3 Morphology of Particles

The approach of uniform density is valid within a restricted range of reciprocal space ranging from $Q = 0$ to a certain value of Q , from which the scattering curve starts to be affected by the density fluctuations inside the particle. Around the direct beam, in the so-called Guinier region, this approach is very good. The intensity curve always shows the exponential decay with Q^2 , as given by (2.9), which in terms of average density is

$$\lim_{Q \rightarrow 0} I(Q) = N I_{Th} (\bar{\rho} - \rho_0)^2 \lim_{Q \rightarrow 0} \langle |\text{FT}\{s(\mathbf{r})\}|^2 \rangle = N I_{Th} (\bar{\rho} - \rho_0)^2 v_p^2 e^{-\frac{1}{3} Q^2 \langle r^2 \rangle} \quad (2.14)$$

where

$$\langle r^2 \rangle = \frac{1}{v_p} \int_{v_p} r^2 dV \quad (2.15)$$

is the mean square radius,⁵ equivalent to that obtained by the discrete summation in (2.10), but with the advantage of being calculated from the particle shape without the need for prior knowledge of the interatomic distances. For example, for a spherical particle of radius a ,

$$R_g^2 = \langle r^2 \rangle = 3a^2/5 \quad \text{and} \quad I(Q)/I(0) = e^{-0.2(Qa)^2}.$$

Note that this is almost the same result of the exponential decay $e^{-0.21(Qa)^2}$ used to adjust the initial part of the scattered intensity curve by a spherical and uniform electron density in Exercise 1.6(b); the slight difference arises from the fact that in the Exercise the scattering at half maximum was used as reference, $I(Qa=1.815)/I(0) = 1/2$, rather than the limit for $Q \rightarrow 0$.

The intensity curve range that can be reproduced by an exponential decay with Q^2 varies with the particle morphology. In most cases, it goes from $Q = 0$ to a value not far beyond $Q = 1/R_g$. This value serves as an estimate of the extent of Guinier region in the intensity curve, from which only information on particle size (radius of gyration) can be extracted.

After the Guinier region, the exponential decay with Q^2 is replaced by a behavior strongly influenced by the particle shape. The extent at Q of this region with particle's morphological information, which is often called Porod region (Guinier 1994), depends on how much larger are the dimensions of the particle in relation to the scale length of the internal density fluctuations. Due to the wide variety of

⁵It is an optional task to demonstrate that $\lim_{Q \rightarrow 0} \langle |\text{FT}\{s(\mathbf{r})\}|^2 \rangle = v_p^2 e^{-\frac{1}{3} Q^2 \langle r^2 \rangle}$. Such demonstration can be found in several books on SAXS, e.g. Giacovazzo (2002), Glatter and Kratky (1982), and Guinier (1994).

systems it is difficult to establish a general rule for the occurrence or not of the Porod region. However, as a rule, it is expected that the morphological analysis is feasible when the particle is dozens of times larger than the size of the molecules composing it.

In the case of particles of uniform density, abrupt interfaces and regular surfaces, (2.13) foresees intensity curves with asymptotic fall of the type $1/Q^n$ where n is an integer⁶ related to the dimensionality of the particle. Analytical solutions for the term $\langle |\text{FT}\{s(\mathbf{r})\}|^2 \rangle$ are possible for specific types of particles, while numerical solutions are necessary in most cases, see, for example, Lindner and Zemb (2002). Here we will make a simple, but quite versatile, numerical approach to demonstrate the main features of the asymptotic behavior in the intensity curves. This demonstration is based on the fact that (2.6) and (2.13) provide nearly the same results in the Q range comprising both Guinier and Porod regions, i.e.

$$I(Q)/I(0) = \frac{1}{V^2} \langle |\text{FT}\{s(\mathbf{r})\}|^2 \rangle \simeq \frac{2}{N(N-1)} \sum_a^{N-1} \sum_{b>a}^N \frac{\sin(Qr_{ab})}{Qr_{ab}} \quad (2.16)$$

as long as the position vectors \mathbf{r} are uniformly distributed within the particle shape (outline) and in sufficient quantity so that the r_{ab} values of adjacent positions are much smaller than the dimensions of the particle.

Through (2.16), using random distributions of position vectors within the chosen particle shape, the following asymptotic behaviors can be verified. Particles with dimension 3 where the ratio between dimensions in three orthogonal directions tends to $1 : 1 : 1$, such as spheres and cubes, the intensity of the interference fringes falls with $1/Q^4$, $n = 4$, Fig. 2.5. In the case of spherical particles, the fall with $1/Q^4$ can be verified analytically from the FT of a sphere, as calculated in Exercise 1.6(b). Sharp reduction in one or two dimensions of the particle eliminates the interference fringes in the Porod's region and changes the value of n . Particles with dimension 2 are those with a planar aspect for which $n = 2$, $1/Q^2$ asymptote. Those with elongated aspects, rod-type, have dimension 1 for which $n = 1$, $1/Q$ asymptote. Figure 2.5 also shows the theoretical scattering curves of particles with ratios $1:1:w$ (dimension 2) and $w:w:1$ (dimension 1) in the limit $w \rightarrow 0$. Curves with asymptotes $1/Q^n$ for larger Q values occur when the particle dimensional aspect (3, 2 or 1) is well defined, i.e. at the $w = 0$ and $w = 1$ limits (solid line curves in Fig. 2.5). In intermediate cases, the range where the $1/Q^n$ behavior occurs is less and less the more the particle proportions deviate from the limiting cases (dashed line curves in Fig. 2.5).

...

⁶Non-integer values occur in particles without defined interfaces, such as macromolecules and materials with fractal properties (Teixeira 1988).

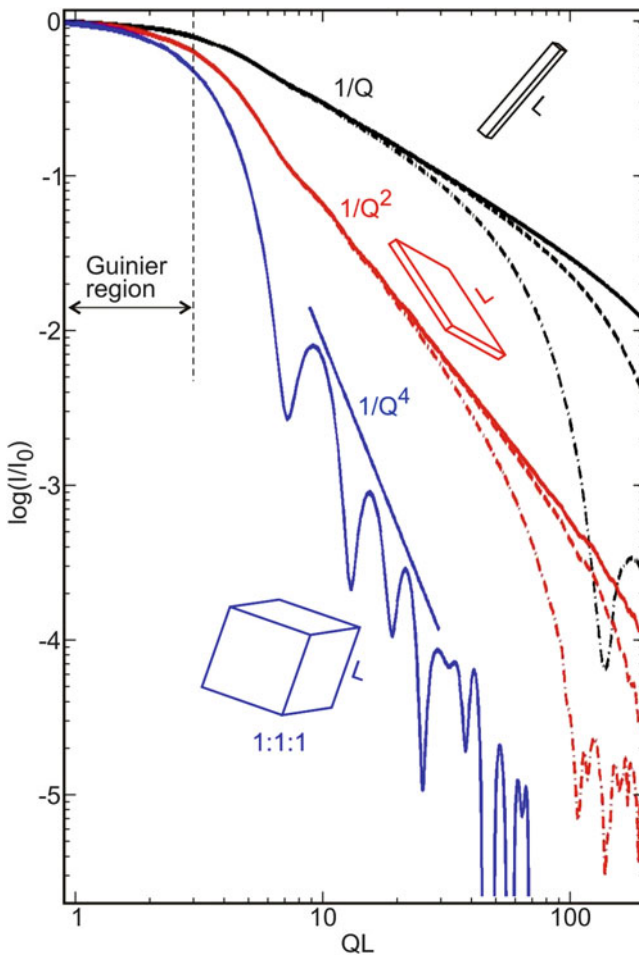


Fig. 2.5 Asymptotic behavior of the intensity scattered by particles with different dimensionalities: 1:1:1 (dimension 3), 1:1: w (dimension 2), and $w:w:1$ (dimension 1) where $w = 1/100$ (straight line), $2/100$ (dashed line), and $5/100$ (dashed with dotted line). Curves calculated numerically by using (2.16) with $N = 2000$ [assintotic.m]

Exercise 2.4. Particles of uniform density and spheroidal shapes. (a) How does the radius of gyration R_g depend on oblate and prolate shapes? (b) When does R_g cease to depend on the ratio w between the smallest and largest dimensions of the particle?
Answer (a): By writing (2.15) in cylindrical coordinates (ρ, ϕ, z) ,

$$\langle r^2 \rangle = \frac{2\pi}{v_p} \int_{-c}^c \int_0^{\rho(z)} (\rho'^2 + z^2) \rho' d\rho' dz .$$

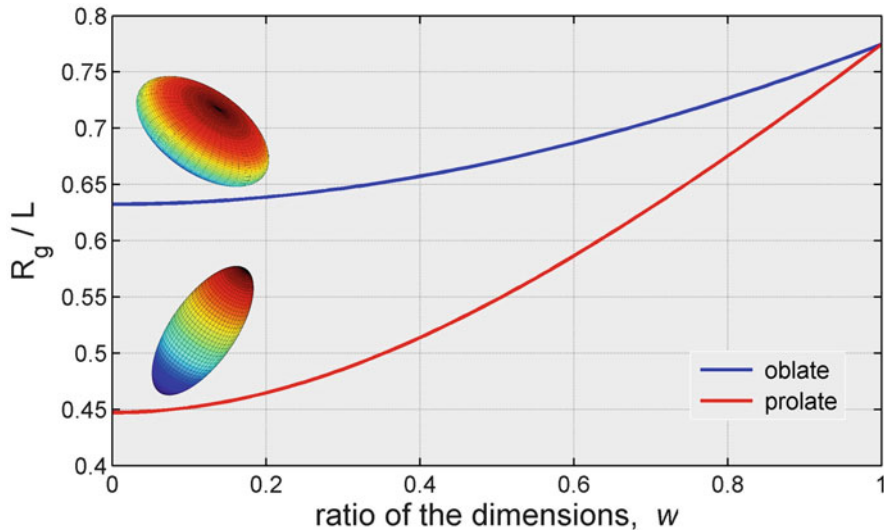


Fig. 2.6 Radius of gyration R_g as a function of ratio w between the smallest and the largest dimension ($2L$). Particles of uniform density and spheroidal shapes, $w = 1$ implies sphere of radius L [exellipsoid.m]

From the equation of an ellipsoid of revolution, $(x/a)^2 + (y/a)^2 + (z/c)^2 = 1$, we have $\rho^2(z) = a^2[1 - (z/c)^2]$ and $v_p = 4\pi a^2 c/3$. The analytical solution of the integral leads to $\langle r^2 \rangle = (2a^2 + c^2)/5$. Oblate shapes: $a = L$, $c = wL$ where $w < 1$, and $R_g^2 = (2 + w^2)L^2/5$. Prolate shape: $c = L$, $a = wL$, and $R_g^2 = (2w^2 + 1)L^2/5$. Answer (b): From the $R_g \times w$ graph, Fig. 2.6, it can be seen that for $w < 0.1$, R_g is already close to the limit values: $\sqrt{2/5} L$ (oblates) and $\sqrt{1/5} L$ (prolates).

...

Suggestion: Calculate the scattering curve by using (2.16) in the Guinier region and numerically obtain the radius of gyration for particles with different dimensionalities.

...

2.3.4 Polydisperse Systems and Dispersion of Size

The kinematic intensity in polydisperse systems, i.e. composed by different particles without interacting with each other, can be treated as the sum of the intensities of monodisperse systems, (2.6) or (2.13). So, $I(Q) = I_{Th} \sum_j N_j P_j(Q)$ where the index j specifies each of the independent systems that comprise the total system

(polydisperse). Within the approaching of particles of uniform density in a solvent of electronic density ρ_0 , $P_j(Q) = (\bar{\rho}_j - \rho_0)^2 \langle |\text{FT}\{s_j(\mathbf{r})\}|^2 \rangle$ and weight

$$C_j(0) = N_j P_j(0) = N_j (\bar{\rho}_j - \rho_0)^2 v_{p,j}^2$$

of the contribution of each system j in the scattered intensity is determined by the number N_j of particles j , and their scattering power in relation to the media. The intensity in polydisperse systems in the limit $Q \rightarrow 0$ remains

$$I(Q) = I(0) e^{-\frac{1}{3} Q^2 R_g^2},$$

but the radius of gyration is given by

$$R_g^2 = \frac{\sum_j C_j(0) \langle r^2 \rangle_j}{\sum_j C_j(0)} \quad (2.17)$$

where $\langle r^2 \rangle_j$ is the mean square radius of the j particles, and $I(0) = I_{Th} \sum_j C_j(0)$.

A very common type of polydisperse system found in many real situations is the one formed by particles with the same electronic density $\bar{\rho}$, but presenting variations in shape and size. This allows rewriting the expression of intensity as

$$I(Q) = I_{Th} (\bar{\rho} - \rho_0)^2 \sum_j N_j \langle |\text{FT}\{s_j(\mathbf{r})\}|^2 \rangle. \quad (2.18)$$

In the most general cases of particles having different morphologies, the analysis of scattering curves is often infeasible. On the other hand, when the particles have the same shape, e.g. spherical particles embedded in a homogeneous liquid or solid matrix, the dispersion of size softens the interference fringes that normally occur in the intensity curve, making it easier to analyze the asymptotic behavior in the Porod region. Determining the size distribution (point of interest in research involving many nanoparticle synthesis) is possible under certain circumstances. When the shape function depends only on the dimensional variable L of the particle, $s_j(\mathbf{r}) \rightarrow s(L, \mathbf{r})$ and $N_j \rightarrow N p(L) dL$ where N is the total number of particles in the system and $p(L)$ is the size distribution function so that $\int_0^\infty p(L) dL = 1$. The intensity in (2.18) is thus given by the integral

$$I(Q) = N I_{Th} (\bar{\rho} - \rho_0)^2 \int_0^\infty p(L) \langle |\text{FT}\{s(L, \mathbf{r})\}|^2 \rangle dL, \quad (2.19)$$

and the radius of gyration in (2.17) becomes

$$R_g^2 = \frac{\int_0^\infty p(L) v_p^2(L) R_g^2(L) dL}{\int_0^\infty p(L) v_p^2(L) dL}. \quad (2.20)$$

$R_g(L)$ is the radius of gyration of the particles whose value of dimensional variable is between L and $L + dL$.

Intensity curves with asymptotes $1/Q^4$ are associated with regular particles without surface fractality and without sharply planar or linear character—ratio between smallest and largest size a lot greater than $1/10$. In such cases, it is possible to show that the integral in (2.19) is

$$N \int_0^\infty p(L) \langle |\text{FT}\{s(L, \mathbf{r})\}|^2 \rangle dL \simeq \frac{2\pi}{Q^4} N \int_0^\infty p(L) A_s(L) dL = 2\pi \frac{N \langle A_s \rangle}{Q^4} = 2\pi \frac{A}{Q^4} \quad (2.21)$$

in the region where the interference fringes are softened by the size distribution $p(L)$. $A_s(L)$ is the surface area of the particles with size L , and $A = N \langle A_s \rangle$ is the total surface area of the N particles, corresponding to the total area of the interface between particles and solvent, that is, between materials with densities $\bar{\rho}$ and ρ_0 .

$$I(Q) = 2\pi I_{Th} (\bar{\rho} - \rho_0)^2 \frac{A}{Q^4} \quad (2.22)$$

is known as the Porod's law and can be observed in several systems consisting of materials with two different electron densities (Craievich 2002).

...

Exercise 2.5. Spherical particles, besides being analytically tractable, quite often occur in the synthesis of nanoparticles. Considering a disperse system of spherical particles with continuously distributed radius around a most likely value a_0 . (a) Make the theoretical demonstration⁷ of Porod's law in (2.22). (b) What is the relationship between visibility of the fringes and dispersion of size (radius)?

Answer (a): When $s(L, \mathbf{r})$ is the shape function of a spherical particle of radius a , it follows from (1.38) that

$$\begin{aligned} \langle |\text{FT}\{s(L, \mathbf{r})\}|^2 \rangle &= v_p^2(a) \Theta^2(Qa) = (4\pi a^3)^2 \left[\frac{\sin(Qa) - (Qa) \cos(Qa)}{(Qa)^3} \right]^2 = \\ &\simeq 8\pi^2 \left[\frac{a^2}{Q^4} + \frac{1}{Q^6} + \left(\frac{a^2}{Q^4} - \frac{1}{Q^6} \right) \cos(2Qa) - \frac{2a}{Q^5} \sin(2Qa) \right]. \end{aligned}$$

Discarding terms with Q^{-5} and Q^{-6} , and substituting this expression in (2.19) with the radius a in the place of the dimensional variable L ,

⁷See Guinier (1994, p. 336).

$$I(Q) \simeq I_{Th} (\bar{\rho} - \rho_0)^2 \frac{2\pi N}{Q^4} \int p(a) 4\pi a^2 [1 + \cos(2Qa)] da \simeq 2\pi I_{Th} (\bar{\rho} - \rho_0)^2 \frac{A}{Q^4} .$$

The higher the dispersion of size distribution and the Q values, the more the cosine contributions tend to cancel each other so that $\int p(a) 4\pi a^2 \cos(2Qa) da \simeq 0$, thus leading to the Porod's formula (or law) as we wanted to demonstrate.

Answer (b): Fringes are no longer visible when $\cos(2Qa)$ ranges from -1 to $+1$ within a small range of the a values, i.e. when $Q > \pi/\Delta a$ where Δa represents the dispersion of values such as the full width at half maximum of the distribution $p(a)$.

Exercise 2.6. Consider a non-Gaussian distribution of spherical particles. (a) Simulate the scattering curve. From what value of Q does the curve become smooth (without fringes)? (b) Compare values of gyration radius R_g and average surface area $\langle A_s \rangle$ with those obtained by Gaussian distributions capable of generating similar scattering curves. In what circumstances is it possible to clearly distinguish between Gaussian and non-Gaussian size distributions?

Answer (a): One of the most common non-Gaussian distribution is the log-normal distribution

$$p(a) = \frac{1}{a \sigma_n \sqrt{2\pi}} e^{-(\ln a - \ln b)^2 / 2\sigma_n^2},$$

whose variable $b = a_0 e^{\sigma_n^2}$ depends on the value of a_0 (most probable radius) and of the standard deviation in logarithmic scale, σ_n . As expected, Exercise 2.5(b), the fringes disappear for $Q > \pi/\Delta a$ where Δa is the full width at half maximum of $p(a)$. As for example, the two distributions shown in Fig. 2.7 (inset), $\Delta a = 23.5 \text{ \AA}$ and 36.3 \AA , which implies that the regions without fringes have $Q > 0.13 \text{ \AA}^{-1}$ and $Q > 0.08 \text{ \AA}^{-1}$, respectively.

Answer (b): Let $p(a) = \frac{1}{\sigma \sqrt{2\pi}} e^{-(a-a_0)^2 / 2\sigma^2}$ be the Gaussian distribution used for the sake of comparison.⁸ In Table 2.1, the parameters of the two distributions resulting in similar curves are compared. The values are no longer compatible when the log-normal distribution is very asymmetric. However, in these cases $\sigma \gtrsim a_0/3$, implying in a significant fraction of particles with null radius ($a = 0$), a fact that can be used as a feasibility criterion of the Gaussian model for describing the size distribution.

...

⁸For large values of σ , such as $\sigma > a_0/3$, the normalization constant is reset so that $\int_0^\infty p(a) da = 1$.

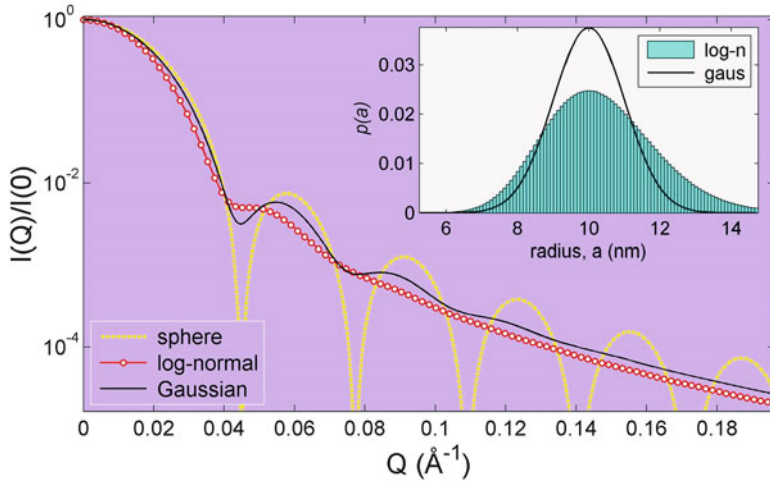


Fig. 2.7 Normalized intensity curves of X-ray scattering by disperse systems of spheres with uniform density and different size distributions (*inset*). Reference curve of the scattering by spheres of radius a_0 (most probable radius of the distributions) is also shown [exlognormal.m]

Table 2.1 Parameters of the log-normal and Gaussian size distributions producing similar scattering curves

a_0 (Å)	Log-normal			Gaussian		
	σ_n	R_g (Å)	$\langle A_s \rangle (\text{\AA}^2)$	σ (Å)	R_g (Å)	$\langle A_s \rangle (\text{\AA}^2)$
50	0.1	42.0	3.3×10^4	5.9	42.0	3.2×10^4
50	0.2	53.2	3.7×10^4	13.7	53.0	3.4×10^4
100	0.3	153.5	1.8×10^5	49	145.1	1.6×10^5
100	0.7	1095	8.8×10^5	397	850	24.1×10^5

R_g and $\langle A_s \rangle$ calculated from (2.20) and (2.21), respectively. For comparison details see routine exlognormal.m

Summary

— Scattering power of discrete particles:

$$P(Q) = \sum_a \sum_b f_a(Q) f_b^*(Q) \frac{\sin(Qr_{ab})}{Qr_{ab}}$$

— Scattering power of uniform particles in solution:

$$P(Q) = (\bar{\rho} - \rho_0)^2 \langle |\text{FT}\{s(\mathbf{r})\}|^2 \rangle$$

— Low angle approach, limit $Q \rightarrow 0$, Guinier region:

$$P(Q) = P(0) \exp\left(-\frac{1}{3}Q^2 R_g^2\right)$$

— Particle's gyration radius, R_g :

$$R_g^2 = \left(\frac{1}{2} \sum_a \sum_b r_{ab}^2\right) / N_{at}^2 \text{ (discrete)} \quad \text{or} \quad R_g^2 = \frac{1}{v_p} \int_{v_p} r^2 dV \text{ (uniform)}$$

— Asymptotic behavior, regular uniform particles, Porod region:

$$P(Q) = 2\pi (\bar{\rho} - \rho_0)^2 A / Q^4$$

— Total surface area of particles with $p(L)$ size distribution:

$$A = N \langle A_s \rangle = N \int_0^\infty p(L) A_s(L) dL$$

— Average gyration radius:

$$R_g^2 = \frac{\int_0^\infty p(L) v_p^2(L) R_g^2(L) dL}{\int_0^\infty p(L) v_p^2(L) dL}$$

— Size distributions:

$$p(L) = \frac{e^{-(L-L_0)^2/2\sigma^2}}{\sigma \sqrt{2\pi}} \text{ (Gaussian)} \quad \text{and} \quad p(L) = \frac{e^{-(\ln L - \ln b)^2/2\sigma_n^2}}{L \sigma_n \sqrt{2\pi}} \text{ (log-normal)}$$

$$b = L_0 \exp(\sigma_n^2)$$

Chapter 3

Complex Systems

Disperse systems represent extreme situations of total absence of correlation between the scattering units. There are internal correlations only.¹ At the other extreme are the crystalline systems where the correlations between the scattering units are constant, resulting in understanding the long-range order in macroscopic scales. Between these two extreme situations are the systems with arbitrary correlations, which are complex systems where there are correlations between the scattering units, but these correlations may vary along the physical length of the systems.

The mathematical description of complex systems requires a formalism that is flexible enough to describe both internal correlations in scattering units with nontrivial structures and possible correlations between the scattering units. In the previous chapter we studied two relatively simple models of scattering units: particles with discrete internal structure and particles of uniform density. However, these models do not cover all the possibilities. There are cases where an atom-by-atom description is unviable, but the internal density fluctuations must be taken into account.

Samples denser than gas and dilute solutions often exhibit diffraction patterns more rich in details than that provided by the simple analysis of the internal structure of the scattering units. For example, in the case of liquids, a discrete electronic density, such as the one in (1.51), allows to describe only the individual scattering of molecules because the internal correlations—intramolecular interatomic distances—are well defined. But a more elaborate formulation is lacking to take into account the mutual interference between molecules in positions with some correlation. The mutual interference is determined by the intermolecular interaction

¹In a gas, the scattering units are molecules and the internal correlations producing interference effects are the interatomic distances r_{ab} , e.g. (2.7). In the case of monatomic gas, the atoms are the scattering units and the internal correlations are the atomic orbitals contributing to the atomic scattering factor, (1.46).

potential, which in case of short-range interactions, the correlations are often purely statistical.

The formulation required to describe the kinematic scattering by any type of sample is obtained by taking as a starting point an arbitrary electron density $\rho(\mathbf{r})$, whose intensity

$$\begin{aligned} I(\mathbf{Q}) &= I_{Th} |\text{FT}\{\rho(\mathbf{r})\}|^2 = I_{Th} \text{FT}\{\rho(\mathbf{r})\} \text{FT}\{\rho(\mathbf{r})\}^* = I_{Th} \text{FT}\{\rho(\mathbf{r}) * \rho(-\mathbf{r})\} \\ &= I_{Th} \text{FT}\{C(\mathbf{u})\}, \end{aligned} \quad (3.1)$$

is written in the most general way possible, making it clear that the intensity in the reciprocal space is the FT of the correlation function

$$C(\mathbf{u}) = \rho(\mathbf{r}) * \rho(-\mathbf{r}) = \int \rho(\mathbf{r})\rho(\mathbf{r} + \mathbf{u}) dV. \quad (3.2)$$

Any correlation between the positions \mathbf{r} of the electronic charges is expressed in the correlation function. The vector \mathbf{u} represents the relative positions between the charges. The higher the value of $C(\mathbf{u})$, the greater the number of times that the separation \mathbf{u} between charges occurs in the sample, which means the greater the number of charges separated by \mathbf{u} . In most cases, charges are atomic electrons and \mathbf{u} is the vector separation between pairs of atoms or atom groups such as molecules and particles.

Note 3.1: Patterson Function

The deduction of the correlation function in (3.2), also called Patterson function, uses the equality $g(u) = f(x) * f^*(-x) = \int f^*(x)f(x+u) dx$. Here we will make a general deduction of this equality whether $f(x)$ is a real or complex function. Given that

$$\text{FT}\{f(x)\}^* = \int f^*(x)e^{-iQx}dx = \int f^*(-x)e^{iQx}dx = \text{FT}\{f^*(-x)\},$$

and recalling that the product of the FTs is equal to the FT of the convolution, (1.32), it is easy to see that

$$\begin{aligned} |\text{FT}\{f(x)\}|^2 &= \text{FT}\{f(x)\}\text{FT}\{f(x)\}^* = \\ \text{FT}\{f(x)\}\text{FT}\{f^*(-x)\} &= \text{FT}\{f(x) * f^*(-x)\} = \text{FT}\{g(u)\}. \end{aligned}$$

On the other hand, it is also true that

$$\text{FT}\{f(x)\}\text{FT}\{f(x)\}^* = \int f(x')e^{iQx'}dx' \int f^*(x)e^{-iQx}dx = \iint f^*(x)f(x')e^{iQ(x'-x)}dx'dx .$$

Replacing x' with $u + x$ and dx' with du , we reach

$$\text{FT}\{f(x)\}\text{FT}\{f(x)\}^* = \int \left[\int f^*(x)f(x+u)dx \right] e^{iQu}du = \text{FT}\{g(u)\} ,$$

thus demonstrating that

$$g(u) = f(x) * f^*(-x) = \int f^*(x)f(x+u)dx = \int f^*(x-u)f(x)dx ,$$

and that $g(u)$ is a symmetric (even) function in the case of $f(x)$ being a real function.

The description by means of the correlation function of the numerous forms of matter to be organized, from an atomic scale all the way to a microscopic one, is what matters from the cinematic intensity point of view. The correlation function is independent of phase factors, namely the determination of $\rho(\mathbf{r})$ depends on the phase of scattered X-ray waves as summarized in (1.53), but $C(\mathbf{u})$ depends only on the intensity, which is a real value with a null phase. Consequently, the correlation function represents the set of all the structural information directly accessible via diffraction (kinematic) experiments of X-rays that can be, in principle, determined by inverse FT of the intensity, Sect. 1.2.1, i.e.

$$C(\mathbf{u}) = \text{FT}^{-1}\{I(\mathbf{Q})/I_{Th}\} = \frac{1}{(2\pi)^3} \int [I(\mathbf{Q})/I_{Th}] e^{-i\mathbf{Q}\cdot\mathbf{u}} dV_Q . \quad (3.3)$$

There is, however, an experimental difficulty in measuring $I(\mathbf{Q})$ across the reciprocal space as required by the integral above. One of the reasons is that the maximum value of Q is limited by energy, as already discussed, (1.49). Even using high energy X-rays to make it possible to measure intensity with large reciprocal vectors (3.3) is a vector integral of volume and, if the sample is not isotropic, it will be necessary to measure the scattered intensity as a function of module Q of the reciprocal vector on different incidence planes, implying in very elaborate experimental procedures. Therefore, besides the type of sample to be analyzed: liquids, colloids, glassy or amorphous materials, polycrystals, crystals, etc., one must keep in mind what information is accessible within the experimental conditions available. The sections and chapters that follow are intended to demonstrate how the correlation function and the intensity behave in various types of samples arranged in an ascending order of the degree of correlation between the scattering units.

3.1 Internal Correlations in Particles

In systems where the scattering units are randomly oriented—absence of preferred orientations—the scattering power $P(Q)$ of each unit corresponds to the average over all orientations and depends only on the module of the vector \mathbf{Q} , such as seen in Chap. 2 for disperse systems of simple particles. This makes it possible to assume that there is an abstract mathematical function equivalent to a spherically symmetric electron density $\rho_s(\mathbf{r})$, such that

$$P(Q) = |\text{FT}\{\rho_s(\mathbf{r})\}|^2 = \left| 4\pi \int \rho_s(r) \frac{\sin Qr}{Qr} r^2 dr \right|^2 \quad (3.4)$$

follows from (1.36). In systems where the particles are in solution, ρ_s has values related to the electron density ρ_0 of the medium, so there is no need to explicitly write the difference $\rho_s - \rho_0$ in the equations below.

Even in the cases of particles with a spherical symmetry where $\rho_s(\mathbf{r})$ corresponds to the particle's actual electron density, there is not an unambiguous choice for the density function since $P(Q)$ involves a quadrature operation, precluding any mathematical recourse from reaching the expression of $\rho_s(r)$ with 100 % reliability. The unambiguous information available on the electron density is an internal correlation function of the particle

$$c(u) = \rho_s(\mathbf{r}) * \rho_s(-\mathbf{r}) = \int \rho_s(\mathbf{r}) \rho_s(\mathbf{r} + \mathbf{u}) dV. \quad (3.5)$$

Since $\rho_s(\mathbf{r})$ is a spherically symmetrical function, $c(u)$ is independent of the direction of the vector \mathbf{u} considered in the integration of $\rho_s(\mathbf{r} + \mathbf{u})$, implying in a simplification in the expression of the particle's scattering power, which is given by

$$P(Q) = \text{FT}\{c(u)\} = 4\pi \int \underbrace{c(u) u^2}_{p(u)} \frac{\sin Qu}{Qu} du = 4\pi \int p(u) \frac{\sin Qu}{Qu} du. \quad (3.6)$$

However, instead of describing the internal correlations of the particle by the function $c(u)$, which always has a maximum value in $u = 0$, Fig. 3.1a, it is more convenient, for purposes of interpretation of the particle's structure, to express the correlations by the distribution of distances between electronic charges,

$$p(u) = c(u) u^2 = \text{FT}^{-1}\{P(Q)\} u^2 = \frac{1}{2\pi^2} \int_0^{Q_f} P(Q) Qu \sin(Qu) dQ, \quad (3.7)$$

Figure 3.1b, usually called Par Distance Distribution Function (PDDF) (Lindner and Zemb 2002).

From the experimental point of view, the determination of $p(u)$ has a limited resolution by the final scattering angle $2\theta_f$, available in a given instrumental

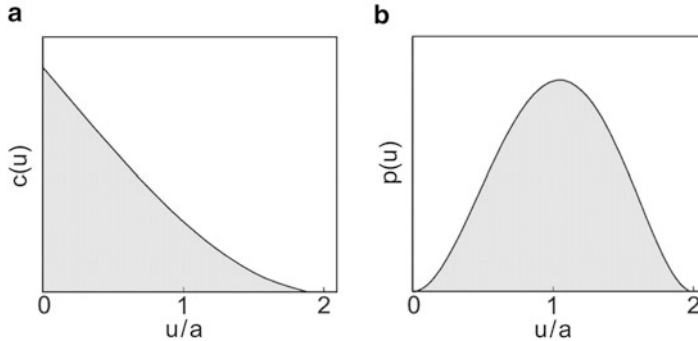


Fig. 3.1 (a) Internal correlation function, $c(u) = \rho_s(r) * \rho_s^*(-r)$, and (b) par distance distribution function (PDDF), $p(u) = c(u) u^2$, for an uniform sphere of radius a

arrangement or considered in the calculation of $P(Q)$, where $Q_f = Q_{max} \sin \theta_f$. Alternatively, curve fitting methods are also used in determining $p(u)$. In cases where prior information about the particle's structure is available, it is possible to write the PDDF in terms of a few adjustable parameters. The particle's scattering power, (3.6), is then calculated as a function of these parameters, which are adjusted in order to reproduce the experimental intensity curve $I(Q) = N I_{Th} P(Q)$ from a sample containing N dispersed particles.

...

Exercise 3.1. General case of spherical particles with radial electron density. (a) Numerically solve the particle's internal correlation function $c(u)$ as given by (3.5). (b) By choosing a thick shell sphere as example, calculate $P(Q)$ from the (3.6), determine $p(u)$ by the inverse FT of $P(Q)$ and compare with the expected PDDF. What is the minimum value of Q_f for the PDDF to be close to the expected one? (c) Generate random positions within the particle's volume and build a histogram of the distances duly weighed with the relative values of the electron density of each position. What is the similarity between histogram and PPDF?

Answer (a): The internal correlation function is an integral of volume that is independent of the direction of the vector \mathbf{u} . Taking $\mathbf{r} = r[\sin \gamma \cos \varphi, \sin \gamma \sin \varphi, \cos \gamma]$ and $\mathbf{u} = u[0, 0, 1]$,

$$c(u) = \int \rho_s(r) \rho_s(|\mathbf{r} + \mathbf{u}|) dV = 2\pi \int_0^\infty \int_0^\pi \rho_s(r) \rho_s(\sqrt{r^2 + u^2 + 2ru \cos \gamma}) r \sin \gamma d\gamma r dr .$$

When changing by variable $z = r^2 + u^2 + 2ru \cos \gamma$, the function

$$p(u) = u^2 c(u) = \pi u \int_0^\infty \rho_s(r) \left[\int_{(r-u)^2}^{(r+u)^2} \rho_s(\sqrt{z}) dz \right] r dr , \quad (3.8)$$

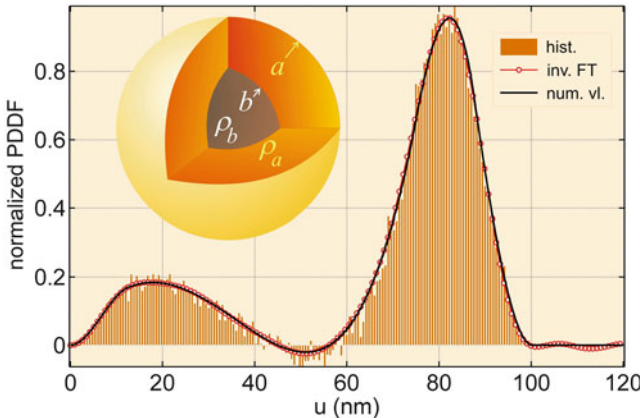


Fig. 3.2 PDDF calculated by different methods: numeric (num. vl.), (3.8); inverse FT of $P(Q)$ (inv. FT), (3.7) with $Q_f = 0.04 \text{ \AA}^{-1}$; and histogram with $N_r = 4000$ random positions (hist.), (3.9). Inset: spherical particle with relative densities $\rho_a = 2$ and $\rho_b = -1$, and radii $a = 50.0 \text{ nm}$ and $b = 37.5 \text{ nm}$ [exshell.m]

can be calculated numerically whatever the mathematical expression of $\rho_s(r)$.

Answer (b): In the case of the particle example illustrated in Fig. 3.2, $p(u) = u^2 \text{FT}^{-1}\{P(Q)\}$ is very close to the numerical values $Q_f \gtrsim 20/a$ where a is the particle's outer radius.

Answer (c): As shown in Fig. 3.2, the histogram

$$n(u) = 2 \sum_{i=1}^{N_r} \sum_{j>i}^{N_r} \rho_s(\mathbf{r}_i) \rho_s(\mathbf{r}_j) \int_u^{u+\Delta u} \delta(u' - r_{ij}) du' , \quad (3.9)$$

tends to be proportional to $p(u)$ the greater the number N_r of random positions \mathbf{r}_i . The integral $\int_u^{u+\Delta u} \delta(u' - r_{ij}) du'$ calculates the number distances $r_{ij} = |\mathbf{r}_i - \mathbf{r}_j|$ with values between u and $u + \Delta u$ where Δu is the bin width of the histogram.

...

3.1.1 Molecules, Proteins, and Discrete Particles in General

Upon comparing the expressions of scattering power in (2.6) and (3.6),

$$P(Q) = 4\pi \int p(u) \frac{\sin Qu}{Qu} du = \sum_{a,b} f_a(Q) f_b^*(Q) \frac{\sin Qr_{ab}}{Qr_{ab}} ,$$

it is easy to see that

$$4\pi p(u) = \sum_{a,b} f_a(Q) f_b^*(Q) \delta(u - r_{ab}) \quad (3.10)$$

provides the exact solution for $P(Q)$. Although it does not correspond to the actual PDDF nor to the one that is experimentally accessible via inverse FT, (3.7), which has no dependence on Q , this expression of $p(u)$ is very useful to simulate scattering curves, as we shall demonstrate in the next topics.

3.1.1.1 Limit of Small Angle

In the limit of small angle, $Q \rightarrow 0$, when the atomic scattering factors are interchangeable with an average value $f_m(0)$,

$$4\pi p(u) = f_m^2(0) \sum_{a,b} \delta(u - r_{ab}) \quad (3.11)$$

is proportional to the histogram of the particle's internal interatomic distances, a fact that makes the calculation of $P(Q)$ more efficient in computational terms, as mentioned in Note 3.1. The root mean square radius, or gyration radius, (2.10), can also be obtained from the function $p(u)$ whereas

$$\frac{\int p(u) u^2 du}{2 \int p(u) du} = \left(\frac{1}{2} \sum_{a,b} r_{ab}^2 \right) / N_{at}^2 = R_g^2. \quad (3.12)$$

Note 3.2: The calculation of $P(Q)$ in proteins and macromolecules with thousands of atoms is done much more efficiently when taking into account the limit of small angle. By replacing (3.11) in (3.6), we have

$$P(Q) = f_m^2(0) \int N(u) \frac{\sin Qu}{Qu} du \quad (3.13)$$

where $N(u) du$ is the number of times that the interatomic distances r_{ab} with values between u and $u + du$ occur in the particle. The `saxs.m` routine reads pdb files (see Sect. 2.3.1) and executes this numerical integral with resolution $du = 0.01 \text{ \AA}$ so as to provide $P(Q)$ and the histogram $N(u)du$.

...

Exercise 3.2. Lysozyme was the second protein structure, the first of the category of enzymes, to be determined by X-ray methods. Understanding the correlations between the physical structure and the biochemical activity of the enzymes was started with lysozyme (Vocadlo et al. 2001). (a) Given the structure of the lysozyme, as in file 2LYZ.pdb (Protein Data Bank: <http://www.pdb.org/>), calculate the curve

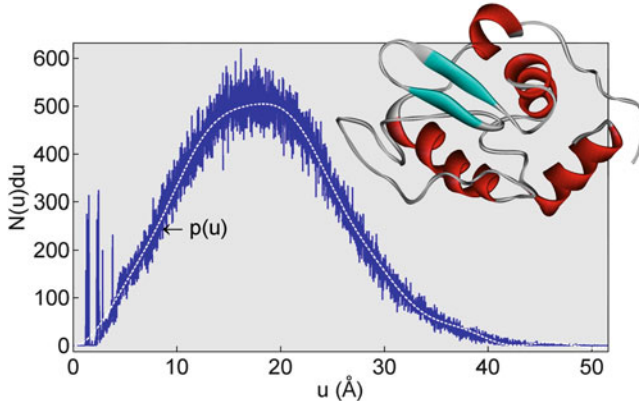


Fig. 3.3 Histogram of interatomic distances in lysozyme. Resolution $du = 0.01 \text{ \AA}$. Inset: amino acid chains of lysozyme (PDB ID: 2LYZ; Protein Data Bank: <http://www.pdb.org/>). The function $p(u)$ (dashed white line) obtained by (3.7), with $Q_f = 0.75 \text{ \AA}^{-1}$, is compared to the histogram [exlysozyme.m]

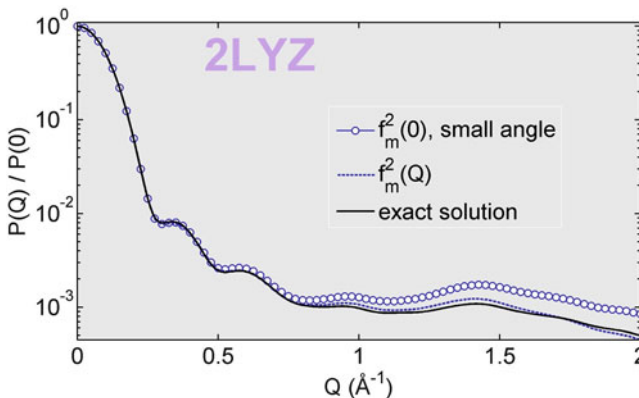


Fig. 3.4 Lysozyme's scattering power calculated by: (1) small angle approach, (3.13); (2) with $f_m^2(Q)$ in the place of $f_m^2(0)$ in the (3.13); and (3) exact solution, (2.6) [exlysozyme.m]

$P(Q)$ from the histogram $N(u)du$ of the interatomic distances, e.g. Fig. 3.3. Up to which value of Q is the small angle approach satisfactory within an accuracy of 10 %? (b) Compare the PDFF determined from the small angle scattering curve with the histogram of the interatomic distances.

Answer (a): In lysozyme, whose gyration radius is $R_g = 14.0 \text{ \AA}$, the small angle approach, where $4\pi p(u) \simeq f_m^2(0) N(u)$, differs from the exact solution gradually with the increase of Q , the relative difference being above 10 % when $Q > 0.75 \text{ \AA}^{-1}$. This value is of the order of ten times larger than the Guinier region, Fig. 3.4. The origin of the systematic increase of the relative difference lies in the fact of the atomic scattering factors decrease as Q increases, which can be remedied by

exchanging $f_m(0)$ for $f_m(Q)$. However, in the case of lysozyme and of any other particle formed by different atoms, the solution with $4\pi p(u) \simeq f_m^2(Q) N(u)$ also fails to coincide with the exact solution out of the small angle interval.

Answer (b): The distances between nearest neighbors are only resolved when $Q_f \rightarrow \infty$, so that $p(u) = u^2 \text{FT}^{-1}\{P(Q)\}$ in the small angle region corresponds to a low resolution histogram, Fig. 3.3.

...

3.1.1.2 General Wide Angle Solution

Outside the limit of small angle, in the event of disperse systems where there are measurable intensities at relatively wide angles, it is convenient to rewrite (3.10) as

$$4\pi p(u) = \sum_a |f_a(Q)|^2 \delta(u) + \sum_{a,b \neq a} f_a(Q) f_b^*(Q) \delta(u - r_{ab}) = \sum_a |f_a(Q)|^2 [\delta(u) + \bar{p}(u)],$$

from where the following equalities are reached²

$$\text{FT} \left\{ \frac{c(u)}{\sum_a |f_a(Q)|^2} \right\} = \underbrace{\text{FT} \left\{ \frac{\delta(u)}{4\pi u^2} \right\}}_{=1} + \text{FT} \left\{ \frac{\bar{p}(u)}{4\pi u^2} \right\} = \frac{P(Q)}{N_{at} f_m^2(Q)} = S(Q). \quad (3.14)$$

Since $S(Q) = 1 + \text{FT}\{\bar{p}(u)/4\pi u^2\}$, the normalized PDDF

$$\bar{p}(u) = \frac{1}{N_{at} f_m^2(Q)} \sum_{a,b \neq a} f_a(Q) f_b^*(Q) \delta(u - r_{ab}), \quad (3.15)$$

is experimentally accessible through the relation

$$\bar{p}(u) = 4\pi u^2 \text{FT}^{-1}\{S(Q) - 1\} = \frac{2}{\pi} \int_0^{Q_f} [S(Q) - 1] Qu \sin(Qu) dQ, \quad (3.16)$$

whose resolution depends on both Q_f and the statistic of photon counting above the background intensity due to, for instance, Compton scattering. But what actually is obtained from the inverse FT operation is something close to

$$\bar{p}(u) = \frac{1}{N_{at} \langle \gamma^2 \rangle} \sum_{a,b \neq a} \gamma_a \gamma_b^* \delta(u - r_{ab}) \quad (3.17)$$

where $\gamma_a = Q_f^{-1} \int_0^{Q_f} f_a(Q) dQ$ and $N_{at} \langle \gamma^2 \rangle = \sum_{a=1}^{N_{at}} |\gamma_a|^2$. In particles composed of different chemical elements, the weights γ_a of the contributions of each element

²Recalling that $p(u) = u^2 c(u)$ and $\sum_a |f_a(Q)|^2 = N_{at} \langle f^2(Q) \rangle = N_{at} f_m^2(Q)$.

are only necessary for a detailed comparison of experimental and theoretical $\bar{p}(u)$ curves obtained from (3.16) and (3.17), respectively. The relative frequencies with which the separations r_{ab} occur in the particle structure can be extracted directly from the experimental curve when the elements have equal or near atomic numbers such that $\gamma_a \gamma_b^*/\langle \gamma^2 \rangle \simeq 1$. Alternatively, a common approach is to take $\gamma_a \gamma_b^*/\langle \gamma^2 \rangle$ by $f_a(0) f_b^*(0)/f_m^2(0)$ since it produces no significant variation in (3.17).

Note 3.3: Considering that $\bar{p}(u)$ is obtained via (3.16). The upper limit of integration, Q_f , introduces oscillations of period $2\pi/Q_f$ in the solution. A resource to minimize these unwanted oscillations is to convolute the solution with a rectangular function of unit area and width equal to the period of the oscillations as shown in Fig. 3.5. The use of this resource is, however, limited to situations where the interatomic distance values have differences greater than the period of the oscillations.

Typical disperse systems where there are measurable intensities at high angles are aggregates in solid or in powder form whose constituent particles do not present preferred orientations. Despite the high concentration of particles, the classification of disperse systems is appropriate because the scattered intensities are characteristic of the internal structure of the particles and the effects of correlations between particles are negligible at wide angles. The most common among these systems are the polycrystalline samples where the particles are crystals of submicroscopic dimensions. Particles with dimensions in submicron scales have high densities of interatomic distances above a few nanometers, making it difficult to accurately identify all distances and limiting the resolution of the structure. Consequently, the

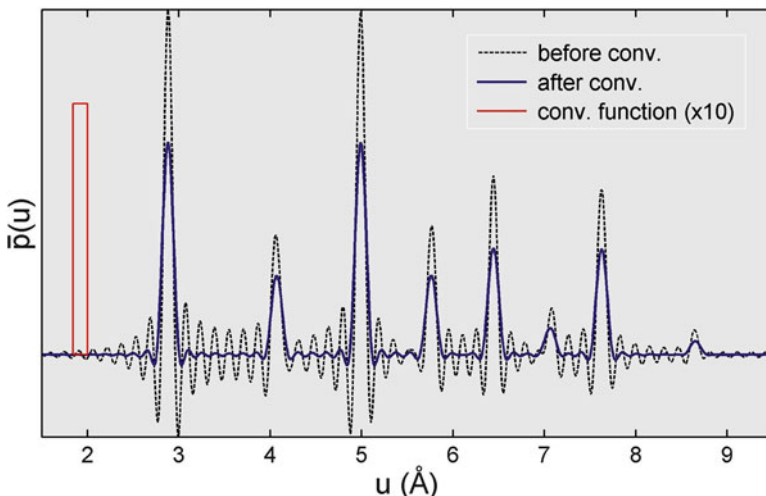


Fig. 3.5 Example of normalized PDDF, (3.16) with $Q_f = 40 \text{ \AA}^{-1}$, before (before conv.) and after (after conv.) of convolving with a rectangular function (red line) of unit area and width $2\pi/Q_f$. Hypothetical structure: gold (Au) nanocrystals with 1 nm in diameter [exgoldnano0.m]

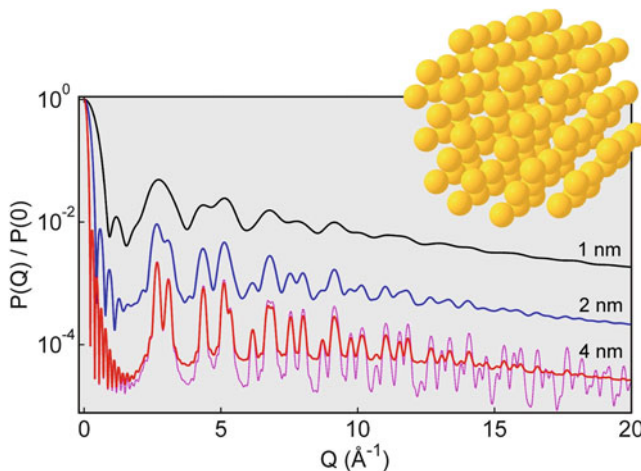


Fig. 3.6 Simulated X-ray scattering by Au nanoparticles with diameters of 1, 2, and 4 nm. Disorder in the atomic positions: 5% (solid lines) and 1% (dashed line) of the minimum interatomic distance (2.88 \AA). Inset: Au nanoparticle with a diameter of 1 nm [exgoldnano1.m]

structural analysis through $\bar{p}(u)$, (3.15), or equivalently by the so-called atomic pair density function (PDF),

$$h(u) = \frac{\bar{p}(u)}{4\pi u^2} = \frac{1}{4\pi u^2 N_a f_m^2(Q)} \sum_{a,b \neq a} f_a(Q) f_b^*(Q) \delta(u - r_{ab}), \quad (3.18)$$

is appropriate for studies of local order of the systems, which means determining the correlations between nearest neighbors (Egami and Billinge 2003). The complete determination of the non-local average structure of polycrystalline samples uses another formalism as we will discuss later.

...

Exercise 3.3. Gold nanoparticles have unique optical and electronic properties, as well as molecular affinities. These are a few reasons that make them the subject of intense research with a wide range of applications in many areas. Assuming spherical nanoparticles with an ordered crystalline structure, simulate the X-ray scattering curve. Note: neglect Compton scattering. (a) What happens in the wide angle region when increasing the diameter of the particles? (b) What is the effect of a small random disorder in the atomic positions? (c) What is the minimum X-ray energy to identify the atomic distances between the nearest neighbors up to 10 \AA ?

Answer (a): Generating atomic positions³

$$\mathbf{r}_a = a_0 [\mathbf{m}, \mathbf{n}, \mathbf{p}] + a_0 \{[0, 0, 0], [1/2, 1/2, 0], [1/2, 0, 1/2], [0, 1/2, 1/2]\}_{\mathbf{m}, \mathbf{n}, \mathbf{p}}$$

within a sphere with the desired diameter of the nanoparticle, where $a_0 = 4.0782 \text{ \AA}$ and $\mathbf{m}, \mathbf{n}, \mathbf{p} \in \mathbb{Z}$, calculate the histogram $N(u)du$ of interatomic distances and then

$$P(Q) = |f_{\text{Au}}(Q)|^2 \int N(u) \frac{\sin Qu}{Qu} du .$$

The increase in diameter gives rise to increasingly more defined diffraction peaks, Fig. 3.6. The widths of the peaks are proportional to the inverse of the diameter. For example, the isolated peak at $Q = 4.36 \text{ \AA}^{-1}$ has a full width at half maximum of $\Delta Q \simeq 7.26/\text{diameter}$, in the same way that the peak around $Q = 0$, as seen in Exercise 1.6, indicating that the widths of the diffraction peaks are related to FT of the particle shape (a nanocrystal in this case).

Answer (b): By adding small random displacements $d\mathbf{r} = [dr_1, dr_2, dr_3]$, to the positions \mathbf{r}_a of the crystalline lattice, it is possible to simulate the effect of disorder in the scattering of X-rays. Figure 3.6 shows scattering curves with $|dr_i| < 0.05 a_0 / \sqrt{2}$, corresponding to 5 % of the smallest interatomic distance. $P(Q) \rightarrow \sum_a |f_a(Q)|^2$ and $S(Q) \rightarrow 1$ the greater the disorder and the value of Q . Quantitatively, the effect is treatable within the Debye–Waller approach (Note 3.4),⁴ leading to

$$S(Q) = 1 + [S_0(Q) - 1] e^{-Q^2 \langle d\mathbf{r}^2 \rangle} \quad (3.19)$$

where $S_0(Q)$ represents the situation without disorder and $\langle d\mathbf{r}^2 \rangle$ is the mean square deviation⁵ around the positions \mathbf{r}_a . For disorder of 5 %, $\langle d\mathbf{r}^2 \rangle = 7 \times 10^{-3} \text{ \AA}^2$.

Answer (c): The scattering curve needs to go beyond $Q_f = 10 \text{ \AA}^{-1}$ to identify all distances up to 10 Å, as in the case of $Q_f = 20 \text{ \AA}^{-1}$, Fig. 3.7. For example, in an experimental setup where the maximum angle of intensity measurement is $2\theta_f = 60^\circ$, it would require photons of 60 keV to reach $Q_f \simeq 20 \text{ \AA}^{-1}$.

...

³The crystalline structure of Au is face-centered cubic (fcc).

⁴See also Egami and Billinge (2003, p. 31), or Als-Nielsen and McMorrow (2001, p. 140).

⁵Mean square deviation: $\langle dx^2 \rangle = \sum_{i=1}^N (x_i - \bar{x})^2 / (N - 1)$.

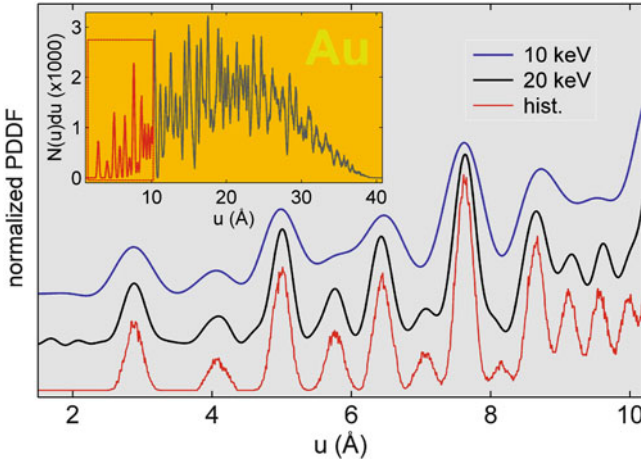


Fig. 3.7 PDDFs extracted from simulated scattering curves in Au nanoparticles and compared to the histogram (hist.) of interatomic distances (inset). Scattering curves with Q ranging from 0 to 10 \AA^{-1} and from 0 to 20 \AA^{-1} require X-rays with minimum energies of 10 keV and 20 keV, respectively. Inset: interatomic distances in a particle with diameter of 4 nm and disorder of 5% (Fig. 3.6) [exgoldnano2.m]

Note 3.4: Approximation of Debye–Waller generalized for disordered and static distributions. In the case of the correlation function, $c(u)$, of a discrete distribution of atoms is such that

$$4\pi u^2 c(u) = \sum_a |f_a(Q)|^2 \delta(u) + \sum_{a, b \neq a} f_a(Q) f_b^*(Q) G(u - r_{ab}),$$

a procedure analogous to that used in (3.14) leads to

$$S(Q) = 1 + \frac{1}{\sum_a |f_a(Q)|^2} \sum_{a, b \neq a} f_a(Q) f_b^*(Q) \text{FT} \left\{ \frac{G(u - r_{ab})}{4\pi u^2} \right\}. \quad (3.20)$$

The distances r_{ab} represent the ideal configuration of the structure without disorder so that $\bar{p}(u)$ as given in (3.15) is a series of delta functions responsible for the function $S_0(Q)$ of the ideal structure. Disorders of a random nature without preference of direction or atomic site cause uncertainties in the values of r_{ab} , transforming the delta function into Gaussian $G(u)$ of unit area and standard deviation $\sigma = \sqrt{2\langle dr^2 \rangle}$ where $\langle dr^2 \rangle$ is the mean square deviation of the atomic positions in relation to the ideal positions. In other words,

$$\delta(u - r_{ab}) \rightarrow G(u) * \delta(u - r_{ab}) = G(u - r_{ab})$$

since they all have the same Gaussian standard deviation, for instance, as seen in the histogram in Fig. 3.7. The FT above has an approximate solution,

Note 3.4: (continued)

$$\text{FT} \left\{ \frac{G(u - r_{ab})}{4\pi u^2} \right\} = \frac{1}{\sigma \sqrt{2\pi}} \int \exp \left[-\frac{(u - r_{ab})^2}{2\sigma^2} \right] \frac{\sin Qu}{Qu} du \simeq \frac{\sin Qr_{ab}}{Qr_{ab}} e^{-\frac{1}{2}Q^2\sigma^2}. \quad (3.21)$$

The minimum values of r_{ab} in solids are of the order of 2 Å, implying that this approximate solution is very good even for σ values as large as 0.2 Å; it can be verified numerically, cf. routine `debye.m`. By replacing the integral solution, (3.21), in (3.20), (3.19) is demonstrated, as well as the validity of the approximation of Debye–Waller in a situation where the disorder is independent of thermal vibrations, Sect. 4.3.1.

3.1.2 Particles of Random Conformation

Up until now we have dealt with systems formed by one (monodisperse) or more (polydisperse) types of particles with deterministic structures: a single electron density function describing all particles of a given type. There are systems, however, whose particles are distinct from each other, without having two identical particles in the entire system. Long chains of monomers, which are known as polymers, are typical examples of systems where the only information available are the average values of the chain conformations in solution.

Mathematical models of the possible conformations are essential for quantitative analysis of the experimental data of radiation scattering by these systems. In the most simple models of random conformations, the positions

$$\mathbf{r}_j = \ell \hat{\mathbf{e}}_j + \mathbf{r}_{j-1}$$

of identical monomers along the chain have separation vectors of constant module, ℓ , but with directions $\hat{\mathbf{e}}_j$ varying within certain limits imposed by the physical feasibility of the models, Fig. 3.8. In the model commonly called random walk (RW), all values of the scalar products $\hat{\mathbf{e}}_j \cdot \hat{\mathbf{e}}_{j-1} \in [-1, 1]$ have equal probabilities, e.g. Fig. 3.9.

The scattering power of X-rays by a single chain with N_m monomers has the exact solution

$$P(\mathbf{Q}) = \sum_{j=1}^{N_m} \sum_{k=1}^{N_m} F_j(\mathbf{Q}) F_k^*(\mathbf{Q}) e^{i\mathbf{Q} \cdot \mathbf{r}_{jk}},$$

in analogy to (2.4). $F_j(\mathbf{Q})$ is the monomer's form factor, as in (1.52), and in the particular orientation of the j -th position in the chain. In disperse systems containing

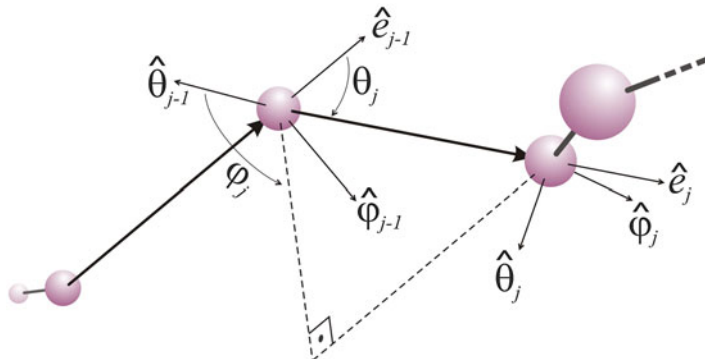


Fig. 3.8 System of relative coordinates $\hat{\theta}_j$, $\hat{\phi}_j$, and \hat{e}_j to describe the junction between monomers of a polymer

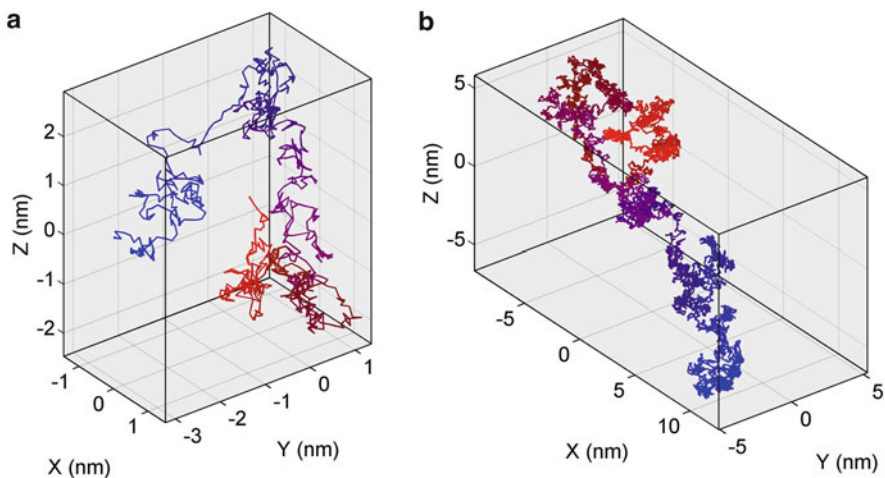


Fig. 3.9 Monomers chains (polymers) generated according to the RW model. (a) Chain of 1000 and (b) 10,000 monomers. For improved view of the polymer's spatial conformation, the color varies from blue to red along the chains. Monomer length $\ell = 0.154 \text{ nm}$ [polymerchain.m]

N chains of N_m monomers each, the form factors are replaced by the monomer's scattering power,

$$F_j(\mathbf{Q})F_k^*(\mathbf{Q}) \rightarrow \langle |F(\mathbf{Q})|^2 \rangle = P_m(Q) = \sum_{a,b}^{N_m} f_a(Q)f_b^*(Q) \frac{\sin Qr_{ab}}{Qr_{ab}},$$

and the kinematic intensity $I(Q) = N I_{Th} P(Q)$ scattered by the system depends on the average chain conformation, which means

$$P(Q) = \langle P(Q) \rangle = P_m(Q) \sum_{j,k} \langle e^{iQ \cdot r_{jk}} \rangle = P_m(Q) \sum_{j,k} \langle \cos(Q \cdot r_{jk}) \rangle \quad (3.22)$$

where $r_{jk} = \mathbf{r}_k - \mathbf{r}_j = \ell (\hat{\mathbf{e}}_{j+1} + \hat{\mathbf{e}}_{j+2} + \cdots + \hat{\mathbf{e}}_k) = \ell \sum_{\alpha=j+1}^k \hat{\mathbf{e}}_\alpha$.

Since there is no long-range order, it is necessary to concern only with the small angle solution that is obtained by the expansion in Taylor series,

$$\langle \cos(Q \cdot r_{jk}) \rangle \simeq 1 - \frac{1}{2} \langle (Q \cdot r_{jk})^2 \rangle = 1 - \frac{1}{2} Q^2 \langle r_{jk}^2 \cos^2 \gamma_{jk} \rangle .$$

In the absence of preferential directions for the vectors \mathbf{r}_{jk} , $\langle r_{jk}^2 \cos^2 \gamma_{jk} \rangle = \langle r_{jk}^2 \rangle \langle \cos^2 \gamma_{jk} \rangle$ and

$$\langle \cos^2 \gamma_{jk} \rangle = \frac{1}{4\pi} \int_0^{2\pi} \int_{-1}^{+1} \cos^2 \gamma_{jk} d(\cos \gamma_{jk}) d\varphi_{jk} = \frac{1}{3} .$$

Substituting in (3.22),

$$\lim_{Q \rightarrow 0} P(Q) = P_m(Q) \sum_{j,k} \left(1 - \frac{1}{6} Q^2 \langle r_{jk}^2 \rangle \right) = P_m(Q) N_m^2 e^{-\frac{1}{3} Q^2 \bar{R}_g^2} , \quad (3.23)$$

thus demonstrating that in the small angle limit, the experimental scattering curve is determined by the mean square gyration radius of the chains $\bar{R}_g^2 = \langle R_g^2 \rangle$. $P_m(Q) \simeq P_m(0)$ in the small angle region since $\bar{R}_g >> \ell$.

In a single chain,

$$r_{jk}^2 = \ell^2 \sum_{\alpha=j+1}^k \sum_{\beta=j+1}^k \hat{\mathbf{e}}_\alpha \cdot \hat{\mathbf{e}}_\beta = \ell^2(k-j) + \ell^2 \sum_{\alpha, \beta \neq \alpha} \hat{\mathbf{e}}_\alpha \cdot \hat{\mathbf{e}}_\beta .$$

But in the specific case of the RW model where the versors $\hat{\mathbf{e}}_\alpha$ are totally independent, the second term of this equation vanishes when calculating the average value of the chains, resulting in $\langle r_{jk}^2 \rangle = \ell^2(k-j)$ and

$$\langle R_g^2 \rangle = \left\langle \frac{1}{2N_m^2} \sum_{j,k} r_{jk}^2 \right\rangle = \frac{\ell^2}{N_m^2} \sum_{j,k>j} (k-j) = \frac{\ell^2}{2N_m^2} \sum_{j=1}^{N_m} j(j-1) \simeq \frac{1}{6} N_m \ell^2 . \quad (3.24)$$

If the length and molecular weight of the monomer is known, the number N_m of monomers in each chain is easily calculated based on the polymer's molecular weight. The compatibility between experimental values of the mean square gyration radius and the values given in (3.24) make it possible to check the validity of the hypothesis of free-junction model (RW model) for a given polymer in solution (Lindner and Zemb 2002).

3.1.2.1 Asymptotic Behavior

Another important characteristic of scattering by particles of random conformations is the asymptotic behavior of $S(Q) = P(Q)/N_m^2 P_m(Q)$ when $Q \rightarrow \infty$. The analysis of this behavior requires solving (3.22) beyond the Guinier region where the intensity curve has exponential decay with Q^2 . In any system where the vectors \mathbf{r}_{jk} have random orientations,

$$\langle \cos(Q \cdot \mathbf{r}_{jk}) \rangle = \frac{\sin Qr}{Qr} * G(r - r_{jk}) .$$

If the values of the modules r_{jk} were well defined, the weight function $G(r - r_{jk})$ would be a delta function and $\langle \cos(Q \cdot \mathbf{r}_{jk}) \rangle = \sin Qr_{jk}/Qr_{jk}$ as calculated in the deduction of (2.6) or by the approximation of Debye–Waller for small deviations, (3.21). On the other hand, if there is large dispersion in the values of r_{jk} , it follows that⁶

$$\langle \cos(Q \cdot \mathbf{r}_{jk}) \rangle \approx e^{-\frac{1}{6} Q^2 \langle r_{jk}^2 \rangle} . \quad (3.25)$$

With $\langle r_{jk}^2 \rangle = \ell^2 |k - j|$ and $\langle R_g^2 \rangle = N_m \ell^2 / 6$, (3.25) when substituted in (3.22) provides⁷

$$S(Q) = 2(e^{-x} - 1 + x)/x^2 \quad \text{where} \quad x = Q^2 \langle R_g^2 \rangle . \quad (3.26)$$

(3.26) implies an asymptotic fall $1/Q^2$, as seen in the Kratky graphs (Glatter and Kratky 1982) in Fig. 3.10. This asymptotic behavior is often observed in polymers and denatured (unfolded) proteins in solution (Barbosa 2008; Lindner and Zemb 2002).

...

Exercise 3.4. Common plastic bags are generally made of polyethylene (PE), chemically speaking it is the most simple polymer with a molecular weight ranging from 100,000 to 200,000 g/mol. The chain $(\text{CH}_2-\text{CH}_2)_n$ is comprised of monomers with a molecular weight of 14 g/mol and a length of $\ell = 0.154 \text{ nm}$ (bonding length C–C). Through computer simulation, check the validity of the Debye formula in (3.26).

Answer: The chain formation rule is given by the recursive relation

⁶The validity of this approximation for different weight functions can be checked by a numerical comparison similar to that performed for verifying (3.21).

⁷Results obtained by the expansion in Taylor series of $\exp(-Q^2 \langle r_{jk}^2 \rangle / 6)$ and using that $\sum_{j=1, k>j}^{N_m} (k-j)^n \simeq N_m^{n+2} / [(n+2)(n+1)]$ for $N_m \rightarrow \infty$. See also Lindner and Zemb (2002, p. 268).

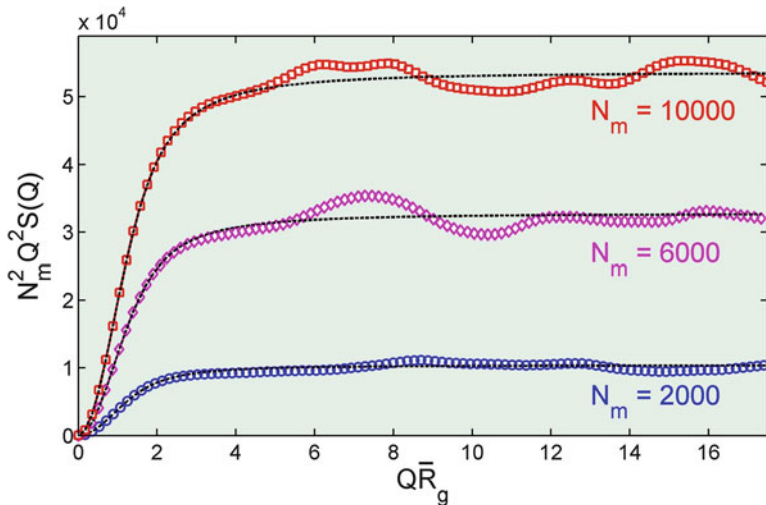


Fig. 3.10 Simulated scattering curves across 500 chains of N_m monomers each, (3.22). Polymer PE, free-junction model, e.g. Fig. 3.9. Theoretical curves (dashed line), (3.26), adjusted with $\bar{R}_g^2 = 7.7, 22.0$, and 37.3 nm^2 [polymerkratky.m]

$$\begin{pmatrix} \hat{\theta}_j \\ \hat{\varphi}_j \\ \hat{\mathbf{e}}_j \end{pmatrix} = \begin{pmatrix} \cos \theta_j \cos \varphi_j & \cos \theta_j \sin \varphi_j & -\sin \theta_j \\ -\sin \varphi_j & \cos \varphi_j & 0 \\ \sin \theta_j \cos \varphi_j & \sin \theta_j \sin \varphi_j & \cos \theta_j \end{pmatrix} \begin{pmatrix} \hat{\theta}_{j-1} \\ \hat{\varphi}_{j-1} \\ \hat{\mathbf{e}}_{j-1} \end{pmatrix} \quad (3.27)$$

where the versors $\hat{\theta}_j$, $\hat{\varphi}_j$, and $\hat{\mathbf{e}}_j$ are defined in Fig. 3.8. In the RW model there are no restrictions in the junction angles, i.e. θ_j and φ_j take on any values in the intervals $[0, \pi]$ and $[0, 2\pi]$, respectively. Examples of chains generated by the RW model are shown in Fig. 3.9.

Simulations of the average scattering generated by hundreds of chains are compared to (3.26) in Fig. 3.10. Despite the limited statistical resolution, the simulated curves follow the behavior foreseen in the theoretical curve for both the chains of low ($28,000 \text{ g/mol}$) and high ($140,000 \text{ g/mol}$) molecular weight. The values of $\langle R_g^2 \rangle = 7.7, 22.0$, and 37.3 nm^2 used to adjust the theoretical curves are very close to the $7.9, 23.7$, and 39.5 nm^2 provided by (3.24).

Although deduced from the RW model, the Debye formula can also describe the scattering curve for other models, such as the model with limitation in the junction angles where $\theta_j = 71 \pm 2^\circ$ and φ_j takes on only three values: 0 or $\pm 120^\circ$. The scattering curves have an asymptotic behavior $1/Q^2$ and the gyration radius determined by the adjustment of the theoretical curves correspond to mean square values, $\langle R_g^2 \rangle$, computed on ensembles containing thousands of virtual chains, as shown in Fig. 3.11.

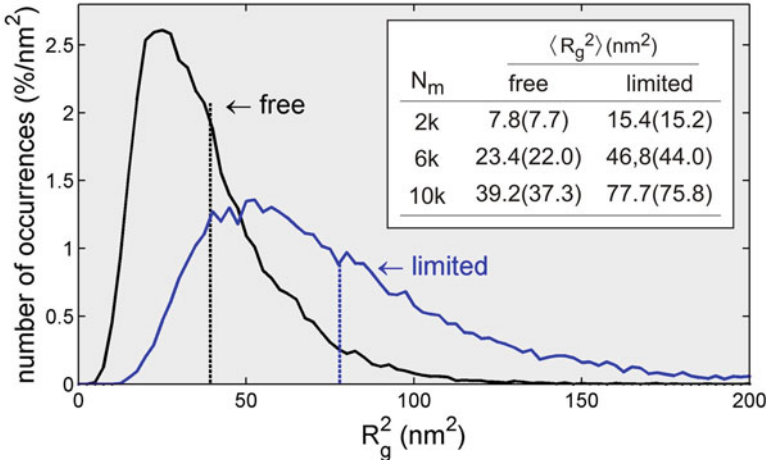


Fig. 3.11 Statistical distributions of the values of R_g^2 in virtual chains generated according to either the free-junction model or limited-junction model ($\theta_j = 71 \pm 2^\circ$ and $\varphi_j \in [-120^\circ, 0, +120^\circ]$). Polymer PE with a molecular weight of 140,000 g/mol. Inset: comparative table between $\langle R_g^2 \rangle$ from the distributions and those obtained by adjusting the scattering curves (values in parentheses), as in Fig. 3.10 [polymerRg.m]

...

Section Summary

— Kinematic intensity

$$I(\mathbf{Q}) = I_{Th} \text{FT}\{C(\mathbf{u})\}$$

— General correlation function (Patterson function)

$$C(\mathbf{u}) = \rho(\mathbf{r}) * \rho(-\mathbf{r}) = \int \rho(\mathbf{r}) \rho(\mathbf{r} + \mathbf{u}) dV$$

— Internal correlation function in systems of dispersed particles

$$c(u) = \rho_s(\mathbf{r}) * \rho_s(-\mathbf{r}) = \int \rho_s(\mathbf{r}) \rho_s(\mathbf{r} + \mathbf{u}) dV$$

— Particle scattering power

$$P(Q) = \text{FT}\{c(u)\} = 4\pi \int c(u) u^2 \frac{\sin Qu}{Qu} du = 4\pi \int p(u) \frac{\sin Qu}{Qu} du$$

— Par Distance Distribution Function (PDDF)

$$p(u) = c(u) u^2 = \text{FT}^{-1}\{P(Q)\} u^2 = \frac{1}{2\pi^2} \int_0^{Q_f} P(Q) Q u \sin(Qu) dQ$$

— Numerical solution for PDDF of spherically symmetric electron densities

$$p(u) = c(u) u^2 = \pi u \int_0^\infty \rho_s(r) \left[\int_{(r-u)^2}^{(r+u)^2} \rho_s(\sqrt{r'}) dr' \right] r dr$$

— PDDF for discrete particles (general solution)

$$p(u) = \frac{1}{4\pi} \sum_{a,b} f_a(Q) f_b^*(Q) \delta(u - r_{ab})$$

— Atomic Pair Density Function (PDF)

$$h(u) = \frac{p(u)}{u^2 N_{at} f_m^2(Q)} = \frac{1}{4\pi u^2 N_{at} f_m^2(Q)} \sum_{a,b \neq a} f_a(Q) f_b^*(Q) \delta(u - r_{ab})$$

3.2 Arbitrary Correlations Between Particles

Arbitrary correlations other than internal ones in particles arise in systems where the potential of interaction affects the way the particles are distributed within the sample's volume. In the simplest situations, the interactions have enough strength to establish some statistical order at short range, but leaving a few degrees of freedom for the relative orientation between non-spherical particles, as in Fig. 3.12. Strong interactions capable of imposing exact orientations are, in most cases, also responsible for the long-range order in systems where the scattered intensities have become intrinsically dependent on the reciprocal vector \mathbf{Q} , and not only on its module, Q . Apart from crystal systems that will be covered in the next chapter, the X-ray scattering by any system of identical particles having effects of mutual interference will be described from the electron density

$$\rho(\mathbf{r}) = \rho_s(\mathbf{r}) * q(\mathbf{r}) . \quad (3.28)$$

With the exception that the function $\rho_s(\mathbf{r})$ is not in principle spherically symmetric, (3.28) can be treated in the same manner as used to describe a discrete distribution of atoms, (1.51), where

$$q(\mathbf{r}) = \sum_{n=1}^N \delta(\mathbf{r} - \mathbf{r}_n) \quad (3.29)$$

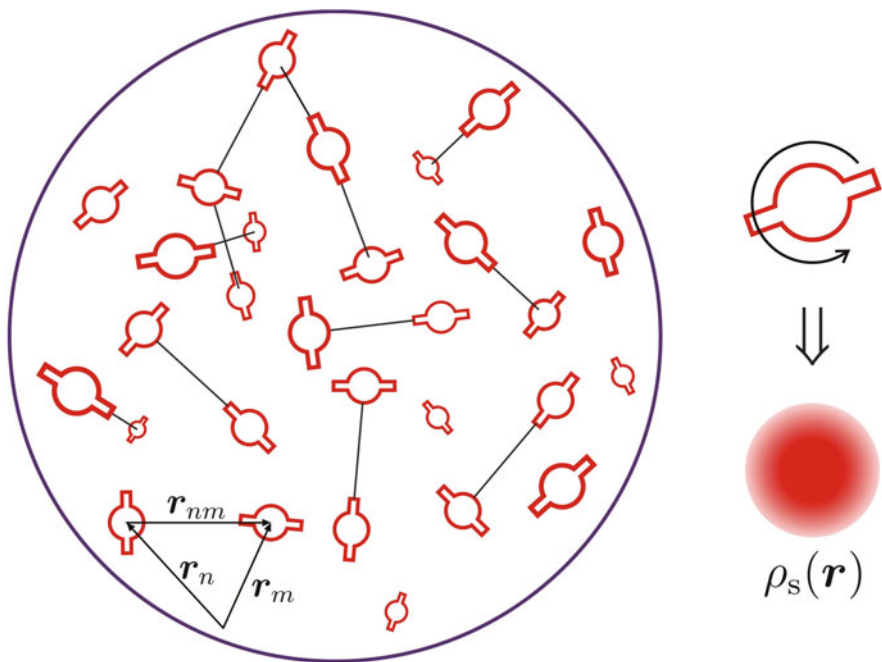


Fig. 3.12 System of non-spherical particles with short range order. r_{nm} is the most probable separation between adjacent particles. A spherically symmetric electron density $\rho_s(\mathbf{r})$ accounts for the scattering of each particle in a random distribution of orientations

provides the instantaneous positions of the N particles within the sample's volume V and $\int_V q(\mathbf{r})dV = N$.

The abstract function $\rho_s(\mathbf{r})$ accounts for both the relative density to the medium and the distribution of orientations such that

$$P(\mathbf{Q}) = \text{FT}\{\rho_s(\mathbf{r}) * \rho_s(-\mathbf{r})\} = \langle \text{FT}\{c(\mathbf{u})\} \rangle \quad (3.30)$$

where $c(\mathbf{u})$ is the internal correlation function of a particle in a given orientation whose average contribution is calculated on the distribution of orientations in the sample. In either the cases of particles with spherical symmetry or as in those where all orientations are equally probable, $P(\mathbf{Q}) = P(Q)$. Otherwise, the scattering will no longer have an azimuthal symmetry around the incident beam direction, reflecting the existence of preferred orientations in the sample.

3.2.1 Mutual Interference

Regardless of the nature of the orientations, whether random, preferential, or highly ordered, the scattering properties of the particles are accounted for in $P(\mathbf{Q})$, while the instantaneous intensity $I(\mathbf{Q})$ scattered by the system will also depend on the correlation function

$$\begin{aligned} C_q(\mathbf{u}) = q(\mathbf{r}) * q(-\mathbf{r}) &= \sum_{n=1}^N \sum_{m=1}^N \delta(\mathbf{u} - \mathbf{r}_{nm}) = N \delta(\mathbf{u}) + \sum_{n, m \neq n} \delta(\mathbf{u} - \mathbf{r}_{nm}) = \\ &= N[\delta(\mathbf{u}) + h(\mathbf{u})] \end{aligned} \quad (3.31)$$

between the relative positions of the particles $\mathbf{r}_{nm} = \mathbf{r}_m - \mathbf{r}_n$. When substituting in the expression of intensity, we have

$$I(\mathbf{Q}) = I_{Th} P(\mathbf{Q}) \text{FT}\{C_q(\mathbf{u})\} = N I_{Th} P(\mathbf{Q}) [1 + \text{FT}\{h(\mathbf{u})\}] . \quad (3.32)$$

The spatial arrangement of particles is essentially characterized by the reduced correlation function

$$h(\mathbf{u}) = \frac{1}{N} \sum_{n, m \neq n} \delta(\mathbf{u} - \mathbf{r}_{nm}) , \quad (3.33)$$

which has a physical meaning similar to the PDF of a particle composed of identical atoms in (3.18), but with two key differences: it depends on the vector \mathbf{u} in cases of non-isotropic systems, and it contains information on the sample volume, which are irrelevant to the study of the particles' interaction properties. In other words, although the expression of $h(\mathbf{u})$ in (3.33) is accurate and contains all the information about the distribution of the particles in the sample, not all the information is of practical interest. The distances between the neighboring particles, which are the smallest r_{nm} values, is the information that is in fact of interest as it characterizes the particle interaction properties. The larger separations reflect only repetitions of these properties, going to the limits imposed by the contour of the sample volume.

3.2.2 Volume Effects

In the absence of correlations, the contribution of the sample volume is restricted to ultra-small angle region around the direct beam as seen in the case of low correlated systems. But with the increase in the degree of correlation between the particles, constructive interferences occur outside the direct beam, generating

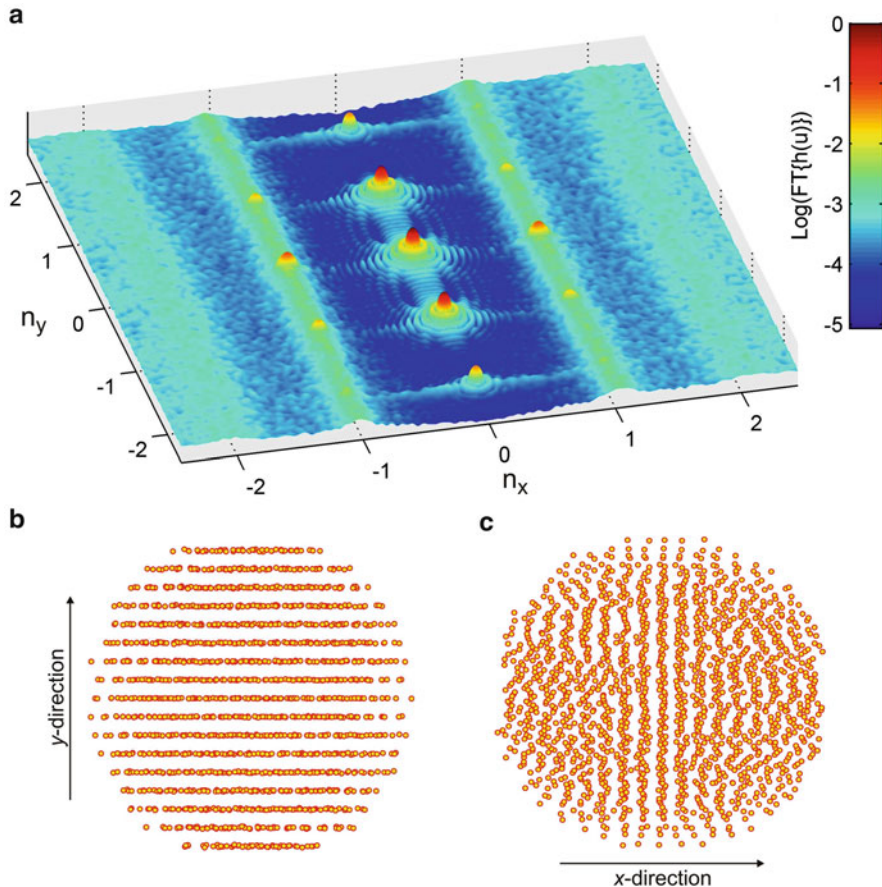


Fig. 3.13 (a) Fourier transform of the function $h(u)$, (3.33), for a system with different degrees of correlation along the directions (b) \hat{y} and (c) \hat{x} , both perpendicular to the incident beam (direction \hat{z}). $n_{x,y} = (a/2\pi) Q_{x,y}$. Volume of the ensemble (sample): cylindrical with a diameter $16a$ (plane xy) and length $6a$. Correlation rule between adjacent particles: $\Delta a/a = 1 + \alpha w$ with $\alpha = 0.2$ and 0.02 along the directions \hat{x} and \hat{y} , respectively, and w takes random values in the interval $[-1, +1]$ [fthofuplotmap.m, fthofuR.m]

diffracted beams with profiles strongly influenced by the sample volume,⁸ or more specifically, by the size of the volume illuminated with coherent radiation. This fact is clearly illustrated in Fig. 3.13. Along the direction y , the positions of the particles are enough correlated to generate a few diffraction peaks at $(n_x, n_y) = (0, \pm 1)$ and $(0, \pm 2)$. The circular ripples around each peak are caused by the volume (size

⁸This phenomenon is analogous to that observed in particles with a crystalline structure, e.g. Exercise 3.3. The larger the particle, the more definite are the diffraction peaks.

and shape) of the ensemble of particles. On the other hand, along the direction x where the correlations do not go beyond the first neighbors, $\text{FT}\{h(\mathbf{u})\}$ produces only mild modulations in the scattered intensity in $n_x = \pm 1$ and ± 2 , but without showing effects caused by the volume of the ensemble. This example illustrates a very common feature in the study of systems with weakly correlated particles where the profiles of the scattered intensities are not affected by the shape of the sample.

Proper treatment of systems with correlated particles is based on the fact that the function $h(\mathbf{u})$ can be written as the product of two functions, i.e.

$$h(\mathbf{u}) = \Omega(\mathbf{u}) \varrho g(\mathbf{u}) = \Omega(\mathbf{u}) \{\varrho [g(\mathbf{u}) - 1] + \varrho\}, \quad (3.34)$$

as demonstrated in detail in Note 3.1. The first function, $\Omega(\mathbf{u})$, carries the dependence with the sample's volume and, because of this, only varies significantly for large values of u , generally of the order of hundreds of microns or even up to a few millimeters. The second function, $g(\mathbf{u})$, varies on a scale of a few angstroms and contains the desired information of the correlations between the particles. Quantitatively, $g(\mathbf{u})$ is also a correlation function, but instead of providing absolute values, it provides the relative frequency with which the vector separation \mathbf{u} occurs in the system in relation to the frequency expected in the case of a disperse system with a density $\varrho = N/V$ of particles. That is to say that by taking any particle as a reference, the probability of finding another particle in the position \mathbf{u} within a volume V/N is equal to $g(\mathbf{u})$. An example of function $g(\mathbf{u})$ is shown in Fig. 3.14.

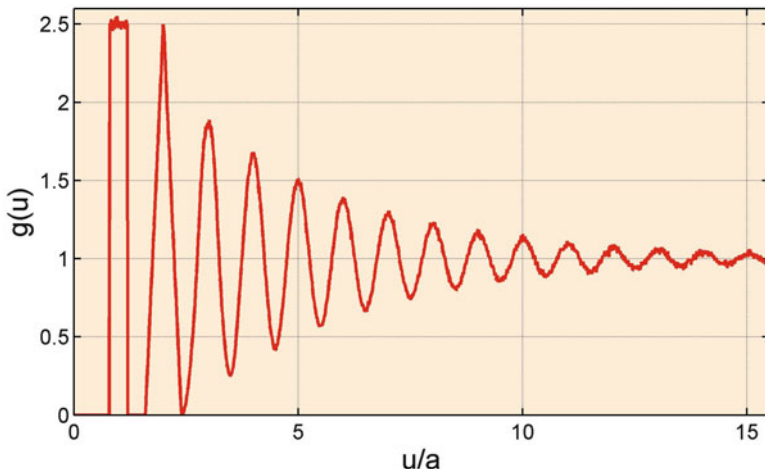


Fig. 3.14 Function $g(\mathbf{u})$ for unidirectional correlation $\Delta a/a = 1+\alpha w$ between adjacent particles, $\alpha = 0.2$ in this example. w represents random values in the interval between -1 and $+1$, which are different for each pair of adjacent particles [exgofu1.m]

Note 3.1: Deduction of Functions $g(\mathbf{u})$ and $\Omega(\mathbf{u})$. When the properties of interaction of the particles in a sample (gas, liquid, or solid) are independent of the sample volume, the particle density can always be written as $q(\mathbf{r}) = q_0(\mathbf{r}) s(\mathbf{r})$ where $q_0(\mathbf{r})$ is the characteristic density of the material and $s(\mathbf{r})$ is the shape function that is 1 or 0 for \mathbf{r} inside or outside of the sample's volume, respectively. The correlation function

$$C_q(\mathbf{u}) = q(\mathbf{r}) * q(-\mathbf{r}) = \int q_0(\mathbf{r}) q_0(\mathbf{r} + \mathbf{u}) s(\mathbf{r}) s(\mathbf{r} + \mathbf{u}) dV = \int_{V\Omega(\mathbf{u})} q_0(\mathbf{r}) q_0(\mathbf{r} + \mathbf{u}) dV$$

only exists within the domain

$$V\Omega(\mathbf{u}) = s(\mathbf{r}) * s(-\mathbf{r}) = \int s(\mathbf{r}) s(\mathbf{r} + \mathbf{u}) dV$$

defined by the volume V of the sample. The function $\Omega(\mathbf{u})$ varies monotonically from 1 to 0 with u ranging from zero to the size of the sample, which means that $\Omega(0) = 1$ since $\int s(\mathbf{r}) s(\mathbf{r}) dV = \int_V dV = V$, and $\Omega(\mathbf{u}) = 0$ if u is greater than the sample's dimension. On a macroscopic scale of variation of the function $\Omega(\mathbf{u})$, the characteristic density is an average density ϱ . However, on a scale of a few angstroms, there are fluctuations $f(\mathbf{r})$ of the average density such that $q_0(\mathbf{r}) = \varrho f(\mathbf{r})$, making it possible to write as

$$C_q(\mathbf{u}) = \int_{V\Omega(\mathbf{u})} \varrho^2 f(\mathbf{r}) f(\mathbf{r} + \mathbf{u}) dV \simeq V\Omega(\mathbf{u}) \varrho^2 \frac{1}{v} \int_v f(\mathbf{r}) f(\mathbf{r} + \mathbf{u}) dV = V\Omega(\mathbf{u}) \varrho^2 g(\mathbf{u}).$$

The volume v is as extensive as necessary so that $g(\mathbf{u})$ does not depend on v and thus contains only the characteristic correlations of the material. In a statistically homogeneous sample, $f(\mathbf{r}) = 1$ and therefore $g(\mathbf{u}) = 1$ for any volume v . Comparing the expression $C_q(\mathbf{u})$ above to (3.31),

$$\underbrace{\varrho V}_{=N} \Omega(\mathbf{u}) \varrho g(\mathbf{u}) = N[\delta(\mathbf{u}) + h(\mathbf{u})]$$

where for $u \neq 0$,

$$h(\mathbf{u}) = \Omega(\mathbf{u}) \varrho g(\mathbf{u}),$$

as used in (3.34).

A few properties of function $\Omega(\mathbf{u})$.

$$\text{FT}\{V\Omega(\mathbf{u})\} = \text{FT}\{s(\mathbf{r}) * s(-\mathbf{r})\} = \text{FT}\{s(\mathbf{r})\} \text{FT}\{s(\mathbf{r})\}^* = |\text{FT}\{s(\mathbf{r})\}|^2 = |W(Q)|^2.$$

Note 3.1: (continued)

The FT of the sample's shape function

$$W(\mathbf{Q}) = \text{FT}\{s(\mathbf{r})\} = \int s(\mathbf{r}) e^{i\mathbf{Q}\cdot\mathbf{r}} dV = \int_V e^{i\mathbf{Q}\cdot\mathbf{r}} dV$$

is equal to V when $\mathbf{Q} = 0$, i.e. $W(0) = V$. Therefore, $|W(0)|^2 = V^2$,

$$\text{FT}\{\Omega(\mathbf{u})\}_{\mathbf{Q}=0} = V, \quad \text{and}$$

$$\int \text{FT}\{\Omega(\mathbf{u})\} dV_q = \int \Omega(\mathbf{u}) \underbrace{\left(\int e^{i\mathbf{Q}\cdot\mathbf{u}} dV_q \right)}_{= \delta(\mathbf{u})} dV_u = \Omega(0) = 1.$$

Because we are dealing with a macroscopic volume ($V \rightarrow \infty$), these last two properties are similar to a delta function, which is

$$\text{FT}\{\Omega(\mathbf{u})\} \simeq \delta(\mathbf{q}).$$

Note: $\mathbf{Q} = 2\pi\mathbf{q}$ and $dV_q = (2\pi)^{-3}dV_Q$, see Sect. 1.2.1.

In the expression of the scattered intensity, both volume and correlation effects come from the FT of (3.34),

$$\text{FT}\{h(\mathbf{u})\} = \text{FT}\{\varrho [g(\mathbf{u}) - 1]\} * \text{FT}\{\Omega(\mathbf{u})\} + \varrho \text{FT}\{\Omega(\mathbf{u})\}. \quad (3.35)$$

The second term, $\varrho \text{FT}\{\Omega(\mathbf{u})\}$, is proportional to the FT's square module of the shape function $s(\mathbf{r})$, see Note 3.1, and is responsible for the scattered intensity profile around the direct beam. In Fig. 3.13, this term produces the circular ripples seen in $(n_x, n_y) = (0, 0)$ since the volume considered there has a circular shape on the beam's perpendicular plane. In real situations of samples with macroscopic volumes, the contribution of this second term can be discarded because $\text{FT}\{\Omega(\mathbf{u})\} = 0$ for $\mathbf{Q} \neq 0$.

The information of the correlations are contained in the convolution term of the two FTs,

$$\text{FT}\{\varrho [g(\mathbf{u}) - 1]\} * \text{FT}\{\Omega(\mathbf{u})\}.$$

In the absence of correlations (disperse systems) where all the separations are equally probable, i.e. $g(\mathbf{u}) = 1$ for any \mathbf{u} , the convolution term is null, leaving only the scattering around $\mathbf{Q} = 0$ given by $\text{FT}\{h(\mathbf{u})\} = \varrho \text{FT}\{\Omega(\mathbf{u})\}$. In a system with long-range order, such as a crystal, $\text{FT}\{\varrho [g(\mathbf{u}) - 1]\}$ produces diffraction peaks that can be more defined than $\text{FT}\{\Omega(\mathbf{u})\}$ in the vector space \mathbf{Q} . As a consequence of this convolution operation, the effects of the diffracting volume will appear in all the

diffraction peaks, as seen in Fig. 3.13a at $(n_x, n_y) = (0, \pm 1)$ and $(0, \pm 2)$. We will return to discuss this situation when dealing with diffraction of X-rays in crystals.

In systems with arbitrary correlations, which in general are correlations between nearest neighbors only, $\text{FT}\{\varrho [g(\mathbf{u}) - 1]\}$ is a much larger function than $\text{FT}\{\Omega(\mathbf{u})\}$, which can be compared to a delta function (Note 3.1). Thus,⁹

$$\text{FT}\{h(\mathbf{u})\} = \text{FT}\{\varrho [g(\mathbf{u}) - 1]\} * \underbrace{\text{FT}\{\Omega(\mathbf{u})\}}_{= \delta(\mathbf{q})} + \varrho \underbrace{\text{FT}\{\Omega(\mathbf{u})\}}_{= 0 \text{ for } Q \neq 0} \simeq \text{FT}\{\varrho [g(\mathbf{u}) - 1]\}, \quad (3.36)$$

justifying the absence of volume effects in the intensities scattered by systems of weakly correlated particles, as seen in the intensities at $n_x = \pm 1$ and ± 2 in Fig. 3.13.

The scattered intensity by systems presenting correlations on length scale of a few neighboring particles is therefore given by

$$I(\mathbf{Q}) = N I_{Th} P(\mathbf{Q}) [1 + \varrho \text{FT}\{g(\mathbf{u}) - 1\}]. \quad (3.37)$$

Although in many systems the particles are in motion, such as in a liquid, the large number of particles ensures instant arrangements statistically equivalent among themselves. Thus, provided that the system is in thermal equilibrium, the dynamics of the particles will not affect the scattered intensity. This means that the intensity curves collected over long periods of time have line profiles that can be simulated based on instantaneous arrangements.

In cases where the scattering power of the particles is known, intensity measurements allow accessing the interference function,¹⁰

$$S(\mathbf{Q}) = \frac{I(\mathbf{Q})}{N I_{Th} P(\mathbf{Q})} = 1 + \varrho \text{FT}\{g(\mathbf{u}) - 1\}, \quad (3.38)$$

thus leading to experimental methods of determining the correlation function $g(\mathbf{u})$.

...

Exercise 3.1. Show analytically that $\sum_{n,m \neq n} \exp(i\mathbf{Q} \cdot \mathbf{r}_{nm}) \propto |\text{FT}\{s(\mathbf{r})\}|^2$ or a system of N noninteracting particles in a volume V , whose contour is defined by the shape function $s(\mathbf{r})$.

Answer: Comparing the FTs of (3.33) and (3.34), and recalling that in the absence of correlations $g(\mathbf{u}) = 1$, it follows from Note 3.1 that

⁹The convolution of two FTs is done in a variable \mathbf{q} , (1.32), and when one of them is a delta function, the other FT remains unchanged.

¹⁰In disperse systems, the structural function $S(\mathbf{Q})$ is associated with the internal structure of the particles, such as in (2.8). In literature, it is common to represent the interference function arising from the mutual interference between particles also with $S(\mathbf{Q})$, which is the same symbol, a similar meaning, but in slightly different context.

$$\frac{1}{N} \sum_{n, m \neq n} e^{i Q \cdot r_{nm}} = \varrho \text{FT}\{\Omega(\mathbf{u})\} = \frac{\varrho}{V} |\text{FT}\{s(\mathbf{r})\}|^2. \quad \text{Q.E.D.}$$

Exercise 3.2. Calculate the interference function $S(Q)$ corresponding to the function $g(\mathbf{u})$ given in Fig. 3.14. Is the result compatible to that seen in Fig. 3.13?

Answer: Assuming that there are correlations along the direction \hat{x} only, so that $g(\mathbf{u}) = g(u_x)$. With $\hat{s} = \hat{z}$ as the incident beam direction, and $\hat{s}' = [\sin \gamma, 0, \cos \gamma]$ the direction of scattered radiation with γ being the scattering angle 2θ ,

$$Q = \frac{2\pi}{\lambda} (\hat{s}' - \hat{s}) = \frac{2\pi}{\lambda} [\sin \gamma, 0, \cos \gamma - 1] = [Q_x, 0, Q_z].$$

Limiting the scattering angle such that $Q_z \approx 0$, and recalling that $g(u_x)$ is an even function, (3.38) leads to

$$S(Q_x) \simeq 1 + 2\varrho_L \int [g(u_x) - 1] \cos(Q_x u_x) du_x \quad (3.39)$$

where ϱ_L stands for a linear density of particles along the direction \hat{x} . The amplitude of the interference signal observed along Q_x in Fig. 3.13 is well reproduced for $\varrho_L \simeq 0.85/a$, as shown in Fig. 3.15.

...

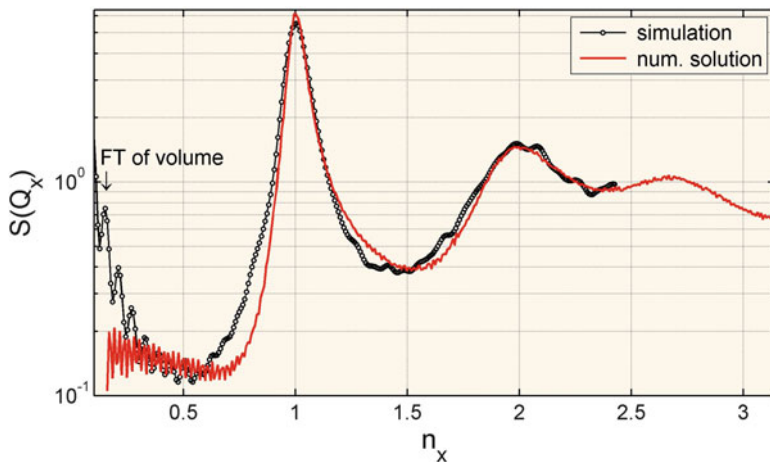


Fig. 3.15 Interference signal as a function of $n_x = (a/2\pi)Q_x$, Fig. 3.13 (simulation), compared to (3.39) (num. solution) [exgofu2.m]

3.2.3 Liquids and Colloidal Suspensions

Systems where the expression of the intensity given in (3.37) is valid are mostly isotropic systems where $g(\mathbf{u}) = g(u)$. The little correlation between the particles—a condition implied in the deduction of (3.37)—comes from weak interaction potentials, unable to induce preferred orientations in the systems. Consequently, the scattered intensity $I(Q) = N I_{Th} P(Q) S(Q)$ depends only on the module Q of the reciprocal vector, just as in

$$S(Q) = 1 + \varrho \text{FT}\{g(u) - 1\} = 1 + 4\pi\varrho \int_0^\infty [g(u) - 1] u^2 \frac{\sin(Qu)}{Qu} du. \quad (3.40)$$

The correlation length scale of the system, u_L , from which $g(u > u_L) = 1$ is the parameter that actually defines the extension, or upper limit, of the integral above.

In situations where $S(Q)$ is experimentally accessible, the function $g(u)$ is obtained by the inverse FT operation, i.e. $\varrho [g(u) - 1] = \text{FT}^{-1}\{S(Q) - 1\}$, whose solution of the angular part ends up as

$$4\pi\varrho u[g(u) - 1] = \frac{2}{\pi} \int_0^{Q_f} [S(Q) - 1] Q \sin(Qu) dQ. \quad (3.41)$$

The integral is truncated in Q_f because of the particular conditions of each instrumental apparatus.

Different names can be found in the literature for function $g(u)$ depending on area of study or sample type. In the study of liquids and colloidal suspensions, $g(u)$ is commonly called radial distribution function (RDF), or also pair correlation function, which can be calculated by the theory of liquids, statistical mechanic methods, and computer simulation (Guinier and Fournet 1955; Hansen and McDonald 1990; Lindner and Zemb 2002). In liquids, when formed by simple molecules where it is possible to estimate $P(Q)$ a priori, experimental intensity data lead to $S(Q)$. That is not the case, for instance, of biological molecules in solution that may present significant morphological changes in relation to the known crystalline structure (Protein Data Bank: <http://www.pdb.org/>). One of the objectives in modeling conformation processes, or unfolding, of proteins in a solution is to estimate $P(Q)$ so as to then arrive at the interference function $S(Q)$ and hence the interaction potential (Barbosa 2008).

...

Exercise 3.3. The peculiar physical properties of water, such as high boiling point, are due to the hydrogen bonds that exist between the molecules. Each molecule is bound to the other three, and the bond equilibrium distance is around 2.8 \AA in liquid water. From an RDF for water at normal temperature and pressure conditions

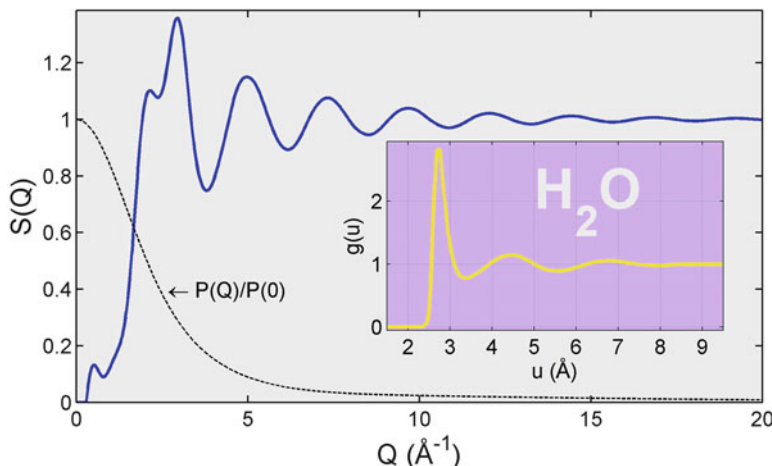


Fig. 3.16 Interference function $S(Q)$ (blue line) for liquid water according to a given RDF shown in the inset. $P(Q) = |f(Q)|^2$ where $f(Q)$ is the atomic scattering factor of the ion O^{2-} for which $|f(0)|^2 \simeq 100$. $\varrho = 3.346 \times 10^{-2}$ molecules/ \AA^3 [exwaterSofQ.m]

(NTP) find: (a) the interference function $S(Q)$; and (b) the scattered intensity over a flat area detector.

Answer (a): With the function $g(u)$ in hands,¹¹ the interference function in Fig. 3.16 is obtained from (3.40) with $\varrho = (N_A \div 18)/\text{cm}^3 = 3.346 \times 10^{-2}$ molecules/ \AA^3 .

Answer (b): In the H_2O molecule the hydrogen electrons complete the 2p orbital of oxygen so that an approximate calculation of the scattering intensity consists in taking into account the atomic scattering factor of ion O^{2-} , routine `ASFQ.m` in Appendix B. The ionic charge produces a significant difference in the interval $Q < 4 \text{\AA}^{-1}$ since $|f_O(0)|^2 \simeq 64$ while $|f_{O^{2-}}(0)|^2 \simeq 100$. Figure 3.17 shows simulated intensity according to $I(Q) = N I_{Th} P(Q) S(Q)$, given in number of photons scattered over the detector area.

...

3.2.4 Radial Distribution Function

Given a static distribution of N particles, such as those generated by computer simulation, the corresponding RDF is obtained by comparing (3.33) and (3.34),

¹¹ Although the general aspects of the RDF of liquid water were taken from Hura et al. (2003), the interference function $S(Q)$, especially in the interval $Q < 2 \text{\AA}^{-1}$, is very sensitive to the accuracy of function $g(u)$. Therefore, the scattering simulated in this exercise should not be considered an exact reproduction of the water's experimental scattering at NTP.

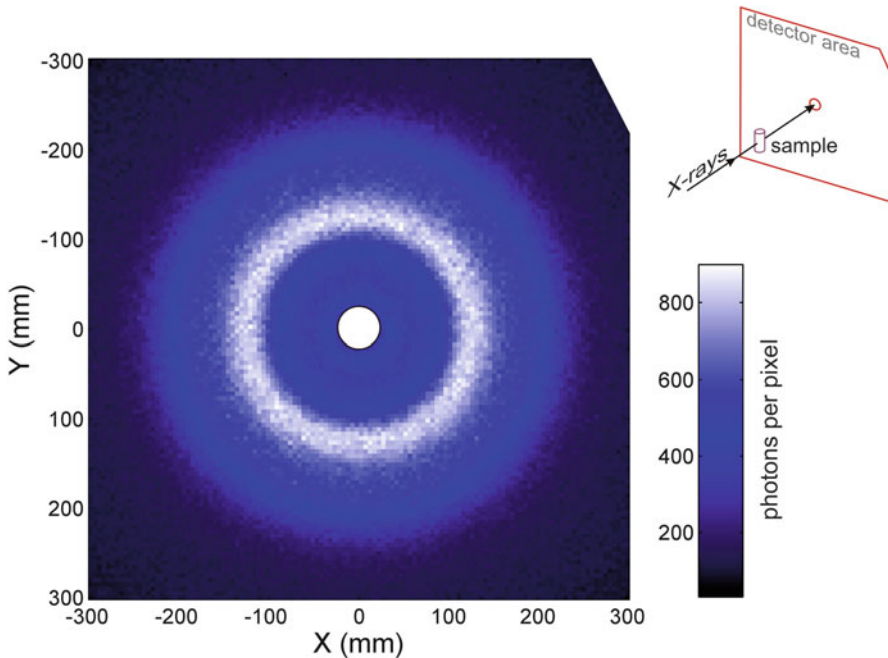


Fig. 3.17 X-ray scattering in liquid water (NTP). Area detector positioned at 37.2 cm from the sample. Image simulation for a statistic of 5×10^6 counts. Photons of 12 keV, pixel of 5 mm [exwaterccd.m]

$$h(\mathbf{u}) = \Omega(\mathbf{u}) \varrho g(\mathbf{u}) = \frac{1}{N} \sum_{n, m \neq n} \delta(\mathbf{u} - \mathbf{r}_{nm}) .$$

As the volume function is close to unit, $\Omega(\mathbf{u}) \simeq 1$, on the variation scale of the function $g(\mathbf{u})$, there is a subset of N' particles whose frequency with which the separations \mathbf{r}_{nm} occur are not affected by the sample's finite volume. Within this subset, isotropic systems¹² have the RDF estimated as

$$g(u) = \frac{1}{4\pi u^2 \varrho N'} \sum_{n=1}^{N'} \sum_{m \neq n}^N \delta(u - r_{nm}) . \quad (3.42)$$

In practice, the numerical calculation of RDF is done with the following recipe. First you calculate the number of separations with values between u and $u + \Delta u$ through the histogram

¹²In isotropic systems, $g(\mathbf{u}) dV_u \rightarrow 4\pi u^2 g(u) du$.

$$H_n(u) = \sum_{m \neq n}^N \int_u^{u+\Delta u} \delta(u' - r_{mn}) du'$$

using as a reference the particle at the center of distribution with a vector position \mathbf{r}_n where $r_{mn} = |\mathbf{r}_m - \mathbf{r}_n|$. Choosing another $N' - 1$ different particles, also around the center of the distribution, we arrive at the average histogram

$$H(u) = \frac{1}{N'} \sum_{n=1}^{N'} H_n(u) .$$

The higher the N' , the better the statistic with which $H(u)$ is determined. But if N' is very large, close to the total number of particles, then the fact of the distribution being finite will be present in $H(u)$ even for values of u as small as the distances between the nearest neighbors.

In a system without correlations, the number of separations between u and $u + \Delta u$, using any particle as a reference, is given by $H_0(u) = \varrho 4\pi u^2 \Delta u$. Then, according to the definition of function $g(u)$, Note 3.1,

$$g(u) = \frac{H(u)}{H_0(u)} = \frac{1}{4\pi u^2 \varrho N' \Delta u} \sum_{n=1}^{N'} H_n(u) . \quad (3.43)$$

It is important to keep in mind that the RDF to be used in (3.40), which is the one responsible for the scattering of X-rays, has to do with very large systems without statistical fluctuations. The statistical fluctuations appear in the sampling process when trying to get to the RDF from small finite set of particles. A strategy to improve the resolution of the RDF is to take the average of several finite distributions frozen in time and statistically equivalent.

...

Exercise 3.4. Generate random positions \mathbf{r}_n within a volume V and exclude one of every two whose separation $r_{mn} = |\mathbf{r}_m - \mathbf{r}_n|$ is less than a certain value d . (a) What is the maximum density of positions that can be obtained with such a criterion of exclusion? (b) How does the finiteness of the distributions affect the RDF calculated by (3.43)?

Answer (a): Generating N_i initial random positions within a volume V and then eliminating one position from every two with a separation less than d , there will be N_f final positions left in the volume where $r_{mn} \geq d$. With $N_i \rightarrow \infty$, N_f tends toward a limit value in accordance with the expression

$$N_f = N_{max}(1 - e^{-\alpha N_i}) . \quad (3.44)$$

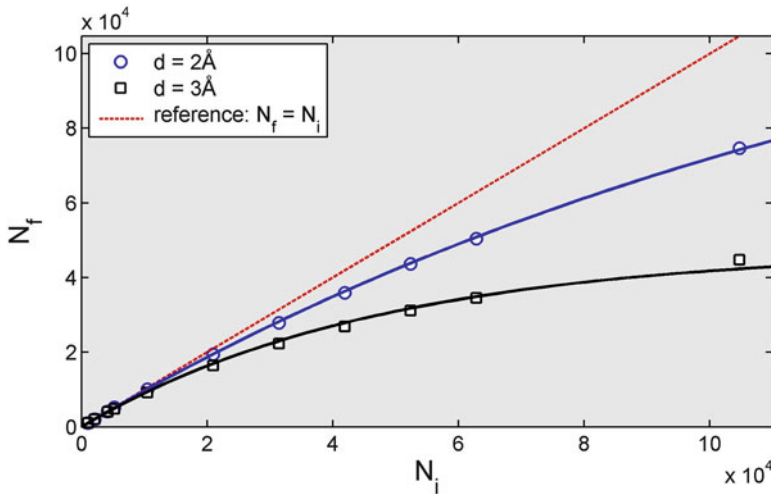


Fig. 3.18 Final number N_f of positions with separations $r_{mn} \geq d$, obtained from the initial distribution of N_i random positions within a spherical volume with a radius of 100\AA . Curves adjusted by (3.44) with $\alpha = 0.7 \times 10^{-5}$ ($d = 2\text{\AA}$) and $\alpha = 2.1 \times 10^{-5}$ ($d = 3\text{\AA}$) [exrdffitting.m]

When $\alpha N_i \ll 1$, $N_f \rightarrow N_i$ so that $N_{max} = \alpha^{-1}$. Figure 3.18 shows the analyses for two values of d , implying in a maximum density of the order of $\varrho = 1.3/v_d$ where $v_d = 4\pi d^3/3$ is the volume of exclusion around each position.

Answer (b): The region $u \gtrsim d$, Fig. 3.19, is very affected by statistical fluctuations, which are minimized by calculating the average histogram $H(u)$, (3.43), on a large number of positions. On the other hand, the more positions are used in relation to the total number in the distribution, the reduction of $g(u)$ due to the finite volume (inset of Fig. 3.19) occurs for continually smaller values of u . In quantitative terms, if the distribution occupies a spherical volume of radius R and the positions considered in $H(u)$ are contained in a sub-volume of radius R' , the decrease of $g(u)$ starts around $u \simeq R - R'$.

Exercise 3.5. Particles in solution may exhibit different behaviors depending on the solvent. (a) Derive the interference function $S(Q)$ between monomers (particles) in a solution of low concentration where the only interaction between them is the limitation imposed by the impenetrability of a monomer in another or, in general, by the existence of Colombian repulsion according to the hard sphere model.¹³ What is the most obvious effect of this limitation/repulsion? (b) If the monomers aggregate forming dimers, what happens to the scattered intensity?

¹³Hard sphere model: interaction potential is zero for $u \geq d$ and infinite for $u < d$ (Hansen and McDonald 1990).

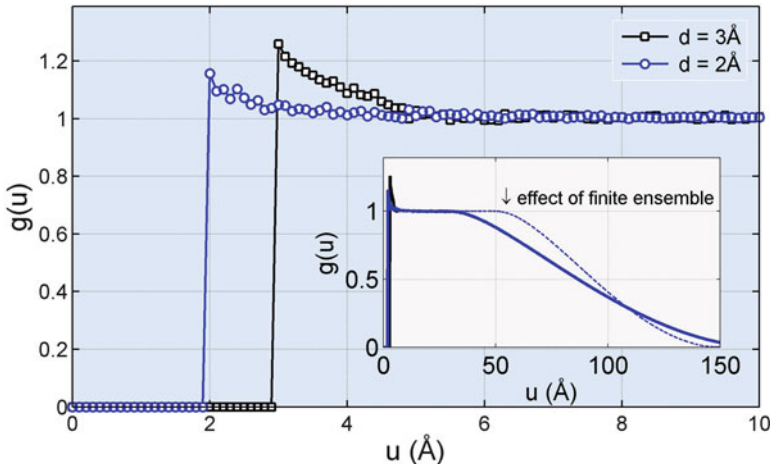


Fig. 3.19 RDFs for finite distributions of positions with separations $r_{mn} \geq d$, within a spherical volume of radius 100 Å containing around 43.4×10^3 ($d = 2$ Å) and 31.1×10^3 ($d = 3$ Å) positions. Inset: RDFs on an extended scale showing effects of finite volume for large values of u ; the average histogram in the (3.43) was calculated using the positions r_n around the center of the distributions in such a way that $r_n < 70$ Å (blue line) and $r_n < 50$ Å (blue dashed line). Each RDF corresponds to the average over ten different distributions statistically equivalent [exrdfplot.m]

Answer (a): The system in question is very similar to systems without correlations (disperse systems) where $g(u) = 1$, except that separations with values $u < d$ do not occur in the system and, therefore, $g(u < d) = 0$ where d is the smallest center-to-center distance possible between two monomers, Fig. 3.20a. It follows from (3.40) that

$$S(Q) = 1 - 4\pi\varrho \int_0^d u^2 \frac{\sin(Qu)}{Qu} du = 1 - 8\varrho v \Theta(Qd), \quad (3.45)$$

$\Theta(Qd) = 3[\sin(Qd) - Qd \cos(Qd)]/(Qd)^3$ corresponds to the FT of a sphere with a radius d as shown in Exercise 1.6(b), and $v = \pi d^3/6$ is the effective volume of a monomer, which is 1/8 of the exclusion volume v_d defined in Exercise 3.4(a).

The greatest repulsion effect between the monomers occurs in the small Q region where $\Theta(Qd) \rightarrow 1$ and $S(Q) \rightarrow S(0) = 1 - 8\varrho v$, causing a negative deflection in the intensity's profile as can be seen in Fig. 3.21. The magnitude of the deflection depends on the packing factor ϱv , which increases with the concentration. See Note 3.2 about the validity of (3.45).

Answer (b): If $I_m(Q) = N I_{Th} P(Q)$ is the intensity scattered by a disperse system of monomers where $\varrho v \ll 1$, the system's dimerization implies in:

$$N P(Q) \rightarrow \frac{N}{2} P_d(Q) \approx N P(Q) \left[1 + \frac{\sin Qd}{Qd} \right]$$

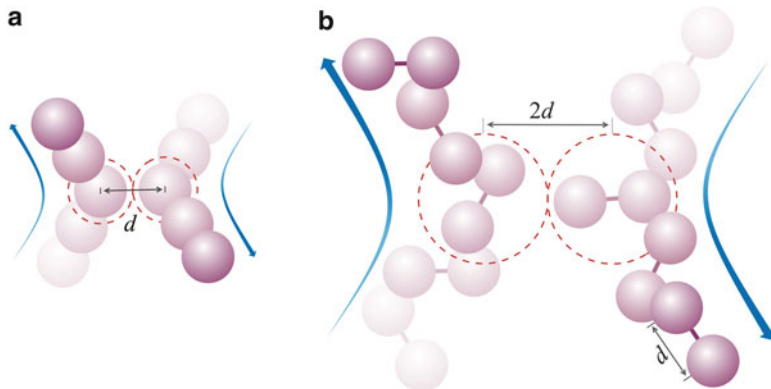


Fig. 3.20 Collision of (a) monomers and (b) dimers with distances of maximum approximation equal to d and $2d$, respectively

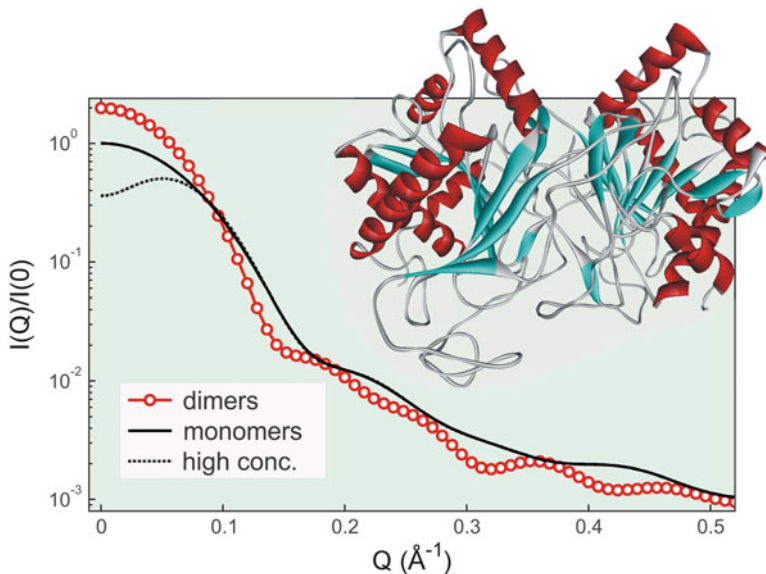


Fig. 3.21 Scattering curves in monomers and dimers. High concentration, $\varrho v = 0.08$, of monomers cause deflection in the scattering curve of around $Q = 0$, while the dimer formation tends to increase the scattering in this region. *Inset:* dimer of the enzyme H166G (PDB ID: 1GUP) taken as an example, gyration radius $R_g = 24.8 \text{ \AA}$ [ex1GUP.m]

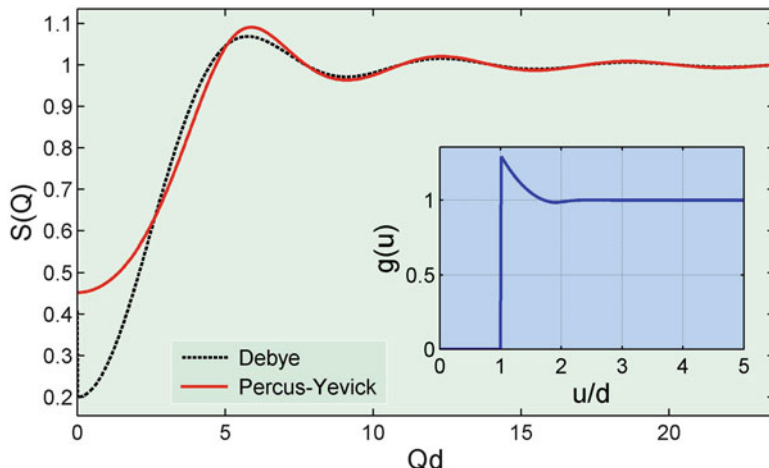


Fig. 3.22 Interference functions for hard spheres with a packing factor $\varrho v = 0.1$. Approximate solution (Debye) where $g(u \geq d) = 1$, (3.45), compared to a solution by statistical mechanics (Percus–Yevick) whose RDF is shown in the *inset* [exhardssphere.m]

provided that d becomes the center-to-center distance of monomers in the dimers and that this distance is much greater than the length scale of variation in the monomer's internal structure when forming a dimer, as depicted in Fig. 3.20b.

The constructive interference of the electric fields scattered by the monomers that form a dimer increases the scattering power $P_d(Q)$ of the dimer by a factor of 4 around $Q = 0$, resulting in a factor of 2 in the increase of intensity due to the number of dimers being half the number of monomers. This effect is general and independent of the validity of the above approach where $P_d(Q) \approx 2P(Q)[1 + \sin(Qd)/Qd]$. See, for example, Fig. 3.21 where the scattering by monomers and dimers are compared.

...

Note 3.2: Packing Factor Without Ordering. Known as the Debye solution (Giacovazzo 2002; Guinier and Fournet 1955), (3.45) is satisfactory in the region $Qd > 2$ only for low concentrations with a packing factor of hard spheres $\varrho v < 0.1$, cf. Fig. 3.22. The approach $g(u \geq d) = 1$ used in the deduction of (3.45) corresponds to a limit situation $\varrho v \rightarrow 0$. As ϱv increases, the value of the RDF just above $u = d$ also increases, as seen in the RDFs in Fig. 3.19. The density limit $\varrho = 1.3/v_d = 0.16/v$, found in Exercise 3.4(a), indicates that packing factors $\varrho v < 0.16$ are possible without there being a structural ordering—the maximum value is 0.74 (close-packing of spheres, crystal systems). Theoretical RDFs for the hard sphere model are obtained through classical statistical mechanics, Percus–Yevick solution (Lindner and Zemb 2002).

3.2.5 Amorphous

Solid materials without atomic ordering are commonly referred to as amorphous. The absence of order does not imply in the absence of short-range correlations, which are responsible for the few relatively well-defined contributions present in the RDF of an amorphous. These correlations are characteristics of more stable chemical bonds in the molecules of the material. Most of the amorphous contain various atomic species, which give rise to various RDFs from and among the various chemical elements present in them. But, in terms of structural analysis by X-rays, what is the relative contribution of each RDF in the radiation scattering and what is the RDF obtained by the Fourier analysis (inverse FT) of the experimental data? These are the questions that we will address in this section.

The RDFs of systems with multiple chemical species follow directly from (3.42) as being

$$g_{\alpha\beta}(u) = \frac{1}{4\pi u^2 \varrho_\beta N'_\alpha} \sum_{a \in \{\alpha\}} \sum_{b \in \{\beta\}}^{N'_\alpha} \delta(u - r_{ab}) . \quad (3.46)$$

N'_α is the subset of atoms of the element α around the center of the sample that makes it possible to calculate the RDF without effects of volume, while ϱ_β is the mean number density of the atoms of the element β , and N_β the number of atoms of this element considered in the calculation of RDF. According to this definition of RDF, the coordination number, which is the number of atoms β in a spherical shell with a radius ranging from u_1 to u_2 around an atom α is given by

$$N_\beta(\alpha) = \varrho_\beta \int_{u_1}^{u_2} 4\pi u^2 g_{\alpha\beta}(u) du . \quad (3.47)$$

To properly consider the contribution of each RDF, it is necessary to use as a starting point the general correlation function in (3.2), which is $C(\mathbf{u}) = \rho(\mathbf{r}) * \rho(-\mathbf{r})$, where the electron density

$$\rho(\mathbf{r}) = s(\mathbf{r}) \sum_\alpha \rho_\alpha(\mathbf{r}) * q_{0\alpha}(\mathbf{r}) , \quad (3.48)$$

contains the explicit representation of the different chemical species present in the sample by the density $\rho_\alpha(\mathbf{r})$ of electrons in the electron cloud of the element α . $\text{FT}\{\rho_\alpha(\mathbf{r})\} = f_\alpha(Q)$ is therefore the atomic scattering factor of this element. In a medium of infinite extension, $q_{0\alpha}(\mathbf{r}) = \varrho_\alpha f_\alpha(\mathbf{r})$ describes the spatial configuration of the atoms α in terms of the fluctuation $f_\alpha(\mathbf{r})$ of the mean number density of these atoms, ϱ_α . The finite extension of volume V scattering radiation with phase coherence is imposed by the shape function $s(\mathbf{r})$. Thus, in a procedure analogous to that used in Note 3.1, for $u \neq 0$, we reach

$$\begin{aligned} C(\mathbf{u}) &= V \Omega(\mathbf{u}) \sum_{\alpha, \beta} f_\alpha(Q) f_\beta^*(Q) \varrho_\alpha \varrho_\beta \frac{1}{v} \int_v f_\alpha(\mathbf{r}) f_\beta(\mathbf{r} + \mathbf{u}) dV = \\ &= V \Omega(\mathbf{u}) \sum_{\alpha, \beta} f_\alpha(Q) f_\beta^*(Q) \varrho_\alpha \varrho_\beta g_{\alpha\beta}(\mathbf{u}) = V \Omega(\mathbf{u}) w^2 g(\mathbf{u}) . \end{aligned} \quad (3.49)$$

The intensity scattered by the sample is given by $I(Q) = I_{Th} \text{FT}\{C(\mathbf{u})\}$, and due to this $\varrho_\alpha(\mathbf{r})$ already appear substituted by $f_\alpha(Q)$ in (3.49) whereas the FT of a convolution results in a product of FTs such as $\text{FT}\{\varrho_\alpha(\mathbf{r}) * \varrho_\beta(-\mathbf{r})\} = f_\alpha(Q) f_\beta^*(Q)$, (1.31).

As every amorphous medium is supposedly isotropic, $g_{\alpha\beta}(\mathbf{u}) = g_{\alpha\beta}(u)$ are the RDFs defined in the (3.46). Furthermore, since in the case of a homogeneous medium where all the interatomic distances are equally probable, $g_{\alpha\beta}(u) = 1$ as well as the total RDF of the system

$$g(u) = \frac{1}{w^2} \sum_{\alpha, \beta} f_\alpha(Q) f_\beta^*(Q) \varrho_\alpha \varrho_\beta g_{\alpha\beta}(u) , \quad (3.50)$$

a condition that is satisfied as long as

$$w^2 = \sum_{\alpha, \beta} f_\alpha(Q) f_\beta^*(Q) \varrho_\alpha \varrho_\beta . \quad (3.51)$$

The non-zero term of the correlation function for $u = 0$ describes the scattering in the case of a system without correlations so that the full expression of the correlation function is

$$C(\mathbf{u}) = \varrho V f_m^2(Q) \delta(u) + V \Omega(\mathbf{u}) w^2 g(u)$$

where $\varrho V = N_{at}$ is the total number of atoms in the volume V and $\varrho = \sum_\alpha \varrho_\alpha$. So,

$$I(Q) = I_{Th} \varrho V f_m^2(Q) S(Q) + I_{Th} \varrho V \langle S(Q, Z) \rangle \quad (3.52)$$

is the intensity scattered by the amorphous where

$$S(Q) = 1 + \frac{w^2}{\varrho f_m^2(Q)} [\text{FT}\{g(u) - 1\} * \text{FT}\{\Omega(\mathbf{u})\} + \text{FT}\{\Omega(\mathbf{u})\}] \quad (3.53)$$

and $\langle S(Q, Z) \rangle = \sum_\alpha \varrho_\alpha S(Q, Z_\alpha) / \varrho$ is the average Compton scattering per atom in the cases when it is necessary to account for the background noise due to incoherent scattering.

In a sample with macroscopic dimensions, the exact shape of the sample ceases to be important since $\text{FT}\{\Omega(\mathbf{u})\} \simeq \delta(q)$, Note 3.1, for any direction of the scattering vector. The structural signal away from the direct beam becomes dependent only

on the Q module of the reciprocal vector, reflecting the isotropy of the amorphous medium, i.e.

$$S(Q) = 1 + \frac{w^2}{\varrho f_m^2(Q)} \text{FT}\{g(u) - 1\} = 1 + 4\pi \frac{w^2}{\varrho f_m^2(Q)} \int_0^\infty [g(u) - 1] u^2 \frac{\sin(Qu)}{Qu} du . \quad (3.54)$$

In the case of amorphous made up by a single element, $w^2 = \varrho^2 |f(Q)|^2$, $f_m^2(Q) = |f(Q)|^2$, and $w/f_m = \varrho$. When there are several elements, it is also possible to use $w/f_m \simeq \varrho$ (a fact that is verified numerically), allowing in general to approximate the expression $S(Q)$ to the one in (3.40).

Inverse FT operation of the experimental curve $S(Q)$,

$$4\pi\varrho u[g(u) - 1] \simeq \frac{2}{\pi} \int_0^{Q_f} [S(Q) - 1] Q \sin(Qu) dQ , \quad (3.55)$$

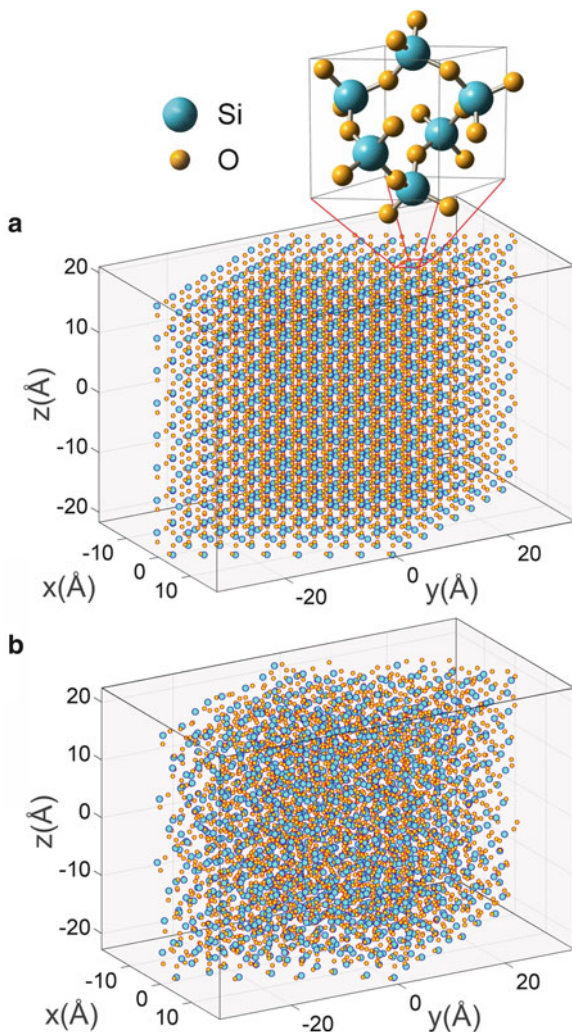
leads to the experimental function $g(u)$. The expression of $g(u)$ in (3.50) is suitable for the calculation of $S(Q)$ since atomic electron densities already appear as atomic scattering factors. But the actual RDF of the system has very little difference with the $g(u)$ calculated for $Q = 0$, which is to say that experimental $g(u)$ is equivalent to the theoretical one calculated with $f_a(0)$, or with $f_a(0) + f'_a(\mathcal{E}) + if''_a(\mathcal{E})$ when atomic resonance effects are relevant. Anyway, it is worth emphasizing that $g(u)$ is not exactly an RDF of atomic positions, but a weighted sum of the various RDFs that exist in a multi-element amorphous, or a RDF of the fluctuation in the average electron density of the material.

3.2.5.1 Crystallization of Amorphous Solids

In order to strengthen the concepts implicit in the equations presented above, (3.46)–(3.55), it would be very useful if we could generate amorphous through computer simulation. But this is a task that requires molecular dynamics calculation where the potentials of the interatomic interactions are taken into account. Still, there is a limitation of the number of atoms that the current computers can deal with these programs. To overcome these difficulties, we have a relatively simple routine, Note 3.4, that generates atomic structures with varying degrees of disorder from a known crystal structure. Here we use as an example of the structure of α -quartz (SiO_2), Fig. 3.23.

Generating disordered structures is one way to obtain RDFs with aspects that are similar to those of an amorphous where only the distances between nearest neighbors are clearly resolved, e.g. Fig. 3.24. However, since each structure represents one of many statistically equivalent regions that make up the macroscopic medium (sample), the absence of preferred orientations of the regions ensures the system's isotropy independently of the degree of ordering. This makes it possible to experience a procedure analogous to the crystallization of the amorphous solids with

Fig. 3.23 Atomic structure of α -quartz (SiO_2): (a) ordered periodic and (b) disordered. *Inset*: unit of repetition of the periodic structure [quartzR.m]



the gradual appearance of diffraction peaks, which show constructive interference conditions occurring at wide angles due to the phenomenon of periodic ordering of the structure. When the regions are large enough, the intensity profiles are obtained from (3.52) and (3.54), as observed in Figs. 3.25 and 3.26 (inset) without effects from the finite sizes of the diffracting regions.

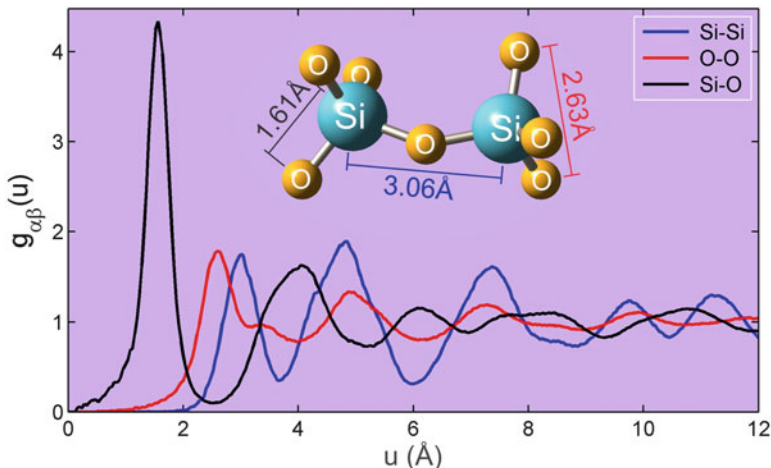


Fig. 3.24 RDFs of the atomic structure of α -quartz with a disorder of 8 %. Insertion: oxygen tetrahedra with silicon in the center and the distances between nearest neighbors [quartzrdfplot.m]

Note 3.4: Disordering Periodic Structures. If \mathbf{a} , \mathbf{b} , and \mathbf{c} stand for the edges of the repeating element, also known as unit cell, of a periodic ordered structure and $\mathbf{r}_a = x_a \mathbf{a} + y_a \mathbf{b} + z_a \mathbf{c}$ are the position vectors of the atoms inside the repeating element, then (x_a, y_a, z_a) are the fractional coordinates along the edges. The convolution of the repeating element with a three-dimensional lattice of points $\mathbf{R}_{m,n,p} = m\mathbf{a} + n\mathbf{b} + p\mathbf{c}$, with $m, n, p \in \mathbb{Z}$, generates a periodic atomic structure of a crystal, as shown in Chap. 4. The disordered structure is obtained from a lattice of points $\mathbf{R}_{m,n,p}$ where adjacent points satisfy the relation

$$\frac{(\mathbf{R}_{m',n',p'} - \mathbf{R}_{m,n,p}) \cdot \mathbf{x}}{|\mathbf{x}|^2} = 1 + \alpha w .$$

The routine `quartzR.m` implements this method of generating disordered structures for the α -quartz whose repeating element, Fig. 3.23 (inset), contains three atoms of silicon and six of oxygen, $\mathbf{a} = a [\cos(\pi/3), \sin(\pi/3), 0]$, $\mathbf{b} = a [\cos(\pi/3), -\sin(\pi/3), 0]$, and $\mathbf{c} = c [0, 0, 1]$ where $a = 4.9134 \text{ \AA}$ and $c = 5.4052 \text{ \AA}$. The volume of the repeating element is $(\mathbf{a} \times \mathbf{b}) \cdot \mathbf{c} = 113 \text{ \AA}^3$. Note: The structures generated by the method are only resources for the practice of introducing X-ray scattering through non-crystalline solids and should not be taken as physically feasible structures.

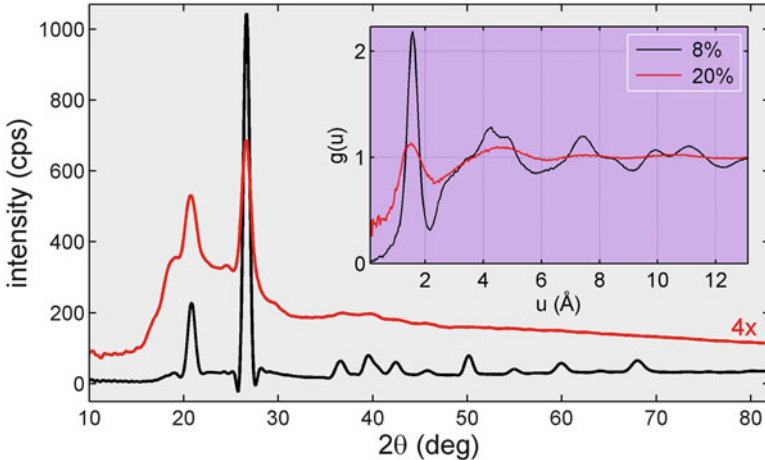


Fig. 3.25 Simulations of the intensities scattered by α -quartz with disorders of 8 % (black line) and 20 % (red line), (3.52) and (3.54). X-rays of 8 keV and flux such that $I_{Th}V\varrho = 1$ cps. Inset: $g(u)$ calculated with $Q = 0$ in (3.50) [quartzlofQ.m]

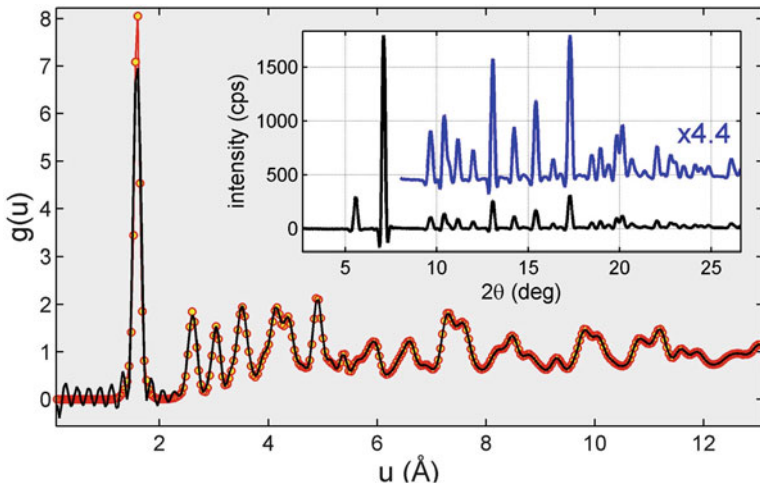


Fig. 3.26 RDF obtained by inverse FT (black line) of $S(Q)$, (3.55), compared to the one calculated (red line with circles) for α -quartz with disorder of 2 %. 30 keV X-rays. Inset: simulation of the intensity scattered with $I_{Th}V\varrho = 1$ cps [quartzgofu.m]

The resolution of the structure from the scattering curve is affected by the experimental Q_f value, (3.55). Figure 3.26 demonstrates that in samples with reasonable levels of crystallization, 2 % of disorder in this example, even with experiments with a large Q_f , of the order of 30 \AA^{-1} , present differences between the experimental $g(u)$ and the theoretical one calculated by (3.50) in the small u region. Through the routine quartzgofu.m that generated Fig. 3.26, other resolution tests

can be done on the basis of both the structure's disorder as well as the Q_f value. The use of convolution function discussed in Note 3.3 minimizes oscillations with period $2\pi/Q_f$, but tends to decrease the resolution of the sharpest contribution in $g(u)$, which can also be checked with the above-mentioned routine.

Structural analysis via RDF, (3.55), is suitable for low order systems like non-crystalline solids where the diffraction peaks show no effects due to finite sample volume. With increasing order, the peaks become sharper and the approach $\text{FT}\{g(u) - 1\} * \text{FT}\{\Omega(\mathbf{u})\} \simeq \text{FT}\{g(u) - 1\}$ taken to reach (3.54) may not be enough to describe the scattered intensity by the system. The RDFs estimated from finite clusters and used to simulate the intensities patterns shown in Figs. 3.25 and 3.26 (inset) give rise to infeasible details such as negative intensities for the clusters with more order. These details should disappear when carrying out the convolution operation above mentioned or, alternatively, by simulating the intensity patterns via PDF, (3.18), with sums over all the atoms of the clusters to account for the effect of finite volume.

In practice, only samples with highly crystalline submicron regions, commonly called crystallites, configure situations where the effects of volume from the diffracting regions are noticeable. But in general there is no reason to study highly crystalline structures through RDF and PDF, which are only useful in the study of local order in systems with some kind of disorder (Egami and Billinge 2003). Local order in crystalline structures are well determined within the formalism of periodic lattices, as will be detailed in the next chapter. Furthermore, this formalism also enables direct association between diffraction peaks and element of periodicity giving rise to each peak. This situation is very different from the analysis by RDF or PDF. For example, in Fig. 3.25, try to find a physical explanation for both the position and the relative intensity of the diffraction peaks observed in $2\theta = 21.0^\circ$ and 26.8° . Notice how difficult it is to do this only from the RDF without any previous notion that you may have about periodic lattices.

...

Exercise 3.6. The only structural information accessible via X-ray scattering is the total RDF, $g(u)$. Determine from the $g(u)$ of SiO_2 (α phase) the coordination number of the first layer of oxygen around the silicon.

Answer: From (3.47),

$$N_{\text{O}}(\text{Si}) = \varrho_{\text{O}} \int_{u_1}^{u_2} 4\pi u^2 g_{\text{SiO}}(u) \, du .$$

In samples with good crystallization (disorder < 8 %, Fig. 3.24), the Si–O bond generates an isolated contribution in the interval $u < 2.2 \text{ \AA}$. Thus, the coordination number of the first layer is obtained in the interval $u_1 = 0$ and $u_2 = 2.2 \text{ \AA}$ where

$$g(u) \simeq \frac{1}{w^2} f_{\text{Si}} f_{\text{O}} \varrho_{\text{Si}} \varrho_{\text{O}} \underbrace{[g_{\text{SiO}}(u) + g_{\text{OSi}}(u)]}_{=2g_{\text{SiO}}(u)}$$

so that

$$N_{\text{O}}(\text{Si}) = \frac{w^2}{2f_{\text{Si}} f_{\text{O}} \varrho_{\text{Si}}} \int_0^{2.2 \text{\AA}} 4\pi u^2 g(u) du .$$

With $V_c = 113 \text{\AA}^3$ being the volume of the repeating element containing 3Si and 6O. Note 3.4, $\varrho_{\text{Si}} = 3/V_c$ and $\varrho_{\text{O}} = 6/V_c$. If $f_{\text{Si}} = 14$ and $f_{\text{O}} = 8$, then we arrive at

$$w^2 = f_{\text{Si}} f_{\text{Si}}^* \varrho_{\text{Si}}^2 + f_{\text{O}} f_{\text{O}}^* \varrho_{\text{O}}^2 + (f_{\text{Si}} f_{\text{O}}^* + f_{\text{Si}}^* f_{\text{O}}) \varrho_{\text{Si}} \varrho_{\text{O}} = 0.6344 \text{\AA}^{-6} .$$

For any $g(u)$ with little disorder, the numerical integral is worth 37.6\AA^3 and therefore

$$N_{\text{O}}(\text{Si}) = \frac{0.6344}{2(14)(8)(3/113)} 37.6 = 4.0 ,$$

which means that, in a radius of up to 2.2\AA around each silicon atom there are four oxygens, as seen in Fig. 3.24 (inset).¹⁴

...

Section Summary

— Intensity scattered by a system of identical particles with effects of mutual interference

$$I(\mathbf{Q}) = N I_{\text{Th}} P(\mathbf{Q}) [1 + \text{FT}\{h(\mathbf{u})\}]$$

— Reduced correlation function of the system

$$h(\mathbf{u}) = \frac{1}{N} \sum_{n,m \neq n} \delta(\mathbf{u} - \mathbf{r}_{nm}) = \Omega(\mathbf{u}) \varrho g(\mathbf{u})$$

— Scattered intensity without effects of volume from the sample

$$I(\mathbf{Q}) = N I_{\text{Th}} P(\mathbf{Q}) [1 + \varrho \text{FT}\{g(\mathbf{u}) - 1\}] = N I_{\text{Th}} P(\mathbf{Q}) S(\mathbf{Q})$$

— Interference function, or structural signal, of isotropic systems

¹⁴For more complex systems there are other methods for extracting the RDFs $g_{\alpha\beta}(u)$ from the experimental data. See, for example, Egami and Billinge (2003, Ch. 3, p. 64).

$$S(Q) = 1 + \varrho \text{FT}\{g(u) - 1\} = 1 + 4\pi\varrho \int_0^\infty [g(u) - 1] u^2 \frac{\sin(Qu)}{Qu} du$$

— Experimental RDF

$$g(u) = 1 + \varrho^{-1} \text{FT}^{-1}\{S(Q) - 1\} = 1 + \frac{1}{2\pi^2 u \varrho} \int_0^{Q_f} [S(Q) - 1] Q \sin(Qu) dQ$$

— Calculation of RDF for static distributions of identical particles

$$g(u) = \frac{1}{4\pi u^2 \varrho N'} \sum_{n=1}^{N'} \sum_{m \neq n}^N \delta(u - r_{nm}) = \frac{1}{4\pi u^2 \varrho N' \Delta u} \sum_{n=1}^{N'} H_n(u)$$

— RDFs of samples with different chemical species (distinct elements)

$$g_{\alpha\beta}(u) = \frac{1}{4\pi u^2 \varrho_\beta N'_\alpha} \sum_{a \in \{\alpha\}}^{N'_\alpha} \sum_{b \in \{\beta\}}^{N'_\beta} \delta(u - r_{ab})$$

— Total RDF of samples with many elements

$$g(u) = \frac{1}{\sum_{\alpha, \beta} f_\alpha(Q) f_\beta^*(Q) \varrho_\alpha \varrho_\beta} \sum_{\alpha, \beta} f_\alpha(Q) f_\beta^*(Q) \varrho_\alpha \varrho_\beta g_{\alpha\beta}(u)$$

Chapter 4

Crystals

The highly ordered matter at a molecular atomic level gives origin to crystals. In the history of modern science, the proof of the crystalline (ordered) form of matter occurred simultaneously with the demonstration that X-radiation was an electromagnetic radiation. One of the most important areas of applied physics, X-ray crystallography, was started by the diffraction of X-rays in a NaCl crystal (Bragg and Bragg 1913; Max von Laue 1913). To it we owe our current knowledge on the atomic structure of materials and proteins, including the structure of the double helix of deoxyribonucleic acid (DNA) (Franklin and Gosling 1953; Watson and Crick 1953; Wilkins et al. 1953).

In the study of non-crystalline materials by X-ray scattering (previous chapters of this book) where the atoms occupy positions not very correlated, structural modeling is difficult, significantly limiting the resolution of the structures analyzed. In crystals, this difficulty does not exist because the atoms are at specific sites, correlated by translation operations on macroscopic scales. The easy spatial description of the crystalline structures led to developing a unique mathematical treatment with specific terminologies for the analysis of crystalline materials. The periodicities present in a given structure, which is the numerous times that the same interatomic distance is repeated along the physical dimension of a crystal, generates intense diffracted beams at high angles, enabling the structural analysis of high resolution with low-flux compact radiation sources. This fact made it possible to accumulate knowledge of the crystalline structures at a time when there were no intense sources of radiation such as the synchrotron sources. These, in turn, have led to the determination with high spatial resolution (of the order of 1–3 Å) of complex structures such as most biological macromolecules known (Protein Data Bank: <http://www.pdb.org/>).

Although the mathematical description of crystals is relatively simple and precise, there are extremely difficult details to be treated theoretically. In the systems discussed previously—low correlated and complex systems—the absence of intense beams scattered at high angles made theoretical treatments possible without the

need to take into account the rescattering of radiation through the systems. In the case of crystals, this approach would only be, strictly speaking, acceptable in very small crystals with submicron dimensions. From a broader perspective, there are a number of factors that corroborate so that the kinematic approach of X-ray diffraction is satisfactory or not. Among the main factors are the size and perfection of the crystal, the coherence length of the radiation, and the photoelectric absorption. Perfect crystals with macroscopic dimensions represent a medium with periodic electron density. The exact description of the X-ray wave propagation in perfect crystals is made from solving Maxwell's Equations in a medium with periodic dielectric susceptibility. This description is given the name of Dynamical Theory of X-ray diffraction in crystals (Authier 2004). Dynamical because it takes into account the coupling of the incident and diffracted waves along the physical dimension of the samples, namely the successive rescattering of the X-ray waves as they propagate in the medium. Imperfections of the crystalline lattice minimize the rescattering of waves with phase coherence, but they do not eliminate possible rescattering of the diffracted intensities. In this chapter we will be seeing the Kinematic Theory, which is valid for small crystals similar to many of the samples used in structural determination. The amplitude of the incident wave is the same for the entire diffracting volume. The X-ray photons interact once with the atoms of the structure and the effects of rescattering and attenuation of the diffracted beams are negligible.

4.1 Elements of X-Ray Crystallography

4.1.1 Unit Cell and Crystalline Lattice

The remarkable feature in the description of the electron density of a crystal is the fact that the physical space is filled by an identical unit of repetition, which receives the name of unit cell, Fig. 4.1. When we take the unit cells and put one next to the other, we have the crystal. Mathematically this is done by the convolution of the electron density of the unit cell

$$\rho_{\text{cel}}(\mathbf{r}) = \sum_a^{N_{\text{at}}} \rho_a(\mathbf{r} - \mathbf{r}_a) , \quad (4.1)$$

with a discrete lattice of virtual points,

$$\mathbf{R}_{mnp} = m\mathbf{a} + n\mathbf{b} + p\mathbf{c} \quad \text{where } n, m, p \in \mathbb{Z} , \quad (4.2)$$

called crystalline lattice. \mathbf{a} , \mathbf{b} , and \mathbf{c} are the edge vectors of the unit cell whose volume is

$$V_{\text{cel}} = \mathbf{a} \cdot (\mathbf{b} \times \mathbf{c}) = \mathbf{b} \cdot (\mathbf{c} \times \mathbf{a}) = \mathbf{c} \cdot (\mathbf{a} \times \mathbf{b}), \quad (4.3)$$

and the positions $\mathbf{r}_a = x_a \mathbf{a} + y_a \mathbf{b} + z_a \mathbf{c}$ of the N_{at} atoms inside the unit cell given in terms of fractional coordinates x_a , y_a , and z_a .

In the expression of crystal's electron density

$$\rho_{\text{cryst}}(\mathbf{r}) = s(\mathbf{r}) \sum_{m,n,p} \rho_{\text{cel}}(\mathbf{r}) * \delta(\mathbf{r} - \mathbf{R}_{mnp}), \quad (4.4)$$

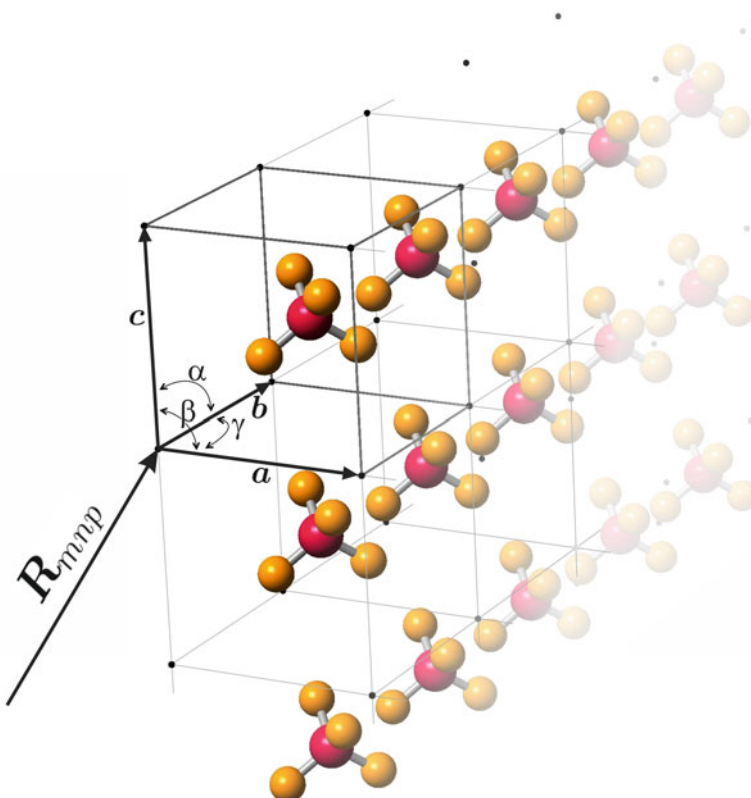


Fig. 4.1 Periodic lattice of points \mathbf{R}_{mnp} and unit cell of edges \mathbf{a} , \mathbf{b} , and \mathbf{c} , showing a tetrahedral group centered on the atomic fractional coordinates $(x, y, z) = (1/2, 1/2, 1/2)$ and with the other atoms at $(x - 0.15, y - 0.15, z - 0.15)$, $(x + 0.15, y + 0.15, z - 0.15)$, $(x + 0.15, y - 0.15, z + 0.15)$, and $(x - 0.15, y + 0.15, z + 0.15)$

the physical dimensions of the diffracting volume¹ are specified by the shape function $s(\mathbf{r})$ [$s(\mathbf{r}) = 1$ or 0 for \mathbf{r} inside or outside the considered volume, respectively], so that the sums of the integers m , n , and p extend from $-\infty$ to $+\infty$. Alternatively, finite sums can be considered, but this creates an extra difficulty in describing samples of different shapes from those defined by the edges of the unit cell.

The crystal's form factor,

$$F_{\text{cryst}}(\mathbf{Q}) = \text{FT}\{\rho_{\text{cryst}}(\mathbf{r})\} = \underbrace{\text{FT}\{\rho_{\text{cel}}(\mathbf{r})\}}_{F(\mathbf{Q})} \sum_{m,n,p} \text{FT}\{\delta(\mathbf{r} - \mathbf{R}_{mnp})\} * \underbrace{\text{FT}\{s(\mathbf{r})\}}_{W(\mathbf{Q})}, \quad (4.5)$$

brings together three different pieces of information to be analyzed separately. The FTs of the unit cell, $F(\mathbf{Q})$, and of the crystal's volume, $W(\mathbf{Q})$, will be discussed later. Here we analyze the FT of the crystalline lattice,

$$\sum_{m,n,p} \text{FT}\{\delta(\mathbf{r} - \mathbf{R}_{mnp})\} = \sum_{m,n,p=-\infty}^{+\infty} e^{i\mathbf{Q} \cdot \mathbf{R}_{mnp}} = \begin{cases} 0 & \text{if } \mathbf{Q} \cdot \mathbf{R}_{mnp} \notin 2\pi \mathbb{Z} \\ \infty & \text{if } \mathbf{Q} \cdot \mathbf{R}_{mnp} \in 2\pi \mathbb{Z}. \end{cases}$$

The reciprocal vectors that satisfy the condition $\mathbf{Q} \cdot \mathbf{R}_{mnp} \in 2\pi \mathbb{Z}$ form a set of vectors \mathbf{Q}_{hkl} called vectors of the crystal's reciprocal lattice, Note 4.1. As for this set of vectors, the sums above behave like delta functions considering that

$$\delta(\mathbf{Q} - \mathbf{Q}_{\text{hkl}}) = \begin{cases} 0 & \text{if } \mathbf{Q} \neq \mathbf{Q}_{\text{hkl}} \\ \infty & \text{if } \mathbf{Q} = \mathbf{Q}_{\text{hkl}}. \end{cases}$$

However, every delta function is normalized, i.e. $\int \delta(\mathbf{Q} - \mathbf{Q}_{\text{hkl}}) dV_Q = 1$. The normalization of the sums, Note 4.1, allows the substitution

$$\sum_{m,n,p} e^{i\mathbf{Q} \cdot \mathbf{R}_{mnp}} \rightarrow \frac{(2\pi)^3}{V_{\text{cel}}} \sum_{\text{h,k,l}} \delta(\mathbf{Q} - \mathbf{Q}_{\text{hkl}}) \quad (4.6)$$

where the new sums, now in h , k , and l , account for all possible vectors of the reciprocal lattice.²

¹The smallest of the crystal volume and the volume defined by radiation coherence lengths. For the sake of textual simplification, we will refer to diffracting volume only as crystal volume.

²Please, do not confuse this k index with the module k of the wavevector, which are distinguished by the used font and by the context in which they appear in the text.

Note 4.1: Reciprocal Lattice. The coherent intensity scattered by a crystal, which is called diffracted intensity, has only sharp maximums for the set $\{\mathbf{Q}_{\text{hkl}}\}$ of reciprocal vectors that are the reciprocal lattice vectors. So,

$$\mathbf{Q} \cdot \mathbf{R}_{mnp} = m\mathbf{Q} \cdot \mathbf{a} + n\mathbf{Q} \cdot \mathbf{b} + p\mathbf{Q} \cdot \mathbf{c} \in 2\pi\mathbb{Z}$$

is only possible for any $\mathbf{Q} \in \{\mathbf{Q}_{\text{hkl}}\}$ and any integer values of m , n , and p , if

$$\mathbf{Q} \cdot \mathbf{a} = 2\pi h, \quad \mathbf{Q} \cdot \mathbf{b} = 2\pi k, \quad \text{and} \quad \mathbf{Q} \cdot \mathbf{c} = 2\pi l \quad \text{where } h, k, l \in \mathbb{Z}.$$

The reciprocal lattice of a crystal as defined by the vectors $\mathbf{Q}_{\text{hkl}} = h\mathbf{a}^* + k\mathbf{b}^* + l\mathbf{c}^*$, corresponds to a lattice of discrete points with indices hkl and base vectors \mathbf{a}^* , \mathbf{b}^* , and \mathbf{c}^* , which satisfy the relationships: $\mathbf{a}^* \cdot [\mathbf{a}, \mathbf{b}, \mathbf{c}] = [2\pi, 0, 0]$, $\mathbf{b}^* \cdot [\mathbf{a}, \mathbf{b}, \mathbf{c}] = [0, 2\pi, 0]$, and $\mathbf{c}^* \cdot [\mathbf{a}, \mathbf{b}, \mathbf{c}] = [0, 0, 2\pi]$. These relations have as their solution

$$\mathbf{a}^* = 2\pi \frac{\mathbf{b} \times \mathbf{c}}{\mathbf{a} \cdot (\mathbf{b} \times \mathbf{c})}, \quad \mathbf{b}^* = 2\pi \frac{\mathbf{c} \times \mathbf{a}}{\mathbf{b} \cdot (\mathbf{c} \times \mathbf{a})}, \quad \text{and} \quad \mathbf{c}^* = 2\pi \frac{\mathbf{a} \times \mathbf{b}}{\mathbf{c} \cdot (\mathbf{a} \times \mathbf{b})}, \quad (4.7)$$

which are vectors that are perpendicular to the faces bc , ac , and ab of the unit cell, and define a reciprocal unit cell with a volume of $V_{\text{cel}}^* = \mathbf{a}^* \cdot (\mathbf{b}^* \times \mathbf{c}^*) = (2\pi)^3 / V_{\text{cel}}$.

— The demonstration of (4.6) requires integration of the triple sum in m , n , and p inside a small volume around a single hkl reciprocal lattice point. Writing $\mathbf{Q} = u\mathbf{a}^* + v\mathbf{b}^* + w\mathbf{c}^*$ such that

$$dV_Q = [du \mathbf{a}^* \cdot (dv \mathbf{b}^* \times dw \mathbf{c}^*)] = V_{\text{cel}}^* du dv dw,$$

and with $u \in [h - \zeta, h + \zeta]$, $v \in [k - \zeta, k + \zeta]$, and $w \in [l - \zeta, l + \zeta]$ where $0 < \zeta \ll 1$, we reach

$$\begin{aligned} & \int \left(\sum_{m,n,p} e^{i\mathbf{Q} \cdot \mathbf{R}_{mnp}} \right) dV_Q = V_{\text{cel}}^* \int \left(\sum_{m,n,p} e^{2\pi i(mu + nv + pw)} \right) du dv dw = \\ &= V_{\text{cel}}^* \int_{h-\zeta}^{h+\zeta} \left(\sum_{m=-\infty}^{+\infty} e^{2\pi imu} \right) du \int_{k-\zeta}^{k+\zeta} \left(\sum_{n=-\infty}^{+\infty} e^{2\pi inv} \right) dv \int_{l-\zeta}^{l+\zeta} \left(\sum_{p=-\infty}^{+\infty} e^{2\pi ipw} \right) dw = \\ &= V_{\text{cel}}^* \int_{h-\zeta}^{h+\zeta} \delta(u-h) du \int_{k-\zeta}^{k+\zeta} \delta(v-k) dv \int_{l-\zeta}^{l+\zeta} \delta(w-l) dw = V_{\text{cel}}^*. \end{aligned}$$

...

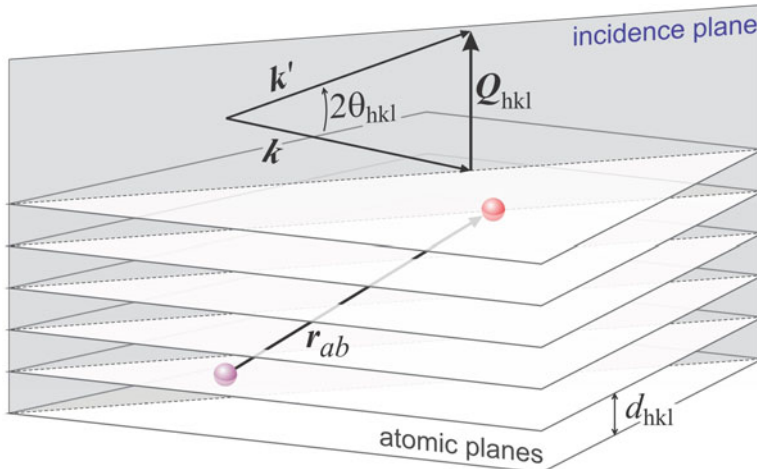


Fig. 4.2 Coherent scattering by atomic planes where $\mathbf{Q}_{\text{hkl}} \cdot \mathbf{r}_{ab} = 2\pi n$, with $n \in \mathbb{Z}$ and $d_{\text{hkl}} = 2\pi / Q_{\text{hkl}}$

Exercise 4.1. Bragg's law is the most famous equation in X-ray crystallography. (a) Show that each reciprocal lattice point (RLP) of indices hkl stands for set of atomic planes perpendicular to the reciprocal vector \mathbf{Q}_{hkl} and that the distance between adjacent planes is worth

$$d_{\text{hkl}} = \frac{2\pi}{Q_{\text{hkl}}} . \quad (4.8)$$

(b) What is the scattering angle associated with each RLP given in terms of the interplanar distance d_{hkl} ?

Answer (a): If \mathbf{Q}_{hkl} is the vector of active diffraction, the phase difference between the fields scattered by any two atoms with vector separation \mathbf{r}_{ab} will be $\Delta\phi = \mathbf{Q}_{\text{hkl}} \cdot \mathbf{r}_{ab}$, as shown in (2.1). Therefore, all atoms contained in the same plane perpendicular to the vector \mathbf{Q}_{hkl} scatter in phase since $\Delta\phi = 0$, as well as those contained in parallel planes separated by nd with $n \in \mathbb{Z}$, such that $\Delta\phi = \mathbf{Q}_{\text{hkl}} nd = 2\pi n$, Fig. 4.2. This requires however that $d = d_{\text{hkl}}$ in (4.8).

Answer (b): According to (1.39), $\mathbf{Q}_{\text{hkl}} = \mathbf{k}' - \mathbf{k}$, $Q_{\text{hkl}} = (4\pi/\lambda) \sin \theta_{\text{hkl}} = 2\pi/d_{\text{hkl}}$, and

$$2 d_{\text{hkl}} \sin \theta_{\text{hkl}} = \lambda , \quad (4.9)$$

which is the Bragg's law³ for the hkl reflection with scattering angle of $2\theta_{\text{hkl}}$, Fig. 4.2.

³The Bragg's law is many times written as $2d \sin \theta = n\lambda$ where d is the interplanar distance, θ the incidence angle with the planes, and $n = 1, 2, 3, \dots$ etc. Note that different values of n are equivalent to consider different RLPs along the plane's normal direction.

Exercise 4.2. Given the crystal lattice parameters, i.e. the edge lengths a , b , and c and the angle values α , β , and γ , Fig. 4.1, write a MatLab routine to calculate d_{hkl} and use it to identify the interplanar distances responsible for the main peaks seen of the intensity pattern of α -quartz in Fig. 3.25.

Answer: The angles between the edges are set so that $\mathbf{a} \cdot \mathbf{b} = ab \cos \gamma$, $\mathbf{a} \cdot \mathbf{c} = ac \cos \beta$, and $\mathbf{b} \cdot \mathbf{c} = bc \cos \alpha$. Using any system of coordinates for describing the edge vectors, for example (the most common choice)

$$\mathbf{a} = a [\sin \beta, 0, \cos \beta], \quad \mathbf{b} = b [\sin \alpha \cos \varphi, \sin \alpha \sin \varphi, \cos \alpha], \quad \text{and} \quad \mathbf{c} = c [0, 0, 1]$$

where $\cos \varphi = (\cos \gamma - \cos \beta \cos \alpha) / \sin \alpha \sin \beta$, the reciprocal lattice vectors \mathbf{a}^* , \mathbf{b}^* , and \mathbf{c}^* are then obtained from (4.7), which leads to

$$d_{\text{hkl}} = \frac{2\pi}{|\mathbf{ha}^* + \mathbf{kb}^* + \mathbf{lc}^*|}. \quad (4.10)$$

This is implemented in routine bragg.m (Appendix B). In the case of α -quartz, for 100 and 011 type of reflections, the routine provides

```
>> bragg(8000, [4.9134 4.9134 5.4052 90 90 120], [1 0 0; 0 1 1]);
Energy = 8000.00eV (1.549813 Å)
d(1,0,0) = 4.25513 Å, thB = 10.4927 deg, 2thB = 20.9855 deg
d(0,1,1) = 3.34342 Å, thB = 13.4013 deg, 2thB = 26.8026 deg
```

Exercise 4.3. The measurements of interplanar distances by X-ray diffraction are compromised by angular $\Delta\theta$ and spectral $\Delta\lambda/\lambda$ resolutions. For a cubic crystal [$a = b = c$, $\alpha = \beta = \gamma = 90^\circ$], how does the resolution $\Delta a/a$ of the lattice parameter depend on both the angular and spectral resolutions?

Answer: The simple application of the theory of errors (Vuolo 1996) to Bragg's law, (4.9), results in

$$\left(\frac{\Delta d}{d}\right)^2 = \left(\frac{\Delta \lambda}{\lambda}\right)^2 + (\cot \theta \Delta \theta)^2. \quad (4.11)$$

In a cubic crystal, $d_{\text{hkl}} = a/\sqrt{h^2 + k^2 + l^2}$ and therefore $\Delta a/a = \Delta d/d$. For photons of energy $\mathcal{E} = 10200 \pm 1 \text{ eV}$ where the scattering angle of reflection 400 was measured at $2\theta = 50.938 \pm 0.008^\circ$,

$$\frac{\Delta d}{d} = \left[\frac{1}{10200^2} + \cot^2\left(\frac{50.938}{2}\right) \left(\frac{0.008}{2} \frac{\pi}{180}\right)^2 \right]^{1/2} = 1.8 \times 10^{-4},$$

implying in $a = 5.653 \pm 0.001 \text{ Å}$.

...

4.1.2 Structure Factors and Diffracted Intensities

The complete determination of the crystal structure of a substance involves two distinct steps: (a) characterize the crystalline lattice, which means to measure the lattice parameters; and (b) assign values to the fractional coordinates of the atoms inside the unit cell. Measurements of the directions of the diffracted beams provide the lattice parameters, while the beam intensity values are essential to obtain the fractional coordinates. The relationship between intensities and fractional coordinates is established by the form factor of the unit cell $F(\mathbf{Q})$, (4.5), which is the amplitude in electron units of the field scattered by the unit cell.

The form factor is given by (1.52) for any \mathbf{Q} vector. But in the reciprocal space of a crystal, the diffracted intensities are highly localized around the hkl nodes of the reciprocal lattice.⁴ Thus structure factors of a crystal are the values of the form factor calculated only for the reciprocal lattice vectors, which is

$$F(\mathbf{Q}) \rightarrow F(\mathbf{Q}_{\text{hkl}}) = F_{\text{hkl}} = \sum_a^{N_{\text{at}}} f_a e^{i\mathbf{Q}_{\text{hkl}} \cdot \mathbf{r}_a} = \sum_a^{N_{\text{at}}} f_a e^{2\pi i (hx_a + ky_a + lz_a)} \quad (4.12)$$

where h , k , and l are integers and $f_a = (f_0 + f' + if'')_a$ such as defined in Sect. 1.4. Note that by allowing non-integer numbers in (4.12) we obtain the form factor of any point in the reciprocal space described in the base \mathbf{a}^* , \mathbf{b}^* , and \mathbf{c}^* .

How localized the diffracted intensities are around the nodes of the reciprocal lattice depends on the crystal volume. Since in (4.5) the FT of the crystal shape, $W(\mathbf{Q}) = \text{FT}\{s(\mathbf{r})\}$, appears convolving the other terms, all of the nodes of the reciprocal lattice gain volume, which increases inversely proportional to the crystal's actual volume. By substituting (4.6) and (4.12) in (4.5), we then arrive at the crystal's form factor⁵

$$F_{\text{cryst}}(\mathbf{Q}) = \frac{(2\pi)^3}{V_{\text{cel}}} \sum_{\text{h.k.l}} F(\mathbf{Q}_{\text{hkl}}) \delta(\mathbf{Q} - \mathbf{Q}_{\text{hkl}}) * W(\mathbf{Q}) = \frac{1}{V_{\text{cel}}} \sum_{\text{h.k.l}} F_{\text{hkl}} W(\mathbf{Q} - \mathbf{Q}_{\text{hkl}}), \quad (4.13)$$

whose square module provides the diffracted intensities.

In most practical situations of applying the Kinematic Theory it is valid to deal with the diffracted intensities as being independent of each other—the situations where this treatment is not valid will be discussed at a later point. This means that the rescattering effects are neglected as well as any other effects arising from the

⁴RLPs are also called nodes in order to emphatically differentiate them from any other point of the reciprocal space to which indices hkl are not integer numbers.

⁵The number $(2\pi)^3$ disappears from (4.13) because the convolution operation, “*”, stands for an integration in dV_q , see (1.32), but becomes one in $dV_Q = (2\pi)^3 dV_q$, which means, $(2\pi)^3 \int \delta(2\pi \mathbf{q}' - \mathbf{Q}_{\text{hkl}}) W(2\pi \mathbf{q} - 2\pi \mathbf{q}') dV_q' = \int \delta(\mathbf{Q}' - \mathbf{Q}_{\text{hkl}}) W(\mathbf{Q} - \mathbf{Q}') dV_Q' = W(\mathbf{Q} - \mathbf{Q}_{\text{hkl}})$.

simultaneous excitation of more than one node of the reciprocal lattice. The intensity distribution in the reciprocal space of a crystal is thus given by

$$I(\mathbf{Q}) = I_{Th} |F_{\text{cryst}}(\mathbf{Q})|^2 \simeq \sum_{h,k,l} I_{hkl}(\mathbf{Q}) \quad (4.14)$$

where

$$I_{hkl}(\mathbf{Q}) = I_{Th} \frac{1}{V_{\text{cel}}^2} |F_{hkl}|^2 |W(\mathbf{Q} - \mathbf{Q}_{hkl})|^2. \quad (4.15)$$

The structure factor amplitudes (or modules), $|F_{hkl}|$, are values experimentally accessible through the kinematic diffraction of X-rays. The number of values required to solve a structure, i.e. estimate the fractional coordinates, depends on the structure's complexity. In relatively simple structures—generally with unit cells of a volume under 1000 \AA^3 containing no more than a few hundred atoms, it is feasible to adjust the atomic positions until the relative intensities of the model structure are consistent with the experimental intensities. Certainly this procedure is not feasible when one wishes to determine the crystalline structure of a protein containing thousands of atoms. Specific methods used in protein crystallography are adequately described in the appropriate literature.⁶ But beyond collecting thousands of intensity values, measurements on samples with resonant or heavy atoms are often necessary.

...

Exercise 4.4. The development of the micro and optoelectronic industry was due to the electronic properties of the semiconductor crystals such as Si and GaAs, which can be synthesized with high degree of crystalline perfection. Compare amplitude and phase of the structure factors of the 002, 004, 111, and $\bar{1}\bar{1}\bar{1}$ reflections of these materials. Interpret the origin of the most important differences. Note: $\bar{h}\bar{k}\bar{l} \Rightarrow -h, -k, \text{ and } -l$.

Answer: Positioning the origin of the crystalline lattice of one of the atoms of the unit cell as illustrated in Fig. 4.3a, the fractional coordinates of both A and B elements are⁷

A : (0, 0, 0), (1/2, 1/2, 0), (1/2, 0, 1/2), (0, 1/2, 1/2), and

B : (1/4, 1/4, 1/4), (3/4, 3/4, 1/4), (3/4, 1/4, 3/4), (1/4, 3/4, 3/4).

⁶See, for example, Giacovazzo (2002, Ch. 9).

⁷Several semiconductors have cubic unit cell with zinc blend or diamond structures, such as GaAs and Si, space groups F43m and Fd $\bar{3}$ m, respectively. See Hahn (2006, Ch. 7.1, pp. 112–717).

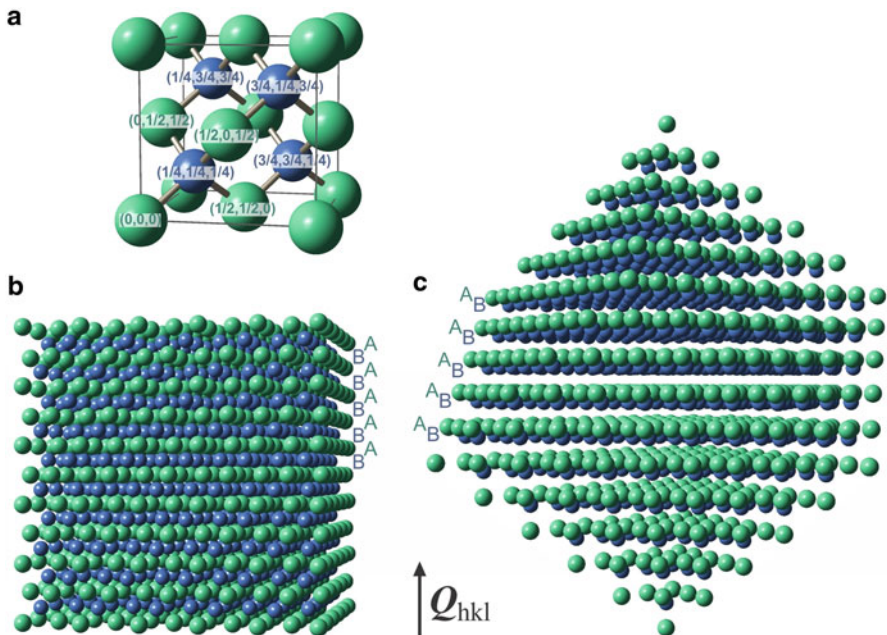


Fig. 4.3 Zinc blend type of cubic structure, space group $F\bar{4}3m$ (Hahn 2006). (a) Unit cell. (b, c) Perspectives of the structure along the directions (b) [001] and (c) [111]. The Q_{hkl} and $Q_{\bar{h}\bar{k}\bar{l}} = -Q_{hkl}$ diffraction vectors see differently the arrangement of the atomic planes along the [111] direction, BA-BA-BA and AB-AB-AB, respectively. In the case of direction [001] the arrangement is always A-B-A-B-A

Substituting in (4.12),

$$F_{hkl} = |F_{hkl}| e^{i\phi_{hkl}} = \begin{cases} 4(f_A + f_B) & \text{if } h+k+l = 4n \\ 4(f_A - f_B) & \text{if } h+k+l = 2(2n+1) \\ 4(f_A \pm if_B) & \text{if } h+k+l = 2n+1 \end{cases} \quad (4.16)$$

where $n \in \mathbb{Z}$. The structure factors for the mentioned reflections are compared in Table 4.1.

The 004 and 111 reflections are more intense in GaAs, Figs. 4.3b and 4.3c, than in Si due to the higher average atomic number of GaAs, i.e. $f_{\text{Ga}} + f_{\text{As}} > 2f_{\text{Si}}$. In Si, as $f_A - f_B = 0$, reflection 002 has zero intensity. In non-centrosymmetric crystals, a few pairs of hkl and $\bar{h}\bar{k}\bar{l}$ reflections⁸ have different perspectives of the structure,

⁸See Friedel and Bijvoet pairs, e.g. Giacovazzo (2002, pp. 170 and 475).

Table 4.1 Structure factors (amplitude and phase) of a few reflections in gallium arsenide and silicon crystals, (4.16)

hkl	GaAs		GaAs*		Si	
	$ F_{\text{hkl}} $	$\phi_{\text{hkl}} (\circ)$	$ F_{\text{hkl}} $	$\phi_{\text{hkl}} (\circ)$	$ F_{\text{hkl}} $	$\phi_{\text{hkl}} (\circ)$
002	24.4	148.0	24.4	-32.0	0.0	—
004	135.2	7.6	135.2	7.6	61.6	1.5
111	125.2	-46.0	146.1	-34.1	60.7	-43.9
$\bar{1}\bar{1}\bar{1}$	146.1	55.9	125.2	44.0	60.7	46.1

GaAs: A = Ga, B = As. GaAs*: A = As, B = Ga. Si: A = B = Si. Values for X-rays of 10,400 eV, approximately 33 eV above the absorption K-edge of Ga [sfactor.m]

such as in the case of reflections 111 and $\bar{1}\bar{1}\bar{1}$ in GaAs, Fig. 4.3c. The imaginary part of the atomic scattering factor has a greater amplitude under resonance, which is a fact that accentuates the differences in intensities of the pairs of reflections susceptible to the absence of a symmetry center. Note that if $f'' = 0$ for all atoms of the structure, $F_{\bar{\text{h}}\bar{\text{k}}\bar{\text{l}}} = F_{\text{hkl}}^*$ and therefore $|F_{\bar{\text{h}}\bar{\text{k}}\bar{\text{l}}}|^2 = |F_{\text{hkl}}|^2$ for any $\bar{\text{h}}\bar{\text{k}}\bar{\text{l}}/\text{hkl}$ pair of reflections regardless of the structure having or not a symmetry center.

Exercise 4.5. In a polar crystal, besides $f'' \neq 0$, what other mathematical property of the structure factors is also necessary for having Friedel pairs with different intensities?

Answer: The structure factor of any reflection can always be written in two parts: one with the real terms of the atomic scattering factors; and the other with the imaginary terms. This leads to

$$F = \sum_a (f + f')_a e^{i\phi_a} + i \sum_a (f'')_a e^{i\phi_a} = F' + iF'' = |F'|e^{i\phi'} + i|F''|e^{i\phi''} = e^{i\phi'} [|F'| + i|F''|e^{i(\phi'' - \phi')}]$$

where $\phi_a = 2\pi(hx_a + ky_a + lz_a)$, see (4.12). The intensities in the Friedel pair are proportional to $|F|^2 = |F'|^2 + |F''|^2 - 2|F'||F''| \sin(\phi'' - \phi')$ and to $|\bar{F}|^2 = |F'|^2 + |F''|^2 + 2|F'||F''| \sin(\phi'' - \phi')$, the latter obtained by swapping ϕ_a with $-\phi_a$. So for $|F|^2$ to be different from $|\bar{F}|^2$, it is also necessary to have $\sin(\phi'' - \phi') \neq 0$, a fact that only occurs for a few reflections in non-centrosymmetric crystals such as reflections with odd indices in III-V semiconductors.

Exercise 4.6. Methods that explore mathematical relationships between the phases of the structure factors, called “direct methods,” contributed to overcoming the phase problem in X-ray crystallography and received the Nobel Prize in Chemistry in 1985 (Hauptman and Karle 1953). Given any three reciprocal lattice vectors, for instance \mathbf{A} , \mathbf{B} , and \mathbf{C} that belong to the set $\{\mathbf{Q}_{\text{hkl}}\}$, what is the mathematical relationship between these vectors so that the triplet of structure factors $F(\mathbf{B})F(\mathbf{C})/F(\mathbf{A})$ has an invariant phase with respect to the choice of origin for atomic fractional coordinates in the unit cell?

Answer: If \mathbf{r}_a stands for atomic positions in the unit cell regarding a certain choice of origin with structure factors $F(\mathbf{Q})$, then

$$F^\dagger(\mathbf{Q}) = \sum_a f_a e^{i\mathbf{Q}\cdot(\mathbf{r}_a + \Delta\mathbf{r})} = e^{i\mathbf{Q}\cdot\Delta\mathbf{r}} F(\mathbf{Q})$$

are the structure factors with the origin shifted by $\Delta\mathbf{r}$ in relation to the previous one. The triplet

$$\frac{F^\dagger(\mathbf{B})F^\dagger(\mathbf{C})}{F^\dagger(\mathbf{A})} = \frac{|F(\mathbf{B})||F(\mathbf{C})|}{|F(\mathbf{A})|} e^{i[\Psi_T + (\mathbf{B} + \mathbf{C} - \mathbf{A}) \cdot \Delta\mathbf{r}]}$$

will have phase $\Psi_T = \phi_B + \phi_C - \phi_A$ invariant under translation of the origin when $\mathbf{A} = \mathbf{B} + \mathbf{C}$. For example, for GaAs crystal with X-rays of 10,400 eV, Table 4.1, the invariant phases of the triplets $F_{111}F_{\bar{1}\bar{1}\bar{1}}/F_{002}$ and $F_{\bar{1}\bar{1}\bar{1}}F_{\bar{1}11}/F_{002}$ are $\Psi_T = 120.0^\circ$ and $\Psi_T = -36.2^\circ$, respectively.⁹

...

4.2 Truncation of the Crystal Lattice

Another important aspect of the kinematic intensity, (4.15), is the dependence on the shape of the crystal. In the crystal structure analysis, the sample size (diffracting volume) varies in a length scale of micrometer. Although small, this scale of size is sufficient for the term $|W(\mathbf{Q} - \mathbf{Q}_{\text{hkl}})|^2$ to not broaden the diffraction conditions to the point of compromising the resolution of the structure. The effects of shape are accentuated with the decrease of scale, making it possible to estimate the dimension of very small crystallites by enlarging the diffraction peaks above the instrumental width, which is a procedure analogous to that of estimating particle sizes in solution by small angle scattering, Sect. 2.3.

In studies of nanostructured materials and surfaces, the truncation of the crystalline lattice, namely, the fact that the crystals have finite dimensions, produces remarkable effects when analyzing the distribution of intensity in the reciprocal space with intense beams. In nanotechnology, many devices contain crystalline materials of nanometer dimensions. The high resolution mapping of the intensity distribution around one node of the reciprocal lattice, i.e. mapping the function $|W(\Delta\mathbf{Q})|^2$, is an important tool for analysis of nanostructured devices (Pietsch et al. 2004). In crystals with surfaces defined at an atomic scale, $|W(\Delta\mathbf{Q})|^2$ distributes the intensity along the normal direction to the surface, allowing diffraction experiments at a grazing incidence with the diffraction vector contained in the surface's plane (Malachias et al. 2011). The approximation in (4.14), of considering the diffracted intensities by different hkl reflections as independent of each other, needs to be

⁹There are experimental methods based on a dynamical theory of X-ray diffraction, which are susceptible to the value of Ψ_T , e.g. Morelhão et al. (2011).

reassessed when $W(\Delta\mathbf{Q})$ is very broad and the fields scattered by adjacent nodes show interference effects, see Exercise 4.8.

...

Exercise 4.7. The smaller the dimensions of a crystal, the larger is the volume of the reciprocal lattice nodes. (a) What is the aspect of the nodes in crystals with thickness of $t = 100 \text{ nm}$? Consider both crystal shapes: rectangular area and circular area. (b) What mathematical function describes the asymptotic drop in intensity along the surface normal direction?

Answer (a): The volume of the nodes is determined by the function $|W(\Delta\mathbf{Q})|^2$ where $\Delta\mathbf{Q} = \mathbf{Q} - \mathbf{Q}_{\text{hkl}}$. In a crystal with rectangular shape, dimensions $L \times L \times t$,

$$\begin{aligned} W(\Delta\mathbf{Q}) = \text{FT}\{s(\mathbf{r})\} &= \int_{-L/2}^{L/2} e^{i\Delta Q_x x} dx \int_{-L/2}^{L/2} e^{i\Delta Q_y y} dy \int_{-t/2}^{t/2} e^{i\Delta Q_z z} dz = \\ &= tL^2 \frac{\sin(\Delta Q_x L/2)}{\Delta Q_x L/2} \frac{\sin(\Delta Q_y L/2)}{\Delta Q_y L/2} \frac{\sin(\Delta Q_z t/2)}{\Delta Q_z t/2}. \end{aligned}$$

The aspect of node in a 3D visualization is shown in Fig. 4.4a.

In the case of a crystal in the shape of a disc, diameter L and thickness t ,

$$\begin{aligned} W(\Delta\mathbf{Q}) &= \int_0^{2\pi} \int_0^{L/2} e^{i\Delta Q_{xy} r \cos\varphi} r dr d\varphi \int_{-t/2}^{t/2} e^{i\Delta Q_z z} dz = \\ &= t W_r(\Delta Q_{xy}) \frac{\sin(\Delta Q_z t/2)}{\Delta Q_z t/2} \end{aligned}$$

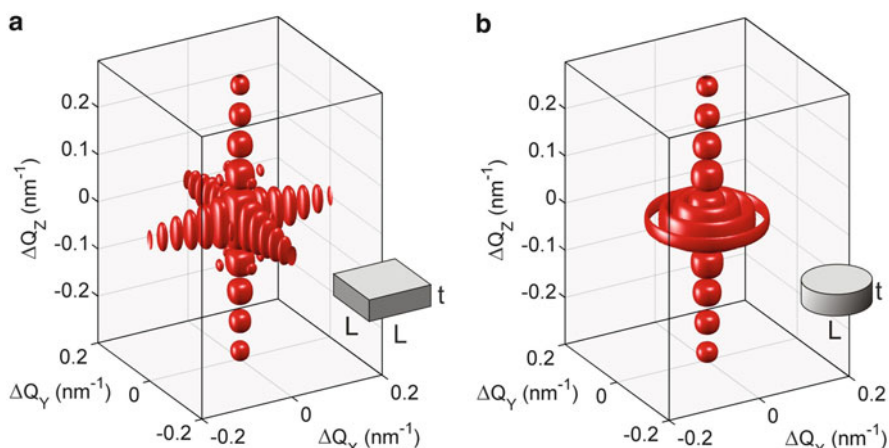


Fig. 4.4 Nodes of the reciprocal lattice in crystals with a thickness $t = 100 \text{ nm}$ and (a) rectangular and (b) disc shape, $L = 2t$. 3D aspect illustrated by isosurfaces of the function $|W(\Delta\mathbf{Q})|$, (4.13) [exrlp3Dview.m]

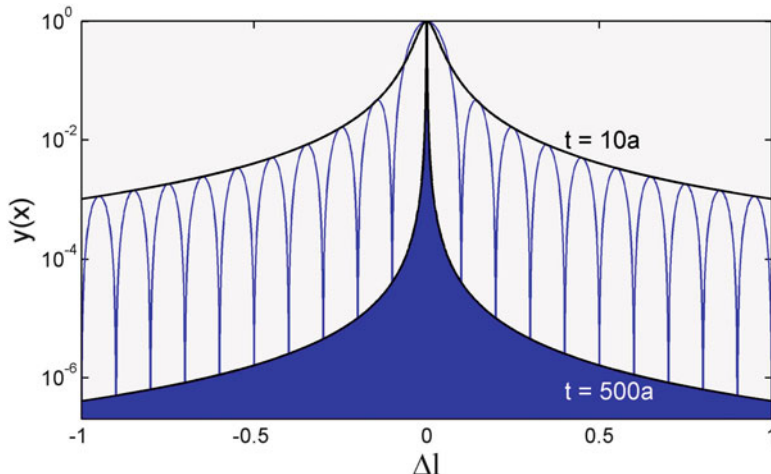


Fig. 4.5 Comparison of Lorentzian function $y(x) = 1/[1 + x^2]$ (black line) with the function $y(x) = |\sin(x)/x|^2$ (blue line). $x = \Delta Q_z t/2$, $\Delta Q_z = 2\pi\Delta l/a$, and $t = Na$ [sincfunction.m]

produces the visualization shown in Fig. 4.4b. $\Delta Q_{xy}^2 = \Delta Q_x^2 + \Delta Q_y^2$, $r^2 = x^2 + y^2$ and the integral in the azimuthal angle φ resolved numerically.

Answer (b): The maximums of the sinc function, $\sin(x)/x$, for $x \neq 0$ fall with $1/x$, while for $x = 0$ the function is 1. The fall in intensity in the longitudinal direction to the thickness t is given by the square module of the sinc function with $x = \Delta Q_z t/2$, item (a), whose maximums are described by a Lorentzian function such as

$$\left| \frac{\sin(\Delta Q_z t/2)}{\Delta Q_z t/2} \right|^2_{\text{maximums}} = \frac{1}{1 + (\Delta Q_z t/2)^2}. \quad (4.17)$$

See comparisons in Fig. 4.5. The period of the maximums, or thickness fringes, is $\Delta Q_z = 2\pi/t$.

Exercise 4.8. The alignment of adjacent nodes of the reciprocal lattice with the normal direction to the crystal surface favors interference effects between the fields diffracted by adjacent nodes. How does the thickness of the crystal affect the validity of the approach implicit in (4.14) for treating separately the diffracted intensities?

Answer: The approach will always be valid independently of the values of F_{hkl} , provided that

$$\left| \sum_{h,k,l} W(Q - Q_{hkl}) \right|^2 - \sum_{h,k,l} |W(Q - Q_{hkl})|^2 = 0.$$

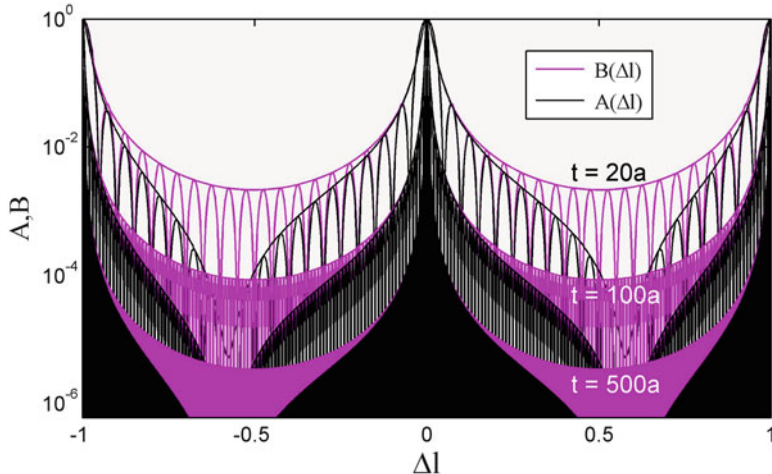


Fig. 4.6 Discrepancies between the functions $A(\Delta l)$ and $B(\Delta l)$, as defined in the text, with crystal thickness t . The envelope curves are obtained by replacing $\sin(x_j)/x_j$ for $1/(1 + ix_j)$ in (4.18) [sincinterference.m]

If the nodes with indexes l and $l \pm 1$ are aligned to the normal direction, the above equation would be reduced to

$$\underbrace{\left| \sum_{j=0,\pm 1} \frac{\sin(x_j)}{x_j} \right|^2}_{A(\Delta l)} - \underbrace{\left| \sum_{j=0,\pm 1} \frac{\sin(x_j)}{x_j} \right|^2}_{B(\Delta l)} = 0 \quad (4.18)$$

where $x_j = \Delta Q_{z,j}t/2 = \pi N(\Delta l - j)$ and $N = t/a$ is the number of unit cells with a lattice parameter $c = a$, in the direction of the crystal's thickness t . In Fig. 4.6, the discrepancies between the terms A and B are compared as a function of thickness. The increase in thickness does not affect the limits of the discrepancies intervals ($|\Delta l| > 1/5$), but requires a signal to noise ratio continually greater in order to measure diffracted intensities in these intervals.

Exercise 4.9. Assuming valid the kinematic approach for crystals with micrometer dimensions, rewrite $I_{hkl}(\mathbf{Q})$, (4.15), in terms of delta functions. What is the value of $I_{hkl}(0)$?

Answer: From the relationships described in Note 3.1 for the volume function $\Omega(\mathbf{u})$,

$$|W(\Delta \mathbf{Q})|^2 = V \text{FT}\{\Omega(\mathbf{u})\} \simeq V \delta_q(\Delta \mathbf{q}) = (2\pi)^3 V \delta_Q(\Delta \mathbf{Q})$$

where $|W(0)|^2 = V^2$ and $\delta_q(0) = (2\pi)^3 \delta_Q(0) = V$. Recalling that if $N = V/V_{\text{cel}}$ is the number of unit cells in the crystal with a volume V and $V_{\text{cel}}^* = (2\pi)^3/V_{\text{cel}}$ is the reciprocal volume of the unit cell, the intensity distribution around a node \mathbf{hkl} can be rewritten as

$$I_{\mathbf{hkl}}(\mathbf{Q}) \simeq I_{Th} |F_{\mathbf{hkl}}|^2 N V_{\text{cel}}^* \delta_Q(\mathbf{Q} - \mathbf{Q}_{\mathbf{hkl}}) \quad (4.19)$$

where $I_{\mathbf{hkl}}(0) = I_{Th} |F_{\mathbf{hkl}}|^2 N^2$.

...

4.3 Atomic Disordering in Crystalline Structures

The mathematical description by the unit cell and periodic lattice convolution, (4.4), generates structures with perfect periodicity since all the unit cells along the crystal are identical. Such perfection accentuates the maximums and minimums of the interference patterns: maximums (constructive interferences) on the nodes of the reciprocal lattice and minimums (destructive interferences) throughout the rest of the reciprocal space. However, if there is a minimum of disorder in the atomic positions, there is a softening of both the constructive and destructive interferences. The intensities of the diffraction peaks decrease while the values of the scattered intensities in the regions outside of the diffraction peaks tend to increase. This is an analogous situation to those demonstrated in Fig. 3.6, Exercise 3.3 (b), and in Fig. 3.25.

4.3.1 Thermal Vibrations

Even at absolute zero temperature, atoms in a solid vibrate according to the fundamental frequencies of the quantum states inherent to the chemical bonds. The higher the temperature, the higher the frequencies and amplitudes of vibration. However, compared to the frequency of the X-rays, of the order of 10^{18} Hz, thermal vibrations are slow movements. Within the temporal coherence of an X-ray beam, something around a few femtoseconds,¹⁰ the atoms of the structure are frozen at slightly different positions than the average positions described by the perfect structure, characterizing instant disorders similar to those addressed in Note 3.4. The main difference is in the fact that the vibrations are not necessarily isotropic (equal in all directions), and neither are the amplitudes equal for all atoms of the

¹⁰Temporal coherence: longitudinal coherence C_L , (1.15), divided by the speed of light, e.g. $\Delta\lambda/\lambda = 10^{-4}$ and $\lambda = 1.54 \text{ \AA}$ $\Rightarrow C_L/c = 2.6 \text{ fs}$ of temporal coherence.

structure. If they were, i.e. isotropic vibrations of the same amplitude, the solution obtained in Note 3.4 and summarized in (3.19) would be sufficient to account for the effects of thermal vibrations in the temporal average of the intensity scattered throughout the structure.

In order to differentiate parameters of disorder by atomic site,¹¹ the starting point becomes the general correlation function of the perfect (average) structure

$$C(\mathbf{u}) = \sum_{a,b} f_a f_b^* \delta(\mathbf{u} - \mathbf{r}_{ab}) = \sum_a |f_a|^2 \delta(u) + \sum_{a,b \neq a} f_a f_b^* \delta(\mathbf{u} - \mathbf{r}_{ab}), \quad (4.20)$$

written directly in terms of the atomic scattering factors so as to provide the kinematic intensity $I(\mathbf{Q}) = I_{Th} \text{FT}\{C(\mathbf{u})\}$. The indexes a and b run along all the structure's atoms. Slight disorders in the atomic positions turn the delta functions into Gaussians functions $G(\mathbf{u} - \mathbf{r}_{ab})$, whose standard deviations η_{ab} , depend on the mean square deviations η_a^2 and η_b^2 of the atomic positions responsible for the separation \mathbf{r}_{ab} , which is $\eta_{ab}^2 = \eta_a^2 + \eta_b^2$. The FTs of the Gaussians¹²

$$\text{FT}\{G(\mathbf{u} - \mathbf{r}_{ab})\} = e^{i\mathbf{Q} \cdot \mathbf{r}_{ab}} e^{-\frac{1}{2} Q^2 (\eta_a^2 + \eta_b^2)}, \quad (4.21)$$

are susceptible only to the mean square deviations in the direction of the diffraction vector $\mathbf{Q} = Q\hat{\mathbf{Q}}$, which requires special attention in the systems with anisotropic disorders where $\eta_a \rightarrow \eta_a(\hat{\mathbf{Q}})$.

(4.21) can be used to reach the following expression of kinematic intensity

$$\begin{aligned} I(\mathbf{Q}) &= I_{Th} \text{FT}\{C(\mathbf{u})\} = I_{Th} \sum_a |f_a|^2 \text{FT}\{\delta(u)\} + I_{Th} \sum_{a,b \neq a} f_a f_b^* \text{FT}\{G(\mathbf{u} - \mathbf{r}_{ab})\} = \\ &= I_{Th} \sum_a |f_a|^2 + I_{Th} \sum_{a,b \neq a} f_a e^{-\frac{1}{2} Q^2 \eta_a^2} f_b^* e^{-\frac{1}{2} Q^2 \eta_b^2} e^{i\mathbf{Q} \cdot \mathbf{r}_{ab}}, \end{aligned} \quad (4.22)$$

which explicitly shows that the disorder in the atomic structure of a solid in relation to the average structure can be treated as an exponential attenuation of the atomic scattering factors present in the term of interference (double sum). In a hypothetical situation of total disorder, $\eta_{a,b} \rightarrow \infty$, there would still be the sum (simple sum) of the individual intensities scattered by the atoms, such as in a disperse system, Chap. 2. In systems with a high degree of disorder, e.g. Fig. 3.25, the contribution of these individual intensities increases the background noise as Q increases, but is limited by the reduction of the atomic scattering factors.

¹¹Further details about atomic disorder parameters are available in Authier (2006, pp. 228–242).

¹²Although (4.21) has an analytical solution, the routine `debye.m` allows numerical verification in one dimension.

In the case of crystalline structures where the amplitudes of the vibrations are very small in relation to the size of the unit cells, the dominant effect is the attenuation of the diffracted intensities; the increase in background noise is negligible. Formally this is demonstrated by rearranging the sums in (4.22) in terms of the N unit cells of the crystal and of the N_{at} atoms present in each unit cell.,,

$$\begin{aligned} I(\mathbf{Q}) &= I_{Th} \sum_{a=1}^{N \times N_{at}} |f_a|^2 (1 - e^{-\frac{1}{2} Q^2 \eta_a^2}) + I_{Th} \left| \sum_{a=1}^{N \times N_{at}} f_a e^{-\frac{1}{2} Q^2 \eta_a^2} e^{i \mathbf{Q} \cdot \mathbf{r}_a} \right|^2 = \\ &= I_{Th} N \sum_{a=1}^{N_{at}} |f_a|^2 (1 - e^{-\frac{1}{2} Q^2 \eta_a^2}) + I_{Th} |F_{\text{cryst}}(\mathbf{Q})|^2 \simeq I_{Th} |F_{\text{cryst}}(\mathbf{Q})|^2. \end{aligned} \quad (4.23)$$

$F_{\text{cryst}}(\mathbf{Q})$ is the form factor of the crystal defined in (4.13), but accounting for the effect of the thermal vibrations in the structure factors

$$F_{hkl} = \sum_a f_a e^{-M_a} e^{2\pi i (hx_a + ky_a + lz_a)} \quad (4.24)$$

through the exponential attenuation with factor

$$M_a = \frac{1}{2} Q^2 \eta_a^2 = 8\pi^2 \eta_a^2 \left(\frac{\sin \theta}{\lambda} \right)^2, \quad (4.25)$$

commonly called the temperature factor or Debye–Waller factor (Authier 2006). The root mean square deviation associated with the a -th atom of the unit cell is in general terms given by $\eta_a^2 = \langle |(\mathbf{r}_a - \langle \mathbf{r}_a \rangle) \cdot \hat{\mathbf{Q}}|^2 \rangle$. The $\langle \dots \rangle$ represent spatiotemporal averages, which are both the temporal average in a single unit cell and an average of all the unit cells of the structure at a given instant of time. The latter case allows you to include disorders of non-thermal origin, such as those induced by defects randomly distributed in the structure.

In a crystalline lattice there are also collective vibrations known as phonons. The collective movement induces correlations between atomic positions that alter the Bragg's law locally, generating very weak diffuse intensities outside the diffractions of the average crystalline lattice. The scattering of X-rays by thermally excited phonons, called Thermal Diffuse Scattering (TDS), has been observed with intense X-ray sources and has given rise to studies of the lattice dynamic in solids (Holt et al. 1999). However, the treatment of thermal vibrations without correlations, i.e., the atoms vibrating independently one from the other, makes it possible to adequately describe the effects of the thermal vibrations in the techniques commonly employed in the study and characterization of crystal structures.

...

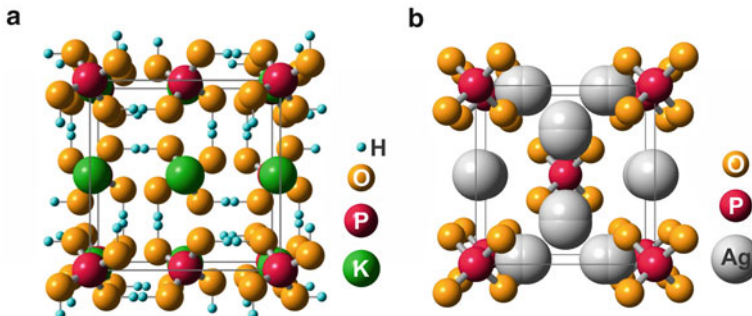


Fig. 4.7 Atomic structure of crystals. (a) Potassium dihydrogen phosphate (KDP), unit cell with 4 KH_2PO_4 molecules. (b) Silver orthophosphate, unit cell with 2 Ag_3PO_4 molecules. View from the crystallographic axis [001]. H and Ag atoms have occupancy factors of 1/2

Exercise 4.10. The potassium dihydrogen phosphate (KDP), Fig. 4.7a, is a soluble salt with numerous applications ranging from the food industry—sports drinks for example—to laser technology. The latter application in the form of single crystals grown by the slow evaporation process from aqueous solution. (a) Build a histogram of the KDP’s structure factors (square modules) plotted as a function of the diffraction vector module Q . What is the attenuation imposed by the thermal vibrations in the histogram’s main contribution? (b) Metal ions present as impurities in the crystal structure tend to occupy interstitial sites surrounded by oxygens. Would it be possible, in principle, to show an increase in disorder of the oxygens only?

Answer (a): The function

$$\mathcal{F}(Q) = \sum_{\text{hkl}} |F_{\text{hkl}}|^2 \delta(Q - Q_{\text{hkl}}) \quad (4.26)$$

represents the histogram of the squared modules of the structure factors shown in Fig. 4.8 where $Q_{\text{hkl}} = 2\pi/d_{\text{hkl}}$. In the case of thermal vibrations of the same magnitude for all atoms of the structure, the factor $e^{-Q^2\eta^2}$ is common for all reflections. The higher is the value of Q , the higher is the attenuation of intensity. For the main contribution that occurs at $Q = 3.218 \text{ \AA}^{-1}$ due to 16 reflections from family 132, see Note 4.2, the attenuation will be around 10 %, 21 %, and 34 % when $\eta = 0.1 \text{ \AA}$, 0.15 \AA , and 0.2 \AA , respectively.

Answer (b): When increasing the disorder of O atoms, the relative variation in the structure factors becomes no longer systematic as in the case of a uniform increase of disorder to all atoms, Fig. 4.9. Therefore, in principle, it would be feasible to show experimentally that O atoms have higher disorder.

Note 4.2: We have used routine `diffraction.m` to calculate, index, and sort the structure factors of a crystal in a given energy. Below is part of the file generated by this routine, taking as an example the structure of the KDP:

X-ray photon energy = 10000.0eV (wavelength = 1.239850Å)										
h	k	l	I _{hkl} (%)	Re{F _{hkl} }	Im{F _{hkl} }	F _{hkl}	fase	th	tth	d _{hkl}
2	0	0	100.0	127.384	4.0551	127.449	1.8	9.5772	19.1543	3.7260
-2	0	0	100.0	127.384	4.0551	127.449	1.8	9.5772	19.1543	3.7260
0	2	0	100.0	127.384	4.0551	127.449	1.8	9.5772	19.1543	3.7260
0	-2	0	100.0	127.384	4.0551	127.449	1.8	9.5772	19.1543	3.7260
1	1	-2	80.8	104.005	47.981i	114.539	24.8	12.3089	24.6179	2.9080
1	-1	2	80.8	104.005	47.981i	114.539	24.8	12.3089	24.6179	2.9080
-1	-1	2	80.8	104.005	47.981i	114.539	24.8	12.3089	24.6179	2.9080
-1	1	2	80.8	104.005	47.981i	114.539	24.8	12.3089	24.6179	2.9080
-1	-1	2	76.8	104.265	-39.946i	111.655	-21.0	12.3089	24.6179	2.9080
1	-1	-2	76.8	104.265	-39.946i	111.655	-21.0	12.3089	24.6179	2.9080
1	1	2	76.8	104.265	-39.946i	111.655	-21.0	12.3089	24.6179	2.9080
-1	1	-2	76.8	104.265	-39.946i	111.655	-21.0	12.3089	24.6179	2.9080
-4	0	-4	64.1	101.980	4.234i	102.067	2.4	29.1423	58.2845	1.2730
4	0	4	64.1	101.980	4.234i	102.067	2.4	29.1423	58.2845	1.2730
-4	0	4	64.1	101.980	4.234i	102.067	2.4	29.1423	58.2845	1.2730
4	0	-4	64.1	101.980	4.234i	102.067	2.4	29.1423	58.2845	1.2730
0	-4	4	64.1	101.980	4.234i	102.067	2.4	29.1423	58.2845	1.2730
0	4	-4	64.1	101.980	4.234i	102.067	2.4	29.1423	58.2845	1.2730
0	4	4	64.1	101.980	4.234i	102.067	2.4	29.1423	58.2845	1.2730
0	-4	-4	64.1	101.980	4.234i	102.067	2.4	29.1423	58.2845	1.2730
.
-6	-8	-2	0.0	0.077	0.367i	0.375	78.2	58.2840	116.5680	0.7288

F000 = 298.747 + 4.345i

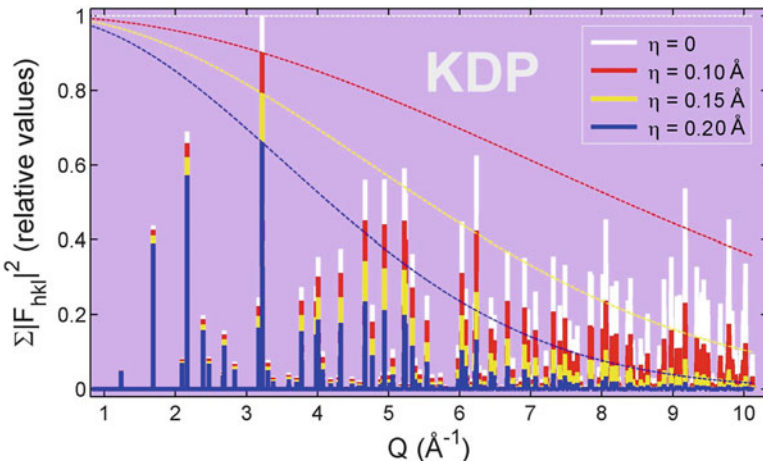


Fig. 4.8 Histograms of the KDP's structure factors without ($\eta = 0$) and with ($\eta = 0.10, 0.15$, and 0.20\AA) root-mean-square displacement of the atomic positions. Curves $e^{-Q^2\eta^2}$ (dashed lines) are shown [kdphistogram.m]

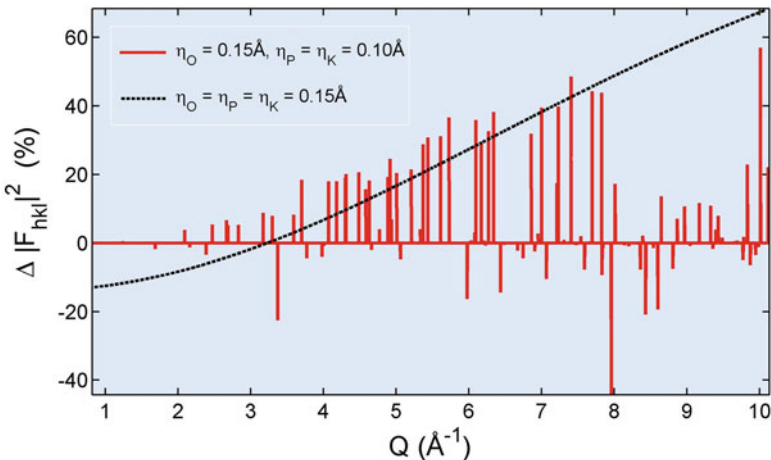


Fig. 4.9 Relative variation of $|F_{hkl}|^2$ with increasing of atomic disorder in KDP. Reference structure with $\eta_P = \eta_K = \eta_O = 0.10 \text{ \AA}$ [kdphistcomp.m]

...

4.3.2 Occupancy Factor

Beyond factors of disorder, the unit cells of a crystal can be different from each other when there are atoms with occupancy factors lower than 1. One of the causes is a greater number of energetically equivalent atomic sites compared with a smaller number of atoms to occupy them. A typical example is silver orthophosphate, a semiconductor with interesting photo oxidative properties (Yi et al. 2010) and whose structure is shown in Fig. 4.7b. Two Ag_3PO_4 molecules provide 6 Ag atoms per unit cell. The symmetry operations of the space group P43n (Hahn 2006) generate 12 sites that are equivalent to site $(x, 0, 1/2)$, grouped into six pairs of sites nearby, such as the pair $(x, 0, 1/2)$ and $(1/2-x, 0, 1/2)$. Thus, if the position of equilibrium would be at $x = 0.25$ the occupancy factor of Ag atoms would be 1, but in the actual structure $x = 0.231$ so that the occupancy factor is worth 1/2. This means that in a snapshot of the structure, Ag atoms with coordinates $(0.231, 0, 1/2)$ occur in 50 % of the unit cells present in the material and with coordinates $(0.269, 0, 1/2)$ in the remaining unit cells. The same happens for the other five pairs of nearby sites so that all the Ag atoms have occupancy factors equal to 1/2.

Another cause of occupancy factors lower than 1 is due to stoichiometry of the elements used for preparing a material. If A and B are chemically equivalent

elements in the structure, the compound with a formula $A_xB_{1-x}[\text{radical}]$ has a fraction x of unit cells containing the element A in a particular site, while this same atomic site will be occupied by the element B in the other unit cells.

In the mathematical expression of the structural factor, such as in (4.24), it is common to omit the occupancy factors, which are implicit in the concept of average unit cell. The full expression of the structure factors, explaining the occupancy factors and the resonance amplitudes, is given by

$$F_{\text{hkl}} = \sum_a (f_0 + f' + if'')_a C_a e^{-M_a} e^{2\pi i (hx_a + ky_a + lz_a)} \quad (4.27)$$

where C_a is the occupancy factor of a -th atom in the structure's average unit cell.

Summary

— Unit cell

edge vectors: \mathbf{a} , \mathbf{b} , and \mathbf{c}

lattice constants and angles: $\mathbf{a} \cdot \mathbf{b} = ab \cos \gamma$, $\mathbf{a} \cdot \mathbf{c} = ac \cos \beta$, and $\mathbf{b} \cdot \mathbf{c} = bc \cos \alpha$

volume: $V_{\text{cel}} = \mathbf{a} \cdot (\mathbf{b} \times \mathbf{c}) = \mathbf{b} \cdot (\mathbf{c} \times \mathbf{a}) = \mathbf{c} \cdot (\mathbf{a} \times \mathbf{b})$

position of the a -th atom: $\mathbf{r}_a = x_a \mathbf{a} + y_a \mathbf{b} + z_a \mathbf{c}$

— Reciprocal lattice vectors ($h, k, l \in \mathbb{Z}$)

$$\mathbf{Q}_{\text{hkl}} = h\mathbf{a}^* + k\mathbf{b}^* + l\mathbf{c}^* = 2\pi h \frac{\mathbf{b} \times \mathbf{c}}{V_{\text{cel}}} + 2\pi k \frac{\mathbf{c} \times \mathbf{a}}{V_{\text{cel}}} + 2\pi l \frac{\mathbf{a} \times \mathbf{b}}{V_{\text{cel}}}$$

— Interplanar distances and Bragg's law

$$d_{\text{hkl}} = \frac{2\pi}{|\mathbf{Q}_{\text{hkl}}|} = \frac{V_{\text{cel}}}{|h(\mathbf{b} \times \mathbf{c}) + k(\mathbf{c} \times \mathbf{a}) + l(\mathbf{a} \times \mathbf{b})|} = \frac{\lambda}{2 \sin \theta_{\text{hkl}}}$$

— Kinematic intensity of the reflection hkl

$$I_{\text{hkl}}(\mathbf{Q}) = I_{\text{Th}} \frac{1}{V_{\text{cel}}^2} |F_{\text{hkl}}|^2 |W(\mathbf{Q} - \mathbf{Q}_{\text{hkl}})|^2$$

— Structure factors

$$F_{\text{hkl}} = \sum_a (f_0 + f' + if'')_a C_a e^{-M_a} e^{2\pi i (hx_a + ky_a + lz_a)}$$

— Temperature or disorder factor (Debye–Waller)

$$M_a = \frac{1}{2} Q^2 \eta_a^2 = 8\pi^2 \eta_a^2 \left(\frac{\sin \theta}{\lambda} \right)^2$$

— Root mean square deviation of the a -th atom in the direction \hat{Q} do the diffraction vector

$$\eta_a^2 = \langle |(\mathbf{r}_a - \langle \mathbf{r}_a \rangle) \cdot \hat{Q}|^2 \rangle$$

Chapter 5

Applications of Kinematic Diffraction

X-ray diffraction is an essential tool for chemical and structural analysis in materials science, geosciences, chemistry, biology, and also in micro- and nanotechnology. The validity of the Kinematic Theory in crystals, as summarized by (4.14), makes the practical applications of this tool a lot easier. Applications of kinematic diffraction are divided into three major types of experimental methods. The first, and probably the most widely used worldwide, is the X-ray diffraction in polycrystals, the popular *powder method*. Unless of geometric factors, polarization, and instrumental effects,¹ the method is basically the experimental measurement of the histogram of the squared modules of structure factors, such as those in Fig. 4.8.

Not less important, although used to a lesser extent, are the diffractometry methods in single crystals. The breaking of the azimuthal symmetry of scattering (around the incident beam) requires appropriated instrumentation for dealing with the inherent 3D geometry of the X-ray diffraction phenomenon in crystals. This has the advantage of the larger number of reflections monitored individually with no contributions from other reflections, but as a disadvantage it has an occasional loss of resolution when working with macroscopic crystals diffracting beyond the limit treatable purely by the kinematic approach.

Finally, the third group of methods also requires knowledge of 3D diffraction geometry, but differing from single crystal diffractometry by the fact that the main object of investigation is the spatial intensity distribution in specific areas of the reciprocal space rather than the directions and relative values of the diffracted intensities. The reciprocal space mapping methods imply in high spatial resolution detection systems that are able to discriminate small changes, in the order of a few seconds of arc, in the directions of the diffracted beams. Important applications of such methods have the purpose of characterizing nanostructured devices. However, to address them directly requires detailed incursion into the universe of these

¹Instrumental effects include several factors that affect the line profile of the diffracted intensities, including angular and spectral resolution, linear absorption by the sample, and crystallite size.

devices (Pietsch et al. 2004), which is outside the scope of this book. The overview of scattering geometry in reciprocal space given below greatly facilitates the understanding of the mapping methods.

5.1 Working in the Reciprocal Space

In scattering techniques at angles greater than a few degrees from the direct beam require minimum notions of 3D geometry involved in the diffraction process. A very efficient way of dealing with this geometry is to work in the reciprocal space where the incident radiation is represented by scattering spheres,² Fig. 5.1. The diffraction phenomenon is associated with the coherent (or elastic) radiation scattering in such a way that the scattered wavevector $\mathbf{k}' = \mathbf{Q} + \mathbf{k}$ has the same module of the incident wavevector, i.e. $|\mathbf{k}'| = |\mathbf{k}|$, a fact that defines the surface of a sphere as the angular dispersion locus of all the physically possible scattered wavevectors \mathbf{k}' . Thus, photons with a wavevector \mathbf{k} will be diffracted by the reciprocal vector \mathbf{Q} when this is secant to the scattering sphere of radius $|\mathbf{k}| = 2\pi/\lambda$.

A polychromatic beam is equivalent to scan a region of reciprocal space with a set of non-concentric spheres with radii continuously varying, Fig. 5.1a; the greater the energy, the lesser the λ and the greater the sphere radius. All diffraction vectors included within the scanning region will diffract, although at different wavelengths

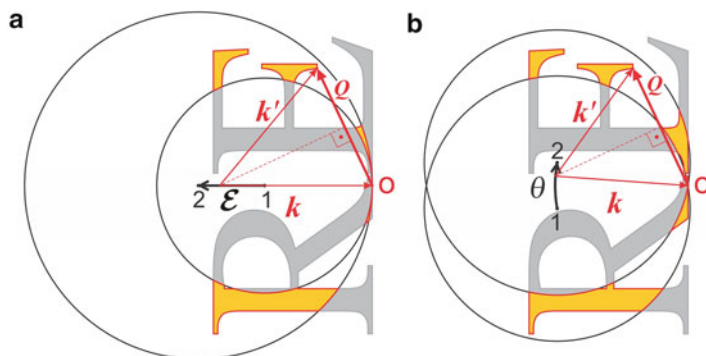


Fig. 5.1 Scattering spheres in: (a) energy scanning with fixed incidence angle; and (b) angle scanning with fixed energy (monochromatic beam). Arrows connecting points 1 and 2 demarcate the trajectories of the spheres center with radius $2\pi/\lambda$ during the scans. The letters RE symbolize regions of non-null values of the function $I(\mathbf{Q})$ in reciprocal space, (4.14), and the highlighted areas symbolize the excited regions in each scanning. Different excitation conditions for the same point in reciprocal space, indicated by the vector \mathbf{Q} , are illustrated

²In crystallography, diffraction geometries in reciprocal space and scattering spheres are, respectively, called Ewald's constructions and reflection spheres, or also Ewald's spheres (Ewald 1969).

depending on which satisfies the diffraction condition: vector \mathbf{Q} secant to the scattering sphere of radius $2\pi/\lambda$. In the case of a monochromatic beam with negligible angular divergence, to scan a reciprocal space region it is necessary to vary the beam incidence angle as in the pictorial situation in Fig. 5.1b.

...

Exercise 5.1. In an experiment with polychromatic radiation, $\hat{\mathbf{z}} = [0, 0, 1]$ is the direction of incidence and $\mathbf{Q} = Q [\sin \alpha \cos \varphi, \sin \alpha \sin \varphi, \cos \alpha]$ is any diffraction vector. Using only vector relations in reciprocal space, find the coordinates of the scattering sphere center exciting vector \mathbf{Q} , the direction of the diffracted beam, and the correlation between α and the scattering angle 2θ .

Answer: From the elastic scattering condition $|\mathbf{k}'|^2 = |\mathbf{k} + \mathbf{Q}|^2 = k^2$, we have that every vector \mathbf{Q} secant to the sphere of radius k will be in a diffraction condition, satisfying the relation

$$\mathbf{k} \cdot \mathbf{Q} = -Q^2/2. \quad (5.1)$$

Since $\mathbf{k} = k\hat{\mathbf{z}}$, the condition of diffraction is summarized as $k \cos \alpha = -Q/2$, which allows us to determine the radius $k = 2\pi/\lambda$ of the scattering sphere exciting the vector \mathbf{Q} . For example, if $\alpha = 120^\circ$ the diffraction condition occurs for $k = Q$, or $\lambda = d_{\text{hkl}}$ in the case of \mathbf{Q} being a vector of the reciprocal lattice of module $2\pi/d_{\text{hkl}}$. The center of the scattering sphere is appointed by the vector antiparallel to the vector of the incident wave, i.e. by $-\mathbf{k}$, which in this case points to the coordinates $(0, 0, -k)$. The direction of the diffracted beam is given by

$$\mathbf{k}' = \mathbf{Q} + \mathbf{k} = [Q \sin \alpha \cos \varphi, Q \sin \alpha \sin \varphi, Q \cos \alpha + k],$$

and since $\alpha > 90^\circ$, $\mathbf{k} \cdot \mathbf{k}' = k^2 \cos 2\theta = \mathbf{k} \cdot (\mathbf{Q} + \mathbf{k}) = k^2 - Q^2/2 = k^2(1 - 2 \cos^2 \alpha)$

$$\Rightarrow 2\theta = 2\alpha - 180^\circ.$$

...

Note 5.1: Vectorial Bragg's Law. When the diffraction vectors correspond to the exact reciprocal lattice vectors, $\mathbf{Q} = 2\pi/d_{\text{hkl}}$ and (5.1) reduces to

$$2\mathbf{k} \cdot \mathbf{Q} = -Q^2 \Rightarrow 2 \frac{2\pi}{\lambda} \cos(90^\circ + \theta) = -\frac{2\pi}{d_{\text{hkl}}} \Rightarrow 2d_{\text{hkl}} \sin \theta = \lambda.$$

...

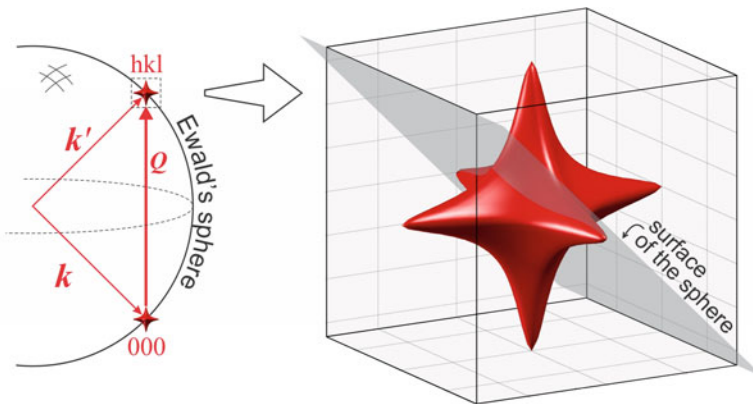


Fig. 5.2 Excitation geometry of a reciprocal lattice node hkl . The diffracted intensity comes from the intersection area between the scattering (Ewald) sphere surface and the reciprocal node volume function $|W(\Delta\mathbf{Q})|^2$, represented here by an isosurface

Exercise 5.2. By varying the angle of incidence of a collimated monochromatic X-ray beam in a small crystal, hkl nodes of the reciprocal lattice touch the scattering sphere generating diffracted beams. (a) What is the scattered intensity during the trajectory of a single node through the surface of the scattering sphere? (b) What is the area under the scattered intensity curve?

Answer (a): Although the intensity distribution in reciprocal space of a crystal is described point-to-point by function $I(\mathbf{Q})$, (4.14), the measurable intensity comes from the sphere surface intersection area with function $|W(\Delta\mathbf{Q})|^2$ responsible for the volume of the nodes, as depicted in Fig. 5.2.

By defining a xyz coordinate system so that the plane of incidence is the plane xz and $\mathbf{Q}_{hkl} = Q_{hkl} [0, 0, 1]$ the reciprocal lattice vector of a given node, then

$$\mathbf{k} = k[\cos \theta, 0, -\sin \theta] \quad \text{and} \quad \mathbf{k}' = k\hat{\mathbf{s}}' = k[\cos \theta', \sin \theta' \sin \varphi', \sin \theta' \cos \varphi'] ,$$

are the possible incident and scattered wavevectors, respectively. At a given angle of incidence θ , the set of reciprocal vectors

$$\mathbf{Q} = \mathbf{k}' - \mathbf{k} = k[\cos \theta' - \cos \theta, \sin \theta' \sin \varphi', \sin \theta' \cos \varphi' + \sin \theta] , \quad (5.2)$$

end on the scattering sphere surface, thus satisfying the condition of elastic scattering. The scattered intensity corresponds to the integral of $I_{hkl}(\mathbf{Q})$, (4.15), on the scattering sphere,

$$I(\theta) = \int I_{hkl}(\mathbf{Q}) d\Omega' = I_{Th} \frac{1}{V_{cel}^2} |F_{hkl}|^2 \int_0^{2\pi} \int_0^\pi |W(\mathbf{Q} - \mathbf{Q}_{hkl})|^2 \sin \theta' d\theta' d\varphi' . \quad (5.3)$$

In general, $|W(\Delta Q)|^2$ is a well-localized function. The maximum occurs when θ and θ' are equal to Bragg's angle and $\varphi' = 0$. Integration intervals in θ' and φ' are thus limited to a small solid angle near the point where Q_{hkl} touches the scattering sphere during the θ scanning. The diffracting crystalline lattice dimensions determine how limited the integration intervals are, the smaller the size of the lattice, the larger the intervals to be considered. In a detector system with open window where all diffracted radiation by a node is accounted, $I_{Th} \rightarrow I_e = \Phi r_e^2 \langle |\mathcal{P}(\hat{s}')|^2 \rangle$ and (5.3) allows accurate numerical solutions within the kinematic approach whatever is the shape of the crystal. Examples of θ scans generating intensity curves with different profiles and same area are shown in Fig. 5.3.

Answer (b): When crossing the sphere surface, all the volume of a reciprocal node will be diffracted so that the area

$$A_{\text{hkl}} = \Delta t \int I(\theta) d\theta = \Delta t I_e \frac{1}{V_{\text{cel}}^2} |F_{\text{hkl}}|^2 \iiint |W(Q - Q_{\text{hkl}})|^2 \sin \theta' d\theta' d\varphi' d\theta , \quad (5.4)$$

under the diffraction curve will be proportional to the radiation count time Δt in each position θ , as well as the volume integral of the function $|W(\Delta Q)|^2$.

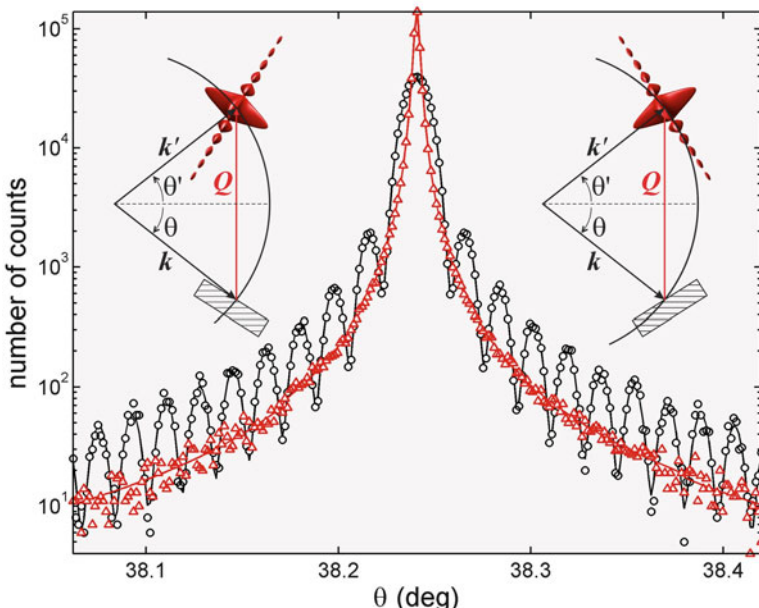


Fig. 5.3 Simulated rocking curves, θ -scans, of the 224 reflection in a GaSb (001) crystal at grazing incidence geometry (circles) and grazing output (up triangles), see Note 5.2. Differences in profiles come from the relative orientation between reciprocal node and scattering sphere (insets). Simulation parameters: crystal with a thickness of $0.5 \mu\text{m}$ and area of $4 \mu\text{m}^2$, $\lambda = 1.540562 \text{\AA}$ and statistics of 5×10^5 counts per curve [rockingcurve.m]

Knowing that,³

$$\int |W(\Delta \mathbf{Q})|^2 dV_Q = (2\pi)^3 V, \quad (5.5)$$

now we only have to find the volume element dV_Q in terms of the variables θ' , φ' , and θ .

Following the same procedure used to find volume elements in non-cartesian coordinates—as in the case of cylindrical and spherical coordinates⁴, it gives that

$$dV_Q = \left| \frac{\partial \mathbf{Q}}{\partial \theta} \cdot \left(\frac{\partial \mathbf{Q}}{\partial \varphi'} \times \frac{\partial \mathbf{Q}}{\partial \theta'} \right) \right| d\theta' d\varphi' d\theta = k^3 [\cos \theta' \sin \theta + \cos \theta \sin \theta' \cos \varphi'] \sin \theta' d\theta' d\varphi' d\theta.$$

The partial derivatives follow directly from (5.2): $\partial \mathbf{Q} / \partial \theta' = k[-\sin \theta', \cos \theta' \sin \varphi', \cos \theta' \cos \varphi']$, $\partial \mathbf{Q} / \partial \varphi' = k \sin \theta' [0, \cos \varphi', -\sin \varphi']$, and $\partial \mathbf{Q} / \partial \theta = k[\sin \theta, 0, \cos \theta]$. As the angular intervals are located around $\theta' \simeq \theta$ and $\varphi' \simeq 0$,

$$\sin \theta' d\theta' d\varphi' d\theta = \frac{dV_Q}{k^3 \sin 2\theta}.$$

Substituting this result together with (5.5) in (5.4), we have

$$A_{hkl} = I_e |F_{hkl}|^2 \frac{N\lambda^3}{\sin 2\theta_{hkl} V_{cel}} \Delta t. \quad (5.6)$$

...

The integrated intensity of the scanning curve, (5.6), is an experimentally measurable quantity. In crystals with N unit cells, the value of the integrated intensity from one reflection to another changes only with the structure factor and scattering angle.⁵ Therefore, regardless of the crystal shape, as long as the entire volume of the reciprocal node crosses the scattering sphere during the scanning curve, the integrated intensity allows us to assign relative values to the $|F_{hkl}|^2$ of the various reflections of a crystal. This fact originates structural analysis methods such as diffractometry of single crystals with monochromatic beam and diffractometry of polycrystals, both capable of solving fractional coordinates, Sect. 4.1.2.

³See Exercise 4.9 or properties of function $\Omega(\mathbf{u})$, Note 3.1.

⁴See Jacobian matrix, e.g. Arfken (1985), or Zachariasen (1945, p. 107).

⁵Angle $2\theta_{hkl}$ in the polarization factor, implicit in the term I_e , and in the geometric factor $1/\sin 2\theta_{hkl}$, also called the Lorentz factor (Als-Nielsen and McMorrow 2001; Giacovazzo 2002).

Note 5.2: Rocking Curves. In thin crystals with rectangular shape, dimensions $L \times L \times T$ where $L \gg T$,

$$|W(\Delta Q)|^2 \simeq V^2 \frac{1}{1 + (\Delta Q'_x L/2)^2} \frac{1}{1 + (\Delta Q'_y L/2)^2} \frac{\sin^2(\Delta Q'_z T/2)}{(\Delta Q'_z T/2)^2},$$

see Exercise 4.7. When the normal direction of the largest face of the crystal is contained in the incidence plane xz , making an angle of θ_n with the diffraction vector Q_{hkl} parallel to the z -axis,

$$\begin{pmatrix} \Delta Q'_x \\ \Delta Q'_z \end{pmatrix} = \begin{pmatrix} \cos \theta_n & -\sin \theta_n \\ \sin \theta_n & \cos \theta_n \end{pmatrix} \begin{pmatrix} \Delta Q_x \\ \Delta Q_z \end{pmatrix}.$$

From (5.2), $\Delta Q_x = k(\cos \theta' - \cos \theta)$, $\Delta Q_y = k\varphi' \sin \theta'$, and $\Delta Q_z = k(\sin \theta' + \sin \theta) - Q_{\text{hkl}}$. By the fact that the dimension L of the crystal along y -axis is large, the angle φ' is too small so that $\sin \varphi' \rightarrow \varphi'$ and $\cos \varphi' \rightarrow 1$. Thus the integral in φ' in (5.3) is $L\lambda / \sin \theta'$, and

$$I(\theta) = I_e N^2 |F_{\text{hkl}}|^2 \frac{\lambda}{L} \int_{\theta-\zeta}^{\theta+\zeta} \frac{1}{1 + (\Delta Q'_x L/2)^2} \frac{\sin^2(\Delta Q'_z T/2)}{(\Delta Q'_z T/2)^2} d\theta',$$

is obtained by numerical solution of the integral in θ' on an interval of width 2ζ around the angle θ . The curves in Fig. 5.3 were obtained for $\theta_n = \pm 32.26^\circ$ and $\zeta = 80\lambda/T \cos \theta$.

5.2 Powder Diffractometry

The easy identification of chemicals substances present in a solid sample consisting of microscopic crystalline grains (crystallites) is one of the most important applications of the diffractometry of polycrystals. When an X-ray beam hits a polycrystalline sample, the diffraction will occur in the crystallites with suitable spatial orientations to satisfy Bragg's law. As the beam is collimated and monochromatic, i.e. low angular divergence and small spectral width, the record of scattering angles 2θ of the diffracted intensities allows determining the interplanar distances $d = \lambda/2 \sin \theta$, (4.9), of the substances present in the sample. As each chemical substance has a characteristic set of interplanar distances, identifying substances which are present there is possible, except for when there are many different substances in the same sample.

Digital catalogs of substances and their interplanar distances are commercially available, both in separate acquisitions and in computer software packages that come with many existing diffractometers in the market. Academic laboratories working with X-ray diffraction, such as the Crystallography Laboratory of the

Physics Institute of the University of São Paulo, in general have these catalogs available that can be used, in principle, by any interested person. Alternatively, a crystallographic information file (CIF) for each of the cataloged substance is available online (Crystallography Open Database: <http://www.crystallography.net/>). Although values of interplanar distances and structure factors are not listed in the CIFs, they can be calculated from the crystallographic information, as implemented in the routines `bragg.m`, `sfactor.m`, and `diffraction.m`.

5.2.1 *Relative Intensities in Polycrystalline Samples*

Other applications of diffractometry of polycrystals are in refining crystallographic information of new materials and studying substances under structural changes in adverse conditions, e.g. temperature and pressure. In many cases you need to register, in addition to the angles 2θ , the relative values of the diffracted intensities, which, ultimately, will determine the fractional coordinates of the atoms in the unit cell. However, accuracy in resolving the structure implies in establishing correlations, free of instrumental effects, among intensity measures and structural factors.

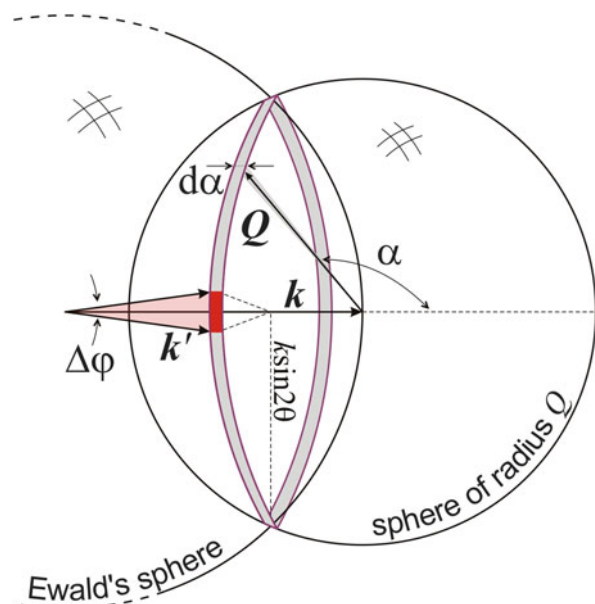
Samples where the crystallites have perfectly random orientation distributions greatly facilitate the solution of structures with high resolution. The preparation of samples requires some care to avoid texturing, which is the induction of preferred orientations. Collecting intensity data in a rotating sample is a common procedure for minimizing texture effects. A second requirement is the constancy of the crystallites number within the diffracting volume. Depending on the particular diffraction geometry used and the shape of the sample, the effective number of crystallites may vary with the instrumental angles, causing correctable systematic variation of the diffracted intensities.⁶ In the simplest situation, samples without textures where the number N_c of crystallites is the same for all the reflections, the relative values of the structure factors, or rather, the histogram of $|F_{hkl}|^2$, e.g. Fig. 4.8, can be inferred from the experimental data of diffracted intensities according to the treatment described below.

5.2.1.1 Geometric Factors

Given \mathbf{Q} as any reciprocal lattice vector of a crystal whose structure is to be analyzed. In a polycrystalline sample of this material, consisting of thousands of randomly oriented crystallites, the set of vectors \mathbf{Q} from all crystallites are evenly distributed over the surface of a sphere of radius Q . Therefore,

⁶For details on diffraction geometry and instrumental effects on the diffracted intensities for polycrystalline sample, see Prince (2006, Ch. 2.3, pp. 42–79).

Fig. 5.4 Reciprocal space of the X-ray diffraction in polycrystalline samples. Each reciprocal lattice vector \mathbf{Q} is represented by a sphere of radius Q , whose intersection with the scattering sphere defines a ring of radius $k \sin 2\theta$ and lateral area $dS = 2\pi Q^2 \sin \alpha d\alpha$ as the locus of all reciprocal vectors of module Q in condition to diffract the incident beam of wavevector \mathbf{k} . The axial acceptance $\Delta\varphi$ of the detector restricts the intensity measures to the diffracted beams with \mathbf{k}' within the fraction $\Delta\varphi/2\pi \sin 2\theta$ of the ring



$dN_c/N_c = (4\pi)^{-1}d\Omega_Q$ corresponds to the fraction of crystallites with vector \mathbf{Q} oriented within the differential solid angle $d\Omega_Q = \sin \alpha d\alpha d\varphi$. When a monochromatic X-ray beam of low divergence hits the sample, the scattering sphere intercepts the sphere of radius Q centered at the reciprocal space origin, defining a ring of lateral area $dS = 2\pi Q^2 \sin \alpha d\alpha$ and radius $k \sin 2\theta$ where $Q = 2k \sin \theta$, as illustrated in Fig. 5.4. The fraction of crystallites in diffraction condition is thus given by the area ratio of the ring and the sphere of radius Q , i.e. $dN_c/N_c = dS/4\pi Q^2 = \frac{1}{2} \cos \theta d\theta$ where $\theta = \alpha - 90^\circ$ (Cullity and Stock 2001). The width $d\theta$ is related to the angular divergence and spectral width of the incident beam.

Intensity measurements are usually limited by the axial acceptance—perpendicular to the instrumental incidence plane—of the detection system. Only the part of the intersection ring scattering inside the detector axial acceptance $\Delta\varphi$ contributes to the intensity measures, Fig. 5.4. The value $\Delta\varphi$ is the same for all reflections, but as the ring radius changes, the relative reduction $\Delta\varphi/2\pi \sin 2\theta$ in the diffracting fraction of crystallites must also be taken into account.

$$\frac{dN_c}{N_c} = \frac{\cos \theta d\theta \Delta\varphi}{4\pi \sin 2\theta} = \frac{d\theta \Delta\varphi}{8\pi \sin \theta} \quad (5.7)$$

is the effective fraction of crystallites responsible for the measured values of the diffracted intensities.⁷

⁷See also Als-Nielsen and McMorrow (2001, p. 157).

5.2.1.2 Area and Line Profile of the Diffraction Peaks

The radiation scattered at a given angle 2θ aggregates contributions from several slightly disoriented crystallites, which is equivalent to scanning a single crystallite through the scattering sphere, as in Fig. 5.3. The integration of the scattered intensity as a function of 2θ corresponds to an intensity measurement with the detector opened, implying that the diffraction peaks of polycrystalline samples have areas that are proportional to the areas of rocking curves of a crystallite, (5.6). Thus, multiplying (5.6) by the effective fraction of crystallites contributing in each reflection, (5.7), we have

$$A_{\text{hkl}} = I_e \left(\sum_n |F_{\text{hkl}}|_n^2 \right) \frac{N_c \langle N \rangle \lambda^3}{8\pi \sin \theta \sin 2\theta V_{\text{cel}}} d\theta \Delta\varphi \Delta t \quad (5.8)$$

as the integrated intensity expression of the reflections in polycrystals. The index n of the sum runs through all reflections with same interatomic distance d_{hkl} , diffracting at $2\theta = 2\sin^{-1}(0.5\lambda/d_{\text{hkl}})$. Note that in some crystals the structure factors in the sum may have slightly different values from each other due to atomic resonance as seen, for instance, in the $|F_{\text{hkl}}|$ table in Note 4.2 for $d = 2.908 \text{ \AA}$.

Having variations of sizes between the N_c crystallites in the sample, the relative values of the structure factor amplitudes are still accessible as long as the average number $\langle N \rangle$ of unit cells per crystallite is constant during the data collection. Within the kinematic limit, the size and shape of the crystallites have little importance to the solution of the structure, except when they are very small or of low crystallinity to the point of affecting the resolution of the diffraction peaks. Accurate measurement of position and area of the peaks are obtained by curve fitting methods. The used line profile functions—Gaussian, Lorentzian, pseudo-Voigt, etc.—are those that best fit the profile of experimental peaks. Moreover, estimating crystallite size is of interest in several studies.

The intrinsic width of the diffraction peaks is related to the mean volume of the reciprocal nodes, $\langle |W(\Delta Q)|^2 \rangle$, calculated over the size and orientation distributions. As $W(\Delta Q)$ is nothing but the FT of a crystallite shape function, the result is analogous to that obtained by small angle scattering in disperse system with size distribution, Sect. 2.3.4. Although the intensities at wide angles are orders of magnitude smaller than at the small angle region, the width of the diffraction peaks is also set within a range around the maximum where the Guinier approximation is satisfactory. In the case of crystallites with shapes not correlated to crystallographic directions, it allows deriving a relationship between the peak width and mean crystallite size from the line profile function

$$\mathcal{L}(\Delta Q) \simeq V^{-2} \lim_{\Delta Q \rightarrow 0} \langle |W(\Delta Q)|^2 \rangle = e^{-\frac{1}{3}(\Delta Q)^2 R_g^2}, \quad (5.9)$$

normalized by height. $\Delta Q = |\mathbf{Q} - \mathbf{Q}_{\text{hkl}}|$ and R_g is the weighted gyration radius of the crystallites as defined in (2.17) for a system of uniform density particles with

distribution of sizes. From the condition $\mathcal{L}(\Delta Q_{1/2}) = 1/2$, we obtain the FWHM (full width at half maximum) in reciprocal space,

$$\beta_Q = 2\Delta Q_{1/2} = 2R_g^{-1} \sqrt{3 \ln(2)} = 2.884/R_g . \quad (5.10)$$

In real space, which is intensity measured as a function of the scattering angle 2θ , the angular FWHM

$$\beta_{2\theta} = \frac{\beta_Q}{(2\pi/\lambda) \cos \theta} = \frac{0.46\lambda}{\cos \theta R_g} \quad (5.11)$$

follows from the relationship $Q = (4\pi/\lambda) \sin \theta$.

In a situation where the value of R_g remains constant for any reflection, all diffraction peaks have the same width β_Q in the reciprocal space. But, in real space, the peaks become wider as the scattering angle increases, reflecting the dependence of the angular FWHM with the term $1/\cos \theta$. In the case of cubic crystallites with edge L , gyration radius $R_g = L/2$, (5.11) provides $\beta_{2\theta} = 0.92\lambda/L \cos \theta$, basically the same result as the popular Scherrer equation used to estimate the crystallite size in powder diffraction (Warren 1990; Zachariasen 1945).

...

Exercise 5.3. Standard samples of polycrystalline silicon are used in calibration of the instrumental widths of many diffractometers. (a) Simulate the silicon diffractogram from the pair distance distribution function (PDDF), (3.10), for a crystallite with dimensions above 10 nm. Are the integrated intensities compatible with the values expected according to (5.8)? (b) By using a pseudo-Voigt function, compare the line profiles of spherical and cubic crystallites of same volume. Are the gyration radii obtained by curve fitting in accordance with the values predicted by (5.10)?

Answer (a): After calculating the PDDF

$$4\pi p(u) = \sum_{a,b} f_a f_b^* \delta(u - r_{ab}) = |f_{Si}(Q)|^2 \sum_{a,b} \delta(u - r_{ab})$$

that is the histogram of interatomic distances r_{ab} , routine `siliconnano.m`, the intensity $I_{PDDF}(Q) = I_{Th} N_c P(Q)$ is obtained as a function of the crystallite scattering power $P(Q) = 4\pi \int p(u) \frac{\sin Qu}{Qu} du$, routine `siliconPofQ.m`. The intensity pattern recorded on an X-ray film using the Debye–Scherrer camera geometry is shown in Fig. 5.5.

From the structure factors, the intensity pattern, or diffractogram, is calculated by

$$I_{XRD}(Q) = K \mathcal{A}(Q) * \mathcal{L}(Q)$$

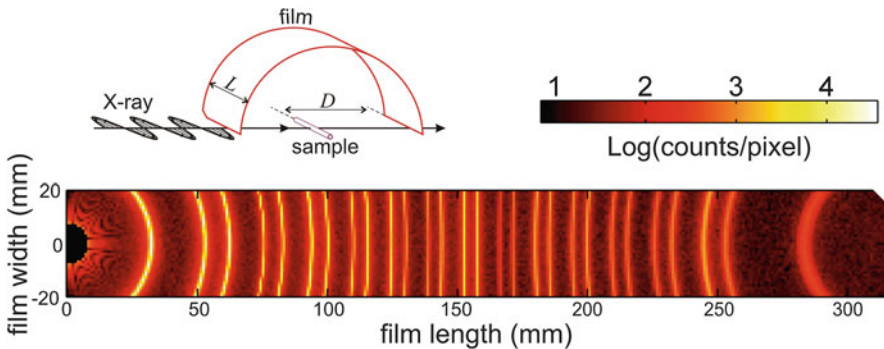


Fig. 5.5 Diffraction pattern of polycrystalline silicon on X-ray film using the Debye–Scherrer camera geometry. $I_{PDDF}(Q)$ for spherical crystallites of diameter 200 Å and disorder of 2 %. Image simulated with statistic of 5×10^6 counts, 12.4 keV X-rays, and σ -polarization. Film radius $D = 100$ mm and pixel size of 1 mm^2 [siliconDScamera.m]

where K contains all the constant terms in a given experiment and

$$\mathcal{A}(Q) = \sum_{\text{hkl}} \frac{|F_{\text{hkl}}|^2}{\sin 2\theta_{\text{hkl}}} Q_{\text{hkl}}^{-1} \delta(Q - Q_{\text{hkl}})$$

takes into account the relative variations of the integrated intensities for the case of σ polarization in which I_e is independent of the scattering angle 2θ . It stands for (5.8) with $\lambda/4\pi \sin \theta$ substituted by Q_{hkl}^{-1} . The hkl sum runs through all reciprocal lattice nodes with negative and positive indexes. When the FWHM β_Q is independent of Q , as assumed in (5.10), the same line profile function of unit area can be used for all peaks, such as the function

$$\mathcal{L}(Q) = x \frac{1}{\sigma \sqrt{2\pi}} e^{-Q^2/2\sigma^2} + (1-x) \frac{2}{\pi} \frac{w}{4Q^2 + w^2}. \quad (5.12)$$

Both parts, Gaussian ($x = 1$) and Lorentzian ($x = 0$), have width β_Q when $\sigma = \beta_Q/2\sqrt{2 \ln 2}$ and $w = \beta_Q$, respectively. As seen in Fig. 5.6, the $I_{XRD}(Q)$ intensity pattern calculated with $8\pi^2\eta_a^2 = 0.35 \text{ \AA}^2$ in the Debye–Waller factor, (4.25), reproduces very well the $I_{PDDF}(Q)$ pattern calculated for a disorder of 2 %, differing only at the end close to $2\theta = 180^\circ$.

Answer (b): Spherical crystallites with diameter D and cubic ones with edge L will have the same volume when $L = D\sqrt[3]{\pi}/6 \simeq 0.8D$. Diffraction peak profiles from PDDFs of crystallites with $D = 200 \text{ \AA}$ ($R_g = 77.5 \text{ \AA}$) and $L = 160 \text{ \AA}$ ($R_g = 80.0 \text{ \AA}$) are shown in Fig. 5.7. Peak fitting with function $\mathcal{L}(Q)$, (5.12), provides $R_g = 82 \text{ \AA}$ and $R_g = 88 \text{ \AA}$ for spherical and cubic crystallites, respectively.

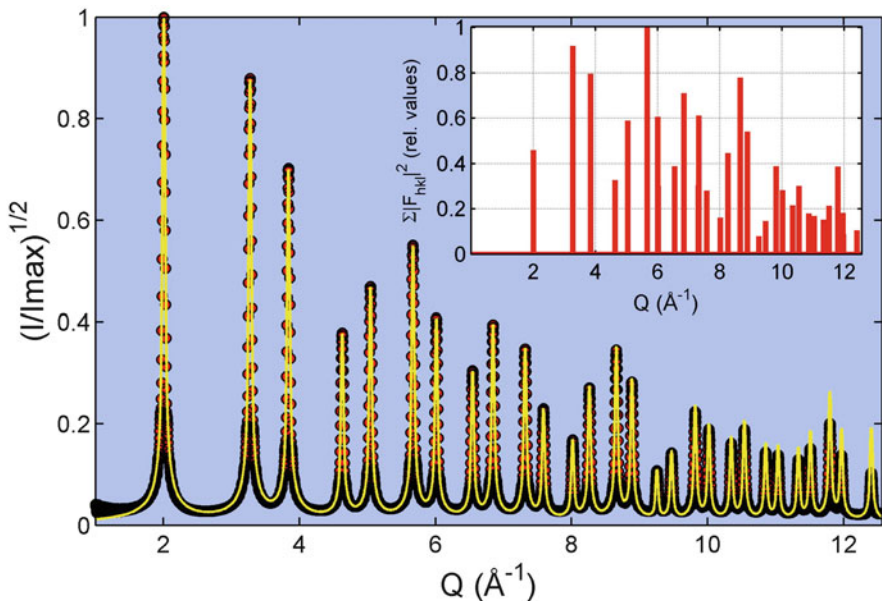


Fig. 5.6 Diffractogram of polycrystalline silicon simulated from distinct approaches: PDDF of spherical crystallites, $I_{PDDF}(Q)$ (circles); and integrated intensities, $I_{XRD}(Q)$ (solid line). Crystallite diameter of 200 Å. Wavelength $\lambda = 1 \text{ \AA}$. Inset: histogram of the structure factors, $\mathcal{F}(Q) = \sum_{hkl} |F_{hkl}|^2 \delta(Q - Q_{hkl})$ [siliconxrdpattern.m]

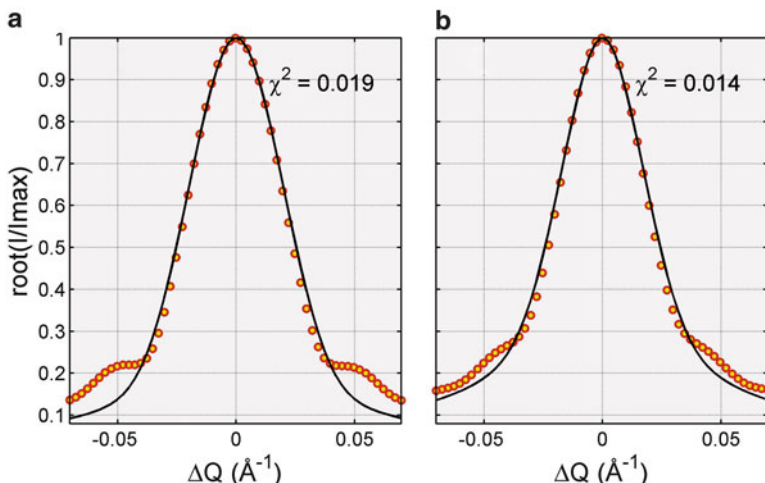


Fig. 5.7 Diffraction peak at $Q = 3.2724 \text{ \AA}^{-1}$ from PDDFs (circles) and best fittings (solid lines) by (5.12): (a) spherical crystallite with diameter of 200 Å and fitting parameters $R_g = 82 \text{ \AA}$ and $x = 0.8$; (b) cubic crystallite with edge of 160 Å and fitting parameters $R_g = 88 \text{ \AA}$ and $x = 0.55$. The least square values, χ^2 , are shown next to each curve [siliconpeakfit.m]

Exercise 5.4. Reflected beam geometry, also known as Bragg–Brentano geometry, is widely used in the diffractometry of polycrystals. The powder samples are packaged in disc like containers with thickness T and extensive surface area, which are much larger than the cross section S_0 of the incident beam. The incidence and scattering directions make an angle θ with the sample’s surface. (a) What is the combined effect of the linear attenuation and variation of illuminated area on the relative intensities? (b) In a polycrystalline silicon sample prepared with 60 % compaction, estimate the minimum thickness so that this combined effect is independent of the angle θ .

Answer (a): An X-ray photon hitting the sample at an angle θ is diffracted by a crystallite at the penetration depth z . The linear path taken from the surface to the crystallite is $z/\sin\theta$, and it is equal to the photon path back to the surface. If μ is the linear attenuation coefficient of the sample, then $e^{-2\mu z/\sin\theta}$ is the photon’s probability of leaving the sample. The decrease in intensity considering all depths within the sample corresponds to the sum of the probabilities, implying in an average thickness

$$T'(\theta) = \int_0^T e^{-2\mu z/\sin\theta} dz = \frac{\sin\theta}{2\mu} [1 - e^{-2\mu T/\sin\theta}] .$$

Since $S_0/\sin\theta$ is the area illuminated by the X-ray beam on the sample’s surface,

$$V'(\theta) = \frac{S_0}{\sin\theta} T'(\theta) = \frac{S_0}{2\mu} [1 - e^{-2\mu T/\sin\theta}] \quad (5.13)$$

is the effective diffracting volume. The variation of the effective volume with the angle θ means that the number of crystallites contributing in the diffracted intensities at different angles varies, but this variation can be discarded in thick samples where $e^{-2\mu T} \ll 1$.

Answer (b): In powder samples, the linear attenuation coefficient $\mu = c \mu_{\text{crystal}}$ depends on the compaction factor c , equal to the mass density ratio between the sample and the material in crystal form (Cullity and Stock 2001). In a silicon crystal, there are 8 atoms per cubic unit cell of edge $a = 5.4309 \text{ \AA}$, and thus, $\mu_{\text{Si}} = 8\sigma(\mathcal{E})/a^3$ where the total cross-section $\sigma(\mathcal{E})$ is a function of the X-ray energy, (1.59).⁸ Considering that the corrections in the relative intensities are negligible when less than 1 %, (5.13) requires $2\mu T > \ln(100) = 4.6$. For characteristic copper radiation $K_{\alpha 1}$, $\mathcal{E} = 8048 \text{ eV}$, $\mu_{\text{Si}} = 14.5 \text{ mm}^{-1}$, and $\mu = 0.6\mu_{\text{Si}} = 8.72 \text{ mm}^{-1}$, which leads to $T > 0.26 \text{ mm}$. When the radiation energy increases, the minimum thickness also increases. For example, $\mathcal{E} = 12398.5 \text{ eV}$ would require $T > 0.935 \text{ mm}$.

...

⁸Routines `fpp.m`, `sgrayleigh.m`, and `sgcompton.m`.

5.3 Single Crystal Diffractometry

Measuring a large number of individual reflections is the main advantage of the single crystal diffractometry, something infeasible in polycrystalline samples. By means of the kinematic diffraction in single crystals, it is possible to assign values related to the structure factor amplitudes individually without overlapping values of those reflections that have interplanar distances that are equal or very close to each other, that is, you have $|F_{\text{hkl}}|^2$ from each hkl reflection instead of their sum as in (5.8). The appropriate experimental conditions for the diffraction of single crystals are those that allow recording diffracted intensities by ideally small crystals where the kinematic approach is valid for all reflections and the linear attenuation effects negligible. The feasibility to meet such conditions depends mainly on the radiation source.

5.3.1 With Monochromatic Radiation

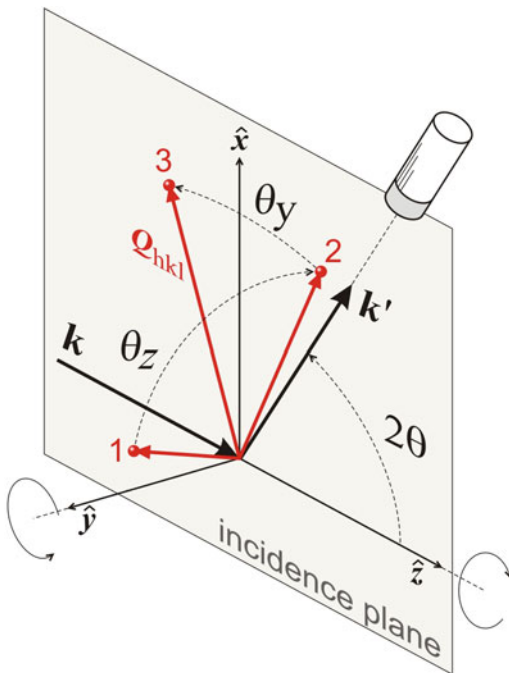
The characteristic radiation—spectral lines of metallic targets employed in X-ray generation by compact sources such as tubes, rotating anodes, and microfocus—has been responsible for the development of single crystal diffractometry with monochromatic radiation. At the cost of a few hundred thousand dollars, research groups may have at their disposal an equipment capable of determining the structure of single crystals. These equipments have goniometric system of good accuracy and mechanical stability to orient spatially the three-dimensional lattice of a crystal in order to automatically measure a large number of reflections.

Although there are variations, the goniometer with a fixed incidence plane is one of the most common. Efficient for crystals of low structural complexity, it consists of three axes for rotating the sample and an axis for positioning the photon counter (one-dimensional detector). From the manual identification of few non-collinear reflections, the sample orientation matrix is established and any reflection, within the mechanical limits of each equipment, can then be measured. After a hkl reflection is chosen, the systematic procedure is to place the diffraction vector on the incidence plane and turn it in this plane until the diffraction condition is satisfied, e.g. Fig. 5.8. With the detector positioned at the scattering angle $2\theta_{\text{hkl}}$, the diffracted intensity is collected during a narrow rocking curve around the exact Bragg diffraction condition. This measure corresponds to the integrated intensity defined in (5.6). Normalized by the radiation counting time, the measure provides the reflection power

$$P_{\text{hkl}} = I_e |F_{\text{hkl}}|^2 \frac{N\lambda^3}{\sin 2\theta_{\text{hkl}} V_{\text{cel}}} , \quad (5.14)$$

sometimes also called integrated intensity for historical reasons.

Fig. 5.8 Goniometry of single crystals illustrating basic rotations to observe a chosen hkl reflection whose reciprocal node is initially in an arbitrary position in the three-dimensional space (position 1): (1) rotation of θ_z around the z -axis, parallel to the incident wavevector k , places the node in the incidence plane xz (position 2); (2) θ_y rotation around the y -axis places the node in the diffraction condition (position 3); (3) detector positioned to monitor the diffracted intensity with wavevector $k' = Q_{hkl} + k$



In the case of crystals with higher structural complexity such as protein crystals, the goniometry with unidimensional photon counter is less efficient due to the large number of reflections to be measured. The rotating crystal method collects the diffracted intensities on film, or area detector type CCD (Charge Coupled Device), during crystal rotation around a single axis, e.g. Fig. 5.12. Besides the higher efficiency in the collection of integrated intensities, the method differs from the previous one by the fact that most reflections occur on an inclined incidence plane with respect to the rotation axis, and therefore the reflection power expression

$$P_{hkl} = I_e |F_{hkl}|^2 \frac{N\lambda^3}{\cos \omega \cos \omega' |\sin(\phi' - \phi)| V_{cel}}, \quad (5.15)$$

see the deduction in Note 5.3, is different from that in (5.14). The angles in this expression are defined in relation to the rotation axis, as in Fig. 5.9. In the particular situation where the incidence plane is perpendicular to the rotation axis, $\omega = \omega' = 0$ and $\phi' - \phi = 2\theta_{hkl}$, which results in (5.14). The many intensity values collected automatically either with unidimensional detector or area detector consist in the set of experimental data available for unraveling the atom fractional coordinates in the unit cell. Structural modeling, feasible for simple structures, and electron density maps are the methods used to solve the structure of a crystal (Giacovazzo 2002).

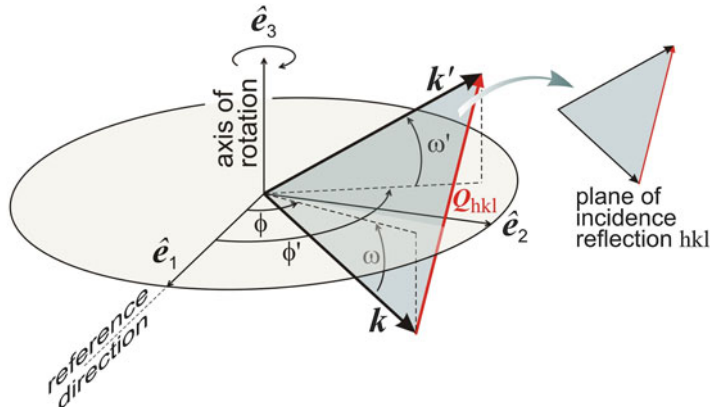


Fig. 5.9 Wavevectors k and k' in spherical coordinates, ω , ϕ , ω' , and ϕ' , defined in relation to the axis \hat{e}_3 of crystal rotation ϕ and an arbitrary reference direction, \hat{e}_1

Note 5.3: Integrated Intensity, Rotating Crystal Method (Zachariasen 1945). Given

$$\mathbf{k} = k[\cos \omega \cos \phi, \cos \omega \sin \phi, \sin \omega] \quad \text{and} \quad \mathbf{k}' = k[\cos \omega' \cos \phi', \cos \omega' \sin \phi', \sin \omega']$$

as the incident and diffracted wavevectors, respectively, described in spherical coordinates in relation to the rotation axis ϕ , Fig. 5.9. Following a procedure that is similar to that used in Exercise 5.2(b), the area under the intensity curve as a function of the rotation angle is

$$A_{hkl} = \Delta t \int I(\phi) d\phi = \Delta t I_e \frac{1}{V_{cel}^2} |F_{hkl}|^2 \iiint |W(\mathbf{Q} - \mathbf{Q}_{hkl})|^2 \cos \omega' d\omega' d\phi' d\phi,$$

whose volume element is calculated by the Jacobian of the transformation: $\mathbf{Q} = \mathbf{k}' - \mathbf{k}$ and

$$dV_Q = \left| \frac{\partial \mathbf{Q}}{\partial \phi} \cdot \left(\frac{\partial \mathbf{Q}}{\partial \phi'} \times \frac{\partial \mathbf{Q}}{\partial \omega'} \right) \right| d\omega' d\phi' d\phi = k^3 \cos \omega \cos \omega' |\sin(\phi' - \phi)| \cos \omega' d\omega' d\phi' d\phi,$$

that is, $\cos \omega' d\omega' d\phi' d\phi = dV_Q/k^3 \cos \omega \cos \omega' |\sin(\phi' - \phi)|$, resulting in

$$A_{hkl} = I_e |F_{hkl}|^2 \frac{N \lambda^3}{\cos \omega \cos \omega' |\sin(\phi' - \phi)| V_{cel}} \Delta t.$$

...

Exercise 5.5. Single crystal goniometers spatially orient the sample's diffraction vectors starting from the orientation matrix. (a) With two crystallographic directions identified beforehand $A = [A_1 A_2 A_3]$ and $B = [B_1 B_2 B_3]$,⁹ find the orientation matrix and the crystalline lattice base vectors, i.e. edge vectors \mathbf{a} , \mathbf{b} , and \mathbf{c} , in an xyz coordinate system where the direction A coincides with the z -axis and direction B is within the xz -plane. (b) In a monoclinic lattice, $\alpha = \gamma = 90^\circ$ and $\beta \neq 90^\circ$, what is the orientation matrix for directions $A = [100]$ and $B = [010]$? (c) With $\mathbf{k} = k\hat{z}$ being the incident wavevector, which are the rotations necessary for reflection 002 to diffract on the xz incidence plane?

Answer (a): Directions A and B correspond to vectors $\mathbf{A} = A_1\mathbf{a} + A_2\mathbf{b} + A_3\mathbf{c}$ and $\mathbf{B} = B_1\mathbf{a} + B_2\mathbf{b} + B_3\mathbf{c}$. Edge vectors, in matrix notation $\mathbf{a} = [a_1, a_2, a_3] = [a_i]$, $\mathbf{b} = [b_i]$, and $\mathbf{c} = [c_i]$, are defined arbitrarily since the unit cell geometry is maintained (see Exercise 4.2). From the directions A and B , an orthonormal basis is created

$$\hat{\mathbf{e}}_1 = \hat{\mathbf{e}}_2 \times \hat{\mathbf{e}}_3, \quad \hat{\mathbf{e}}_2 = \mathbf{A} \times \mathbf{B} / |\mathbf{A} \times \mathbf{B}|, \quad \text{and} \quad \hat{\mathbf{e}}_3 = \mathbf{A} / |\mathbf{A}|. \quad (5.16)$$

The orientation matrix $\mathcal{M} = [e_{ij}]$ formed by coefficients of the versors $\hat{\mathbf{e}}_i = [e_{i1}, e_{i2}, e_{i3}]$, projects the edge vectors on the orthonormal basis, $\mathbf{a} = e_{ij}a_j\hat{\mathbf{e}}_i$, $\mathbf{b} = e_{ij}b_j\hat{\mathbf{e}}_i$, and $\mathbf{c} = e_{ij}c_j\hat{\mathbf{e}}_i$.¹⁰ In the absence of rotations, $\hat{\mathbf{e}}_i = [\delta_{ij}]$ where $\delta_{ij} = 1$ (or 0) if $i = j$ (or $i \neq j$) and the edge vector components, in row matrix notation, are represented by $\mathbf{a} = [e_{1j}a_j, e_{2j}a_j, e_{3j}a_j] = [e_{ij}a_j]$, $\mathbf{b} = [e_{ij}b_j]$ and $\mathbf{c} = [e_{ij}c_j]$.

Answer (b): Starting from the arbitrary base $\mathbf{a} = a[\sin \beta, 0, \cos \beta]$, $\mathbf{b} = b[0, 1, 0]$, and $\mathbf{c} = c[0, 0, 1]$ (Exercise 4.2). $\mathbf{A} = \mathbf{a}$ and $\mathbf{B} = \mathbf{b}$ imply that

$$\mathcal{M} = \begin{pmatrix} 0 & 1 & 0 \\ -\cos \beta & 0 & \sin \beta \\ \sin \beta & 0 & \cos \beta \end{pmatrix},$$

resulting in the new base $\mathbf{a} = a[0, 0, 1]$, $\mathbf{b} = b[1, 0, 0]$, and $\mathbf{c} = c[0, \sin \beta, \cos \beta]$ where \mathbf{a} (direction A) $\parallel \hat{z}$ and \mathbf{b} (direction B) $\in xz$, Fig. 5.10a.

Answer (c): Given $\mathcal{R}_X(\theta_x)$, $\mathcal{R}_Y(\theta_y)$, and $\mathcal{R}_Z(\theta_z)$ as the sample rotation operations whose senses follow the “right hand” rule. Redirecting the orthonormal basis according to matrix $\mathcal{R} = [R_{ij}]$, $\hat{\mathbf{e}}_i = [R_{ij}]$ and replacing in the result of item (a), we have $\mathbf{a} = [e_{ij}a_jR_{ik}]$, $\mathbf{b} = [e_{ij}b_jR_{ik}]$, and $\mathbf{c} = [e_{ij}c_jR_{ik}]$. With null rotations, $\mathbf{Q}_{002} = 2\mathbf{c}^* = (\frac{4\pi}{c \sin \beta})[0, 1, 0]$ are the initial diffraction vector coordinates. Putting it in the xz -plane requires a rotation of -90° around the z -axis, followed by a rotation of θ_{002} around the y -axis to get the exact diffraction condition. So, $\mathbf{Q}_{002} = (\frac{4\pi}{c \sin \beta})[\cos \theta_{002}, 0, -\sin \theta_{002}]$, generating the diffracted beam $\mathbf{k}' = \mathbf{Q}_{002} + \mathbf{k} = \mathbf{k}$

⁹Equal sign used only to associate letter/label to a crystallographic direction whose indexes are given in brackets.

¹⁰Einstein sum convention, for example, $\mathbf{a} = e_{ij}a_j\hat{\mathbf{e}}_i = \sum_{i,j=1}^3 e_{ij}a_j\hat{\mathbf{e}}_i = (e_{11}a_1 + e_{12}a_2 + e_{13}a_3)\hat{\mathbf{e}}_1 + (e_{21}a_1 + e_{22}a_2 + e_{23}a_3)\hat{\mathbf{e}}_2 + (e_{31}a_1 + e_{32}a_2 + e_{33}a_3)\hat{\mathbf{e}}_3 = (\mathbf{a} \cdot \hat{\mathbf{e}}_1)\hat{\mathbf{e}}_1 + (\mathbf{a} \cdot \hat{\mathbf{e}}_2)\hat{\mathbf{e}}_2 + (\mathbf{a} \cdot \hat{\mathbf{e}}_3)\hat{\mathbf{e}}_3$.

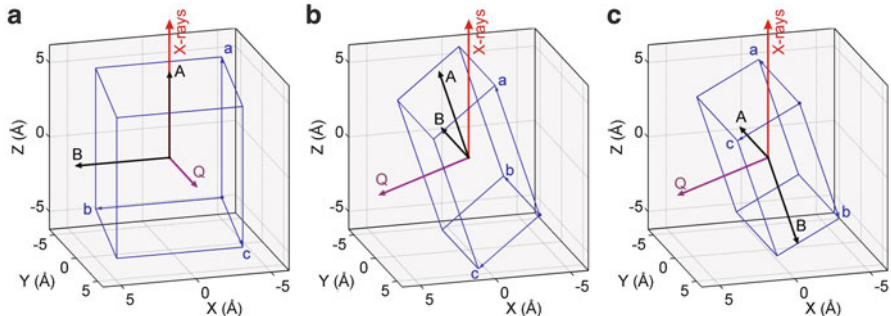


Fig. 5.10 Monoclinic unit cell oriented in the laboratory's xyz coordinate system. (a) Null rotations, orientation matrix defined with the direction $A = [100]$ parallel to the incident X-ray beam and the direction $B = [010]$ contained in the xz -incidence plane. (b, c) Reciprocal vector \mathbf{Q}_{002} in diffraction condition, rotations (b) $\mathcal{R}_Y(\theta_{002}) \mathcal{R}_Z(-90^\circ)$ and (c) $\mathcal{R}_Y(90^\circ + \theta_{002}) \mathcal{R}_X(90^\circ)$. Lattice parameters: $a = 9.462 \text{ \AA}$, $b = 8.392 \text{ \AA}$, $c = 5.221 \text{ \AA}$, $\alpha = \gamma = 90^\circ$ e $\beta = 110.18^\circ$. $\lambda = 1.540562 \text{ \AA}$ e $\theta_{002} = 18.3227^\circ$. Vectors A , B , and Q indicated by arrows with arbitrary lengths [orientcryst.m]

$[\sin 2\theta_{002}, 0, \cos 2\theta_{002}]$ on the xz -plane. The rotations matrix is

$$\mathcal{R} = \mathcal{R}_Y(\theta_{002}) \mathcal{R}_Z(-90^\circ) = \begin{pmatrix} 0 & \cos \theta_{002} & \sin \theta_{002} \\ -1 & 0 & 0 \\ 0 & -\sin \theta_{002} & \cos \theta_{002} \end{pmatrix},$$

Figure 5.10b. Alternatively, rotations $\mathcal{R}_Y(90^\circ + \theta_{002}) \mathcal{R}_X(90^\circ)$ also put the vector \mathbf{Q}_{002} in the diffraction condition, Fig. 5.10c.

Exercise 5.6. In a rotating crystal experiment, calculate the spherical coordinates of the wavevectors in Fig. 5.9 for a given reflection hkl and preselected rotation axis. Answer: Rotating axis and reference direction specified by the crystallographic directions A and B , respectively. In the orthonormal basis $\hat{\mathbf{e}}_i$, (5.16), $\mathbf{k} = k[\cos \omega \cos \phi, \cos \omega \sin \phi, \sin \omega]$ and $\mathbf{k}' = k[\cos \omega' \cos \phi', \cos \omega' \sin \phi', \sin \omega']$. The angle ω is fixed and determined by the experimental setup: rotating axis at $90^\circ - \omega$ from the incident wavevector direction. The angle ϕ depends on the diffraction vector Q of the reflection in question. Projecting the vector on the orthonormal base, $\mathbf{Q}_e = [\mathbf{Q} \cdot \hat{\mathbf{e}}_i] = Q[\sin \alpha_Q \cos \phi_Q, \sin \alpha_Q \sin \phi_Q, \cos \alpha_Q]$, the angle ϕ is obtained from (5.1),

$$\mathbf{k} \cdot \mathbf{Q}_e = -kQ \sin \theta \Rightarrow \cos(\phi - \phi_Q) = \cos(\Delta\phi) = -\frac{\sin \theta + \sin \omega \cos \alpha_Q}{\cos \omega \sin \alpha_Q}.$$

Table 5.1 Spherical coordinates of the wavevectors \mathbf{k} and \mathbf{k}' , Fig. 5.9

hkl	α_Q	ϕ_Q	ω	ϕ	ω'	ϕ'	$ \sin(\phi' - \phi) $
204	53.432	-90.000	-18.894	174.045	0.000	199.778	0.434
				5.955		340.222	0.434
137	50.613	-18.435	-18.894	232.318	14.056	274.521	0.672
				90.812		48.609	0.672
222	75.304	-45.000	-18.894	209.993	-9.318	247.170	0.604
				60.007		22.830	0.604
226	51.804	-45.000	-18.894	209.993	9.318	247.170	0.604
				60.007		22.830	0.604
040	90.000	0.000	0.000	244.117	0.000	295.883	0.786
				115.883		64.117	0.786

Rotating axis [001], reference direction [010], $\lambda = 1.480506 \text{ \AA}$, tetragonal lattice, $a = b = 6.783 \text{ \AA}$ and $c = 18.288 \text{ \AA}$ [rotatcrys.m]

Note that in a complete 360° rotation the reciprocal node of a reflection crosses the scattering sphere twice, corresponding to the positions $\phi = \phi_Q \pm \Delta\phi$. In each position, $\mathbf{k}' = [\mathbf{k}'_i] = \mathbf{Q}_e + \mathbf{k}$. So, $\sin \omega' = k'_3/k$ and $\tan \phi' = k'_2/k'_1$. See examples in Table 5.1.

...

The X-ray flux obtained from compact sources imposes a limit on the minimum size of the crystals to be studied. Even using optimized focal optics for flux gain, the crystals must have dimensions greater than several tens of microns so that it is possible to collect intensities from a significant number of reflections. However, in crystals larger than a few microns, the relative experimental intensity values may differ from the predicted values by the Kinematics Theory. Corrections for linear attenuation are feasible, but correcting the data for dynamical diffraction effects is, in practice, impossible. There are several aspects that make complex the dynamical calculation, but the main difficulty is the lack of an exact approach for crystals that are neither perfect nor ideally imperfect (Warren 1990; Zachariasen 1945), that is, for real crystals. Thus, because of lack of alternatives, data are analyzed within the kinematic approach, (5.14) or (5.15), being aware that dynamical diffraction effects are one more factor in addition to the intrinsic difficulties stemming from the lack of information on the structure factor phases compromising the structural resolution.

5.3.2 With Polychromatic Radiation

The high gain of flux provided by synchrotron sources certainly allows data collection in very small crystals. However, in addition to the high flux, these sources also provide an intense continuous spectrum, which greatly favors the

diffractometric of single crystals with polychromatic radiation where the reflections occur simultaneously and the integrated intensities are obtained without the need to rotate the sample. This combination of facilities enables experiments with temporal resolution, which are available in some synchrotron laboratories. On the other hand, the insignificant continuous spectrum of compact sources, commonly called *Bremsstrahlung*, restricts the use of the method—which is internationally known as the Laue method (Max von Laue 1913)—to simple applications such as checking of crystalline state in natural and synthetic crystals, identification of crystallographic axes symmetry, and experiments for teaching purposes.

...

Exercise 5.7. What is the diffracted power by a hkl node when diffraction experiments in single crystals are made with polychromatic radiation and fixed direction of incidence?

Answer: Similar calculation to the integrated intensity with monochromatic radiation, Exercise 5.2(b). The difference is the fact that the reciprocal node volume is scanned by endless scattering spheres associated with continuous wavelengths of the incident radiation. Given $\mathbf{k} = k[1, 0, 0]$ as the incident wavevector and

$$\mathbf{Q} = \mathbf{k}' - \mathbf{k} = k[\cos \theta' - 1, \sin \theta' \sin \varphi', \sin \theta' \cos \varphi'] \quad (5.17)$$

as the set of all reciprocal vectors ending on the surface of the scattering sphere with radius $k = 2\pi/\lambda$ when passing by the center of the hkl node. $\theta' = 2\theta$ is the scattering angle. To represent the wavelength variation, we create a dimensionless variable ϵ , so that $k \rightarrow (1 + \epsilon)k$. Then,

$$I(\epsilon) = \int I_{\text{hkl}}(\mathbf{Q}) d\Omega' = I_{\text{Th}} \frac{1}{V_{\text{cel}}^2} |F_{\text{hkl}}|^2 \int_0^{2\pi} \int_0^\pi |W(\mathbf{Q} - \mathbf{Q}_{\text{hkl}})|^2 \sin \theta' d\theta' d\varphi'$$

is the scattered intensity at the wavelength $\lambda/(1 + \epsilon)$, and the total diffracted intensity (with open detector)

$$A_{\text{hkl}} = \Delta t \int I(\epsilon) d\epsilon = \Delta t I_e \frac{1}{V_{\text{cel}}^2} |F_{\text{hkl}}|^2 \iiint |W(\mathbf{Q} - \mathbf{Q}_{\text{hkl}})|^2 \sin \theta' d\theta' d\varphi' d\epsilon, \quad (5.18)$$

is analogous to the area under the intensity curve which, in this case, is a function of the dimensionless variable. Using the Jacobian of the transformation of variables, the volume element in the reciprocal space

$$dV_Q = \left| \frac{\partial \mathbf{Q}}{\partial \epsilon} \cdot \left(\frac{\partial \mathbf{Q}}{\partial \varphi'} \times \frac{\partial \mathbf{Q}}{\partial \theta'} \right) \right| d\theta' d\varphi' d\epsilon = 2k^3 \sin^2 \theta \sin \theta' d\theta' d\varphi' d\epsilon,$$

is written in terms of the variables θ' , φ' , and ϵ . Only the partial derivative $\partial \mathbf{Q} / \partial \epsilon = \mathbf{Q}$ is different from those used in the deduction of (5.6). Substituting in (5.18)

$$\sin \theta' d\theta' d\varphi' d\epsilon = \frac{dV_Q}{2k^3 \sin^2 \theta}$$

and recalling that $\int |W(\Delta \mathbf{Q})|^2 dV_Q = (2\pi)^3 V$, (5.5), we obtain the diffracted power

$$P_{\text{hkl}}(\lambda) = \frac{A_{\text{hkl}}}{\Delta t} = I_e |F_{\text{hkl}}|^2 \frac{N\lambda^3}{2 \sin^2 \theta_{\text{hkl}} V_{\text{cel}}} = I_e N |F_{\text{hkl}}|^2 \left(\frac{2\lambda d_{\text{hkl}}^2}{V_{\text{cel}}} \right). \quad (5.19)$$

The value of λ , satisfying the condition of diffraction for a given hkl node, depends on the angle between the diffraction vector and the direction of incidence, e.g. Exercise 5.1. Furthermore, there is the variation of flux with the wavelength, $\Phi(\lambda) = w(\lambda)\Phi_{\max}$, whose weight function $w(\lambda)$, is defined by the particularities of each radiation source. In most cases, this variation implies only in $I_e \rightarrow w(\lambda)I_e$ in (5.19), where $I_e = \langle |\mathcal{P}(\hat{s}')|^2 \rangle r_e^2 \Phi_{\max}$.

Exercise 5.8. The lithium metal (Li) has a unique role in automotive batteries and mobile phone technologies in addition to the use in medicine. The most important natural source of Li is spodumene mineral, $\text{LiAl}(\text{SiO}_3)_2$, often found in crystalline form, monoclinic system.¹¹ Simulate the polychromatic diffraction pattern of spodumene on an X-ray film. Note: neglect linear attenuation, Compton scattering, and rescattering effects (dynamical diffraction).

Answer: In a given crystal orientation, the reciprocal lattice vectors \mathbf{Q}_{hkl} in the laboratory reference system xyz are obtained from the base $\mathbf{a} = [e_{ij}a_j R_{ik}]$, $\mathbf{b} = [e_{ij}b_j R_{ik}]$, and $\mathbf{c} = [e_{ij}c_j R_{ik}]$, see Exercise 5.5(c). With $\mathbf{k} = k\hat{s}$ as the incident wavevector,

$$\mathbf{Q}_{\text{hkl}} \cdot \hat{s} < 0 \quad \text{and} \quad \lambda = -4\pi \mathbf{Q}_{\text{hkl}} \cdot \hat{s} / Q_{\text{hkl}}^2 \in [\lambda_{\min}, \lambda_{\max}]$$

are the diffraction conditions of the reflection hkl. The diffracted beam will have orientation $\hat{s}' = (\lambda/2\pi) \mathbf{Q}_{\text{hkl}} + \hat{s}$ and relative power given by (5.19), which is

$$P_{\text{hkl}} \propto w(\lambda) \langle |\mathcal{P}(\hat{s}')|^2 \rangle \frac{\lambda |F_{\text{hkl}}|^2}{Q_{\text{hkl}}^2}.$$

In the case of a cylindrical film with radius D , with axis along the y -direction, and incident beam parallel to the direction z ($\hat{s} = [0, 0, 1]$), Fig. 5.11 (inset), the diffracted intensities at coordinates (X_f, Y_f) on the film are given by

$$X_f = D \arctan(-s'_1/s'_3) \quad \text{and} \quad Y_f = D \tan[\arcsen(s'_2)].$$

Figure 5.11 shows the diffraction pattern with the reciprocal vectors \mathbf{Q}_{00l} at 10° from the incidence direction (170° from \hat{s}). In this example, $\lambda_{\max} = 2\lambda_{\min} = 2 \text{ \AA}$, and the

¹¹COD ID: 2003129 (Crystallography Open Database: <http://www.crystallography.net/>).

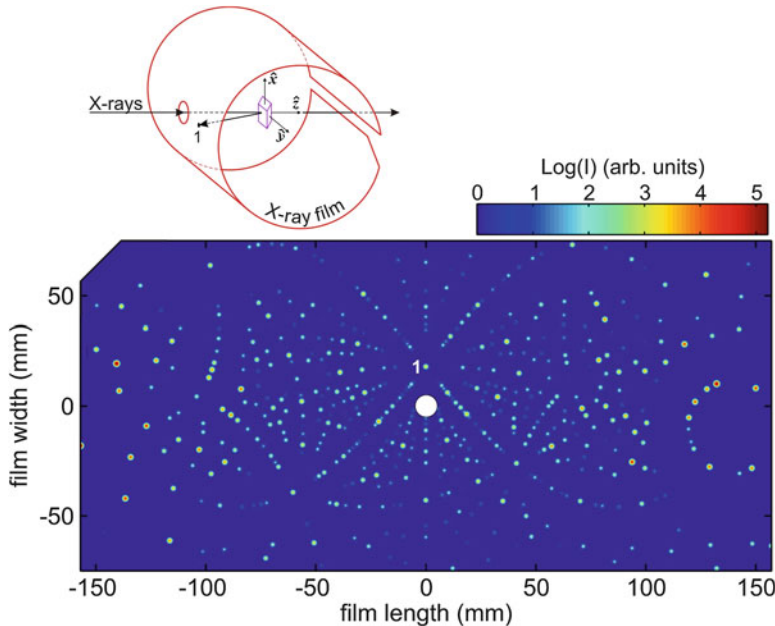


Fig. 5.11 Polychromatic diffraction pattern, spodumene crystal. Orientation: $A = [100]$, $B = [001]$, and $\mathcal{R} = R_X(10^\circ) \mathcal{R}_Y(90^\circ)$. All $00l$ reflections, with $l > 0$, contribute at the point 1 indicated [lauemethod.m]

spectrum has constant weight in the interval given, i.e. $w(\lambda) = 1$ if $\lambda_{min} \leq \lambda \leq \lambda_{max}$ or otherwise $w(\lambda) = 0$. Below there are a few indexes of the reflections seen in Fig. 5.11, routine lauemethod.m:

spodumen.in, $A = [1 0 0]$, $B = [0 0 1]$, TH = [10.000 90.000 0.000]							
h	k	l	$ F_{hkl} ^2$	$wl(A)$	$Phkl$	X (mm)	Y (mm)
-2	-2	1	15679.2(100.0%)	1.414618	163960.8	-140.745	19.482
0	2	0	5467.6(34.9%)	1.457256	123872.3	-157.080	-18.199
3	-1	0	9752.6(62.2%)	1.466306	106920.3	132.351	10.299
5	3	1	13401.2(85.5%)	1.606282	30197.4	93.953	-25.506
-3	1	1	1784.0(11.4%)	1.746826	24652.4	-127.186	-9.068
-2	4	1	8237.9(52.5%)	1.439858	24103.1	-136.616	-42.121
1	-1	0	480.9(3.1%)	1.306717	22767.4	150.059	8.217
5	-3	1	13136.7(83.8%)	1.167313	20555.7	117.719	28.233
-3	-1	1	1758.9(11.2%)	1.070540	15076.0	-139.580	7.168
-3	3	1	3389.4(21.6%)	1.256694	14815.1	-134.311	-23.363
-6	0	4	5751.4(36.7%)	1.547614	11698.1	-84.180	7.934
4	0	0	1518.6(9.7%)	1.508597	11274.8	122.467	2.037
0	0	6	2040.1(13.0%)	1.608684	1933.2	0.000	18.199
0	0	8	327.5(2.1%)	1.206513	130.9	0.000	18.199

...

5.4 Protein Crystals

Large unit cells, with dimensions of tens of angstroms, have reciprocal spaces with high density of reciprocal lattice nodes, approximately 1000 times the density observed in inorganic crystals. Figure 5.12 shows a situation where about 3000 reflections diffract in the small solid angle comprehended by the flat area detector with a diameter of 10 and 60 cm distant from the sample. The low crystallographic symmetry of the rotating axis allows each reflection to contribute separately in the simulated image with angular resolution of 0.2 mrad.

When working with protein crystals it is common to save the structural information in Cartesian coordinates, atomic positions (X_a , Y_a , Z_a) instead of fractional coordinates (x_a , y_a , z_a). The conversion matrix \mathbb{S} , between Cartesian and fractional coordinates is set from the position vector

$$\mathbf{r}_a = x_a \mathbf{a} + y_a \mathbf{b} + z_a \mathbf{c} = X_a \hat{\mathbf{x}} + Y_a \hat{\mathbf{y}} + Z_a \hat{\mathbf{z}}$$

of any atom in the crystal unit cell, written in both coordinate systems, so that

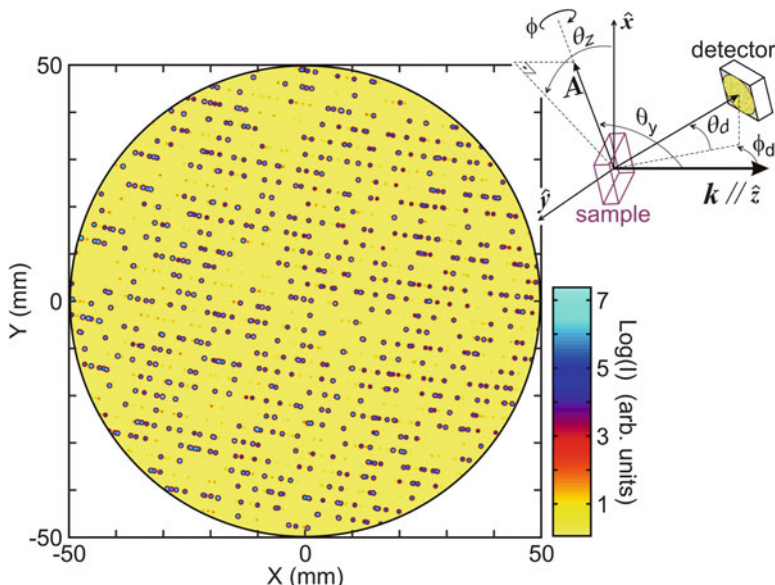


Fig. 5.12 Rotating crystal method. Simulated diffraction pattern of crystallized insulin (PDB ID: 1TRZ) with characteristic $CuK_{\alpha 1}$ radiation ($\lambda = 1.540562 \text{ \AA}$). Rotating axis $A = [5\ 1\ 0]$, in the orientation $\theta_y = 60^\circ$ and $\theta_z = 30^\circ$. Flat area detector distant 60 cm from the sample in the azimuth $\phi_d = -30^\circ$ and null elevation $\theta_d = 0$, pixel size $125 \mu\text{m}$. Note 5.4 [rotcrystmethod.m]

$$\begin{pmatrix} x_a \\ y_a \\ z_a \end{pmatrix} = \mathbb{S} \begin{pmatrix} X_a \\ Y_a \\ Z_a \end{pmatrix} \quad \text{where} \quad \mathbb{S}^{-1} = \begin{pmatrix} \mathbf{a} \cdot \hat{\mathbf{x}} & \mathbf{b} \cdot \hat{\mathbf{x}} & \mathbf{c} \cdot \hat{\mathbf{x}} \\ \mathbf{a} \cdot \hat{\mathbf{y}} & \mathbf{b} \cdot \hat{\mathbf{y}} & \mathbf{c} \cdot \hat{\mathbf{y}} \\ \mathbf{a} \cdot \hat{\mathbf{z}} & \mathbf{b} \cdot \hat{\mathbf{z}} & \mathbf{c} \cdot \hat{\mathbf{z}} \end{pmatrix} \quad (5.20)$$

is determined by the unit cell edge vectors.

Note 5.4: Simulation of the Rotating Crystal Method

The diffracted wavevectors are easily described in the orthonormal basis $\hat{\mathbf{e}}_i$ linked to the rotary axis A , (5.16) and Exercise 5.6. However, the method simulation requires the directions of diffracted beams in the laboratory's coordinate system xyz . Given $\mathbf{k} = k[0, 0, 1]$ as the incident wavevector, $\hat{\mathbf{s}}_d = [\sin \theta_d, -\cos \theta_d \sin \phi_d, \cos \theta_d \cos \phi_d]$ as the versor pointing towards the detector's flat area center, and $\mathcal{R}(\theta_z, \theta_y) = \mathcal{R}_Z(\theta_z) \mathcal{R}_Y(\theta_y)$ the rotation matrix orienting the rotating axis in the laboratory system, Fig. 5.12 (inset). Once calculated the azimuth ϕ in which each reflection diffracts, e.g. Table 5.1, the components of vector $\mathbf{k}' = k\hat{\mathbf{s}}' = [k'_i]$ in the laboratory system will be

$$[k'_i] = \mathcal{R}(\theta_z, \theta_y) \mathcal{R}_Z(180^\circ - \phi) [k'_j]^t_e .$$

The diffracted beam will hit the detector when $\arccos(\hat{\mathbf{s}}' \cdot \hat{\mathbf{s}}_d)$ is less than the detector acceptance angle. The relative powers of diffracted beams follow from (5.15),

$$P_{hkl} \propto \langle |\mathcal{P}(\hat{\mathbf{s}}')|^2 \rangle \frac{|F_{hkl}|^2}{\cos \omega \cos \omega' |\sin(\phi' - \phi)|} .$$

In the case of unpolarized radiation, $\langle |\mathcal{P}(\hat{\mathbf{s}}')|^2 \rangle = (1 + \cos^2 2\theta)/2$ where $\cos(2\theta) = k'_3/k$. The procedures described herein are implemented in the `rotcrystmethod.m` routine used to generate the diffraction pattern in Fig. 5.12 and the list of reflections partially reproduced below.

h, k, l	$ F_{hkl} ^2$	Phkl	X (mm)	Y (mm)	
12, -23, -1	919422.70 (100.0%)	2667065.73	-47.515	13.476	1
3, 19, -1	694493.92 (75.5%)	1876024.97	-37.151	0.957	2
10, -21, 7	770889.27 (83.8%)	1839258.43	-16.195	-19.746	3
13, -24, -2	643284.58 (70.0%)	1794722.38	-32.784	23.814	4
11, -23, 1	618235.38 (67.2%)	1724044.52	-47.218	-3.445	5
11, -23, -2	621384.64 (67.6%)	1705207.66	-43.754	-4.239	6
2, 19, 1	592249.67 (64.4%)	1603440.13	-45.486	-13.758	7
0, 22, 2	689227.01 (75.0%)	1590654.36	-18.511	-41.785	8
3, 17, 4	548023.93 (59.6%)	1520421.00	-46.116	-3.699	9
11, -19, 6	522253.31 (56.8%)	1513256.49	-48.902	10.404	10
.	
5, 1, 12	0.00 (0.0%)	0.01	-9.564	-30.612	2959

In the crystallization process, the unit cells may contain a few biological functional units, which are molecular complexes responsible for the active form of the protein in organisms. The functional units are grouped forming asymmetric units, and these form the unit cells. Crystallographic symmetry operations (Hahn 2006) describe the spatial distribution of the asymmetric units in the unit cell. Therefore, the essential information about protein crystals are: (1) the conversion matrix \mathbb{S} containing the lattice parameters information; (2) Cartesian coordinates of the atoms in the asymmetric unit, e.g. “ATOM” and “HETATM” records in *.pdb files, Sect. 2.3.1; and (3) the symmetry operations that, when applied to the fractional coordinates of the asymmetric unit, provide the fractional coordinates of all other atoms in the unit cell. With this information in hand, the X-ray diffraction in the crystal can be calculated and compared with experimental results.

...

Exercise 5.9. Insulin is found in the human body either as monomers or hexamers, being the former the active form. The structure of insulin crystals varies depending on the crystallization process. In general, the asymmetrical units are dimers of the functional unit (monomer), and the hexagonal unit cell is formed by three hexamers (groups of three dimers). Given the lattice parameters of an insulin crystal, $a = b = 80.638 \text{ \AA}$, $c = 37.782 \text{ \AA}$, $\alpha = \beta = 90^\circ$, and $\gamma = 120^\circ$, find the conversion matrix \mathbb{S} . (b) In the asymmetric unit, an atom has Cartesian coordinates $[X, Y, Z] = [8.209, 20.582, 3.556] \text{ \AA}$. What are the fractional coordinates $[x, y, z]$ of the nine equivalent atoms. Note: use symmetry operations of group 146 for hexagonal axis (Hahn 2006).

Answer (a): In an arbitrary orthogonal basis, $\mathbf{a} = a[1, 0, 0]$, $\mathbf{b} = b[\cos \gamma, \sin \gamma, 0]$, and $\mathbf{c} = c[0, 0, 1]$, Exercise 4.2. The conversion matrix is obtained by substituting these vectors in (5.20) and calculating the inverse matrix, i.e.,

$$\mathbb{S}^{-1} = \begin{pmatrix} a & b \cos \gamma & 0 \\ 0 & b \sin \gamma & 0 \\ 0 & 0 & c \end{pmatrix} \Rightarrow \mathbb{S} = \begin{pmatrix} 0.012401 & 0.007160 & 0.000000 \\ 0.000000 & 0.014320 & 0.000000 \\ 0.000000 & 0.000000 & 0.026468 \end{pmatrix}.$$

Answer (b): Since the Cartesian coordinates are given in the same arbitrary basis used for the edge vectors, the fractional coordinates of the chosen atom in the asymmetric unit are $[x, y, z] = [X, Y, Z]\mathbb{S}^t = [0.24916, 0.29472, 0.09412]$. The symmetry operations without translation form the hexamer 1, whereas the translations $[2/3, 1/3, 1/3]$ and $[1/3, 2/3, 2/3]$ form hexamers 2 and 3. Thus,

hexamer 1	hexamer 2	hexamer 3
x, y, z	$x + 2/3, y + 1/3, z + 1/3$	$x + 1/3, y + 2/3, z + 2/3$
$-y, x - y, z$	$-y + 2/3, x - y + 1/3, z + 1/3$	$-y + 1/3, x - y + 2/3, z + 2/3$
$-x + y, -x, z$	$-x + y + 2/3, -x + 1/3, z + 1/3$	$-x + y + 1/3, -x + 2/3, z + 2/3$

are the atom equivalent positions in each hexamer of the unit cell.

Note 5.5: Reading PDB Files. The routine `pdbcoordfrac.m` reads `*.pdb` files and lists the atom fractional coordinates in the unit cell, including occupancy and temperature factors.

...

Summary

- Scattering sphere and Bragg cone

$$|\mathbf{Q} + \mathbf{k}|^2 = k^2 \quad \text{or} \quad \mathbf{k} \cdot \mathbf{Q} = -Q^2/2$$

- Diffraction power (integrated intensity) of hkl reflection in crystallites, rotation axis \perp to the incidence plane

$$P_{\text{hkl}} = I_e K \frac{|F_{\text{hkl}}|^2}{\sin 2\theta_{\text{hkl}}} , \quad K = N\lambda^3 V_{\text{cel}}^{-1}$$

- Diffraction power of polycrystalline (powder) samples

$$P(Q) = I_e K \sum_{\text{hkl}} \frac{|F_{\text{hkl}}|^2}{\sin 2\theta_{\text{hkl}}} Q_{\text{hkl}}^{-1} \delta(Q - Q_{\text{hkl}}) , \quad K = \frac{1}{2} N_c \langle N \rangle \lambda^2 d\theta \Delta\phi V_{\text{cel}}^{-1}$$

- Diffraction power of hkl reflection, rotating crystal method (monochromatic radiation)

$$P_{\text{hkl}} = I_e K \frac{|F_{\text{hkl}}|^2}{\cos \omega \cos \omega' |\sin(\phi' - \phi)|} , \quad K = N\lambda^3 V_{\text{cel}}^{-1}$$

- Diffraction power of hkl reflection, Laue method (polychromatic radiation)

$$P_{\text{hkl}}(\lambda) = I_e K w(\lambda) \frac{\lambda |F_{\text{hkl}}|^2}{Q_{\text{hkl}}^2} , \quad K = 8\pi N V_{\text{cel}}^{-1}$$

Chapter 6

Dynamical Diffraction

What is the validity of the kinematic approach?... How do the dynamical diffraction effects affect the relative intensities of a crystal?... How narrow are the diffraction curves in perfect single crystals?... Here are some frequently asked questions on X-ray crystallography. In this chapter, the simplest approach of dynamical diffraction, known as Darwin–Prins dynamical theory (Als-Nielsen and McMorrow 2001; Warren 1990), will be revisited. Although restricted to symmetric reflection geometry, it allows us to understand basic principles of the phenomenon, contributing to the development of easy to implement calculation routines without long incursions through the complex approach of the dynamical diffraction general theory (Authier 2004; Batterman and Cole 1964; Ewald 1969; Weckert and Hümmel 1997).

Within the vast universe of X-radiation modern applications, the dynamical diffraction has well-defined niches where the knowledge of general approaches is essential. More specific literature is indicated for those who need to work in these niches. (1) In the diffraction imaging techniques, the contrast observed in the images originates from the differences between the kinematic and dynamical intensities, e.g. Fig. 6.1. The perfect crystalline lattice undergoes dynamical diffraction, whereas small deformed regions, diffracting in kinematic regime, produce more intense contributions (Authier 2004; Bowen and Tanner 1998). (2) In X-ray optics, single crystals are often used in intense beam conditioning. After interacting with a perfect single crystal, the exact beam properties, such as energy passband and polarization, are described within the dynamical theory (Als-Nielsen and McMorrow 2001; Authier 2004). (3) In nanostructured devices such as those used in optoelectronic, active regions of low dimensionality are often deposited/grown on single crystal substrates. The high resolution structural characterization of the active region can be completed within the kinematic approach. But, in general, the dynamical diffraction occurring on the substrate also needs to be taken into account (Bowen and Tanner 1998; Pietsch et al. 2004). (4) Standing waves methods. In the dynamical diffraction scheme, a pattern of standing waves is formed within the crystal. It is possible

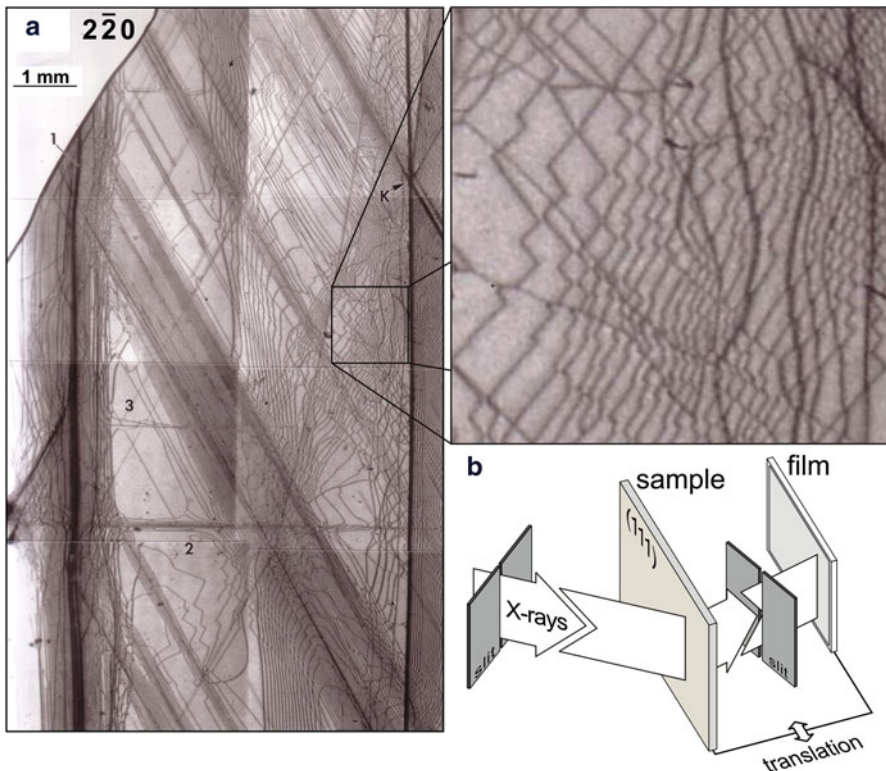


Fig. 6.1 (a) X-ray topography in silicon slab with face (111) and thickness of 100 μm . The contrast comes from the difference in intensity between kinematic (dark lines) and dynamical (lighter areas) diffraction. In the extended area, the zig-zag lines indicate reactions between defects in the crystalline lattice (Morelhão et al. 2000). (b) Transmission geometry of the Laue topographic camera used in the experiment: film records diffracted-transmitted beam during sample translation. Courtesy from S. L. Morelhão and S. Mahajan in a study conducted at Carnegie Mellon University, Pittsburgh (1995)

to estimate the resonant atoms in the structure by varying the position of this pattern using the incidence angle (Authier 2004). (5) The only method able to experimentally measure invariant triplet phases, see Exercise 4.6, is based on interference of multiple waves diffracted within the crystal, an inherently dynamical effect (Chang 1984; Morelhão et al. 2015; Weckert and Hümmer 1997).

6.1 Recursive Equations

The watershed event between the dynamical and kinematic theories is whether to consider or not the changes that the X-ray waves undergo when they travel in the crystalline medium. Let R_1 and T_1 be the electric field reflection and

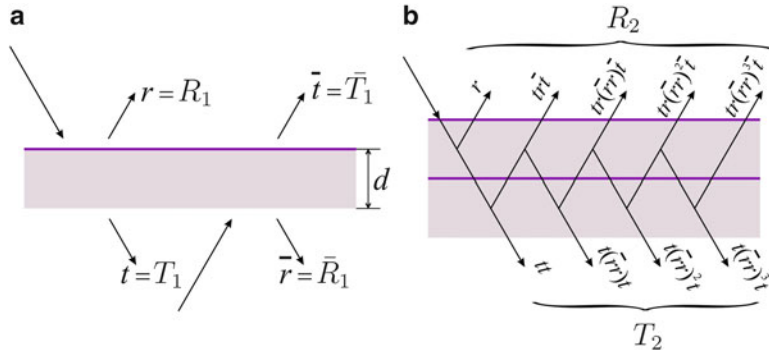


Fig. 6.2 Reflection and transmission coefficients for X-ray wave by (a) one and (b) two crystallographic planes

transmission coefficients for a single crystalline lattice plane of thickness d . As each crystallographic plane of a reflection hkl may comprise several atomic layers, e.g. Fig. 4.3, these coefficients depend on which side the plane is illuminated. Thus, R_1 and \bar{T}_1 will be the coefficients when the plane is illuminated by the opposite side, Fig. 6.2a. Within the plane wave approximation, with an illuminated area much larger than thickness d , the reflection is specular, which means that incident and reflected waves make the same angle θ with the crystalline plane.

From a theoretical point of view, there are several differences between dynamical and kinematic diffraction, even in the case of diffraction by crystals as thin as the thickness of only two planes, i.e. crystals of thickness $2d$. Considering the confined field by multiple reflections between planes, Fig. 6.2b, the reflection and transmission coefficients become

$$R_2 = R_1 + T_1 R_1 \bar{T}_1 \sum_{n=0}^{\infty} (\bar{R}_1 R_1)^n = R_1 \left(1 + \frac{T_1 \bar{T}_1}{1 - \bar{R}_1 R_1} \right) \quad \text{and}$$

$$T_2 = T_1 T_1 \sum_{n=0}^{\infty} (\bar{R}_1 R_1)^n = \frac{T_1 T_1}{1 - \bar{R}_1 R_1}. \quad (6.1)$$

From the Darwin–Prins' theory,¹ we have the coefficients

$$R_1 = -ig(\mathbf{Q}) e^{i\phi}, \quad \bar{R}_1 = -ig(-\mathbf{Q}) e^{i\phi} \quad \text{and} \quad T_1 = \bar{T}_1 = [1 + ig(0)] e^{i\phi} \quad (6.2)$$

¹The reflected and transmitted fields by planes of atoms with thickness comparable to the wavelength are deduced in many textbooks, see, for example, James (1948), Warren (1990), and Als-Nielsen and McMorrow (2001).

given as a function of

$$g(\mathbf{Q}) = \frac{r_e \lambda d}{\sin \theta V_{\text{cel}}} C F(\mathbf{Q}) = \Gamma C F(\mathbf{Q}) \quad (6.3)$$

and of the phase $\phi = -kd \sin \theta$. $F(\mathbf{Q})$ is the structure factor for the diffraction vector \mathbf{Q} , whose direction is normal to the planes, and having module $Q = 2k \sin \theta$ where $k = 2\pi/\lambda$. The polarization factor $C = \langle |\mathcal{P}(\hat{\mathbf{e}}, 2\theta)|^2 \rangle^{1/2}$ is 1 in the polarization σ and in transmission coefficients, in the polarization π it is $|\cos(2\theta)|$, see Sect. 1.1.1.

In the kinematic approach, the multiple reflections are neglected, $\sum_{n=0} (\bar{R}_1 R_1)^n \rightarrow 1$, and the transmitted fields are unchanged; only the wave phase evolution is taken into account as it crosses each plane, so that $T_1 = \bar{T}_1 = e^{i\phi}$. This results in $R_2 = R_1 + T_1 R_1 \bar{T}_1 = R_1(1 + e^{2i\phi})$ and $T_2 = e^{2i\phi}$. The total constructive interference between the reflected fields occurs when $\phi = m\pi$, which is an equivalent condition to Bragg's law, $2d \sin \theta = m\lambda$.

The dynamical treatment, in addition to considering the rescattering by planes, which are irrelevant in very thin crystals, the transmitted fields are corrected by the term $ig(0)$, which adds two important effects: photoelectric absorption and a tiny displacement of the Bragg angle. More precisely,

$$1 + ig(0) = 1 - \Gamma \sum_a f_a'' + i\Gamma \sum_a [f_a(0) + f_a'] \simeq \left(1 - \Gamma \sum_a f_a'' \right) e^{i\Delta} \quad (6.4)$$

once $\Gamma \approx 10^{-5} - 10^{-7}$. The negative real term is responsible for reducing the transmitted wave amplitude, while the imaginary term causes a small increment Δ in the phase, and therefore in the constructive interference condition, which becomes $\phi + \Delta = m\pi$, or

$$2d \sin \theta = \lambda(m + \Delta/\pi). \quad (6.5)$$

Both effects are accentuated in thick crystals, where the diffraction curve width is of the order of Bragg's angle displacement and the curve profile is susceptible to absorption.

Having in hand the reflection and transmission coefficients by a set of $N/2$ planes, (6.1) can be recursively used to obtain the coefficients of N planes, that is,

$$R_N = R_{N/2}(1+T_N), \quad \bar{R}_N = \bar{R}_{N/2}(1+T_N), \quad \text{and} \quad T_N = \frac{T_{N/2}^2}{1 - \bar{R}_{N/2}R_{N/2}}. \quad (6.6)$$

Examples of reflectivity curves are shown in Fig. 6.3, $|R_N(\theta)|^2$ calculated through these recursive equations for crystals with different numbers of planes. In the limit case when $N \rightarrow \infty$,

$$R(\theta) = \lim_{N \rightarrow \infty} R_N(\theta), \quad (6.7)$$

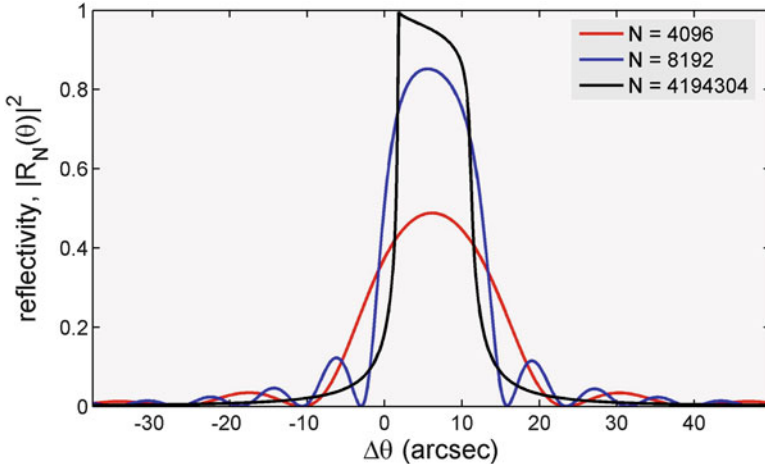


Fig. 6.3 Reflectivity curves in crystals with N planes, (6.6). Symmetrical reflection 220 Ge, $d_{220} = 2.000 \text{ \AA}$, 10 keV X-rays and polarization σ . $\Delta\theta = \theta - \theta_{220}$ [rcdarwinprinsplot.m]

the curve converges to a profile with peculiar characteristics: asymmetric profile with maximum reflectivity less than or equal to 1 occurring at the left of the peak width, whose center is displaced from the exact Bragg's angle by $\Delta\theta \simeq \lambda\Delta/2\pi d \cos\theta$, as obtained from (6.5).

The reflectivity curve asymmetry in thick crystals has its origin in the photoelectric absorption. In the hypothetical situation of total absence of absorption, the curve would be symmetrical with total reflection (maximum equals 1) taking place within an angular range of the order of the FWHM itself² whose value is estimated by the expression

$$W_{\text{dyn}} \simeq \frac{2}{3} \sqrt{|R_1 \bar{R}_1|} \tan\theta = \frac{2}{3} \Gamma C \sqrt{|F_{\text{hkl}} F_{\bar{\text{hkl}}}|} \tan\theta . \quad (6.8)$$

The fact that W_{dyn} is a function of $|F_{\text{hkl}} F_{\bar{\text{hkl}}}|$ implies that the reflections hkl and $\bar{\text{hkl}}$ have the same FWHM, irrespective of atomic resonances and absence of symmetry center in the crystal. (6.8) is empirical and valid in the limit $N \rightarrow \infty$, which can be checked with the recursive formula in (6.6).

...

²The FWHM of the diffraction curve in the dynamical regime, thick crystals, is slightly different from the intrinsic width or Darwin's width, e.g. Als-Nielsen and McMorrow (2001, p. 184).

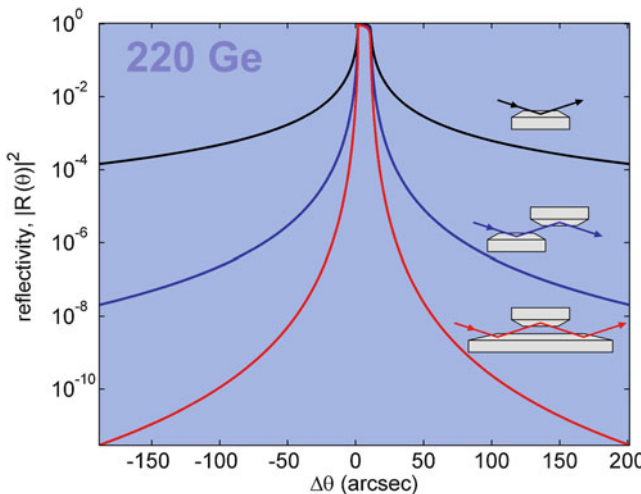


Fig. 6.4 Reflectivity curves in single crystals after 1, 2, and 3-bounces (reflections) [rcdarwinprins.m]

Exercise 6.1. Monocrystalline blocks with channel cut are often employed in X-ray optics. Investigate the angular acceptance of the diffraction condition as a function of the number n of bounces that the X-ray beam performs within the channel cut.

Answer: Assuming a perfect parallelism between the crystallographic planes at each side wall of the channel, the reflectivity after n bounces will be $|R(\theta)|^{2n}$, (6.7). As the reflectivity is close to 100 % within the width W_{dyn} , the central region of the curve is barely affected by the number of bounces, but the intensities at the curve shoulders are strongly reduced. For example, if in a given $\Delta\theta$ the reflectivity is 1 % in a simple reflection ($n = 1$), it will be 0.01 % and 0.0001 % in channel cuts of two and three bounces, respectively, Fig. 6.4.

Exercise 6.2. Under kinematic diffraction, the intensities are proportional to the structure factors square modules, $I_{\text{hkl}} \propto |F_{\text{hkl}}|^2$, so that the difference in the structure factors of a Friedel's pair generates the anomalous signal

$$\Lambda = \frac{I_{\text{hkl}} - I_{\bar{\text{hkl}}}}{I_{\text{hkl}} + I_{\bar{\text{hkl}}}} = \frac{|F_{\text{hkl}}|^2 - |F_{\bar{\text{hkl}}}|^2}{|F_{\text{hkl}}|^2 + |F_{\bar{\text{hkl}}}|^2} .$$

Non-null signs ($\Lambda \neq 0$) indicate absence of symmetry center in the crystal structure, see Exercises 4.4 and 4.5. By comparing reflectivity curves of a Friedel's pair, figure out if Λ can be determined via dynamical diffraction in perfect single crystals?

Answer: Taking as an example the $11\bar{7}/\bar{1}\bar{1}\bar{7}$ pair in GaAs, below and above the absorption edge of Ga at 10,367 eV. Under kinematic diffraction, the intensity profile is determined by crystal thickness, 324 nm in the case shown in Fig. 6.5a. Only curve intensity changes, one increasing and the other decreasing, as the energy

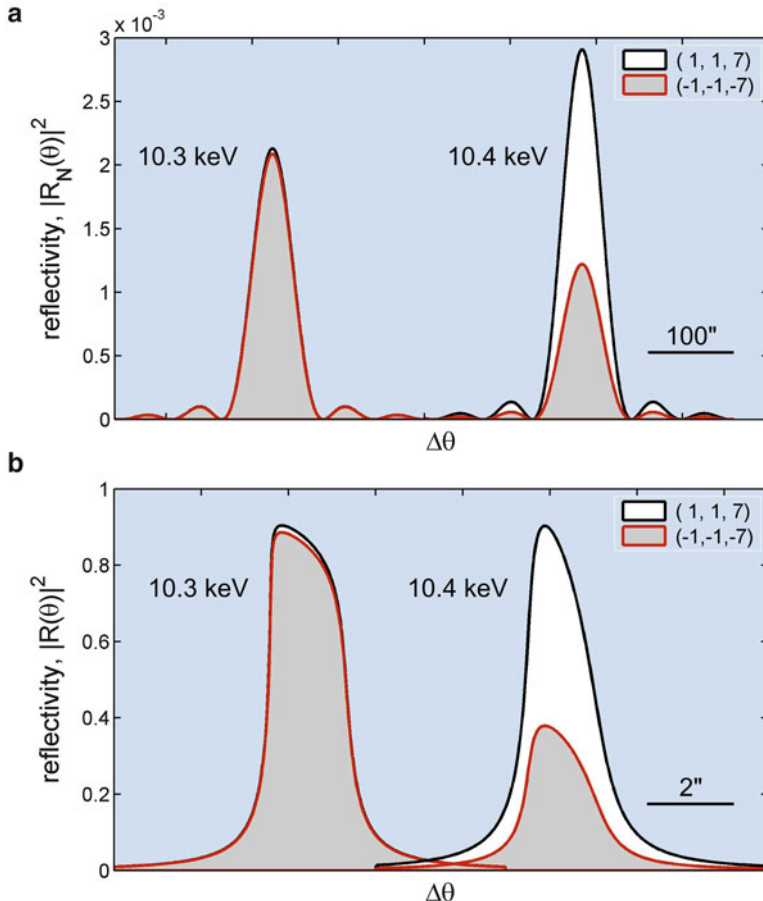


Fig. 6.5 Reflectivity curves of the 117 and $\bar{1}\bar{1}7$ reflections in GaAs crystals with faces (117) and thicknesses (a) 324 nm ($N = 2^{12}$ planes) and (b) 1 cm ($N = 2^{27}$ planes). Polarization σ , X-ray energies indicated next to the curves, which are displaced in $\Delta\theta$ axis for better viewing. Simulations using recursive formula in (6.6) [exanomalousignal.m]

goes above the edge, reflecting the fact that the kinematic intensity is proportional to the structure factor square module.

Under dynamical diffraction, Fig. 6.5b, both reflectivity curves below the edge (10,300 eV) already have maximum close to 1. Consequently, at the energy above the edge (10,400 eV), the intensity of one of the curves is practically unchanged, whereas the intensity of the other curve decreases. There are also changes in the line profiles below and above the edge. But, despite the change in line profile and the fact that the curves are no longer directly proportional to the structure factor square modules, the ratio between the curves follows the ratio $|F_{117}|^2/|F_{\bar{1}\bar{1}7}|^2 = 2.383$.

Therefore, the anomalous signal Λ , which in this case is 41 %, is a measurable value regardless of kinematic or dynamical diffraction.

6.1.1 Standing Waves

In thick crystals, the reflection coefficients have amplitude and phase as in

$$R(\theta) = |R(\theta)| e^{i[\Omega(\theta) + \varphi_{\text{hkl}}]} . \quad (6.9)$$

The phase contains two terms: the phase φ_{hkl} of the structure factor $F_{\text{hkl}} = |F_{\text{hkl}}| \exp(i\varphi_{\text{hkl}})$; and the dynamic phase $\Omega(\theta)$ that varies from 180° to 0 as the incidence angle θ increases through the reflectivity curve, Fig. 6.6. Since the reflectivity is close to 1, the interference between the incident and reflected waves gives rise to a standing wave pattern within the crystal. When $\Omega = 180^\circ$, the phase φ_{hkl} set the maximums of the standing waves pattern at the lower electron density layer of the plane (hkl). On the other hand, with the dynamic phase varying to $\Omega = 0$, the pattern maximums move to the layer of higher electron density, thus increasing the photoelectric absorption.³

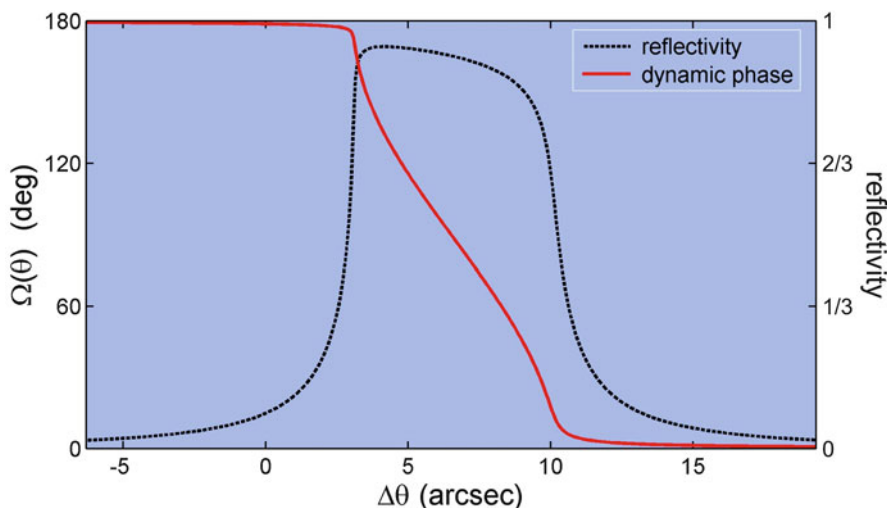


Fig. 6.6 Dynamic phase $\Omega(\theta)$ as a function of the reflectivity curve (right scale). Silicon 111, 8 keV X-rays [dynamicphase.m]

³See Authier (2004, Ch. 16) for detailed discussion on the standing waves phenomenon.

The displacement of the standing wave pattern is responsible for the asymmetry of the dynamical reflectivity curves. In general, the higher the density gradient through the thickness of the crystallographic plane, the greater the asymmetry of the reflectivity curve. For example, in crystals with diamond-like structure, e.g. Si and Ge, or zinc blend type, e.g. GaAs and InAs, the electron density of planes (220) is concentrated in a single layer of atoms. That's the reason why the reflectivity curve in Fig. 6.3 has an enhanced maximum on the left side of the curve. The same is not true for planes (111), which are formed by two atom layers slightly displaced from each other, e.g. Fig. 4.3b, making the density gradient less sharp and smoothing the asymmetry of the reflectivity curve as seen in Fig. 6.6.

In protein crystals, the large number of atoms per unit cell tends to smooth the electron density gradient through the thickness of the crystallographic plane. Consequently, the reflectivity curves have rounded maximums even in cases of strong reflections, e.g. inset in Fig. 6.7a, losing the typical asymmetry observed in crystals with small unit cells. However, measuring intrinsic profiles in perfect protein crystals, with lowermost FWHMs ($W_{\text{dyn}} < 1 \mu\text{rad}$) due to the enormous volume of the unit cells, is a considerable instrumental challenge.

6.2 Kinematic Limit

According to the Kinematic Theory, Chap. 5, the reflection power is always proportional to the number of unit cells in the crystal, (5.14), (5.15), and (5.19). This means that in reflection geometry the area of the reflectivity curve, or just integrated reflectivity,

$$P_N = \int |R_N(\theta)|^2 d\theta , \quad (6.10)$$

increases linearly with the number of crystallographic planes within the validity limit of the kinematic approach. In other words, $P_N \simeq (P_{j+1} - P_j)(N - j) + P_j$ when both N and j are small numbers. Deviation from this linear behavior is, at first, a separator criterion between the kinematic and dynamical diffraction, indicating that absorption and/or rescattering effects start to set in. Computer simulation of the reflectivity curve via recursive formula provides the simplest way to graph the integrated reflectivity P_N , as a function of the number N of diffracting planes or crystal thickness Nd . For instance, Fig. 6.7 illustrates the behavior of P_N in the cases of strong and weak reflections. See Note 6.1 to convert the geometric progression of thickness, (6.6), to the arithmetic progression necessary for analyzing the integrated reflectivity behavior.

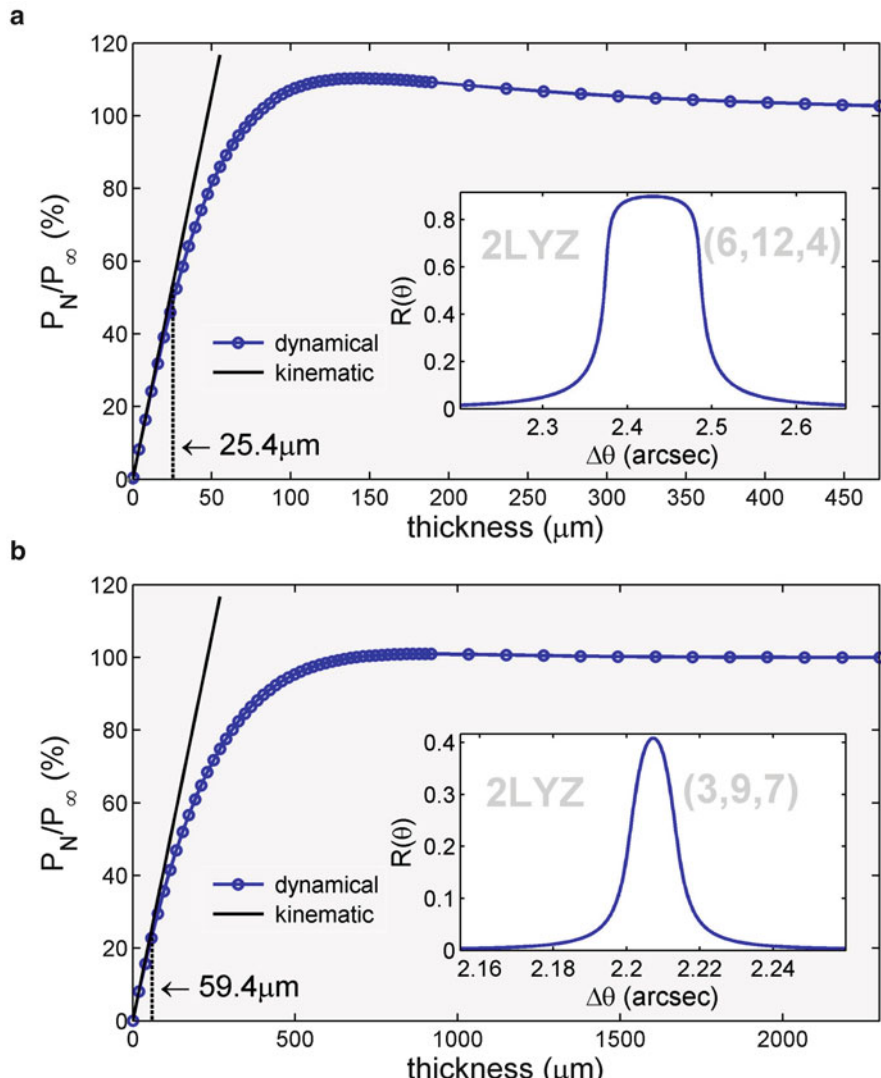


Fig. 6.7 Integrated reflectivity, (6.10), as a function of crystal thickness. Lysozyme crystal (PDB ID: 2LYZ), reflections (a) 6 12 4 and (b) 3 9 7. X-rays of 12 keV and σ -polarization. Vertical dashed lines indicate 10 % deviation from linear behavior (kinematic limit). Inset: reflectivity curves under dynamical diffraction, (6.7) [kinematiclimit.m]

Note 6.1: Reflection and Transmission Coefficients for Crystals of Any Thickness. Consider a scheme similar to that shown in Fig. 6.2b where the planes represent systems containing different numbers of identical crystallographic planes: System A, upper plane, with coefficients R_A , \bar{R}_A , and T_A ; and system B, lower plane, with coefficients R_B , \bar{R}_B , and T_B . Taking into account the multiple reflections at the interface between the systems, the AB system coefficients will be

$$R_{AB} = R_A + R_B \frac{T_A^2}{1 - \bar{R}_A R_B}, \quad \bar{R}_{AB} = \bar{R}_B + \bar{R}_A \frac{T_B^2}{1 - \bar{R}_A R_B} \quad \text{and} \quad T_{AB} = \frac{T_A T_B}{1 - \bar{R}_A R_B}. \quad (6.11)$$

The reflectivity of N planes, when $\log_2(N) \notin \mathbb{N}^*$, is obtained by writing the number N in binary basis, calculating the coefficients for the thicknesses that corresponds to the digits 1 through (6.6), and getting the final coefficients by applying (6.11) to the coefficients from the different thicknesses. For instance, $N = 100$ equals to 1100100 in binary base, then the coefficients for 2^6 , 2^5 , and 2^2 planes come from (6.6), while for 96 and 100 planes the coefficients are obtained from (6.11). This procedure is implemented in routine rcdarwinprins.m.

...

Exercise 6.3. Investigate the kinematic limit as a function of unit cell size, energy, photoelectric absorption, and reflection power. What are the most favorable conditions for a satisfactory kinematic analysis of the diffracted intensities?

Answer: By taking as a reference for the kinematic limit the 10 % deviation of integrated reflectivity P_N from the linear behavior, the various factors affecting the kinematic approach validity are analyzed in Table 6.1. Crystals with a large unit cells, such as protein crystals, have extended kinematic limits, in general two orders of magnitude larger than inorganic crystals. The increase in the energy of X-rays tends to extend the kinematic limit, except when it excites an absorption edge as in GaAs. In most cases, strong reflections have a kinematic limit lower than weak reflections. Therefore, in general, the kinematic treatment should provide satisfactory results when, for a given energy, the larger crystal dimension is smaller than the kinematic limit of the most intense reflection measured.

...

6.3 Refraction Index for X-Rays

Of tremendous importance in X-ray optics, studies of surfaces, and phase imaging techniques is the refraction index for X-rays. When the incident wave crosses an

Table 6.1 Validity threshold of kinematic approach for many crystals, strong (*) and weak (†) reflections

Crystal	h	k	l	<i>Nd</i> (μm)	
				8 keV	12 keV
Lysozyme *	6	12	4	17.1	25.4
Lysozyme †	3	9	7	24.6	59.4
GaAs *	4	0	0	0.64	0.38
GaAs †	2	0	0	0.88	0.32
Insulin *	3	17	4	24.1	40.3
Insulin †	6	8	13	34.7	69.4
LaMnO ₃ *	0	0	4	0.25	0.32
LaMnO ₃ †	2	1	0	0.28	0.44

Criterion: thickness Nd in which the integrated reflectivity deviates 10 % from linear behavior, e.g. Fig. 6.7 [kinematiclimit.m]

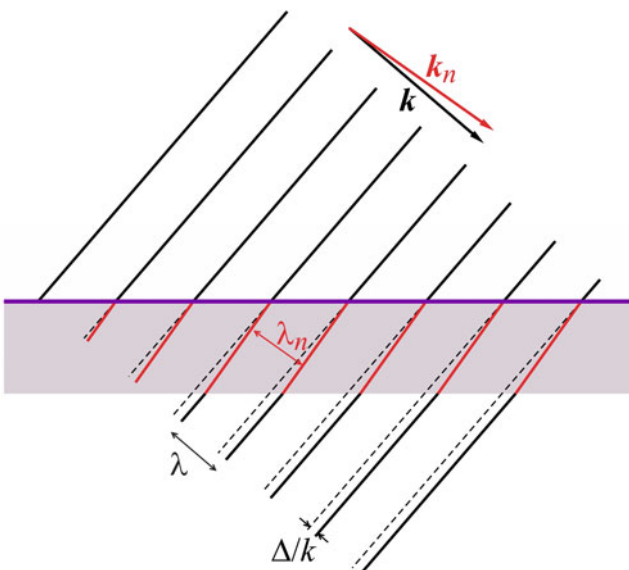


Fig. 6.8 X-ray wavefronts when crossing an atomic plane

atomic plane, the phase increment Δ in (6.4) shifts forward the wavefronts by Δ/k , as illustrated in Fig. 6.8. Inside the plane thickness, the wavevector \mathbf{k}_n shows slightly different module and direction regarding the wavevector \mathbf{k} in vacuum. This can be described in terms of a refraction index, which is deduced here from the transmission coefficient T_1 under normal incidence condition when

$$T_1 = [1 + ig(0)]e^{i\phi} = e^{i[g(0)+\phi]} = e^{-inkd}.$$

The minus signal is due to the choice of phase signal made in (1.33) for the incident X-ray wave. From (6.3) with $\sin \theta = 1$, the above equality becomes

$$\frac{r_e \lambda d}{V_{\text{cel}}} F(0) - kd = -nkd$$

that provides the refraction index

$$n = 1 - \frac{r_e \lambda^2}{2\pi V_{\text{cel}}} \sum_a [f_a(0) + f'_a] - i \frac{r_e \lambda^2}{2\pi V_{\text{cel}}} \sum_a f''_a = 1 - \gamma - i\beta. \quad (6.12)$$

In non-crystalline materials, the unit cell volume V_{cel} is replaced by a generic volume V with the sum running over all atoms inside this volume.

Real and imaginary parts of the refraction index have distinct physical meanings. The imaginary part accounts for photoelectric absorption so that $|e^{-i(1-\gamma-i\beta)kx}|^2 = e^{-\mu x}$ where

$$\mu = 2\beta k = \frac{2r_e \lambda}{V} \sum_a f''_a = \frac{1}{V} \sum_a \sigma_a \quad (6.13)$$

is the linear attenuation coefficient according to the definition of the atomic absorption cross-section in (1.70). The real part accounts for refraction itself. Under oblique incidence at an angle θ with the interface between vacuum and material medium, the wavevectors components parallel to the interface are equal (Snell's law): $k \cos \theta = k_n \cos \theta_n$. With $k_n = (1 - \gamma)k$, the propagation direction inside the medium is $\cos \theta_n = \cos \theta / (1 - \gamma)$. It implies in total reflection with critical angle θ_c for which $\cos \theta_c = 1 - \frac{1}{2}\theta_c^2 = 1 - \gamma$, and therefore

$$\theta_c = \sqrt{2\gamma}. \quad (6.14)$$

Total external reflection for X-ray has very important practical consequences. One is that it makes possible to focus X-ray beams impinging on a surface at small glancing angles, giving rise to optical devices (X-ray mirrors) extensively employed in synchrotron facilities and commercial diffractometers. Studies of surfaces by means of grazing incidence techniques are other applications of the phenomenon (Als-Nielsen and McMorrow 2001; Malachias et al. 2011; Pietsch et al. 2004). For instance, just above the critical angle, the specular reflected intensity is still enough to probe the electron density profile in depth a few hundred nanometers below the surface. Since it is independent of the crystalline state of the sample, X-ray specular reflectometry is also useful for studying nanostructured thin films of amorphous materials (Morelhão et al. 2002). On the other hand, X-ray imaging of soft tissues exploit either the tiny deflection or phase shift of the X-ray wave when crossing the interface of two medium with difference in electron density. In quantitative values, this deflection is about 1 μrad for X-rays of 20 keV and density variations of 10 % with respect to the water density (Antunes et al. 2006).

...

Exercise 6.4. To improve performance of X-ray mirrors, metallic coated glass surfaces are often used. Compare the critical angles of glass surfaces with and without a thin layer of gold. Assume a glass of amorphous α -quartz.

Answer: In any case, the critical angle comes from (6.14) and (6.12). For glass,

$$\gamma = \frac{r_e \lambda^2}{2\pi} \frac{2(Z + f')_{\text{Si}} + 3(Z + f')_{\text{O}}}{V_{\text{cell}}} = \frac{r_e \lambda^2}{2\pi} \frac{52 + 2f'_{\text{Si}} + 3f'_{\text{O}}}{113 \text{ \AA}^3},$$

and for gold,

$$\gamma = \frac{r_e \lambda^2}{2\pi} \frac{4(Z + f')_{\text{Au}}}{V_{\text{cell}}} = \frac{r_e \lambda^2}{2\pi} \frac{316 + 4f'_{\text{Au}}}{67.8 \text{ \AA}^3}.$$

Critical angles for glass and gold surfaces are compared in Fig. 6.9.

In general, atomic resonance rule a small contribution to θ_c , as seen in Fig. 6.9, so that f' is neglectable when calculating γ . Since Z/V_{cell} is equivalent to $\rho N_A/M$ as in (1.58), the real part of the refraction index can be calculated as

$$\text{Real}\{n\} = 1 - \frac{r_e \lambda^2 N_A}{2\pi M} \rho. \quad (6.15)$$

Just to recall, N_A is the Avogadro's number, M is the molar mass, and ρ is the mass density of the material.

...

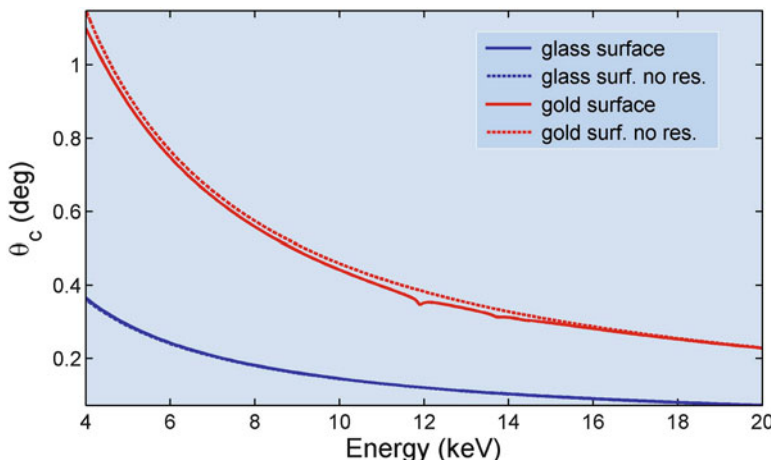


Fig. 6.9 Critical angle for total external X-ray reflection in glass and gold coated surfaces. Effect of neglecting the atomic resonance correction term f' is also shown [excritangle.m]

Summary

— Reflection and transmission coefficients for a lattice plane of thickness d

$$\boxed{R_1 = -i \Gamma C F(Q) e^{i\phi} \quad \text{and} \quad T_1 = [1 + i \Gamma C F(0)] e^{i\phi}}$$

$$\phi = -kd \sin \theta$$

— Recursive equations, coefficients for crystals of thickness Nd

$$\boxed{R_N = R_{N/2}(1 + T_N), \quad \bar{R}_N = \bar{R}_{N/2}(1 + T_N), \quad \text{and} \quad T_N = \frac{T_{N/2}^2}{1 - \bar{R}_{N/2}R_{N/2}}}$$

— Integrated reflectivity

$$\boxed{P_N = \int |R_N(\theta)|^2 d\theta}$$

— Dynamical reflectivity curve $|R(\theta)|^2$ and phase shift $\Omega(\theta)$

$$\boxed{\lim_{N \rightarrow \infty} R_N(\theta) = R(\theta) = |R(\theta)| \exp \{i[\Omega(\theta) + \varphi_{hkl}]\}}$$

— Kinematic limit

$$\boxed{\frac{P_N}{(P_{j+1} - P_j)(N - j) + P_j} < 0.9}$$

for $j < 1000$

— Refraction index for X-rays

$$\boxed{n = 1 - \frac{r_e \lambda^2}{2\pi V} \sum_a [f_a(0) + f'_a] - i \frac{r_e \lambda^2}{2\pi V} \sum_a f''_a = 1 - \gamma - i\beta}$$

— Critical angle for total external reflection

$$\boxed{\theta_c = \sqrt{2\gamma} = \left(\frac{r_e \lambda^2}{\pi V} \sum_a [f_a(0) + f'_a] \right)^{1/2} \simeq \left(\frac{r_e \lambda^2 N_A}{\pi M} \rho \right)^{1/2}}$$

Chapter 7

Worked Examples

Even after reading all previous chapters of this book, someone can still be insecure on how to carry out X-ray data analysis for the first time. For this reason, we have prepared this chapter with a few simple examples to show in detail all the steps that are necessary for analyzing intensity data. After downloading the original data files from <http://xraybook.if.usp.br/> and saving them in the same directory of your computer together with some of the MatLab routines given in Appendix B, you will be able to reproduce exactly the analysis described herein. In the following sections, Matlab codes and the figures that they generate are interleaved for a better understanding of each topic.

7.1 PDDF Analysis of Lysozyme

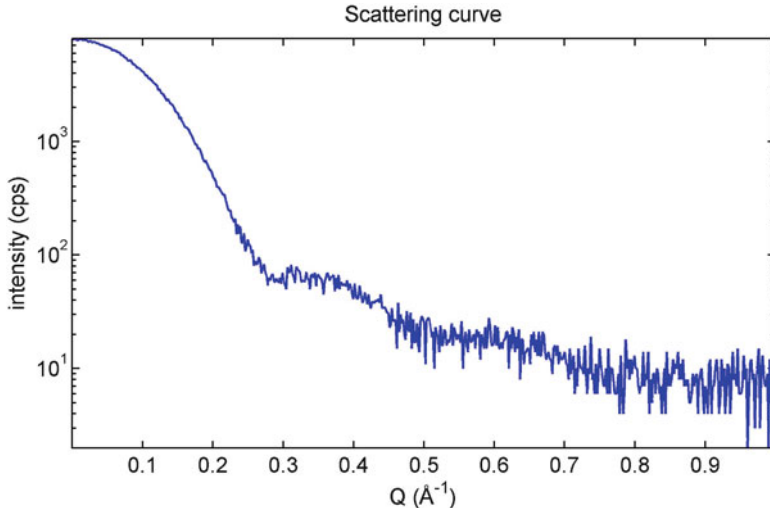
In a disperse system of large molecules where measurable intensities are within the small angle region only, the analysis can be carried out by inverse Fourier Transform of the scattering curve, which provides the PDDF of the molecules as in (3.7). To facilitate this first Fourier analysis, the intensity data is already given as a function of the reciprocal vector module Q with nearly constant increment dQ that simplifies the integration in the interval of Q from 0 to Q_f . This analysis is divided into three major parts as detailed below.

7.1.1 Contents

- Loading intensity data
- Inverse Fourier Transform (FT)
- Gyration radius

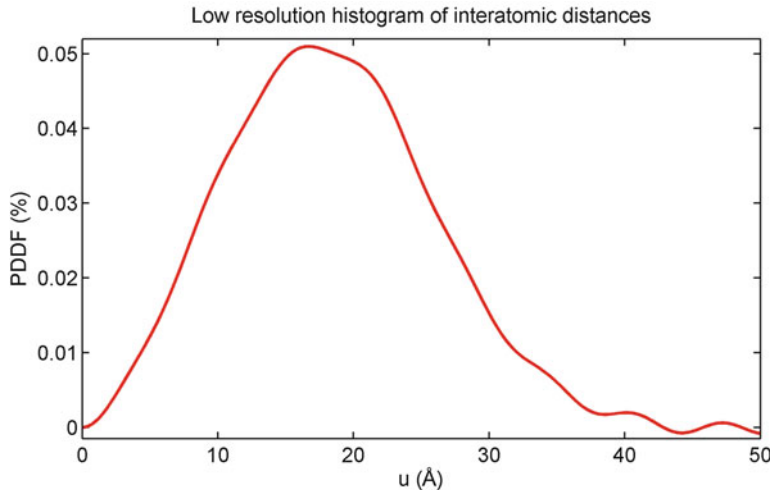
7.1.2 Loading Intensity Data

```
S=load('lysozymeIofQ.dat'); % <-- from http://xraybook.
if.usp.br/
Q=S(:,1); I=S(:,2)';
semilogy(Q,I,'LineWidth',1.5)
xlabel(['Q (' char(197) '^{-1})'])
ylabel('intensity (cps)')
title('Scattering curve')
```



7.1.3 Inverse Fourier Transform

```
U = 0:0.01:50;
Nu = size(U,2);
Nq = size(Q,2);
dQ = Q(3)-Q(2);
A = (dQ/(2*pi*pi))*I.*Q;
p = size(I,Nu);
for n=1:Nu
    u = U(n);
    p(n) = sum(u*A.*sin(u*Q)); % <-- inverse FT integral
end;
S = 0.01*sum(p);
plot(U,p/S,'r','LineWidth',2)
xlabel(['u (' char(197) ')'])
ylabel('PDF (%)')
title('Low resolution histogram of interatomic distances')
```



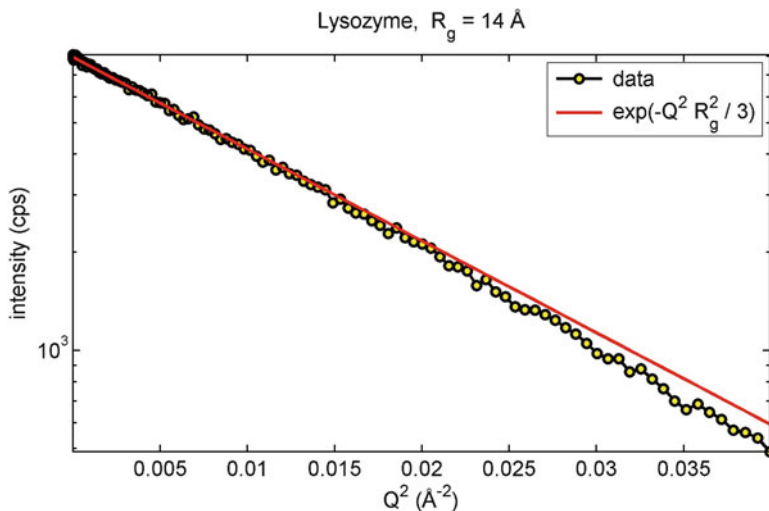
7.1.4 Gyration Radius

```
Rg2 = 0.5*sum(p.*U.*U) / sum(p);
Rg = sqrt(Rg2);
X = Q(Q<.2); X2 = X.*X;
Y = I(1)*exp((-Rg2/3)*X2);
semilogy(X2,I(Q<.2),'ko',X2,Y,'r','MarkerSize',6,
'MarkerFaceColor','y','LineWidth',2)
xlabel(['Q^2 (' char(197) '^{-2})'])
ylabel('intensity (cps)')
legend(' data',' exp(-Q^2 R_g^2 / 3)')
title(['Lysozyme, R_g = ' num2str(0.1*round(10*Rg)) ' ' char
(197)])
```

7.2 PDF Analysis of Gold Nanoparticles

Although similar, the Fourier analysis of intensity data collected at high angles is a little different from the previous one. The particles must have some internal order to provide measurable intensities at high angles, then the focus of analysis is the structural function $S(Q)$ that leads to the normalized PDDF as defined in (3.16) or to the pair density function (PDF) in (3.18).

The content of the analysis below applies to intensity data collected with uniform increments in the scattering angle 2θ . By using the relation $Q = (4\pi/\lambda) \sin \theta$, the intensity curve $I(Q)$ as a function of Q is obtained. The raw structural function is estimated as $S(Q) = I(Q)/f_m^2(Q)$ where $f_m^2(Q)$ is the mean square atomic scattering factor of the particle. Background intensity not related to the internal structure of the



particles should be subtracted and the curve $S(Q)$ normalized so that the background intensity of statistical noise fluctuates around 1. The Fourier analysis is then carried out by integrating $S(Q) - 1$ in the available Q interval, but with dQ varying from one data point to the other. When the intensity data at the small angle region is missing, the normalized PDDF shows positive and negative values, as seen in this example. Otherwise it will show positive values only that are proportional to the occurrence frequency of interatomic distances, e.g. inset of Fig. 3.7. The PDF signal at end of the Fourier analysis displays relative values related to the coordination number (Exercise 3.2), which is the number of neighbors within a spherical shell of radius u and thickness du .

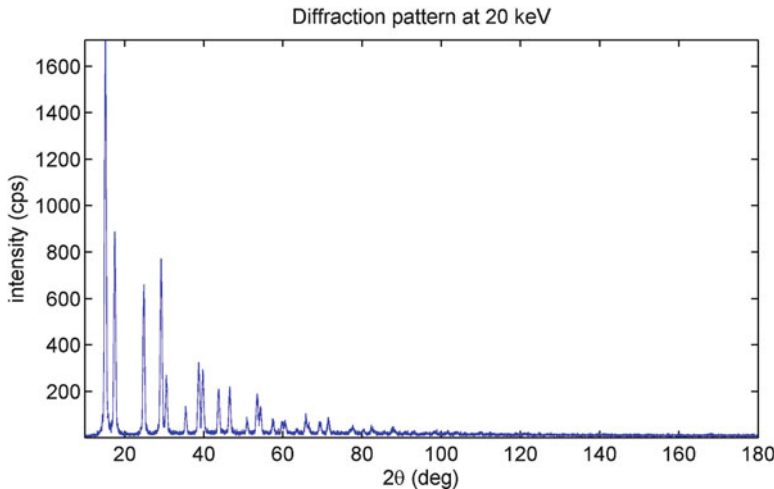
7.2.1 Contents

- Loading intensity data
- Structural function $S(Q)$
- Background correction
- Normalizing $S(Q)$
- Fourier analysis

7.2.2 Loading Intensity Data

```
S=load('goldnan080r5.dat'); % <-- from http://xraybook.if.usp.br/
tth=S(:,1)'; I=S(:,2)';
plot(tth,I)
```

```
xlabel('2\theta (deg)')
ylabel('intensity (cps)')
title('Diffraction pattern at 20 keV')
```

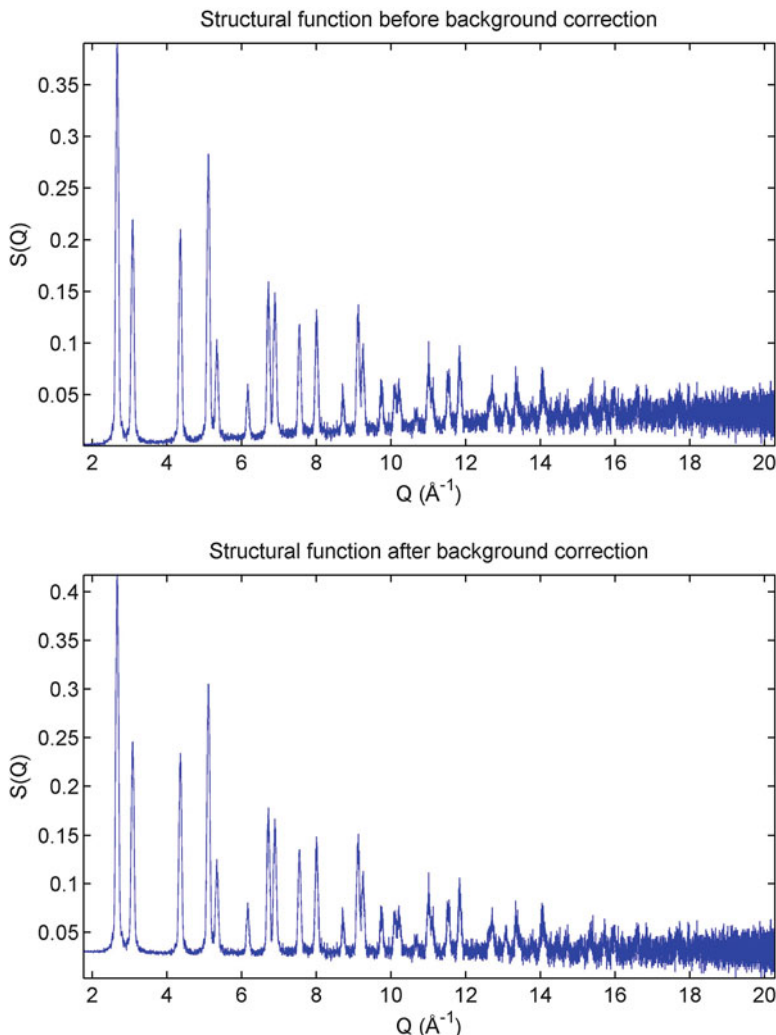


7.2.3 Structural Function $S(Q)$

```
Q = (4*pi/0.62)*sind(0.5*tth); % <-- wavelength 0.62Å (20keV X-rays)
f=asfQ('Au',(0.25/pi)*Q); % <-- scattering factor of Au atom
S = I./(f.*f);
plot(Q,S)
xlabel(['Q (' char(197) '^{-1})'])
ylabel('S(Q)')
title('Structural function before background correction')
```

7.2.4 Background Correction

```
a= (0.03-0.0016)/14; % <-- manual correction with a straight line
bckg = [(0.03-0.0016)-a*(Q(Q<=16)-2) zeros(size(Q(Q>16)))] ;
S = S + bckg; % alternatively, routine backadj.m can
plot(Q,S) % be used as in the next example
xlabel(['Q (' char(197) '^{-1})'])
ylabel('S(Q)')
title('Structural function after background correction')
```

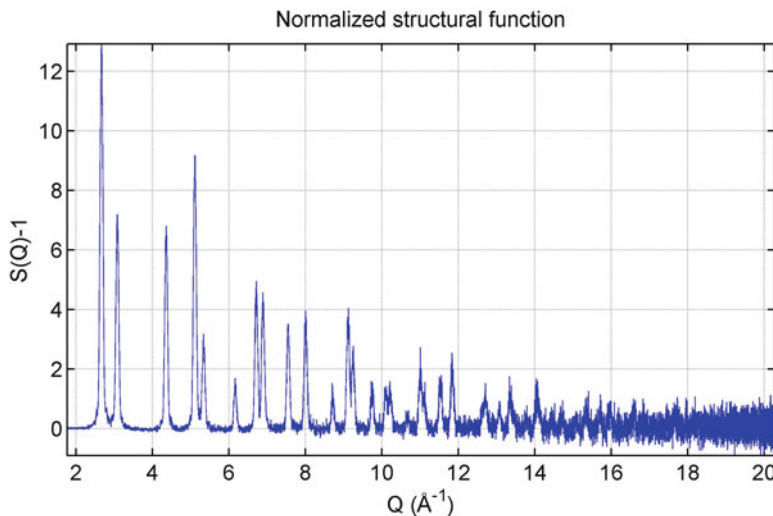


7.2.5 Normalizing $S(Q)$

```

S_1 = 33.3333*S-1;      % <-- so that S(Q) has statistical noise around 1
plot(Q,S_1)               % and then S(Q)-1 has it around 0
grid
xlabel(['Q (' char(197) '^{-1}')'])
ylabel('S(Q)-1')
title('Normalized structural function')

```



7.2.6 Fourier Analysis

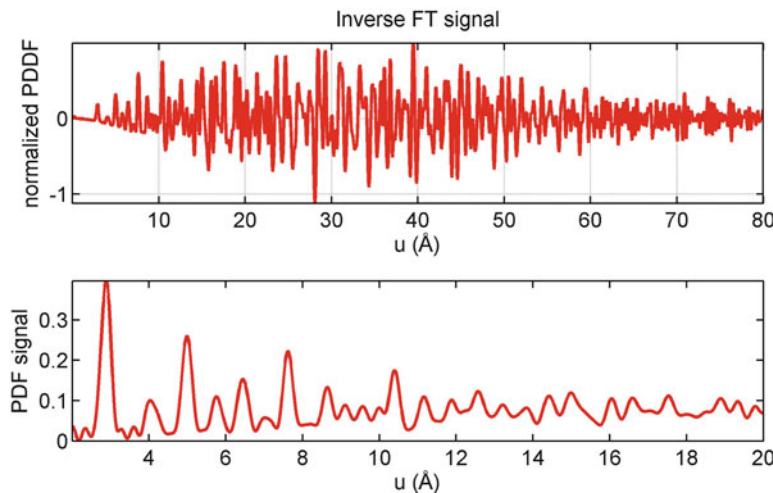
```

U = 0:0.01:80;
Nu = size(U,2);
Nq = size(Q,2);
dQ = [Q(2)-Q(1) Q(2:Nq)-Q(1:Nq-1)];
A = (2/pi)*S_1.*Q.*dQ;
p = zeros(1,Nu);
for n=1:Nu
    u = U(n);
    p(n) = sum(u*A.*sin(u*Q));
end;
subplot(2,1,1)
plot(U,p*(1/max(p)),'r','LineWidth',2)
grid
xlabel(['u (' char(197) ')'])
ylabel('normalized PDDF')
title('Inverse FT signal')
subplot(2,1,2)
N = U>2 & U<20.01;
pdf = p(N)./(4*pi*U(N).*U(N));
pdf = pdf-min(pdf);
plot(U(N),pdf,'r','LineWidth',2)
xlabel(['u (' char(197) ')'])
ylabel('PDF signal')

```

7.3 XRD Analysis of Alumina

Very often we face the problem of identifying compounds present in a polycrystalline (powder) sample. This example teaches how to proceed for comparing an experimental XRD pattern with the simulated one for a compound that is



expected to be present in the sample. From a Crystallographic Information File (CIF) available on the internet for the expected compound, the input crystal data file `*.in` for routine `sfactor.m` is created. The procedure is analogous to that used in routine `kdpcoorfrac.m`, the major difference is due to the operations of symmetry specified in each CIF. In the case of alumina, CIF with COD ID 2300448 (Crystallography Open Database: <http://www.crystallography.net/>), the input file `Al2O3.in` should look like this

```
4.7582 4.7582 12.9897 90.0000 90.0000 120.0000
Al3+ 0.0000 0.0000 0.3523 1.00 0.263
Al3+ 0.0000 0.0000 0.1477 1.00 0.263
Al3+ 0.0000 0.0000 0.6477 1.00 0.263
Al3+ 0.0000 0.0000 0.8523 1.00 0.263
Al3+ 0.6667 0.3333 0.6856 1.00 0.263
Al3+ 0.6667 0.3333 0.4810 1.00 0.263
Al3+ 0.6667 0.3333 0.9810 1.00 0.263
Al3+ 0.6667 0.3333 0.1856 1.00 0.263
Al3+ 0.3333 0.6667 0.0190 1.00 0.263
Al3+ 0.3333 0.6667 0.8144 1.00 0.263
Al3+ 0.3333 0.6667 0.3144 1.00 0.263
Al3+ 0.3333 0.6667 0.5190 1.00 0.263
O2- 0.3062 0.0000 0.2500 1.00 0.168
O2- 0.0000 0.3062 0.2500 1.00 0.168
O2- 0.6938 0.6938 0.2500 1.00 0.168
O2- 0.6938 0.0000 0.7500 1.00 0.168
O2- 0.0000 0.6938 0.7500 1.00 0.168
O2- 0.3062 0.3062 0.7500 1.00 0.168
O2- 0.9729 0.3333 0.5833 1.00 0.168
O2- 0.6667 0.6395 0.5833 1.00 0.168
O2- 0.3605 0.0271 0.5833 1.00 0.168
O2- 0.3605 0.3333 0.0833 1.00 0.168
O2- 0.6667 0.0271 0.0833 1.00 0.168
O2- 0.9729 0.6395 0.0833 1.00 0.168
O2- 0.6395 0.6667 0.9167 1.00 0.168
O2- 0.3333 0.9729 0.9167 1.00 0.168
O2- 0.0271 0.3605 0.9167 1.00 0.168
O2- 0.0271 0.6667 0.4167 1.00 0.168
O2- 0.3333 0.3605 0.4167 1.00 0.168
```

```
02-. 0.6395 0.9729 0.4167 1.00  0.168
```

Note: the used symbols for atoms and ions are those defined in routine `asfQ.m`.

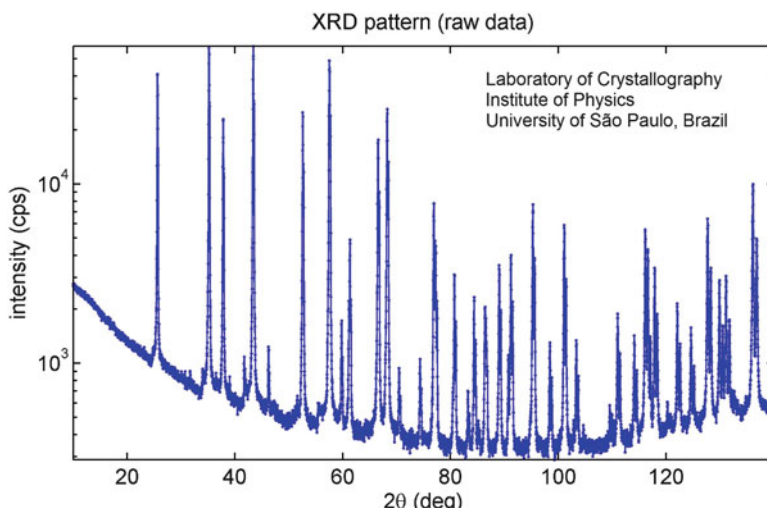
In the analysis below, the background intensity is flattened with the help of routine `backadj.m`, and the XRD pattern simulated by routine `diffractogram.m` that uses the list of structure factors saved in file `Al2O3E8048.sft` by routine `diffraction.m`. Although the experimental pattern has contributions of $\text{Cu}K_{\alpha 1}$ and $\text{Cu}K_{\alpha 2}$ radiations, the same list of structure factors is used for both wavelengths.

7.3.1 Contents

- Loading intensity data
- Adjusting the background intensity
- XRD pattern simulation from a CIF
- Comparison of experimental and simulated patterns

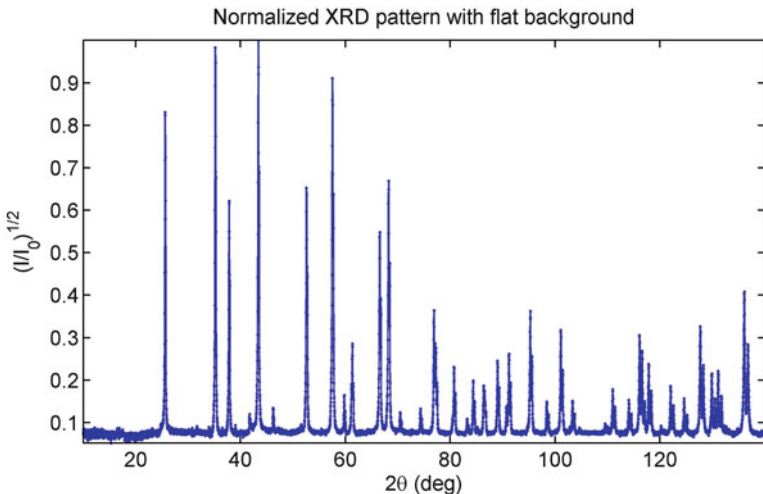
7.3.2 Loading Intensity Data

```
S=load('xrdalumina.dat'); % <- from http://xraybook.if.usp.br/
tth=S(:,1); I=S(:,2);
semilogy(tth,I,'-b','LineWidth',1)
xlabel('2\theta (deg)')
ylabel('intensity (cps)')
title('XRD pattern (raw data)')
```



7.3.3 Adjusting the Background Intensity

```
% B = backadj(tth,ginput); % <-- uncomment to select a few
% save('alumina\_backadj.dat','B','ascii'); % background data points and
B = load('alumina_backadj.dat'); % to save alumina_backadj.dat
Bmin = min(B);
Ib = I-B + Bmin;
Bmin = Bmin/max(Ib);
Ib = Ib*(1/max(Ib));
plot(tth,sqrt(Ib),'-b.','LineWidth',1)
xlabel('2\theta (deg)')
ylabel('(I/I_0)^{1/2}')
title('Normalized XRD pattern with flat background')
```



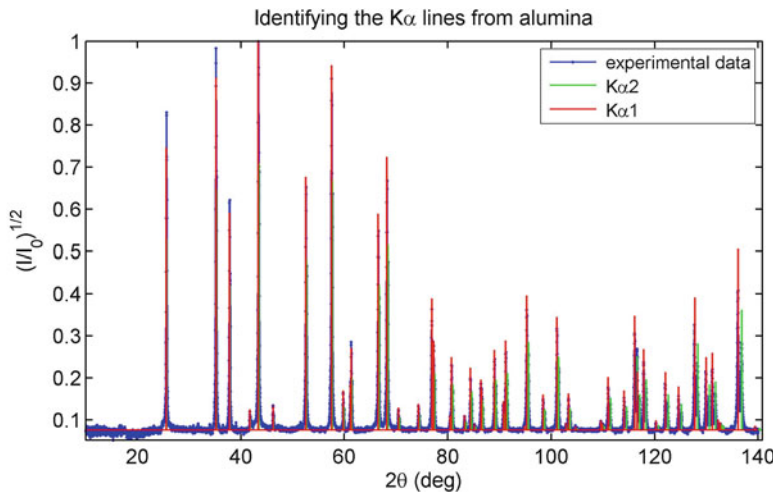
7.3.4 XRD Pattern Simulation from a CIF

```
wl1 = 1.540462; % <-- wavelength of CuK_alpha1 (Angstrom)
wl2 = 1.54439; % <-- wavelength of CuK_alpha2 (Angstrom)
yscale = 1.0; % <-- manual adjustment of intensity
xshift = -0.01; % <-- manual adjustment of position
% diffraction(1.540562,'Al2O3.in',0); % <-- to save file Al2O3E8048.sft
P = diffractogram('Al2O3E8048.sft',500,.4,0);
N = P(:,2) > min(tth) & P(:,2) < max(tth);
X = P(N,2);
Y = P(N,4).* (0.5*(1+cosd(X).^2)); % <-- polarization correction
Y = (1/max(Y))*Y;
Y = yscale*(1-Bmin)*Y;
Y2 = 0.5*Y + Bmin; % <-- intensity of Kalpha2 lines
Y = Y + Bmin;
X2 = 2*asind((wl2/wl1)*sind(0.5*X));
plot(tth,sqrt(Ib),'-b.',X2+xshift,sqrt(Y2),'g',...
     X+xshift,sqrt(Y),'r','LineWidth',1)
xlabel('2\theta (deg)')
```

```

ylabel('(I/I_0)^{1/2}')
title('Identifying the K\alpha lines from alumina')

```



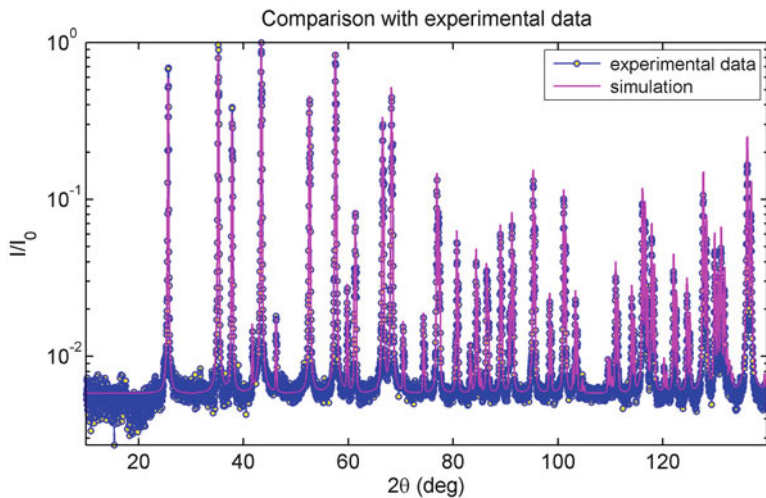
7.3.5 Comparison of Experimental and Simulated Patterns

```

Q1 = (4*pi/wl1)*sind(.5*tth);
Q2 = (4*pi/wl2)*sind(.5*tth);
Q = P(:,1); Iq = P(:,3);
Ntth = size(tth,2);
Is = zeros(1,Ntth);
for n = 1:Ntth
    V = find(Q>Q1(n));
    x = getI(Q1(n),Q(V(1)-1),Q(V(1)),Iq(V(1)-1),Iq(V(1)));
    V = find(Q>Q2(n));
    Is(n) = x + 0.5*getI(Q2(n),Q(V(1)-1),Q(V(1)),Iq(V(1)-1),Iq(V(1)));
end;
Is = Is.* (0.5*(1+cosd(tth).^2)); % <- polarization correction
Is = yscale*((1-Bmin)/max(Is))*Is + Bmin;
semilogy(tth,Ib,'-b.',tth+xshift,Is,'m','LineWidth',1)
xlabel('2\theta(theta (deg)')
ylabel('I/I_0')
title('Comparison with experimental data')

function Y=getI(x,xa,xb,ya,yb)
Y = (yb-ya)*(x-xa)/(xb-xa) + ya;

```



...

Suggestion: Evaluate the agreement between experimental and simulated patterns when varying the Debye–Waller factor and lattice parameters. These changes are made in the file Al2O3.in. Changes in the line profile of the peaks are made in the call of routine diffractogram.m.

...

7.4 Measurement of Absorption Edge

Emission spectra of X-ray generators can be measured by Bragg diffraction in crystals with a known structure. The spectral resolution depends on the experimental setup, but it is possible even with low power generators used in equipment for teaching purposes. Due to the continuous spectrum of sealed X-rays tubes, absorption edges of metal foils are easily observed. On the other hand, metal sheets with specific absorption edges are used as filters for removing unwanted spectral lines from the metal target of a given tube. For instance, a molybdenum tube produces K_{α} (17.44 keV) and K_{β} (19.65 keV) lines when the high voltage applied in the tube is a little above 20 kV (Mo K-edge). A slightly lighter element, Zr in this case, has the K edge precisely between the target element K lines. In this experiment carried out on the Leybold X-ray apparatus, the Mo tube emission spectra at 30 kV is recorded after diffracting in a NaCl (100) crystal, reflection 200

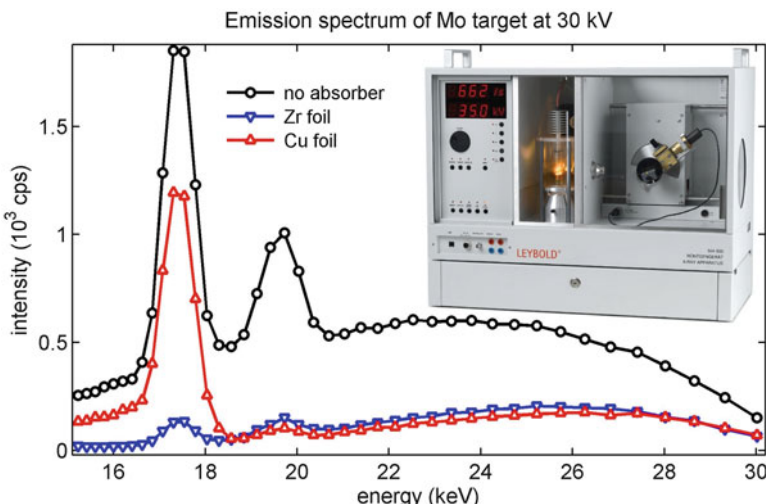
for which $2d_{200} = 5.6402 \text{ \AA}$. By inserting metal foils of known thicknesses in the beam path, the foils absorption spectra are also recorded. The equation for linear attenuation coefficient $\mu = (N_A \rho/A) \sigma$, is applied to measure the total attenuation cross-section $\sigma = \sigma_a + \sigma_R + \sigma_C$ as defined in (1.59). N_A is the Avogadro's number, ρ is the mass density of the metal foil, and A the atomic weight. The experimental values of σ are then compared to theoretical values for the photoelectric absorption cross-section, σ_a , provided by routine `fpp.m`.

7.4.1 Contents

- Experimental data
- Transmission coefficients
- Photoelectric absorption cross-section

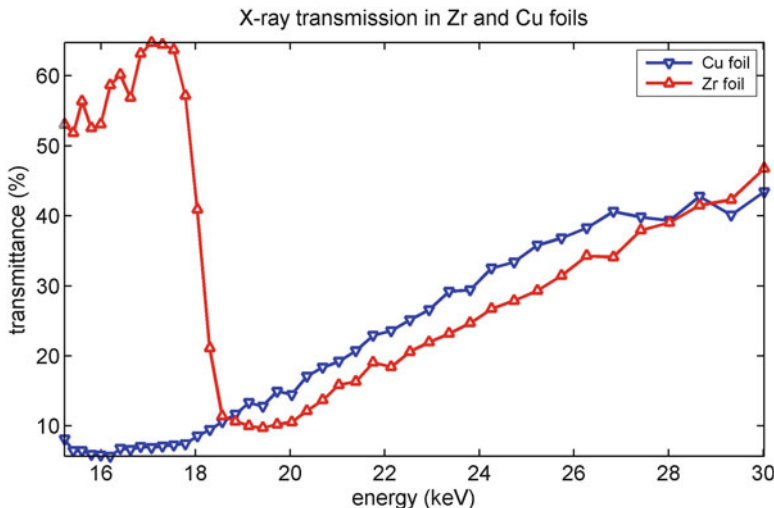
7.4.2 Experimental Data

```
M = load('zirconium_kedge.dat'); % <-- from http://xraybook.if.usp.br/
X = M(:,1)'; I0 = M(:,2)'; Iz = M(:,3)'; Ic = M(:,4)';
E = 12.3985./ (5.6402*sind(X)); % <-- converting diffraction angle in energy
% with 2*d_hkl = 5.6402 Angstrom
plot(E,0.001*I0,'-ko',E,0.001*Ic,'-bv',E,0.001*Iz,'-r^',...
'MarkerFaceColor','w','LineWidth' ,2)
xlabel('energy (keV)')
ylabel('intensity (10^3 cps)')
title('Emission spectrum of Mo target at 30 kV')
```



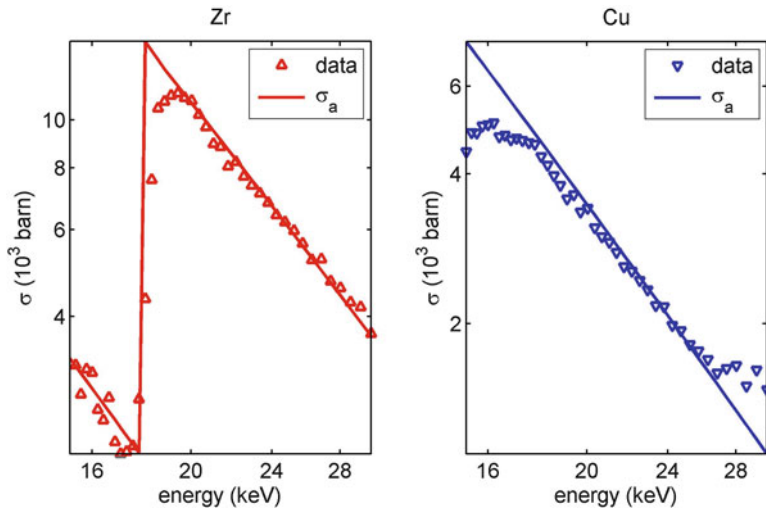
7.4.3 Transmission Coefficients

```
Tc = Ic./I0; Tz = Iz./I0;
plot(E,100*Tc,'-bv',E,100*Tz,'-r^','MarkerFaceColor','w','LineWidth',2)
xlabel('energy (keV)')
ylabel('transmittance (%)')
title('X-ray transmission in Zr and Cu foils')
```



7.4.4 Photoelectric Absorption Cross-Section

```
xc = 0.0067; %<- Cu filter parameters: foils thickness (cm),
Ac = 63.55; rhoc = 8.92; % atomic weight (g/mol), and density (g/cm3)
xz = 0.0048; %<- Zn filter parameters: foils thickness (cm),
Az = 91.22; rhoz = 6.49; % atomic weight (g/mol), and density (g/cm3)
NA = 6.022e+23; %<- Avogadro's number
f = fpfpp('Cu',E);
sga_Cu = 0.001*f(:,4); %<- Cu photoelectric absorption cross-section
f = fpfpp('Zr',E);
sga_Zr = 0.001*f(:,4); %<- Zn photoelectric absorption cross-section
sg_Cu = (-Ac*le+21/(xc*NA*rhoc))*log(Tc);
sg_Zr = (-Az*le+21/(xz*NA*rhoz))*log(Tz);
subplot(1,2,1)
loglog(E,sg_Zr,'r^',E,sga_Zr,'r','MarkerFaceColor','w','LineWidth',2)
xlabel('energy (keV)')
ylabel('sigma (10^3 barn)')
title('Zr')
subplot(1,2,2)
loglog(E,sg_Cu,'bv',E,sga_Cu,'b','MarkerFaceColor','w','LineWidth',2)
xlabel('energy (keV)')
ylabel('sigma (10^3 barn)')
title('Cu')
```



Suggestion: Evaluate the contribution of X-ray scattering to the linear attenuation coefficients. Coherent and incoherent (Compton) scattering cross-sections, σ_R and σ_C , can be obtained from routines `sgrayleigh.m` and `sgcompton.m`, respectively.

Appendix A

Electric Dipole Radiation by a Free Electron

From the Maxwell's equations, the electric and magnetic fields,

$$\mathbf{E} = c\mathbf{B} \times \hat{\mathbf{r}} \quad \text{and} \quad \mathbf{B} = \nabla \times \mathbf{A} , \quad (\text{A.1})$$

of the radiation generated by any current density \mathbf{J} are described from the potential vector

$$\mathbf{A}(\mathbf{r}, t) = \frac{1}{4\pi\epsilon c^2} \int \frac{\mathbf{J}(\mathbf{r}', t')}{|\mathbf{r} - \mathbf{r}'|} dV' \simeq \frac{1}{4\pi\epsilon c^2 r} \int \mathbf{J}(\mathbf{r}', t') dV' . \quad (\text{A.2})$$

The simplification $|\mathbf{r} - \mathbf{r}'| \simeq r$ is valid for point sources, or very far away, in relation to the radiation observation point $\mathbf{r} = r\hat{\mathbf{r}}$ at the time instant $t = t' + r/c$. In the case of a single electron oscillating with speed \mathbf{v} at the origin, the above integral reduces to

$$\int \mathbf{J}(\mathbf{r}', t') dV' = -e\mathbf{v}(t') . \quad (\text{A.3})$$

When $\hat{\mathbf{z}}$ is set as the electron oscillation direction, i.e. $\mathbf{v} = v\hat{\mathbf{z}}$,

$$A_x(\mathbf{r}, t) = 0, \quad A_y(\mathbf{r}, t) = 0, \quad A_z(\mathbf{r}, t) = \frac{-ev(t')}{4\pi\epsilon c^2 r} \quad \text{and} \\ \mathbf{B} = \nabla \times \mathbf{A} = \hat{\mathbf{x}} \frac{\partial A_z}{\partial y} - \hat{\mathbf{y}} \frac{\partial A_z}{\partial x} . \quad (\text{A.4})$$

The partial derivatives are obtained as follows:

$$\frac{\partial A_z}{\partial x} = \frac{-e}{4\pi\epsilon c^2} \left[v \frac{\partial}{\partial x} \left(\frac{1}{r} \right) + \frac{1}{r} \frac{\partial v}{\partial x} \right] = \frac{-e}{4\pi\epsilon c^2} \left[-\frac{v}{r^2} \frac{\partial r}{\partial x} + \frac{1}{r} \frac{\partial v}{\partial t'} \frac{\partial t'}{\partial x} \right] \quad (\text{A.5})$$

where

$$\frac{\partial r}{\partial x} = \frac{\partial}{\partial x} \left(\sqrt{x^2 + y^2 + z^2} \right) = \frac{x}{r} \quad \text{and} \quad \frac{\partial t'}{\partial x} = \frac{\partial}{\partial x} \left(t - \frac{\sqrt{x^2 + y^2 + z^2}}{c} \right) = -\frac{1}{c} \frac{x}{r}. \quad (\text{A.6})$$

Therefore,

$$\frac{\partial A_z}{\partial x} = \frac{-e}{4\pi\epsilon c^2} \left[-\frac{v x}{r^3} - \frac{x \dot{v}}{c r^2} \right] \simeq \frac{e \dot{v}}{4\pi\epsilon c^3} \frac{x}{r^2} \quad \text{and} \quad \frac{\partial A_z}{\partial y} \simeq \frac{e \dot{v}}{4\pi\epsilon c^3} \frac{y}{r^2}, \quad (\text{A.7})$$

where the derivative in y is obtained by similar deduction. Replacing (A.7) in (A.1),

$$\mathbf{B} = \frac{e \dot{v}}{4\pi\epsilon c^3} \frac{y\hat{x} - x\hat{y}}{r^2} = \frac{-e \dot{v}}{4\pi\epsilon c^3} \frac{\hat{z} \times \hat{r}}{r} \quad \text{and} \quad (\text{A.8})$$

$$\mathbf{E} = c\mathbf{B} \times \hat{\mathbf{r}} = \frac{e \dot{v}}{4\pi\epsilon c^2} \frac{\hat{r} \times \hat{z} \times \hat{r}}{r}. \quad (\text{A.9})$$

Representing the electron oscillation direction by $\hat{\mathbf{e}}$ and the radiation observation direction by $\hat{\mathbf{s}}'$, we come to the general expression

$$\mathbf{E}(\mathbf{r}, t) = \hat{\mathbf{s}}' \times \hat{\mathbf{e}} \times \hat{\mathbf{s}}' \frac{e \dot{v}(t')}{4\pi\epsilon r c^2} = \mathcal{P}(\hat{\mathbf{s}}') \frac{e \dot{v}(t')}{4\pi\epsilon r c^2} \quad (\text{A.10})$$

where $\mathcal{P}(\hat{\mathbf{s}}') = \hat{\mathbf{s}}' \times \hat{\mathbf{e}} \times \hat{\mathbf{s}}'$ is the vector polarization factor introduced in Sect. 1.1.1, (1.5). The other term of (A.10) is the amplitude of scattering given in (1.8), with R and \ddot{z} in place of r and \dot{v} , respectively.

Appendix B

MatLab Routines

MatLab®—The Language of Technical Computing, is the high-level language and interactive environment used for developing most routines of this book. Simple and compact, the language made it possible for more than 80 routines to be attached here. Other MatLab advantages are easy manipulation of matrixes and graphical interfaces, and the possibility of calling programs written in other languages such as C, C++, Java, and Fortran. An example of program in C++ is the routine `saxs.c` that is available in the supporting information at the book’s website. For more information on MatLab, go to <http://www.mathworks.com/products/matlab/>.

Supporting Information for routines and worked exercises can be found at the book’s webpage <http://xraybook.if.usp.br/>.

1. `asfQ.m`

```
function f=asfQ(atom,x)
%%%%%%%%%%%%%%%%%%%%%%%%%%%%%%%%%%%%%
% Calculate atomic scattering factors, f0
%%%%%%%%%%%%%%%%%%%%%%%%%%%%%%%%%%%%%
% Input:
% atom = element symbol, e.g. 'Ga'
% x = sen(theta)/lambda = 0.25*Q/pi (m-by-n array) (1/Angstrom)
% Output:
% f0(x) = c + sum_i ai * exp(-bi*x^2) i=1,2,3,4
% in a m-by-n matrix format.
% Coefficients a1, a2, a3, a4, b1, b2, b3, b4, and c
% from file f0_CromerMann.dat available at http://xraybook.if.usp.br/
%%%%%%%%%%%%%%%%%%%%%%%%%%%%%%%%%%%%%
x = x.*x;
sizeA = size(atom,2);
mmax = cromermann(0);
m = 1; CM=zeros(1,9); ctr = 1;
while ((ctr == 1) && (m < mmax + 1))
    line = cromermann(m);
    aux = find(line(1:8)==‘ ’);
    n = aux(1);
    if (n==sizeA+1)
        X = line(1:n-1);
        if (X==atom)
            CM = sscanf(line(9:size(line,2)),'%f');
            ctr = 0;
```

```

    end;
end;
m = m + 1;
end;
if (ctr==1) disp([' Element ' atom ' not found!!!']); return; end;
f = CM(1)*exp(-CM(5)*x) + CM(2)*exp(-CM(6)*x) + CM(3)*exp(-CM(7)*x) + CM(4)*exp(-CM(8)*x) + CM(9);

function line=cromermann(mn)
M = [
'C      2.310000  0.020000  1.588600  0.865000 20.843900 10.207500  0.568700 51.651200  0.215600';
'Ga     15.235400  6.700600  4.359100  2.962300  3.066900  0.241200 10.780500 61.413500  1.718900';
'Ga3+   12.692000  6.698830  6.066920  1.006600  2.812620  0.227890  6.364410 14.412200  1.535450';
'As     16.672300  6.070100  3.431300  4.277900  2.634500  0.264700 12.947900 47.797200  2.531000';
% Complete matrix of coefficients is available on the book's webpage
if (mn==0), line = size(M,1);
else      line = M(mn,:);
end;

```

2. assintotic.m

```

function M=assintotic(a,b,c,Qi,Qf,N,Na)
%%%%%%%%%%%%%%%%%%%%%%%%%%%%%%%%%%%%%
% Small-angle scattering of particles with rectangular dimensions %
% Input: %
% a,b,c = particles dimensions (Angstrom) %
% Qi,Qf = Q-range, initial and final values (1/Angstrom) %
% N = number of points in the scattering curve %
% Na = number of random positions within particle's volume a x b x c %
% Output: M = [Q; I]'; N-by-2 array with the curve intensity x Q %
% Usage: Z=assintotic(10,10,100,0.008,2,0,200,1000); %
%%%%%%%%%%%%%%%%%%%%%%%%%%%%%%%%%%%%%
N = fix(N);
if (N>1), dQ = (Qf-Qi)/N; else disp('      >>> Insufficient number of points!!!'); end;
Q = Qi:dQ:Qf;
Nq = size(Q,2);
R = [a*rand(Na,1) b*rand(Na,1) c*rand(Na,1)];
I = zeros(1,Nq);
for n=1:Na
    for m = n+1:Na
        Rnm = R(m,:)-R(n,:);
        QR = sqrt(Rnm*Rnm')*Q;
        I = I + sin(QR)./QR;
    end;
end;
M = [Q; I]';

```

3. backadj.m

```

function B=backadj(X,M)
%%%%%%%%%%%%%%%%%%%%%%%%%%%%%%%%%%%%%
% To adjust background noise of XRD pattern %
% Input: %
% X = x-axis (2theta or Q) values of the raw data %
% M = ginput <- MatLab command to get (x,y) coordinates by clicking %
%      on the figure window %
% Output B = background noise in the raw data, estimated by linear %
%      interpolating the points obtained from the ginput command %
%%%%%%%%%%%%%%%%%%%%%%%%%%%%%%%%%%%%%
N=size(M,1);
xa = M(1,1); ya = M(1,2);
B=zeros(size(X));
for n=2:N
    xb = M(n,1); yb = M(n,2);
    Nx = X-xa & X==xb;
    B(Nx) = (X(Nx)-xa)*((yb-ya)/(xb-xa)) + ya;
    xa = xb; ya = yb;
end;

```

4. benzeneonpsp.m

```

function I=benzeneonpsp(thx,thy,thz,D,L,pixel,wl,prn)
%%%%%%%%%%%%%%%%%%%%%%%%%%%%%%%%%%%%%
% Intensity pattern of a molecule on cylindrical film (X-ray detector) %
% Molecule: aromatic ring with 6 carbon atoms %
% Input: %
% thx, thy, and thz molecule rotation angles (deg) %
% film radius D and length 2L, and size of pixel (mm) %
% wl = wavelength (Angstrom) ou energy (eV) %
% prn = 0 to suppress image preview %

```

```
% Output: I = intensity on the pixel array
% Secondary routines required: asfQ.m
% Usage:
% >> I=benzenesaxsp(30,0,90,50,200,2,20000,1);
%%%%%%%%%%%%%%%
rad = pi / 180;
deg = 1/rad;
if (wl < 1000) E = 12398.5 / wl; else E = wl; wl = 12398.5 / E; end;
aux = 2 * pi / wl;
s = [1 0 0];
e = [0 0 1];
dz = pixel;
n = floor(2*pi/dz);
LimZ = 0.5*ndz;
Z = -LimZ:dz:LimZ;
Nz = size(Z,2);
dphi = pixel / D;
n = floor(pi/dphi);
LimPhi = 0.5*(2*n-1)*dphi;
phi = -LimPhi:dphi:LimPhi;
Nphi = size(phi,2);
D2 = D*D;
aux1 = D2*dz*dphi;
Rn = i*benzene([thx thy thz]*rad);
for nz = 1:Nz
    z = Z(nz);
    invr = 1/sqrt(z*z+D2);
    DOmega = aux1*invr*invr*invr;
    X(1:Nphi,nz)=z;
    for np = 1:Nphi
        y = phi(np);
        cphi = cos(y);
        sphi = sin(y);
        sprime = invr*[D*cphi D*sphi z];
        p = cross(sprime,cross(e,sprime));
        p = p * p';
        Q = aux * (sprime - s);
        modQ(np,nz) = norm(Q);
        modQ(np,nz) = norm(Q);
        F = sum(exp(Q.*Rn));
        Ic(np,nz) = p*F*conj(F)*DOmega;
        Ic(np,nz) = p*F*conj(F)*DOmega;
        Y(np,nz)= y*deg;
    end;
end;
f = asfQ('C',(25/pi)*modQ);
I = real(f.*f.*Ic);
if (prn~0)
    hfi=figure(1);
    clf
    set(hfi,'InvertHardcopy', 'off','Color','w')
    surf(X,Y,log10(I))
    axis image
    shading interp
    set(gca,'FontSize',14,'Color',[0.93 0.93 0.93],'LineWidth',1)
    set(gca,'YTick',[ -180 -120 -60 0 60 120 180 ],'ZTick',[ ],'DataAspectRatio',[1 1 0.3])
    colormap(jet)
    colorbar('XColor','k','FontSize',14,'Location','East','LineWidth',1)
    xlabel('file axis, z (mm)', 'FontSize',18,'Rotation',21)
    ylabel('2\theta (\circ)', 'FontSize',18)
    text(-1160,-2020,400,'Log(I)', 'FontSize',14)
end;

function Rn=benzene(Or)
thx = Or(1); thy = Or(2); thz = Or(3);
ra=1.4;
th = [0 60 120 180 240 300] * (pi/180) + thx;
r = ra*[zeros(1,6); cos(th); sin(th)];
cthz = cos(thz);
sthz = sin(thz);
cth = cos(thy);
sth = sin(thy);
Ry = [cth 0 -sth; 0 1 0; sth 0 cth];
Rz = [cthz -sthz 0; sthz cthz 0; 0 0 1];
Rz = Rz*Ry*r;
```

5. benzenesaxs1.m

```
function M=benzenesaxs1(D,L,pixel,wl)
%%%%%%%%%%%%%%%
% Small angle X-ray scattering by
% a disperse system of benzene molecules
% Input:
%   radius D (mm) and width 2L (mm) of the film (cylindric geometry)
%   pixel size (mm)
%   wl = wavelength (Angstrom) or energy (eV)
% Output M = [tht Ir Ic]
%           |   |
%           |   | incoherent (Compton) intensity
```

```

% | coherent intensity
% | angle of scattering (deg)
% Secondary routines required: asfQ.m and csfQ.m
% Usage:
% >> benzenesaxs1(50,50,2,20000)
%%%%%%%%%%%%%%%
if (wl < 1000) E = 12398.5 / wl; else E = wl; wl = 12398.5 / E; end;
d = 1.4; % C-C bond length (Angstrom)
s = [1 0 0]; % incident beam direction
e = [0 0 1]; % polarization (electric wavefield direction)
dz = pixel;
n = floor(2*L/dz);
LimZ = 0.5*n*dz;
Z = -LimZ:dz:LimZ;
Nz = size(Z,2);
dphi = pixel / D;
n = floor(pi/dphi);
LimPhi = 0.5*(2*n-1)*dphi;
phi = -LimPhi:phi:LimPhi;
Nphi = size(phi,2);
D2 = D*D;
aux1 = D2*dz*dphi;
for nz = 1:Nz
    z = Z(nz);
    invr = 1/sqrt(z*z+D2);
    DOmega = aux1*invr*invr*invr;
    X(1:Nphi,nz)=z;
    for np = 1:Nphi
        y = phi(np);
        Y(np,nz)= D*y;
        cphi = cos(y);
        sphi = sin(y);
        sprime = invr*[D*cphi D*sphi z];
        p = cross(sprime,cross(e,sprime));
        P2(np,nz) = (p * p')*DOmega;
        Q(np,nz) = norm(sprime - s); % |s'-s|
    end;
end;
Q(Q==0)=1e-8;
f=asfQ('C',(0.5/wl)*Q); % (1/4pi)*(2pi/wl)*|s'-s|
f = 6*(f.*f);
S=csfQ('C',(0.5/wl)*Q);
nphalf = round(0.5*Nphi);
for nz = 1:Nz
    for np = 1:nphalf
        m = (nz-1)*Nphi + np;
        f2(np,nz)=f(m);
        fc(np,nz)=6*S(m,2);
    end;
    for np=nphalf+1:Nphi
        m = (nz-1)*Nphi + np;
        f2(np,nz)=f(m);
        fc(np,nz)=0;
    end;
end;
Qd = (2*pi*d/wl)*;
SdeQ = sin(Qd)./Qd;
Qd = (2*pi*d*sqrt(3)/wl)*Q;
SdeQ = SdeQ + sin(Qd)./Qd;
Qd = (4*pi*d/wl)*Q;
SdeQ = 1+ 2*SdeQ + sin(Qd)./Qd;
A = f2.*SdeQ;
I = P2.* (A + fc);
nz0 = round(0.5*Nz);
IzS = (1/6).*A(1:nphalf,nz0);
IzC = (1/6).*fc(1:nphalf,nz0);
h1=figure(1);
clf
set(h1,'InvertHardcopy', 'off','Color','w')
surf(X,Y,log10(I))
axis image
shading interp
view(90,90)
set(gca,'Position',[0.165 0.5 0.775 0.45], 'FontSize',14,'LineWidth',1)
set(gca,'YTick',[-150 -120 -90 -60 -30 0 30 60 90 120 150], 'ZTick',[], 'DataAspectRatio',[1 1 0.3])
box on
colormap(hot)
colorbar('XColor','k','FontSize',14,'Location','NorthOutside','LineWidth',1,'Position',
[0.54 0.405 0.38 0.05])
xlabel('film width (mm)', 'FontSize',18)
ylabel('2\thetaeta ({\circ})', 'FontSize',18)
text(0,0,500,'Log(I)', 'FontSize',14)
h2=figure(2);
clf
set(hf2,'InvertHardcopy', 'off','Color','w')
semilogy(-Y(1:nphalf,nz0),IzS,'k',-Y(1:nphalf,nz0),IzC,'--r','LineWidth',2)
set(gca,'FontSize',14,'Color',[1 0.95 0.87],'LineWidth',1)
xlabel('2\thetaeta ({\circ})', 'FontSize',18)
ylabel('|f_C(Q)|^2S(Q)', 'FontSize',18)

```

```

text(90,8,'Compton \downarrow','Color','r','FontSize',18)
axis tight
grid
M = [-Y(i:nphalf,nz0) Izs IzC];

```

6. benzenesaxs2.m

```

function M=benzenesaxs2(wl)
%%%%%%%%%%%%%%%%%%%%%%%%%%%%%%%%%%%%%
%           SAXS: structural function of the benzene molecule %
% Input: %
%   wl = wavelength (Angstrom) or energy (eV) %
% Output M = [Q; SofQ; SofQ1; SofQ2; SofQ3]'; %
%           |   |   |   |   |   |
%           |   |   |   |   |   interference pattern of each atomic pair %
%           |   |   |   |   |   |
%           |   |   |   |   |   structural function %
%           |   |   |   |   |   |
%           reciprocal vector module (1/Angstrom) %
%%%%%%%%%%%%%%%%%%%%%%%%%%%%%%%%%%%%%
if (wl < 1000) E = 12398.5 / wl; else E = wl; wl = 12398.5 / E; end;
d = 1.4; % C-C bond length (Angstrom)
Qmax = (4*pi/wl);
dQ = Qmax/1000;
Q = 0:dQ:Qmax;
Q(1) = 1e-8;
Qd1 = d*Q;
Qd2 = (d*sqrt(3))*Q;
Qd3 = (2*d)*Q;
SofQ1 = sin(Qd1)./Qd1;
SofQ2 = sin(Qd2)./Qd2;
SofQ3 = sin(Qd3)./Qd3;
SofQ = 1+2*(SofQ1+SofQ2)+SofQ3;
hf1=figure(1);
clf
set(hf1,'InvertHardcopy', 'off','Color','w')
semilogy(Q,2+SofQ1,'--m',Q,1.5+SofQ2,'--r',Q,1+SofQ3,'--b','LineWidth',1)
legend(' 140pm',' 243pm',' 280pm')
hold on
semilogy(Q,SofQ,'k','LineWidth',1.5);
hold off
set(gca,'FontSize',14,'Color',[1 0.95 0.87],'LineWidth',1,'YTick',[0.7 0.8 0.9 1 1.5 2 2.5 3])
xlabel('Q (A^{-1})','FontSize',18)
ylabel('S(Q)', 'FontSize',18)
axis([0 Qmax 0.98*min(SofQ) 3.2])
grid
M = [Q; SofQ; SofQ1; SofQ2; SofQ3]';

```

7. bragg.m

```

function M=bragg(wl,A,H)
%%%%%%%%%%%%%%%%%%%%%%%%%%%%%%%%%%%%%
% Input: %
%   wl = wavelength (Angstrom) or energy (eV) %
%   A = [a b c alpha beta gamma], lattice parameters (Angstrom and deg) %
%   H = [h1 k1 l1; h2 k2 l2; ...], reflection indexes %
% Output M = [ E   wl   0   0;
%             d   thB 2thB Vc]
%             |   |   |   |
%             |   |   |   |   unit cell volume (Angstrom^3)
%             |   |   |   |   2theta Bragg (deg)
%             |   |   |   |   theta Bragg (deg)
%             |   |   |   |   interplane distance (Angstrom)
% Usage:
% >> bragg(1.54, [], []);
% >> bragg(8000, [4.9134 4.9134 5.4052 90 90 120], [1 0 0; 0 1 1]);
%%%%%%%%%%%%%%%%%%%%%%%%%%%%%%%%%%%%%
rad = pi / 180;
deg = 1/rad;
if (wl < 1000) E = 12398.5 / wl; else E = wl; wl = 12398.5 / E; end;
fprintf('   Energy = %.2feV (%.6f A)\n',E,wl);
if isempty(A) M = [E wl]; return; else M(1,:) = [E wl 0 0]; end;
nm = size(A);
if (nm(1)*nm(2)==1)
    A(1:3) = A(1)*ones(1,3);
    A(4:6) = [90 90 90];
elseif (nm(1)*nm(2)==2)
    A(1:3) = [A(1) A(1) A(2)];
    A(4:6) = [90 90 90];
end;
A(4:6) = A(4:6)*rad;
cosphi = cos(A(6)) - cos(A(5))*cos(A(4));
cosphi = cosphi / (sin(A(5))*sin(A(4)));
sinphi = sqrt(1-cosphi*cosphi);
a1 = A(1) * [sin(A(5)) 0 cos(A(5))];
```

```

a2 = A(2) + [sin(A(4))*cosphi sin(A(4))*sinphi cos(A(4))];
a3 = A(3) * [ 0 0 1];
alr = cross(a2,a3);
Vc = alral';
alr = alr/Vc;
a2r = cross(a3,a1)/Vc;
a3r = cross(a1,a2)/Vc;
Nr = size(H,1);
for n=1:Nr
    q = H(n,1)*alr + H(n,2)*a2r + H(n,3)*a3r;
    d = 1/sqrt(q*q');
    sinth = 0.5*w1/d;
    if (sinth > 1)
        fprintf('      d(%d,%d,%d) = %7.5f A (reflection not allowed for this energy!!!)\n',H(n,1),H(n,2),H(n,3),d);
        M(n+1,:) = [ d 0 0 Vc];
    else
        th = asin(sinth)*deg;
        tth = 2*th;
        fprintf('      d(%d,%d,%d) = %7.5f A,   thB = %6.4f deg,   2thB = %6.4f deg\n',H(n,1),H(n,2),H(n,3),d,th,tth);
        M(n+1,:) = [ d th tth Vc];
    end;
end;

```

8. csfQ.m

```

function S=csfQ(atom,X)
%%%%%%%%%%%%%%%%%%%%%%%%%%%%%%%%%%%%%
% Linear interpolation of tabulated values of the
% incoherent (Compton) scattering function, S(x,Z)
%
% Input:
%   atom = element symbol from 'H' to 'Cs' (Z from 1 to 55)
%   X = sin(th)/lambda = 0.25*Q/pi (1/Angstrom), e.g. X=0:0.05:2;
%
% Output S = [x f]
%           | |
%           | interpolated values of S(x,Z)
%           sen(th)/lambda (1/Angstrom)
%
% Tabulated values S(x,Z) from file IncohScattFunction.txt available at
% http://xraybook.if.uesp.br/
%%%%%%%%%%%%%%%%%%%%%%%%%%%%%%%%%%%%%
X(X<0)=0; X(X>2)=2;
s=size(X); NofX=s(1)*s(2);
sizeA = size(atom,2);
W(1,: ) = [ 1. 2. 3. 4. 5. 6. .7 .8 .9 1.0 1.5 2.0];
mmax = hubbell(0);
m = 1; W(2,: )=zeros(1,12); ctr = 1;
while ((ctr == 1) & (m < mmax+1))
    line = hubbell(m);
    aux = find(line(1:8)==' ');
    n = aux(1);
    if (n==sizeA+1)
        A = line(1:n-1);
        if (A==atom)
            W(2,: ) = sscanf(line(9:size(line,2)),'%f');
            ctr = 0;
        end;
    end;
    m = m + 1;
end;
if (ctr==1)
    disp([' Element ' atom ' not found!!! Using Cs instead...']);
    W(2,: ) = sscanf(line(9:size(line,2)),'%f');
end;
NofW = 12;
for nx = 1:NofX
    x = X(nx);
    x2 = 0; f = 0;
    nw = 1;
    while (nw <= NofW)
        x1 = x2; y = f;
        x2 = W(1,nw); f = W(2,nw);
        if (x2 > x)
            f = (f - y) * (x - x1) / (x2 - x1) + y;
            nw = NofW;
        end;
        nw = nw + 1;
    end;
    S(nx,: ) = [x f];
end;

function line=hubbell(m)
M = [
'C 1.039 2.604 3.643 4.184 4.478 4.690 4.878 5.051 5.208 5.348 5.781 5.930';
'N 1.080 2.858 4.097 4.792 5.182 5.437 5.635 5.809 5.968 6.113 6.630 6.860';
'O 0.977 2.799 4.293 5.257 5.828 6.175 6.411 6.596 6.755 6.901 7.462 7.764';

```

```
'Ca 3.105 5.690 7.981 9.790 11.157 12.163 12.953 13.635 14.256 14.830 16.921 17.970'];
% Complete table of theoretical values is available on the book's webpage
if (m==0), line = size(M,1);
else line = M(m,:);
end;
```

9. debye.m

```
function debye(ct,Qf,rab,sg)
%%%%%%%%%%%%%%%%%%%%%%%%%%%%%%%%%%%%%
% Comparison of numerical solutions of F = FT(G(u-rab)) %
% with usual approximations %
%
% Input: %
%   ct = 1 for F = G(u-rab).sin(Qu)/Qu, 2 for F = G(u-rab).sin(Qu), and %
%         3 for F = G(u-rab).cos(Qu) %
%   Qf = upper limit of Q-range (1/Angstrom) %
%   rab = a value of interatomic distance (Angstrom) %
%   sg = Gaussian standard deviation (Angstroms), %
%         G(u-rab) = exp[-(u-rab)^2/2sg^2] %
%%%%%%%%%%%%%%%%%%%%%%%%%%%%%%%%%%%%%
if (sg < 0.005)
    disp(' >>> Standard deviation too small, use sg > 0.005 A!!!!')
    return;
end;
if (rab >= 50)
    disp(' >>> Interatomic distance too large, use rab < 50 A!!!!')
    return;
end;
Nu = 10000;
Umax = 200;
du = Umax/Nu;
U = 0:du:Umax;
U(1) = 1e-8;
Nq = 500;
dq = Qf/Nq;
Q = 0:dq:Qf;
Q(1)=1e-8;
Nq = size(Q,2);
G = (du/(sg*sqrt(2*pi)))*exp((-0.5/sg^2)*(U-rab).^2);
Y = zeros(1,Nq);
if (ct==1)
    for n = 1:Nq
        Qu = Q(n)*U;
        Y(n) = sum(G.*sin(Qu)./Qu);
    end;
    Qrab = rab*Q;
    dqm = sg/sqrt(2);
    Y2 = exp(-(dqm^2*(Q.*Q))).*(sin(Qrab)./Qrab);
    ytext = 'FT\{G(u-rab)/4\pi u^2\}';
elseif (ct==2)
    for n = 1:Nq
        Qu = Q(n)*U;
        Y(n) = sum(G.*sin(Qu));
    end;
    Qrab = rab*Q;
    dqm = sg/sqrt(2);
    Y2 = exp(-(dqm^2*(Q.*Q))).*sin(Qrab);
    ytext = 'imag[FT\{G(u-rab)\}]';
else
    for n = 1:Nq
        Qu = Q(n)*U;
        Y(n) = sum(G.*cos(Qu));
    end;
    Qrab = rab*Q;
    dqm = sg/sqrt(2);
    Y2 = exp(-(dqm^2*(Q.*Q))).*cos(Qrab);
    ytext = 'real[FT\{G(u-rab)\}]';
end;
hfi=figure(1); clf; set(hfi,'InvertHardcopy', 'off','Color','w');
plot(Q,Y,'r',Q,Y2,'.b','LineWidth',2)
axis tight
set(gca,'FontSize',14,'Color',[0.93 0.93 0.93],'LineWidth',1)
xlabel('Q (A^{-1})','FontSize',18)
ylabel(ytext,'FontSize',18)
legend(' numerical solution',' DW approximation')
```

10. diffraction.m

```

function M=diffraction(wl,fname,prn)
%%%%%%%%%%%%%%%%%%%%%%%%%%%%%%%%%%%%%
% List of structure factors Phkl %
% Input %
% wl = wavelength (Angstrom) or energy (eV) %
% fname = crystal data file (*.in) or structure factor list (*.sft) %
% prn = 1 open figure window for |Phkl|^2 x Q %
% Output M = [Q; tth; pl]'; n-by-3 array histogram x Q or x 2theta %
% save file list (*.sft) when fname has extension *.in %
% Secondary routines required: sfactor.m %
% Usage: M=diffraction(10000,'KDP0.in'); %
%%%%%%%%%%%%%%%%%%%%%%%%%%%%%%%%%%%%%
if (wl < 1000), E = 12398.5 / wl; else E = wl; wl = 12398.5 / E; end;
rad = pi / 180;
M = [0 0];
n = regexp(fname,'.in', 'once');
if isempty(n)
    if isempty(regexp(fname,'.sft', 'once'))
        disp('      >>> File type unkown!!!!')
        return;
    else
        fidin = fopen(fname,'r');
        if (fidin==1)
            disp(['      >>> File ' fname ' not found!!!!'])
            return;
        end;
        for n=1:6, line = fgets(fidin); end;
        n = 0;
        while (line(2)==' ')
            n = n + 1;
            F2(n,1) = sscanf(line(47:57),'%f')^2;
            Dhkl(n,1) = sscanf(line(84:91),'%f');
            line = fgets(fidin);
        end;
        fclose(fidin);
    end;
else
fout = [fname(1:n-1) 'E' num2str(round(E)) '.sft'];
fidin = fopen(fname,'r');
if (fidin==1)
    disp(['      >>> File ' fname ' not found!!!!'])
    return;
end;
line = fgets(fidin);
P = sscanf(line,'%f');
if (size(P,2)==6)
    disp('      >>> Line 1: a b c alpha beta gamma');
    fclose(fidin);
    return;
end;
fclose(fidin);
P(4:6) = P(4:6)*rad;
cosphi = cos(P(6)) - cos(P(5))*cos(P(4));
cosphi = cosphi / (sin(P(5))*sin(P(4)));
sinphi = sqrt(1-cosphi*cosphi);
a1 = P(1) * [sin(P(5)) 0 cos(P(5))];
a2 = P(2) * [sin(P(4))*cosphi sin(P(4))*sinphi cos(P(4))];
a3 = P(3) * [0 0 1];
alr = cross(a2,a3);
Vc = alr*al';
alr = alr/Vc;
a2r = cross(a3,a1)/Vc;
a3r = cross(alr,a2)/Vc;
hmax = floor(2.0 / (wl * sqrt(alr*alr')));
kmax = floor(2.0 / (wl * sqrt(a2r*a2r')));
lmax = floor(2.0 / (wl * sqrt(a3r*a3r')));
H = [-hmax:-1 1:hmax];
K = [-kmax:-1 1:kmax 0];
L = [-lmax:-1 1:lmax 0];
m = 0; two_wl = 2/wl;
Nmax = (2*hmax+1)*(2*kmax+1)*(2*lmax+1);
HKL= zeros(Nmax,3); thBragg = zeros(Nmax,1); Dhkl = zeros(Nmax,1);
for nh = 1:2:hmax
    for nk = 1:2:kmax+1
        for nl = 1:2:lmax+1
            h = H(nh); k = K(nk); l = L(nl);
            q = h*alr + k*a2r + l*a3r;
            modq = sqrt(q*q');
            if (modq>two_wl)
                m = m + 1;
                HKL(m,:) = [h k l];
                thBragg(m,1) = asin(0.5*modq*wl)/rad;
                Dhkl(m,1) = 1.0 / modq;
            end;
        end;
    end;
end;

```

```

h=0;
for nk = 1:2*kmax
    for nl = 1:2*lmax
        k = K(nk); l = L(nl);
        q = k*a2r + l*a3r;
        modq = sqrt(q*q');
        if (modq>two_wl)
            m = m + 1;
            HKL(m,:) = [h k l];
            thBragg(m,1) = asin(0.5*modq*wl)/rad;
            Dhkl(m,1) = 1.0 / modq;
        end;
    end;
k = 0;
for nl = 1:2*lmax
    l = L(nl);
    q = l*a3r;
    modq = sqrt(q*q');
    if (modq>two_wl)
        m = m + 1;
        HKL(m,:) = [h k l];
        thBragg(m,1) = asin(0.5*modq*wl)/rad;
        Dhkl(m,1) = 1.0 / modq;
    end;
end;
Nn = m;
F = sfactor(wl, fname, [HKL; 0 0 0]);
F0 = F(Nr+1);
F = F(1:Nr);
F2 = real(F.*conj(F));
NF = F2>0.1;
F2 = F2(NF); F = F(NF); HKL = HKL(NF,:); thBragg = thBragg(NF); Dhkl = Dhkl(NF);
Nr = size(F2,1);
clear NF;
invF2max = 100/max(F2);
X = F2;
Nmax = [];
for m=1:Nr
    Nmax = [Nmax; find(X==max(X))];
    X(Nmax)=0;
end;
Nmax=Nmax(1:Nr);
HKL = HKL(Nmax,:);
Dhkl = Dhkl(Nmax);
F = F(Nmax);
F2 = F2(Nmax);
thBragg = thBragg(Nmax);
clear Nmax X;
fidout = fopen(fout,'w');
fprintf(fidout,'n X-ray photon energy = %6.1feV (wavelength = %8.6fA)      Ihkl = |Fhkl|^2\n',E,wl);
fprintf(fidout,'-----|-----|-----|-----|-----|-----|-----|\n');
fprintf(fidout,'| h   k   l | Ihkl(%%) |      FH |      phase | th   tth   dhkl |\n');
fprintf(fidout,'-----|-----|-----|-----|-----|-----|-----|\n');
for m=1:Nr
    x = real(F(m,1));
    y = imag(F(m,1));
    ph = atan2(y,x)/rad;
    th = thBragg(m);
    fprintf(fidout,'| %3d %3d %3d | %5.1f | %9.3f %9.3fi %9.3f %6.1f | %7.4f %8.4f %7.4f |\n',...
        HKL(m,1),HKL(m,2),HKL(m,3),invF2max*F2(m),x,y,sqrt(F2(m)),ph,th,2*th,Dhkl(m,1));
end;
fprintf(fidout,'-----|-----|-----|-----|-----|-----|-----|\n');
fprintf(fidout,'F000 = %5.3f %5.3fi\n',real(F0),imag(F0));
fclose(fidout);
end;
Nr = size(Dhkl,1);
Umax = 1.5*max(Dhkl);
du = 0.0002;
U = 0:du:Umax;
p = zeros(size(U));
for n=1:Nr, k = floor(Dhkl(n)/du)+1; p(k) = p(k) + F2(n); end;
dmin = 0.5*wl;
Nth = find(U<dmin);
Q = (2*pi)./U(Nth);
p = p(Nth);
Qmax = 4*pi/wl;
tth = (2/rad)*asin(Q/Qmax);
M = [Q; tth; p];
if (prn==1)
    hf1=figure(1); clf; set(hf1,'InvertHardcopy', 'off','Color','w')
    plot(Q,p/max(p),'b','LineWidth',3)
    axis([0.98*min(Q) 1.02*max(Q) -0.02 1.02])
    set(gca,'FontSize',14,'Color',[0.93 0.93 0.93],'FontName','Arial','LineWidth',1)
    xlabel('Q (A^{-1})','FontSize',18)
    ylabel('\Sigma|F_{hkl}|^2 (relative values)','FontSize',18)
end;

```

11. diffractogram.m

```

function M=diffractogram(fname,Rg,xpv,prn)
%%%%%%%%%%%%%%%%%%%%%%%%%%%%%%%%%%%%%
% X-ray powder diffraction pattern %
% Input: %
%   fname = *.sft, list of structure factors from routine diffraction.m %
%   Rg = crystallite gyration radius (Angstrom) %
%   xpv = pseudo-Voigt line profile function %
%         1 for Gaussian and 0 for Lorentzian %
%   prn = 1 for figure window %
% Output M = [Q; tth; I; p; pF]', n-by-4 array with I(Q) and I(tth) %
% intensity curves, and histograms of Ahkl and |Fhkl|^2 %
% Usage: M=diffractogram('SIE12399.sft',85,0.4,1);
%%%%%%%%%%%%%%%%%%%%%%%%%%%%%%%%%%%%%
M = [0 0];
if isempty(regexp(fname,'.sft', 'once')), disp(' >>> Unknown file type!!!'); return; end;
fid = fopen(fname,'r');
if (fid==1), disp(' >>> File ' fname ' not found!!!'); return; end;
line = fgets(fid);
line = fgets(fid);
N1=find(line=='=');
N2=find(line==',');
wl = sscanf(line(N1(2)+1:N2(2)+6),'%f');
for n=1:4, line = fgets(fid); end;
n0;
while (line(2)==' ')
n = n + 1;
F2(n,1) = sscanf(line(47:57),'%f')^2;
d(n,1) = sscanf(line(84:91),'%f');
tth(n,1) = sscanf(line(74:83),'%f');
line = fgets(fid);
end;
fclose(fid);
Nr = n;
A = d.*F2./sin(d(tth));
Qhkl = (2*pi)./d;
Qmax = (4*pi)/wl;
dQ = Qmax/50000;
Q = 0:dQ:Qmax;
p = zeros(size(Q)); pF = p;
for n=1:Nr
k = floor(Qhkl(n)/dQ)+1;
p(k) = p(k) + A(n);
pF(k) = pF(k) + F2(n);
end;
Qmin = 0.5*min(Qhkl);
N = Q>0;
Q = Q(N);
p = p(N);
pF = pF(N) * (1/max(pF));
Nq = size(Q,2);
sg = sqrt(1.5)/Rg;
bq = sqrt(12*log(2))/Rg;
if (bq<2*dQ), I = p;
else
m = floor(50*bq/dQ);
X = (-m:m)*dQ;
X2 = X.*X;
PV = ((xpv*(sg*sqrt(2*pi)))*exp((-1/(2*sg*sg))*X2));
PV = PV + ((2*(1-xpv)*bq/pi)./(4*X2+bq*bq));
pt = [p(1)*ones(1,m) p p(Nq)*ones(1,m)];
I = zeros(1,Nq);
for n=1:Nq
I(n) = sum(PV.*pt(n:2*m+n));
end;
end;
clear pt;
I = I*(1/max(I));
tth = 2*a sind(Q*(1/Qmax));
M = [Q; tth; I; p; pF]';
if (prn==1)
hfi=figure(1);
clf
set(hfi,'InvertHardcopy', 'off','Color','w')
plot(Q,I,'k','LineWidth',2)
axis([Qmin Qmax -0.02 1.02])
set(gca,'FontSize',14,'Color',[0.93 0.93 0.93],'LineWidth',1)
xlabel('Q (Å^{-1})','FontSize',18)
ylabel('normalized intensity','FontSize',18)
grid
end;
```

12. dynamicphase.m

```

function dynamicphase(wl, fname, H)
%%%%%%%%%%%%%%%%%%%%%%%%%%%%%%%%%%%%%
%           Dynamic phase across the reflectivity curve %
%
% Input:
%   wl = wavelength (Angstrom) or energy (eV)
%   fname = crystal data information, file '*.in'
%   H = [h k l] reflection indexes
% Secondary routines required: sfactor.m and rcdarwinprins.m
% Usage: dynamicphase(8000,'Si.in',[1 1 1])
%%%%%%%%%%%%%%%%%%%%%%%%%%%%%%%%%%%%%
if (wl < 1000), E = 12398.5 / wl; else E = wl; wl = 12398.5 / E; end;
F = sfactor(E,fname,H(1,:));
if (F*conj(F)<1), disp('      >>> Forbidden or very weak reflection!!!'); return; end;
S=rcdarwinprins(E,fname,H,2^30,0).';
X=S(1,:);
Y = S(2,:).*conj(S(2,:));
xc = sum(X.*Y)/sum(Y);
range = sum(abs(X-xc).*Y)/sum(Y);
Xmin = xc-3*range;
Xmax = xc+3*range;
Yi = real(S(2,:));
W = atan2(Yi,Yr)*(180/pi);
Fr = real(F);
Pi = imag(F);
phi = atan2(Fi,Fr)*(180/pi);
if (W(1)<0), N = find(W<0); W(N) = W(N) + 360; end;
W = W-phi;
N = find(W<-90); W(N) = W(N) + 360;
Wmin = min(W);
if (Wmin<0), Wmin = 0; end;
Wmax = max(W);
Ymax = max(Y);
if (Ymax>0.5), Ymax = 1; else Ymax = 1.02*Ymax; end;
if (Wmax<180), Wmax = 180; end;
hf1=figure(1); clf; set(hf1,'InvertHardcopy', 'off','Color','w')
plot(X,Y,(Wmax/Ymax),'--k',X,W,'-r','LineWidth',2)
axis([Xmin Xmax Wmin Wmax])
set(gca,'YTick',[0 60 120 180],'FontSize',14,'Color',[.7 .78 1],'LineWidth',1)
xlabel('Delta(theta (arcsec))','FontSize',18)
ylabel('Omega(theta) (deg)','FontSize',18)
legend(' reflectivity',' dynamic phase')

```

13. ex1GUP.m

```

function ex1GUP
%%%%%%%%%%%%%%%%%%%%%%%%%%%%%%%%%%%%%
% Plots scattering curves of monomers and dimers of %
%   mutant enzyme H166G (PDB ID: 1GUP) %
%
% Required files: 1GUPmono.pdb and 1GUPdime.pdb %
% 1GUPmono.pdb = records "ATOM" from 1 to 2784 of file 1GUP.pdb %
% 1GUPdime.pdb = records "ATOM" from 1 to 5551 of file 1GUP.pdb %
% Both files are available at http://xraybook.if.ues.br/
%%%%%%%%%%%%%%%%%%%%%%%%%%%%%%%%%%%%%
d = 54; % exclusion distance (Angstrom)
rhov = 0.08; % packing factor
Ssaxs('1GUPmono.ndu',2,1000,0); % use '1GUPmono.pdb' in the 1st run
Qm = S(1,:);
Pm = S(2,:);
invPmax = 1/max(Pm);
Pm = Pm * invPmax;
PmS = Pm.*((1-(8*rhov)*tfpsphere(d*Qm));
Ssaxs('1GUPdime.ndu',2,1000,0); % use '1GUPdime.pdb' in the 1st run
Qd = S(1,:);
Pd = (0.5*invPmax)*S(2,:);
N=1:4:size(Qd,2);
hf1=figure(1);
clf
set(hf1,'InvertHardcopy', 'off','Color','w')
semilogy(Qd(N),Pd(N),'-ro',Qm,Pm,'k',Qm,PmS,'-.k','LineWidth',2,'MarkerSize',7,'MarkerFaceColor','w');
axis tight
set(gca,'FontSize',14,'Color',[0.890196 0.941176 0.901961],'Box','on','LineWidth',1)
xlabel('Q (A^{-1})','FontSize',18)
ylabel('I(Q)/I(0)','FontSize',18)
legend(' dimers',' monomers',' high conc.')
axis([-0.01 .52 8e-4 2.4])

function Z=tfpsphere(u)
u(u<0)=1e-8;
u3 = u.*u.*u;
Z = 3*((sin(u)-u.*cos(u))./u3);

```

14. ex1N5U.m

```

function ex1N5U
%%%%%%%%%%%%%%%%%%%%%%%%%%%%%%%%%%%%%
% Plot SAXS curve generated by routine sакс.c for human albumin (1N5U.pdb) %
% and saved in file 'sакс1N5U_0to30E8keV.dat' available at %
% http://xraybook.if.usp.br/ %
%%%%%%%%%%%%%%%%%%%%%%%%%%%%%%%%%%%%%
M = load('sакс1N5U_0to30E8keV.dat');
Q = M(:,1)';
P = M(:,2)';
S = M(:,3)';
Rg = 27.8916;
alpha = -Rg^2/3;
N=find(Q<=0.2);
jmax = size(N,2);
m = 5;
Q2 = Q(N(1:m:jmax)).*Q(N(1:m:jmax));
Ps = log10(P(N(1:m:jmax)));
hfi=figure(1);
clf
set(hfi,'InvertHardcopy','off','Color','w')
plot(Q2,Ps,'bo','MarkerFaceColor','w','MarkerSize',6,'LineWidth',1.5)
hold on
plot([0 0.02],log10(P(1)*[1 exp(alpha*0.02)]),'r--','LineWidth',1.5)
hold off
axis([0 .04 6.9 9.1]);
grid
legend('P(Q)', 'P(0)exp(-R_g^2/3)', 'Location', 'SouthWest')
set(gca,'FontSize',14,'Color',[0.855 0.702 1],'LineWidth',1)
set(gca,'YTick',[7 7.5 8 8.5 9])
xlabel('Q (A^{-2})','FontSize',14);
ylabel('log(P)', 'FontSize',14);
text(0.017,log10(1.3e7), 'R_g = 27.9 A', 'FontSize',16, 'Color', 'r')
ha2=axes('Position',[.41 .496 .48 .40]);
semilogy(Q,P,'b','LineWidth',2)
hold on
semilogy([.2 .2],[1e+5 1.2e+9], '--k','LineWidth',1)
hold off
set(ha2,'FontSize',14,'Color',[0.973 0.973 0.973],'LineWidth',1)
set(ha2,'YTick',[1e+5 1e+6 1e+7 1e+8 1e+9])
xlabel('Q (A^{-1})','FontSize',18)
ylabel('P(Q)', 'FontSize',18)
axis tight
text(.5,1e+8,'1N5U','FontSize',36,'Color',[0.7 0.7 0.7],'FontWeight','bold')

```

15. exabscs.m

```

function exabscs(atom,Emin,Emax)
%%%%%%%%%%%%%%%%%%%%%%%%%%%%%%%%%%%%%
% Absorption edge in log-log graphic %
%%%%%%%%%%%%%%%%%%%%%%%%%%%%%%%%%%%%%
% Input:
% atom = element symbol, e.g. 'Ag'
% Emin, Emax = energy range (keV)
% Secondary routines required: fpfpp.m
% Usage: exabscs('Kr',7,30)
%%%%%%%%%%%%%%%%%%%%%%%%%%%%%%%%%%%%%
Emin = abs(Emin); Emax = abs(Emax);
if (Emin>500), Emin = 0.001*Emin; Emax = 0.001*Emax; end;
if (Emax>Emin), x=Emax; Emax = Emin + 0.01; Emin = x; end;
if (Emin<1), Emin = 1; end;
if (Emax>70), Emax = 70; end;
E = Emin:0.01:Emax;
NE = size(E,2);
M = fpfpp(atom,1000*E);
Y = M(:,4)';
Np = 1:40:NE;
X = E(Np);
X0 = E;
nfind(M(:,2)==min(M(:,2)),1);
dE = E(3)-E(2);
Edge = E(n);
if (Edge-E(1) > 5), n1 = find(abs(E-Edge+5)<dE,1);
else n1 = 1;
end;
if (E(NE)-Edge > 5), n2 = find(abs(E-Edge-5)<dE,1);
else n2 = NE;
end;
if (n-n1 < 12) disp(' Emin too close of the edge!!!'); return; end;
if (n2-n < 12) disp(' Emax too close of the edge!!!'); return; end;
Xb = log(X0(1:n-10)); Xa = log(X0(n+10:NE));
Yb = log(Y(1:n-10)); Ya = log(Y(n+10:NE));
Ybi = interp1(Xb,Yb,Xb);
Ab = (Ybi(2)-Ybi(1))/(Xb(2)-Xb(1));
labelAb = [' \leftarrow \{it n\} = ' num2str(0.01*round(100*Ab))];
Yai = interp1(Xa,Ya,Xa);
Aa = (Yai(2)-Yai(1))/(Xa(2)-Xa(1));

```

```

labelAa = [' \leftarrow \{it n\} = num2str(0.01*round(100*Aa));';
hf1=figure(1);
clf
set(hf1,'InvertHardcopy', 'off','Color','w')
loglog(exp(Xb),exp(Ybi),'b',exp(Xa),exp(Yai),'r','LineWidth',2)
hold on
loglog([min(Xb) max(Xa)], [min(Ybi) max(Yai)],'k','LineWidth',2)
loglog(X,Y(Np),'ko','MarkerFaceColor','w','MarkerSize',6,'LineWidth',1)
hold off
set(gca,'FontSize',14,'Color',[0.93 0.93 0.93],'LineWidth',1)
ylabel('(\sigma_a / ( barn))','FontSize',18)
xlabel('Energy (keV)', 'FontSize',18)
axis tight; grid
nb = round(0.2*(1:n-10));
na = round(0.3*(n+10:N));
text(X0(nb),Y(nb),labelAb,'FontSize',18,'Color','b')
text(X0(na),Y(na),labelAa,'FontSize',18,'Color','r')
fprintf('\n Edge = %0.3f keV\n',Bedge)
Bbi = Y(n-10)/X0(n-10)^Ab;
fprintf(' below edge: %0.5g^{%0.5f}\n',Bbi,Ab);
Bai = Y(n+10)/X0(n+10)^Aa;
fprintf(' above edge: %0.5g^{%0.5f}\n',Bai,Aa);

```

16. ex anomalousignal.m

```

function ex anomalousignal
%%%%%
% Reflectivity curves below and above the Ga K-edge (@ 10360eV) %
% Secondary routines required: rcdarwinsprins.m %
% Required files: GaAs.in %
%%%%%
%rcdarwinsprins(10300,'GaAs.in',[1 1 7],4096,0).'
X1=S(1,:);
N = find(X1>-180 & X1<180);
X1=X1(N);
Y1=S(2,N).*conj(S(2,N));
Y1b=S(3,N).*conj(S(3,N));
S=rcdarwinprins(10400,'GaAs.in',[1 1 7],4096,0).';
X2=S(1,:);
X2=X2(N);
Y2=S(2,N).*conj(S(2,N));
Y2b=S(3,N).*conj(S(3,N));
c1 = [.87 .92 .98]; c2 = [.86 .86 .86]; c3 = [.85 .16 .0];
hf1=figure(1); clf; set(hf1,'InvertHardcopy', 'off','Color','w')
area(X1-180,Y1,'EdgeColor',c3,'FaceColor','w','LineWidth',2)
area(X2+180,Y2,'EdgeColor','k','FaceColor','w','LineWidth',2)
area(X2+180,Y2b,'EdgeColor',c3,'FaceColor',c2,'LineWidth',2)
hold off
axis([-360 400 0 3e-3])
set(gca,'FontName','Arial','FontSize',14,'Color',c1,'LineWidth',1)
xlabel('(\Delta\theta)', 'FontSize',18)
ylabel('reflectivity, |R_N(\theta)|^2','FontSize',18)
legend(' ( 1, 1, 7)', ' (-1,-1,-7)')
%rcdarwinsprins(10300,'GaAs.in',[1 1 7],2^30,0)';
X1=S(1,:);
N = find(X1>-1 & X1<8);
X1=X1(N);
Y1=S(2,N).*conj(S(2,N));
Y1b=S(3,N).*conj(S(3,N));
S=rcdarwinprins(10400,'GaAs.in',[1 1 7],2^30,0).';
X2=S(1,:);
N = find(X2>-1 & X2<8);
X2=X2(N);
Y2=S(2,N).*conj(S(2,N));
Y2b=S(3,N).*conj(S(3,N));
hf2=figure(2); clf; set(hf2,'InvertHardcopy', 'off','Color','w')
area(X1-3,Y1,'EdgeColor',c3,'FaceColor',c2,'LineWidth',2)
area(X2+3,Y2,'EdgeColor','k','FaceColor','w','LineWidth',2)
area(X2+3,Y2b,'EdgeColor',c3,'FaceColor',c2,'LineWidth',2)
hold off
axis([-4 11 0 1])
set(gca,'FontName','Arial','FontSize',14,'Color',c1,'LineWidth',1)
xlabel('(\Delta\theta)', 'FontSize',18)
ylabel('reflectivity, |R(\theta)|^2','FontSize',18)
legend(' ( 1, 1, 7)', ' (-1,-1,-7)')

```

17. exasf.m

```

function exasf
%%%%%
%           Atomic scattering factors for atoms and ions
%           with X-rays of two different energies
%
%
% Secondary routines required: asfQ.m
%%%%%
S1=asftth(20000,'Ga');
S2=asftth(20000,'Ga3+');
S3=asftth(8000,'Ga');
S4=asftth(8000,'Ga3+');
nsize(S1,1);
hf1=figure(1);
clf
set(hf1,'InvertHardcopy', 'off','Color','w')
plot(S1(:,1),S1(:,2),'b','LineWidth',1)
set(gca,'FontSize',14,'Color',[0.93 0.93 0.93],'LineWidth',1)
hold on
plot(S2(:,1),S2(:,2),'r','LineWidth',1)
plot(S3(:,1),S3(:,2),'bo','MarkerFaceColor','w','MarkerSize',4,'LineWidth',1)
plot(S4(:,1),S4(:,2),'r','MarkerFaceColor','w','MarkerSize',4,'LineWidth',1)
hold off
xlabel('Q (A^{-1})','FontSize',18)
ylabel('atomic scattering factor, f(Q)','FontSize',18)
axis([0 21 5 32])
legend('Ga (20kev)', 'Ga^{3+} (20kev)', 'Ga (8kev)', 'Ga^{3+} (8kev)')
hf1=figure(2);
clf
set(hf1,'InvertHardcopy', 'off','Color','w')
plot(S2(:,3),S2(:,4),'--r',S2(:,3),-S2(:,4),'--r','LineWidth',2)
set(gca,'FontSize',14,'Color',[0.93 0.93 0.93],'LineWidth',1)
hold on
plot(S1(:,3),S1(:,4),'b',S1(:,3),-S1(:,4),'b','LineWidth',2)
plot(S4(:,3),S4(:,4),'--r',S4(:,3),-S4(:,4),'--r','LineWidth',2)
plot(S3(:,3),S3(:,4),'b',S3(:,3),-S3(:,4),'b','LineWidth',2)
plot([-1 1],[0 0],'k',[0 0],[1 -1],'k','LineWidth',1)
hold off
xlabel('x','FontSize',18)
ylabel('y','FontSize',18)
xmin=min([S1(n,3) S2(n,3) S3(n,3) S4(n,3)]);
xmax=max([S1(1,2) S2(1,2) S3(1,2) S4(1,2)]);
ymax=max(max([S1(:,4) S2(:,4) S3(:,4) S4(:,4)]));
ymin=-ymax;
axis(1.12*[xmin xmax ymin ymax])
text(-10,8,' \leftarrowarrow 8keV','FontSize',18,'Color','k')
text(-4.5,-3,' \leftarrowarrow 20keV','FontSize',18,'Color','k')
text(30.5,4,' \downarrowarrow ','FontSize',18,'Color','b')
text(30,7,'Ga','FontSize',18,'Color','b')
text(20,0.5,' Ga^{3+} \rightarrowarrow ','FontSize',18,'Color','r')
grid

function S=asftth(wl,atom)
if (wl > 100) wl = 12398.5 / wl; end;
dx = 0.01;
x = [0:dx:1];
tth = 2.*asin(x);
x = (1/wl)*x;
f = asfQ(atom,x);
S(:,1) = (4*pi)*x;
S(:,2) = f;
S(:,3) = f .* cos(tth);
S(:,4) = f.* sin(tth);

```

18. excompton.m

```

function M=excompton(wl)
%%%%%
% Coherent and incoherent (Compton) intensities scattered by
% one electron with different probability density functions.
%
% I) |psi(r)|^2 constant within a sphere of radius a=0.5A
%
% II) |psi(r)|^2 of the hydrogen 1s orbital
%
% wl = wavelength (Angstrom) or energy (eV)
%%%%%
if (wl < 100) E = 12398.5 / wl; else E = wl; wl = 12398.5 / E; end;
a = 0.53; % Bohr radius (Angstrom)
tth = (0:0.005:1)*pi;
tth(1)=1e-6;
x = cos(tth);
P2 = 0.5*(1*x.*x);
Qa = (4*pi*a/wl)*sin(0.5*tth);
tth = tth * (180/pi);
x2 = Qa.*Qa;
x = 3*(sin(Qa)-Qa.*cos(Qa))./(x2.*Qa);
fI2 = x.*x;

```

```

Icoer1 = P2.*fI12;
Icompl = P2.*(1-fI12);
x = 1+0.25*x2;
x = 1./(x.*x);
fII2 = x.*x;
Icoer2 = P2.*fII2;
Icomp2 = P2.*(1-fII2);
hf1=figure(1);
clf
set(hf1,'InvertHardcopy','off','Color','w')
plot(tth,Icoer1,'b',tth,Icoer2,'r','LineWidth',2)
hold on
plot(tth,Icompl,'b- ',tth,Icomp2,'r--',tth,Icoer1+Icompl,'k- .','LineWidth',1.5)
hold off
set(gca,'FontSize',14,'Color',[0.854902 0.701961 1],'LineWidth',1,'YTick',[0 0.2 0.4 0.6 0.8 1.0])
ylabel('I(Q) / \Phi r_e^2 d\Omega\omega ','FontSize',18)
xlabel('2\theta (\circ)', 'FontSize',18)
axis tight
text(40,0.8,' \leftarrow I_{Th}', 'FontSize',18, 'Color', 'k')
M = [tth; Icoer1; Icompl; Icoer2; Icomp2];
X=(0:0.01:4)*a;
XX = X.*X;
Y1 = (3/a^3)*XX(X<=a);
n = size(Y1,2)+1;
Y1(n) = 0;
Y2 = (4/a^3)*(XX.*exp(-(2/a)*X));
ha2=axes('Position',[.70 .25 .19 .37]);
plot(X(1:n),Y1,'b',X,Y2,'r','LineWidth',2)
set(ha2,'FontSize',14,'Color',[0.9 0.9 1])
ylabel('4\pi r^2 |\psi(r)|^2 (A^{-1}) ', 'FontSize',14)
xlabel('r (A)', 'FontSize',14)
axis tight
text(0.5,4,' \leftarrow I', 'FontSize',18, 'Color', 'b', 'FontName', 'Times')
text(0.8,1,' \leftarrow II', 'FontSize',18, 'Color', 'r', 'FontName', 'Times')

```

19. excritangle.m

```

function excritangle
%%%%%%%%%%%%%%%%%%%%%%%%%%%%%%%%%%%%%
% Critical angle for total external reflection in %
% gold and glass (amorphous alpha-quartz) surfaces %
% Secondary routines required: fpfpp.m %
%%%%%%%%%%%%%%%%%%%%%%%%%%%%%%%%%%%%%
E = 4:0.1:20; % energy range (keV)
deg = 180/pi;
wl = 12.3985./E;
rewl2_pi = (2.818e-5*wl.*wl/pi);
f = fpfpp('Si',E);
fpSi = f(:,2)';
f = fpfpp('O',E);
fpO = f(:,2)';
f = fpfpp('Au',E);
fpAu = f(:,2)';
Yglass = (1/113)*rewl2_pi .* (52 + 2*fpSi + 3*fpO);
Yglass = sqrt(Yglass)*deg;
Yglass0 = (52/113)*rewl2_pi;
Yglass0 = sqrt(Yglass0)*deg;
Ygold = (1/67.8)*rewl2_pi .* (316 + 4*fpAu);
Ygold = sqrt(Ygold)*deg;
Ygold0 = (316/67.8)*rewl2_pi;
Ygold0 = sqrt(Ygold0)*deg;
hf = figure; clf; set(hf,'InvertHardcopy','off','Color','w')
plot(E,Yglass,'b',E,Yglass0,'--b',E,Ygold,'r',E,Ygold0,'--r','LineWidth',2)
set(gca,'FontSize',14,'LineWidth',1);
axis tight;
xlabel('Energy (keV)', 'FontSize',18)
ylabel('|\theta_c (deg)|', 'FontSize',18)
legend(' glass surface', ' glass surf. no res.', ' gold surface', ' gold surf. no res.')

```

20. excsf.m

```

function excsf(atom,E1,E2,p)
%%%%%%%%%%%%%%%%%%%%%%%%%%%%%%%%%%%%%
% Coherent and incoherent scattering by an atom %
% comparison for two different energies %
%%%%%%%%%%%%%%%%%%%%%%%%%%%%%%%%%%%%%
% Input:
% atom = element symbol, e.g. 'C'
% E1,E2 = two energy values (keV)
% p = 0, 1, and 2 for sigma-, pi-, and non-polarized X-rays
% Secondary routines required: asfQ.m and csfQ.m %

```

```
% Usage:
% >> excsf('C',8,20,0);
%%%%%%%%%%%%%%%
if (B1>500) E1 = 0.001*abs(B1); end;
if (E2>500) E2 = 0.001*abs(E2); end;
labelE1 = [num2str(round(B1)) 'keV'];
labelE2 = [num2str(round(E2)) 'keV'];
tth = (0:1:360)*(pi/180);
if (p==1)
    P2 = cos(tth)';
    P2 = P2.*P2';
    labelP = '(pi polarization';
elseif (p==2)
    P2 = cos(tth)';
    P2 = 0.5*(1+P2.*P2);
    labelP = 'unpolarized';
else
    P2 = ones(size(tth,2),1);
    labelP = '\sigma polarization';
end;
S1=asfxQ(B1,atom,tth,P2);
S2=csfxQ(B1,atom,tth,P2);
S3=asfxQ(B2,atom,tth,P2);
S4=csfxQ(B2,atom,tth,P2);
xmax = S1(1,2); xmin = min(S4(:,3)); ymax = max(S1(:,4)); ymin = -ymax;
hfl=figure(1);
clf
set(hfl,'InvertHardcopy','off','Color','w')
plot(S1(:,3),S1(:,4),'b','LineWidth',2)
set(gca,'FontSize',14,'Color',[0.93 0.93 0.93],'LineWidth',1,'Position',[0.13 0.02 0.775 0.9])
hold on
plot(S2(:,3),S2(:,4),'-b','LineWidth',1)
plot(S3(:,3),S3(:,4),'r','LineWidth',2)
plot(S4(:,3),S4(:,4),'-r','LineWidth',1)
plot([-1 1],[0 0],'k',[0 0],[1 -1],'k','LineWidth',1)
hold off
xlabel('x','FontSize',18)
ylabel('y','FontSize',18)
axis image
axis([1.2*xmin 1.05*xmax 1.1*ymin 1.1*ymax])
text(0,0,atom,'FontSize',36,'Color',[0.855 0.702 1],'FontWeight','bold')
grid
legend([' coherent ' labelE1],[' compton ' labelE1],[' coherent ' labelE2],[' compton ' labelE2])
title(['(atom ',' labelP,'FontSize',18)

function S=asfxQ(wl,atom,tth,P2)
wl = 12.3985 / wl;
x = sin(0.5*tth)/wl;
S(:,1) = (4*pi) * x;
F = asfQ(atom,x)';
F2(:,1) = F.*F.*P2';
S(:,2) = F2';
S(:,3) = F2 .* cos(tth)';
S(:,4) = F2 .* sin(tth');

function S=csfxQ(wl,atom,tth,P2)
wl = 12.3985 / wl;
x = sin(0.5*tth)/wl;
S(:,1) = (4*pi) * x;
Y = csfQ(atom,x);
F = Y(:,2).*P2';
S(:,2) = F';
S(:,3) = F .* cos(tth)';
S(:,4) = F .* sin(tth');
```

21. ellipsoid.m

```
function exellipsoid
X=0:0.01:1;
Nx = size(X,1);
W2 = X.*X;
Rg2 = sqrt(0.2*(2*w2 + 1)); % olate
Rg1 = sqrt(0.2*(2 + w2)); % prolate
hfl=figure(1);
clf
set(hfl,'InvertHardcopy','off','Color','w')
plot(X,Rg1,'b',X,Rg2,'r','LineWidth',2)
axis([0 1 0.4 0.8])
set(gca,'FontSize',14,'Color',[0.93 0.93 0.93],'LineWidth',1)
legend(' oblate',' prolate',4)
xlabel('ratio of the dimensions, {\it w}', 'FontSize',18);
ylabel('R_g / L', 'FontSize',18);
grid
```

22. exexafs.m

```

function exexafs
%%%%%%%%%%%%%%%%%%%%%%%%%%%%%%%%%%%%%
% EXAFS with 4 neighbors %
%%%%%%%%%%%%%%%%%%%%%%%%%%%%%%%%%%%%%
M = fpfpp('Mn',6000:2:9000);
E = M(:,1)';
NE = size(M,1);
Sga = 0.001*M(:,4)';
nb = find(M(:,2)==min(M(:,2)));
EB = M(nb,1);
K = E(nb)-EB; % kinetic energy of the photoelectron (eV)
co = 0.512315; % units [Angstrom^{-1}] [eV^{-1/2}]
ke = co * sqrt(K);
ke(1) = 1e-6;
ke2 = ke.*ke;
ke3 = ke2.*ke;
Nk = size(ke,2);
kmax = 5;
aux = exp(2) / kmax^2;
Rke_ke = (aux*ke2).*exp((-2/kmax)*ke);
Rke_ke = Rke./ke;
pke = 2*(exp((-0.05)*ke)-1.1);
R = 5;
xy = R*[0.5 0.5; -0.5 -0.5; 0.3 -0.3; -0.3 0.3]; % atomic coordinates in the xy plane (Angstrom)
Nat = size(xy,1);
for n = 1:Nat
    rn = sqrt(xy(n,:)*xy(n,:));
    chi(n,:) = Rke_ke.*sin((2*rn)*ke + pke)/(rn*rn);
    chi10(n,:) = Rke_ke.*sin((2*rn)*ke + 10*pke)/(rn*rn);
    Rn(n) = rn;
end;
Chi = sum(chi,1);
Chi10 = sum(chi10,1);
hf1=figure(1);
clf
set(hf1,'InvertHardcopy','off','Color','w')
plot(ke,Chi.*ke3,'r','LineWidth',2)
set(gca,'FontSize',14,'Color',[1 0.95 0.87],'LineWidth',1)
 xlabel('k_e (A^{-1})','FontSize',18)
 ylabel('k_e^3 \chi(k_e)','FontSize',18)
axis tight
Sgp = [Sga(1:nb-1) Sga(nb:NE).*(1+Chi)];
E=0.001*E;
hf2=figure(2);
clf
set(hf2,'InvertHardcopy','off','Color','w')
loglog(E,Sga,'-k',E(nb:NE),Sgp(nb:NE),'r','LineWidth',2)
set(gca,'FontSize',14,'Color',[1 0.95 0.87],'LineWidth',1)
 set(gca,'XTick',[6 7 8 9], 'YTick',[6 8 10 20 40])
 xlabel('Energy (keV)','FontSize',18)
 ylabel('\sigma_a (10^3 barn)','FontSize',18)
 text(8.6,37.5,'Mn','FontSize',36,'Color',[0.871 0.49 0],'FontWeight','bold')
 axis tight
 grid
 ha1=gca;
 navg = round((nb+NE)/3);
ha2=axes('Position',[.35 .18 .4 .4]);
loglog(E(nb-3:navg),Sga(nb-3:navg),'-k',E(nb:navg),Sgp(nb:navg),'r','LineWidth',2)
set(ha2,'FontSize',14,'Color',[0.973 0.973 0.973])
 axis tight
 set(ha2,'XTick',[],'YTick',[])
 xx = get(ha2,'XLim')*[1 0 0 1 1; 0 1 1 0 0];
 yy = get(ha2,'YLim')*[1 1 0 0 1; 0 0 1 1 0];
 axes(ha1);
 hold on
 plot(xx,yy,'k','LineWidth',1)
 hold off
 axes(ha2);
dx = R/500;
X = 0:dx:R;
Nx = size(X,2);
twoIX = (2*i)*X;
dk = [ke(2:Nk)-ke(1:Nk-1) ke(Nk)-ke(Nk-1)];
chidk = ke3.*Chi.*dk;
chi10dk = ke3.*Chi10.*dk;
for nx = 1:Nx
    Z = exp(twoIX(nx)*ke);
    rho(nx) = sum(Z.*chidk);
    rho10(nx) = sum(Z.*chi10dk);
end;
rho = sqrt(rho.*conj(rho));
irmax = 1/max(rho);
rho10 = sqrt(rho10.*conj(rho10));
hf3=figure(3);
clf
set(hf3,'InvertHardcopy','off','Color','w')
plot(X,irmax*rho,'k',X,irmax*rho10,'--b','LineWidth',2)

```

```

set(gca,'FontSize',14,'Color',[.961 .922 .922],'LineWidth',1,'YTickLabel',[])
 xlabel('interatomic distance, u (A)', 'FontSize',18)
 ylabel('F(u) (arb. units.)', 'FontSize',18)
 axis tight
 grid
 legend(' small variation, \delta_n ',' huge variation, 10\delta_n')
 hold on
 for n=1:Nat
 plot([Rn(n) Rn(n)], [0 1], 'r', 'LineWidth',1)
 end;
 hold off
hf4=figure(4);
clf
 set(hf4,'InvertHardcopy', 'off','Color','w')
 ha4a=axes('Position',[0.1 0.2 0.38 0.6]);
 set(ha4a,'FontSize',14,'Color',[.961 .922 .922],'LineWidth',1);
 plot(k_e,pke,'r','LineWidth',2)
 set(ha4b,'YTick',[0 .2 .4 .6 .8])
 xlabel('k_e (A^{-1})', 'FontSize',18)
 ylabel('R_n (A)', 'FontSize',18)
 axis tight
grid
ha4b=axes('Position',[0.6 0.2 0.38 0.6]);
set(ha4b,'FontSize',14,'Color',[.961 .922 .922],'LineWidth',1);
plot(k_e,Rke,'r','LineWidth',2)
set(ha4b,'YTick',[0 .2 .4 .6 .8])
 xlabel('k_e (A^{-1})', 'FontSize',18)
 ylabel('R_n (A)', 'FontSize',18)
axis tight
grid

```

23. exexafsmap.m

```

function exexafsmap
%%%%%%%%%%%%%%%%%%%%%%%%%%%%%%%%%%%%%%%
% EXAFS with 4 neighbors %
%%%%%%%%%%%%%%%%%%%%%%%%%%%%%%%%%%%%%%
E = 200; % eV
R = 5; % Angstrom
rad = pi / 180;
k = 0.512315*sqrt(E);
dr = R / 100;
M = -R:dr:R;
Np = size(M,2);
xy = [0 0; 0.5 0.5; -0.5 -0.5; 0.3 -0.3; -0.3 0.3] * R;
for n = 1:5 modR(n) = sqrt(xy(n,:)*xy(n,:)); end;
psh = k * modR;
an = 0.1; kan = k * an;
A = [i i i i]/[1 modR(2:5)];
for n = 1:Np
y = M(n);
for m = 1:Np
x = M(m);
for nn = 1:5
ra2 = [x y] - xy(nn,:);
ra = sqrt(ra2*ra2');
if (ra<an) ra = an; end;
kr = k * ra;
arg = kr + psh(nn);
den = kan / kr;
psi(nn) = A(nn) * exp(i*arg) * den;
end;
z = sum(psi);
Z(n,m) = z*conj(z);
X(n,m) = x; Y(n,m) = y;
end;
end;
logZ = log10(Z);
hf1=figure(1);
clf
set(hf1,'InvertHardcopy', 'off','Color','w')
surf(X,Y,logZ)
axis tight
shading interp
set(gca,'FontSize',14,'Color',[0.93 0.93 0.93],'LineWidth',1)
set(gca,'ZTick',[],'DataAspectRatio',[.15 .15 1])
colormap(jet)
view(150,30)
xlabel('x (A)', 'FontSize',18,'Rotation',18)
ylabel('y (A)', 'FontSize',18,'Rotation',-45)
colorbar('XColor','k','FontSize',14,'Location','East','LineWidth',1)
text(0,0,1,'log(P)', 'FontSize',18,'Rotation',90)

```

24. exfpfpp.m

```

function Z=exfpfpp(atom,Emin,Emax)
% Coherent scattering cross-section (Rayleigh) with atomic resonance
% Input:
%   atom = element symbol, e.g. 'Se'
%   Emin,Emax = energy range from Emin to Emax (keV)
% Output Z = [E' f' f" sga sgR sgRr]
%   |   |   |   |
%   |   |   |   | cross-section with resonance (barn)
%   |   |   |   | cross-section without resonance (barn)
%   |   |   |   | absorption cross-section (barn)
%   |   |   |   | imaginary term (in electron number)
%   |   |   |   | real term (in electron number)
%   |   |   |   | energy (eV)
% Secondary routines required: asfQ.m and fpfpp.m
% Usage:
% >> Z=exfpfpp('Se',3,23);
%
Emin = abs(Emin); Emax = abs(Emax);
if (Emax < Emin) E = Emax; Emax = Emin; Emin = E; end;
if (Emax>500) Emin = 0.001*Emin; Emax = 0.001*Emax; end;
if (Emax<1) Emin = 1; end;
if (Emax>70) Emax = 70; end;
if (Emax-Emin<0.020) E = [Emin Emin+0.01]; dE = 0.01;
else E = Emin:0.01:Emax; dE = E(3)-E(2);
end;
NE = size(E,2);
M = fpfpp(atom,1000*E);
rad = pi/180;
re = 2.818e-15;           % (m)
hc = 12.3985;             % (keV.A)
invWL = E/hc;
dttb = 0.2;                % (deg)
TTB = 0:dttb:180;          % (deg)
X = TTB * rad;
dx = dttb * rad;
aux1 = pi * re * re * dx * 1e+28;
SinG = sin(X);
PSinG = (2-SinG.*SinG).*SinG;
for nn = 1:NE
  fres = M(nn,2:3);
  f = asfQ(atom,invWL(nn)*sin(0.5*X));
  fr = f + fres(1) + i*fres(2);
  f = f.*f;
  fr = fr.*conj(fr);
  I(nn) = aux1*sum(PSinG.*f);
  Ir(nn) = aux1*sum(PSinG.*fr);
end;
Z = M;
c = size(Z,2);
Z(:,c+1:c+2) = [I; Ir]';
hfl=figure(1);
clf
set(hfl,'InvertHardcopy', 'off','Color','w')
plot(E,I,'k--',E,Ir,'k','LineWidth',2)
set(gca,'FontSize',14,'Color',[0.854902 0.701961 1],'LineWidth',1)
ylabel('sigma_R (barn)', 'FontSize',18)
xlabel('Energy (keV)', 'FontSize',18)
axis tight
legend(' without res.', ' with res.',3)
n=find(M(:,2)==min(M(:,2)));
if isempty(n)
  n1 = 1; n2 = NE; n = (n1+n2)/2;
else
  Edge = E(n);
  if (Edge-E(1) > 5)
    n1 = find(abs(E-Edge)<dE);
  else n1 = 1;
  end;
  if (E(NE)-Edge > 5)
    n2 = find(abs(E-Edge-5)<dE);
  else n2 = NE;
  end;
end
n1 = n1(1); n2 = n2(1);
ha2=axes('Position',[.48 .45 .4 .4]);
plot(E(n1:n2),M(n1:n2,2),'b',E(n1:n2),M(n1:n2,3),'r','LineWidth',2)
set(ha2,'FontSize',14,'Color',[0.93 0.93 0.93])
ylabel('resonant amplitude', 'FontSize',14)
xlabel('Energy (keV)', 'FontSize',14)
axis tight
legend('f \prime', 'f \prime\prime',4)

```

25. exgofu1.m

```

function M=exgofu1(d,N)
%%%%%
% Function g(u) for one-dimensional correlation %
%
% Input: %
% d, degree of disorder along one direction, Da/a = 1 + d*(2*rand-1) %
% N, statistic of (2N-1)^2 counts per point %
% Output: M = [U; g]'; n-by-2 array %
% Usage: M = exgofu1(.2, 200); %
%%%%%
NN = 2*N + 1; % value of NN limited by available RAM memory
X = zeros(NN,NN,NN);
X(:,:,1) = d*(2*rand(NN)-1);
if (N>0)
    X(:,:,2) = X(:,:,1) + 1 + d*(2*rand(NN)-1);
    X(:,:,3) = X(:,:,1) - 1 + d*(2*rand(NN)-1);
    if (N>1)
        for n = 2:N
            X(:,:,2*n) = X(:,:,2*(n-1)) + 1 + d*(2*rand(NN)-1);
            X(:,:,2*n+1) = X(:,:,2*(n-1)+1) - 1 + d*(2*rand(NN)-1);
        end;
    end;
end;
V = (sum(sum(X(:,:,NN-1)))-sum(sum(X(:,:,NN))))/NN^2;
xmin=min(min(X(:,:,NN)));
xmax=max(max(X(:,:,NN-1)));
Umax = 1.02*(xmax-xmin)/du;
du = 0.01;
U = 0:du:Umax;
px = zeros(1,size(U,2));
for n=1:NN
    for m=1:NN
        r0 = X(n,m,1);
        for l=1:NN
            k = fix(abs(X(n,m,l)-r0)/du) + 1;
            px(k) = px(k) + 1;
        end;
    end;
end;
g = (1/(2*du*px(1)))*px;
Nu = size(px,2);
hfi=figure(1);
clf
set(hfi,'InvertHardcopy', 'off','Color','w')
plot(U(2:Nu),g(2:Nu),'r','LineWidth',2)
axis tight
grid
set(gca,'FontSize',14,'Color',[1 0.949 0.867],'LineWidth',1)
xlabel('u/a','FontSize',18)
ylabel('g(u)','FontSize',18)
M=[10*U(2:Nu); g(2:Nu)]';

```

26. exgofu2.m

```

function exgofu2
%%%%%
% To compare scattering data simulation from ensemble of particles with %
% the interference function obtained from g(u) %
%
% Required files: fthofu_N8d20sphereito20.dat and exgofu.dat %
% Files generated by routines fthofu.m and exgofu1.m, and available at %
% http://xraybook.if.usp.br/
%%%%%
I = load('fthofu_N8d20sphereito20.dat');
A = 150; pixel = 0.5; D = 600; wl = 1; % same values used in routine fthofu.m
Qx = (2*pi/wl)*sin(atan((-A:pixel:A)/D));
detc = 300;
Ix = sum(I(301-detc:301+detc,:,:))/(2*detc+1);
M = find(Qx>0);
Ix = Ix(M);
Qx = Qx(M);
M=find(Qx>1);
Ixmin = min(Ix(M));
Dlx = max(Ix(M))-Ixmin;
M=load('exgofu.dat');
Um=M(1,:);
g=M(2,:);
Nu = size(U,2);
twop1 = 2*pi;
dq = 0.005;
Q=0.1:dq:2;
Nq = size(Q,2);
du = U(3)-U(2);
G = g-1;
for nq = 1:Nq

```

```

q = Q(nq);
S(nq) = sum(G.*cos(q*U));
end;
rho = 0.17;
S = 1 + (rho*du)*S;
aux=pi/pi;
hfi=figure(1);
clf
set(hfi,'InvertHardcopy', 'off','Color','w')
semilogy(aux*Qx,Ix,'-ko','MarkerFaceColor','w','MarkerSize',3,'LineWidth',1)
hold on
semilogy(aux*Q,S,'-r','LineWidth',1.5)
hold off
axis([0.1 3.14 .1 6.4])
set(gca,'FontSize',14,'Color',[1 0.97 0.92],'LineWidth',1)
xlabel('n_x','FontSize',18)
ylabel('S(Q_x)','FontSize',18)
grid
legend(' simulation',' num. solution')
text(.1,.1,3,' FT of volume','FontSize',14)
text(.1,1,' \downarrow','FontSize',14)

```

27. exgoldnano0.m

```

function Z=exgoldnano0(Qf)
%%%%%%%%%%%%%%%%%%%%%%%%%%%%%%%%%%%%%
% Resolution of PDDF by inverse FT in gold nanoparticles %
% Input: %
% Qf = upper limit of the inverse FT integral (1/Angstrom) %
% Output Z = [U; h; Pu'];
% | |
% | PDDF after convolution with rectangular function %
% | PDDF as obtained from inverse FT %
% | interatomic distance (Angstrom) %
% Required files: 'goldnano10r05.pdu' from http://xraybook.if.usp.br/
% File generated by routine goldnano.m %
% Usage: Z = exgoldnano0(40);
%%%%%%%%%%%%%%%%%%%%%%%%%%%%%%%%%%%%%
M=load('goldnano10r05.pdu');
U = M(1,:);
p = M(2,:);
if (U(1)==0), U(1) = 1e-8; end;
dQ = Qf/5000;
Q = 0:dQ:Qf;
Q(1) = 1e-8;
Nq = size(Q,2);
S = zeros(1,Nq);
for n=1:Nq
    Qu = Q(n)*U;
    S(n) = sum(p.*sin(Qu)./Qu));
end;
S = (1/p(1))*S;
Nu = size(U,2);
F = (2*dQ/pi)*((S-1).*Q);
for n = 1:Nu
    u = U(n);
    h(n) = sum((u*F).*sin(u*Q));
end;
du = U(3)-U(2);
wl = 2*pi/Qf;
Nw = floor(0.5*wl/du);
for n=1:Nu
    nmin = n-Nw;
    nmax = n+Nw;
    if ((nmin<1) Pu(n) = sum(h(1:nmax))/nmax;
    elseif (nmax>Nu) Pu(n) = sum(h(nmin:Nu))/(Nu-nmin+1);
    else Pu(n) = sum(h(nmin:nmax))/(2*Nw+1);
    end;
end;
hfi=figure(1); clf; set(hfi,'InvertHardcopy', 'off','Color','w')
plot(U,h,'-k','LineWidth',1)
hold on
plot(U,Pu,'Color',[0 0 .5],'LineWidth',1.5)
plot([2-wl 2 2+w1 2-w1],[0 0 1 0]*(10/wl),'r','LineWidth',1)
hold off
set(gca,'FontSize',14,'Color',[0.93 0.93 0.93],'LineWidth',1)
set(gca,'YTick',[])
xlabel('u (A)','FontSize',18)
ylabel('P(u)','FontSize',18)
legend(' before conv. ',' after conv. ',' conv. function (x10)')
axis([1.5 9.5 min(h) max(h)])
Z = [U; h; Pu];

```

28. exgoldnano1.m

```

function exgoldnano1(Qf)
%%%%% Scattering power, P(Q), of gold nanoparticles with different diameters %%
% Input:
% Qf = maximum reciprocal vector module (1/Angstrom) %
% Secondary routines required: asfQ.m %
% Required files: goldnano10r5.pdu, goldnano20r5.pdu,
% goldnano40r5.pdu, and goldnano40r1.pdu %
% Files generated by routine goldnano.m, and %
% available at http://xraybook.if.usp.br/ %
% Usage: exgoldnano1(20)
%%%%%
M10=goldnanopdq('goldnano10r5.pdu',Qf);
M20=goldnanopdq('goldnano20r5.pdu',Qf);
M40=goldnanopdq('goldnano40r5.pdu',Qf);
M41=goldnanopdq('goldnano40r1.pdu',Qf);
hf1=figure(1); clf; set(hf1,'InvertHardcopy', 'off','Color','w')
semilogy(M10(:,1),M10(:,2),'k','LineWidth',1.5)
hold on
semilogy(M20(:,1),M20(:,2),'b','LineWidth',1.5)
semilogy(M41(:,1),M41(:,2),'-m','LineWidth',1.5)
semilogy(M40(:,1),M40(:,2),'r','LineWidth',1.5)
hold off
axis([-0.01*Qf 0.9*min(M41(:,2)) 1.1])
set(gca,'FontSize',14,'Color',[0.93 0.93 0.93],'LineWidth',1)
set(gca,'YTick',[1e-4 1e-2 1])
xlabel('Q (A^{-1})','FontSize',18)
ylabel('P(Q) / P(0)','FontSize',18)
legend(' 1 nm',' 2 nm',' 4 nm',' 4 nm')
legend(' 1 nm',' 2 nm',' 4 nm',' 4 nm')

function M=goldnanopdq(fname,Qf)
S=load(fname)';
U = S(1,:);
p = S(2,:);
if (U(1)==0) U(1) = 1e-8; end;
dQ = Qf/5000;
Q = 0:dQ:Qf; O(1) = 1e-8;
Nq = size(Q,2);
f = asfQ('Au',(0.25/pi)*Q);
f = f.*p;
for n=1:Nq
    Qu = Q(n)*U;
    Y(n) = f(n) * sum(p.*sin(Qu)./Qu));
end;
Y = (1/max(Y))*Y;
Y(Y<1e-6) = 1e-6;
M = [Q; Y]';

```

29. exgoldnano2.m

```

function exgoldnano2(E1,E2,Nph)
%%%%% Comparison of PDDF extracted from P(Q) curves with different energies %%
% Input:
% E1,E2 = photon energies (keV) %
% Nph = number of counts in the P(Q) curve %
% Secondary routines required: asfQ.m and photonstatistic.m %
% Required files: goldnano40r5.pdu from http://xraybook.if.usp.br/
% Usage: exgoldnano2(10,20,1e6)
%%%%%
fname = 'goldnano40r5.pdu';
if (E1>500), E1 = 0.001*E1; end;
if (E2>500), E2 = 0.001*E2; end;
Qf1 = 1.0135*E1;
Qf2 = 1.0135*E2;
G=load(fname)';
U = G(1,:);
p = G(2,:);
Nu=size(U,2);
M1 = goldnanopdu(fname,Qf1,Nph);
Pul1 = M1(:,2)';
Pu1max = max(Pul1);
M2 = goldnanopdu(fname,Qf2,Nph);
Pu2 = M2(:,2)';
Pu2max = max(Pu2);
if (Pu1max>Pu2max)
    Pu2 = (Pu1max/Pu2max)*Pu2;
    pmax = Pu1max/max(p(2:Nu));
else
    Pu1 = (Pu2max/Pu1max)*Pu1;
    pmax = Pu2max/max(p(2:Nu));
end;
N = find(U<10.2, 1, 'last' );
Pu1max = max(Pul1(1:N));

```

```

Pu2max = max(Pu2(1:N));
Pu1min = min(Pu1(1:N));
Pu2min = min(Pu2(1:N));
if (Pu1max>Pu2max) Ymax = Pu1max;
else Ymax = Pu2max;
end;
if (Pu1min<Pu2min) Ymin = Pu1min;
else Ymin = Pu2min;
end;
DY = Ymax-Ymin;
hf1=figure(1); clf; set(hf1,'InvertHardcopy', 'off','Color','w')
plot(U(1:N),Pu1(1:N)+0.5*DY,'b','LineWidth',1.5)
hold on
plot(U(1:N),Pu2(1:N)+0.25*DY,'k','LineWidth',1.5)
plot(U(2:N),pmax*p(2:N),'r','LineWidth',1.0);
hold off
axis([1.5 U(N) [Ymin Ymax]+[-0.02 1.02]*DY])
set(gca,'FontSize',14,'Color',[0.93 0.93 0.93],'LineWidth',1)
set(gca,'YTick',[])
xlabel('u (A)', 'FontSize',18)
ylabel('normalized PDDF', 'FontSize',18)
legend([' num2str(E1)' ' keV'], [' num2str(E2)' ' keV'], ' hist.')
pmax = max(p);
hal=axes('Position',[.2 .532 .38 .35]);
plot(U,p,'Color',[.5 .5 .5],'LineWidth',1);
set(hal,'FontSize',14,'Color',[1 .8 0])
ylabel('N(u)du (x1000)', 'FontSize',14)
 xlabel('u (A)', 'FontSize',14)
 axis([1.2 max(U) -0.03*pmax 1.02*pmax])
hold on
plot(U(2:N),p(2:N),'r','LineWidth',1);
plot([1.5 10.25 10.25 1.5], [-0.015 -0.015 0.85 0.85 0.85 -0.015]+pmax,'--r','LineWidth',1)
hold off
text(0.8*pmax,U,0.8*pmax,'Au','FontSize',36,'Color',[1 1 0],'FontWeight','bold')

function PdeU=goldnanopdu(fname,Qf,Nph)
Moload(fname);
U = M(1,:);
p = M(2,:);
if (U(1)==0) U(1) = 1e-8; end;
dQ = Qf/5000;
Q = 0:Qf:Qf;
Q(1) = 1e-8;
Nq = size(Q,2);
f = asfQ('Au',(0.25/pi)*Q);
f = f.*f;
for n=1:Nq
Qu = Q(n)*U;
P(n) = f(n)*sum(p.*sin(Qu)./Qu));
end;
Ps=photostatistic(P,Nph);
S = f(1)*(Ps./f);
Nu = size(U,2);
F = (2*dQ/pi)*((S-1).*Q);
for n = 1:Nu
u = U(n);
h(n) = sum((u.*F).*sin(u.*Q));
end;
du = U(3)-U(2);
w1 = 2*pi/df;
Nw = floor(0.5*w1/du);
for n=1:Nu
nmin = n-Nw;
nmax = n+Nw;
if (nmin<1) Pu(n) = sum(h(1:nmax))/nmax;
elseif (nmax>Nu) Pu(n) = sum(h(nmin:Nu))/(Nu-nmin+1);
else Pu(n) = sum(h(nmin:nmax))/(2*Nw+1);
end;
end;
PdeU = [U; Pu]';

```

30. exhardsphere.m

```

function exhardsphere(d,x)
%%%%%%%%%%%%%%%%%%%%%%%%%%%%%%%%%%%%%
% Debye approach versus Percus-Yevick solution for %
% Ornstein-Zernick equation with hard sphere potential %
% Input: %
% d - the shortest distance between two particles %
% x = packing factor (from 0 to 0.4) %
% Usage: %
% >> exhardsphere(3,0.08) %
%%%%%%%%%%%%%%%%%%%%%%%%%%%%%%%%%%%%%
d = abs(d);
x = abs(x); if (x>0.4) x = 0.4; end;
vp = (pi/6)*d^3; % volume occupied by each particle (1/8 of the exclusion volume)
rho = x/vp; % density of partiles

```

```

Umax = 5*d;
du = d/100;
U = 0:du:Umax;
U(1)=1e-8;
Ud = U/d;
Nu = size(U,2);
aux1 = (1-x)^4;
aux2 = -(1+0.5*x)^2 / aux1;
aux1 = (1+2*x)^2 / aux1;
C = (-0.5*x*aux2)*(Ud.*Ud.*Ud) - (6*x*aux2)*Ud - aux1;
C(U>d) = 0;
Qmax = 6 * (5*pi/2) / (2*d);
dq = Qmax/2000;
Q = 0:dq:Qmax;
Q(1) = 1e-8;
Nq = size(Q,2);
G = (4*pi*du)*C.*U;
TFC = zeros(1,Nq);
for n=1:Nq
    q = Q(n);
    TFC(n) = sum(G.*sin(q*U))/q;
end;
S = 1./(1-rho*TFC);
Y = rho*(TFC.*TFC).*S;
F = (dq/(2*pi*pi))*Y.*Q;
invFTY = zeros(1,Nu);
for n=1:Nu
    u=U(n);
    invFTY(n) = sum(F.*sin(u*Q))/u;
end;
g = invFTY + C + 1;
g(Ud)=0;
Qd = Q*d;
T = tfsphere(Qd);
Sp = 1-(8*rho*v*p)*T;
Smin = min(Sp);
Smax = max(Sp);
dS = Smax-Smin;
Smin = Smin-0.05*dS;
Smax = Smax+0.05*dS;
hfi=figure(1);
clf
set(hfi,'InvertHardcopy', 'off','Color','w')
plot(Qd,Sp,'-k',Qd,S,'r','LineWidth',2)
set(gca,'FontSize',14,'Color',[0.89 0.94 0.9],'FontName','Arial','LineWidth',1)
legend('Debye','Percus-Yevick','Location','SouthWest')
xlabel('Qd','FontSize',18);
ylabel('S(Q)','FontSize',18);
axis([0 max(Qd) Smin Smax])
ha2=axes('Position',[.533 .251 .338 .4]);
plot(Ud,g,'b','LineWidth',2)
set(ha2,'FontSize',14,'Color',[0.729 0.831 0.957],'FontName','Arial','LineWidth',1)
xlabel('u/d','FontSize',18)
ylabel('g(u)','FontSize',18)
gmax = max(g);
axis([0 max(Ud) 0 1.05*gmax])
grid

function Z=tfsphere(u)
u(u==0)=1e-8;
u3 = u.*u.*u;
Z = 3*((sin(u)-u.*cos(u))./u3);

```

31. exkk.m

```

function exkk(atom)
%%%%%
% Effects of exafs in the resonance amplitude: f' +if'
% (model of 4 neighbors)
% Input: atom = element symbol, e.g. 'Fe'
%%%%%
dE = 2; % eV
E=0:dE:70000; % eV
NE = size(E,2);
M = fppp(atom,E);
nb = find(M(:,2)==min(M(:,2)));
Eb = M(nb,1);
K = E(nb:NE)-Eb; % kinetic energy of the photoelectron (eV)
co = 0.512315; % units [Angstrom^{-1}] [eV^{-1/2}]
ke = co * sqrt(K);
ke(1) = 1e-6;
Nk = size(ke,2);
kmax = 5;
aux = exp(2) / kmax^2;

```

```
Rke_ke = aux.*exp((-2/kmax)*ke));
pke = 2*(exp((-0.05)*ke)-1.1);
xy = 5*[0.5 0.5; -0.5 -0.5; 0.3 -0.3; -0.3 0.3]; % atomic coordinates in the xy plane (Angstrom)
Nat = size(xy,1);
for n = 1:Nat
    rn = sqrt(xy(n,:)*xy(n,:));
    chi(n,:) = Rke_ke.*sin((2*rn)*ke + pke)/(rn*rn);
end;
Chi = sum(chi,1);
fpp0 = M(:,3)';
fpp = [fpp0(1:nb-1) fpp0(nb:NE).*(1+Chi)];
Dfp = fpp - fpp0;
W = E(1:NE-1) + 0.5*dE;
W2 = W.*W;
xDfpdx = (E.*Dfp)*( -2*dE/pi);
E2 = E.*E;
for nw=1:NE-1;
    X = E2-W2(nw);
    Dfp(nw)=sum(xDfpdx./X);
end;
nearedge = find(abs(E-(Eb+250))<1000);
X = 0.001*E(nearedge);
Xw = 0.001*w(nearedge);
fp0 = M(nearedge,2)';
fpp0 = fpp0(nearedge);
fp0 = fp0(nearedge);
fp1 = fp0+M(nearedge+1,2)');
fp1 = 0.5*(fp0+M(nearedge+1,2')) + Dfp(nearedge);
hf1=figure(1);
clf
set(hf1,'InvertHardcopy','off','Color','w')
plot(X,fp0,'.w',X,fp0,'-w',Xw,fp1,'b',X,fpp1,'r','LineWidth',2)
set(gca,'FontSize',14,'Color',[0.854902 0.701961 1],'LineWidth',1)
ylabel('resonance amplitude','FontSize',18)
xlabel('Energy (keV)','FontSize',18)
axis tight
legend('f\prime isolated atom','f\prime prime isolated atom',...
'f\prime \chi(E) \neg 0','f\prime\prime\prime \chi(E) \neg 0',4)
text(0.001*Eb,0,atom,'FontSize',36,'Color',[0.93 0.93 0.93],'FontWeight','bold')
```

32. exlognormal.m

```
function M=exlognormal(a0,sn,sg,Npt)
%%%%%%%%%%%%%%%%%%%%%%%%%%%%%%%%%%%%%
% SAXS of spherical particles with size distribution %
% comparison of Gaussian and log-normal distributions %
%%%%%%%%%%%%%%%%%%%%%%%%%%%%%%%%%%%%%
% Input:
% a0 = most probable radius (Angstrom)
% sn = standard deviation in log scale of the log-normal distribution
% sg = standard deviation of Gaussian distribution (in Angstrom)
% Npt = number of points in the scattering curve
% Output M = [Q; I; Ig];
%           |   |
%           |   saxs curve for a Gaussian distribution
%           |   saxs curve for a log-normal distribution
%           reciprocal vector module
% Usage:
% >> M=exlognormal(100,.15,10,500);
%%%%%%%%%%%%%%%%%%%%%%%%%%%%%%%%%%%%%
Nmin = 5; % number of visible minima
Wg = 2*sg*sqrt(2*log(2));
amin = a0-2*Wg;
if (amin<0) amin = 1; end;
amax = a0+2*Wg;
Wn = 2*sn*sqrt(2*log(2));
b = a0*exp(sn*sn);
logb = log(b);
amin = exp(logb-Wn);
amax = exp(logb+Wn);
Wn = exp(logb+0.5*Wn)-exp(logb-0.5*Wn);
if (amin>amin) amin = amin; end;
if (amax>amax) amax = amax; end;
Qmax = Nmin * (5*pi/2) / (2*a0);
dx = (amax-amin)/100;
aux = 0.8*pi/Qmax;
if (dx > aux) dx = aux; end;
a = amin:dx:amax;
X = a-a0;
logX = log(a/b);
logX2 = logX.*logX;
auxx1 = -1/(2*sn*sn);
auxx2 = dx/(sn*sqrt(2*pi));
L = auxx2*(exp(auxx1*logX2)./a);
Ng = size(L,2);
dQ = Qmax/Npt;
Q = 0:dQ:Qmax;
```

```

Q(1) = 1e-8;
aux = 4*pi/3;
for n = 1:Ng
    aj = a(n);
    vj = aux * aj * aj * aj;
    u = aj*0;
    x = vj*tfsphere(u);
    Y(n,:) = x.*x;
end;
I = L*x;
v0 = aux * a0 * a0 * a0;
u = a0 * Q;
x = v0 * tfsphere(u);
I0 = (x.*x);
aux = -1.0 / (2*sg*sg);
G = exp(aux * (X.*X));
sumG = sum(G);
G = (1/sumG)*G;
Ig = G*Y;
I = I*(1/max(I));
I0 = I0*(1/max(I0));
Ig = Ig*(1/max(Ig));
res = 100*abs(sum(abs(log(Ig)-log(I)))/sum(log(I)));
res = -3*log(I(3)/I(2))/(Q(3)*Q(3)-Q(2)*Q(2));
x = sqrt(x);
y = -3*log(Ig(3)/Ig(2))/(Q(3)*Q(3)-Q(2)*Q(2));
y = sqrt(y);
a2 = a.*a;
vp2 = (4*pi/3) * (a2.*a);
vp2 = vp2.*vp2;
RgL = 0.6*sum(L.*vp2.*a2)/sum(L.*vp2);
RgG = sqrt(RgL);
RgG = sqrt(RgG);
AsL = (4*pi)*sum(L.*a2);
AsG = (4*pi)*sum(G.*a2);
fprintf(' log-normal: Rg = %3.1f(%3.1f)A, As = %5.3eA^2,fwhm=%3.1fA\n',RgL,x,AsL,Wn)
fprintf(' Gaussian: Rg = %3.1f(%3.1f)A, As = %5.3eA^2,fwhm=%3.1fA\n',RgG,y,AsG,Wg)
fprintf(' residue = %5.3f\n',res)
Npt5 = 1:5:Npt;
hfl=figure(1);
clf
set(hfl,'InvertHardcopy', 'off','Color','w')
semilogy(Q,I0,'y--','LineWidth',2)
hold on
semilogy(Q,Npt5,I(Npt5),'-ro','MarkerFaceColor','w','MarkerSize',4,'LineWidth',1)
semilogy(Q,Ig,'k','LineWidth',1)
hold off
axis([0 max(Q) 0.8*min(min([I; Ig])) 1.1])
set(gca,'FontSize',14,'Color',[0.854902 0.701961 1])
ylabel('I(Q)/I(0)', 'FontSize',18)
xlabel('Q (A^-1)', 'FontSize',18)
legend('sphere',' log-normal',' Gaussian',4)
M = [0; I; Ig];
h1=axes('Position',[.48 .532 .38 .37]);
hb=bar(0.1*a,L,1);
hold on;
plot(0.1*a,G,'k','LineWidth',1);
hold off;
colormap cool
set(h1,'FontSize',12,'Color',[0.97 0.97 0.97])
ylabel('{\it p(a)}')
xlabel('radius, {\it a} (nm)')
axis tight
legend(' log-n',' gaus')

function Z=tfsphere(u)
u3 = u.*u.*u;
Z = 3*((sin(u)-u.*cos(u))./u3);

```

33. exlysozyme.m

```

function exlysozyme
%%%%%%%%%%%%%%%%%%%%%%%%%%%%%%%%%%%%%
% Comparison of exact and approximate solutions for the SAXS curve %
% Files required: %
% - saxs2LYZ_0to180E20keV.dat (generated by routine saxs.c) %
% - saxs2LYZ_0to40E5keV.dat (generated by routine saxs.c) %
% - 2LYZ.ndu (generated by routine histogram.m) %
% also available at http://xraybook.if.usp.br/ %
% Secondary routines required: saxs.m and invftpofq.m %
%%%%%%%%%%%%%%%%%%%%%%%%%%%%%%%%%%%%%
Msaxs('2LYZ.ndu',2,80,0);
M(:,2)=M(:,2)*(1/max(M(:,2)));
Qmax = max(M(:,1));

```

```

Pmin = min(M(:,2));
S=load('saxs2LYZ_0to180E20keV.dat');
smax = max(S(:,2));
Ns=find(S(:,1)<=Qmax);
ymin = S(max(Ns),2)/smax;
if (Pmin<ymin) ymin=Pmin; end;
X=M(:,1)*(0.25/pi);
fmQ = 193*asfQ('N',X)+613*asfQ('C',X)+185*asfQ('O',X)+10*asfQ('S',X);
fmQ = fmQ.*fmQ;
hf1=figure(1); clf; set(hf1,'InvertHardcopy','off','Color','w')
semilogy(M(:,1),(fmQ.*M(:,2))/fmQ(1),'--b','LineWidth',1.5)
semilogy(S(:,1),S(:,2)/smax,'k','LineWidth',1.5)
hold off
axis([0 Qmax 0.9*ymin 1.1])
set(gca,'FontSize',18,'Color',[0.93 0.93 0.93],'YTick',[0.001 0.01 0.1 1],'LineWidth',1)
xlabel('Q (A^{-1})','FontSize',18)
ylabel('P(Q) / P(0)','FontSize',18)
legend('f_m^2(0), small angle','f_m^2(Q)', 'exact solution',1)
text(0.45,0.5,'saxsLYZ_0to40E8keV.dat',0.75,52,1000);
N=invftpq('saxsLYZ_0to40E8keV.dat',0.75,52,1000);
H=load('2LYZ.ndu');
n = size(H,1);
du = H(3,1)-H(2,1);
Hsum = sum(H(2:n,2))*du;
Hmax = max(H(2:n,2));
hf2=figure(2); clf; set(hf2,'InvertHardcopy','off','Color','w')
plot(H(2:n,1),H(2:n,2),'b','LineWidth',1)
hold on
plot(N(:,1),Hsum*N(:,2),'--k','LineWidth',1.5)
hold off
axis([0 H(n,1) [-0.02 1.02]*Hmax])
set(gca,'FontSize',18,'Color',[0.93 0.93 0.93],'LineWidth',1)
xlabel('u (A) ','FontSize',18)
ylabel('N(u)du','FontSize',18)
text(8,250, ' \leftarrow p(u)', 'Color','k','FontSize',18)

```

34. exrdf.m

```

function M=exrdf(R0,d,N)
%%%%%%%%%%%%%%%%%%%%%%%%%%%%%%%%%%%%%
% RDF according to the hard sphere model
% numerical simulation based on random distribution of positions
%%%%%%%%%%%%%%%%%%%%%%%%%%%%%%%%%%%%%
% Input:
% R0 = volume radius of the distribution (Angstrom)
% d = minimum separation distance between positions (Angstrom)
% 2N = approximated number of initial positions in the volume
% Output: M = [U, g], g(u) in a n-by-2 array
% Usage: M=exrdf(100,2,4000);
%%%%%%%%%%%%%%%%%%%%%%%%%%%%%%%%%%%%%
time=clock; fprintf(' %1.0fh%1.0fm%1.0fs\n',time(4:6))
NN=N;
d2 = d*d;
R0 = R0+R0;
R = R0*(2*rand(N,3)-1);
R2 = sum(R.*R,2);
R = R(R2<=R02,:);
N = size(R,1);
for n=1:N
    rn = R(n,:);
    for m=n+1:N
        rnm = R(m,:)-rn;
        rnm2 = rnm * rnm';
        if (rnm2<d2)
            R(m,:) = R(m,:) + 4*R0;
        end;
    end;
end;
R2 = sum(R.*R,2);
R = R(R2<=R02,:);
N = size(R,1);
V = (4*pi/3)*R0^3;
rho = N / V;
Umax = 2*R0;
du = 0.1;
U = 0:du:Umax;
U(1) = 1e-8;
Nu = size(U,2);
p = zeros(1,Nu);
R2 = sum(R.*R,2);
Mj = find(R2<0.25*R02); % 0.25 => 50% of R0 or 0.49 => 70% of R0
Nj = size(Mj,1);
for nn=1:Nj
    n = Mj(nn);
    rn = R(n,:);

```

```

for m=1:n-1
    rmn = R(m,:)-rn;
    k = fix(sqrt(rmn * rmn')/du)+1;
    p(k) = p(k) + 1;
end;
for m=n+1:N
    rmn = R(m,:)-rn;
    k = fix(sqrt(rmn * rmn')/du)+1;
    p(k) = p(k) + 1;
end;
g = p./(4*pi*rho*Nj*du*(U.*U));
M = [U; g];
fprintf(' N=%1.0f, n=%1.0f, Nj=%1.0f, rho=%10.8f\n',NN,N,Nj,rho)
time=clock; fprintf(' %1.0fh%1.0fm%1.0fs\n',time(4:6))

```

35. exrdfitting.m

```

function exrdfitting(a,b)
%%%%%%%%%%%%%%%%%%%%%%%%%%%%%%%%%%%%%
% NF x Ni curve adjusted by NF = Nmax*[1-exp(-alpha*Ni)] %
% Input:
% a,b = alpha values for the two data sets given below %
% Usage: exrdfitting(0.7e-5,2,1e-5) %
%%%%%%%%%%%%%%%%%%%%%%%%%%%%%%%%%%%%%
% Data sets from routine exrdfd.m with d = 2 and 3, e.g. exrdf(100,d,1000);
N=[ 2 4 8 10 20 40 60 80 100 120 200]*1000;
n(1,:)=[1013 2047 4098 5171 10065 19451 27886 35914 43662 50446 74620]; % d = 2
n(2,:)=[1028 2019 3997 4864 9219 16403 22345 26913 31125 34530 44749]; % d = 3
%-----
R0 = 100;
V = (4*pi/3) * R0^3;
d = [2 3];
vp = (pi/6)*(d.*d.*d);
N = N * (pi/6);
X=0:1000:110000;
na = 1/a;
Ya = na*(1-exp(-a*X));
nb = 1/b;
Yb = nb*(1-exp(-b*X));
fprintf(' rho(2)=%5.3f/v_p e rho(3)=%5.3f/v_p\n', (na/V)*vp(1), (nb/V)*vp(2))
hfi = figure(1);
clf
set(hfi,'InvertHardcopy','off','Color','w')
plot(N,n(1,:),'bo',N,n(2,:),'ks',N,N,'--r','MarkerFaceColor','w','MarkerSize',8,'LineWidth',1.5)
legend(' d = 2A',' d = 3A',' reference: N_f = N_i',2)
hold on
plot(X,Ya,'b',X,Yb,'k','LineWidth',2)
hold off
set(gca,'FontSize',14,'Color',[0.93 0.93 0.93],'LineWidth',1)
axis tight
xlabel('N_i','FontSize',18)
ylabel('N_f','FontSize',18)

```

36. exrdfplot.m

```

function exrdfplot
%%%%%%%%%%%%%%%%%%%%%%%%%%%%%%%%%%%%%
% Plot RDFs generated by the hard sphere model %
% Required file: exrdfplot.dat %
% File generated by routine exrdf.m (see text for details), and %
% available at http://fap.if.usp.br/~morelhaoxrayphysicsbook.html %
%%%%%%%%%%%%%%%%%%%%%%%%%%%%%%%%%%%%%
S = load('exrdfplot.dat');
U1 = S(1,:); g1 = S(2,:); % <- exrdf(100,2,2e+5) with R' = 50% of R0
U2 = S(3,:); g2 = S(4,:); % <- exrdf(100,3,2e+5) with R' = 50% of R0
U3 = S(5,:); g3 = S(6,:); % <- exrdf(100,2,2e+5) with R' = 70% of R0
hfi = figure(1);
clf
set(hfi,'InvertHardcopy','off','Color','w')
plot(U2,g2,'-ks','MarkerFaceColor','w','MarkerSize',6,'LineWidth',1.5)
hold on
plot(U1,g1,'-bo','MarkerFaceColor','w','MarkerSize',6,'LineWidth',1.5)
hold off
set(gca,'FontSize',14,'Color',[.87 .92 .98],'LineWidth',1)
axis([0 10 0 1.39])
 xlabel(' (A) ','FontSize',18)
 ylabel('g(u) ','FontSize',18)
legend(' d = 3A',' d = 2A')
grid

```

```

hal=axes('Position',[.481 .24 .38 .38]);
plot(U2,g2,'k',U1,g1,'b','LineWidth',2);
hold on
plot(U3,g3,'-b','LineWidth',1)
hold off
set(hal,'FontSize',16,'Color',[.97 .97 .97])
ylabel('g(u)', 'FontSize',16)
xlabel('u (A)', 'FontSize',16)
axis([10 150 0 1.39])
text(50,1.1,'downarrow effect of finite ensemble','FontSize',12)
grid

```

37. exrlp3Dview.m

```

function exrlp3Dview(L,T,vlevel,disc)
%%%%%%%%%%%%%%%%%%%%%%%%%%%%%%%%%%%%%
% Generates 3D visualization of reciprocal lattice nodes in thin crystal %
% with rectangular or circular area %
% Input: %
%   L = lateral dimension (nm) %
%   T = thickness (nm) %
%   vlevel = isosurface level value, between 0 and 1 %
%   disc = 1 for crystals with circular area, otherwise rectangular area %
% Usage: exrlp3DView(200,100,0.038,1)
%%%%%%%%%%%%%%%%%%%%%%%%%%%%%%%%%%%%%
Nc = 6;
dQ = 1 / 2^Nc;
QrangeXY = (-1:dQ:1)*(40/L);
QrangeZ = (-1:dQ:1)*(30/T);
[Qx,Qy,Qz]=meshgrid(QrangeXY, QrangeXY, QrangeZ);
Qx(Qx==0)=1e-8;
Qy(Qy==0)=1e-8;
Qz(Qz==0)=1e-8;
if (disc==1)
    R=L/2;
    T=T/2;
    Nq = size(Qx,1);
    dphi = pi/500;
    phi=0:dphi:2*pi-dphi;
    cphi=cos(phi);
    cphi(cphi==0)=1e-8;
    Qxy = sqrt(Qx(:,:,1).*Qx(:,:,1)+Qy(:,:,1).*Qy(:,:,1));
    Wxy = zeros(Nq);
    for n=1:Nc
        for m=1:Nq
            a = Qxy(n,m)*cphi;
            x = a.*R;
            x = exp(x).*(1-x)-1;
            x = x ./ (a.*a);
            Wxy(n,m) = sum(x).*dphi;
        end;
    end;
    Wxy = (1/(pi*R*conj(R)))*Wxy;
    W = cat(3,Wxy,Wxy);
    for n=1:Nc, W = cat(3,W,W); end;
    W = cat(3,W,Wxy);
    W = W.*sin(T*Qz)./(T*Qz);
else
    L=L/2;
    T=T/2;
    W = sin(L*Qx)./(L*Qx);
    W = W.*sin(L*Qy)./(L*Qy);
    W = W.*sin(T*Qz)./(T*Qz);
end;
W = sqrt(W.*conj(W));
hfl = figure(1);
clf
set(hfl,'InvertHardcopy','off','Color','w')
P = patch(isosurface(Qx,Qy,Qz,W,vlevel),'FaceColor','red','EdgeColor','none');
isonormals(Qx,Qy,Qz,W,P)
view(3)
daspect([1 1 1])
axis tight
camlight
camlight(-80,-10)
lighting phong
set(gca,'FontSize',14,'Color',[0.97 0.97 0.97],'Box','on','LineWidth',1,'FontName','Arial')
grid
view(-30,25)
xlabel('Q_X (nm^{-1})','FontSize',18)
ylabel('Q_Y (nm^{-1})','FontSize',18)
zlabel('Q_Z (nm^{-1})','FontSize',18)

```

38. exsgc.m

```

function M=exsgc(atom,Emin,Emax,Np)
%%%%%%%
% Incoherent scattering cross-section (Compton), sg_C
% comparison of analytical x numerical solutions
%
% Input:
% atom = element symbol, from 'H' to 'Cs' (Z from 1 to 55)
% Emin,Emax = energy range from Emin to Emax (eV or keV)
% Np = number of points in the sg_C x E curve
% Output M = [E sg1 sg2]
%           |   |
%           |   cross-section (barn), analytical solution
%           |   cross-section (barn), numerical solution
%           |   energy (keV)
% Secondary routines required: csfQ.m and sgcompton.m
% Usage:
% >> Mexsgc('Ca',1,20,50);
%%%%%%%
Emin = abs(Emin); Emax = abs(Emax);
if (Emax < Emin), E = Emax; Emx = Emin; Emin = E; end;
if (Emax>500), Emin = 0.001*Emin; Emax = 0.001*Emax; end;
if (Emin<1), Emin = 1; end;
if (Emax>25), Emax = 25; end;
if (Np<2), Np=2; end;
dE = (Emax-Emin)/(Np-1);
E = Emin:dE:Emax;
NE = size(E,2);
rad = pi/180;
re = 2.817940285e-15; % (m)
hc = 12.3985; % (keV.A)
invWL = E/hc;
dtth = 0.2; % (deg)
TTH = 0:dtth:180; % (deg)
X = TT*rad;
dx = dtth * rad;
aux1 = pi * re * re * dx * 1e+28;
SinG = sin(X);
PSinG = (2-SinG.*SinG).*SinG;
for nn = 1:NE
    S = csfQ(atom,invWL(nn)*sin(0.5*X));
    M(nn,1) = E(nn);
    M(nn,2) = aux1*sum(PSinG.* (S(:,2)));
end;
S = sgcompton(atom,E);
M(:,3) = S(:,2);
hfi=figure(1);
clf
set(hfi,'InvertHardcopy','off','Color','w')
plot(E,M(:,3),'k','LineWidth',2)
hold on
plot(E,M(:,2),'bo','MarkerFaceColor','w','MarkerSize',6,'LineWidth',1.5)
hold off
set(gca,'FontSize',14,'Color',[0.854902 0.701961 1],'LineWidth',1)
ylabel('sigma_C (barn)', 'FontSize',18)
xlabel('Energy (keV)', 'FontSize',18)
axis tight; grid
legend(' analytical',' numerical',4)
n = round(0.5*NE);
text(E(n),M(n,3),atom,'FontSize',36,'Color',[0.98 0.98 0.98],'FontWeight','bold')

```

39. exsgr.m

```

function M=exsgr(atom,Emin,Emax,Np)
%%%%%%
% Coherent scattering cross-section (Rayleigh), sg_R
% comparison of analytical x numerical solutions
%
% Input:
% atom = element symbol, e.g. 'O'
% Emin,Emax = energy range from Emin to Emax (eV or keV)
% Np = number of points in the sg_R x E curve
% Output M = [E sg1 sg2]
%           |   |
%           |   cross-section (barn), analytical solution
%           |   cross-section (barn), numerical solution
%           |   energy (keV)
% Secondary routines required: asfQ.m and sgrayleigh.m
% Usage:
% >> Mexsgr('O',2,20,50);
%%%%%%
Emin = abs(Emin); Emax = abs(Emax);
if (Emax < Emin) E = Emax; Emx = Emin; Emin = E; end;
if (Emax>500) Emin = 0.001*Emin; Emax = 0.001*Emax; end;
if (Emax<2) Emx = 2; end;
if (Emax>70) Emax = 70; end;
if (Np<2) Np=2; end;

```

```

dE = (Emax-Emin) / (Np-1);
E = Emin:dE:Emax;
NE = size(E,2);
rad = pi/180;
re = 2.817940285e-15; % (m)
hc = 12.3985; % (keV.A)
invWL = E/hc;
dtth = 0.2; % (deg)
TTH = 0:dtth:180; % (deg)
X = TTH * rad;
dx = dtth * rad;
aux1 = pi * re * re * dx * 1e+28;
Ntth = size(X,2);
SinG = sin(X);
PSinG = (2-SinG.*SinG).*SinG;
for nn = 1:NE
    f = asfQ(atom,invWL(nn)*sin(0.5*X));
    f = f.*f;
    M(nn,1) = E(nn);
    M(nn,2) = aux1*sum(PSinG.*f);
end;
S = sgrayleigh(atom,E);
M(:,3) = S(:,2);
hf1=figure(1);
clf
set(hf1,'InvertHardcopy', 'off','Color','w')
plot(E,M(:,3),'k','LineWidth',2)
hold on
plot(E,M(:,2),'bo','MarkerFaceColor','w','MarkerSize',6,'LineWidth',1.5)
hold off
set(gca,'FontSize',14,'Color',[0.854902 0.701961 1],'LineWidth',1)
ylabel('Sigma_R ( barn)', 'FontSize',18)
xlabel('Energy (keV)', 'FontSize',18)
axis tight; grid
legend(' analytical', ' numerical',1)
n = round(0.5*NE);
text(E(n),M(n,3),atom,'FontSize',36,'Color',[0.98 0.98 0.98],'FontWeight','bold')

```

40. exshell.m

```

function S=exshell(a,b,rhoa,rhob)
%%%%%%%%%%%%%%%%%%%%%%%%%%%%%%%%%%%%%
%           Pair distance distribution function (PDDF) in
%           particles like hollow sphere
%%%%%%%%%%%%%%%%%%%%%%%%%%%%%%%%%%%%%
% Input:
%   a and b, external and internal radius (Angstrom)
% rhoa: density for b < r < a
% rhob: density for 0 < r < b
% Output S = [U; pnu; p; ph]';
%           |   |   |
%           |   |   PDDF via histogram
%           |   |   PDDF via inverse FT
%           |   |   PDDF via numerical integral
%           |   internal distances (Angstrom)
% Usage:
% >> S = exshell(500,375,2,-1);
%%%%%%%%%%%%%%%%%%%%%%%%%%%%%%%%%%%%%
if (b==a) b = 0.5 * a; elseif (b>a) c = a; a = b; b = c; end;
M=Pdeq(a,b,rhoa,rhob,5);
Q = M(1,:);
P0 = M(2,:);
dQ = Q(3)-Q(2);
Umax = 2.4*a;
du = Umax/1000;
U = 0:du:Umax;
U(1) = 1e-6;
Nu = size(U,2);
A = (dQ/(2*pi*pi))*(P0.*Q);
for n=1:Nu
    u = U(n);
    p(n) = sum(A.*sin(Q*u));
end;
pnu=pdeunum(U,a,b,rhoa,rhob);
Nat = 4000;
rand('state',sum(100*clock));
X = 2*rand(Nat,3)-1;
X2 = sum(X.*X,2);
N = find(X2<=1);
R = X(N,:);
r = sqrt(X2(N));
N = size(R,1);
R = a*R;
ps = rhoa*ones(1,N);
ps(r<=b/a)=rhob;
ph=zeros(1,Nu);
for n=1:N

```

```

for m=n+1:N
    D = R(m,:)-R(n,:);
    d = sqrt(D*D');
    k = floor(d/du)+1;
    ph(k) = ph(k)+ps(m)*ps(n);
end;
end;
ph = 2*ph;
Nmax = find(pnu==max(pnu));
pnumax = sum(pnu(Nmax-10:Nmax+10))/20;
pmax = sum(p(Nmax-10:Nmax+10))/20;
phmax = sum(ph(Nmax-10:Nmax+10))/20;
pnu = pnu/pnumax;
p = p/pmax;
ph = ph/phmax;
N = 1:7:Nu;
Nh = 1:5:Nu;
hfi=figure(1);
clf
set(hfi,'InvertHardcopy', 'off','Color','w')
bar(U(Nh),ph(Nh),'FaceColor',[.87 .49 0], 'EdgeColor','w')
hold on
plot(U(N),p(N),'-ro','MarkerFaceColor','w','MarkerSize',4,'LineWidth',1)
plot(U,pnu,'k','LineWidth',1)
hold off
set(gca,'FontSize',14,'Color',[1 .97 .92])
axis tight
ylabel('p(u)', 'FontSize',18)
xlabel('u (A)', 'FontSize',18)
legend(' hist.', ' inv. FT', ' num. vl.')
hal=axes('Position',[.14 .532 .3 .37]);
P0 = P0/max(P0);
semilogy(Q,P0,'r','LineWidth',2)
set(hal,'FontSize',14,'Color',[0.9 0.9 1])
ylabel('P(Q)', 'FontSize',14)
xlabel('Q (A^-{1})', 'FontSize',14)
axis([Q(1) max(Q) 0.9e-5 1.1])
axis([Q(1) max(Q) 0.9e-5 1.1])
S = [U; pnu; p; ph];

```

```

function M=PdeQ(a,b,rhoa,rhob,Nmin)
Qmax = Nmin * (5*pi/2) / (2*a);
dQ = Qmax/2000;
Q = 0:dQ:Qmax;
Q(1) = 1e-8;
Va = 4*pi*a*a/3;
Vb = 4*pi*b*b/3;
F = (Va*rhoa) * tfsphere(Q*a) - (Vb*(rhoa-rhob)) * tfsphere(Q*b);
P = F.*conj(F);
M = [Q; P];

```

```

function Z=tfsphere(u)
u3 = u.*u.*u;
Z = 3*((sin(u)-u.*cos(u))./u3);

```

```

function M=pdeunum(U,a,b,rhoa,rhob)
Rmax = 1.1*a;
dr = Rmax/1000;
R = 0:dr:Rmax;
Nr = size(R,2);
invw = 10 / dr;
Y = rhoef(R,a,b,rhoa,rhob,invw);
Nu = size(U,2);
rhoRdr = (pi*dr)*(R.*Y);
for n=1:Nu
    u = U(n);
    for m=1:Nr
        r = R(m);
        z1 = (r-u); z1 = z1*z1;
        z2 = (r+u); z2 = z2*z2;
        dz = (z2-z1) / 400;
        Z = z1:dz:z2;
        Yz = rhoef(sqrt(Z),a,b,rhoa,rhob,invw);
        A(m) = dz * sum(Yz);
    end;
    C(n) = sum(rhoRdr.*A)/u;
end;
M = C.*U.*U;

```

```

function Y = rhoef(R,a,b,rhoa,rhob,invw)
Y = (1./((1 + exp(invwx*(R - a)))).*((rhoa-rhob)./(1 + exp(invwx*(b - R))))+rhob);

```

41. exsphere.m

```

function M=exsphere
%%%%%%%%%%%%%%%%%%%%%%%%%%%%%%%%%%%%%
% Scattering by uniform sphere %
%%%%%%%%%%%%%%%%%%%%%%%%%%%%%%%%%%%%%
uhalf = 1.8149;
alpha = log(2)/uhalf^4;
U = 0:0.01:20; U(1) = 1e-6;
Y = tfsphere(U);
Z = exp(-alpha*(U.*U));
hfi=figure(1);
clf
set(hfi,'InvertHardcopy', 'off','Color','w')
plot(U,Z,'x-',[U,Y,'b',[1.815],[0.5],'ko','LineWidth',2,'MarkerFaceColor','w','MarkerSize',9)
set(gca,'FontSize',14,'Color',[0.854902 0.701961 1],'LineWidth',1)
 xlabel('Qa','FontSize',18)
 ylabel('I(Qa) / I(0)','FontSize',18)
text(0.35,0.505,' Qa = 1.815 \rightarrow','FontSize',18)
axis([0 5 0 1.01])
ha2=axes('Position',[.48 .48 .4 .4]);
plot(U,log10(Z),'r-',[U,log10(Y),'b'],'LineWidth',1)
set(ha2,'FontSize',14,'Color',[0.9 0.9 1])
 xlabel('Qa')
 ylabel('log(I)')
axis([0 20 -5 0.02])
M = [U; Y; Z];

```

42. exwaterccd.m

```

function exwaterccd(E,Qf,N)
%%%%%%%%%%%%%%%%%%%%%%%%%%%%%%%%%%%%%
% X-ray diffraction of liquid water on a CCD area detector %
%%%%%%%%%%%%%%%%%%%%%%%%%%%%%%%%%%%%%
% Input:
% E = X-ray energy (keV)
% Qf = rec. vector module (1/Angstrom) limited by sample-ccd distance %
% N > 999, diffraction pattern with statistic of N counts %
% Secondary routines required: exwaterSofQ.m %
% Usage:
% >> exwaterccd(12,4,5e6)
%%%%%%%%%%%%%%%%%%%%%%%%%%%%%%%%%%%%%
A = 300; % square screen detector of lateral size 2A (mm)
pixel = 5; % pixel size (mm)
if (E>500) E = 0.001*E; end;
Qfmax = E*pi*sin(0.5*atan(30/5)); %--> % to limit Qf so that the minimum %
if (Qf>Qfmax) Qf = Qfmax; end; % sample-ccd distance is D = 5 cm %
M = exwaterSofQ(Qf,0); %%%%%%%%%%%%%%%%%%%%%%%%%%%%%%%%%%%%%%
Q = M(1,:);
PS = M(2,:);
D = A / tan(2*asin(Qf/E));
X = 0:pixel:A;
Y = -A:pixel:0;
Nx = size(X,2);
twopi_wl = 2*pi*E/12.3985;
for n=1:Nx
    for m=1:Nx
        v = [X(n) Y(m) D];
        v = v / sqrt(v*v');
        cg = v(3);
        v = v - [0 0 1];
        q = twopi_wl*sqrt(v*v');
        DQ = abs(Q-q);
        nn=find(DQ==min(DQ));
        I(m,n) = PS(nn(1))* cg*cg*cg; % to account for effective pixel size
    end;
end;
beye=zeros(Nx);
for n=1:Nx
    eye(n,Nx+1-n) = 1;
end;
I = [I*beye I];
I = [I; eye*I];
if (N>999) I = photonstatistic(I,N); end;
hfi=figure(1);
clf
set(hfi,'InvertHardcopy', 'off','Color','w')
set(gca,'FontSize',14,'Color','k','LineWidth',1)
imagesc([-A A],[-A A,I])
blackbluemap = [zeros(1,64) 0:1/63:1; zeros(1,64) 0:1/63:1; 0:1/63:1 ones(1,64)];
colormap(blackbluemap)
axis image

```

```

view(0,90)
colorbar('YColor','k','FontSize',14,'Location','East','LineWidth',1)
xlabel('X (mm)', 'FontSize',18)
ylabel('Y (mm)', 'FontSize',18)
text(0,0,200,'photons per pixel','FontSize',16,'Rotation',90)

```

43. exwaterSofQ.m

```

function M=exwaterSofQ(Qf,prn)
%%%%%%%%%%%%%%%%%%%%%%%%%%%%%%%%%%%%%
% Interference function S(Q) from published RDF of water %
%
% Input: %
%   Qf = rec. vector module (1/Angstrom), upper limit of S(Q) integral %
%   prn = 1 for graphic output (figure window) %
% Output: M=[Q; I]; %
%           | %
%           | normalized intensity, I(Q)/NI_{TH} = P(Q)S(Q) %
%           | reciprocal vector module (1/Angstrom) %
% Secondary routines required: asfQ.m %
% Required files: gotwater.dat %
% File available at http://xraybook.if.usp.br/ %
% Usage: %
% >> M=exwaterSofQ(20,1);
%%%%%%%%%%%%%%%%%%%%%%%%%%%%%%%%%%%%%
GofU=load('gotwater.dat');
U=GofU(:,1);
g=GofU(:,2);
clear GofU;
g(g<0)=0;
U(1)=1e-8;
du=U(3)-U(2);
dq=Qf/1000;
Q=0:dq:Qf;
Q(1)=1e-8;
Nq=size(Q,2);
alpha=max(U)^3/(3*sum(g.*U.*U)*du);
rho=1e-24*6.022e+23/18/alpha;
Gudu=(4*pi*rho*du)*(g-1).*U;
for n=1:Nq
    q=Q(n);
    S(n)=1+sum(Gudu.*sin(q.*U))/q;
end;
S(S<0)=0;
f=ASFQ('O2-',(0.25/pi)*Q);
f2=f.*f;
if(prn==1)
hfi=figure(1);
clf
set(hfi,'InvertHardcopy','off','Color','w')
plot(Q,S,'b','LineWidth',2)
set(gca,'FontSize',14,'Color',[0.93 0.93 0.93],'LineWidth',1)
hold on
plot(Q,f2/f2(1),'--k','LineWidth',1)
hold off
xlabel('Q (A^{-1})','FontSize',18)
ylabel('S(Q)', 'FontSize',18)
text(2.5,4,'leftarrow P(Q)/P(0)','FontSize',14,'Color','k')
axis([0 Qf 0 1.02*max(S)])
hal=axes('Position',[.481 .282 .38 .38]);
plot(U,g,'y','LineWidth',2);
set(hal,'FontSize',14,'Color',[.85 .7 1])
set(hal,'XTick',[2 3 4 5 6 7 8 9])
ylabel('g(u)','FontSize',14)
xlabel('A','FontSize',14)
axis([11.5 9.5 -.05 2.95])
text(5,2,'H_20','FontSize',36,'Color',[.93 .93 .93],'FontWeight','bold')
grid
end;
M=[Q; f2.*S];

```

44. fpfpp.m

```

function M=fpfpp(A,EE)
%%%%%%%%%%%%%%%%%%%%%%%%%%%%%%%%%%%%%
% Linear interpolation of tabulated values of %
% atomic resonance amplitude, f' and f" %
%
% Input: %
%   A = element symbol, e.g. 'Se' %
%   EE = energy values (m-by-n array) (eV) %
% Output: M = [E f' f" sgal]
%           | | |
%           | | absorption cross-section (barn) %
%           | | imaginary term (electron number) %
%           | | real term (electron number) %

```

```
%           energy (eV)
% Routine available for download at http://xraybook.if.usp.br/
%%%%%
s=size(EE); NofE=s(1)*s(2);
if (EE>NofE), EE = 1000*EE; end;
aux = 2000 * 2.818 * 12398.5;
W = dispersion(atomm(A));
NofW = size(W,1);
if (NofW == 1)
    disp([' Element ' A ' unknown!!!']);
    M = [0 0 0];
    return;
end;
EE(EE<=0) = 0.1;
M = zeros(NofE,4);
for ne = 1:NofE
    E = EE(ne);
    nw = 1; ctr = 0;
    E2 = 0; fal = W(nw,2); fa2 = W(nw,3);
    while (nw < NofW)
        E1 = E2; x = fal; y = fa2;
        E2 = W(nw,1); fal = W(nw,2); fa2 = W(nw,3);
        if (E2 > E)
            fal = (fal - x) + (E - E1) / (E2 - E1) + x;
            fa2 = (fa2 - y) + (E - E1) / (E2 - E1) + y;
        nw = NofW; ctr = 1;
        end;
        nw = nw + 1;
    end;
    if (ctr==0), fal = W(nw-1,2); fa2 = W(nw-1,3); end;
    M(ne,:) = [E fal fa2 aux*fa2/E];
end;

function nm=atomm(A)
% This function is available at the book's webpage

function Z=dispersion(nm)
% This function is available at the book's webpage
```

45. fthofu.m

```
function R=fthofu(N,d,cyl,fnm,prn)
%%%%%
% Fourier Transform of function h(u) for a volumetric ensemble of
% particles with anisotropic correlations
% Input:
% N, the ensemble has nearly (2N+1)x(2N+1)x7 particles
% d, degree of disorder along the X direction, Da/a = 1 + d*(2*rand-1)
% cyl = 1 for cylindrical volume, otherwise rectangular volume
% fnum = 1, 2,... (ID number of the output file),
%       0 to suppress FT calculation and file saving
% prn = 0 to suppress graphic output
% Output R(n,:)= [X Y Z] 3D coordinates of the particles
%       file with n-by-n array of FT{Cq(u)} values on detector pixels
% Usage:
% >> R = fthofu(2,0.2,1,1,1);
a0 = 10; % average particle-to-particle distance (Angstrom)
dy = 0.1*d;
N = round(abs(N));
NN = 2*N + 1;
X = zeros(NN,NN,NN);
Y = zeros(NN,NN,NN);
Z = zeros(NN,NN,NN);
X(:,:,1) = d*(2*rand(NN)-1);
Y(:,:,1) = dy*(2*rand(NN)-1);
Z(:,:,1) = zeros(NN);
h = 0;
if (N>0)
    X(:,:,2) = X(:,:,1) + 1 + d*(2*rand(NN)-1);
    X(:,:,3) = X(:,:,1) - 1 + d*(2*rand(NN)-1);
    Y(:,:,2) = Y(:,:,1) + 1 + dy*(2*rand(NN)-1);
    Y(:,:,3) = Y(:,:,1) - 1 + dy*(2*rand(NN)-1);
    Z(:,:,2) = Z(:,:,1) + 1;
    Z(:,:,3) = Z(:,:,1) - 1;
    h = [0 1 -1];
    if (N>1)
        for n = 2:N
            X(:,:,2*n) = X(:,:,2*(n-1)) + 1 + d*(2*rand(NN)-1);
            X(:,:,2*n+1) = X(:,:,2*(n-1)+1) - 1 + d*(2*rand(NN)-1);
            Y(:,:,2*n) = Y(:,:,2*(n-1)) + 1 + dy*(2*rand(NN)-1);
            Y(:,:,2*n+1) = Y(:,:,2*(n-1)+1) - 1 + dy*(2*rand(NN)-1);
            Z(:,:,2*n) = Z(:,:,2*(n-1)) + 1;
            Z(:,:,2*n+1) = Z(:,:,2*(n-1)+1) - 1;
            h(2*n:2*n+1) = [h -n];
        end;
```

```

    end;
end;
NN = N+1;
nn = 0;
for n=1:NN
    for m=1:NN
        for p=1:NN
            nn = nn + 1;
            R(nn,:) = [X(N0-h(p),N0+h(m),n) Y(N0-h(p),N0-h(n),m) Z(N0+h(n),N0+h(m),p)];
        end;
    end;
end;
clear X Y Z;
R = a0*R;
if (cyl == 1)
    rai02 = max(max(R));
    rai02 = rai02*raio2;
    R = R(sum(R.*R,2)<raio2,:);
end;
R = R(R(:,3).*R(:,3)<1000,:);
if (fnum==0)
    Nr = size(R,1);
    twopi_wl = 2*pi/1; % wavelength of 1 Angstrom (X-ray of 12.4 keV)
    A = 150; % square screen detector of lateral size 2A (mm)
    D = 600; % sample-detector distance (mm)
    pixel = 0.5; % pixel size (mm)
    X = -A:pixel:A;
    Y = A:-pixel:-A;
    Nx = size(X,2);
    for n=1:Nx XX(n,:)=X; YY(:,n)=Y'; end;
    for n=1:Nx
        for m=1:Nx
            S = [XX(1,n) YY(m,1) D];
            S = S / sqrt(S*S') - [ 0 0 1];
            Q(m,n,:)= twopi_wl*S;
        end;
    end;
time=clock; fprintf(' %2.0fh%2.0fm%2.0fs\n',time(4:6))
C = zeros(size(Q,1),size(Q,2));
for n=1:Nr
    for m=n+1:Nr
        r = R(m,:)-R(n,:);
        C = C + cos(Q(:,:,1)*r(1)+Q(:,:,2)*r(2)+Q(:,:,3)*r(3));
    end;
end;
C = (2/Nr)*C+1;
time=clock; fprintf(' %2.0fh%2.0fm%2.0fs\n',time(4:6))
if (prn~0)
    surf(XX,YY,log(C))
    shading interp
    axis image
    set(gcf,'InvertHardcopy','off','Color','w')
    set(gca,'ZTick',[],'FontSize',14,'Color',[0.93 0.93 0.93],'LineWidth',1)
    xlabel(' X (mm)', 'FontSize',18)
    ylabel(' Y (mm)', 'FontSize',18)
    zlabel('log(I)', 'FontSize',18)
    view(-14,30)
end;
if (cyl == 1)
    save(['fthofu_N num2str(N) ' d' num2str(100*d) 'sphere' num2str(fnum) '.dat'],'C','-ascii');
else
    save(['fthofu_N num2str(N) ' d' num2str(100*d) 'square' num2str(fnum) '.dat'],'C','-ascii');
end;
end;

```

46. fthofuplotmap.m

```

function fthofuplotmap
%%%%%%%%%%%%%%%%%%%%%%%%%%%%%%%%%%%%%
% Surface map of TF[h(u)] as a function of Qx and Qy %
%%%%%%%%%%%%%%%%%%%%%%%%%%%%%%%%%%%%%
% Required file: fthofu_N8d20sphere1to20.dat %
% File generated by routine fthofu.m %
% and available at http://xraybook.if.usp.br/ %
%%%%%%%%%%%%%%%%%%%%%%%%%%%%%%%%%%%%%
I = load('fthofu_N8d20sphere1to20.dat'); I = I/max(max(I));
A = 150; pixel = 0.5; D=600; % same values used in routine fthofu.m
Q = 20*sin(0.5*atan((-A:pixel:A)/D)); % Qmax normalized by a0/(2*pi)
for n=1:size(Q,2)
    Qx(n,:) = Q;
    Qy(:,n) = -Q';
end;
hfi = figure(1);
clf
set(hfi,'InvertHardcopy','off','Color','w')
surf(Qx,Qy,log10(I))
shading interp
axis image

```

```

view(-14,30)
set(gca,'Position',[0.05 0.07 0.85 0.9], 'LineWidth',1)
set(gca,'FontSize',14,'Color',[0.93 0.93 0.93])
set(gca,'ZTick',[],'DataAspectRatio',[0.03 0.03 0.4],'YTick',[-2 -1 0 1 2],'XTick',[-2 -1 0 1 2])
colormap(jet)
colorbar('kColor','k','FontSize',14,'Location','East','LineWidth',1)
xlabel('n_x','FontSize',18)
ylabel('n_y','FontSize',18)
text(2,0,0,'Log(FT\{h(u)\})','FontSize',16,'Rotation',90)

```

47. fthofuR.m

```

function fthofuR(N,d,cyl)
%%%%%%%%%%%%%%%%%%%%%%%%%%%%%%%%%%%%%
% 3D plot of the ensemble of particles generated by routine fthofu.m %
% Secondary routines required: fthofu.m %
% Input parameters N, d, and cyl defined in the required routine %
%%%%%%%%%%%%%%%%%%%%%%%%%%%%%%%%%%%%%
a0 = 10; % same value used in routine fthofu.m
R = (1/a0)*fthofu(N,d,cyl,0,0);
hf1=figure(1); clf; set(hf1,'InvertHardcopy', 'off','Color','w')
subplot(1,2,2)
plot3(R(:,1),R(:,2),R(:,3),'ro','MarkerFaceColor','y','MarkerSize',3,'LineWidth',.6)
axis image
axis([-9 9 -9 9 -7 7])
view(0,60)
set(gca,'FontSize',14,'Color','w','LineWidth',1)
set(gca,'ZTick',[],'YTick',[])
xlabel('X/a','FontSize',14)
hold on
plot3([-8 -6],[-8 -8],[-6 -6],'r','LineWidth',2)
text(-6,-8,-6,'x')
plot3([-8 -8],[-8 -6],[-6 -6],'b','LineWidth',2)
text(-8,-6,-6,'y')
plot3([-8 -8],[-8 -8],[-6 -4],'k','LineWidth',2)
text(-8,-8,-4,'z')
hold off
subplot(1,2,1)
plot3(R(:,1),R(:,2),R(:,3),'ro','MarkerFaceColor','y','MarkerSize',3,'LineWidth',.6)
axis image
axis([-9 9 -9 9 -7 7])
view(90,60)
set(gca,'FontSize',14,'Color','w','LineWidth',1)
set(gca,'XTick',[],'ZTick',[])
ylabel('Y/a','FontSize',14)
hold on
plot3([6 8],[-8 -8],[-6 -6],'r','LineWidth',2)
text(8,-8,-6,'x')
plot3([6 6],[-8 -6],[-6 -6],'b','LineWidth',2)
text(6,-6,-6,'y')
plot3([6 6],[-8 -8],[-6 -4],'k','LineWidth',2)
text(6,-8,-4,'z')
hold off

```

48. goldnano.m

```

function M=goldnano(D,desord)
%%%%%%%%%%%%%%%%%%%%%%%%%%%%%%%%%%%%%
% Histogram of interatomic distances, or PDDF, in %
% gold nanoparticles with crystalline structure %
%%%%%%%%%%%%%%%%%%%%%%%%%%%%%%%%%%%%%
% Input:
% D = particle diameter (Angstrom) %
% desord = atomic disorder in percentage (%) of the distance 2.88 A %
% Output M = [U; p];
% | |
% | histogram (number of occurrences between u and u+du) %
% | interatomic distances (Angstrom) %
% Usage: M = goldnano(20,5);
%%%%%%%%%%%%%%%%%%%%%%%%%%%%%%%%%%%%%
if (D>100), disp('Warning!!! Delay time can be very long for D > 100 Angstroms'); end;
a=4.0782; % lattice parameter (Angstrom) of gold fcc crystals
if (D<a), D = a; end;
N = fix(D/a)+1;
Nc = 0;
for m=0:N-1
    for n=0:N-1
        for p=0:N-1
            Nc = Nc + 1;
            R(Nc,:) = [m n p]; % lattice points
        end;
    end;
end;

```

```

        end;
    end;
    if (Nc==0), Nc = 1; R(1,:) = [0 0 0]; end;
    R=a*R;
    X = a*[0 0 0; .5 .5 0; .5 0 .5; 0 .5 .5]; % atomic coordinates regarding each lattice point
    Nx = size(X,1);
    for n=2:Nx
        for m=1:Nc
            R((n-1)*Nc+m,:) = R(m,:) + X(n,:);
        end;
    end;
    Nat = size(R,1);
    Cm = sum(R(:,1))/Nat;
    X = R - Cm*ones(Nat,3);
    X2 = sum(X.*X,2);
    NN = X2<0.25*D*D;
    R = X(NN,:);
    Nat = size(R,1);
    R = R + (0.01*desord*a/sqrt(2))*(1-2*rand(Nat,3));
    c0 = fix(clock);
    hora = [num2str(c0(4)) ':' num2str(c0(5)) ':' num2str(c0(6))];
    disp([' goldnano started at ' hora])
    Umax=1.02*D;
    du = 0.01;
    U = 0:du:Umax;
    Nu = size(U,2);
    pzzeros(1,Nu);
    for n=1:Nat
        for m=n+1:Nat
            r = R(n,:)-R(m,:);
            k=fix(sqrt(r*r)/du)+1;
            p(k) = p(k) + 1;
        end;
    end;
    p = 2*p;
    p(1) = Nat;
    plot(U,p,'r','LineWidth',2)
    M = [U; p];
    c1 = fix(clock);
    hora = [num2str(c1(4)) ':' num2str(c1(5)) ':' num2str(c1(6))];
    disp([' goldnano ended at ' hora])
    Dc = c1-c0;
    if (Dc(6)<0), Dc(6)=60+Dc(6); Dc(5)=Dc(5)-1; end;
    if (Dc(5)<0), Dc(5)=60+Dc(5); Dc(4)=Dc(4)-1; end;
    if (Dc(4)<0), Dc(4)=24+Dc(4); end;
    hora = [num2str(Dc(4)) ':' num2str(Dc(5)) ':' num2str(Dc(6))];
    disp([' Time delay ' hora ' (h:m:s)'})

```

49. histogram.m

```

function M=histogram(fname,prn)
%%%%%%%%%%%%%%%%%%%%%%%%%%%%%%%%%%%%%
% Histogram of interatomic distances, or PDDF, of
% molecules catalogued in the Protein Data Bank
%%%%%%%%%%%%%%%%%%%%%%%%%%%%%%%%%%%%%
% Input:
% fname = pdb text file, *.pdb, or saved files *.ndu
% if *.ndu, it calculates the histogram and generate file *.ndu
% if *.ndu, it just plots the histogram
% prn = 0 to suppress graphic window
% Output M = [U; p];
%           |
%           | histogram
%           | interatomic distances (Angstrom)
% Usage: M = histogram('2LYZ.pdb',1);
%%%%%%%%%%%%%%%%%%%%%%%%%%%%%%%%%%%%%
M = [0 0];
n1 = regexp(fname,'.pdb'); n2 = regexp(fname,'.ndu');
if isempty([n1 n2]), disp(' >>> Unknown file type!!!'); return; end;
fidin = fopen(fname,'r');
if (fidin==1), disp([' >>> File ' fname ' not found!!!']); return; end;
if isempty(n1)
    M = load(fname);
    U = M(:,1)';
    p = M(:,2)';
    Nu = size(U,2);
    soma = sum(p);
    N = round(sqrt(soma));
    RgII = sqrt(0.5*sum(p.*U.*U)/soma);
    RgI = 0;
    fclose(fidin);
else
    fout = [fname(1:n1-1) '.ndu'];
    fidin = fopen(fname,'r');
    line = fgets(fidin);
    n = 0;
    while (line>=-1)
        switch line(1:5)

```

```

case {'ATOM'} % use "case {'ATOM ','HETATM'}" to read both "ATOM" and "HETATM" records
    n = n + 1;
    R(n,:) = sscanf(line(31:54),'%f');
    A(n,:) = line(77:78);
end;
line = fgets(fidin);
end;
fclose(fidin);
N = size(R,1); Nchem = 0; AA = zeros(N,1); NA = 1;
while ~isempty(NA)
    n = NA(1);
    Mn = A(n,1)==A(:,1) & A(n,2)==A(:,2);
    Nchem = Nchem + 1;
    AA(Mn) = Nchem;
    Atom(Nchem,:) = A(n,:);
    NA = find(AA==0);
end;
for n=1:Nchem, fprintf('    %1.0f %s',size(find(AA==n),1),Atom(n,:)); end;
fprintf('\n');
Umax = 0;
for n=1:N
    for m=n+1:N
        r = R(m,:)-R(n,:);
        r2 = r*r';
        if (r2>Umax) Umax = r2; end;
    end;
end;
Umax = 1.02*sqrt(Umax);
du = 0.01;
U = 0:du:Umax;
Nu = size(U,2);
p=zeros(1,Nu);
soma = 0;
for n=1:N
    for m=n+1:N
        r = R(m,:)-R(n,:);
        r2 = r*r';
        soma = soma + r2;
        k = floor(sqrt(r2)/du)+1;
        p(k) = p(k)+1;
    end;
end;
p = 2*p; p(1)=N;
RgI = sqrt(soma)/N;
RgII = sum(U.*U.*p)/sum(p);
RgII = sqrt(0.5*RgII);
M = [U; p]';
save(fout,'M','ascii');
end;
if (prn~=0)
    hf1=figure(1); clf; set(hf1,'InvertHardcopy', 'off','Color','w')
    plot(U(2:Nu),p(2:Nu),'b','LineWidth',1)
    axis([0 U(Nu) [-0.02 1.02]*max(p(2:Nu))])
    set(gca,'FontSize',14,'Color',[0.93 0.93 0.93])
    xlabel('u (Å)', 'FontSize',18)
    ylabel('N(u)', 'FontSize',18)
end;
fprintf('    Protein: %s\n',fname(1:find(fname=='.')-1))
if (RgI==0), fprintf('    Nat = $1.0f, Rg = %3.1fA\n',N,RgII);
    else fprintf('    Nat = $1.0f, Rg = %3.1f(%3.1f)A\n',N,RgI,RgII);
end;

```

50. invftpofq.m

```

function M=invftpofq(fname,Qf,Umax,Nu)
%%%%%%%%%%%%%%%%%%%%%%%%%%%%%%%%%%%%%
% Inverse Fourier Transform of the molecule's scattering power, P(Q)
% Input:
%   fname = file with Q and P in columns 1 and 2 (Q values in Angstrom)
%   Qf = upper limit to calculate the inverse FT
%   Umax = maximum interatomic distance (Angstrom)
%   Nu = number of points in the calculated PDDF
% Output  M = [U; p]';
%           |
%           | PDDF
%           | interatomic distances (Angstrom)
% Usage: N=invftpofq('saxs2LYZ_0a40E8keV.dat',0.75,52,1000);
% File saxs2LYZ_0a40E8keV.dat from http://xraybook.if.usp.br/
%%%%%%%%%%%%%%%%%%%%%%%%%%%%%%%%%%%%%
S=load(fname)';
Q = S(1,:);
P = S(2,:);
Nq = size(Q,2);
dQ = Q(3)-Q(2);
if (Qf < Q(Nq))

```

```

n = find(abs(Q-Qf)<=0.5*dQ);
Q = S(1,1:n);
P = S(2,1:n);
end;
du = Umax/N;
U = 0:du:Umax;
Nu = size(U,2);
aux = dQ / (2*pi*pi);
for n = 1:Nu
    u = U(n);
    Qu = u*Q;
    p(n) = aux*sum(P.*Qu.*sin(Qu));
end;
pint = sum(p)*du;
p = (1/pint)*p;
M=[U; p]';

```

51. kdpcoordfrac.m

```

function kdpcoordfrac(etaP,etaK,etaO, fname, p)
%%%%%%% KDP crystal data file with root-mean-square displacements %%%
% Input:
% etaP, etaK, etaO: rms (Angstrom) for P, K, and O atoms
% p = 1 to save file fname.in
% Usage: kdpcoordfrac(0.15,0.15,0.15,'KDP15',1)
% Source: http://www.crystallography.net/, cod ID: 9007582
%%%%%%% %%%%
etaP = etaP*etaP; etaK = etaK*etaK; etaO = etaO*etaO;
P = [7.4521 7.4521 6.974 90.0 90.0 90.0]; % lattice parameters
Rf(1:4,:) = [0 0 0; 1/2 0 3/4; 1/2 1/2 1/2; 0 1/2 1/4]; % P atoms
Rf(5:8,:) = [0 0 1/2; 1/2 0 1/4; 1/2 1/2 0; 0 1/2 3/4]; % K atoms
x = 0.1484; y = 0.0826; z = 0.1259;
Rf(9:16,:) = [x, y, z; -x, -y, z; y, -x, -z; -y, x, -z;... % O atoms
               -x + 1/2, y, -z + 3/4; x + 1/2, -y, -z + 3/4;...
               -y + 1/2, -x, z + 3/4; y + 1/2, x, z + 3/4];
Rf(17:24,:) = Rf(9:16,:)+0.5*ones(8,3);
Nat = size(Rf,1);
N = Rf>1;
Rf(N) = Rf(N) - 1;
N = Rf<0;
Rf(N) = Rf(N) + 1;
OcupFactor = ones(Nat,1);
Bfactor = (8*pi*pi)*(etaP*ones(4,1); etaK*ones(4,1); etaO*ones(16,1));
Rf = [Rf OcupFactor Bfactor];
SYM = ['P ' ; 'K ' ; 'O2-'];
A = [4 4 16];
nn = size(A,2);
L = A(1);
for m2=size(A,2), L = [L sum(A(1:n))]; end;
nn=0;
for n1:size(L,2)
    LL(n,:)= [nn+1 L(n)];
    nn = L(n);
end;
if (p == 1, fid = fopen([fname '.in'], 'w'); else fid = 1; fprintf('\n'); end;
fprintf(fid, '%.4f %.4f %.4f %.4f %.4f %.4f\n', P(1),P(2),P(3),P(4),P(5),P(6));
for nn=1:size(A,2)
    at = SYM(nn,:);
    a = LL(nn,1); b = LL(nn,2);
    for m=a:b
        fprintf(fid, '%s %.4f %.4f %.4f %.4f %.4f %.4f\n', at,Rf(m,1),Rf(m,2),Rf(m,3),OcupFactor(m),Bfactor(m));
    end;
end;
if (p == 1, fclose(fid); else fprintf('\n'); end;

```

52. kdphistcomp.m

```

function kdphistcomp
%%%%%%% Variation in structure factor square modules with disorder %%%
% Required files: KDP10E10000.sft and KDP150xE10000.sft
% Files generated by routines diffraction.m and kdpcoordfrac.m, and
% available at http://xraybook.if.usp.br/
% Secondary routines required: diffraction.m
%%%%%%% %%%%
fname1 = 'KDP10E10000.sft'; %etaK=etaP=etaO=0.1 (reference)
fname2 = 'KDP150xE10000.sft'; %etaK=etaP=0.1; etaO=0.15;
E = 10000; etal = 0.1; eta2 = 0.15;
I1 = diffraction(E,fname1,0);
I2 = diffraction(E,fname2,0);
N = I2(:,1)==I1(:,1);
Q12 = I2(N,1)';

```

```

pl = I1(N,3)';
pl = pl/max(pl);
p2 = I2(N,3)';
p2 = p2/max(p2);
Dp21 = zeros(size(Q12));
N = pl*0.02;
Dp21(N) = 100*(pl(N)-p2(N))./pl(N);
Q = Q12(pl==max(pl));
aux = -(eta2^2-etal^2);
Y21 = 100*(1-exp(aux*(Q12.*Q12 - Q.*Q)));
hf1=figure(1); clf; set(hf1,'InvertHardcopy', 'off','Color','w')
plot(Q12,Dp21,'r',Q12,Y21,'-k','LineWidth',2)
set(gca,'FontSize',14,'Color',[0.87 0.92 0.98],'Box','on','LineWidth',1)
axis tight
xlabel('Q (A^-1)', 'FontSize',18)
ylabel('Delta |F_{hkl}|^2 (%)', 'FontSize',18)
legend(' \eta_O = 0.15A, \eta_P = \eta_K = 0.10A, ' '\eta_O = \eta_P = \eta_K = 0.15A')

```

53. kdphistogram.m

```

function kdphistogram
%%%%%%%%%%%%%%%%%%%%%%%%%%%%%%%%%%%%%
% Histograms of |Phkl|^2 x Q for KDP with Debye-Waller factor %
% Required files: KDP0E10000.sft, KDP10E10000.sft, KDP15E10000.sft, and %
% KDP20E10000.sft %
% Files generated by routines diffraction.m and kdpcoordfrac.m, and %
% available at http://xraybook.if.usp.br/ %
% Secondary routines required: diffraction.m %
%%%%%%%%%%%%%%%%%%%%%%%%%%%%%%%%%%%%%
E=10000; % X-ray energy (eV) used to calculate files *.sft
hf1=figure(1); clf; set(hf1,'InvertHardcopy', 'off','Color','w')
I = diffraction(E,'KDP0E10000.sft',0);
Q = I(:,1)';
p = I(:,3)';
pmax = max(p);
p = p/pmax;
plot(Q,p,'w','LineWidth',3)
axis([0.98+min(Q) 1.02+max(Q) -0.02 1.02])
set(gca,'FontSize',14,'Color',[0.85 0.7 1.0], 'LineWidth',1)
xlabel('Q (A^-1)', 'FontSize',18)
ylabel('|\Sigma|F_{hkl}|^2 (relative values)', 'FontSize',18)
hold on
I = diffraction(E,'KDP10E10000.sft',0);
Q = I(:,1)';
p = I(:,3)'/pmax;
plot(Q,p,'r','LineWidth',3)
I = diffraction(E,'KDP15E10000.sft',0);
Q = I(:,1)';
p = I(:,3)'/pmax;
plot(Q,p,'y','LineWidth',3)
I = diffraction(E,'KDP20E10000.sft',0);
Q = I(:,1)';
p = I(:,3)'/pmax;
plot(Q,p,'b','LineWidth',3)
legend(' \eta = 0, ' '\eta = 0.10 A, ' '\eta = 0.15 A, ' '\eta = 0.20 A')
plot(Q,ones(size(Q)), '-w','LineWidth',1)
aux = -0.1*0.1;
plot(Q,exp(aux*Q.*Q), '-r','LineWidth',1)
aux = -0.15*0.15;
plot(Q,exp(aux*Q.*Q), '--y','LineWidth',1)
aux = -0.2*0.2;
plot(Q,exp(aux*Q.*Q), '--b','LineWidth',1)
hold off
text(5.5,.85,'KDP', 'FontSize',36,'Color',[.93 .93 .93], 'FontWeight','bold')

```

54. kinematiclimit.m

```

function Z=kinematiclimit(E,fname,H)
%%%%%%%%%%%%%%%%%%%%%%%%%%%%%%%%%%%%%
% Integrated reflectivity via recursive equations %
% Input: %
% E = energy (eV) or wavelength (Angstrom) %
% fname = file *.in with crystal data information %
% H = [h k l] reflection indexes %
% Secondary routines required: rcdarwinprins.m %
% Usage: Z=kinematiclimit(10000,'GaAs.in',[1 1 1]); %
%%%%%%%%%%%%%%%%%%%%%%%%%%%%%%%%%%%%%
M = rcdarwinprins(E,fname,H,0,0);
V = M(1);
d = M(2);
if (V>1000), N = [1 2]*2^8; else N = [1 2]*2^7; end;
S=rcdarwinprins(E,fname,H,N(1),0)';
Idyn(1) = sum(S(2,:).*conj(S(2,:)))*(S(1,2)-S(1,1));
S=rcdarwinprins(E,fname,H,N(2),0)';

```

```

Idyn(2) = sum(S(2,:).*conj(S(2,:)))*(S(1,2)-S(1,1));
alpha = (Idyn(2)-Idyn(1))/(N(2)-N(1));
Sd=rcdarwinprins(E,fname,H,2^30,0)';
maxIdyn = sum(Sd(2,:).*conj(Sd(2,:)))*(Sd(1,2)-Sd(1,1));
Nkin = maxIdyn/alpha;
dN = Nkin/12;
N = [N (1:1:48)*dN];
dN = Nkin/2;
N = [N N(size(N,2))+(1:1:12)*dN];
m = size(N,2);
Idyn = [Idyn zeros(1,m-2)];
for n=3:m
    S=rcdarwinprins(E,fname,H,N(n),0)';
    Idyn(n) = sum(S(2,:).*conj(S(2,:)))*(S(1,2)-S(1,1));
end;
Idyn = Idyn*(100/maxIdyn);
X = N*(d/10000);
alpha = (Idyn(2)-Idyn(1))/(X(2)-X(1));
Ikin = alpha*x;
Nk = find(Ikin<120);
DI = 100*(Ikin-Idyn)./Idyn;
n = find(DI>10, 1 );
if (n>1)
    Xc = ((X(n)-X(n-1))/(DI(n)-DI(n-1)))*(10-DI(n-1)) + X(n-1);
else Xc = d*Nkin/20000;
end;
Z = [X; Idyn]';
hfl=figure(1); clf; set(hfl,'InvertHardcopy','off','Color','w')
plot(X,Idyn,'bo',X(Nk),Ikin(Nk),'k',[Xc Xc],[0 alpha*Xc],'-k','LineWidth',2)
axis([0 max(X) 0 120])
set(gca,'FontSize',14,'Color',[.97 .97 .97],'LineWidth',1)
xlabel('thickness (\mu m)', 'FontSize',18)
ylabel('P_N/P_\infty(\mu m)', 'FontSize',18)
legend('dynamical', 'kinematic')
fprintf('      10% deviation at %6.3f \mu m\n', Xc)
text(Xc,10,['\leftarrow num2str(round(Xc*10)/10) '\mu m'],'FontSize',18)
ha2=axes('Position',[.47 .25 .4 .40]);
ha2=axes('Position',[.47 .25 .4 .40]);
X=Sd(1,:);
Y = Sd(2,:).*conj(Sd(2,:));
xc = sum(X.*Y)/sum(Y);
range = sum(abs(X-xc).*Y)/sum(Y);
Xmin = xc-3*range;
Xmax = xc+3*range;
plot(X,Y,'b','LineWidth',2)
axis([Xmin Xmax 0 1.02*max(Y)])
set(ha2,'FontSize',14,'Color',[1 1 1],'FontName','Arial','LineWidth',1)
 xlabel('|\Delta(theta) /arcsec|', 'FontSize',16)
 ylabel('R(\theta)', 'FontSize',16)
 nlabel=fname(1:find(fname=='.')-1);
 rlabel=['(' num2str(H(1)) ',' num2str(H(2)) ',' num2str(H(3)) ')'];
 text(xc-0.7*range, 0.75*max(Y),nlabel,'FontSize',24,'Color',[0.86 0.86 0.86],'FontWeight','bold')
 text(xc+0.6*range, 0.55*max(Y),rlabel,'FontSize',24,'Color',[0.86 0.86 0.86],'FontWeight','bold')

```

55. lauemethod.m

```

function lauemethod(fname,A,B,TH)
%%%%%%%%%%%%%%%%%%%%%%%%%%%%%%%%%%%%%
% Laue method
%
% Input:
%   fname: file *.in with crystal data information (see sfactor.m)
%   A = [A1,A2,A3] crystallographic direction aligned to the z axis
%   B = [B1,B2,B3] reference direction in the xz plane
%   TH = [thx,thy,thz] rotation matrix R=Rx(thx)Ry(thy)Rz(thz)
% Output file *.laue with list of hkl reflection power and
% spot coordinates on the X-ray film
% Secondary routines required: asfQ.m and ffpmp.m
%
% Usage:
% lauemethod('spodumen.in',[1 0 0],[0 0 1],[10 90 0])
% lauemethod('Si.in',[1 1 1],[-1 -1 2],[0 0 0])
%%%%%%%%%%%%%%%%%%%%%%%%%%%%%%%%%%%%%
wlmin = 1; wlmax = 2; % continuous spectrum, constant intensity approach
% wavelength between wlmin and wlmax (Angstrom)
Lg = 75; % half film width (mm)
D = 50; % film radius (mm),
e = [0 1 0]; % polarization, electric field vibration direction
pix = .2; % film pixel (mm)
sg = 2*pix; % size of diffraction spots, half width at 61% of the maximum
rad = pi / 180;
twopis = 2*pi*i;
hc = 12398.5;
c0 = fix(clock);
code = [num2str(c0(1)) num2str(c0(2)) num2str(c0(3)) num2str(c0(4)) num2str(c0(5)) num2str(c0(6))];
n = regexp(fname,'.in');
if isempty(n) disp(' >>> Unknown file type!!!!'); return; end;
fidin = fopen(fname,'r');
if (fidin==-1) disp(' >>> File ' fname ' not found!!!!'); return; end;

```

```

fout = [fname(1:n-1) code '.laue'];
line = fgets(fidin);
P = sscanf(line,'%f');
if (size(P,2)==6) disp('      >>> Linha 1: a b c alpha beta gamma'); return; end;
n = 0;
line = fgets(fidin);
while (line<=-1)
    n = n + 1;
    w = find(line==' ');
    atm(n,:)= ' ';
    atm(n,1:w-1) = line(1:w-1);
    if isempty(regexp('abcdefghijklmnopqrstuvwxyz',atm(n,2)))
        atomsym(n,:)=[1 w-1];
    else atomsym(n,:)=[2 w-1]; end;
    Rat(n,:)= sscanf(line(w+1:size(line,2)),'%f');
    line = fgets(fidin);
end;
fclose(fidin);
Nat = n; Nchem = 0; AA = zeros(Nat,1); NA = find(AA==0);
while ~isempty(NA)
    n = NA(1);
    M = find(atm(n,1)==atm(:,1) & atm(n,2)==atm(:,2) & atm(n,3)==atm(:,3) & atm(n,4)==atm(:,4));
    Nchem = Nchem + 1;
    AA(M) = Nchem;
    NA = find(AA==0);
    acod(Nchem,:)= atm(n,:);
    asym(Nchem,:)= atomsym(n,:);
end;
clear atm atomsym;
P(4:6) = P(4:6)*rad;
cosphi = cos(P(6)) - cos(P(5))*cos(P(4));
cosphi = cosphi / (sin(P(5))*sin(P(4)));
sinphi = sqrt(1-cosphi*cosphi);
a1 = P(1) * [sin(P(5)) 0 cos(P(5))];
a2 = P(2) * [sin(P(4))*cosphi sin(P(4))*sinphi cos(P(4))];
a3 = P(3) * [0 0 1];
vecA = A(1)*a1 + A(2)*a2 + A(3)*a3;
vecB = B(1)*a1 + B(2)*a2 + B(3)*a3;
e3 = vecA/norm(vecA);
e2 = cross(vecA,vecB);
e2 = e2/norm(e2);
e1 = cross(e2,e3);
M = [e1; e2; e3]';
thx = TH(1)*rad;
thy = TH(2)*rad;
thz = TH(3)*rad;
Rx = [1 0 0; 0 cos(thx) -sin(thx); 0 sin(thx) cos(thx)];
Ry = [cos(thy) 0 sin(thy); 0 1 0; -sin(thy) 0 cos(thy)];
Rz = [cos(thz) -sin(thz) 0; sin(thz) cos(thz) 0; 0 0 1];
R = Rx*Ry*Rz;
MR = M*R';
a = a1*MR;
b = a2*MR;
c = a3*MR;
air = cross(b,c);
Vc = air*a';
air = air/Vc;
a2r = cross(c,a)/Vc;
a3r = cross(a,b)/Vc;
hmax = floor(2.0 / (wlmin * norm(air)));
kmax = floor(2.0 / (wlmin * norm(a2r)));
lmax = floor(2.0 / (wlmin * norm(a3r)));
H = [-hmax:hmax];
K = [-kmax:kmax];
L = [-lmax:lmax];
m = 0;
for nh = 1:2*hmax+1
    for nk = 1:2*kmax+1
        for nl = 1:2*lmax+1
            h = H(nh); k = K(nk); l = L(nl);
            q = h*air + k*a2r + l*a3r;
            if (q(3)<0)
                q2 = q*q';
                w1 = -2*q(3)/q2;
                if ((wl<w1max) && (wl>wlmin))
                    sp = wl*q + [0 0 1];
                    z = D*tan(asin(sp(2)));
                    if (z*z<Lg*Lg)
                        m = m + 1;
                        HKL(m,:)= [h k l];
                        WL(m,1)= wl;
                        Yf(m,1)= z;
                        Xf(m,1)= D*atan2(sp(1),-sp(3));
                        Phkl2(m,1)= sfactorQ(Nchem,acod,asym,hc/wl,sqrt(q2),AA,twopii,Rat,[h k l]);
                        p = cross(sp,cross(e,sp));
                        p = p * p';
                        Ahkl(m,1)= p*w1*Phkl2(m)/q2;
                    end;
                end;
            end;
        end;
    end;
end;

```

```

        end;
    end;
end;
Nrefl = m;
X = Ahkl1;
Nmax = [];
while (sum(X)>0)
    NN = find(X==max(X));
    X(NN) = 0;
    Nmax = [Nmax; NN];
end;
Nrefl = size(Nmax,1);
HKL = HKL(Nmax,:);
WL = WL(Nmax);
Yf = Yf(Nmax);
Xf = Xf(Nmax);
Phkl2 = Phkl2(Nmax);
Ahkl1 = Ahkl1(Nmax);
clear Nmax X;
invF2max = 100/max(Phkl2);
invAmax = 100/max(Ahkl1);
fidout = fopen(fout,'w');
fprintf(fidout,'n %s, A = [%2d %2d %2d], B = [%5.3f %5.3f %5.3f]\n',...
    fname,A(1),A(2),A(3),B(1),B(2),B(3),TH(1),TH(2),TH(3));
fprintf(fidout,'-----|-----|-----|-----|\n');
fprintf(fidout,' | h k l | Phkl|^2 | w(A) | Phkl X(mm) Y(mm) |\n');
fprintf(fidout,'-----|-----|-----|-----|\n');
for m=1:Nrefl
    fprintf(fidout,' | %3d %3d %3d | %7.1f(%5.1f%) | %8.6f | %9.1f %9.3f %9.3f | \n',HKL(m,1),HKL(m,2),...
        HKL(m,3),...
        Phkl2(m),invF2max*Phkl2(m),WL(m),Ahkl1(m),Xf(m),Yf(m));
end;
fprintf(fidout,'-----|-----|-----|-----|\n');
fclose(fidout);

Nx = floor(pi*D/pix);
Ny = floor(Lg/pix);
perimeter = Nx*pix;
width = Ny*pix;
Z = zeros(2*Ny+1,2*Nx+1);
for m=1:Nrefl
    nx = fix(Xf(m)/pix)+Nx+1;
    ny = fix(Yf(m)/pix)+Ny+1;
    Z(ny,nx) = Z(ny,nx) + Ahkl1(m);
end;
Ng = floor(10*sg/pix);
Xg = (-Ng:Ng)*pix;
Xg = Xg.*Xg;
for nx=1:2*Ng+1
    for ny=1:2*Ng+1
        Xg2(ny,nx) = Xg(ny) + Xg(nx);
    end;
end;
G = (1/(sg*sg*2*pi))*exp((-1/(2*sg*sg))*Xg2);
Zg = [zeros(2*Ny+1+2*Ng,Ng) zeros(Ng,2*Nx+1); Z zeros(Ng,2*Nx+1)] zeros(2*Ny+1+2*Ng,Ng);
for nx=1:2*Nx+1
    for ny=1:2*Ny+1
        Z(ny,nx) = sum(sum(G.*Zg(ny:2*Ng+ny,nx:2*Ng+nx)));
    end;
end;
h1=figure(1); clf; set(h1,'InvertHardcopy','off','Color','w')
imagesc(perimeter*[-1 1],width*[-1 1],log10(Z+1))
axis image
set(gca,'Ydir','normal','FontName','Arial','FontSize',14,'LineWidth',1)
colorbar jet;
colorbar('FontSize',14,'Location','EastOutside','LineWidth',1)
ylabel('film width (mm)', 'FontSize',18)
xlabel('film length (mm)', 'FontSize',18)
text(1.274*perimeter,-width/3,5000,'Log(I) (arb. units)', 'FontSize',14,'Rotation',90)

function F2 = sfactorQ(Nchm,acod,asym,E,Q,AA,twopii,R,H)
for n=1:Nchm
    aux = fpfp(acod(n,1:asym(n,1)),E);
    fres(n) = aux(2)+li1*aux(3);
end;
x = 0.5*Q;
x2 = x*x;
F = 0;
for n=1:Nchm
    fn = asfQ(acod(n,1:asym(n,2)),x) + fres(n);
    NA=find(AA==n)';
    F = F + fn*sum(exp(twopii*(R(NA,1:3)*H')).*R(NA,4).*exp((-x2)*R(NA,5)));
end;
F2 = F*conj(F);

```

56. orientcryst.m

```

function orientcryst(wl,P,A,B,TH,H)
% Alignment of Single Crystals
%
% Input:
%   wl = wavelength (Angstrom) or energy (eV)
%   P = [a b c alpha beta gamma] parameters of the unit cell (in Angstrom and degree)
%   A = [A1,A2,A3] crystallographic direction parallel to the z axis (incident beam)
%   B = [B1,B2,B3] reference direction in the xz plane
%   TH = [thx,thy,thz], orientation matrix R=Rx(thx)Ry(thy)Rz(thz)
%   H = [h k l] reflection indexes, use TH = [1] or [] to orient reflection hkl with
%       chi or phi alignment, respectively
%
% Usage:
% orientcryst(1.540562,[9.4620 8.3920 5.2210 90.00],[1 0 0],[0 1 0],[0 0 0],[0 0 2])
% orientcryst(1.540562,[9.4620 8.3920 5.2210 90.00],[1 0 0],[0 1 0],[],[0 0 2])
% orientcryst(1.540562,[9.4620 8.3920 5.2210 90.00],[1 0 0],[0 1 0],[1],[0 0 2])
%%%%%
rad = pi / 180;
if (wl < 1000), E = 12398.5 / wl; else E = wl; wl = 12398.5 / E; end;
if isempty(P), return; end;
nm = size(P);
if (nm(1)*nm(2)==1)
    P(1:3) = P(1)*ones(1,3);
    P(4:6) = [90 90 90];
elseif (nm(1)*nm(2)==2)
    P(1:3) = [P(1) P(1) P(2)];
    P(4:6) = [90 90 90];
end;
P(4:6) = P(4:6)*rad;
cosphi = cos(P(6)) - cos(P(5))*cos(P(4));
cosphi = cosphi / (sin(P(5))*sin(P(4)));
sinphi = sqrt(1-cosphi*cosphi);
    a1 = P(1) * [sin(P(5)) 0 cos(P(5))];
    a2 = P(2) * [sin(P(4))*cosphi sin(P(4))*sinphi cos(P(4))];
    a3 = P(3) * [0 0 1];
    vecA = A(1)*a1 + A(2)*a2 + A(3)*a3;
    vecB = B(1)*a1 + B(2)*a2 + B(3)*a3;
    e3 = vecA/norm(vecA);
    e2 = cross(vecA,vecB);
    e2 = e2/norm(e2);
    e1 = cross(e2,e3);
M = [e1; e2; e3];
a = a1*M;
b = a2*M;
c = a3*M;
    alr = cross(b,c);
    Vc = alr*a';
    alr = alr/Vc;
    a2r = cross(c,a)/Vc;
    a3r = cross(a,b)/Vc;
Q = H(1,1)*alr + H(1,2)*a2r + H(1,3)*a3r;
modQ = norm(Q);
if (size(TH,2)==3)
    thx = TH(1)*rad;
    thy = TH(2)*rad;
    thz = TH(3)*rad;
    Rx = [1 0 0; 0 0 cos(thx) -sin(thx); 0 sin(thx) cos(thx)];
    Ry = [cos(thy) 0 sin(thy); 0 1 0; -sin(thy) 0 cos(thy)];
    Rz = [cos(thz) -sin(thz) 0; sin(thz) cos(thz) 0; 0 0 1];
    R = Rx*Ry*Rz;
else
    thbragg = asin(0.5*wl*modQ);
    if isempty(TH)
        thy = pi/2-acos(Q(3)/modQ) + thbragg;
        x = Q(1); y = Q(2);
        thz = -atan2(y,x);
        Rx = [cos(thz) -sin(thz) 0; sin(thz) cos(thz) 0; 0 0 1];
        Ry = [cos(thy) 0 sin(thy); 0 1 0; -sin(thy) 0 cos(thy)];
        R = Ry*Rz;
    fprintf(' Chi alignment: R = RyRz, thz = %9.4f, thy = %9.4f,
            thBragg = $9.4f\n',thz/rad,thy/rad,thbragg/rad)
    else
        thy = acos(Q(1)/modQ) + thbragg;
        x = Q(2); y = Q(3);
        thz = 0.5*pi - atan2(y,x);
        Rx = [1 0 0; 0 0 cos(thx) -sin(thx); 0 sin(thx) cos(thx)];
        Ry = [cos(thy) 0 sin(thy); 0 1 0; -sin(thy) 0 cos(thy)];
        R = Ry*Rx;
    fprintf(' Phi alignment: R = RyRx, thx = %9.4f, thy = %9.4f,
            thBragg = $9.4f\n',thx/rad,thy/rad,thbragg/rad)
    end;
end;
MR = M*R';
a = a1*MR;
b = a2*MR;
c = a3*MR;
    alr = cross(b,c);
    Vc = alr*a';

```

```

    alr = alr/Vc;
    a2r = cross(c,a)/Vc;
    a3r = cross(a,b)/Vc;
    Q = H(1,1)*alr + H(1,2)*a2r +H(1,3)*a3r;
    O = [ 0 0 0 ];
    d = a + b + c;
    A = b + c;
    B = a + c;
    C = a + b;
    D = 0.5*d;
    modD = 1.5*norm(D);
    vecA = modDe3*MR;
    vecB = modD*el1*MR;
    Q = modD*(Q/norm(Q));
    hf1 = figure(1); clf; set(hf1,'InvertHardcopy','off','Color','w')
    vector(O,a,-D,'b',1,' a');
    hold on
    vector(O,b,-D,'b',1,' b');
    vector(O,c,-D,'b',1,' c');
    vector(O,[ 0 0 1.5*modD],[ 0 0 ],'r',2,' \uparrowarrow X-rays ');
    vector(O,Q,[ 0 0 ],'m',2,' Q');
    vector(O,vecB,[ 0 0 ],'k',2,' B');
    vector(O,vecA,[ 0 0 ],'k',2,' A');
    vector(B,a,-D,'b',1,[ 1 ]);
    vector(B,C,-D,'b',1,[ 1 ]);
    vector(B,B,-D,'b',1,[ 1 ]);
    vector(C,a,-D,'b',1,[ 1 ]);
    vector(C,B,-D,'b',1,[ 1 ]);
    vector(C,d,-D,'b',1,[ 1 ]);
    vector(A,b,-D,'b',1,[ 1 ]);
    vector(A,c,-D,'b',1,[ 1 ]);
    vector(A,d,-D,'b',1,[ 1 ]);
    plot3(modD*[ 1 -1 1 -1 -1 1 ],modD*[ -1 -1 1 1 -1 -1 ],modD*[ 1 1 1 -1 -1 -1 ],'k','LineWidth',1 )
    plot3(modD*[ -1 -1 ],modD*[ -1 -1 ],modD*[ 1 -1 ],'k','LineWidth',1 )
    plot3(-D(1),-D(2),-D(3),'b.')
    axis image
    axis(modD*[ -1 1 -1 1 -1 1 ])
    hold off
    text(0,0,0,'O')
    set(gca,'FontSize',18,'Color',[ 0.97 0.97 0.97 ],'LineWidth',1)
    grid
    xlabel('X (A)', 'FontSize',18)
    ylabel('Y (A)', 'FontSize',18)
    zlabel('Z (A)', 'FontSize',18)
view(164,18)

function vector(A,B,T,cor,linha,nome)
V = [(A+T)' (B+T)' ];
plot3(V(1,:),V(2,:),V(3,:),cor,'LineWidth',linha)
if ~isempty(nome)
    text(V(1,2),V(2,2),V(3,2),nome,'Color',cor,'FontSize',18)
end;
```

57. pdbboxdfrac.m

```

function pdbboxdfrac(fname,OP)
%%%%%%%%%%%%%%%%%%%%%%%%%%%%%%%%%%%%%
% To generate crystal data information files (*.in) from %
% *.pdb file format (see http://www.wwpdb.org/) %
%%%%%%%%%%%%%%%%%%%%%%%%%%%%%%%%%%%%%
% Input: %
% fname = *.pdb file %
% OP = space group number %
% Output: save file *.in as described in routine sfactor.m %
% Usage: %
% >>> pdbboxdfrac('1TRZ.pdb',146) %
%%%%%%%%%%%%%%%%%%%%%%%%%%%%%%%%%%%%%
n = regexp(fname,'.pdb');
if isempty(n), disp(' >>> Unknown file type!!!!'); return; end;
fout = [fname(1:-1) '.in'];
fidin = fopen(fname,'r');
if (fidin==1), disp(' >>> File \' fname \' not found!!!!'); return; end;
line = fgets(fidin); n=0; m=0;
while (line>=1)
    switch line(1:5)
        case {'CRYST'}
            P = sscanf(line(7:54),'%f');
        case {'SCALE'}
            m = m + 1;
            SC(m,:) = sscanf(line(11:40),'%f');
        case {'ATOM ','HETAT'}
            n = n + 1;
            Rf(n,: ) = [(SC*sscanf(line(31:54),'%f'))' sscanf(line(55:66),'%f')];
            A(n,:) = line(77:78);
    end;
    line = fgets(fidin);
end;
fclose(fidin);
```

```

N = size(Rf,1); Nchem = 0; Achem = zeros(N,1); NA = 1;
while ~isempty(NA)
    n = NA(1);
    Mn = find(A(n,1)==A(:,1) & A(n,2)==A(:,2));
    Nchem = Nchem + 1;
    OCF(Nchem) = sum(Rf(Mn,4));
    Achem(Mn) = Nchem;
    if (A(n,1)~=' ')
        Atom(Nchem,:) = [A(n,1) lower(A(n,2))];
    else
        Atom(Nchem,:) = [A(n,2) ' '];
    end;
    NA = find(Achem==0);
end;
fprintf(' Atoms in the asymmetric unit with occupation factor (...)\n');
for n=1:Nchem
    x = size(find(Achem==n),1);
    fprintf(' %1.0f(%4.2f)%s',x,OCF(n)/x,Atom(n,:));
end;
fprintf('\n');
fid = fopen('fout','w');
fprintf(fid,'%6.4f %6.4f %6.4f %6.4f %6.4f\n',P(1),P(2),P(3),P(4),P(5),P(6));
for n=1:N
    R = symop(OP,Rf(n,1:3));
    for m=1:size(R,1)
        fprintf(fid,'%s %8.4f %8.4f %8.4f %6.3f %6.2f\n',Atom(Achem(n),:),R(m,1),R(m,2),R(m,3),Rf(n,4),Rf(n,5));
    end;
end;
fclose(fid);

function R=symop(OP,Rf)
X=Rf(1); Y=Rf(2); Z=Rf(3);
switch OP
    case {4}
        R(1,:) = [X,Y,Z; -X,Y+1/2, -Z];
    case {18}
        R(1,:) = [X,Y,Z; -X,-Y,Z; -X+1/2,Y+1/2, -Z; X+1/2,-Y+1/2, -Z];
    case {96}
        R = [ X, Y, Z; -X, -Y, Z; -Y+1/2,X+1/2,Z+3/4; Y+1/2,-X+1/2, Z+1/4;
              -X+1/2,Y+1/2,-Z+3/4; X+1/2,-Y+1/2,-Z+1/4; Y, X, -Z, -Y, -X,-Z+1/2];
    case {146}
        R = [ X, Y, Z; -Y, X-Y, Z; X-Y, Z; -X+Y, -X, Z;
              X+2/3,Y+1/3,Z+1/3; -Y+2/3,X-Y+1/3,Z+1/3; -X+Y+2/3,-X+1/3,Z+1/3;
              X+1/3,Y+2/3,Z+2/3; -Y+1/3,X-Y+2/3,Z+2/3; -X+Y+1/3,-X+2/3,Z+2/3];
    case {169}
        R = [ X, Y, Z; -Y, X-Y,Z+1/3; -X+Y,-X,Z+2/3;
              -X,-Y,Z+1/2; Y,-X+Y,Z+5/6; X-Y, X,Z+1/6];
    case {197}
        R = [ X, Y, Z; -X,-Y, Z; -X,Y, -Z; X,-Y,-Z; Z, X, Y; Z,-X,-Y;
              -Z,-X,Y; -Z, X,-Y; Y,Z, X,-Y; Z,-X; Y,-Z,-X; -Y,-Z, X];
        R = [R; R+0.5*ones(12,3)];
    case {...} % include other "case" to add an operation symmetry
        % from 230 space groups, see "International Tables for
        % Crystallography (2006). Vol. A, ch. 7.1, pp. 112-717
    otherwise, R = [X,Y,Z];
end;

```

58. photonsonpsp.m

```

function I=photonsonpsp(thx,thy,thz,D,L,pixel,wl,N)
%%%%%%%%%%%%%%%%%%%%%%%%%%%%%%%%%%%%%
% Intensity pattern with statistic of N counts
% Input:
% thx, thy, thz, D, L, pixel, and wl defined in routine benzeneonpsp.m
% N = number of photons (counts) scattered on the film
% Output: I = counts on the pixel array
% Secondary routines required: benzeneonpsp.m and photonstatistic.m
% Usage:
% >> I = photonsonpsp(30,0,90,50,200,2,20000,1e+4);
%%%%%%%%%%%%%%%%%%%%%%%%%%%%%%%%%%%%%
dz = pixel;
n = floor(2*L/dz);
LimZ = 0.5*n*dz;
Y=benzeneonpsp(thx,thy,thz,D,L,pixel,wl,0);
I=photonstatistic(Y,N)+1;
h1=figure(1);
clf
set(h1,'InvertHardcopy', 'off','Color','w')
imagesc([-LimZ LimZ],[-1 1]*D*pi,log10(I))
axis image
set(gca,'FontSize',14,'LineWidth',1,'YTick',[-150 -100 -50 0 50 100 150])
colormap(hot)
colorbar('XColor','k','YColor','k','FontSize',14,'Location','East','LineWidth',1)
 xlabel('film width (nm)', 'FontSize',18)
 ylabel('film length (nm)', 'FontSize',18)
text(0,0.5000,'Log(número de fótons / pixel)', 'FontSize',18,'Rotation',90,'Color','k')

```

59. photonstatistic.m

```
function Z=photonstatistic(M,N)
soma = sum(sum(M));
M = M*(1/soma);
Z = zeros(size(M));
for np = 1:N
    aux = 0; photon = rand; nn = 0;
    while (aux<photon)
        nn = nn + 1;
        aux = aux + M(nn);
    end;
    Z(nn) = Z(nn) + 1;
end;
```

60. polymer.m

```
function M=polymer(Nm,jct,sofq)
%%%%%%%%%%%%%%%%%%%%%%%%%%%%%%%%%%%%%
%           Scattering curve S(Q) of a polymer or
%           its gyration radius Rg
%%%%%%%%%%%%%%%%%%%%%%%%%%%%%%%%%%%%%
% Input:
%   Nm = number of monomers in the chain
%   jct = 1 for limited junction, otherwise free junction (RW model)
%   sofq = 0 for gyration radius
% Output: M = [Q; S]', S(Q) curve           if sofq ~= 0
%         M = Rg2, mean square radius (Angstrom^2) if sofq = 0
% Secondary routines required: polymerchain.m
% Usage:
% >> M = polymer(2000,0,1);
%%%%%%%%%%%%%%%%%%%%%%%%%%%%%%%%%%%%%
L = 1.54; % monomer length (Angstrom)
R = 10*polymerchain(Nm,jct,0);
Rg2theo = Nm*L/6;
if (sofq==0)
    Qmax = 18/sqrt(Rg2theo);
    dQ = Qmax/100;
    Q = 0:dQ:Qmax;
    Q(1) = 1e-8;
    Nq = size(Q,2);
    S = zeros(1,Nq);
    for jj=1:Nm
        rj = R(jj,1);
        for kk = jj+1:Nm
            rjk = R(kk,1)-rj;
            S = S + cos(rjk*Q);
        end;
    end;
    S = 2*S;
    M = [Q; S]';
else
    M = sum(sum(R.*R))/Nm;
end;
```

61. polymerchain.m

```
function R=polymerchain(Nm,jct,prn)
%%%%%%%%%%%%%%%%%%%%%%%%%%%%%%%%%%%%%
% Virtual chain of monomers with free or limited junction
%%%%%%%%%%%%%%%%%%%%%%%%%%%%%%%%%%%%%
% Input:
%   Nm = number of monomers in the chain
%   jct = 1 for limited junction, otherwise free junction (RW model)
%   prn = 0 to suppress graphic window
% Output: R, array of 3D coordinates of the monomers
% Usage:
% >> R = polymerchain(1000,0,1);
%%%%%%%%%%%%%%%%%%%%%%%%%%%%%%%%%%%%%
L = 0.154; % monomer length (nm)
if (jct==1)
    phi = [-1 0 1]*(2*pi/3);
    T = [(71+2*(2*rand(Nm,1)-1))*(pi/180) phi fix(2.99999999999*rand(Nm,1))+1]';
else
    T = [pi*rand(Nm,1) (2*pi)*rand(Nm,1)];
end;
R(1,:) = [0 0 0];
M = eye(3);
for n=1:Nm
    st = sin(T(n,1));
    ct = cos(T(n,1));
    sp = sin(T(n,2));
    cp = cos(T(n,2));
    M = [ct*cp ct*sp -st; -sp cp st*sp ct]*M;
    R(n+1,:) = R(n,:)+L*M(3,:);
end;
```

```

Nm = Nm + 1;
rc = sum(R)/Nm;
R(:,1) = R(:,1)-rc(1);
R(:,2) = R(:,2)-rc(2);
R(:,3) = R(:,3)-rc(3);
if (prn==0)
n24;
Ncor = 0.02*(0:1:n)';
n = n + 1;
C = [zeros(n,1) zeros(n,1) 1-Ncor;
      Ncor zeros(n,1) 0.5*ones(n,1);
      0.5*ones(n,1) zeros(n,1) 0.5-Ncor;
      0.5+Ncor zeros(n,1) zeros(n,1)];
x = Nm/100;
hf1 = figure(1); clf; set(hf1,'InvertHardcopy','off','Color','w')
plot3(R(1,1),R(1,2),R(1,3),'b.')
hold on
for nn2:Nm
    plot3(R(n-1:n,1),R(n-1:n,2),R(n-1:n,3),'Color',C(fix((n-1)/x)+1,:),'LineWidth',1.2)
end;
plot3(R(Nm,1),R(Nm,2),R(Nm,3),'r.')
hold off
set(gca,'FontSize',14,'Color',[0.93 0.93 0.93],'Box','on','LineWidth',1)
axis image
axis tight; grid
xlabel('X (nm)', 'FontSize',18)
ylabel('Y (nm)', 'FontSize',18)
zlabel('Z (nm)', 'FontSize',18)
end;

```

62. polymerkratky.m

```

function polymerkratly
%%%%%%%%%%%%%%%%%%%%%%%%%%%%%%%%%%%%%
% Comparison of structural function S(Q) for systems of %
% polymers with different weight %
% Required files: 'polymer2k_1to500.dat', 'polymer6k_1to500.dat', and %
% 'polymer10k_1to500.dat' %
% Files generated by routine polymersystem.m, and available at %
% http://xraybook.if.usp.br/
%%%%%%%%%%%%%%%%%%%%%%%%%%%%%%%%%%%%%
fn2 = 'polymer2k_1to500.dat'; Nma = 2000;
fn6 = 'polymer6k_1to500.dat'; Nmb = 6000;
fn10 = 'polymer10k_1to500.dat'; Nmc = 10000;
fnc = load(fn2);
M = load(fnc)';
Qa=M(1,:);
Sa=M(2,:);
M = load(fnb)';
Qb=M(1,:);
Sb=M(2,:);
M = load(fnc)';
Qc=M(1,:);
Sc=M(2,:);
L = 1.54; % monomer length (Angstrom)
Rg2a = 770;
Rg2b = 2200;
Rg2c = 3730;
Ua = Rg2a*(Qa.*Qa);
Ub = Rg2b*(Qb.*Qb);
Uc = Rg2c*(Qc.*Qc);
Ya = 2*(exp(-Ua)-1+Ua)./(Ua.*Ua);
Ya(1) = 1;
Ya = Ya*Sa(1);
Yb = 2*(exp(-Ub)-1+Ub)./(Ub.*Ub);
Yb(1) = 1;
Yb = Yb*Sb(1);
Yc = 2*(exp(-Uc)-1+Uc)./(Uc.*Uc);
Yc(1) = 1;
Yc = Yc*Sc(1);
hf1 = figure(1);
clf
set(hf1,'InvertHardcopy','off','Color','w')
N=1:size(Qa,2);
Ur=sqrt(Ua(N));
Q2 = Qa(N).^2;
plot(Ur,Sa(N).*Q2,'-bo',Ur,Ya(N).*Q2,'--k','MarkerFaceColor','w','MarkerSize',6,'LineWidth',1.5)
N=1:size(Qb,2);
Ur=sqrt(Ub(N));
Q2 = Qb(N).^2;
plot(Ur,Sb(N).*Q2,'-rs',Ur,Yb(N).*Q2,'--k','MarkerFaceColor','w','MarkerSize',6,'LineWidth',1.5)
N=1:size(Qc,2);
Ur=sqrt(Uc(N));
Q2 = Qc(N).^2;
plot(Ur,Sc(N).*Q2,'-rs',Ur,Yc(N).*Q2,'--k','MarkerFaceColor','w','MarkerSize',6,'LineWidth',1.5)
hold off
set(gca,'FontSize',14,'Color',[0.894 0.941 0.902],'LineWidth',1)

```

```

xlabel('QR_g','FontSize',18)
ylabel('N_m^2Q^2S(Q)','FontSize',18)
text(13,47000,'N_m = 10000','FontSize',18,'Color','r')
text(13,26000,'N_m = 6000','FontSize',18,'Color','m')
text(13,5000,'N_m = 2000','FontSize',18,'Color','b')
axis([0 17.5 0 5.9e+4])

```

63. polymerRg.m

```

function polymerRg(N,Nm)
%%%%%%%%%%%%%%%%%%%%%%%%%%%%%%%%%%%%%
% Statistical distribution of gyration radius for %
% free and limited junction models %
% Ensemble: N polymers with Nm monomers each %
% Secondary routines required: polymer.m %
% Usage: %
% >> polymerRg(1000,2000) %
%%%%%%%%%%%%%%%%%%%%%%%%%%%%%%%%%%%%%
for n=1:N
    Ra(n,1)=polymer(Nm,0,0);
    Rb(n,1)=polymer(Nm,1,0);
end;
Ra = 0.01*Ra;
Rb = 0.01*Rb;
du = 20/8;
Umax = max(Ra);
Ua = 0:du:Umax;
p = zeros(size(Ua));
for n=1:N
    k = fix(Ra(n)/du)+1;
    p(k) = p(k) + 1;
end;
pa = (100/du) * p / sum(p);
Rg2a = sum(Ra)/N;
xa=find(abs(Ua-Rg2a)<du);
N = size(Rb,1);
Umax = max(Rb);
Ub = 0:du:Umax;
p = zeros(size(Ub));
for n=1:N
    k = fix(Rb(n)/du)+1;
    p(k) = p(k) + 1;
end;
pb = (100/du) * p / sum(p);
Rg2b = sum(Rb)/N;
xb=find(abs(Ub-Rg2b)<du);
hfl = figure(1);
clf
set(hfl,'InvertHardcopy','off','Color','w')
plot([Rg2a Rg2a],[0 pa(xa(1))],'-k',Ua,pa,'-k. ','LineWidth',2)
hold on
plot([Rg2b Rg2b],[0 pb(xb(1))],'-b',Ub,pb,'-b. ','LineWidth',2)
hold off
set(gca,'FontSize',14,'Color',[0.93 0.93 0.93],'LineWidth',1)
xlabel('R_g^2 (nm^2)', 'FontSize',18)
ylabel('number of occurrences (/nm^2)', 'FontSize',18)
text(Rg2a,pa(xa(1)), ' \leftarrow free','FontSize',18,'Color','k')
text(Rg2b,pb(xb(1)), ' \leftarrow limited','FontSize',18,'Color','b')
axis tight

```

64. polymersystem.m

```

function polymersystem(fname,Nm,jct,N)
%%%%%%%%%%%%%%%%%%%%%%%%%%%%%%%%%%%%%
% Scattering curve S(Q) by systems of polymers %
%%%%%%%%%%%%%%%%%%%%%%%%%%%%%%%%%%%%%
% Input %
% fname = output file name %
% Nm = number of monomers in each polymer %
% jct = 1 for limited junction, otherwise free junction (RW model) %
% N = number of polymers in the system %
% Output file fname with the S(Q) curve for the system of N polymers %
% Secondary routines required: polymer.m %
% Usage: %
% >> polymersystem('polymer2k_1a500.dat',2000,0,500) %
%%%%%%%%%%%%%%%%%%%%%%%%%%%%%%%%%%%%%
for n=1:N
    M=polymer(Nm,jct,1);
    Y(:,n)=M(:,2);
end;
S = sum(Y,2)/N;
M = [M(:,1) S];
save(fname,'M','-ascii')

```

65. quartzgofu.m

```

function M=quartzgofu(E,tthmax,conv)
%%%%%%%%%%%%%%%%%%%%%%%%%%%%%%%%%%%%%
%   RDF obtained by inverse FT of the interference function S(Q) in
%   a cluster of disordered alpha-quartz
%
% Input:
%   E, energy (keV)
%   tthmax, maximum scattering angle (from 10 to 180 deg)
%   conv = 1 to convolve g(u) with a rectangular function of unit area
%         and width 2*pi/Qf
%
% Output: M=[U; g]'; g(u) curve
%
% Secondary routines required: quartzIofQ.m
%
% Required files: clusterN12d2_1to10.dat and clusterN12d2gofu.dat
%                 from http://xraybook.if.usp.br/
%
% Usage: M=quartzgofu(30,180,0);
%%%%%%%%%%%%%%%%%%%%%%%%%%%%%%%%%%%%%
if (E>100, E = 0.001*E; end; wl = 12.3985/E;
Qmax = 4*pi/wl;
if (tthmax<10), disp('Wide angle scattering, from 10 to 180 deg!!!'); return;
elseif (tthmax>180), tthmax = 180;
end;
QF = Qmax*sind(0.5*tthmax);
S=quartzIofQ(wl,0,'clusterN12d2_1to10.dat');
Nq = S(:,1)<=QF;
Q = S(Nq,1)';
I = S(Nq,2)';
S = S(Nq,3)';
GofU = load('clusterN12d2gofu.dat');
U = GofU(:,1)';
g0 = GofU(:,2)';
hfi=figure(1); clf; set(hfi,'InvertHardcopy', 'off','Color','w')
plot(U,g0,'-ro','LineWidth',1,'MarkerFaceColor','y','MarkerSize',5)
set(gca,'FontSize',14,'FontName','Arial','Color',[0.93 0.93 0.93],'LineWidth',1)
xlabel('u (A)', 'FontSize',18)
ylabel('g(u)', 'FontSize',18)
U=U(Us0.1);
Nu = size(U,2);
Np = Q*0.7;
Q = Q(Np); S=S(Np);
rho = 9/113.01;
dQ = (Q(3)-Q(2))/(2*pi*pi*rho);
g = zeros(1,Nu);
for n=1:Nu
    u=U(n);
    g(n) = 1+(dQ/u)*sum((S-1).*Q.*sin(Q*u));
end;
if (conv==1)
    du = U(3)-U(2);
    wdt = 2*pi/Qf;
    Nw = floor(0.5*wdt/du);
    gexp = zeros(1,Nu);
    for n=1:Nu
        nmin = n-Nw;
        nmax = n+Nw;
        if (nmin<1), gexp(n) = sum(g(1:nmax))/nmax;
        elseif (nmax>Nu), gexp(n) = sum(g(nmin:Nu))/(Nu-nmin+1);
        else gexp(n) = sum(g(nmin:nmax))/(2*Nw+1);
        end;
    end;
    g=gexp;
end;
hold on
plot(U,g,'k','LineWidth',1.5)
hold off
gmax = max(g0);
aux = max(g);
if (aux>gmax), gmax=aux; end;
gmin = min(g);
if (gmin<0), gmin=0; end;
dg = 0.02*(gmax-gmin);
axis([0.1 13.1 gmin-dg gmax+dg])
TTh = 2*asind(Q/Qmax);
Imin = min(I);
Imax = max(I);
DI = 0.02*(Imax-Imin);
ha2=axes('Position',[.4 .45 .48 .43]);
plot(TTh,I,'k','LineWidth',2)
set(ha2,'FontSize',14,'FontName','Arial','Color',[1 1 1],'LineWidth',1)
grid
xlabel('2 theta (deg)');
ylabel('intensity (cps)');
axis([TTh(1) 0.2*max(TTh) Imin-DI Imax+DI])
N = Q*2.12;
alpha = 0.75*Imax/max(I(N));
hold on;
plot(TTh(N),alpha*I(N)+0.25*Imax,'b','LineWidth',2)
hold off;
text(0.15*max(TTh),0.5*Imax,[' x' num2str(0.1*round(10*alpha))], 'FontSize',18, 'Color', 'b')
M = [U; g]';

```

66. quartzIofQ.m

```

function M=quartzIofQ(wl,prn, fname)
%%%%%
% Calculates S(Q) and I(Q) for clusters of disordered alpha-quartz %
% Input: %
%   wl = wavelength (Angstrom) or energy (eV) %
%   prn = 0 to suppress graphic window %
%   fname = file of RDFs in a n-by-5 array format (see quartzrdf.m), e.g. %
%           'clusterN12dX_1to10.dat' from http://xraybook.if.usp.br/ %
% Output M=[Q; I; S]'; n-by-3 array for I(Q) and S(Q) curves %
% Secondary routines required: asfQ.m, fpfp.m, and csfq.m %
% Usage: M=quartzIofQ(1.54,1,'clusterN12d20_1to10.dat'); %
% Note: resonant and Compton scatterings are included. %
%%%%%
if (wl < 100), E = 12398.5 / wl; else E = wl; wl = 12398.5 / E; end;
Qmax = 4*pi/wl;
S=load(fname);
U = S(:,1)';
Uc = 21.07; y = exp(-5.2e-5*(U-Uc).^2.505); y(U<Uc)=1;
y = 1 - y; % <-| correction explained in routine quartzrdfplot.m
gsi = S(:,3)'*y; gox = S(:,4)'*y; gsoxi = S(:,5)'*y;
Vc = 113.01; % unit cell volume (Angstrom^3) containing 3Si and 6O
rhoSi = 3/Vc;
rhoOx = 6/Vc;
rho = rhoSi + rhoOx;
dQ = Qmax/5000;
Q = 0:dQ:Qmax;
Q(1) = 1e-8;
Nq = size(Q,2);
Z = fpfp('Si',E);
fsi = asfQ('Si',(0.25/pi)*Q) + Z(1,2) + li*Z(1,3);
Z = fpfp('O',E);
fox = asfQ('O',(0.25/pi)*Q) + Z(1,2) + li*Z(1,3);
ASi = real(fsi.*conj(fsi));
AOx = real(fox.*conj(fox));
fm2 = (1/3)*ASi + (2/3)*AOx;
ASi = (rhoSi*rhoSi)*ASi(1);
AOx = (rhoOx*rhoOx)*AOx(1);
ASi0x = (rhoSi*rhoOx)*real(fox(1).*conj(fsi(1)));
AOxSi = (rhoOx*rhoSi)*real(fox(1).*conj(fsi(1)));
w2 = (ASi+AOx+ASi0x+AOxSi);
g = (ASi*gsi + AOx*gox + ASi0x*gsoxi + AOxSi*goxsi)/w2;
du = U(3)-U(2);
% GofU = [U; g]; save('clusterN12d2gofu.dat','GofU','-ascii'); % uncomment to save the total RDF
aux = 4*pi*durrho;
S=zeros(1,Nq);
for n=1:Nq
    q = Q(n);
    S(n) = 1 + (aux/q)*sum((g - 1).*sin(q*U).*U);
end;
Np = Q>0.7;
Q = Q(Np); S=S(Np); fm2=fm2(Np);
TTh = 2*pi*sin(Q/Qmax);
C = (1/3)*csfq('Si',(0.25/pi)*Q)+(2/3)*csfq('C',(0.25/pi)*Q);
I = fm2.*S + C(:,2)';
M=[Q; I; S]';
if (prn~0)
    Imin = min(I);
    Imax = max(I);
    DI = 0.02*(Imax-Imin);
    hfi=figure(1);
    clf
    set(hfi,'InvertHardcopy', 'off','Color','w')
    plot(TTh,I,'k','LineWidth',2)
    set(gca,'FontSize',14,'FontName','Arial','Color',[0.93 0.93 0.93],'LineWidth',1)
    xlabel('2theta (deg)', 'FontSize',18);
    ylabel('intensity (cps)', 'FontSize',18);
    axis([TTh(1) 180 Imin-DI Imax+DI])
    Nu = U*0.1;
    ha2=axes('Position',[.45 .4 .43 .48]);
    plot(U(Nu),g(Nu),'k','LineWidth',2)
    set(ha2,'FontSize',14,'FontName','Arial','Color',[0.85 0.7 1],'LineWidth',1)
    grid
    xlabel('u (A)')
    ylabel('g(u)')
    axis([0.1 13.1 0 1.02*max(g(Nu))])
end;

```

67. quartzR.m

```

function XYZ=quartzR(N,d,prn)
%%%%%
% Three-dimensional cluster of disordered alpha-quartz %
% Input: %
%   N, cluster with 9*(2N+1)^3 atoms (1/3 of silicon and 2/3 of oxygen) %
%   d = degree of disorder %

```

```

% prn = 0 to suppress graphic window
% Output XYZ, array of 3D atomic coordinates
% Usage:
% >> XYZ = quartzR(4, 0.02, 1);
%%%%%%%%%%%%%%%
NN = 2*N + 1;
X = zeros(NN,NN,NN);
Y = zeros(NN,NN,NN);
Z = zeros(NN,NN,NN);
X(:,:,1) = d*(2*rand(NN)-1);
Y(:,:,1) = d*(2*rand(NN)-1);
Z(:,:,1) = d*(2*rand(NN)-1);
h = 0;
if (N>0)
    X(:,:,2) = X(:,:,1) + 1 + d*(2*rand(NN)-1);
    X(:,:,3) = X(:,:,1) - 1 + d*(2*rand(NN)-1);
    Y(:,:,2) = Y(:,:,1) + 1 + d*(2*rand(NN)-1);
    Y(:,:,3) = Y(:,:,1) - 1 + d*(2*rand(NN)-1);
    Z(:,:,2) = Z(:,:,1) + 1 + d*(2*rand(NN)-1);
    Z(:,:,3) = Z(:,:,1) - 1 + d*(2*rand(NN)-1);
    h = [0 1 -1];
    if (N>1)
        for n = 2:N
            X(:,:,2*n) = X(:,:,2*(n-1)) + 1 + d*(2*rand(NN)-1);
            X(:,:,2*n+1) = X(:,:,2*(n-1)+1) - 1 + d*(2*rand(NN)-1);
            Y(:,:,2*n) = Y(:,:,2*(n-1)) + 1 + d*(2*rand(NN)-1);
            Y(:,:,2*n+1) = Y(:,:,2*(n-1)+1) - 1 + d*(2*rand(NN)-1);
            Z(:,:,2*n) = Z(:,:,2*(n-1)) + 1 + d*(2*rand(NN)-1);
            Z(:,:,2*n+1) = Z(:,:,2*(n-1)+1) - 1 + d*(2*rand(NN)-1);
            h(2*n:2*n+1) = [n -n];
        end;
    end;
end;
N0 = N+1;
nn = 0;
R = zeros(NN*NN*NN,3);
for n=1:NN
    for m=1:NN
        for p=1:NN
            nn = nn + 1;
            R(nn,:) = [X(N0-h(p),N0+h(m),n) Y(N0-h(p),N0-h(n),m) Z(N0+h(n),N0+h(m),p)];
        end;
    end;
end;
clear X Y Z;
Nr = size(R,1);
a = 4.9134;
c = 5.4052;
G = [0.5*a -sqrt(3)*a/2 0; 0.5*a +sqrt(3)*a/2 0; 0 0 c];
R = R*G;
H = [2*N:-2:0 1:2:(2*N-1)];
n=0; NN2 = NN*NN;
S = zeros(1,NN2*NN);
for jz = 1:NN
    for jx = 1:NN
        for jy = 1:NN
            n = n + 1;
            S(n) = H(jz)+1 + H(jx)*NN2 + H(jy)*NN;
        end;
    end;
end;
Rfrac = [ 0.4699 0.0000 0.66666667; % fractional coordinates of %
          0.0000 0.4699 0.33333333; % 3Si and 6O %
          1-0.4699 1-0.4699 0.0000000; %
          0.4141 0.2681 0.7854000; %
          1-0.2681 0.1460 0.45206667; %
          1-0.1460 1-0.4141 0.11873333; %
          0.2681 0.4141 1-0.78540000; %
          1-0.4141 1-0.1460 1-0.11873333; %
          0.1460 1-0.2681 1-0.45206667];
Nat = size(Rfrac,1);
nnm = 0; ncell = 0; RR = zeros(Nr*Nat,3);
for jz = 1:NN-1
    Az = NN2*(jz-1);
    for jx = 1:NN-1
        Ax = NN*(jx-1);
        for jy = 1:NN-1;
            n = Az+Ax+jy;
            R0 = R(S(n),:);
            M = [R(S(NN+n),:) -R0; R(S(n+1),:) -R0; R(S(NN2+n),:) -R0];
            for nn = 1:Nat
                nnm = nnm + 1;
                RR(nnm,:) = Rfrac(nn,:)*M + R0;
            end;
            ncell = ncell + 1;
            atot = (ncell-1)*Nat;
            aux = (ncell-1)*3;
            Nsi(1+aux:+aux) = (1:3) + atot;
            Nox(1+2*aux:6+2*aux) = (4:9) + atot;
        end;
    end;
end;

```

```

        end;
    end;
end;
XYZ = [RR(Nsi,:); RR(Nox,:)];
if (prn~0)
    hfi=figure(1);
    clf
    set(hfi,'InvertHardcopy', 'off','Color','w')
    set(gca,'FontSize',14,'FontName','Arial','LineWidth',1)
    plot3(RR(Nsi,1),RR(Nsi,2),RR(Nsi,3),'bo','MarkerFaceColor','c','MarkerSize',5,'LineWidth',.6)
    hold on
    plot3(RR(Nox,1),RR(Nox,2),RR(Nox,3),'ro','MarkerFaceColor','y','MarkerSize',3,'LineWidth',.6)
    hold off
 xlabel('x (A)', 'FontSize',18)
 ylabel('y (A)', 'FontSize',18)
 zlabel('z (A)', 'FontSize',18)
 legend(' Si', ' O')
 grid
 axis image
 view(60,20)
 set(gca,'Color',[.97 .97 .97], 'Box','on')
end;

```

68. quartzrdf.m

```

function M=quartzrdf(N,d,prn)
%%%%%%%%%%%%%%%%%%%%%%%%%%%%%%%%%%%%%
%          RDFs in clusters of disordered alpha-quartz
%
% Input:
%   N, cluster with 9*(2N+1)^3 atoms (1/3 of silicon and 2/3 of oxygen)
%   d = degree of disorder
%   prn = 0 to suppress graphic window
%
% Output  M = [U; gsi; gox; gsiox; gosxi];
%           |   |   |   |
%           rdfs Si-Si, O-O, Si-O, and O_Si
%           interatomic distances (Angstrom)
%
% Secondary routine required: quartzR.m
%
% Usage:
% >> M = quartzrdf(4,0.02,1);
%%%%%%%%%%%%%%%%%%%%%%%%%%%%%%%%%%%%%
cc=clock; fprintf('%1.0fh%1.0fm%1.0fs\n',cc(4:6))
RR = quartzR(N,d,0);
Nr = size(RR,1);
n = round(Nr/3);
NSi = 1:n; Nox = n+1:Nr;
a = 4.9134; c = 5.4052; % lattice parameters (Angstrom)
Vc = c*a*a*sind(120); % unit cell volume (Angstrom)
rhoSi = 3/Vc;
rhoOx = 6/Vc;
Radius2 = 0.5*N*a;
Radius2 = Radius2*Radius2;
R2 = sum(RR(Nsi,:).*RR(Nsi,:),2);
Naux = R2<=Radius2;
RSi = RR(Nsi(Naux,:));
NSi_ref = size(RSi,1);
R2 = sum(RR(Nox,:).*RR(Nox,:),2);
Naux = R2<=Radius2;
ROX = RR(Nox(Naux,:));
Nox_ref = size(ROX,1);
NSi_tot = size(NSi,2);
Nox_tot = size(Nox,2);
Umax = 2*(2N+1)*c;
du = 0.005;
U = 0:du:Umax; U(1)=le-8;
fourpiduU2 = 4*pi*du*(U.*U);
p = zeros(size(U));
for m = 1:NSi_ref
    R = RSi(m,:);
    for n = 1:Nox_tot
        dR = RR(NSi(n,:))-R;
        k = fix(sqrt(dR*dR')/du) + 1;
        p(k) = p(k) + 1;
    end;
end;
p(1)=0;
gsi = p./(rhoSi*NSi_ref*fourpiduU2);
p = zeros(size(U));
for m = 1:Nox_ref
    R = ROX(m,:);
    for n = 1:Nox_tot
        dR = RR(Nox(n,:))-R;
        k = fix(sqrt(dR*dR')/du) + 1;
        p(k) = p(k) + 1;
    end;
end;
p(1)=0;
gox = p./(rhoOx*Nox_ref*fourpiduU2);

```

```

p = zeros(size(U));
for m = 1:Nsi_ref
    R = RSi(m,:);
    for n = 1:NOx_tot
        dr = RR(Nox(n))-R;
        k = fix(sqrt(dr*dr')/du) + 1;
        p(k) = p(k) + 1;
    end;
end;
gsiox = p./(rhoOx*Nsi_ref*fourpiduU2);
p = zeros(size(U));
for m = 1:NOx_ref
    R = ROx(m,:);
    for n = 1:Nsi_tot
        dr = RR(Nsi(n))-R;
        k = fix(sqrt(dr*dr')/du) + 1;
        p(k) = p(k) + 1;
    end;
end;
goxsi = p./(rhoSi*NOx_ref*fourpiduU2);
M = [U; gsi; gox; gsiox; goxsi];
fprintf(' N=%1.0f, d=%4.2f, Nr=%1.0f, Nsi_ref=%1.0f\n',N,d,Nr,Nsi_ref,NOx_ref)
cc=clock; fprintf(' %1.Ofh%1.0fm%1.Ofs\n',cc(4:6))
if (prn>=0)
    hf1=figure(1); clf; set(hf1,'InvertHardcopy','off','Color','w')
    set(gca,'FontSize',14,'FontName','Arial','LineWidth',1)
    plot(U,gsi,'b',U,gox,'r',U,gsiox,'--m',U,goxsi,'-c','LineWidth',1)
    xlabel('u (A)', 'FontSize',18)
    ylabel('g_{\alpha\beta}(u)', 'FontSize',18)
    grid
    legend('gsi','g ox','gsiox','goxsi')
end;

```

69. quartzrdfplot.m

```

function quartzrdfplot
%%%%%%%%%%%%%%%%%%%%%%%%%%%%%%%%%%%%%
% Shows the RDFs from a cluster of disordered alpha-quartz %
% Required file: clusterN12d8_1to10.dat from http://xraybook.if.usp.br/ %
% File generated by routine quartzrdf.m %
%%%%%%%%%%%%%%%%%%%%%%%%%%%%%%%%%%%%%
Soload('clusterN12d8_1to10.dat');
U = S(:,1)'; gsi = S(:,2)'; gox = S(:,3)'; gsiox = S(:,4)'; goxsi = S(:,5)';
Uc = 2.07; y = exp(-5.2e-5*(U-Uc).^2.505); % empirical values
y(U<Uc)=1; % <-- % For correcting the RDFs gab(u) due to finite %
y = 1 - y; % cluster size. Use y = 0 to see what happens. %
hf1 = figure(1); % cluster size. Use y = 0 to see what happens. %
clf % cluster size. Use y = 0 to see what happens. %
set(hf1,'InvertHardcopy','off','Color','w')
plot(U,gsi*y,'b',U,gox*y,'r',U,0.5*(gsiox+goxsi)+y,'k','LineWidth',2)
legend('Si-Si','O-O','Si-O')
set(gca,'FontSize',14,'FontName','Arial','Color',[.85 .7 1],'LineWidth',1)
xlabel('u (A)', 'FontSize',18)
ylabel('g_{\alpha\beta}(u)', 'FontSize',18)

```

70. rcdarwinprins.m

```

function M=rcdarwinprins(wl,fname,H,N,prn)
%%%%%%%%%%%%%%%%%%%%%%%%%%%%%%%%%%%%%
% Reflectivity curves of dynamical diffraction %
% Input: %
% wl = wavelength (Angstrom) or energy (eV) %
% fname: file *.in with crystal data information (see sfactor.m) %
% H = [h k l] reflection indexes %
% N = number of crystallographic planes (Bragg planes) %
% prn = 1 for figure window %
Output M = [X; R; R_p; T]' for N>0, otherwise M = [ E wl 0 0 %
| | | | d thB 2thB Vc] %
| | | transmission coefficient %
| | | reflection coefficient, crystal face (-h,-k,-l) %
| | | reflection coefficient, crystal face (h,k,l) %
| incidence angle (arcsec), relative to the Bragg angle %
Secondary routines required: bragg.m and sfactor.m %
exemplo: M=rcdarwinprins(10400,'GaAs.in',[1 1 1],30,1);
%%%%%%%%%%%%%%%%%%%%%%%%%%%%%%%%%%%%%
C = 1; % for sigma-polarization, C = abs(cos(2*thB)) for pi-polarization
rad = pi / 180;
re = 2.818e-5;
if (wl < 1000), E = 12398.5 / wl; else E = wl; wl = 12398.5 / E; end;
M=vcell(wl,fname,H);
V = M(2,4);
d = M(2,1);
if (N<0), return; end;
sinthB = 0.5*wl/d;

```

```

if (sinthB>1) disp(' Inaccessible reflection!!!'); return; end;
thB = asin(sinthB);
Gamma = re*wl*d/(sinthB*V);
F = sfactor(wl,fname,[H; -H; 0 0 0]);
if (F(1)*conj(F(1))<1), disp(' Forbidden or very weak reflection!!!'); return; end;
r = -1i*Gamma*aC*F(1);
r_ = -1i*Gamma*aC*F(2);
t = 1+1i*Gamma*aC*F(3);
thC = asin(0.5*(1+angle(t)/pi)*wl/d);
Dth = thC-thB;
Nd = d*N; % crystal thickness
Dw = (2/3)*tan(thB)*sqrt(abs(r*r_));
CurveWidth = wl / (2.0 * cos(thB) * Nd); % dynamical width
if (CurveWidth>Dw), CurveWidth = Dw; end; % kinematic width
if (CurveWidth>Dw), CurveWidth = Dw; end;
Range = 20 * CurveWidth;
if (Range<Dth), Range = 2*abs(Dth); end;
dth = CurveWidth / 100;
TH = thC + (-Range:dth:Range);
TH=TH(TH>0 & TH<0.5*pi);
expPHI = exp((-2*pi*d*li/wl)*sin(TH));
R1 = r*expPHI;
R1_ = r_*expPHI;
T1 = t*expPHI;
bin=dec2bin(N);
Nn = size(bin,2)-find(bin=='1');
RT = coef(R1,R1_,T1,Nn(1));
R = RT(1,:);
R_ = RT(2,:);
T = RT(3,:);
for nn=2:size(Nn,2)
    RT = coef(R1,R1_,T1,Nn(nn));
    RB = RT(1,:);
    RB_ = RT(2,:);
    TB = RT(3,:);
    Z = 1./(1 - R_ .* RB);
    R = R + RB .* T .* T .* Z;
    R_ = RB_ + R_ .* TB .* TB .* TB .*Z;
    T = T .* TB .* Z;
end;
X = (TH-thB)*(3600/rad);
M = [X; R; R_; T].';
if (prn==1)
    Y = R.*conj(R);
    Ymax = max(Y);
    n2 = find(X==min(X(Y>0.5*Ymax)));
    n1 = n2-1;
    if (n1>0), x1 = (X(n2)-X(n1))*(0.5*Ymax-Y(n1))/(Y(n2)-Y(n1))+X(n1);
    else x1 = 0;
    end;
    n1 = find(X==max(X(Y>0.5*Ymax))), n2 = n1+1;
    if (n2<size(X,2)+1), x2 = (X(n2)-X(n1))*(0.5*Ymax-Y(n1))/(Y(n2)-Y(n1))+X(n1);
    else x2 = 0;
    end;
    Yb = R_.*conj(R_);
    Ybmax = max(Yb);
    ratio = max([Ymax Ybmax])/min([Ymax Ybmax]);
    Ymax = max([Ymax Ybmax]);
    Xmax = max(X);
    Xmin = min(X);
    hfi=figure(1); clf; set(hfi,'InvertHardcopy', 'off','Color','w')
    plot(X,Y,'-k',X,Yb,'-k','LineWidth',2)
    hold on
    plot([0 0],[0 1.05*Ymax],'-k','LineWidth',.5)
    hold off
    axis([Xmin Xmax 0 1.05*Ymax])
    set(gca,'FontSize',14,'Color',[0.7 0.78 1],'LineWidth',1)
    xlabel('\Delta(theta (arcsec)'),'FontSize',18)
    ylabel('reflectivity, |R_N(\thetaeta)|^2','FontSize',18)
    title(['(fname ', E = ' num2str(E) 'eV1,'FontSize',18)
    refIH = [' (' num2str(H(1)) ',' num2str(H(2)) ',' num2str(H(3)) ')'];
    refIHb = [' (' num2str(-H(1)) ',' num2str(-H(2)) ',' num2str(-H(3)) ')'];
    legend(refIH,refIHb);
    fprintf('      Crystal thickness (%d planes) = %4.2e um\n',N,Nd/10000)
    fprintf('      Dynamical width = %5.3f", FWHM = %5.3f" (%4.2f urad)\n',...
    Dw*3600/rad,abs(x2-x1),abs(x2-x1)*(rad1e+6/3600))
    fprintf('      Peak shift = %5.3f"\n',Dth*3600/rad)
    fprintf('      Reflectivity ration = %8.6f\n',ratio)
    fprintf('      Anomalous signal = %5.2f%\n',100*(ratio-1)/(ratio+1))
end;

function V=vcell(wl,fname,H)
n = regexp(fname,'in','once');
if isempty(n), disp(' >>> Unknow file type!!!'), return; end;
fidin = fopen(fname,'r');
if (fidin==-1), disp([' >>> File ' fname ' not found!!!']); return; end;
line = fgets(fidin);
P = sscanf(line,'%f');
if (size(P,2)==6), disp(' >>> Line 1: a b c alpha beta gamma'); return; end;
fclose(fidin);
V = bragg(wl,P,H);

```

```

function RT=coef(R,R_,T,m)
n=0;
while (n<m)
    n = n + 1;
    T = (T.*T)./(1 - R.*R_);
    aux = 1 + T;
    R = R.*aux;
    R_ = R_.*aux;
end;
RT = [R; R_; T];

```

71. rcdarwinprinsplot.m

```

function rcdarwinprinsplot
%%%%%%%%%%%%%%%%%%%%%%%%%%%%%%%%%%%%%
% Comparison of dynamical reflectivity curves from %
% crystals with different thicknesses %
% Secondary routine required: rcdarwinprins.m %
% Required files: Ge.in %
%%%%%%%%%%%%%%%%%%%%%%%%%%%%%%%%%%%%%
E = 10000; % X-ray energy (eV)
fname = 'Ge.in'; % crystal data file as required by sfactor.m
H = [2 2 0]; % reflection indexes
Nn = [12 13 22]; % 2^Nn = number of crystallographic planes
M1=rcdarwinprins(E,fname,H,2^Nn(1),0);
M2=rcdarwinprins(E,fname,H,2^Nn(2),0);
M3=rcdarwinprins(E,fname,H,2^Nn(3),0);
Y1 = M1(:,2).*conj(M1(:,2));
Y2 = M2(:,2).*conj(M2(:,2));
Y3 = M3(:,2).*conj(M3(:,2));
nc = Y1==max(Y1);
Xmin = 0.2*min(M3(:,1));
Xmax = -Xmin + 2*nc;
hfl=figure(1); clf; set(hfl,'InvertHardcopy', 'off','Color','w')
plot(M1(:,1),Y1,'r','LineWidth',2)
hold on
plot(M2(:,1),Y2,'b','LineWidth',2)
plot(M3(:,1),Y3,'k','LineWidth',2)
hold off
axis([Xmin Xmax 0 1])
set(gca,'FontSize',14,'Color',[0.97 0.97 .97],'LineWidth',1)
 xlabel('Delta(theta (arcsec)', 'FontSize',18)
 ylabel('reflectivity, |R_N(theta)|^2', 'FontSize',18)
title(['[fname ', E = ' num2str(E) 'eV, H = (' num2str(H(1)) ',' num2str(H(2)) ',' num2str(H(3)) ')'],
'FontSize',18)
legend(['N = ' num2str(2^Nn(1))],['N = ' num2str(2^Nn(2))],['N = ' num2str(2^Nn(3))])

```

72. rockingcurve.m

```

function S=rockingcurve(wl,a0,H,Nph)
%%%%%%%%%%%%%%%%%%%%%%%%%%%%%%%%%%%%%
% Rocking curves of cubic (001) crystals in reflection geometry %
% Input: %
% wl = wavelength (Angstrom) or energy (eV) %
% a0 = lattice parameter of cubic crystals, e.g. GaSb (a0 = 6.0966A) %
% H = [h k l], reflection index %
% Nph > 1000 for statistic of Nph counts %
% Output S = [TH Y1 Y2], n-by-3 array where TH = bragg angle, and %
% Yn = rocking curve at low (n=1) and high (n=2) incidence angle %
% Secondary routines required: bragg.m and photonstatistic.m %
% Usage: S=rockingcurve(1.540562,6.0966,[2 2 4],1e5);
%%%%%%%%%%%%%%%%%%%%%%%%%%%%%%%%%%%%%
rad = pi / 180;
thm = acos(H(3)/sqrt(H.*H)); % angle between diffraction vector and surface normal
M = bragg(wl,a0,H);
M(2,2) = M(2,2)*rad;
if (M(2,2)==0 || thm>M(2,2)), S=0; disp(' >> Not in reflection condition!!!!'); return; end;
A0 = wl.^2./sin(2*M(2,2));
R1=curve(M,thm,a0);
Z1=photonstatistic(R1(:,2),Nph);
aux1 = max(Z1)/max(R1(:,2));
if (thm<rad)
    ctr=1;
    S = R1;
else ctr=2;
    R2=curve(M,-thm,a0);
    Z2=photonstatistic(R2(:,2),Nph);
    aux1 = max(Z2)/max(R2(:,2));
    S = [R1 R2(:,2)];
end;
dth = R1(2,1)-R1(1,1);
A1=sum(R1(:,2))*dth;
R1(:,2) = R1(:,2) * aux1;

```

```

if (ctr==1)
    fprintf(' curve_area/crystal_volume = %4.2f (A^3), wl^3/sen(2thB) = %4.2f (A^3)\n',A1,A0);
else
    A2=sum(R2(:,2))*dth;
    R2(:,2) = R2(:,2) * aux2;
    fprintf(' curve_area/crystal_volume = %4.2f (A^3), wl^3/sen(2thB) = %4.2f (A^3)\n',0.5*(A1+A2),A0);
end;
X = R1(:,1)*1/(rad);
hf1 = figure(1); clf; set(hf1,'InvertHardcopy','off','Color','w')
if (ctr==1)
    semilogy(X,R1(:,2),'-k',X,Z1,'ko','LineWidth',1);
else
    semilogy(X,R1(:,2),'-k',X,Z1,'ko',X,R2(:,2),'-r',X,Z2,'ro','LineWidth',1);
end;
axis tight
set(gca,'FontSize',14,'Color',[0.97 0.97 0.97],'Box','on','LineWidth',1,'FontName','Arial')
xlabel('theta (deg)','FontSize',18)
if (Nph>1000)
    ylabel('number of counts','FontSize',18)
else
    ylabel('intensity (arb. units)','FontSize',18)
end;

function R=curve(M,thn,a0)
wl = M(1,2);
d = M(2,1);
thB = M(2,2);
k = 2*pi/wl;
Qmax = 2*k;
Qmod = 2*pi/d;
cth = cos(thn);
sth = sin(thn);
L=20000; % crystal lateral dimension (Angstrom)
T=5000; % thickness (Angstrom)
if (L<10000), L = 10000; end;
if (T>5000), T = 5000; end;
Qrange = 100/T;
x = (Qmod-Qrange)/Qmax;
thmin = asin(x);
x = (Qmod+Qrange)/Qmax;
if (x>1)
    thmax = asin(x);
else
    thmax = 0.5*pi;
end;
dth = (thmax-thmin)/250;
TH = thmin:dth:thmax;
a = 0.05;
b = 10;
Dth = (thmin:a*dth:thmax)-thB;
Dth = b*Dth; dthp = (a*b)*dth;
Nth = size(TH,2);
ksth = k*sin(TH);
kcth = k*cos(TH);
T_2 = 0.5*T;
L_2 = 0.5*L;
Y = zeros(1,Nth);
for n=1:Nth
    THp = TH(n) + Dth;
    sTHp = sin(THp);
    DQz = k*sTHp*ksth(n)-Qmod;
    DQx = k*cos(THp)-kcth(n);
    DQxc = L_2*(DQx*sth - DQz*sth);
    DQzc = T_2*(DQx*sth + DQz*sth);
    Z = sin(DQzc)./DQzc;
    Z = (Z.*Z)./(1+(DQxc.*DQxc));
    Y(n) = sum(Z);
end;
V = L*L*T;
N = V/A0^3;
Y = (N*N*wl*dthp/L)*Y;
R = [TH; Y];

```

73. rotatcrys.m

```

function L=rotatcrys(wl,P,A,B,iangle,H)
%%%%%%%%%%%%%%%%%%%%%%%%%%%%%%%%%%%%%
%   Polar coordinates of wavevectors k and k' in azimuthal scanning
% Input:
%   wl = wavelength (Angstrom) or energy (eV)
%   P = [a b c alpha beta gamma] lattice parameters (Angstrom and deg)
%   A, B = axis of rotation and reference direction
%   iangle = incidence angle (deg), angle between k and A is 90+iangle
%   H = [h1 k1 l1; h2 k2 l2; ...] reflection indexes
% Output L = [ hkl alpha phi w phi w' phi' ]
%           | | | | | | | | wavevector k' polar coordinates (deg)
%
```

```

%           |   |   | wavevector k polar coordinates (deg) %
%           |   Q vector polar coordinates (deg) %
%           reflection indexes %
%
% Usage: %
% Lerotatccryst(8374.5,[6.7830 18.2880],[0 0 1],[0 1 0],-18.8941,[2 0 4]); %
% Lerotatccryst(8374.5,[6.7830 18.2880],[0 0 1],[0 1 0],0,[0 4 0]); %
%%%%%%%%%%%%%%%
rad = pi / 180;
deg = 1/rad;
if (wl < 1000), E = 12398.5 / wl; else E = wl; wl = 12398.5 / E; end;
if isempty(P), L = [E wl]; return; end;
nm = size(P);
if (nm(1)*nm(2)==1)
    P(1:3) = P(1)+ones(1,3);
    P(4:6) = [90 90 90];
elseif (nm(1)*nm(2)==2)
    P(1:3) = [P(1) P(1) P(2)];
    P(4:6) = [90 90 90];
end;
P(4:6) = P(4:6)*rad;
cosphi = cos(P(6)) - cos(P(5))*cos(P(4));
cosphi = cosphi / (sin(P(5))*sin(P(4)));
sinphi = sqrt(1-cosphi*cosphi);
a1 = P(1) * [sin(P(5)) 0 cos(P(5))];
a2 = P(2) * [sin(P(4))*cosphi sin(P(4))*sinphi cos(P(4))];
a3 = P(3) * [0 0 1];
air = cross(a2,a3);
Vc = air*air';
air = air/Vc;
a2r = cross(a3,a1)/Vc;
a3r = cross(a1,a2)/Vc;
omega = -iangle;
Nr = size(H,1);
w0 = omega*rad;
vecA = A(1)*a1 + A(2)*a2 + A(3)*a3;
vecB = B(1)*a1 + B(2)*a2 + B(3)*a3;
e3 = vecA/norm(vecA);
e2 = cross(vecA,vecB);
e2 = e2/norm(e2);
e1 = cross(e2,e3);
M = [e1; e2; e3]';
m = 0;
fprintf('\n' );
fprintf(' -----hkl-----alphaQ-----phiQ-----omega-----phi-----omegat-----phit---\n');
for n=1:Nr
    Q = H(n,1)*air + H(n,2)*a2r + H(n,3)*a3r;
    modQ = norm(Q);
    sindh = 0.5*wl*modQ;
    if (sindh <= 1)
        Qe = Q*M;
        cosalphaQ = Qe(3)/modQ;
        alphaQ = acos(cosalphaQ)*deg;
        sinalphaQ = sqrt(1-cosalphaQ^2);
        x = Qe(1); y = Qe(2);
        phiQ = atan2(y,x);
        cw = cos(w0);
        sw = sin(w0);
        x = sindh*sw*cosalphaQ;
        x = -x/(cw*sinalphaQ);
        if (abs(x)<1)
            x = acos(x);
            phi = phiQ + [-x x];
            phi = atan2(sin(phi),cos(phi));
            cphi = cos(phi);
            sphi = sin(phi);
            if (phi(1)<0) phi(1) = 2*pi + phi(1); end;
            if (phi(2)<0) phi(2) = 2*pi + phi(2); end;
            k = (1/wl)*[cw*cphi' cw*sphi' sw*ones(2,1)];
            kp = k(1,:)+Qe;
            wp1 = asin(wl*kp(3));
            x = kp(1); y = kp(2);
            phi1 = atan2(y,x);
            if (phi1<0) phi1 = 2*pi + phi1; end;
            kp = k(2,:)+Qe;
            wp2 = asin(wl*kp(3));
            x = kp(1); y = kp(2);
            phi2 = atan2(y,x);
            if (phi2<0) phi2 = 2*pi + phi2; end;
            m = m + 1;
        L(m,:) = [H(n,:); alphaQ phiQ*deg omega phi(1)*deg wp1*deg phi1*deg];
        m = m + 1;
        L(m,:) = [H(n,:); alphaQ phiQ*deg omega phi(2)*deg wp2*deg phi2*deg];
    end;
end;
Nm = m; m = 0;
while (m<Nm-1)
    m = m + 1;
    fprintf(' (%3.0f,%3.0f,%3.0f): %9.4f %9.4f %9.4f %9.4f %9.4f %9.4f\n',...

```

```

L(m,1), L(m,2), L(m,3), L(m,4), L(m,5), L(m,6), L(m,7), L(m,8), L(m,9)) ;
m = m + 1;
fprintf(' %9.4f %9.4f\n', L(m,7), L(m,9));
fprintf(' -----');
end;

```

74. rotcrystmethod.m

```

function rotcrystmethod(wl, fname, A, TH, THd)
%%%%%%%%%%%%%%%%%%%%%%%%%%%%%%%%%%%%%%%
% Rotating crystal method
%
% Input:
%   wl = wavelength (Angstrom) or energy (eV)
%   fname = file *.in with crystal data information, see sfactor.m or
%   pdfcoorfrac.m (protein crystals)
%   A = [A1,A2,A3] crystallographic direction of the rotating axis
%   TH = [thx,thz] rotation matrix R=Rz(thz)Ry(thy) to orient the
%   rotating axis direction A so that omega = 90-thy (deg)
%   THd = [th1,th2], angle of elevation of the detector area center
%   from yz plane and azimuth around the x axis (deg)
% Output file *.rcm with list of hkl reflection power and
% spot coordinates on the flat area detector
% Secondary routines required: sfactor.m
% Usage: rotcrystmethod(1.540562,'1TRZ.in',[5 1 0],[60 30],[0 -30])
%%%%%%%%%%%%%%%%%%%%%%%%%%%%%%%%%%%%%%%
D = 600; % sample-detector distance (mm)
Rd = 100; % radius of the flat sensor area (mm)
pix = 0.1; % pixel (mm)
sg = 2*pix; % size of diffraction spots, half width at 61% of the maximum
osc = 180; % interval of angular precession is 2osc (deg)
rad = pi / 180; osc = osc * rad;
if (wl<1000) E = 12398.5 / wl; else E = wl; wl = 12398.5 / E; end;
invwl = 1/wl;
if (sum(abs(A))==0) disp(' >>> Invalid rotation axis!!!'); return;
else B=A; B(find(abs(B)==min(abs(B)),1))=50;
end;
cthD = cos(atan(Rd/D));
thD = THd(1)*rad;
phid = THd(2)*rad;
sdD = [sin(thD) -cos(thD)*sin(phid) cos(thD)*cos(phid)];
xD = D*[0 cos(phid) sin(phid)];
yD = D*[cos(thD) sin(thD)*sin(phid) -sin(thD)*cos(phid)];
c0 = fix(clock);
code = [num2str(c0(1)) num2str(c0(2)) num2str(c0(3)) num2str(c0(4)) num2str(c0(5)) num2str(c0(6))];
n = regexp(fname,'.in');
if isempty(n) disp(' >>> Unknown file type !!!'); return; end;
fidin = fopen(fname,'r');
if (fidin==1) disp(' >>> File ' fname ' not found!!!'); return; end;
fout = [fname(1:n-1) 'E' num2str(round(E)) 'eV' code '.rcm'];
line = fgets(fidin);
P = sscanf(line,'%f');
if (size(P,2)==6) disp(' >>> Line 1: a b c alpha beta gamma'); return; end;
n = 0;
line = fgets(fidin);
while (line>=-1)
    n = n + 1;
    w = find(line==' '); w = w(1);
    atm(n,:)= ' ';
    atm(n,1:w-1)= line(1:w-1);
    if isempty(regexp('abcdefghijklmnoprstuvwxyz',atm(n,2)))
        atomsym(n,:)= [1:w-1];
    else atomsym(n,:)= [2:w-1]; end;
    Rat(n,:)= sscanf([line(w+1:size(line,2)),'%f']);
    line = fgets(fidin);
end;
fclose(fidin);
Nat = n; Nc = 0; Ac = zeros(Nat,1); NA = find(Ac==0);
while ~isempty(NA)
    n = NA(1);
    Mc = find(atm(n,1)==atm(:,1) & atm(n,2)==atm(:,2) & atm(n,3)==atm(:,3) & atm(n,4)==atm(:,4));
    Nc = Nc + 1;
    Ac(Mc) = Nc;
    NA = find(Ac==0);
    acod(Nc,:)= atm(n,:);
    asym(Nc,:)= atomsym(n,:);
end;
clear atm atomsym;
P(4:6) = P(4:6)*rad;
cosphi = cos(P(6)) - cos(P(5))*cos(P(4));
cosphi = cosphi / (sin(P(5))*sin(P(4)));
sinphi = sqrt(1-cosphi*cosphi);
a1 = P(1) * [sin(P(5)) 0 cos(P(5))];
a2 = P(2) * [sin(P(4))*cosphi sin(P(4))*sinphi cos(P(4))];
a3 = P(3) * [0 0 1];
alr = cross(a2,a3);
Vc = alr*a1';

```

```

alr = alr/Vc;
a2r = cross(a3,a1)/Vc;
a3r = cross(a1,a2)/Vc;
vecA = A(1)*a1 + A(2)*a2 + A(3)*a3;
vecB = B(1)*a1 + B(2)*a2 + B(3)*a3;
e3 = vecA/norm(vecA);
e2 = cross(vecA,vecB);
e2 = e2/norm(e2);
e1 = cross(e2,e3);
M = [e1; e2; e3]';
thy = TH1'*rad;
thz = TH2'*rad;
Ry = [ cos(thy) 0 sin(thy); 0 1 0; -sin(thy) 0 cos(thy)];
Rz = [cos(thz) -sin(thz) 0; sin(thz) cos(thz) 0; 0 0 1];
wlR = wl*(Rz*Ry);
Rzphi = eye(3);
w0 = 0.5*pi - thy;
hmax = floor(2.0 / (wl * norm(alr)));
kmax = floor(2.0 / (wl * norm(a2r)));
lmax = floor(2.0 / (wl * norm(a3r)));
H = [-hmax:hmax];
K = [-kmax:kmax];
L = [-lmax:lmax];
Lt = zeros(1,6);
m = 0;
for nh = 1:2*hmax+1
    for nk = 1:2*kmax+1
        for nl = 1:2*lmax+1
            h = H(nh); k = K(nk); l = L(nl);
            Q = h*a1r + k*a2r + l*a3r;
            modQ = norm(Q);
            sinth = 0.5*wl*modQ;
            if (sinth <= 1 & sinth > 0)
                Qe = Q*M;
                cosalphaQ = Qe(3)/modQ;
                sinalphaQ = sqrt(1-cosalphaQ^2);
                x = Qe(1); y = Qe(2);
                phiQ = atan2(y,x);
                cw = cos(w0);
                sw = sin(w0);
                x = sinth*sw*cosalphaQ;
                y = cw*sinalphaQ;
                if (abs(x)<=abs(y))
                    phi = atan2(sin(phi),cos(phi));
                    cphi = cos(phi);
                    sphi = sin(phi);
                    veck = invwl*[cw*cphi' cw*sphi' sw*ones(2,1)];
                    kp = veck(1,:)+Qe;
                    thz = pi - phi(1); cthz = cos(thz); sthz = sin(thz);
                    Rzphi(1:2,:) = [cthz -sthz 0; sthz cthz 0];
                    kpxy = kp*(wl*Rzphi)';
                    ckpsD = kpxy*D';
                    if (ckpsD>cthd & abs(phi)<osc)
                        m = m + 1;
                        x = wl*kp(3);
                        g = cw*sqrt(1-x*x);
                        x = kp(1); y = kp(2);
                        g = g*abs(sin(atan2(y,x)-phi(1)));
                        g = 0.5*(1+kpxy(3)*kpxy(3))/g;
                        Lt(m,:) = [h k l g (1/ckpsD)*(kpxy*xD' kpxy*yD')];
                    end;
                    kp = veck(2,:)+Qe;
                    thz = pi - phi(2); cthz = cos(thz); sthz = sin(thz);
                    Rzphi(1:2,:) = [cthz -sthz 0; sthz cthz 0];
                    kpxy = kp*(wl*Rzphi)';
                    ckpsD = kpxy*D';
                    if (ckpsD>cthd & abs(phi)<osc)
                        m = m + 1;
                        x = wl*kp(3);
                        g = cw*sqrt(1-x*x);
                        x = kp(1); y = kp(2);
                        g = g*abs(sin(atan2(y,x)-phi(2)));
                        g = 0.5*(1+kpxy(3)*kpxy(3))/g;
                        Lt(m,:) = [h k l g (1/ckpsD)*(kpxy*xD' kpxy*yD')];
                    end;
                end;
            end;
        end;
    end;
end;
if (m==0) disp('      >>> No available reflection!!!'); return; end;
Nrefl = m;
X = sfactor(wl, fname, Lt(:,1:3));
Phkl2 = X.*conj(X)';
Phkl = Phkl2.*Lt(:,4);
clear X;
X = Phkl;
Nmax = [];

```

```

while (sum(X)>0);
    NN = find(X==max(X));
    X(NN) = 0;
    Nmax = [Nmax; NN];
end;
Nrefl = size(Nmax,1);
Lt = Lt(Nmax,:);
Phkl2 = Phkl2(Nmax);
Phkl = Phkl(Nmax);
clear Nmax X;
invP2max = max(Phkl2);
if (invP2max>1e-8) invP2max = 100/invP2max; else disp('    >>> Forbidden reflections only!!!'); return; end;
c0=clock;
fidout = fopen(fout,'w');
fprintf(fidout,'InCrystal: %s\n',fname);
fprintf(fidout,'Date and Time: %d/%d/%d - %d:%d:%d.%f\n',c0(2),c0(3),c0(1),c0(4),c0(5),c0(6));
fprintf(fidout,'Energy = %6.2f eV (%8.6f A)\n',E,wl);
fprintf(fidout,'Rotating axis A = [%5.3f %5.3f %5.3f], orientation thy = %5.3f and thz = %5.3f\n',
    A(1),A(2),A(3),TH(1),TH(2));
fprintf(fidout,'Detector area radius, Rd = %5.1f mm\n',Rd);
fprintf(fidout,'Sample-detector distance, D = %5.1f mm\n',D);
fprintf(fidout,'Detector elevation and azimuth, thd = %5.3f and phid = %5.3f\n',thD/rad,phiD/rad);
fprintf(fidout,'-----|-----|-----|-----|\n');
fprintf(fidout,' h   k   l | |Phkl|^2 | Phkl      X (mm)      Y (mm) | \n');
fprintf(fidout,'-----|-----|-----|\n');
m = 1;
while (Phkl(m)>1 && m < Nrefl)
    fprintf(fidout,'| %3.0f %3.0f %3.0f | %5.3e(%5.1f%) | %5.3e %10.3f %10.3f | %d\n',...
        Lt(m,1),Lt(m,2),Lt(m,3),Phkl2(m),invP2max*Phkl2(m),Phkl(m),Lt(m,5),Lt(m,6),m);
    m = m + 1;
end;
fprintf(fidout,'-----|-----|-----|\n');
fclose(fidout);
Xf = Lt(:,5); Yf = Lt(:,6);
Nx = floor(Rd/pix); Ny = Nx;
Ld = (2*Nx+1)*pix;
Z = zeros(2*Nx+1);
for m=1:Nrefl
    nx = fix(Xf(m)/pix)+Nx+1;
    ny = fix(Yf(m)/pix)+Ny+1;
    Z(ny,nx) = Z(ny,nx) + Phkl(m);
end;
Ng = floor(10*sg*pix);
Xg = (-Ng:Ng)*pix;
Xg = Xg.*Xg;
for nx=1:2*Ng+1
    for ny=1:2*Ng+1
        Xg2(ny,nx) = Xg(ny) + Xg(nx);
    end;
end;
G = (1/(sg*sg*2*pi))*exp((-1/(2*sg*sg))*Xg2);
Zg = [zeros(2*Ny+1+2*Ng,Ng) [zeros(Ng,2*Nx+1); Z; zeros(Ng,2*Nx+1)] zeros(2*Ny+1+2*Ng,Ng)];
for nx=1:2*Nx+1
    for ny=1:2*Ny+1
        Z(ny,nx) = sum(sum(G.*Zg(ny:2*Ng+ny,nx:2*Ng+nx)));
    end;
end;
thc = (1:360)*rad;
Xc = Rd * cos(thc);
Yc = Rd * sin(thc);
h1=figure(1); clf; set(h1,'InvertHardcopy', 'off','Color','w')
imagesc(Ld*[-.5 .5],Ld*[-.5 .5],log10(Z+1))
hold on
plot(Xc,Yc,'k','LineWidth',1)
plot([-5 5],[0 0],'r-',[0 0],[-5 5],'r-','LineWidth',2)
hold off
axis image
set(gca,'YDir','normal','FontName','Arial','FontSize',18,'Box','on','LineWidth',1)
Ni = 64; VFLIP = zeros(Ni,Ni);
for n = 1:Ni m = Ni - (n-1); VFLIP(n,m) = 1; end;
colormap(VFLIP*gray);
colorbar('FontSize',14,'Location','manual','Position',[.84 .11 .05 .725],'LineWidth',1)
ylabel('Y (mm)')
xlabel('X (mm)')
text(0,0,5000,'Log(I) (arb. units)','FontSize',14,'Rotation',90)

```

75. saxs.c

```

%%%%%%%%%%%%%%%
% Calculates P(Q) by using all records "ATOM" and "HETATM"
% from a pdb file (*.pdb)
% Usage details of this C++ routine as well as the routine itself is
% available at http://xraybook.if.usp.br/
%%%%%%%%%%%%%%

```

76. saxe.m

```

function M=saxe(fname,Qf,Nq,prn)
%%%%%
% Scattering power of molecules in the small angle limit (SAXS curve)
% Input:
%   fname = pdb text file, *.pdb, or saved files *.ndu
%   Qf = maximum Q value, ranging from 0 to Qf (1/Angstrom)
%   Nq = number of points in the P(Q) curve
%   prn = 0 to suppress graphic window
% Output M = [Q; P];
% Secondary routines required: histogram.m
% Usage:
% >>> M = saxe('1N5U.pdb',0.35,1000,0);
% >>> M = saxe('2LYZ.ndu',2,80,0);
%%%%%
S=histogram(fname,0)';
U = S(1,:);
p = S(2,:);
Nu = size(U,2);
du = (U(Nu)-U(1))/(Nu-1);
if (U(1)==0) U(1) = 1e-8; end;
dQ = Qf/Nq;
Q = 0:dQ:Qf; Q(1) = 1e-8;
Nq = size(Q,2);
aux = 4*pi*du;
for n=1:Nq
    Qu = Q(n)*U;
    P(n) = aux * sum(p.* (sin(Qu) ./Qu));
end;
M = [Q; P];
if (prn==0)
    hfi=figure(1);
    clf
    set(hfi,'InvertHardcopy', 'off','Color','w')
    semilogy(Q,P,'k','LineWidth',2);
    axis tight
    set(gca,'FontSize',14,'Color',[0.93 0.93 0.93])
    xlabel('Q (A^{-1})','FontSize',18)
    ylabel('P(Q) / P(0)','FontSize',18)
end;

```

77. factor.m

```

function Fhkl=sfactor(wl,fname,H)
%%%%%
% Structure Factor of hkl reflections
% Input:
%   wl = wavelength (Angstrom) or energy (eV)
%   fname = input crystal data, file *.in
%   H = [h1 k1 l1; h2 k2 l2;...], n-by-3 array of reflection indexes
% Output Fhkl=[F1; F2;...], n-by-1 array of complex structure factors
% Secondary routines requires: asfQ.m and fpfpp.m
% Usage:
% >>> sfactor(10400,'AsGa.in',[0 0 2; 0 0 4; 1 1 1; -1 -1 -1])
% Format of crystal input file (*.in)
% 1st line:
%   a b c alpha beta gamma
% 2nd line and onwards:
%   At xa ya za foo fdw
%   | | | | |
%   | | | | Debye-Waller factor, 8*pi^2*u^2>
%   | | | | occupation factor
%   | fractional coordinates
%   atom symbol, as written in routines asfQ.m and fpfpp.m
% Example of *.in file: GaAs.in
% 5.6534 5.6534 5.6534 90.0 90.0 90.0
% Ga 0.0 0.0 0.0 1.0 0.0
% Ga 0.5 0.5 0.0 1.0 0.0
% Ga 0.0 0.5 0.5 1.0 0.0
% Ga 0.5 0.0 0.5 1.0 0.0
% As 0.25 0.25 0.25 1.0 0.0
% As 0.75 0.75 0.25 1.0 0.0
% As 0.75 0.25 0.75 1.0 0.0
% As 0.25 0.75 0.75 1.0 0.0
%%%%%
if (wl < 1000) E = 12398.5 / wl; else E = wl; wl = 12398.5 / E; end;
n = regexp(fname, '.in', 'once');
if isempty(n)
    disp(' Unknow file type!!!')
    return;
end;
fidin = fopen(fname,'r');
if (fidin==-1)
    disp([' >>> File ' fname ' not found!!!!'])
    return;

```

```

end;
line = fgets(fidin);
P = sscanf(line,'%f');
if (size(P,2)~=6)
    disp('      >>> Line 1: a b c alpha beta gamma'); return;
end;
n = 0;
line = fgets(fidin);
while (line<=-1)
    n = n + 1;
    w = find(line==' '); w = w(1);
    atm(n,:) = '   ';
    atm(n,1:w-1) = line(1:w-1);
    if isempty(regexp('abcdefghijklmnopqrstuvwxyz',atm(n,2), 'once'))
        atomsym(n,:)=1:w-1;
    else atomsym(n,:)=2:w-1; end;
R(n,:) = sscanf(line(w+1:size(line,2)),'%f');
line = fgets(fidin);
end;
fclose(fidin);
Nat = n; Nchem = 0; A = zeros(Nat,1); NA = find(A==0);
while ~isempty(NA)
    n = NA(1);
    M = atm(n,1)==atm(:,1) & atm(n,2)==atm(:,2) & atm(n,3)==atm(:,3) & atm(n,4)==atm(:,4);
    Nchem = Nchem + 1;
    A(M) = Nchem;
    NA = find(A==0);
    acod(Nchem,:) = atm(n,:);
    asym(Nchem,:) = atomsym(n,:);
end;
clear atm atomsym;
cosphi = cosd(P(6)) - cosd(P(5))*cosd(P(4));
cosphi = cosphi / (sind(P(5))*sind(P(4)));
sinphi = sqrt(1-cosphi*cosphi);
a1 = P(1) * [sind(P(5)) 0 cosd(P(5))];
a2 = P(2) * [sind(P(4))*cosphi sind(P(4))*sinphi cosd(P(4))];
a3 = P(3) * [0 1];
alr = cross(a2,a3);
VC = alr*a1';
alr = alr/VC;
a2r = cross(a3,a1)/VC;
a3r = cross(al1,a2)/VC;
hmax = 2.0 / (wl * sqrt(alr*a2r'));
kmax = 2.0 / (wl * sqrt(a2r*a2r'));
lmax = 2.0 / (wl * sqrt(a3r*a3r'));
fres = zeros(Nchem,1);
for n=1:Nchem
    aux = fpfpp(acod(n,1:asym(n,1)),E);
    fres(n) = aux(2)+1i*aux(3);
end;
if isempty(H)
    F=0;
    for n=1:Nchem
        NA= A==n; m = sum(R(NA,4));
        F = F + m * (asfQ(acod(n,1:asym(n,2)),0) + fres(n));
    end;
    Phkl = F;
    return;
end;
twopii = 2*pi*i;
Nhkl = size(H,1);
Phkl = zeros(Nhkl,1);
for m=1:Nhkl
    h = H(m,1); k = H(m,2); l = H(m,3);
    if (hmax>abs(h) && kmax>abs(k) && lmax>abs(l))
        q = h*a1r + k*a2r + l*a3r;
        x = 0.5*sqrt(q*q');
        x2 = x*x;
        F = 0;
        for n=1:Nchem
            fn = asfQ(acod(n,1:asym(n,2)),x) + fres(n);
            NA = A==n;
            F = F + fn*sum(exp(R(NA,1:3)*(twopii*[h; k; l])).*R(NA,4).*exp((-x2)*R(NA,5)));
        end;
        else F=0;
        end;
    Phkl(m,:)= F;
end;

```

78. sgcompton.m

```

function Z=sgcompton(A,E)
%%%%%
% Incoherent (Compton) scattering cross-section %
% Input: %
%   A = element symbol, e.g. 'Ca' %

```

```

%   E = energy values (m-by-n array) (keV)
% Output  Z = [E sgc]
%           | |
%           | cross-section (barn)
%           energy (keV)
% Analytical function:
%   sgr(E) = exp{ c0 + c1*[log(E)]^1 + c2*[log(E)]^2 + c3*[log(E)]^3}
%
% Coefficients c0, c1, c2, and c3 from file CrossSectionCompton.txt
% available at http://xraybook.if.usp.br/
%%%%%%%%%%%%%%%
if (E(1)>500), E = 0.001*E; end;
sizeA = size(A,2);
mmax = mcmaster(0);
m = 1; C=zeros(1,4); ctr = 1;
while ((ctr == 1) & (m < mmax+1))
    line = mcmaster(m);
    aux = find(line(1:7)==' ');
    n = aux(1);
    if (n==sizeA+1)
        X = line(1:n-1);
        if (X==A)
            C = sscanf(line(7:size(line,2)),'%f');
            ctr = 0;
        end;
    end;
    m = m + 1;
end;
X = log(E);
X2 = X.*X;
X = C(1) + C(2)*X + C(3)*X2 + C(4)*(X2.*X);
X = exp(X);
nn = size(E);
Z = zeros(nn(1)*nn(2),2);
for n=1:nn(1)*nn(2), Z(n,:)= [E(n) X(n)]; end;

function line=mcmaster(nn)
M = [
'C      -0.9828799960   1.4668999900   -0.2937400040   0.0155999996';
'N     -1.2368999700   1.7451000200   -0.3546600040   0.0198700000';
'O     -1.7367999600   2.1768999100   -0.4490500090   0.0264730007';
'Si    -0.4149700110   1.3487000500   -0.2223100070   0.0084196003';
'Ar    -0.6821100120   1.7428000000   -0.3176499900   0.0156469997';
'Ca    -0.0982419998   1.3283000000   -0.2137500050   0.0077306000'];
% Complete matrix of coefficients is available on the book's webpage
if (nn==0), line = size(M,1);
else      line = M(nn,:);
end;

```

79. sgrayleigh.m

```

function Z=sgrayleigh(A,E)
%%%%%%%%%%%%%%%
%   Coherent scattering cross-section (Rayleigh), sg_R
%
% Input:
%   A = element symbol, e.g. 'Ca'
%   E = energy values (m-by-n array) (keV)
% Output: Z = [E sgr]
%           | |
%           | cross-section (barn)
%           energy (keV)
% Analytical function:
%   sgr(E) = exp{ c0 + c1*[log(E)]^1 + c2*[log(E)]^2 + c3*[log(E)]^3}
%
% Coefficients c0, c1, c2, and c3 from file CrossSectionRayleigh.txt
% available at http://xraybook.if.usp.br/
%%%%%%%%%%%%%%%
if (E(1)>500), E = 0.001*E; end;
sizeA = size(A,2);
mmax = mcmaster(0);
m = 1; C=zeros(1,4); ctr = 1;
while ((ctr == 1) && (m < mmax+1))
    line = mcmaster(m);
    aux = find(line(1:7)==' ');
    n = aux(1);
    if (n==sizeA+1)
        X = line(1:n-1);
        if (X==A)
            C = sscanf(line(7:size(line,2)),'%f');
            ctr = 0;
        end;
    end;
    m = m + 1;
end;
X = log(E);
X2 = X.*X;

```

```

X = C(1) + C(2)*X + C(3)*X2 + C(4)*(X2.*X);
X = exp(X);
nn = size(E);
for n=1:nn(1)*nn(2); Z(n,:)= [E(n) X(n)]; end;

function line=mcmaster(nn)
M = [
'C      3.10859990 -0.26058000 -0.27197000  0.01351800';
'N      3.47760010 -0.21575999 -0.28887001  0.01513100';
'O      3.77239990 -0.14854001 -0.30712000  0.01673000';
'Si     4.64680004  0.16278000 -0.35856000  0.01969300';
'Ar     5.21080017  0.13562000 -0.34720999  0.01843300'];
% Complete matrix of coefficients is available on the book's webpage
if (nn==0), line = size(M,1);
else    line = M(nn,:);
end;

```

80. siliconDScamera.m

```

function siliconDScamera(D,L,pixel,wl,Nph)
%%%%%%%%%%%%%%%%%%%%%%%%%%%%%%%%%%%%%
% X-ray powder diffraction pattern of silicon %
% Debye-Scherrer camera %
%%%%%%%%%%%%%%%%%%%%%%%%%%%%%%%%%%%%%
% Input:
%   film radius D (mm), width L (mm), and size of pixel (mm)
%   wl = wavelength (Angstrom) or energy (eV)
%   Nph > 1000 for pattern with statistic of N counts
% Secondary routines required: bragg.m, asfQ.m, fpfpp.m,
%                               siliconPofQ.m, and photonstatistic.m
% Required files: siliconnanoD200r.pdu
% File generated by routine siliconnano.m, see http://xraybook.if.usp.br/
% Usage: siliconDScamera(100,40,1,1.5e+6)
%%%%%%%%%%%%%%%%%%%%%%%%%%%%%%%%%%%%%
E=bragg(wl,[],[]);
wl = E(2);
E = E(1);
s = [1 0 0]; % incidence direction
e = [0 1 0]; % polarization (electric field vibration direction)
dy = pixel;
n = floor(L/dy);
LimY = 0.5*n*dy;
Y = -LimY:dy:0;
Ny = size(Y,2);
dphi = pixel / D;
n = floor(pi/dphi);
LimPhi = 0.5*(2*n-1)*dphi;
phi = 0:dphi:LimPhi;
Nphi = size(phi,2);
D2 = D*D;
aux1 = D2*dy*dphi;
Q = zeros(Ny,Nphi); XX = Q; YY = Q; P2 = Q;
for ny = 1:Ny
    y = Y(ny);
    invr = 1/sqrt(y*y+D2);
    DOmega = aux1*invr*invr*invr;
    YY(ny,1:Nphi)=y;
    for np = 1:Nphi
        z = phi(np);
        XX(ny,np)= D*z;
        cphi = cos(z);
        sphi = sin(z);
        sprime = invr*[D*cphi y D*sphi];
        p = cross(sprime,cross(e,sprime));
        P2(ny,np) = (p * p')*DOmega;
        Q(ny,np) = norm(sprime - s); % |s'-s|
    end;
end;
Q = (2*pi/wl)*Q;
M=siliconPofQ('siliconnanoD200r.pdu',Q);
M(Q<-5)=0;
I = M.*P2;
beye=zeros(Ny-1);
for n=1:Ny-1, beye(n,Ny-n) = 1; end;
I = [1; beye*I(1:Ny-1,:)];
XX = [XX; beye*XX(1:Ny-1,:)];
YY = [YY; -beye*YY(1:Ny-1,:)];
hfl=figure(1); clf; set(hfl,'InvertHardcopy', 'off','Color','w')
if (Nph>1000)
    I=photostatistic(I,Nph);
    I(I==0)=1;
    imagesc([0 D*pi],[-LimY LimY],log10(I))
    axis image
    textlabel = 'Log(counts)';
else
    surf(XX,YY,log10(I+1))
    axis image
    shading interp

```

```

    view(0,90)
    textlabel = 'Log(I) (arb. units)';
end;
set(gca,'FontName','Arial','FontSize',14,'LineWidth',1)
colormap(hot)
colorbar('XColor','k','FontSize',14,'Location','NorthOutside','LineWidth',1,'Position',
[0.54 0.405 0.38 0.05])
ylabel('film width (mm)', 'FontSize',18)
xlabel('film length (mm)', 'FontSize',18)
text(0,0,5000,textlabel,'Color','w','FontSize',18)

```

81. siliconnano.m

```

function M=siliconnano(D,amp,sph)
%%%%%
% PDDF in nanocrystal of silicon
%
% Input:
%   D = particle diameter (Angstrom)
%   amp = atomic displacement in percentage (%) of the distance 2.35 A
%   sph == 1 for spherical particle, otherwise cubic with edge of 0.8D
% Output M = [U; p], n-by-2 array
%           U = interatomic dist. (Angstrom) and p = PDDF
% Usage: M = siliconnano(200,2,1);
%%%%%
if (D>200), disp(' Warning!!! Delay time can be very long for D > 200 Angstroms'); end;
if (sph==1), D = 0.8*D; end;
a0=5.4309; % silicon lattice parameter (Angstrom)
if (D<a0), D = a0; end;
N = fix(D/a0)+1;
Nc = 0; R=zeros((N-1)^3,3);
for m=0:N-1
    for n=0:N-1
        for p=0:N-1
            Nc = Nc + 1;
            R(Nc,:) = [m n p]; % lattice position
        end;
    end;
end;
if (Nc==0), Nc = 1; R(1,:) = [0 0 0]; end;
R=a0*R;
X = a0*[ 0 0 0; .5 .5 0; .5 0 .5; 0 .5 .5;
.25 .25 .25; .75 .75 .25; .75 .25 .75; .25 .75 .75]; % fractional coordinates
Nx = size(X,1);
for n=2:Nx
    for m=1:Nc
        R((n-1)*Nc+m,:) = R(m,:) + X(n,:);
    end;
end;
Nat = size(R,1);
Cn = sum(R(:,1))/Nat;
X = R - Cn*ones(Nat,3);
if (sph==1)
    X2 = sum(X.*X,2);
    NN = X2<0.25*D*D;
    R = X(NN,:);
    Nat = size(R,1);
    Umax = 1.02*D;
    fname = ['siliconnanod' num2str(round(D)) 'r' num2str(round(amp)) '.pdu'];
else
    Umax = (1.732*1.05)*D;
    fname = ['siliconnanol' num2str(round(D)) 'r' num2str(round(amp)) '.pdu'];
end;
R = R + (0.01*amp*a0*sqrt(3)/4)*(1-2*rand(Nat,3));
du = 0.001;
U = 0:du:Umax;
Nu = size(U,2);
p=zeros(1,Nu);
for n=1:Nat
    for m=n+1:Nat
        r = R(n,:)-R(m,:);
        k=fix(sqrt(r*r')/du)+1;
        p(k) = p(k) + 1;
    end;
end;
p = 2*p;
p(1) = Nat;
M = [U; p];
save(fname,'M','-ascii');

```

82. siliconpeakfit.m

```

function siliconpeakfit(q0,Rg1,xpv1,Rg2,xpv2)
%%%%%%%%%%%%%%%%%%%%%%%%%%%%%%%%%%%%%
% Peak fitting with pseudo-Voigh function
%
% Input:
%   q0 = peak center (1/Angstrom)
%   Rg1, Rg2 = gyration radius (Angstrom)
%   xpv1, xpv2 = pseudo-Voigt for Gaussian(0)/Lorentzian(1) parameter
% Secondary routines required: siliconPofQ.m
% Required files: siliconnanoD200r2.pdu and siliconanoL160r2.pdu
% Files generated by routine siliconnano.m, see http://xraybook.if.usp.br %
% Usage: siliconpeakfit(3.2724,82,0.8,88,0.55)
%%%%%%%%%%%%%%%%%%%%%%%%%%%%%%%%%%%%%
Qmax = 2*sqrt(12*log(2))/min([Rg1 Rg2]); dq = 0.0025;
DQ = -Qmax:dq:Qmax;
Ia = siliconPofQ('siliconanoD200r2.pdu',q0+DQ);
Ia = Ia / max(Ia);
Ya = pseudovoigt(DQ,Rg1,xpv1);
d = Ia-Ya;
gof1 = sum(d.*d);
gof1text = ['\chi^2 = ' num2str(0.001*round(1000*gof1))];
Ib = siliconPofQ('siliconanoL160r2.pdu',q0+DQ);
Ib = Ib / max(Ib);
Ib = pseudovoigt(DQ,Rg2,xpv2);
d = Ib-Yb;
gof2 = sum(d.*d);
gof2text = ['\chi^2 = ' num2str(0.001*round(1000*gof2))];
hf1=figure(1); clf; set(hf1,'InvertHardcopy', 'off','Color','w')
subplot(1,2,1)
set(gca,'Position',[0.09 0.16 0.4 0.83])
plot(DQ,sqrt(Ia),'ro',DQ,sqrt(Ya),'k','LineWidth',1.5)
axis([min(DQ) max(DQ) 0.08 1])
set(gca,'FontSize',14,'Color',[0.97 0.97 0.97],'LineWidth',1)
xlabel('|\Delta Q| (A^{-1})','FontSize',18)
ylabel('root(I/I_{max})','FontSize',18)
text(0.2*max(DQ),.9,gof1text,'FontSize',16)
text(0.9*min(DQ),.95,'(a)','FontSize',20)
grid
subplot(1,2,2)
set(gca,'Position',[0.55 0.16 0.4 0.83])
plot(DQ,sqrt(Ib),'ro',DQ,sqrt(Yb),'k','LineWidth',1.5)
axis([min(DQ) max(DQ) 0.08 1])
set(gca,'YTickLabel',[],'FontSize',14,'Color',[0.97 0.97 0.97],'LineWidth',1)
xlabel('|\Delta Q| (A^{-1})','FontSize',18)
text(0.2*max(DQ),.9,gof2text,'FontSize',16)
text(0.9*min(DQ),.95,'(b)','FontSize',20)
grid

```

```
function Y=pseudovoigt(DQ,Rg,xpv)
```

```

xpv = abs(xpv);
if (xpv>1), xpv = 1; end;
sg = sqrt(1.5)/Rg;
bq = sqrt(12*log(2))/Rg;
X2 = DQ.*DQ;
Y = (xpv/(sg*sqrt(2*pi)))*exp((-1/(2*sg*sg))*X2);
Y = Y + (2*(1-xpv)*bq/pi)./(4*X2+bq*bq);
Y = Y * (1/max(Y));

```

83. siliconPofQ.m

```

function P=siliconPofQ(fname,Q)
%%%%%%%%%%%%%%%%%%%%%%%%%%%%%%%%%%%%%
% Scattering power P(Q) of silicon nanocrystals
%
% Input:
%   Q = n-by-m array with reciprocal vector modules (1/Angstrom)
%   fname = file .pdu, PDFF from routine siliconnano.m
% Output P, n-by-m array with P(Q) values
% Secondary routines required: astfQ.m and fppfpp.m
% Usage: P=siliconPofQ('siliconanoD200r2.pdu',[0:0.001:12.565]);
%%%%%%%%%%%%%%%%%%%%%%%%%%%%%%%%%%%%%
n = regexp(fname,'pdu','once');
if isempty(n), disp(' >>> Unknown file type!!!!'); P=0; return; end;
S=load(fname)';
U = S(1,:);
P = S(2,:);
U(U==0) = 1e-8;
Nn = size(Q);
P = zeros(Nn(1),Nn(2));
Nq = Nn(1)*Nn(2);
Qf = max(max(Q));
Q(Q==0)=1e-8;
fres = fppfpp('Si',Qf/1.0135e-3);
f = astfQ('Si',(0.25/pi)*Q) + fres(2) + li*fres(3);

```

```

f2 = real(f.*conj(f));
for n=1:Nq
    Qu = Q(n)*U;
    P(n) = f2(n) * sum(p.*(sin(Qu)./Qu));
end;

```

84. siliconxrdpattern.m

```

function siliconxrdpattern
%%%%%%%%%%%%%%%%%%%%%%%%%%%%%%%%%%%%%
% Comparison between simulated XRD patterns from %
% PDFP and Fhkl values %
% Secondary routines required: siliconPofQ.m and diffractogram.m %
% Required files: siliconnanoD200r2.pdu and SiE12399.sft %
% File generated by routine siliconnano.m and diffraction.m, %
% see http://xraybook.if.usp.br/
%%%%%%%%%%%%%%%%%%%%%%%%%%%%%%%%%%%%%
Qf = 1.0135*12.3985; % for X-rays of 12.3985 keV
dQ = Qf/5000;
Q = (1:dQ:Qf);
Y = siliconPofQ('siliconnanoD200r2.pdu',Q); % load('siliconpofqD200r2.dat');
Y = (1/max(Y))*Y;
M = diffractogram('SiE12399.sft',85,.4,0);
hf1=figure(1); clf; set(hf1,'InvertHardcopy', 'off','Color','w')
plot(Q,sqrt(Y),'-ko','MarkerSize',6,'MarkerFaceColor','r','MarkerEdgeColor','auto','LineWidth',1)
hold on; plot(M(:,1),sqrt(M(:,3)),'y','LineWidth',1.5); hold off
axis([min(Q) max(Q) 0 1.0])
set(gca,'FontSize',14,'Color',[0.7 0.78 1],'LineWidth',1)
xlabel(['Q (' char(197) '^{-1}')'], 'FontSize',18)
ylabel('(\Gamma/\Gamma_{max})^{1/2}', 'FontSize',18)
ha2=axes('Position',[.5 .55 .385 .36]);
plot(M(:,1),M(:,5),'r','LineWidth',3)
set(ha2,'FontSize',12,'Color',[1 1 1], 'FontName','Arial','LineWidth',1)
grid
xlabel(['Q (' char(197) '^{-1}')'])
ylabel('|\Sigma|F_{hkl}|^2 (rel. values)')
axis tight

```

85. sincfunction.m

```

function sincfunction
%%%%%%%%%%%%%%%%%%%%%%%%%%%%%%%%%%%%%
% Comparison of functions %
% squared sinc, y(x)=|sin(x)/x|^2, and Lorentzian, y(x)=1/(1+x^2) %
%%%%%%%%%%%%%%%%%%%%%%%%%%%%%%%%%%%%%
a = 1; % lattice parameter
Ng = 1000; % number of points in each curve
dq = 1/Ng;
L = -1:dq:1; % reflection index (00L)
Qz = (2*pi/a)*L; % z component of diffraction vector
Nq = size(Qz,2);
Qz(Qz==0)=1e-8;
N=10; % number of unit cell along crystal thickness
t = N*a;
Qt = 0.5*t*Qz;
Z10 = 1./(1+Qt.*Qt);
Y = sin(Qt)./Qt;
Y10 = Y.*Y;
N=500;
t = N*a;
Qt = 0.5*t*Qz;
Z500 = 1./(1+Qt.*Qt);
Y = sin(Qt)./Qt;
Y500 = Y.*Y;
hf1=figure(1); clf; set(hf1,'InvertHardcopy', 'off','Color','w')
semilogy(L,Y10,'b',L,Y500,'b','LineWidth',1)
hold on
semilogy(L,Z10,'k',L,Z500,'k','LineWidth',1.5)
hold off
axis([L(1) L(Nq) 0.5*min(Z500) 1])
set(gca,'FontSize',14,'Color',[0.97 0.97 0.97],'FontName','Arial','Box','on','LineWidth',1)
xlabel('Delta t', 'FontName','Times','FontSize',20);
ylabel('y(x)', 'FontSize',18);
text(.4,0.01,'t = 10a', 'FontSize',16);
text(.4,.6e-6,'t = 500a', 'FontSize',16,'Color','w');

```

86. sincinterference.m

```

function sincinterference
%%%%%%%%%%%%%%%%%%%%%%%%%%%%%%%%%%%%%
% Interference of sinc functions in the range L-1 to L+1 %
%%%%%%%%%%%%%%%%%%%%%%%%%%%%%%%%%%%%%
NL = 1000; % number of points in each curve
dl = 1/NL;
DL = -1:dl:1; % range of index L of reflection HKL
N=20; % number of unit cells along crystal thickness
Ya = curva(DL,N);
N=100;
Yb = curva(DL,N);
N=500;
Yc = curva(DL,N);
hfi=figure(1); clf; set(hfi,'InvertHardcopy','off','Color','w')
semilogy(DL,Ya(3,:),'m',DL,Ya(1,:),'k','LineWidth',1)
legend('B(\Delta_l)', 'A(\Delta_l)')
hold on
semilogy(DL,Ya(4,:),'m',DL,Ya(2,:),'k','LineWidth',1)
semilogy(DL,Yb(3,:),'m',DL,Yb(4,:),'m',DL,Yb(1,:),'k',DL,Yb(2,:),'k','LineWidth',1)
semilogy(DL,Yc(3,:),'m',DL,Yc(4,:),'m',DL,Yc(1,:),'k',DL,Yc(2,:),'k','LineWidth',1)
hold off
axis([DL(1) max(DL) .6e-6 1])
set(gca,'FontSize',14,'Color',[0.97 0.97 0.97],'FontName','Times','Box','on','LineWidth',1)
 xlabel('|\Delta_l|', 'FontSize',20);
 ylabel('A,B', 'FontSize',18);
 text(.42,0.004,'t = 20a', 'FontSize',16);
 text(.42,5e-5,'t = 100a', 'FontSize',16,'Color','w');
 text(.42,2e-6,'t = 500a', 'FontSize',16,'Color','w');

function Y=curva(DL,N)
N=2*floor(0.5*N); % sin(x)/x = 1/(1+ix) works for N even
aux = pi*N;
DQzt_2 = aux*(DL+1);
L = sncltz(DQzt_2);
DQzt_2 = aux*DL;
C = sncltz(DQzt_2);
DQzt_2 = aux*(DL-1);
R = sncltz(DQzt_2);
A = L(1,:)+C(1,:)+R(1,:);
Y(1,:) = A.*A;
A = L(2,:)+C(2,:)+R(2,:);
Y(2,:) = A.*conj(A);
Y(3,:) = L(1,:).*L(1,:)+C(1,:).*C(1,:)+R(1,:).*R(1,:);
Y(4,:) = L(2,:).*conj(L(2,:))+C(2,:).*conj(C(2,:))+R(2,:).*conj(R(2,:));

function M=sncltz(x)
x(x==0)=1e-8;
M(1,:)=sin(x)./x;
M(2,:)=1./(1+li*x);

```

Bibliography

- Als-Nielsen, J., McMorrow, D.: Elements of Modern X-Ray Physics. Wiley, New York (2001)
- Antunes, A., Safatle, A.M.V., Barros, P.S.M., Morelhão, S.L.: X-ray imaging in advanced studies of ophthalmic diseases. *Med. Phys.* **33**, 2338–2343 (2006). doi:10.1118/1.2207135
- Arfken, G.: Mathematical Methods for Physicists. Academic, Orlando (1985)
- Authier, A.:Dynamical Theory of X-Ray Diffraction, revised edn. Oxford University, Oxford (2004)
- Authier, A. (ed.): International Tables for Crystallography, vol. D, online edition (2006). <http://onlinelibrary.wiley.com/book/10.1107/97809553602060000001/toc>
- Barbosa, L.R.S.: Small angle X-ray scattering study of biological relevant systems. Ph.D. Thesis, Institute of Physics, University of São Paulo (2008). <http://www.teses.usp.br/teses/disponiveis/43/43134/tde-20032009-101046/pt-br.php>
- Batterman, B.W., Cole, H.: Dynamical diffraction of X-rays by perfect crystals. *Rev. Mod. Phys.* **36**, 681–717 (1964)
- Bowen, D.K., Tanner, B.K.: High Resolution X-Ray Diffractometry and Topography. Taylor & Francis, London (1998)
- Bragg, W.H., Bragg, W.L.: The reflexion of X-rays by crystals. *Proc. R. Soc. Lond. A* **88**, 428–438 (1913). doi: 10.1098/rspa.1913.0040. www.nobelprize.org/nobel_prizes/physics laureates/1915/
- Cattani, M.S.D.: X-Ray Scattering by Atoms: Basic Equations. Institute of Physics, University of São Paulo, São Carlos (2011). <http://publica-sbi.if.usp.br/PDFs/pd1668.pdf>
- Chang, S.-L.: Multiple Diffraction of X-Rays in Crystals. Springer, Berlin (1984)
- Cohen-Tannoudji, C., Diu, B., Laloë, F.: Quantum Mechanics, vol. 2. Wiley, New York (1978)
- Coppens, P.: International Tables for Crystallography, vol. B, online edition, cap. 1.2, pp. 10–23 (2010). <http://onlinelibrary.wiley.com/book/10.1107/97809553602060000001/toc>
- Craievich, A.: Small-angle X-ray scattering by nanostructured materials. In: Sakka, S. (ed.) Handbook of Sol-Gel Science and Technology: Processing, Characterization and Applications, vol. II, pp. 161–189. Kluwer Academic, New York (2002)
- Cullity, B.D., Stock, S.R.: Elements of X-Ray Diffraction, 3rd edn. Prentice-Hall, Upper Saddle River (2001)
- Egami, T., Billinge, S.J.L. (eds.): Underneath the Bragg Peaks. Pergamon, Oxford (2003)
- Chapman, H.N., et al.: Femtosecond x-ray protein nanocrystallography. *Nature* **470**, 73–77 (2011)
- Ewald, P.P.: Introduction to the dynamical theory of X-ray diffraction. *Acta Crystallogr. A* **25**, 103–108 (1969)
- Franklin, R.E., Gosling, R.G.: Molecular configuration in sodium thymonucleate. *Nature* **171**, 740–741 (1953). doi:10.1038/171740a0

- Giacovazzo, C. (ed.): Fundamentals of Crystallography, 2nd edn. Oxford University, Oxford (2002)
- Glatter, O., Kratky, O. (eds.): Small Angle Scattering of X-Rays. Academic, London (1982)
- Guinier, A.: X-ray Diffraction: In Crystals, Imperfect Crystals, and Amorphous Bodies. Dover, New York (1994)
- Guinier, A., Fournet, G.: Small-Angle Scattering of X-Rays. Wiley, New York (1955)
- Hahn, T. (ed.): International Tables for Crystallography, vol. A, online edition (2006). <http://onlinelibrary.wiley.com/book/10.1107/97809553602060000001/toc>
- Hansen, J.-P., McDonald, I.R.: Theory of Simple Liquids, 2nd edn. Academic, London (1990)
- Hauptman, H.A., Karle, J.: Solution of the phase problem I. The centrosymmetric crystal. A.C.A. Monograph No.3. Polycrystal Book Service, New York (1953). http://www.nobelprize.org/nobel_prizes/chemistry/laureates/1985/
- Holt, M., Wu, Z., Hong, H., Zschack, P., Jemian, P., Tischler, J., Chen, H., Chiang, T.-C.: Determination of phonon dispersions from x-ray transmission scattering: the example of silicon. *Phys. Rev. Lett.* **83**, 3317–3319 (1999)
- Hubbell, J.H., Veigle, W.J., Briggs, E.A., Brown, R.T., Cromer, D.T., Howerton, R.J.: Atomic form factors, incoherent scattering functions, and photon scattering cross sections. *J. Phys. Chem. Ref. Data* **4**, 471–538 (1975)
- Hura, G., Russo, D., Glaeser, R.M., Head-Gordon, T., Krack, M., Parrinello, M.: Water structure as a function of temperature from x-ray scattering experiments and ab initio molecular dynamics. *Phys. Chem. Chem. Phys.* **5**, 1981–1991 (2003)
- James, R.W.: The Optical Principles of the Diffraction of X-rays, 1st edn. G. Bell & Sons Ltd, London (1948)
- Lindner, P., Zemb, T. (eds.): Neutrons, X-Rays and Light: Scattering Methods Applied to Soft Condensed Matter. Elsevier, Amsterdam (2002)
- Lovesey, S.W., Collins, S.P.: X-Ray Scattering and Absorption by Magnetic Materials. Oxford University, Oxford (1996)
- Malachias, A., Freitas, R., Morelhão, S.L., Magalhães Paniago, R., Kycia, S., Medeiros-Ribeiro, G.: X-ray diffraction methods for studying strain and composition in epitaxial nanostructured systems. In: Haight, R., Ross, F.M., Hannon, J.B. (eds.) Handbook of Instrumentation and Techniques for Semiconductor Nanostructure Characterization, vol. 1, pp. 211–279. World Scientific, Washington, D.C. (2011). doi:10.1142/9789814322843_0006
- Morelhão, S.L., Amirkhanyan, Z.G., Rémedios, C.M.R.: Absolute refinement of crystal structures by X-ray phase measurements. *Acta Crystallogr. A* **71** (2015). doi:10.1038/171740a0
- Morelhão, S.L., Brito, G.E.S., Abramof, E.: Nanostructure of sol.gel films by X-ray specular reflectivity. *Appl. Phys. Lett.* **80**, 407–409 (2002). doi:10.1063/1.1436271
- Morelhão, S.L., Härtwig, J., Meier, D.L.: Dislocations in dendritic web silicon. *J. Cryst. Growth* **213**, 288–298 (2000)
- Morelhão, S.L., Remédios, C.M.R., Freitas, R.O., dos Santos, A.O.: X-ray phase measurements as a probe of small structural changes in doped nonlinear optical crystals. *J. Appl. Crystallogr.* **44**, 93–101 (2011)
- Stöhr, J.: NEXAFS Spectroscopy. Springer, Berlin (1992)
- McMaster, W.H., Grande, N.K.D., Mallett, J.H., Hubbell, J.H.: Compilation of X-ray cross sections. Lawrence Livermore National Laboratory Report UCRL-50174 Section II Revision I (1969). Available from National Technical Information Services L-3, U.S. Dept. of Commerce. <http://cars9.uchicago.edu/~newville/mcbook/>
- Newville, M.: The Fundamentals of XAS, Chicago (2004). <http://xafs.org/Tutorials>
- Pietsch, U., Holý, V., Baumbach, T.: High-Resolution X-Ray Scattering: From Thin Films to Lateral Nanostructures, 2nd edn. Springer, New York (2004)
- Pirenne, M.H.: The Diffraction of X-Rays and Electrons by Free Molecules. Cambridge University, Cambridge (1946)
- Prince, E. (ed.): International Tables for Crystallography, vol. C, online edition (2006). <http://onlinelibrary.wiley.com/book/10.1107/97809553602060000001/toc>
- Teixeira, J.: Small-angle scattering by fractal systems. *J. Appl. Crystallogr.* **21**, 781–785 (1988)

- Vocadlo, D.J., Davies, G.J., Laine, R., Withers, S.G.: Catalysis by hen egg-white lysozyme proceeds via a covalent intermediate. *Nature* **412**, 835–838 (2001)
- von Laue, M.: Eine quantitative prufung der theorie fur die interferenzerscheinungen bei rontgenstrahlen. *Ann. Phys.* **346**, 989–1002 (1913). doi:10.1002/andp.19133461005. http://www.nobelprize.org/nobel_prizes/physics/laureates/1914/
- Vuolo, J.H.: Fundamentos da Teoria de Erros, 2^a edn. Edgard Blucher, São Paulo (1996)
- Warren, B.E.: X-Ray Diffraction. Dover Books on Physics, New York (1990).
- Watson, J.D., Crick, F.H.C.: A structure for deoxyribose nucleic acid. *Nature* **171**, 737–738 (1953). doi:10.1038/171737a0. www.nobelprize.org/nobel_prizes/medicine/laureates/1962/
- Weckert, E., Hümmer, K.: Multiple-beam X-ray diffraction for physical determination of reflection phases and its applications. *Acta Crystallogr. A* **53**, 108–143 (1997)
- Wilkins, M.H.F., Stokes, A.R., Wilson, H.R.: Molecular structure of deoxypentose nucleic acids. *Nature* **171**, 738–740 (1953). doi:10.1038/171738a0
- Yi, Z., Ye, J., Kikugawa, N., Kako, T., Ouyang, S., Stuart-Williams, H., Yang, H., Cao, J., Luo, W., Li, Z., Liu, Y., Withers, R.L.: An orthophosphate semiconductor with photooxidation properties under visible-light irradiation. *Nat. Mater.* **9**, 559–564 (2010)
- Zachariasen, W.H.: Theory of X-Ray Diffraction in Crystals. Wiley, New York (1945)

Index

A

Absorption, X-ray, 1. *See also* Photoelectric absorption
atomic resonance, 42–45
semi-classical approach of, 45–48
cross-section, 39–41, 43–47
for Kr, 48
modulation in, 53–54
Kramers–Kronig relations, 48–50
linear attenuation coefficient, 39–42
and scattering cross-section, 40–42
modulation by rescattering of photoelectrons, 50–56
Absorption edge measurement, 206–209
experimental data, 207
photoelectric absorption cross-section, 208–209
transmission coefficients, 208
 α -quartz
atomic structure, 120–121
RDF of, 121
critical angle of, 192–193
disordering periodic structures, 121–123
Alumina, XRD analysis of. *See* X-ray diffraction (XRD) analysis of alumina
Amorphous solids, 116
coordination number, RDF, 117
correlation function, 118
crystallization (*see* Crystallization)
effect of interference in, 40
periodic structures, disordering, 121
Amplitude
resonance, 42, 44–47, 148
modulation, 56

scattering, 212
of atoms, 23, 26, 28
and polarization, 3
and radiation field, 5–6
structure factor, 135–137, 160, 165
Anomalous scattering factors. *See* Dispersion correction terms
Arbitrary correlations
amorphous solid, 116
coordination number, RDF, 117
correlation function, 118
crystallization (*see* Crystallization)
periodic structures, disordering, 121
liquids and colloidal suspensions
RDF, 109
in water, 109–111
mutual interference, 102
non-spherical particles, 100–101
radial distribution function
intensity scattered, 116
 N particles distribution, 111
numerical calculation, 112
packing factor, 116
random positions, generation, 112–113
repulsion effect, 113–115
volume effects
deduction, functions, 105–106
Fourier transform, 103
interference function calculation, 108
scattered intensity, 107
unidirectional correlation, function, 104
ASFQ.m routine, 24, 110, 203, 213–214
assintotic.m routine, 214
Asymptotic behavior, 72, 73, 75, 97–99

- Atomic form factor. *See* Atomic scattering factor
- Atomic planes
coherent scattering by, 132
X-ray wavefronts crossing, 190
- Atomic resonance, 42–45
absorption cross-section for Kr, 48
and refraction index, 192
semi-classical approach of, 45–48
- Atomic scattering factor, 23–24, 26–27, 42
coherent scattering cross-section for Se, 44–45
with dispersed correction, 43
for Ga, 26, 27
- Atoms
Compton scattering by, 33–36
isolated, coherent scattering cross-section for, 27–28
spherically symmetrical, 23–27
- Attenuation coefficient. *See* Linear attenuation coefficient
- B**
- backadj.m routine, 203, 214
- Benzene molecule, scattering by, 32–33
- benzeneonpsp.m routine, 32, 214–215
- benzenesaxs1.m routine, 215–217
- benzenesaxs2.m routine, 217
- Biot–Savart law, 2
- Bragg–Brentano geometry, 164
- bragg.m routine, 133, 158, 217–218
- Bragg’s angle, 155, 182, 183
- Bragg’s law, 132, 133, 144, 182
- Bremsstrahlung. *See* Lae method
- C**
- Calcium, Compton scattering cross-section for, 35
- Carbon, coherent/incoherent intensities scattered by, 36
- Cauchy’s integral theorem, 49
- CIF. *See* Crystallographic information file (CIF)
- Classical electron radius, 6
- Coherence lengths, 8–11
- Coherent scattering, 2, 12
by atomic planes, 132
of atoms, 23–24
cross-section
- effect of atomic resonance in, 44–45
for isolated atoms, 27–28
- interference phenomena of, 40
of one electron, 19–21
- Complex systems
arbitrary correlations (*see* Arbitrary correlations)
internal correlations (*see* Internal correlations)
mathematical description of, 81
- Compton effect, 1–2, 20, 33–35, 41
- Compton scattering, 1–2, 19–22, 64–66, 89, 119, 209
by atoms, 33–36
intensity, 20–21
- Convolution of functions, 16
- Correlation function, 82–83, 93, 102, 104–105, 107, 117–118, 143
internal, 84–85, 101
pair (*see* Radial distribution function (RDF))
- Critical angle for total external reflection, 191
in glass surfaces, 192
- Cromer–Mann coefficients, 24–25
- Cross-section
absorption, 39–41, 43–47
for Kr, 48
modulation in, 53–54
- coherent scattering
effect of atomic resonance, 44–45
for isolated atoms, 27–28
monoatomic gas, 60, 61
parametric equation, 27
for Se, 45
- Compton scattering, 35
parametric equation, 34
- linear attenuation, 40–42
- photoelectric absorption, 50–52
for absorption edge measurement, 208–209
- Thomson scattering, 6–7
- Crystalline lattice
atomic disordering in
occupancy factor, 147–148
thermal vibrations, 142–144
- FT of, 130
- phonons, 144
- thermal diffuse scattering, 144
- truncation of, 138–139
- Crystallization, of amorphous solids, 119
 α -quartz, 120–122
inverse FT, 122
structural analysis, 123–124

- Crystallographic information file (CIF), 158
XRD pattern simulation from, 204–205
- Crystallography. *See* X-ray crystallography
- Crystals
- atomic disordering
 - occupancy factor, 147–148
 - thermal vibrations, 142–144
 - coherent intensity, 131
 - crystalline lattice, 129
 - diffracted intensities, 131, 134–135
 - electron density, 129
 - form factor, 130, 134, 144
 - FT of crystalline lattice, 130
 - kinematic intensity, 138, 143
 - reciprocal lattice point, 131, 132, 134
 - reciprocal lattice vector, 131, 133, 134, 153, 154, 158, 159
 - reciprocal space of, 135
 - reflectivity curves in, 182–185
 - structure factors, 134
 - amplitude, 135, 137
 - phases (direct methods), 137
 - truncation of crystal lattice, 138–139
 - unit cell, 128
- X-ray diffraction, difficulties, 127–128
- csfQ.m routine, 34, 218–219
- D**
- Darwin–Prins dynamical theory, 179, 181
- Data analysis
- absorption edge, measurement of, 206–209
 - PDDF analysis of lysozyme, 195–197
 - PDF analysis of gold particles, 197–201
 - XRD analysis of alumina, 201–206
- debye.m routine, 94, 219
- Debye–Waller factor, 93–94, 97, 144, 162, 206
- Diffracted intensity, 131, 134
- Diffraction imaging techniques, 179–180
- diffraction.m routine, 146, 158, 203, 220–221
- Diffraction pattern
- crystallized insulin, 174
 - polychromatic, spodumene crystal, 173
 - of polycrystalline silicon, 162
- Diffractogram, polycrystalline silicon, 161, 163
- diffractogram.m routine, 203, 206, 222
- Diffractometry. *See* Single crystal diffractometry
- Dirac delta function, 15
- Dispersion correction terms, 44
- Dynamical diffraction
- kinematic limit, 187–190
 - recursive equations, 180–187
- reflection/transmission coefficients by crystallographic planes, 181–182
- refraction index for X-rays, 190–193
- dynamicphase.m routine, 186, 223
- E**
- Elastically bound electron, 45–48
- Elastic scattering. *See* Thomson scattering
- Electric dipole radiation, 2
 - by free electron, 211–212
- Electron density
- of atoms, 23
 - crystals, 129
 - of molecules, 28–29
 - with radial symmetry, form factor for, 17
 - small angle scattering, 69–70
 - spherical particles, 85–86
 - uniform spherical, relative intensity scattered by, 18
 - volumetric electron density function, 13
- Ewald's spheres. *See* Scattering spheres
- ex1GUP.m routine, 115, 223
- ex1N5U.m routine, 70, 224
- exabscs.m routine, 224–225
- EXAFS. *See* Extended XAFS (EXAFS)
- exanomalousignal.m routine, 185, 225
- exasf.m routine, 26–27, 226
- excompton.m routine, 226–227
- excritangle.m routine, 192, 227
- excsf.m routine, 36, 227–228
- exellipsoid.m routine, 228
- exexafsmap.m routine, 230
- exexafs.m routine, 53, 229–230
- exfpfpp.m routine, 231
- exgoful.m routine, 104, 232
- exgofu2.m routine, 108, 232–233
- exgoldnano0.m routine, 90, 233
- exgoldnano1.m routine, 92, 234
- exgoldnano2.m routine, 93, 234–235
- exhardsphere.m routine, 117, 235–236
- exkk.m routine, 236–237
- exlognormal.m routine, 78, 237–238
- elysozyme.m routine, 88, 238–239
- exrdffitting.m routine, 113, 240
- exrdf.m routine, 239–240
- exrdfplot.m routine, 114, 240–241
- exrlp3Dview.m routine, 241
- exsgc.m routine, 242
- exsgr.m routine, 242–243
- exshell.m routine, 86, 243–244
- exsphere.m routine, 18, 245
- Extended XAFS (EXAFS), 54–55
- exwaterccd.m routine, 111, 245–246
- exwaterSofQ.m routine, 110, 246

F

- Fluorescence, 1, 38, 42–43, 53
 Form factor, 14, 16–17, 29
 atomic (*see* Atomic scattering factor)
 crystals, 130, 134, 144
 molecular, 31, 63
 single electron scattering, 19
 for spherically symmetric electron density, 17
 for uniform sphere, 17
 Fourier analysis, 54–55
 in PDF analysis of gold particles, 201
 Fourier transform (FT), 15–18
 of convolution and product, 16
 of crystalline lattice, 130
 inverse, 15, 83, 85–87, 89, 109, 117, 119,
 122, 196–197
 Four-reflection monochromator, 4–5
 fpfpp.m routine, 44, 164, 207, 246–247
 Free electrons
 electric dipole radiation by, 211–212
 interaction, 1–11
 coherence lengths, 8–11
 polarization effects, 2–5
 radiation field, 5–8
 X-ray scattering by distribution of, 12–22
 distributions of one electron and
 Compton scattering, 19–22
 Fourier transform, 15–18
 Friedel's pair, 184
 FT. *See* Fourier transform (FT)
 fthofu.m routine, 247–248
 fthofuplotmap.m routine, 103, 248–249
 fthofuR.m routine, 103, 249
 Full width at half maximum (FWHM),
 160–162

G

- GaAs crystals, reflectivity curves for, 185
 Gallium, atomic scattering factor for, 26, 27
 Gases
 ideal, effect of interference in, 40
 monoatomic (*see* Monoatomic gas)
 goldnano.m routine, 249–250
 Gold nanoparticles
 PDDFs, 93
 wide angle, 91–92
 X-ray scattering, 91–92
 Gold particles, PDF analysis of. *See* Pair
 density function (PDF)
 Goniometer, 165–166, 168
- Grazing incidence techniques, 138, 155, 191
 Gyration radius, in PDDF analysis of
 lysozyme, 197

H

- histogram.m routine, 250–251

I

- Ideal gas, effect of interference in, 40
 Incident wave, X-ray, 2
 Incoherent scattering. *See* Compton scattering
 Inelastic scattering. *See* Compton scattering
 Integrated intensity, 156, 160, 165, 167
 Integrated reflectivity of crystals, 187–188
 Intensity, scattering, 3–4, 6–7, 14. *See also*
 Kinematic intensity
 arbitrary correlations, 107, 116
 coherent, 27, 28
 Compton scattering, 2, 20–21
 crystals
 coherent intensity, 131
 kinematic intensity, 138, 143
 relative intensity scattered by uniform
 spherical electron density, 18
 single electron, 19
 by single molecule, 29–32

Interference, 12

- dispersed molecules, 64
 mutual interference, 81–82
 self-interference, 19–20

Internal correlations

- molecules, proteins, and discrete particles,
 86–87
 limit of small angle, 87–89
 wide angle solution, 89–94

PDDF, 84

- random conformation particles
 asymptotic behavior, 97–99
 polymers (*see* Polymers)
 scattering power, 84
 spherical particles, radial electron density,
 85–86

spherically symmetrical function, 84

- Interplanar distances, 132, 133, 157–158, 165
 Inverse Fourier transform, 15, 83, 85–87, 89,
 109, 117, 119, 122, 196–197

invftpofq.m routine, 251–252

- Ionization, effect on scattering amplitude, 26
 Iron, modulation of resonance amplitude of, 56
 Isotropic vibrations, 142–143

J

Joule heating effect, 38

K

KDP. *See* Potassium dihydrogen phosphate (KDP)
kdcoordfrac.m routine, 202, 252
kdphistcomp.m routine, 252–253
kdphistogram.m routine, 253
Kinematic diffraction
 vs. dynamical diffraction, 179–180
 powder diffractometry
 crystallographic information file, 158
 polycrystalline samples, relative intensities, 158–161
protein crystals, 174–176
reciprocal space
 coherent radiation, 152
 Ewald's spheres (*see* Scattering spheres)
 scattering spheres, 152
reflection/transmission coefficients, 182
single crystal diffractometry
 monochromatic radiation, 165–167
 polychromatic radiation, 170–171
validity, 189–190
Kinematic intensity, 59
dispersed molecules
 coherent intensity scattered by N molecules, 63
 interference pattern, 64
 molecule form factor, 63
 scattered intensity by single molecule, 63
 scattering power, 64
 structural function, 64
general expression of, 59
monoatomic gas
 beam transverse coherence length, 61
 coherent scattering cross-section, 60, 61
 Fourier transform, 60
small angle scattering
 dispersion of size, 74–78
 macromolecules, 68–69
 morphology of particles, 71–74
 particles of uniform density, 69–70
 polydisperse systems, 74–78
Kinematic limit, 187–190
kinematiclimit.m routine, 188, 190, 253–254
Kramers–Kronig relations, 43, 48–50, 55
Krypton, absorption cross-section for, 48

L

Laue method, 171
lauemethod.m routine, 173, 254–256
Linear attenuation, and scattering cross-section, 40–42
Linear attenuation coefficient, 39–42
Longitudinal coherence length, 9–11
Lorentz factor, 156
Lysozyme
 integrated reflectivity in, 188
 interatomic distances, 88
 PDDF (*see* Pair distance distribution function (PDDF), lysozyme analysis)
 scattering power, 88–89

M

Manganese, modulation in absorption cross-section of, 53–54
Maxwell's equations, 5, 211
Molecular form factor, 31
Molecules
 dispersed
 coherent intensity scattered by N molecules, 63
 form factor, 63
 interference pattern, 64
 scattered intensity by single molecule, 63
 scattering power, 64
 structural function, 64
 scattering by, 28–33
Monoatomic gas
 beam transverse coherence length, 61
 coherent scattering cross-section, 60, 61
 Fourier transform, 60
 scattering angle, 60
Monochromatic radiation
 charge coupled device, 166
 goniometer, 165, 168
 high structural complexity crystals, 166
 integrated intensity, 165
 low structural complexity crystals, 165
 reflection power (*see* Integrated intensity)
 rotating crystal method, 166, 167
Monocrystalline blocks with channel cut, 184
Mutual interference, 81–82

N

Near-edge X-ray absorption spectrum (NEXAFS), 53
Nodes. *See* Reciprocal lattice points (RLPs)

O

`orientcryst.m` routine, 257–258
 Oxygen, coherent scattering cross-section for, 28

P

Pair correlation function. *See* Radial distribution function (RDF)
 Pair density function (PDF), analysis of gold particles, 197–201
 background correction, 199–200
 Fourier analysis, 201
 loading intensity data, 199
 normalizing $S(Q)$, 200–201
 structural function $S(Q)$, 199
 Pair distance distribution function (PDDF), 84, 161–163
 lysozyme analysis, 195–197
 gyration radius, 197
 inverse Fourier transform, 196–197
 loading intensity data, 196
 Parametric equation, 24
 of coherent scattering cross-section, 27
 of Compton scattering cross-section, 34
 Patterson function, 82–83
`pdbcoordfrac.m` routine, 175, 177, 258–259
 PDDF. *See* Pair distance distribution function (PDDF)
 PDF. *See* Pair density function (PDF)
 Phase problem, 28–33
 Phonons, 144
 Photoelectric absorption, 40
 and dynamical diffraction, 182, 183
 modulation by rescattering of, 50–56
 cross-section of Mn, 52–53
 scattering properties by neighboring atoms, 53
 and refraction index, 191
 Photoelectrons, 38, 40, 42, 47
 wavevector with kinetic energy, 50–51
 Photon–electron interaction, 19–20
 Photon energy, 1
`photonusonpsp.m` routine, 259
`photostatistic.m` routine, 260
 Polarization coefficient, 22
 Polarization effects, on free electron radiation, 2–4
 electron in forced vibration, 3
 Polychromatic radiation, 170–171
 Polycrystals, relative intensities in, 158–164
`polymerchain.m` routine, 95, 260–261
`polymerkratky.m` routine, 98, 261–262
`polymer.m` routine, 260

`polymerRg.m` routine, 99, 262

Polymers
 plastic bags, 97–98
 RW model, 96
 scattering power, 94–95
`polymersystem.m` routine, 262
 Porod’s law, 76
 Potassium dihydrogen phosphate (KDP), 145–147
 Powder diffractometry of polycrystals
 area profile of diffraction peaks, 160–161, 163
 geometric factors, 158–159
 line profile of diffraction peaks, 160–161, 163
 Probability density function, 19–21

Q

Quantum electrodynamics (QED), 19
`quartzgofu.m` routine, 122, 263
`quartzIoF.Q.m` routine, 122, 264
`quartzrdf.m` routine, 266–267
`quartzrdfplot.m` routine, 121, 267
`quartzR.m` routine, 120, 121, 264–266

R

Radial distribution function (RDF), 109
 atomic structure of α -quartz, 121
 intensity scattered, 116
 N particles distribution, 111
 numerical calculation, 112
 packing factor, 116
 random positions, generation, 112–113
 repulsion effect, 113–115
 Radiation–electron elementary interaction. *See* Free electron interaction
 Radiation field, in free electron interaction, 5–8, 14
 Radius of gyration, 67, 75
`rddarwinprins.m` routine, 184, 189, 267–269
`rddarwinprinsplot.m` routine, 183, 269
 RDF. *See* Radial distribution function (RDF)
 Reciprocal lattice, crystals, 130, 131
 Reciprocal lattice points (RLPs), 131, 132, 134
 Reciprocal node, 154–156, 166, 170, 171
 Reciprocal space, 152–154, 159, 161, 171, 174
 Recursive equations, 180–187
 standing waves, 186–187
 Reflected beam geometry. *See* Bragg–Brentano geometry

Reflection power. *See* Integrated intensity
Reflectivity curves, in crystals, 182–185
 dynamic phase as function of, 186
Refraction index for X-rays, 190–193
 critical angle for total external reflection in
 glass surfaces, 192–193
 wavefronts crossing atomic plane, 190
Relative intensities in polycrystals, 158–164
Resonance. *See* Atomic resonance
RLPs. *See* Reciprocal lattice points (RLPs)
rockingcurve.m routine, 269–270
Rocking curves, 155, 157, 160
Root mean square deviation, atomic positions,
 144, 146
rotatcryst.m routine, 270–272
Rotating crystal method, 166, 167, 174, 175
rotcrystmethod.m routine, 175, 272–274

S

SAXS. *See* Small angle X-ray scattering
 (SAXS)
saxs.c routine, 68, 70, 274
saxs.m routine, 87, 275
Scalar polarization factor, 4
Scattering spheres, 152, 153, 159, 160
Schrödinger equation, 51
Selenium, coherent scattering cross-section for,
 44–45
Self-interference, 19–20
sfactor.m routine, 158, 202, 275–276
sgcompton.m routine, 34, 42, 164, 209,
 276–277
sgrayleigh.m routine, 27, 42, 164, 209,
 277–278
siliconDScamera.m routine, 278–279
siliconnano.m routine, 161, 279
siliconpeakfit.m routine, 280
siliconPofQ.m routine, 161, 280–281
siliconxrddpattern.m routine, 281
sincfunction.m routine, 281
sincinterference.m routine, 282
Single crystal diffractometry
 monochromatic radiation
 goniometer, 165
 high structural complexity, 166
 low structural complexity, 165
 rotating crystal method, 166, 167
 polychromatic radiation, 170–171
Single electron scattering, 19–22
 form factor, 19
 intensities, 19, 21
Small angle scattering
 macromolecules

 pdb format, 68
 protein data bank, 68
Morphology of particles
 asymptotic behaviors, 72, 73
 exponential decay, 71
 Guinier region, 71, 72
 Porod region, 71, 72
 spherical particle, 71
Particles of uniform density
 electron density, 69–70
 small angle X-ray scattering, 70
Polydisperse systems
 average gyration radius, 67, 75
 dispersion of size, 75
 intensity, 75
 Porod's law, 76
 property of, 67
Small angle X-ray scattering (SAXS), 70
Snell's law, 191
Solids. *See* Amorphous solids
Spheriosymmetrical atoms, 23–27
Spheriosymmetric electron density, form factor
 for, 17
Standing waves methods, 179–180, 186–187
Synchrotron, 3, 33, 41, 43, 54, 170, 191

T

TDS. *See* Thermal diffuse scattering (TDS)
Temperature factor. *See* Debye–Waller factor
Thermal diffuse scattering (TDS), 144
Thickness of crystals
 and integrated reflectivity, 187–188
 and reflection and transmission coefficients,
 189
Thomson scattering, 1–2, 6–7, 19
 differential cross-section of, 6
 total cross-section of, 7
 by volumetric distribution of free
 electrons, 13
Thomson scattering length. *See* Classical
 electron radius
Transverse coherence length, 9–10

V

Vectorial Bragg's law, 153
Vector polarization factor, 3, 212
Volumetric electron density function, 13

W

Wavevectors, 152, 154, 167, 169, 170, 175

X

- X-ray absorption fine structure (XAFS), 50
X-ray absorption near-edge spectroscopy (XANES), 53
X-ray absorption spectroscopy, 40
X-ray crystallography, 28–29. *See also* Crystals
crystalline lattice, 129
crystal's electron density, 129
crystal's form factor, 130
diffracted intensities, 134–135
FT of crystalline lattice, 130
structure factors, 134–135
unit cell, 128
X-ray diffraction (XRD) analysis of alumina, 201–206
background intensity, adjusting, 204
comparison of experimental and simulated patterns, 205–206
loading intensity data, 203
pattern simulation from CIF, 204–205
X-ray optics, 179, 184, 190
X-ray specular reflectometry, 191